



UNIVERSIDAD DE GRANADA

FACULTAD DE FARMACIA

DEPARTAMENTO DE QUÍMICA FARMACÉUTICA Y ORGÁNICA

PROGRAMA DE DOCTORADO EN FARMACIA

TESIS DOCTORAL

SÍNTESIS DE NUEVOS COMPUESTOS INHIBIDORES DE GLICOLATO OXIDASA. APLICACIÓN EN HIPEROXALURIA PRIMARIA Y EVALUACIÓN BIOLÓGICA

DOCTORANDA

MARÍA DOLORES MOYA GARZÓN

DIRECTORA

DRA. MÓNICA DÍAZ GAVILÁN

GRANADA, 6 DE SEPTIEMBRE DE 2019

Editor: Universidad de Granada. Tesis Doctorales
Autor: María Dolores Moya Garzón
ISBN: 978-84-1306-303-4
URI: <http://hdl.handle.net/10481/57135>

La doctoranda / *The doctoral candidate* María Dolores Moya Garzón y la directora de la tesis / and the thesis supervisor Dra. Mónica Díaz Gavilán.

Garantizamos, al firmar esta tesis doctoral, que el trabajo realizado por el doctorando bajo la dirección de la directora de la tesis y hasta donde nuestro conocimiento alcanza, en la realización del trabajo, se han respetado los derechos de otros autores a ser citados, cuando se han utilizado resultados o publicaciones.

/

Guarantee, by signing this doctoral thesis, that the work has been done by the doctoral candidate under the direction of the thesis supervisors and, as far as our knowledge reaches, in the performance of the work, the rights of other authors to be cited (when their results or publications have been used) have been respected.

Lugar y fecha/ *Place and date*: Granada, 1 de Julio de 2019

Directora de la tesis / *Thesis supervisor*

Doctorando / *Doctoral Candidate*

Firmado / *Signed*

Firmado / *Signed*

“Nothing in life is to be feared, it is only to be understood. Now is the time to understand more, so that we may fear less”

Maria Skłodowska-Curie

Agradecimientos

Aunque parecía algo lejano en el horizonte y daba la sensación de que nunca iba a llegar, después de tanto trabajo y esfuerzo, llega el fin de una etapa. Por eso, es momento de dar las gracias a todas aquellas personas que me han acompañado durante este intenso viaje.

En primer lugar a Mónica, que me ha sabido dirigir para completar con éxito este largo camino. Gracias por confiar en mí para formar parte de este proyecto, por enseñarme y acompañarme a lo largo de estos años con tanta ilusión y entusiasmo.

A José Antonio, que ha sido mucho más que un tutor para mí durante todos estos años. Gracias por todos los consejos y ayuda recibidos.

A Guille, sin duda, mi compañero y amigo. Sin él, el día a día en el laboratorio habría sido una misión imposible. Gracias por las charlas, los cafés, las risas, y sobre todo, por la amistad. Pero no todo ha sido trabajar, también hemos compartido buenos momentos fuera del laboratorio, que espero que una vez pasado el agobio de las tesis se repitan.

A todos los demás miembros del grupo BIO-250 y del Departamento de Química Farmacéutica y Orgánica. A Juan, que me introdujo al mundo de la Química Orgánica allá por segundo de carrera y que fue el primero que me animó a formar parte de este grupo de investigación. A Paco, por su ayuda como tutor en el máster y sus consejos y a Pepe, por los buenos momentos en el laboratorio.

A todos los demás compañeros que han pasado por el grupo: Javi, Manoli, María Gracia, Silvia, los compañeros de México...también al resto de compañeros del departamento: Angélica, Fabio, Jose, Nerea...gracias por los buenos ratos que hemos compartido juntos.

Al Centro Instrumentación Científica de la Universidad de Granada, especialmente a los técnicos Samuel, y Alí y Huda, por toda la ayuda prestada durante estos años.

Al Prof. Eduardo Salido, por haberme dado la oportunidad de realizar una enriquecedora estancia en Tenerife que tanto valor ha dado a mi tesis. También al resto de miembros de su grupo, especialmente a Cristina y a Bárbara, por su incansable ayuda con los ensayos biológicos a lo largo de estos años. También Orfan Biotech, especialmente a Miguel, por toda su ayuda y paciencia, así como los

conocimientos que me supo transmitir durante mi estancia, y a Alicia, mi compañera tanto dentro como fuera del laboratorio durante esa etapa.

Al Dr. Angel Pey, por su gran ayuda con la producción y purificación de enzimas que tanto han contribuído a nuestra investigación.

Gracias también a las entidades que han financiado esta tesis doctoral, especialmente a la OHF (*Oxalosis and Hyperoxaluria Foundation*), tanto por el contrato de investigación concedido como las ayudas a congresos, y a la Universidad de Granada por la concesión de un contrato predoctoral FPU del plan propio.

Al Prof. Mario van der Stelt, por haberme brindado la oportunidad de realizar mi estancia internacional en la Universidad de Leiden, y también a la Dra. Marjolein Soethoudt, quien me enseñó a trabajar en el apasionante mundo de la proteómica.

A mi amiga Verónica, por haberme acompañado desde desde la infancia en esta y en cada una de las etapas vividas.

A mis farmacéuticas Laura y Teresa: a pesar de haber estado a muchos km de distancia durante los últimos años, me han acompañado durante la tesis apoyándome y dándome fuerza en todo momento.

A toda mi familia, por haberme apoyado y dado ánimos para llegar al final de este largo camino.

Y por supuesto a Antonio, que ha sido mi pilar fundamental durante todos estos años. Por todos los momentos en los que me ha acompañado (y aguantado) y por los que aún quedan por venir!

Quality criteria to apply for the degree of “International PhD” by the University of Granada

To apply for the mention of “International Doctorate”, this doctoral thesis is supported by:

1. One international internship: Short-term stay at the Leiden Institute of Chemistry (Leiden University, The Netherlands), under the supervision of Prof. Mario van der Stelt, Professor of Molecular Physiology. This stay was performed from the 1st of May to the 31st of July of 2017 and was funded by “Convocatoria de movilidad internacional de estudiantes de doctorado”, Universidad de Granada (2016-2017). Project: “Photoaffinity labeling experiments with a THC-based probe performed on neuronal cells to identify off-target proteins of THC (tetrahydrocannabinol)”.

2. One published scientific article in a relevant journal in the field of the doctoral thesis scope. This published article includes part of the doctoral thesis results.

Moya-Garzón, M. D.; Martín Higuera, C.; Peñalver, P.; Romera, M.; Fernandes, M. X.; Franco-Montalbán, F.; Gómez-Vidal, J. A.; Salido, E.; Díaz-Gavilán, M. Salicylic Acid Derivatives Inhibit Oxalate Production in Mouse Hepatocytes with Primary Hyperoxaluria Type 1. *Journal of Medicinal Chemistry* **2018**, *61* (16), 7144–7167.

Impact Factor (JCR 2018): 6.054. Medicinal Chemistry: 3/61 (Q1)

3. According to the University of Granada criteria to obtain an “International PhD” degree, this doctoral thesis has been written and will be partially defended in English. Additionally, and following the requirement of the University of Granada, some parts of the document (abstract and conclusions) have also been written in Spanish.

Grants and Funding

The PhD candidate María de los Dolores Moya Garzón is grateful to the funding sources that have made this doctoral thesis possible:

- “Ayuda para la Formación de Profesorado Universitario (FPU)”. Plan Propio de la Universidad de Granada (2013).
- “Convocatoria de movilidad internacional de estudiantes de doctorado”. Universidad de Granada (2016-2017).
- Programa “Estancias Breves en centros de investigación nacionales y extranjeros”. Universidad de Granada (2017-2018).
- This work has been funded by BIO-250 group projects from the Oxalosis and Hyperoxaluria Foundation (OHF Research Grant Program 2013), from the University of Granada (“Proyectos de Investigación precompetitivos”, convocatoria 2017, ref. PP2016-PIP05) and from the Ministerio de Ciencia, Innovación y Universidades (Proyectos de I+D+i “Retos Investigación”, convocatoria 2018, ref. RTI2018.098560.B.C21).
- Prof. Mario van der Stelt group from the University of Leiden and Prof. Eduardo Salido group from the University of la Laguna, for hosting and providing scientific material and assistance to the PhD candidate.

Index

Quality criteria to apply for the degree of “International PhD” by the University of Granada	9
Grants and Funding.....	11
Index	13
Abstract	19
Resumen.....	21
Abbreviations.....	23
1. Objectives.....	29
2. Introduction.....	33
2.1. Biological background.....	33
2.1.1. Hyperoxaluria	33
2.1.1.1. Primary hyperoxalurias	33
2.1.1.1.1. Primary hyperoxaluria type 1 (PH1).....	35
2.1.1.1.2. Primary hyperoxaluria type 2 (PH2).....	37
2.1.1.1.3. Primary hyperoxaluria type 3 (PH3).....	38
2.1.1.2. Secondary hyperoxaluria	38
2.1.2. Treatments approaches in PH1.....	40
2.1.2.1. Current treatment approaches	40
2.1.2.1.1. Symptomatic approaches.....	40
2.1.2.1.2. Curative approaches	42
2.1.2.2. Future treatment approaches	43
2.1.2.2.1. Gene therapy	43
2.1.2.2.2. Cell Therapy.....	43
2.1.2.2.3. Pharmacological chaperones.....	43
2.1.2.2.4. Mistargeting correctors	44
2.1.2.2.5. Enzyme replacement therapy	44
2.1.2.2.6. Substrate-reduction therapy	45
2.1.3. Glycolate oxidase (GO).....	48
2.1.3.1. GO inhibition for the treatment of PH1	49
2.1.4. Lactate dehydrogenase (LDH)	53
2.1.4.1. LDHA inhibitors	55

2.1.4.2. LDHA inhibition for the treatment of PH	57
2.1.5. Salicylic acid derivatives	59
2.2. Chemical background	62
2.2.1. Suzuki-Miyaura cross-coupling reaction	62
2.2.2. Reductive amination	64
3. Results and discussion	69
3.1. Oxamic acids and homologous derivatives	71
3.1.1. 2-Oxoacetic acid derivatives and 3-oxopropanoic acid derivatives	77
3.1.1.1. 2-Oxoacetic acid derivatives.....	77
3.1.1.2. 3-Oxopropanoic acid derivatives	79
3.1.2. 4-Oxobutanoic acid derivatives	80
3.1.3. Discussion	81
3.2. Salicylic acid derivatives	82
3.2.1. Commercial salicylic acid derivatives	83
3.2.1.1. Results.....	83
3.2.1.2. Discussion.....	89
3.2.2. Preliminary design, synthesis and biological evaluation of salicylic acids.....	90
3.2.2.1. Non-salicylic derivatives	91
3.2.2.1.1. Results and discussion	91
3.2.2.2. Heteroarylsalicylates	96
3.2.2.2.1. Results	96
3.2.2.2.2. Discussion	106
3.2.2.3. Biphenyl or Arylsalicylate Analogues.....	110
3.2.2.3.1. Results	110
3.2.2.3.2. Discussion	116
3.2.2.4. Discussion on the preliminary results for salicylic acid derivatives.....	118
3.2.3. Salicylic acid derivatives containing two-atom nitrogen-based spacers.....	120
3.2.3.1. Results.....	120
3.2.3.2. Discussion.....	129
3.2.4. Chemical modifications on the formyl group of MDMG-409	130
3.2.4.1. Reductive amination: Results on the synthesis of aminomethylfuryl derivatives of MDMG-409.....	130
3.2.4.2. Aldol condensation: Results on the synthesis of α,β -unsaturated derivatives.	135

3.4.2.3. Results of the biological evaluation of aminomethylfuryl and α,β -unsaturated carbonyl derivatives of MDMG-409.	136
3.4.2.2. Discussion on the biological activity of aminomethylfuryl and α,β -unsaturated carbonyl derivatives of MDMG-409	141
3.3. LDH inhibition	143
3.3.1. Results	144
3.3.1.1. Evaluation of aminomethylfuryl derivatives and α,β -unsaturated carbonyl derivatives against <i>h</i> LDH.	145
a) <i>h</i> LDHA isoenzyme.....	145
b) <i>h</i> LDHB isoenzyme	147
3.3.1.2. Evaluation of derivatives with two-atom nitrogen-based spacers against <i>h</i> LDH.	148
3.3.2. Discussion	149
4. Conclusions	153
4. Conclusiones	155
5. Experimental section.....	159
5.1. General Experimental Methods	159
5.1.1. Chemistry.....	159
5.1.2. Biology	160
5.1.3. HPLC Methods.....	160
5.1.3.1. HPLC methods for Purity Determination	160
5.1.3.2. HPLC methods for colorimetric interferences	161
5.2. General synthetic procedures	162
5.2.1. General synthetic procedure 1: Aniline acylation with ethyl 2-chloro-2-oxoacetate and ethyl 3-chloro-3-oxopropanoate.	162
5.2.2. General synthetic procedure 2: Aniline acylation with succinic anhydride.....	162
5.2.3. General synthetic procedure 3: Basic hydrolysis of ethyl esters.....	162
5.2.4. General synthetic procedure 4: Boc deprotection.	162
5.2.5. General synthetic procedure 5: Suzuki–Miyaura (SM) cross-coupling.	163
5.2.5.1. Method A	163
5.2.5.2. Method B	163
5.2.5.3. Method C	164
5.2.5.4. Method D	164
5.2.6. General synthetic procedure 6: Reductive amination.....	164
5.2.6.1. Method A	164

5.2.6.2. Method B	165
5.2.6.3. Method C	165
5.3. Synthesis of oxamic acid derivatives	166
5.3.1. Synthesis of biphenyl compounds	166
5.3.2. Synthesis of ethyl 2-amino-2-oxoacetate derivatives (ethyloxamates) and ethyl 3-amino-3-oxopropanoate derivatives.....	169
5.3.3. Synthesis of 2-oxoacetic and 3-oxopropanoic acid derivatives	173
5.3.4. Synthesis of 4-oxobutanoic acid derivatives from succinic anhydride	178
5.4. Synthesis of salicylic acid derivatives	181
5.4.1. Synthesis of non-salicylic derivatives and heteroarylsalicylates	181
5.4.2. Synthesis of salicylic acid derivatives containing two-atom nitrogen-based spacers.....	194
5.4.2.1. Synthesis of salicylate derivatives containing flexible methylamino linkers... 194	
5.4.2.2. Synthesis of salicylate derivatives containing rigid imino and azo linkers.....	203
5.4.3. Synthesis of derivatives of the lead compound MDMG-409.....	205
5.4.3.1. Synthesis of aminomethylfuryl derivatives of MDMG-409.	205
5.4.3.2. Synthesis of α,β -unsaturated carbonyl derivatives of MDMG-409.	214
5.5. Synthesis of chemical probes derived from MDMG-409	216
5.6. Biological evaluation of the compounds.....	220
5.6.1. Enzymatic assays	221
5.6.1.1. Glycolate oxidase	221
5.6.1.1.1. Glycolate oxidase production	221
Method A for GO production (University of La Laguna)	221
Method B for GO production (University of Granada).....	222
5.6.1.1.2. Glycolate oxidase colorimetric assay.....	223
5.6.1.1.3. Glycolate oxidase fluorometric assay	224
5.6.1.1.4. Interference tests in the GO enzymatic assay	225
Test for colorimetric interferences	225
Test for interferences by HRP inhibition (colorimetric assay).	226
Test for Interferences by HRP Inhibition (fluorometric assay).....	226
5.6.1.2. LDH enzymatic assay	227
5.6.1.2.1. LDH enzymatic assay (absorbance assay)	227
5.6.1.2.2. LDH enzymatic assay (fluorometric assay).....	227
General information	227
Detailed procedure.....	228

5.6.2. Cell culture assay.....	229
5.6.2.1. <i>Agxt1</i> ^{-/-} primary hepatocytes isolation and culture.....	229
5.6.2.2. Cell viability and cytotoxicity.....	229
5.6.2.3. Oxalate determination	229
5.6.2.4. Interference test of the cell culture assay	230
5.7. <i>In silico</i> studies.....	231
5.8. Statistical analysis	232
6. Appendices	235
6.1. <i>In silico</i> predictions.....	235
6.2. Analysis of interferences	256
6.3. Metabolic profiling.....	259
6.4. International short-term stay.....	262
6.5. Rights and permissions	269
6.6. NMR Spectra	270
7. Bibliography.....	351

Abstract

Primary hyperoxaluria type 1 (PH1) is an inborn error of liver metabolism caused by a deficiency in the hepatic enzyme alanine-glyoxylate aminotransferase (AGT), which is in charge of glyoxylate detoxification. The consequent accumulation of the substrate, glyoxylate, leads to its oxidation into oxalate mainly by the enzyme lactate dehydrogenase (LDH) in the cytosol and, in a minor extent, by glycolate oxidase (GO) in the peroxisome. GO also catalyzes glyoxylate production from glycolate. Since oxalate constitutes an end-product of the metabolism, once the renal excretion is exceeded, it starts depositing as insoluble calcium oxalate crystals that initially damage kidneys and liver, and ends causing systemic oxalosis, being the combined kidney-liver transplantation the unique healing option for these patients. One of the current approaches aiming at the search of a non-surgical treatment for the disease is the substrate reduction therapy (SRT). In this sense, GO has been validated as a safe and efficient target for SRT in a PH1 mouse model. On that basis, and considering the structural requirements previously established for the development of GO inhibitors, two new families of GO inhibitors have been prepared: oxamic acid derivatives and salicylic acid derivatives. All of them share a common structure with a polar head, either salicylic acid or oxamic acid-based, and a hydrophobic side chain, for which different substitution options have been explored. Thus, a total of 70 compounds have been synthesized, purified, and characterized, as well as evaluated against isolated GO and in hyperoxaluric mouse hepatocytes, so as to determine their efficacy on oxalate diminution. Within the oxamic acid derivatives, *N*-octiloxamic acid, an established GO inhibitor, was used as reference for the development of three new sub-families: 2-oxoacetic, 3-oxopropanoic, and 4-oxobutanoic acid derivatives. Regarding the salicylic acid derivatives, the furylsalicylates initially synthesized resulted to be moderate GO inhibitors. These furylsalicylates served as a base for structural modulation, so that the introduction of both flexible and rigid spacers between the polar head and the side chain was explored, as well as different side chain options. As a result, potency against GO was considerably improved. Docking studies allowed the binding mode prediction of the salicylic acid derivatives with GO, and this, along with the biological data gathered for these compounds, led to the establishment of preliminary structure-activity relationships for salicylates with activity as GO inhibitors and capacity to decrease oxalate production on cell culture. In fact, salicylates resulted

to be efficient agents decreasing oxalate in cultures, with EC_{50} values at the low micromolar range. For some compounds, discrepancies between the activity against GO and the phenotypic effect in cells were observed. Thus, to determine the existence of alternative biological targets whereby these compounds might be exerting their biological effect, representative compounds were tested against LDH, which is also involved in oxalate production. As a result, salicylic acid derivatives, specifically aminomethylfuryl derivatives, have been identified as potent dual GO/LDH inhibitors. This, along with their drug-like structure and easy two-step synthesis, makes them promising candidates for the development of a multi-target approach for the treatment of PH1.

Resumen

La hiperoxaluria primaria tipo 1 (HP1) es una enfermedad rara hereditaria causada por un déficit de la enzima hepática alanina-glioxilato aminotransferasa (AGT), encargada de la detoxificación de glioxilato. Como consecuencia, se produce una acumulación de su sustrato, el glioxilato, que pasa a ser oxidado a oxalato principalmente por la enzima lactato deshidrogenasa (LDH) en el citoplasma, y en menor medida, por la enzima glicolato oxidasa (GO), en el peroxisoma. La enzima GO, además, cataliza la producción de glioxilato a partir de glicolato. Dado que el oxalato constituye un producto final del metabolismo, una vez superada la capacidad de excreción renal, comienza a formar depósitos insolubles de oxalato cálcico afectando inicialmente a hígado y riñón, y extendiéndose finalmente a nivel sistémico, siendo el trasplante renal y hepático la única opción curativa para estos pacientes. La terapia de reducción de sustrato (SRT) destaca entre las estrategias actuales que persiguen la búsqueda de un tratamiento no quirúrgico para la enfermedad. En este sentido, la enzima GO ha sido validada como una diana eficiente y segura para la terapia de reducción de sustrato en un modelo de HP1 de ratón. En base a ello, y considerando los requisitos estructurales previamente establecidos para los inhibidores de GO, se ha llevado a cabo la preparación de dos nuevas familias de este tipo de inhibidores: los derivados de ácido oxámico y los derivados de ácido salicílico. En la estructura de todos ellos se ha mantenido una cabeza polar, ya sea derivada de ácido oxámico o salicílico, y una cadena lateral hidrofóbica, para la cual se han explorado diferentes opciones de sustitución. Así, se ha llevado a cabo la síntesis, purificación y caracterización de un total de 70 compuestos, así como su evaluación biológica frente a la enzima GO aislada y en hepatocitos de ratón hiperoxalúrico, con objeto de determinar su eficacia en la reducción de oxalato. Dentro de los derivados de ácido oxámico, el ácido *N*-octiloxámico, un inhibidor GO de referencia, se tomó como modelo para el desarrollo de tres subfamilias de compuestos: derivados del ácido 2-oxoacético, 3-oxopropanoico y 4-oxobutanoico. En cuanto a los derivados de ácido salicílico, los furilsalicilatos inicialmente sintetizados demostraron ser inhibidores de GO moderados. Estos furilsalicilatos sirvieron como base para la modulación estructural, de forma que se exploró la introducción de espaciadores tanto rígidos como flexibles entre la cabeza polar y la cola hidrofóbica, así como diferentes opciones de cadena lateral. Como resultado, se consiguió mejorar en gran medida la potencia contra GO. Gracias a los estudios de *docking* se pudo predecir el modo de unión de

los derivados de ácido salicílico a la enzima GO, y esto, junto a la información biológica obtenida para estos compuestos, permitió el establecimiento de relaciones estructura actividad preliminares para salicilatos inhibidores de GO y con capacidad para reducir la producción de oxalato en cultivos celulares. De hecho, los salicilatos han resultado ser agentes eficaces en la reducción de oxalato en cultivos, con valores de CE_{50} en el rango micromolar bajo. Para algunos compuestos se observaron discrepancias entre la actividad contra la enzima GO y la actividad fenotípica en células. Por ello, con objeto de determinar posibles dianas biológicas alternativas mediante las cuales estos compuestos podrían estar ejerciendo su efecto biológico de reducción de oxalato, algunos compuestos representativos fueron evaluados frente a la enzima LDH, también implicada en la producción de oxalato. Como resultado, los derivados de ácido salicílico, en concreto los aminometilfuril derivados, han sido identificados como potentes inhibidores dobles GO/LDH. Esto, junto con su estructura *drug-like* y su sencilla síntesis en dos pasos usando la reacción de Suzuki y la aminación reductora, los convierte en compuestos prometedores para el desarrollo de una aproximación multi-diana para abordar el tratamiento de HP1.

Abbreviations

AAV	Adeno-associated virus
ADME	Absorption, distribution, metabolism and excretion
AGT	Alanine-glyoxylate aminotransferase
AGT-Ma	<i>Major</i> haplotype of alanine-glyoxylate aminotransferase
AGT-Mi	<i>Minor</i> haplotype of alanine-glyoxylate aminotransferase
AOA	Aminooxyacetic acid
ASA	Acetylsalicylic acid
Boc	<i>tert</i> -Butyloxycarbonyl
CCPST	4-Carboxy-5-[(4-chlorophenyl)-sulfanyl]-1,2,3-thiadiazole
cDNA	Complementary deoxyribonucleic acid
CDST	4-Carboxy-5-dodecylsulfanyl-1,2,3-triazole
COX	Cyclooxygenase
DAO	D-Aminoacid oxidase
DCHBS	Sodium 3,5-dichloro-2 hydroxybenzenesulfonate
DCIP	Dichloroindophenol
DECA	Dequalinium chloride
DMF	Dimethylformamide
EC ₅₀	Half maximal efficacy concentration
EDC	1-Ethyl-3-(3-dimethylaminopropyl)carbodiimide
ERT	Enzyme replacement therapy
ESRT	End-stage renal disease
ESWL	Extracorporeal shock wave lithotripsy

FAD	Flavin adenine dinucleotide
FDA	Food and Drug Administration
FMN	Flavin mononucleotide
GFR	Glomerular filtration rate
GO	Glycolate oxidase, from human (<i>hGO</i>) or mouse (<i>mGO</i>)
GOi	Glycolate oxidase inhibitor
GRHPR	Glyoxylate reductase/hydroxypyruvate reductase
HOBt	Hydroxybenzotriazole
HOGA	4-Hydroxy-2-oxoglutarate aldolase
HPLC	High-performance liquid chromatography
HRP	Horseradish peroxidase
HTS	High-throughput screening
IC ₅₀	Half maximal inhibitory concentration
K_i	Inhibition constant
LDH	Lactate dehydrogenase
Mp	Melting point
mRNA	Messenger ribonucleic acid
MTS	Mitochondrial targeting sequence
NAD	Nicotinamide adenine dinucleotide
NF- κ B	Transcription factor nuclear factor-kappa-B
NSAID	Nonsteroidal anti-inflammatory drug
OMIM	Online Mendelian Inheritance in Man
PAL	Photoaffinity labeling
PH	Primary Hyperoxaluria

PL	Pyridoxal
PLP	Pyridoxal 5'-phosphate
PM	Pyridoxamine
PN	Pyridoxine
rt	Room temperature
SA	Salicylic acid
siRNA	Small interfering RNA
SRT	Substrate reduction therapy
TACA	4-Carboxy-5-(1-pentyl)hexylsulfanyl-1,2,3-triazole
TFA	Trifluoroacetic acid
THC	Tetrahydrocannabinol
THF	Tetrahydrofuran
TKP	3-Decyl-2,5-dioxo-4-hydroxy-3-pyrroline
t_R	Retention time

1. Objectives

1. Objectives

Primary hyperoxaluria type 1 is a rare genetic disease related to disorders in glyoxylate metabolism that lead to oxalate accumulation. Combined kidney-liver transplantation constitutes the only healing treatment, and therefore the development of a pharmacological approach is required. This doctoral thesis aims at developing novel glycolate oxidase inhibitors as substrate reduction therapy for the treatment of the disease. Hence, on the basis of the previously established requirements for glycolate oxidase inhibition, different families of compounds were synthesized, characterized and biologically evaluated. The simultaneous targeting of different enzymes involved in a pathological process reinforces the efficacy of drug therapies. Thus, we preferably searched for the development of novel glycolate oxidase inhibitors with beneficial off-target effects; it means multi-target drugs able to inhibit more than one of the enzymes involved in the pathological production of oxalate. Lactate dehydrogenase, which can transform the same substrate as glycolate oxidase, was our main alternative target.

1. Synthesis, purification and characterization of oxamic acids and homologous derivatives.

- 1.1. Synthesis of 2-oxoacetic acid derivatives.
- 1.2. Synthesis of 3-oxopropanoic acid derivatives.
- 1.3. Synthesis of 4-oxobutanoic acid derivatives.

2. Synthesis, purification and characterization of salicylic acid derivatives.

- 2.1. Synthesis of non-salicylic derivatives.
- 2.2. Synthesis of heteroarylsalicylates.
- 2.3. Synthesis of arylsalicylates.

3. Structural modulation of salicylic derivatives by introduction of linkers: Synthesis, purification and characterization of salicylates containing two-atom nitrogen-based spacers.

- 3.1. Synthesis of salicylate derivatives containing flexible methylamino linkers.
- 3.2. Synthesis of salicylate derivatives containing rigid imino and azo linkers.

1. Objectives

4. **Structural modulation of the furylsalicylate MDMG-409: Synthesis, purification and characterization of 5-aminomethyl-2-furyl and α,β -unsaturated carbonyl derivatives.**
5. **Synthesis of chemical probes derived from compounds MDMG-409 and MDMG-672.**
6. **Production and purification of recombinant *mGO* and *hGO* enzymes.**
7. ***In vitro* evaluation of the synthesized compounds against recombinant *mGO* and *hGO* enzymes.**
 - 7.1. Inhibition percentage at a single dose and IC_{50} determination using a colorimetric assay.
 - 7.2. Inhibition percentage at a single dose and IC_{50} determination using a fluorometric assay.
 - 7.3. Test for interferences in the GO colorimetric and fluorometric assays.
8. ***In vitro* evaluation of the synthesized compounds against recombinant *hLDHA* and *hLDHB* enzymes.**
 - 8.1. Inhibition percentage at a single dose and IC_{50} determination using a fluorometric assay.
 - 8.2. Test for interferences in the LDH fluorometric assay.
9. **Determination of preliminary structure-activity relationships (SAR) for the GO and LDH inhibition activities of salicylates and their capacity to decrease oxalate production on hyperoxaluric hepatocytes.**

2. Introduction

2. Introduction

2.1. Biological background

2.1.1. Hyperoxaluria

The term **hyperoxaluria** is defined as a rise in the levels of oxalate in urine, which increases the risk of appearance of urinary stones. The first clinical case was described in 1925 by Lepoutre,¹ but it was not until 1957 when the difference between primary and secondary hyperoxaluria was established, with the cases reported by Archer et al.² According to the origin of the overproduction of oxalate, primary and secondary hyperoxaluria can be distinguished. Thus, in primary hyperoxaluria there is an overproduction of oxalate with normal dietary absorption of this metabolite, whilst in secondary hyperoxaluria, an increase in the intestinal absorption of oxalate occurs.³

2.1.1.1. Primary hyperoxalurias

Primary hyperoxalurias (PHs) comprise a group of rare autosomal recessive diseases related to glyoxylate metabolism that result in an endogenous overproduction of oxalate, with a normal dietary absorption of this metabolite.⁴⁻⁶

Oxalate constitutes an end-product of metabolism that cannot be metabolized in mammals and needs to be excreted in urine, so that in PH patients the urinary oxalate excretion levels are above 0.5 mmol/1.73 m² of body-surface area per day, usually even more than 1 mmol/1.73 m² (being the normal oxalate excretion lower than 0.5 mmol/1.73 m² per day).⁶

Despite the fact that the overproduction of oxalate mainly comes from the liver, it is excreted through the kidneys, being filtered at the glomerulus and secreted by the renal tubules. Thus, once the excretion capacity is exceeded, oxalate begins to precipitate in the form of highly insoluble calcium oxalate crystals, thereby causing urolithiasis (calculi in the kidney or urinary tract) and/or nephrocalcinosis (deposition of crystals in the renal parenchyma),^{4,6} which produce inflammatory and fibrotic responses. This, combined with secondary complications like infections and urinary obstructions, usually leads to end-stage renal disease (ESRD).⁶ Kidneys result progressively damaged,

affecting the glomerular filtration rate (GFR), which is diminished to 30-45 mL per minute per 1.73 m² of body-surface area. Hence, the kidneys are unable to efficiently eliminate oxalate, producing an increase in plasma. Once the oxalate levels reach saturation, it begins to precipitate in all tissues, mainly in skeleton, causing systemic oxalosis.⁷

Depending on the involved genes, three types of PHs can be identified, although the genetic cause for PH remains unknown for a short number of patients:⁸

- Primary hyperoxaluria type 1 (PH1, MIM#259900), caused by mutations in the gene *AGXT* (MIM*604285), coding for the enzyme alanine-glyoxylate aminotransferase (AGT).
- Primary hyperoxaluria type 2 (PH2, MIM#260000), caused by mutations in the gene *GRHPR* (MIM*604296), coding for the enzyme glyoxylate reductase/hydroxypyruvate reductase (GRHPR).
- Primary hyperoxaluria type 3 (PH3, MIM#613616), caused by mutations in the gene *HOGA1* (MIM*613597, also known as *DHDPSL*), coding for the enzyme 4-hydroxy-2-oxoglutarate aldolase (HOGA).

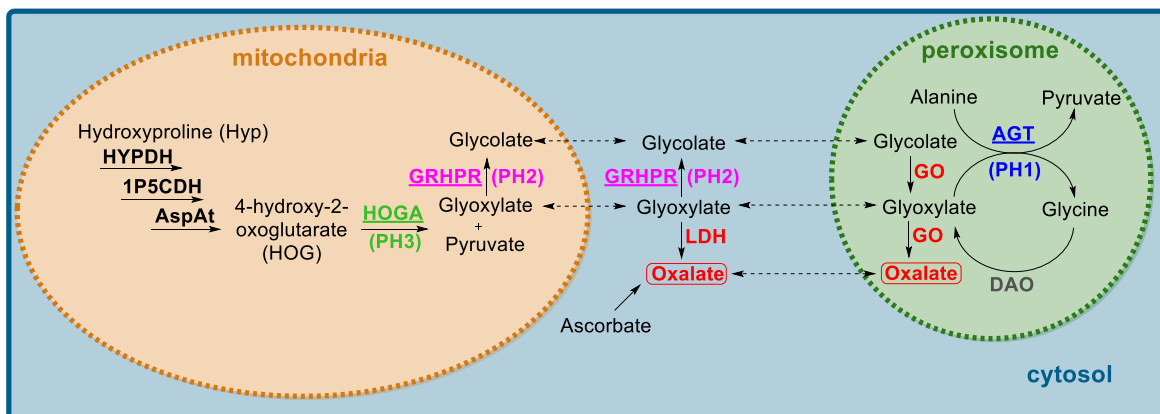


Figure 1. Glyoxylate metabolic pathway showing the enzymes involved in the three types of primary hyperoxaluria. AGT: Alanine-glyoxylate aminotransferase; GO: Glycolate oxidase; GRHPR: Glyoxylate reductase/hydroxypyruvate reductase; DAO: D-Aminoacid oxidase; LDH: Lactate dehydrogenase; HYPDH: Hydroxyproline dehydrogenase; 1P5CDH: Δ^1 -Pyrroline-5-carboxylate dehydrogenase; AspAT: Aspartate aminotransferase; HOGA: 4-Hydroxy-2-oxoglutarate aldolase 1.

2.1.1.1.1. Primary hyperoxaluria type 1 (PH1)

In 1986, for the first time, mutations in the *AGXT* gene were associated with the deficit of AGT that leads to PH1.⁹ AGT, a liver-specific peroxisomal enzyme, is in charge of glyoxylate detoxification. In a transamination reaction following a ping-pong mechanism, and using pyridoxal phosphate (PLP) as cofactor, L-alanine and glyoxylate are transformed into pyruvate and glycine. This last one is water soluble and can be easily excreted in urine (Figure 2).¹⁰

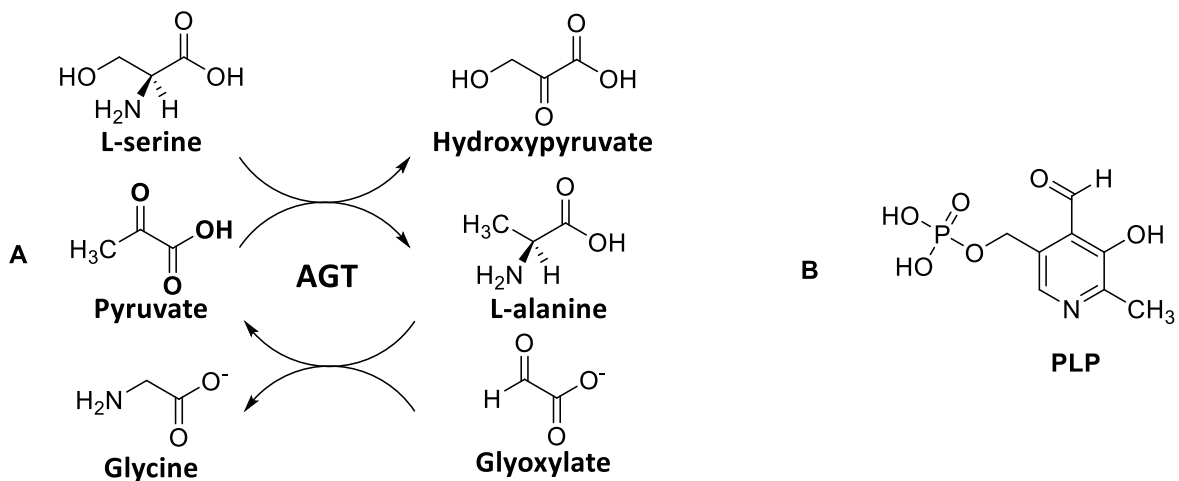


Figure 2. A. Transamination reaction catalyzed by AGT. B. Chemical structure of the cofactor PLP.

However, when there is a diminished AGT activity caused by deficient, absent or mistargeted AGT, an accumulation of glyoxylate occurs, which is then oxidized to oxalate by the enzymes glycolate oxidase (GO) in the peroxisome and lactate dehydrogenase A (LDHA) in the cytosol.¹¹

Alanine-glyoxylate aminotransferase (AGT)

AGXT gene, located in chromosome 2 (2p37.3), encodes for AGT, a homodimeric protein formed by two 43 KDa subunits (392 aminoacids each), each one binding a pyridoxal 5'-phosphate (PLP, the active form of Vitamin B6) molecule as cofactor.⁸

For *AGXT* gene, approximately 200 pathogenic mutations have been described so far, including 120 missense and nonsense mutations, 24 splice mutations and 58 indels.¹²

In order to explain the consequences of the mutations in *AGXT*, four main mechanisms have been described: mitochondrial mistargeting, protein aggregation, catalytic defects and synthesis defects.⁸ Depending on the mutations affecting both alleles, different levels of residual activity of AGT can exist, although in most cases the mutations are missense and lead to a dramatic loss of enzymatic activity in the peroxisome.¹³

There are two polymorphic variants for AGT: the *major* haplotype (AGT-Ma) and the *minor* haplotype (AGT-Mi). The *minor* haplotype is less frequent, appearing in a 20% of the European and North American population,¹⁴⁻¹⁶ and basically consists in two single amino acid substitutions (p.Pro11Leu and p.Ile340Met), along with other genomic changes.¹⁷

The main consequences for the p.Pro11Leu change are:¹⁷

- Reduction of specific catalytic activity.
- Creation of a mitochondrial targeting sequence (MTS) which directs a 5% of the AGT to the mitochondria.
- AGT becomes more sensitive to the adverse effects of some common PH1 mutations.

The real impact of the *minor* allele appears when it is combined with pathological mutations, mainly the p.Gly170Arg substitution. This mutation, which is present in one third of PH1 patients, affects to the protein dimerization in the cytoplasm, increasing its mistargeting to the mitochondria.⁸

Among all registered PH patients, approximately 70% of them have PH1, 10% have PH2, 10% have PH3, and the remaining 10% corresponds to patients having an unidentified genetic cause.¹⁸ Given these statistics, the epidemiological information available mainly refers to PH1.⁸

The estimated prevalence of PH1 ranges from 1 to 3 per million population, and the approximate incidence is 1 out of 120000 live births per year in Europe and North America.^{19,20} A higher incidence of PH1 has been identified in geographically isolated regions like the Canary Islands due to founder effect,^{21,22} and also in countries where consanguineous marriages are frequent, like Kuwait²³ or Tunisia.²⁴

Nevertheless, given the similarity between the clinical manifestations of PH and common kidney stone disease, the existence of misdiagnosis seems plausible.⁸

2.1.1.1.2. Primary hyperoxaluria type 2 (PH2)

Primary hyperoxaluria type 2 is produced by a deficiency in the enzyme glyoxylate reductase-hydroxypyruvate reductase (GRHPR), which is responsible for the reduction of glyoxylate into glycolate and hydroxypyruvate into D-glycerate. Under these circumstances, LDH oxidizes glyoxylate and hydroxypyruvate to oxalate and L-glycerate, respectively, appearing both abnormally in urine.⁸ For that reason, PH2 was firstly designated as L-glyceric aciduria,²⁵ and it was not until 1991²⁶ that the glyoxylate reductase (GR) activity was identified as the probable responsible for the overproduction of oxalate in this disease. In 1999, *GRHPR* was identified as the responsible gene for PH2.^{27,28}

Thus, in PH2, high levels of L-glyceric acid can be detected in urine, establishing the diagnostic difference between PH1 and PH2.²⁶ Nevertheless, it has been suggested that the disease could be misdiagnosed, due to the occurrence of PH2 cases in which severe L-glyceric aciduria is not observed.²⁹

GRHPR presents a widespread distribution, although its abundance is higher in hepatocytes, mainly in the cytosol, but also in the mitochondria.³⁰ Nonetheless, GRHPR is also expressed in other tissues, being the particular case of the renal tubules of probable contribution to the mechanisms of kidney damage in PH2.⁸ Furthermore, this wide distribution of GRHPR³¹ could also compromise the effectiveness of renal transplant in PH2 patients.³² PH2 presents a less severe course than PH1³³ and accounts for 10% of all PH cases.¹⁸

The publication of the first crystalline structure for human GRHPR complexed with the substrate and cofactor NADPH contributed to a better understanding of the substrate specificity, the catalytic mechanism for this enzyme, and the effects of mutations causing PH2.³⁴

The *GRHPR* gene is located in chromosome 9 (9q12) and encodes for a protein of 328 amino acids which forms homodimers of 73 KDa.^{27,28} Regarding the mutations affecting *GRHPR* gene, 16 missense mutations, 8 splice mutations and 19 indels have been described in the PH mutation database,¹² resulting in diminished protein expression and reduced catalytic activity.⁸

2.1.1.1.3. Primary hyperoxaluria type 3 (PH3)

Primary hyperoxaluria type 3 (PH3) is caused by the deficiency in the liver specific mitochondrial enzyme 4-hydroxy-2-oxoglutarate aldolase (HOGA), encoded by gene *HOGA1*. This PH subtype was described in 2010,³⁵ when mutations in the gene *DHDPSL* (coding for dihydrodipicolinate synthase-like, later known as 4-hydroxy-2-oxoglutarate aldolase) were identified as responsible for PH3.³² HOGA takes part in the hydroxyproline degradation pathway, breaking down 4-hydroxy-2-oxoglutarate (HOG) into pyruvate and glyoxylate.³⁶

The *HOGA1* gene, located in chromosome 10 (10q24.2), encodes for the mitochondrial enzyme HOGA, a protein of 327 aminoacids that forms 72 kDa dimers and 144 kDa tetramers.⁸

Among PHs, PH3 is the one that presents the least severe symptoms and only one case of ESRD has been reported so far,¹⁸ although an earlier onset has been noted for this type of PH.^{18,37}

According to the PH mutation database, 27 missense mutations, 4 splice site mutations and 3 indels have been described for *HOGA1*,¹² which cause misfolding, aggregation, and degradation of the protein.³⁸

Mutations in *HOGA1* cause a decreased HOGA activity, which could have different consequences.³⁶ In theory, the deficiency in HOGA would lead to a decreased glyoxylate production in the mitochondria; therefore, two plausible explanations have been proposed in order to justify the overproduction of oxalate in PH3.⁷ On the one hand, HOG could be transformed into glyoxylate by a different cytosolic aldolase, and subsequently, glyoxylate would be oxidized into oxalate by LDH.³⁷ On the other hand, it has been suggested that the accumulated HOG could inhibit the GR activity of the mitochondrial GRHPR, raising the level of glyoxylate and leading to its oxidation into oxalate, as happens in PH2.³⁸ The recent development of a mouse model of PH3 might help to understand the detailed molecular mechanisms involved in PH3.³⁹

2.1.1.2. Secondary hyperoxaluria

Secondary hyperoxaluria is caused by an excess of the dietary intake of oxalate or by an increase of the intestinal absorption of this metabolite. This hyperoxaluria form tends to be milder, with urinary oxalate excretion levels below 1 mmol/1.73 m² per day,

although sometimes it may result in ESRD and systemic oxalosis. Diseases related to fat malabsorption, such as short bowel syndrome, chronic inflammatory bowel disease or cystic fibrosis rise the risk of suffering secondary hyperoxaluria.⁴⁰

2.1.2. Treatments approaches in PH1

Given the similarity between the clinical manifestations of PH1 and those of idiopathic kidney stone disease, PH1 remains sometimes unrecognized for years, hampering an early diagnosis and a suitable treatment for each patient. The diagnosis is made by genetic testing, which also helps to implement the most appropriate treatment, approaching to the personalized medicine.⁴¹

Two main types of treatments for PH1 can be distinguished: the **symptomatic** and the **curative treatments**. Furthermore, promising **future approaches** are currently being studied.^{42,43} Symptomatic treatments pursue the maintenance of renal function preventing crystal formation and deposition by raising the fluid intake, administering crystallization inhibitors, or with medical procedures such as dialysis and kidney transplantation. Curative treatments aim at recovering the AGT activity. Pyridoxine (PN) intake works for some PH1 patients, but for those unresponsive to pyridoxine treatments, liver transplantation is the only curative option. However, in many cases, by the time an appropriate diagnosis is done, severe kidney damage is already produced and double kidney-liver transplantation becomes necessary.

2.1.2.1. Current treatment approaches

2.1.2.1.1. Symptomatic approaches

This therapy, which does not represent a healing option, aims at preventing calcium oxalate formation and deposition and should be implemented as soon as a PH1 diagnosis is done.⁴³

The **fluid intake** must be increased to at least 3 L/m²/day and, simultaneously, crystallization inhibitors such as potassium and sodium citrate should be administered at a dose of 0.10-0.15 g/kg/day.⁴³ Pyridoxine treatment, with a starting dose of 5 mg/kg/day, has shown to be effective in 30% of PH1 patients, usually when the mutation Gly170Arg is present.⁴⁴ With respect to **diet**, no special considerations regarding oxalate intake need to be born in mind, since the main source of oxalate in PH1 patients is endogenous and comes from liver. However, an excessive intake of vitamin C should be avoided, as it can be converted to oxalate.⁴³ On top of that, the consumption of food rich in hydroxyproline should be limited, since the hydroxyproline catabolism contributes to endogenous oxalate production.⁴⁵

Another option for conservative treatment is the increase of **intestinal oxalate consumption** through the use of oxalate degrading bacteria and enzymes.⁴² Besides kidneys, oxalate excretion takes place in the intestinal tract through the anion exchanger SLC26A6, what has prompted the study of mechanisms to increase intestinal oxalate excretion in order to reduce the levels of this metabolite.⁴⁶ These include the oral administration of oxalate degrading bacteria, such as *Oxalobacter formigenes*, which has shown to effectively reduce oxalate levels in PH1 models.^{47,48} However, no conclusive results were reached in different clinical trials with PH1 patients.⁴⁹⁻⁵¹ Another option is the administration of oxalate degrading enzymes, as the case of *Bacillus subtilis* oxalate decarboxylase. This enzyme, which transforms oxalate into formate and carbon dioxide, has also been successfully proved in a PH1 mouse model, showing its ability to reduce hyperoxaluria.⁵²

Dialysis can also be used to remove oxalate from blood, given its low molecular weight (90 Da). However, in PH1, oxalate is produced at a rate of 4-7 mmol/1.73 m²/day, whilst dialysis is only able to remove 1-2 mmol/1.73 m²/day, so that oxalate starts accumulating in the organism when an advanced state of the disease is reached, like in the case of ESRD.⁴³ Thus, the indications of this procedure are limited to restricted cases: it can be used in the waiting time for organ transplantation, to decrease oxalate levels after liver transplant or when organ transplantation is not a possibility in developing countries.⁵

Isolated kidney transplantation is considered as a temporary solution when no other option is available, since the deposition of oxalate continues deteriorating the transplanted kidney.⁵ Nevertheless, in the case of selected patients responsive to pyridoxine, isolated kidney transplantation is being studied as a possible option.⁵³

Finally, **surgical interventions** to treat urolithiasis are not recommended unless there are obstructions, infections or multiple urolithiasis. In contrast, procedures like extracorporeal shock wave lithotripsy (ESWL) have been used to fragment the stones and allow their clearance.⁴³ However, given the high risk of stone re-growth from an incomplete stone clearance in ESWL,⁵⁴ this technique has been replaced by endoscope when there are multiple stones.⁵⁵

2.1.2.1.2. Curative approaches

Regarding the curative approaches, only two strategies are approved, which are the administration of vitamin B6 and liver transplantation.

Pyridoxine administration

The administration of vitamin B6 (pyridoxine), which is the PLP precursor (AGT cofactor), was contemplated as a possible treatment for PH1 since the cause of the disease was identified in 1986.⁹ Approximately 30% of PH1 patients are responsive for this treatment, especially those who carry the p.Gly170Arg or p.Phe152Ile mutations in the *AGXT* gene.^{44,56} In spite of this fact, it is considered as a recommended conservative treatment in all PH1 patients, on the grounds that it constitutes a safe treatment that contributes to preserving the renal function until organ transplantation is possible.⁴³ However, this treatment can be only applied in PH1 patients, but not in PH2 or PH3.⁴³

The recommended starting dose is 5 mg/kg/day, and patients are considered to be responsive for the treatment if the reduction of oxalate excretion in urine exceeds 30%.⁴²

Liver transplantation

Liver transplantation constitutes the only permanent curative option for confirmed PH1 patients, since the replacement of this organ restores the normal activity of AGT, specifically located in liver. However, the success of this procedure depends on the stage of the disease. Due to the frequently advanced kidney damage by the moment surgery is performed, double kidney-liver transplantation is often preferred,⁸ which implies lifelong immunosuppressive treatments with a survival rate of 86%, 80%, and 69% at 1 year, 5 years, and 10 years, respectively.⁵⁷

This therapeutic option can only be applied to PH1 patients: in the case of PH2, GRHPR presents a wide distribution, and in PH3 the less severe course does not require this type of treatment.⁵⁸

2.1.2.2. Future treatment approaches

2.1.2.2.1. Gene therapy

Liver-directed gene therapy seems a desirable approach for PH1, as this disease is exclusively caused by mutations in the *AGXT* gene. Recombinant adeno-associated viral (AAV) vectors have been used to deliver the *AGXT* cDNA to the liver of *Agxt1^{-/-}* mice, restoring AGT activity and therefore correcting PH1.⁵⁹ Alternatively, the administration of helper-dependent adenoviral (HDA) vectors encoding AGT to *Agxt1^{-/-}* mice was also able to restore functional AGT levels.⁶⁰ Despite these studies show the high potential of this technique, drawbacks as the high vector dose required to achieve an adequate transduction efficiency need to be considered.⁴²

2.1.2.2.2. Cell Therapy

This approach aims at restoring liver function by repopulating the organ with fully functional hepatocytes from a donor, reestablishing normal AGT activity without the need for liver transplantation. This strategy could be particularly useful in patients with advanced liver deterioration, as in the case of infantile PH1, since the transfused hepatocytes would grow more easily than the damaged host hepatocytes.⁶¹ Despite this approach has already been successfully used in one young PH1 patient,⁶² this technique still needs to be improved before its implementation as PH1 treatment.⁶¹

However, as happens with liver transplantation, the availability of donors is limited, and long-term immunosuppression would still be required.⁶³ Recently, human induced pluripotent stem cells (iPSCs) derived from PH1 patients were generated,⁶⁴ which could be used in autologous cell transplantation. Although this type of treatment would avoid the need for immunosuppression, the transplanted hepatocytes would still present proliferative disadvantages with respect to resident cells.⁶³ In animal models, this problem has already been overcome by the use of hepatic irradiation to undermine the proliferation of the host hepatocytes.^{65,66}

2.1.2.2.3. Pharmacological chaperones

Pharmacological chaperones are small molecules that help to restore the proper structure of a misfolded protein. Both cofactors and substrate analogs can be used as pharmacological chaperones in misfolding diseases.⁶⁷

Regarding the use of **cofactors** as pharmacological chaperones in PH1, PLP, which is the AGT cofactor, has shown to be able to correct the effect of folding mutations of AGT.⁶⁸ Despite these beneficial effects found for pyridoxine, an excess of this molecule could lead to an undesirable AGT inactivation, hence, reducing glyoxylate detoxification in cells. After supplementation with pyridoxine, it is transformed into PLP (AGT cofactor) and pyridoxine 5'-phosphate (PNP), and when this last one binds to AGT, an inactive AGT-PNP complex is formed. This fact could explain the reason why most patients respond at lower doses of pyridoxine (<10 mg/kg/day). Besides pyridoxine, the use of other B6 vitamers such as pyridoxamine (PM) and pyridoxal (PL) has been investigated, showing more effectiveness than pyridoxine in rescuing PN-responsive variants F152I-Mi and G170R-Mi in a PH1 cellular model.^{69,70}

On the other hand, **substrate analogues** are also able to act as pharmacological chaperones. They are frequently competitive inhibitors that present high binding affinity and specificity for the enzyme. In this regard, the AGT inhibitor aminooxyacetic acid (AOA) has shown to correct the effects of pathogenic AGT variants.⁴² These facts establish the proof-of-principle for the use of pharmacological chaperones in the treatment of PH1, although further research needs to be done to provide more specific molecules.⁷¹

2.1.2.2.4. Mistargeting correctors

The aim of this strategy is to redirect the AGT carrying the Gly170Arg-Mi mutation, wrongly targeted to the mitochondria, to the peroxisome. Treatment with dequalinium chloride (DECA), an FDA-approved drug, has shown to restore trafficking of mutant AGT from mitochondria to peroxisome, giving as a result a reduction of oxalate production.⁷² Besides, a high-throughput screening (HTS) assay has been developed with the aim of identifying pharmacological chaperones that could restore the AGT functionality correcting its misrouting.⁷³

2.1.2.2.5. Enzyme replacement therapy

In this approach, which has already been used in enzymatic deficits such as phenylketonuria⁷⁴ or lysosomal storage disorders,⁷⁵ the affected or absent enzyme due to mutations is replaced by a functional one.

To this end, in PH1, AGT has been successfully conjugated to the polyethylene glycol-polyglutamic acid (PEG-PGA) block-co-polymer, without affecting the enzyme functionality. The administration of this conjugate to a cellular model of PH1 restored the AGT normal activity, and therefore, the glyoxylate detoxification.⁷⁶

Besides that, the consensus approach has been used to design an improved AGT version, with applications in gene therapy and enzyme replacement therapy. This resulting AGT-RHEAM included five key single point mutations (p.Q23R/ p.S.48H/ p.D52E/ p.V.113A/ p.I340M) and presented improved thermal and kinetic stability, as well as increased catalytic activity compared to the wild type.⁷⁷ Recently, the preclinical efficacy of this construct has been tested *in vitro* and *in vivo* in a mouse PH1 model (*Agxt1*^{-/-}) using a mRNA-based approach. As a result, a 40% reduction in urinary oxalate was achieved, suggesting the potential of this therapy.⁷⁸

2.1.2.2.6. Substrate-reduction therapy

Substrate reduction therapy (SRT) constitutes an useful approach in inborn errors of metabolism characterized by substrate accumulation, as it is the case of PH1.⁷⁹

Aforementioned, in PH1, the loss of function of AGT leads to the harmful accumulation of the substrate, glyoxylate, in the peroxisome of hepatocytes. As a result, glyoxylate is oxidized to oxalate by GO (among other enzymes), being GO also responsible for the oxidation of glycolate to glyoxylate. For this reason, it was suggested that the inhibition of GO could lead to a reduction of the amount of glyoxylate to a point where residual AGT activity would be enough to prevent substrate accumulation.⁸⁰ Providing insights to this fact, it was found out that the absence of GO in two brothers as a result of a mutation in the gene *Hao1* resulted in asymptomatic glycolic aciduria as sole manifestation, what emphasizes the safety of a possible treatment based on GO inhibition.⁸¹

Recently, the enzyme GO has been validated as a safe and efficient target for SRT in PH1, using small molecules. The study was carried out in a mouse model of PH1. In it, GO-deficient mice (*Hao1*^{-/-}) did not present adverse phenotypic effects, and double KO mice (*Agxt1*^{-/-}*Hao1*^{-/-}) showed lower levels of oxalate excretion when compared to hyperoxaluric mice (*Agxt1*^{-/-}). Furthermore, the small GO inhibitor (GOi) CCPST, which showed IC₅₀ = 43.5 μM and K_i = 20.3 μM against purified recombinant mouse GO (*mGO*), significantly reduced the production of oxalate on *Agxt1*^{-/-} mouse hepatocytes

in vitro [EC_{50} (24 h) = 25.3 μ M, EC_{50} (48 h) = 33 μ M, EC_{50} (72 h) = 34 μ M]. *In vivo* studies were also performed: oral administration of CCPST to *Agxt1^{-/-}* mice resulted in a 30-50% reduction in urine oxalate. However, in this study it was also stated that the high dose required for the treatment with CCPST could lead to unwanted side effects, and thus, the need of more potent GOi's was emphasized.⁸⁰

Besides, using a high throughput cell-based assay, the GO inhibitory activity of compounds belonging to the LOPAC (library of pharmacologically active compounds) and the NPC (NCATS Pharmaceutical Collection) libraries was assessed. As a result, the compounds potassium dichromate, sodium dichromate, and colistimethate were identified as novel GOi's showing IC_{50} values of 0.096, 0.108, and 2.3 μ M, respectively (Figure 3).⁸²

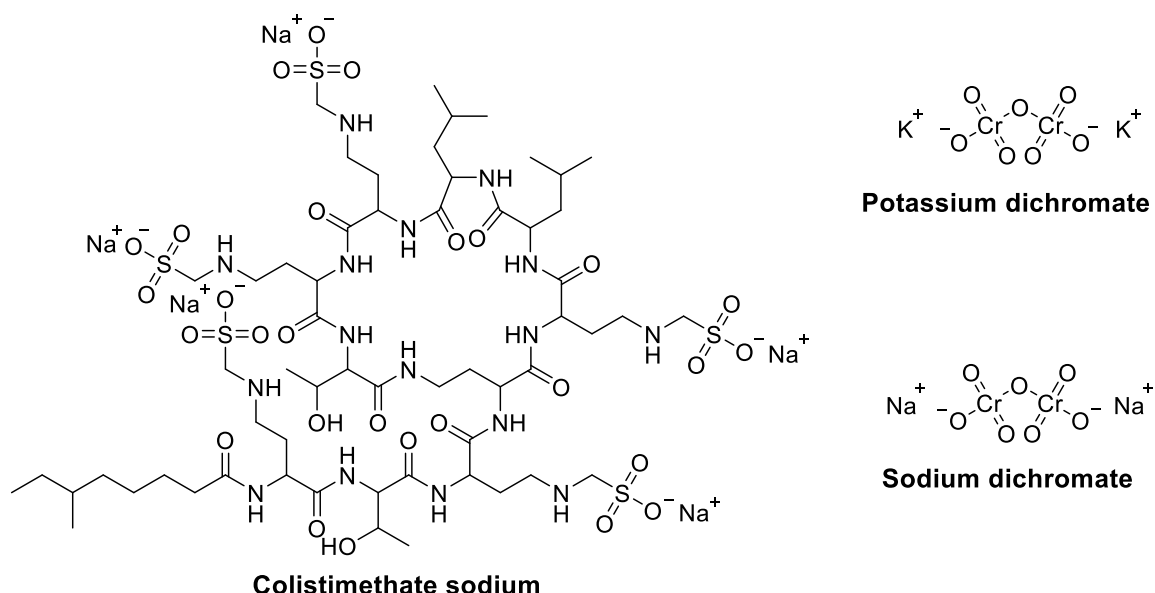


Figure 3. Structure of the glycolate oxidase inhibitors colistimethate, potassium dichromate and sodium dichromate.

Apart from GO, HYPDH (hydroxyproline dehydrogenase) has been proposed as a target for SRT in PH1. Hydroxyproline, coming from the diet, constitutes one of the main sources for glyoxylate in the organism. The enzyme PRODH2 (Proline dehydrogenase 2), later named as HYPDH, is mostly expressed in liver and kidneys, and takes part in the hydroxyproline metabolism in the mitochondria, giving glyoxylate and pyruvate as final products (Figure 1). HYPDH catalyzes the first step of hydroxyproline catabolism, oxidizing this metabolite into Δ^1 -pyrroline-3-OH-5-carboxylate (3-OH-P5C) in a FAD-dependent reaction.⁵⁸

HYPDH has been proposed as a target for SRT to treat the three types of PH, since its inhibition would diminish the production of glyoxylate. Besides, its deficiency in humans has been previously described without pathological effects.^{83,84} Small proline-like inhibitors for HYPDH have also been prepared, and their IC₅₀ values on isolated enzyme were found to be around 0.30 mM.⁸⁵ No data in cells have yet been published for this type of inhibitors.

Apart from GO and HYPDH inhibition using small molecules, development of siRNA^{45,86–89} and antisense oligonucleotides against these enzymes are currently under research.⁹⁰ Better ADME properties and an easier delivery into affected cells favor small molecules over nucleotide molecules. However, it is also possible that synergistic effects could arise from small drug/siRNA co-administration.

Finally, CRISPR/Cas9 technology has also been recently applied to target GO as a strategy for SRT. An AAV-based CRISPR/Cas9 vector was developed and systemically administered in a PH1 model of *Agxt1*^{-/-} mice to target GO. As a result, a long-term GO inhibition was achieved, normalizing the levels of oxalate excreted in urine and preventing the appearance of nephrocalcinosis, without signs of toxicity. Hence, this strategy constitutes a promising alternative for PH1 treatment, which could also be focused to PH2 and PH3 by targeting the corresponding enzymes.⁹¹

2.1.3. Glycolate oxidase (GO)

The flavoenzyme glycolate oxidase (GO) belongs to the α -hydroxy acid oxidase enzyme family and requires flavin mononucleotide (FMN) as cofactor. GO presents a low substrate specificity and is able to metabolize small molecules such as glycolate and glyoxylate, but also long chain α -hydroxy acids including as 2-hydroxy octanoate (2-OH-8) and 2-hydroxy palmitate (2-OH-16) (Figure 4).⁹²

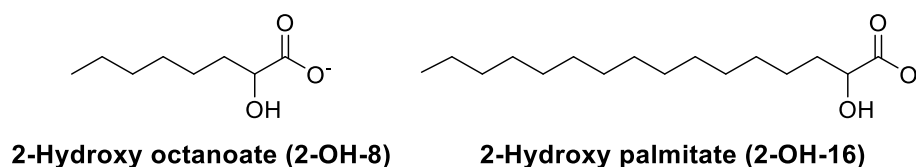


Figure 4. Structure of known glycolate oxidase substrates 2-hydroxy octanoate (2-OH-8) and 2-hydroxy palmitate (2-OH-16).

The general reaction catalyzed by GO can be divided into two half-reactions. In the first half-reaction, glycolate is oxidized into glyoxylate in a reaction catalyzed by FMN, which is reduced. In the second half reaction, reduced FMN is reoxidized by O_2 , forming hydrogen peroxide (H_2O_2) (Figure 5).^{93,94}

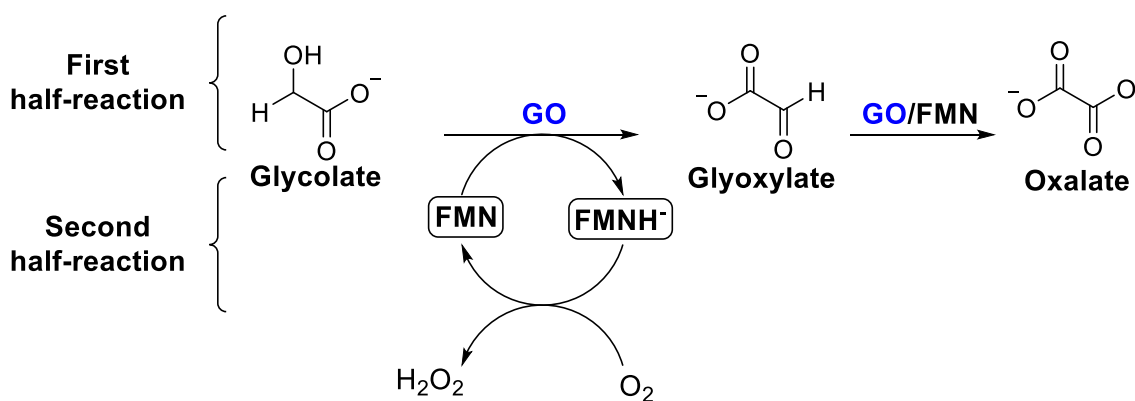


Figure 5. Reaction catalyzed by GO.

In 1953, GO was for the first time identified as the responsible for the oxidation of glycolic and L-lactic acids in plants,⁹⁵ and its structure was later elucidated in spinach.^{94,96} This prompted research efforts to discover GOi's, given their interest as herbicides.⁹⁴

In humans, GO is encoded by *HAOX1* gene (located in chromosome 20p12.3),⁹⁷ and constitutes a homotetramer formed by four 41 kDa monomers, each of them

containing 370 aminoacids.^{97,98} In humans, it is specifically expressed in hepatocytes, and is responsible for stone formation in PHs.⁹⁸

2.1.3.1. GO inhibition for the treatment of PH1

Since the role of GO in glyoxylate metabolism was suggested,⁹⁹ the possibility of using GOi's for the treatment of PH1 was contemplated and multiple small-molecules acting as GOi's have been identified.

GOi's were initially developed to exploit their herbicide action, what prompted the structural study of the spinach GO (sGOX) co-crystallized with the GOi's **TACA** [4-carboxy-5-(1-pentyl)hexylsulfanyl-1,2,3-triazole] and **TKP** (3-decyl-2,5-dioxo-4-hydroxy-3-pyrroline) (Figure 6).⁹⁴ Later on, the crystal structure of human GO (*hGO*) was elucidated,^{92,98} and co-crystallization studies were performed with the GOi's **CDST**⁹² and **CCPST** (Figure 6).¹⁰⁰ The information gathered in these studies has revealed the importance of conserved amino acids at the active site of GO: Tyr26, Trp110, Tyr132, Arg167, Lys236, His260 and Arg263.

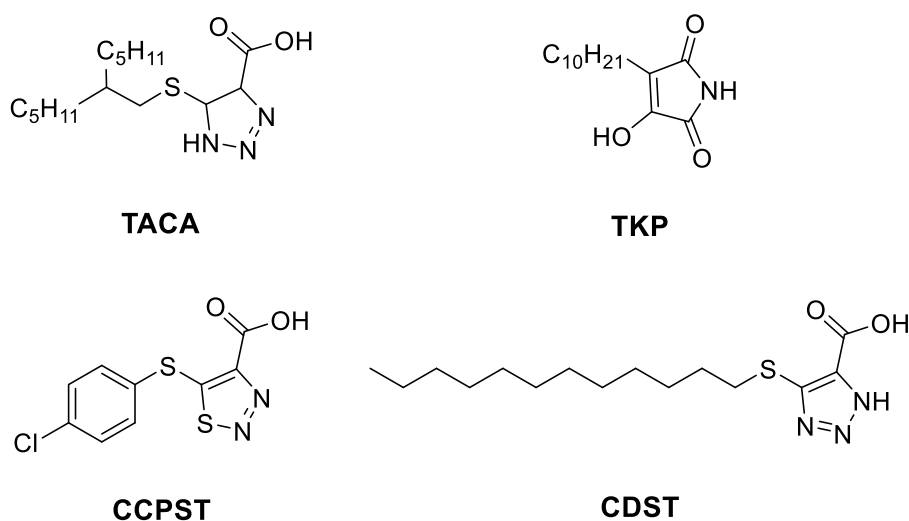


Figure 6. Structure of the known glycolate oxidase inhibitors **TACA**, **TKP**, **CCPST** and **CDST**.

These facts have allowed the establishment of structure-activity relationships for GOi's. In general terms, a GOi comprises two main parts:⁹²

- A polar head that enters the GO active site and mimics the substrate interactions establishing interactions with key amino acids.

- A side chain, whether aromatic or aliphatic, that hangs from the polar head and remains in the access channel establishing hydrophobic interactions causing a disorder that prevents its closure.

The polar head bears an acidic functionality, and it has been shown that the presence of a protonated heteroatom located β with respect to the acidic function is beneficial.^{100,101} Several polar heads have been studied, including α -hydroxy acids¹⁰²⁻¹⁰⁴, α -keto acids¹⁰⁵ and oxamates (Figure 7).^{103,104}

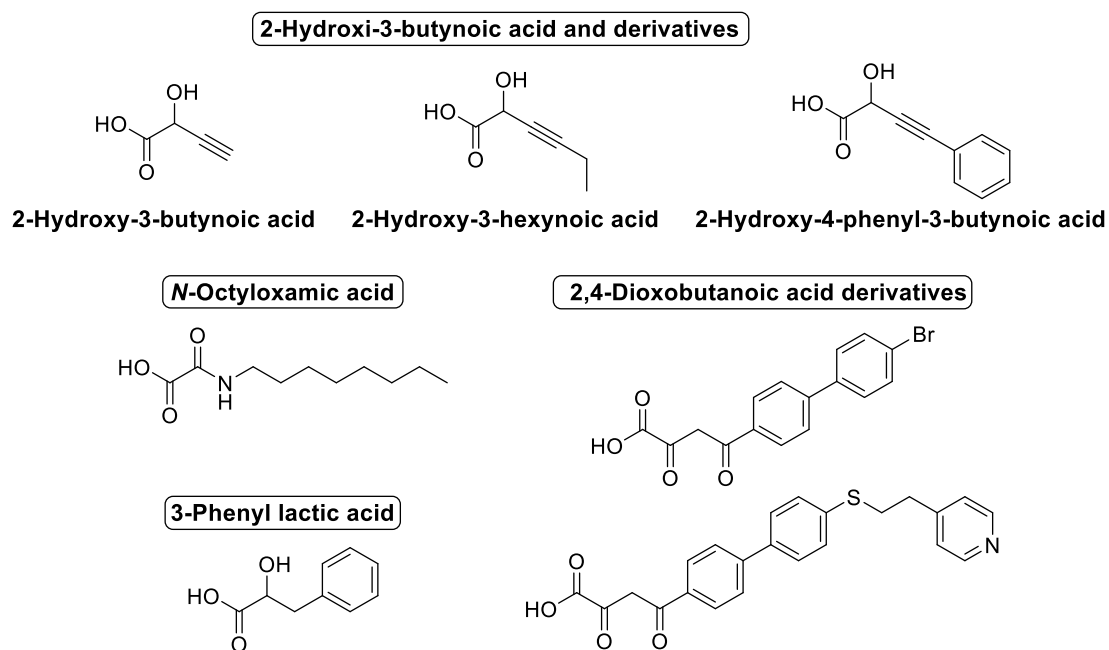


Figure 7. Structure of some known glycolate oxidase inhibitors.

In addition, the presence of flat, electron rich fragments in the polar head stabilize the ternary complex enzyme-cofactor-substrate by π - π interactions with FMN flavin ring.¹⁰²⁻¹⁰⁵

According to crystallographic data,^{92,100} **CDST** and **CCPST** mimic glyoxylate interactions in the active site of *hGO* (Figure 8). Carboxyl groups of **CDST**, **CCPST**, and **glyoxylate** overlay interacting with residues **Arg167**, **Arg263**, and **Tyr26**, while the N atoms at position 3 of the heterocyclic rings of **CDST** and **CCPST** overlay with the keto group in glyoxylate and interact with **His260**. Since the thiadiazole ring of **CCPST** does not carry a proton and neither does the **glyoxylate** keto group, the interaction of these two molecules would require the protonation of **His260**, and this would contribute to the weaker binding of **CCPST** compared to **CDST**.¹⁰¹ **CDST** and **CCPST** also

establish hydrogen bonds to **Tyr132** via the ring N2. This group of amino acids constitute the first of the two binding regions for GOi's.

The side chain of the inhibitor establishes hydrophobic interactions with the second binding region, which is constituted by variable amino acids for each GOi. In the case of **CCPST** and **CDST**, these types of interactions are established with residues **Trp110**, **Leu205**, and **Tyr208**. In addition, within this second binding site, flexible chains such as the one of **CDST** would help to a better accommodation of the inhibitor.¹⁰¹

As mentioned before, several small-molecule GOi's have been described so far, and the possibility of using them for the treatment of PH1 has been previously suggested. However, none of these molecules has been found to be useful for the treatment of PH patients. Possible reasons for this include the unfavorable physicochemical properties that these molecules present, as the case of **CDST**,⁹² which presents poor aqueous solubility while being a potent GOi ($K_i = 15$ nM).

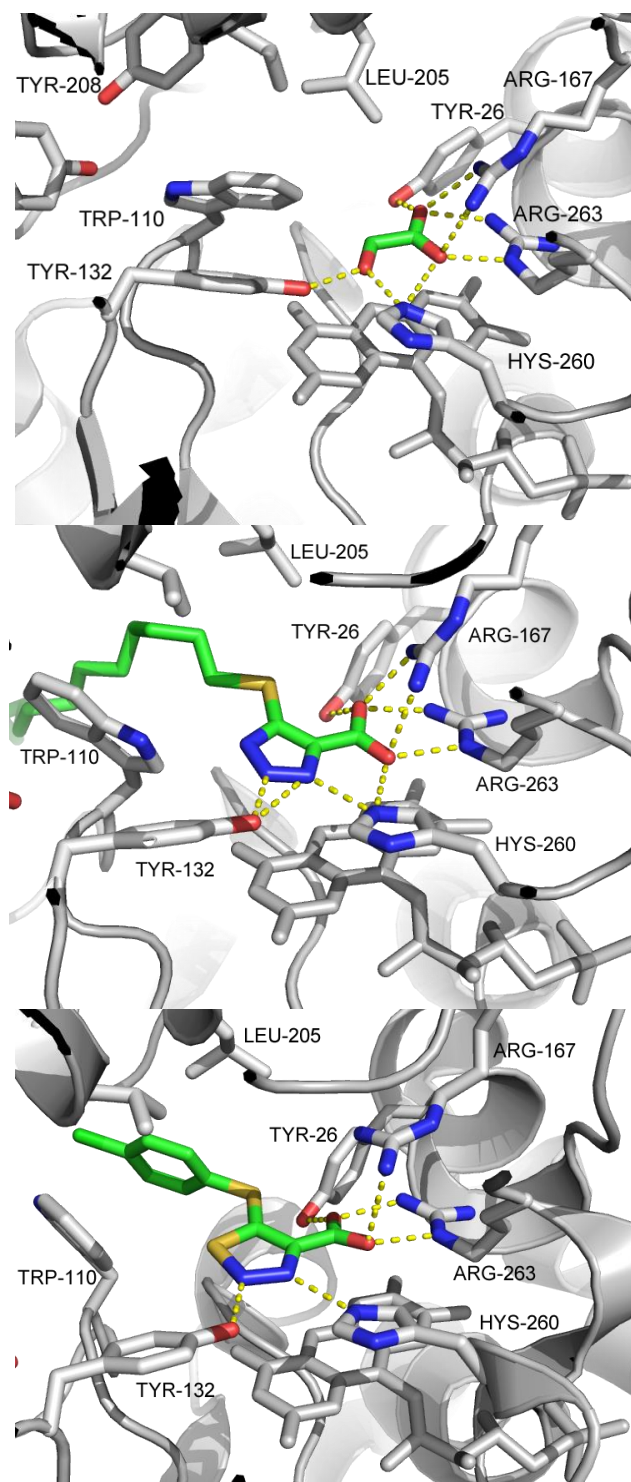


Figure 8. Interactions of **glyoxylate** (up), **CDST** (middle), and **CCPST** (bottom) in *hGO* active site. Obtained from crystallographic data (PDBid: 2RDU; 2RDT and 2W0U, respectively).

2.1.4. Lactate dehydrogenase (LDH)

Human lactate dehydrogenase (*h*LDH) is a tetrameric enzyme formed by two major subunits, LDHA and LDHB, encoded by genes *LDHA* (11p15.1) and *LDHB* (12p12.1), respectively, and named as M (muscle) and H (heart) for the organs from which they are obtained. The combination of these two subunits results in five different isoenzymes, either homotetramers or hybrid tetramers depending on the type of combination, which are named as follows: A4 (LDH5), A3B1 (LDH4), A2B2 (LDH3), A1B3 (LDH2) and B4 (LDH1).¹⁰⁶

LDH is an oxidoreductase enzyme that catalyzes the reversible reaction of conversion of pyruvate into lactate with the concomitant interconversion of NADH to NAD⁺ (Figure 9).¹⁰⁶

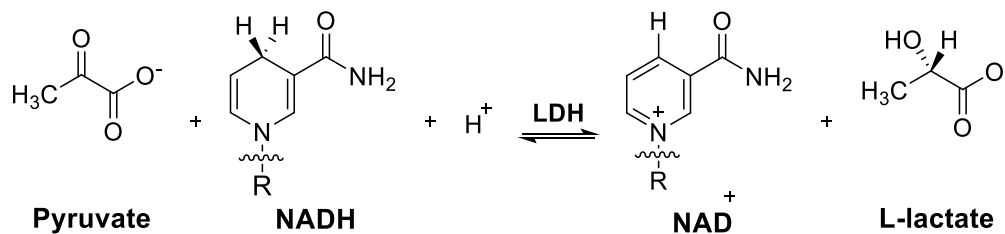


Figure 9. Reaction catalyzed by LDHA (Adapted from ref. ¹⁰⁷).

In humans, LDH5 (A4, LDHA) and LDH1 (B4, LDHB) constitute homotetramers exclusively formed by four A or B subunits, and containing 332 or 334 amino acids each, respectively. LDHA is located in anaerobic tissues such as skeletal muscle and liver, while LDHB can be found in aerobic tissues like heart muscle.¹⁰⁷

*h*LDHA presents a higher affinity for pyruvate than *h*LDHB does, being more efficient for pyruvate reduction in anaerobic conditions, as in hypoxic tumors. In contrast, *h*LDHB favors the reverse reaction and catalyzes the oxidation of lactate under aerobic conditions.¹⁰⁸

It has been shown that LDHA plays an important role in the energetic metabolism of tumor cells. The “Warburg effect”¹⁰⁹ was defined in 1956 as the metabolic switch from oxidative phosphorylation (OXPHOS) towards anaerobic glycolysis observed in tumor cells, even under oxygenated conditions: In normal cells, under aerobic conditions, glucose catabolism originates pyruvate which finally gives CO₂, allowing the entrance of acetyl-Co-A in the citric acid cycle. In contrast, in tumor cells, the hypoxic environment favors fermentation of glucose into lactate: pyruvate is reduced into

lactate in a reaction catalyzed by LDH and coupled to NADH, which is oxidized into NAD^+ (Figure 10).^{106,108}

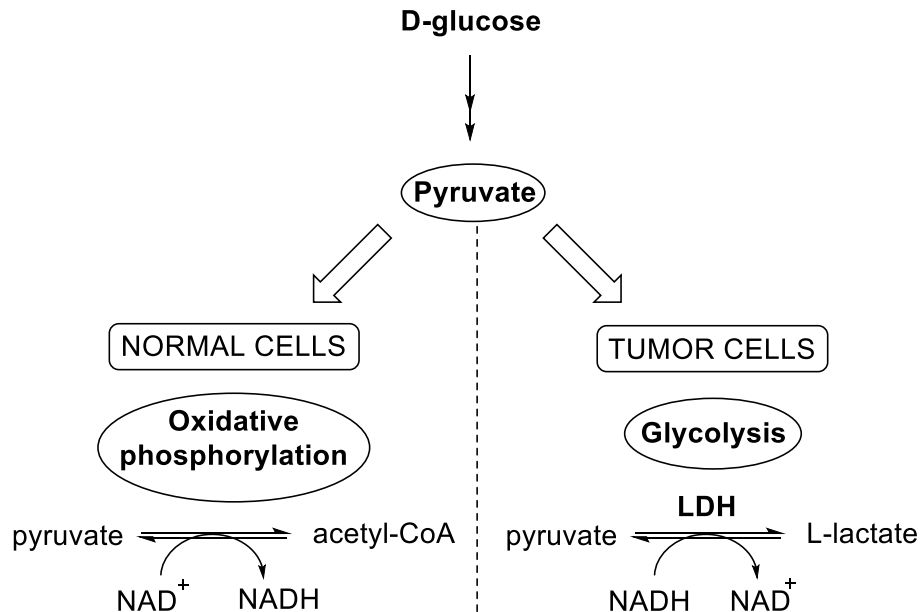


Figure 10. Metabolic pathway of pyruvate in normal cells and tumor cells. (Adapted from ref. ^{108,110})

These facts have led to the consideration of *h*LDHA as an attractive target for cancer therapy,¹¹¹ what has triggered the development of several classes of small-molecule *h*LDHA inhibitors.¹⁰⁸ This is supported by the fact that *h*LDHA inhibition constitutes a safe strategy for cancer therapy, since mutations leading to the loss of LDHA function have shown to cause only exertional myoglobinuria.^{112,113}

The crystallographic studies carried out over LDHA have revealed that there are two main domains in the enzyme: the larger domain, which constitutes the cofactor binding site and is formed by residues 20-162 and 248-266, and the mixed α/β substrate binding domain (smaller domain), including residues 163-247 and 267-331.¹⁰⁷ Crystallographic data have also shown that the active site locates in a deep cavity with narrow access that hosts both the substrate (pyruvate) and the cofactor (NADH). This constitutes a very polar position with a high content in cationic residues (arginines), which is in line with the structural characteristics of the LDHA inhibitors discovered so far: a carboxylate group is often presented with a nearby hydroxyl or carbonyl carbon atom, mimicking the natural substrates lactate and pyruvate (α -hydroxy acid and α -keto acid, respectively).¹¹⁰

There is a high grade of conservation of the amino acids on the active site, suggesting that the differences in kinetics properties between LDHA and LDHB rely on variations of charged surface residues, which interfere with the value of pK_a of His192. This His192 constitutes a key amino acid located in the active site that has shown to determine the different K_M value for pyruvate of both isoforms. This amino acid needs to be protonated before pyruvate binding, and in a later step, a proton from His192 will be transferred to the substrate.¹⁰⁷

2.1.4.1. LDHA inhibitors

Given the importance of selective *h*LDHA inhibition in oncology, important progress has been made in the discovery of small-molecule *h*LDHA inhibitors. Besides **oxamate** (Figure 11), a structural isoster of pyruvate and a well-established *h*LDHA competitive inhibitor,¹¹⁴ several families belonging to different chemical classes have been developed. However, only a few of these molecules have reached preclinical and clinical stages. A brief summary of the main families of *h*LDHA inhibitors is shown below (Figure 12).¹⁰⁸ Moreover, key amino acids for substrate interaction have been revealed by the analysis of the ternary complexes NADH-LDH-pyruvate¹¹⁰ and NADH-LDH-oxamate.^{107,115}

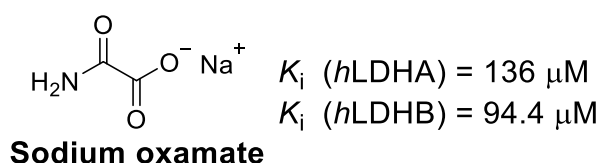


Figure 11. Structure and K_i values of **sodium oxamate**.

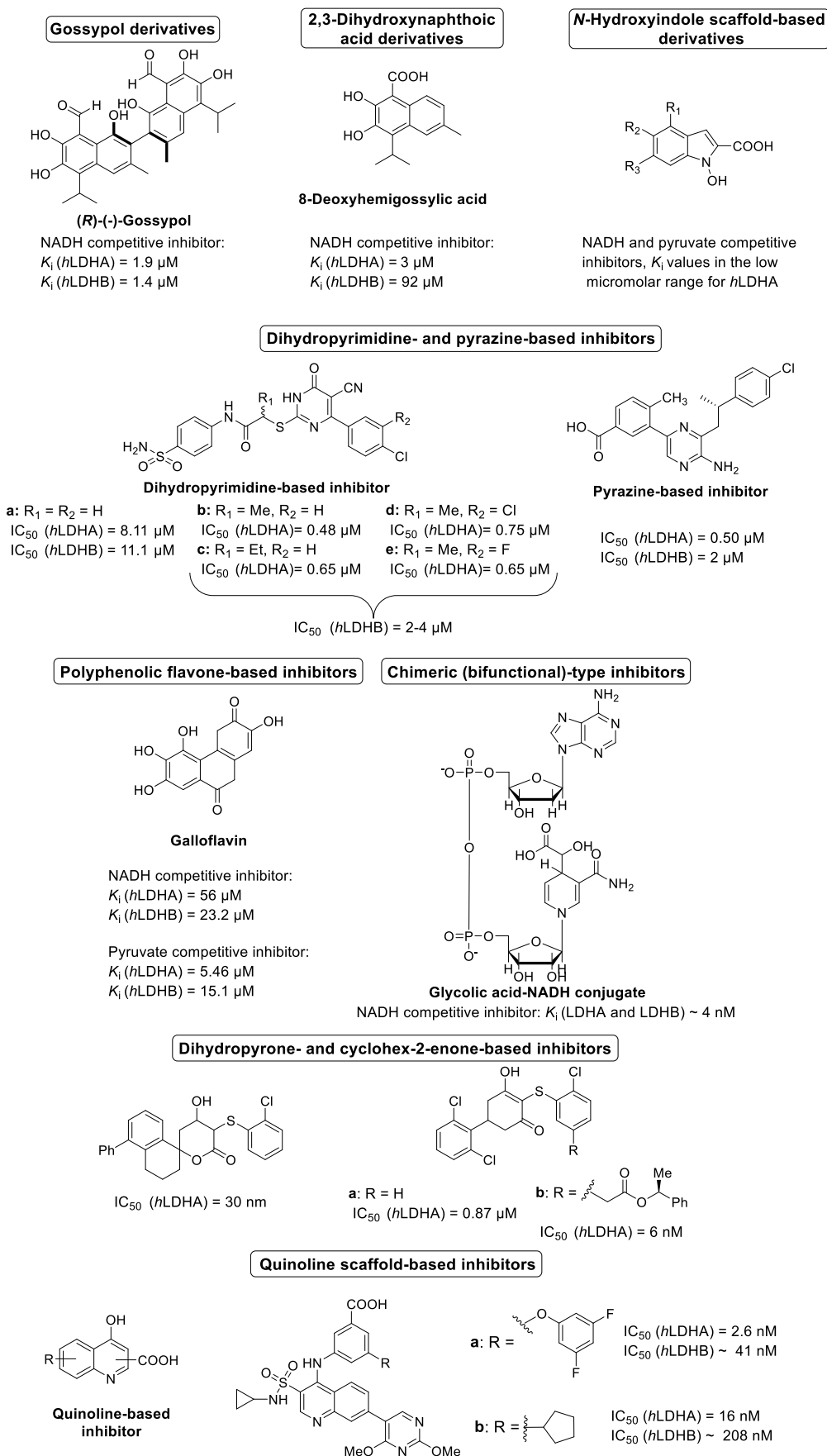


Figure 12. Review of known LDHA and LDHB inhibitors.

2.1.4.2. LDHA inhibition for the treatment of PH

LDHA plays an important role in the last step of glyoxylate metabolism, converting glyoxylate to oxalate in the cytoplasm of hepatocytes. Thus, specific LDHA inhibition has been proposed as a promising strategy for the treatment of PHs.¹¹⁶

In fact, by the use of siRNA-mediated silencing technology, LDHA was inhibited in *Agxt1^{-/-}* and *Grhpr^{-/-}* mice, PH1 and PH2 models respectively. The siRNA was conjugated with *N*-acetylgalactosamine (GalNAc) to specifically target hepatic LDHA, so as to avoid the potential undesired effects of LDHA inhibition in muscle, skin or uterus. As a result, an efficient oxalate decrease was achieved, preventing the deposition of calcium oxalate crystals in mice models and also in non-human primates, providing *in vivo* evidence of the potential of this technique.¹¹⁶

The effects of GalNAc-conjugated siRNA against GO were also evaluated in the same PH1 model. The results obtained suggest that the achievement of a critical level of GO silencing is necessary in order to significantly reduce urinary oxalate concentrations, whilst in the case of LDH, a proportional relationship between LDH inhibition and oxalate reduction exist. In other words, a higher reduction of GO expression compared to LDH was necessary to achieve the same effect on oxalate reduction, and a metabolic adaptation process was proposed in order to explain this lower efficiency of siRNA against GO.¹¹⁶ This fact correlates with previous studies suggesting that GO may not play a major role in the glyoxylate to oxalate conversion.¹¹

In a different recent study, GalNAc-LDHA siRNA was evaluated again in PH1 and PH2 mice models (*Agxt1^{-/-}* and *Grhpr^{-/-}*, respectively). As a result, urinary oxalate excretion was decreased by 75% on *Agxt1^{-/-}* mice and 32% on *Grhpr^{-/-}* mice, showing the potential of LDHA inhibition for the treatment of PHs.¹¹⁷

Very recently, stiripentol (Figure 13) has been identified as a promising LDHA inhibitor with application in the treatment of PH.¹¹⁸ This antiepileptic drug is currently used for treatment of Dravet syndrome, a severe myoclonic epilepsy of infancy. In a recent study developed in 2015, this drug was shown to target LDHA in neurons *in vitro*,¹¹⁹ thereby prompting the study of its possible applications in PH1. Thus, stiripentol has shown to decrease LDH-mediated oxalate synthesis by hepatocytes *in vitro*. *In vivo* experiments were also performed, finding that orally administered stiripentol significantly reduced excreted oxalate in rats. Besides, it has been administered to a young PH1 patient, resulting in a two-thirds oxalate reduction without

the presence of side effects, and hence, establishing stiripentol as a promising therapy for the treatment of PH.¹¹⁸

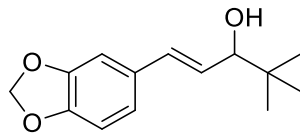


Figure 13. Structure of the LDHA inhibitor stiripentol.

Additionally, although not proven yet, CRISPR/Cas9 directed to LDHA inhibition has already been suggested as an attractive therapeutic option to treat PHs.⁹¹

2.1.5. Salicylic acid derivatives

Salicylic acid (SA), or 2-hydroxybenzoic acid (Figure 14), is a widely studied plant hormone that regulates important functions such as thermogenesis¹²⁰ and disease resistance.^{121,122} Several targets have been already identified for SA in plants, displaying different grades of affinity, but many of them still remain undiscovered.¹²³

Acetylsalicylic acid (ASA) (Figure 14), commonly known as aspirin, is the acetylated derivative of SA. This compound constitutes one of the most widely used medications worldwide to treat pain, inflammation, fever and to prevent undesired clotting.¹²⁴ ASA presents a half-life of approximately 20 min, since it suffers hydrolysis in aqueous solution: once it is administered, it is rapidly deacetylated to give SA.^{125,126}

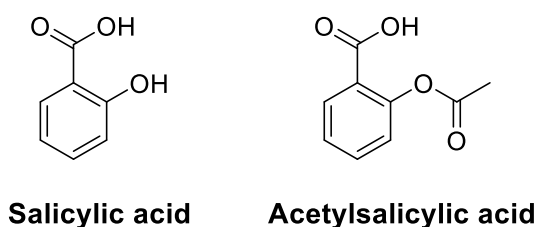


Figure 14. Structures of salicylic acid (SA) and acetylsalicylic acid (ASA).

In 1971, it was stated for the first time that a group of nonsteroidal anti-inflammatory drugs (NSAIDs), including SA and ASA, were able to inhibit the enzyme COX. The mechanism of action for ASA was also then discovered: ASA acetylates a serine in the active site of COX, irreversibly inhibiting the enzyme.¹²⁷ This fact establishes the difference between ASA, an irreversible inhibitor of COX, and other NSAIDs such as diclofenac and ibuprofen (Figure 15), which are reversible inhibitors that exert their effect competing with arachidonic acid for the active site.^{124,128}

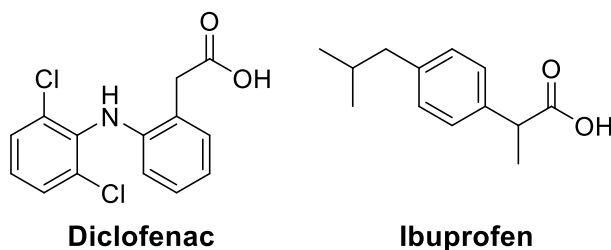


Figure 15. Structures of the NSAIDs diclofenac and ibuprofen.

COX is involved in the synthesis of prostaglandins from arachidonic acid. Prostaglandins are lipid compounds that present hormone-like effects in animals, producing pain, inflammation, fever and swelling.¹²³ In humans, two isoenzymes of

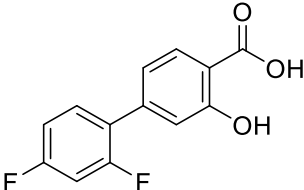
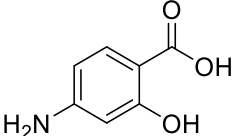
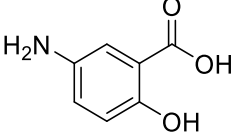
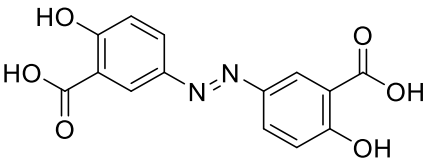
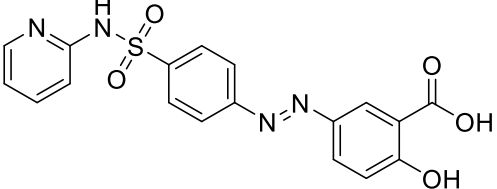
COX were initially identified: COX-1 (constitutively expressed), COX-2 (induced by pro inflammatory agents).¹²⁹ Afterwards, COX-3 was described as a variant of COX-1.¹³⁰

SA, while being a weak COX inhibitor,¹²⁷ presents almost the same pharmacological effects as the irreversible inhibitor ASA. It was demonstrated that *in vivo*, SA presents almost the same anti-inflammatory effect as ASA.¹³¹ However, the results were quite different in the *in vitro* experiments, wherein SA showed to be a weak inhibitor of prostaglandin synthesis (weak COX inhibitor), compared to ASA.^{127,132} This curious fact has led to the study of the exact mechanism of action of SA, since additional targets must be involved in the anti-inflammatory exerted by this drug.¹³³

The detailed mechanism of action for SA and ASA still remains undetermined, and it has been proposed that the effects of SA must be mediated by other targets, apart from COX. Throughout the last decades, several potential targets related to inflammation and energetic metabolism were described for SA, ASA and other salicylates.¹²³ Some mechanisms of action for SA have already been identified, being noteworthy the inhibition of the transcription factor nuclear factor-kappa-B (NF-κB): it regulates the expression of cytokines involved immune and inflammatory responses, such as IL-1, IL-6, interferon β and TNF-α.¹³⁴

Besides ASA and SA, other salicylates, some of them NSAID, are widely used for the treatment of diverse diseases. A brief summary of the applications of salicylates is shown in Table 1.¹²⁴

Table 1. Structure and applications of some salicylic acid derivatives. Data have been collected from references within text.

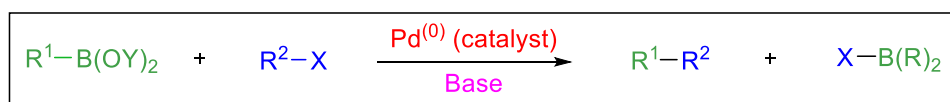
Name	Structure	Application
Diflunisal		Pain killer Antipyretic
4-Aminosalicylic acid		Tuberculosis
Mesalazine (5-Aminosalicylic acid)		Inflammation of the digestive tract ulcerative colitis (UC)
Olsalazine		Inflammatory bowel disease
Sulfasalazine		Inflammatory bowel disease Rheumatoid arthritis Enthesitis-related arthritis

2.2. Chemical background

2.2.1. Suzuki-Miyaura cross-coupling reaction

The Suzuki-Miyaura cross-coupling constitutes one of the most efficient reactions for the construction of C-C bonds in organic synthesis. It is a powerful tool widely used nowadays both in laboratory and industry for the synthesis of olefins, styrenes and biphenyls, given its great functional group tolerance and substrate scope.¹³⁵⁻¹⁴⁴ It was firstly reported by Akira Suzuki in 1979,¹⁴⁵ who received the Nobel Prize in Chemistry in 2010 together with R. F. Heck and E. Negishi for their work on the discovery of palladium-catalyzed cross-coupling reactions.¹⁴⁶

The reaction was initially described for organoboron compounds (such as 1-alkenylboranes), reacting with halides (such as 1-alkenyl, 1-alkynyl or aryl halides), in the presence of a base and with Pd(0) acting as a catalyst.^{145,147} Its scope was later extended to a wider variety of halides and also triflates acting as substrates for the oxidative addition of Pd(0) (Figure 16).¹⁴⁸⁻¹⁵⁰



R^1, R^2 = aryl, alkyl, alkenyl, alkynyl

Y = H, alkyl

X = Cl, Br, I, OTf

Base = Na_2CO_3 , Ba(OH)_2 , K_3PO_4 , Cs_2CO_3 , K_2CO_3

Figure 16. General scheme of Suzuki-Miyaura cross-coupling reaction.

The catalytic cycle for the coupling reaction involves three main steps: oxidative addition, transmetalation and reductive elimination, being the transmetalation step the less extensively studied.^{140,151} (Figure 17):

- 1. Oxidative addition.** The halide or triflate reacts with the Pd(0) catalyst to yield the Pd(II) complex (organopalladium complex). This constitutes the rate-determining step of the catalytic cycle and, for the halide, the reactivity decreases in the order $\text{I} > \text{OTf} > \text{Br} > \text{Cl}$. This step occurs with retention of configuration.
- 2. Transmetalation.** First, the base reacts with the previous organopalladium complex. Another molecule of base reacts with the organoboron reagent activating it by the formation of a more nucleophilic boronate complex, and therefore facilitating the later transfer of the organic group from boron to palladium. Now the

transmetalation occurs, and the organic group is transferred from the boronate complex to the palladium.

3. Reductive elimination. The Pd(II) intermediate undergoes reductive elimination, releasing the final product by carbon-carbon bond formation and regenerating to the catalytically active Pd(0).

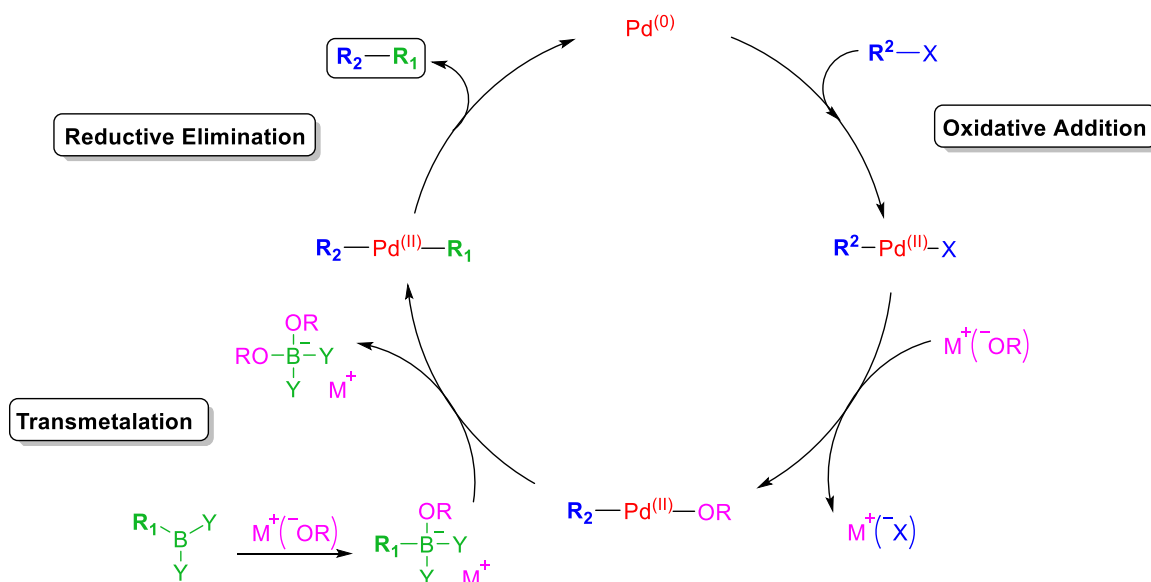


Figure 17. Catalytic cycle for the Suzuki-Miyaura cross-coupling reaction (adapted from references within text).

Traditionally, this coupling involves the use of a ligand, usually a phosphine, which activates the palladium forming a palladium-ligand complex that acts as catalyst. These complexes are frequently sensitive to air and moisture, and therefore this type of reactions need to be performed under oxygen-free conditions to prevent side reactions.¹⁵² Phosphine-free conditions have also been developed using *N*-heterocyclic carbenes,^{153,154} palladacycles,^{155,156} amines,^{157,158} imines,^{159,160} pyrazoles,¹⁶¹ triazoles^{162,163} ...

Efficient ligand-free conditions using Pd-encapsulated catalysts have also been introduced.^{164,165} This type of heterogeneous palladium catalysts are less air sensitive can be easily removed by filtration, allowing an easier purification process and the recycling of the catalyst. The increasing interest for the ligand-free conditions is also supported by the economic and environmental benefits of these systems.¹⁶⁴⁻¹⁶⁷ In accordance with this, conditions in the presence of water as a solvent have also been introduced.^{164,165,168-172}

2.2.2. Reductive amination

Amines constitute an integral part of biologically relevant molecules in nature such as nucleic acids, amino acids, neurotransmitters or alkaloids. They also occupy a central role in organic chemistry, serving as bases and key intermediates, and can be found in multiple drugs. Given the importance of these compounds, several methods for their preparation have been developed, being reductive amination one of the best studied tools for the synthesis of different types of amines.¹⁷³

Reductive amination of carbonyl compounds is nowadays a widely used method for the synthesis of primary, secondary and tertiary amines. This transformation occurs when a carbonyl compound is exposed to an amine that contains at least one N-H bond: an imine or iminium ion is formed through a condensation reaction, and its latter reduction yields the alkylated amine with a new C-N bond formed over carbonyl carbon of the aldehyde or ketone (Figure 18).¹⁷⁴

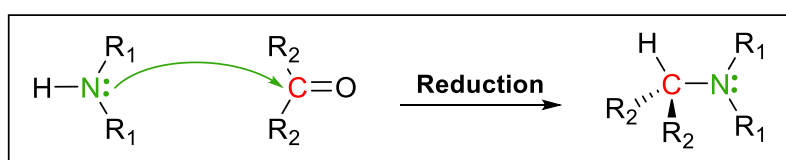


Figure 18. Simplified mechanism of reductive amination (adapted from references within text).

Thus, two well-defined steps can be distinguished in this transformation (Figure 19).^{151,174}

- First, a condensation reaction occurs between the amine and the carbonyl compound, whether an aldehyde or a ketone, to yield the corresponding imine (for NH₃ and primary amines) or iminium ion (for secondary amines), according to the starting material used. The slightly acidic pH value (6-7), at which the reaction is usually carried out, favors the protonation of the imine, resulting in the formation of the iminium ion.
- Afterwards, the previously formed carbon-nitrogen double bond, is reduced by catalytic hydrogenation (hydrogen in the presence of a catalyst) or by addition of special hydride reagents.

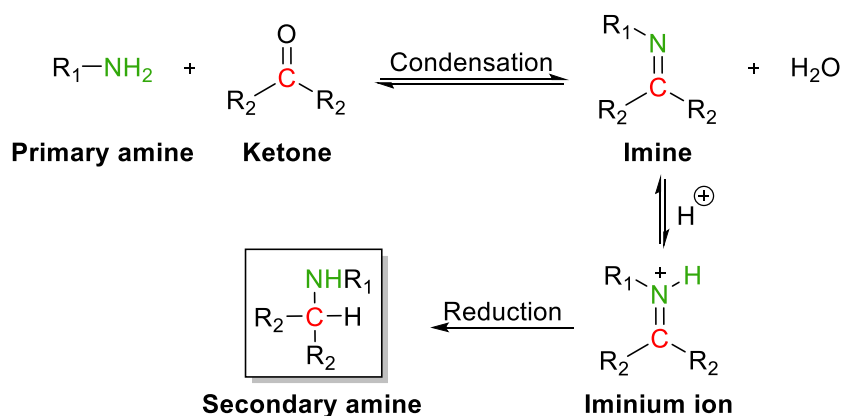


Figure 19. Reductive amination with a primary amine (adapted from references within text).

Two synthetic approaches can be used to conduct this transformation. Reductive amination is described as direct when the carbonyl compound and the amine are directly mixed with the reducing agent that will ultimately reduce the intermediate imine or iminium ion formed. The other method is called stepwise or indirect reductive amination, and involves the isolation of the intermediate imine or iminium ion and its latter reduction in a separate step.^{173,175}

The choice of one or the other approach determines the type of reducing agent that should be used: if the direct approach is followed, a reducing agent that selectively reduces the imine/iminium ion over the carbonyl compound needs to be used. In the case of the indirect approach, the election of this reagent does not constitute a key point, since no competition with the carbonyl compound will occur in the reduction step.

Direct reductive amination is usually the method of choice, and as mentioned before, both catalytic hydrogenation or hydride reducing agents can be utilized.¹⁷³

Catalytic hydrogenation constitutes an economical, convenient and efficient reduction method. However, it can lead to undesirable mixtures of products when double or triple bonds or reducible functional groups are also present in the molecule.^{176,177}

The other method for reduction is based on the use of **hydride reducing agents**. Initially, sodium borohydride (NaBH_4) was used as reducing agent, although its use was limited given its nonselective reduction mechanism: sodium borohydride rapidly reduce ketones and aldehydes.¹⁷⁸ Afterwards, the use of sodium cyanoborohydride (NaBH_3CN) as selective reducing agent was reported.¹⁷⁹ This reagent presented good stability in acid solutions and its selectivity could be guided according to the pH value: at pH 3-4 sodium cyanoborohydride efficiently reduces aldehydes and ketones, whilst

at pH 6-8 imines are preferentially reduced.¹⁷³ However, toxic byproducts are formed during the purification step, such as HCN and NaCN, leading to the development of alternative reducing agents. In 1989, a new procedure for reductive amination was introduced with the use of sodium triacetoxyborohydride [NaBH(OAc)₃], which was then established as a convenient and effective reducing agent. This allowed circumventing the toxicity issues associated to the use of sodium cyanoborohydride.¹⁸⁰

When carrying out reductive amination of aldehydes with primary amines, the dialkylation product may be the desired compound, and it can be directly obtained using the amine as the limiting reagent and adding two or more aldehyde equivalents. However, frequently, dialkylation occurs as a side reaction, and in those cases, it can be suppressed by the addition of an amine excess. Increasing the rate of imine formation by using solvents such as methanol (MeOH), tetrahydrofuran (THF) and dichloroethane (DCE), in which the imine formation occurs faster, is another option to overcome this problem.^{180,181}

3. Results and discussion

3. Results and discussion

Within this doctoral thesis, 70 final compounds along with their corresponding synthesis intermediates have been prepared. All the compounds prepared by the doctoral candidate are named **MDMG-**. Compounds named **BIO-** have been prepared by other researchers belonging to our group or have been obtained from commercial sources, in which case it will be specified. These compounds belong to two main structural families: oxamic acid derivatives and salicylic acid derivatives. For all the final compounds included in this study, the *mGO* inhibitory activity was evaluated using a colorimetric assay in the presence of glycolate as substrate. The addition of the chromogen sulfonated-DCIP or DCHBS, and 4-aminoantipyrine, in a coupled horseradish peroxidase (HRP) reaction, yields a chromogen whose absorbance is measured at 515 nm.⁸⁰

Initially, the inhibitory activity on recombinant *mGO* was assessed at 25 μM , and the IC_{50} value was calculated for those compounds presenting the best percentages of inhibition at a single dose. Potency against *hGO* was also evaluated for the most potent compounds over *mGO*. The capacity to diminish oxalate production on hyperoxaluric mice primary hepatocytes was assessed for the most active *mGOi*'s in a cell-based assay: *Agxt1*^{-/-} hepatocytes are supplemented with glycolate, which is metabolized to glyoxylate by *GO*, and this one is finally oxidized to oxalate by *LDH*, mainly. Afterwards, excreted oxalate is quantified from the extracellular medium using a colorimetric assay.⁸⁰ When an effective *GOi* is added, the oxidation from glycolate to glyoxylate is blocked, and a decrease of oxalate release is then observed. *In silico* calculations about the binding mode inside *hGO* have also been obtained for representative compounds.

mGO was initially chosen as a high-quality tool to perform the screening of potential *GOi*'s, assuring the comparability of the findings when escalating the biological testing to the available PH1 model of *Agxt1*^{-/-} hepatocytes. Besides, *mGO* and *hGO* share 89.5% of sequence identity,⁹⁷ what would allow a safe translation of the results into a human setting. On the other hand, binding mode predictions were performed inside *hGO*, allowing the comparison of the results with **glyoxylate**, **CCPST**, and **CDST** available crystallographic data.¹⁰⁰ In the last stages of this research, recombinant *hGO* was also available to perform the enzymatic assays, so that the most potent compounds on *mGO* were also evaluated as *hGO* inhibitors. At one point, interferences

3. Results and discussion

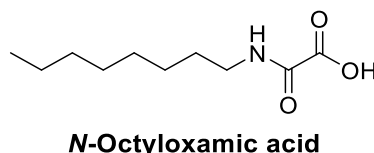
with the GO inhibition colorimetric assay were detected for some compounds, forcing the implementation of an alternative fluorometric method for the enzymatic evaluation.

Finally, the most active GOi's have also been evaluated against LDH, looking for double GO/LDH inhibitors as interesting tools against two key enzymes of glyoxylate metabolism. Both LDHA and LDHB isoenzymes have been tested given the importance of developing selective inhibitors of the hepatic isoenzyme. For LDH evaluation, a kinetic fluorometric method has been implemented.

In order to discard too lipophilic molecules which could be retained in the cellular membrane, the theoretical partition coefficients, expressed as $\log P_{th}$, were calculated for representative compounds.

3.1. Oxamic acids and homologous derivatives

As mentioned before, in previous studies, α -hydroxy acids,^{102–104} α -keto acids¹⁰⁵ and oxamates^{103,104} have been explored as polar heads for the development of GOi's. As a result, compounds such as *N*-octyloxamic acid (Figure 20) were identified as novel GOi's. This compound, bearing a carboxylic acid as polar head, as well as an ionizable amino group in β position, met the structural requirements stated for GOi's, and showed a notable IC₅₀ value of 3 μ M over *hGO*.¹⁰⁴ However, neither *N*-octyloxamic acid nor related compounds became promising drug candidates, probably due to their unfavourable physico-chemical properties. In the case of the *N*-octyloxamic acid, an eight-carbon aliphatic chain hangs from the polar head, conferring the molecule a lipophilicity level that may hamper passing through cell membranes due to the limited solubility in the biological environment.

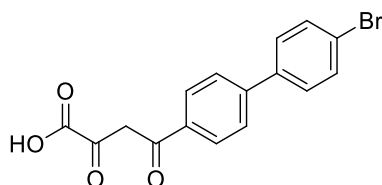


***N*-Octyloxamic acid**

Figure 20. Structure of *N*-octyloxamic acid.

With the aim of obtaining improved versions of this type of compounds, we planned the replacement of the long aliphatic chain present in *N*-octyloxamic acid by a biphenyl fragment that would allow multiple substitution options in order to modulate the lipophilicity of the molecule. In fact, this moiety is already present in other GOi's, such as the 2,4-dioxobutanoic acid derivatives (Figure 21).¹⁰⁵ Besides, the introduction of such fragment would promote the establishment of π - π interactions with the FMN flavin ring. Both activated and deactivated aromatic rings were introduced in the side chain, in order to explore their influence in the biological activity.

Since 2,4-dioxobutanoic acid derivatives have also been described as GOi's,¹⁰⁵ we contemplated the possibility of spacing the two carbonyl groups in the molecule through the introduction of 1 or 2 methylene groups between them, and therefore obtaining malonic and succinic acid derivatives apart from the oxamic acid derivatives already proposed.



4-(4'-Bromobiphenyl-4-yl)-2,4-dioxobutanoic acid

Figure 21. Example of 2,4-dioxobutanoic acid derivative.¹⁰⁵

This way, we could explore the ideal distance between the two carbonyl groups. Thus, biphenyl compounds derived from 4-phenylaniline, carrying different types of activating and deactivating groups, were synthesized (**A-C**, Figure 22).

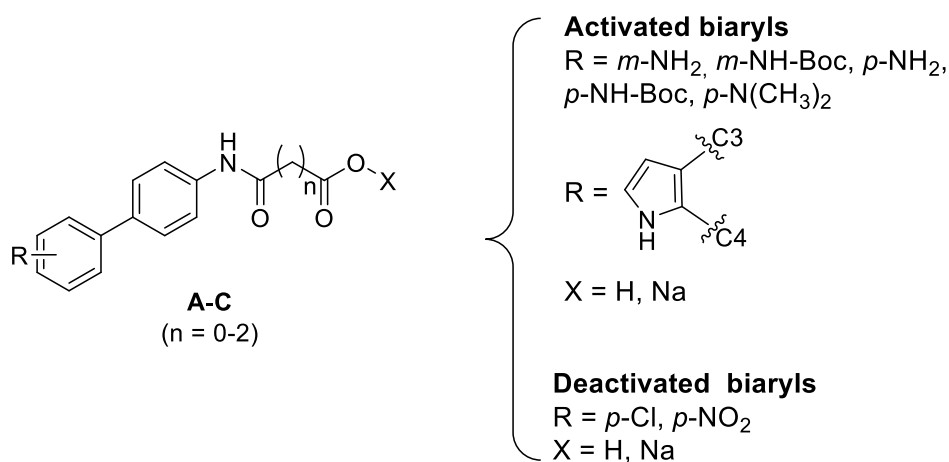
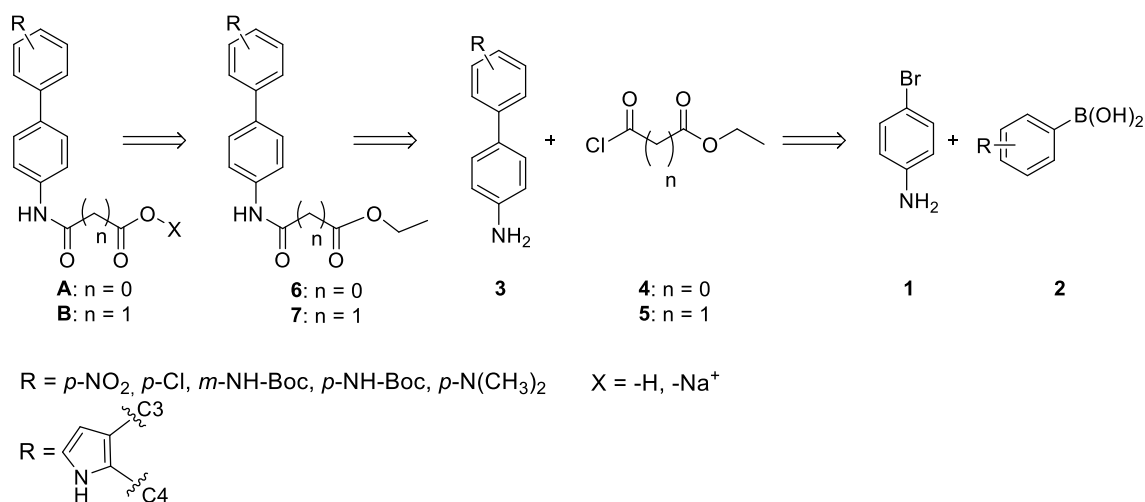


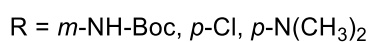
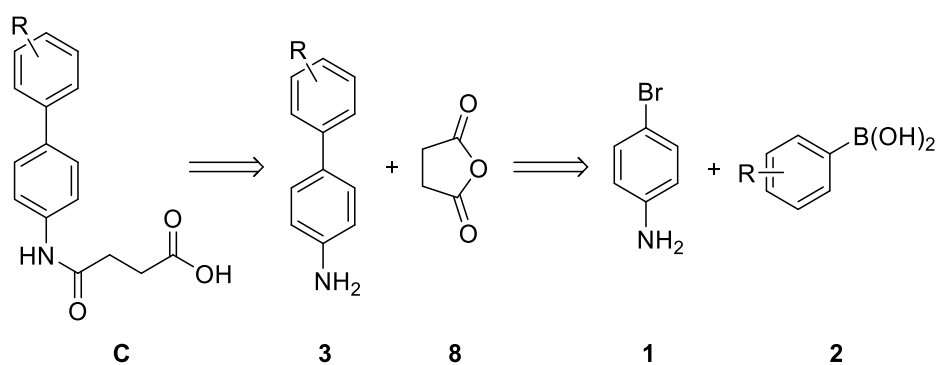
Figure 22. General structure of the synthesized biphenyl compounds (**A-C**). Both activating and deactivating groups were introduced in *m*- and *p*- positions. Compounds were obtained as carboxylic acids or their corresponding salts, and 0 (**A**), 1 (**B**) or 2 (**C**) methylene groups were introduced as spacers between the carbonyl groups.



Scheme 1. Retrosynthetic scheme followed for the synthesis of 2-oxoacetic and 3-oxopropanoic acid derivatives (**A** and **B**, respectively).

As can be seen in the retrosynthetic analysis (Scheme 1), 2-oxoacetic and 3-oxopropanoic acid derivatives (**A** and **B**, respectively) were synthesized in three easy synthetic steps. First, the biaryl moiety was synthesized through Suzuki-Miyaura cross-coupling reaction between *p*-bromoaniline (**1**), and the corresponding arylboronic acid (**2**). The resulting 4-phenylaniline derivative (**3**) was acylated using the acylating agents ethyl 2-chloro-2-oxoacetate (**4**) or ethyl 3-chloro-3-oxopropanoate (**5**) to yield the acylated ester derivatives (**6** and **7**, respectively), which were finally hydrolyzed to afford the final compounds as carboxylic acids or their corresponding salts. In some cases, additional modifications were carried out over the side chain to obtain additional compounds.

In the case of 4-oxobutanoic acid derivatives (**C**), a similar but shorter retrosynthetic scheme was followed (Scheme 2). The biaryl side chain was equally built by Suzuki-Miyaura cross-coupling reaction between *p*-bromoaniline (**1**) and the corresponding arylboronic acid (**2**). The resulting 4-phenylaniline derivative (**3**) was acylated with succinic anhydride (**8**) to afford the final compound as a free carboxylic acid. Again, in some cases, further modifications were carried out over the side chain to obtain different compounds.

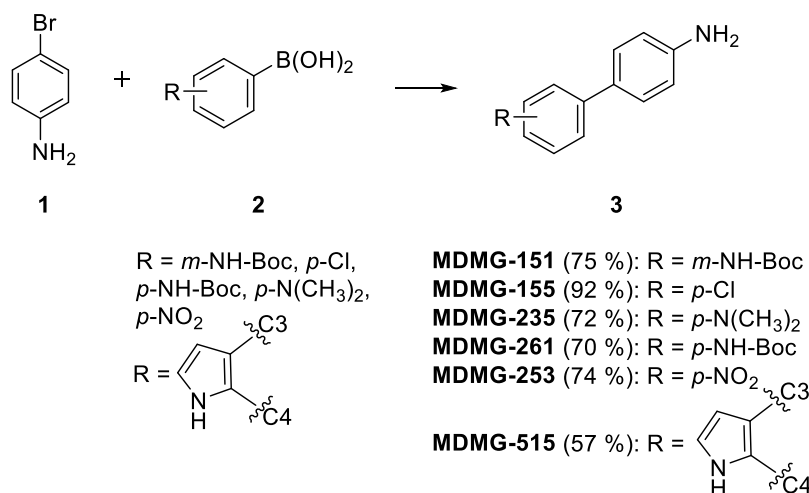


Scheme 2. Retrosynthetic scheme followed for the synthesis of 4-oxobutanoic acid derivatives (**C**).

The first step is common for both retrosynthetic approaches, and consists of the synthesis of the intermediate biaryl moiety through Suzuki-Miyaura cross-coupling reaction between the aryl halide (**1**) and different arylboronic acids (**2**) (Scheme 3).

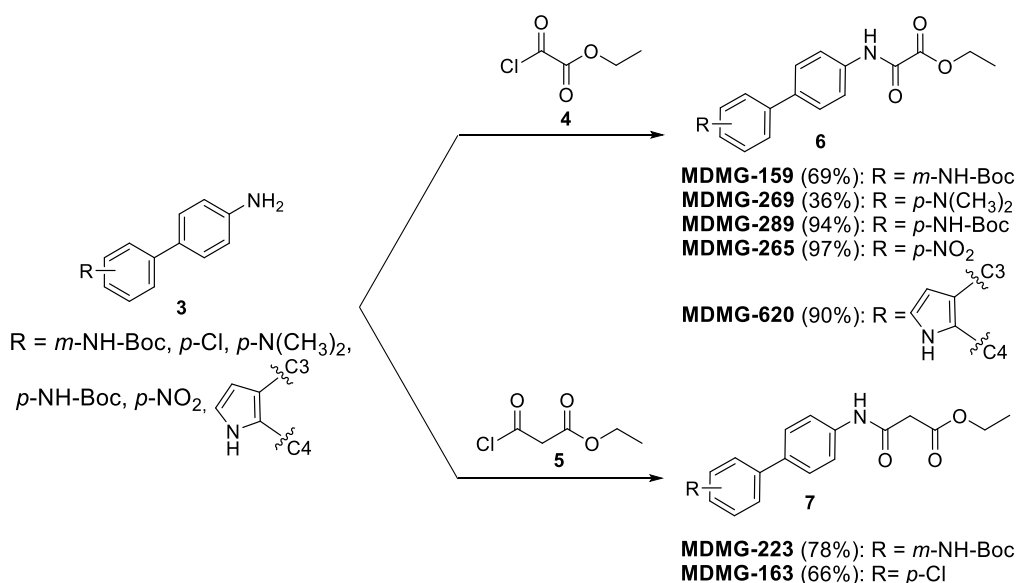
Six intermediate 4-phenylaniline derivatives type **3** (Scheme 3) were synthesized following this strategy. Both activating and deactivating groups were introduced in *ortho*- and *meta*- positions at the biphenyl moiety. In order to explore the influence of the electronic properties of the side chain in the biological activity, four options for

electron-rich rings (**MDMG-151**, **MDMG-261**, **MDMG-235**, **MDMG-515**) and two for electron-poor rings (**MDMG-155** and **MDMG-253**) were introduced as hydrophobic tails.

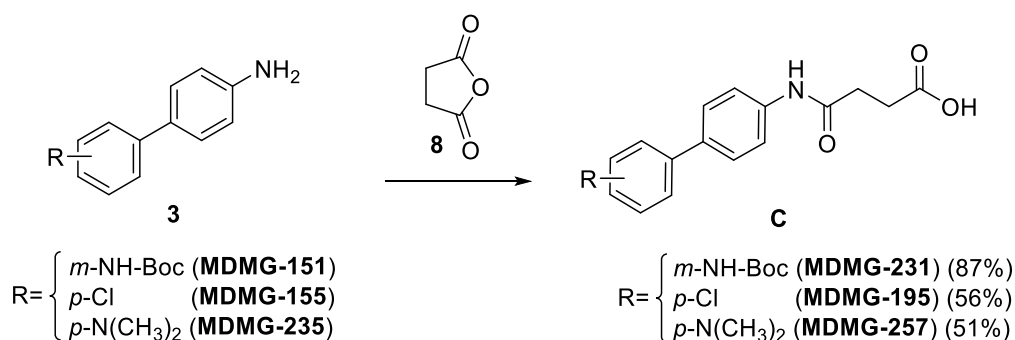


Scheme 3. Suzuki reaction between *p*-bromoaniline and different arylboronic acids to yield the corresponding 4-phenylaniline derivatives. Isolated yields are shown in parenthesis. Reaction conditions: 4-Bromoaniline (1 equiv), boronic acid (1.2 equiv), Pd(OAc)₂ (5 mol%), triphenylphosphine (15 mol%), K₂CO₃ (3 equiv), DMF/H₂O 1/1, microwave, 100/150 °C, 3h (see 5.2.5. General synthetic procedure 5A). Isolated yields are shown in parenthesis.

The next step is the aniline acylation with the corresponding acylating agent, either **4**, **5** or **8**, giving rise to the precursor esters ethyl 2-amino-2-oxoacetates (type **6**), ethyl 3-amino-3-oxopropanoates (type **7**) and the final 4-oxobutanoic acids (type **C**), respectively (Schemes 4 and 5).

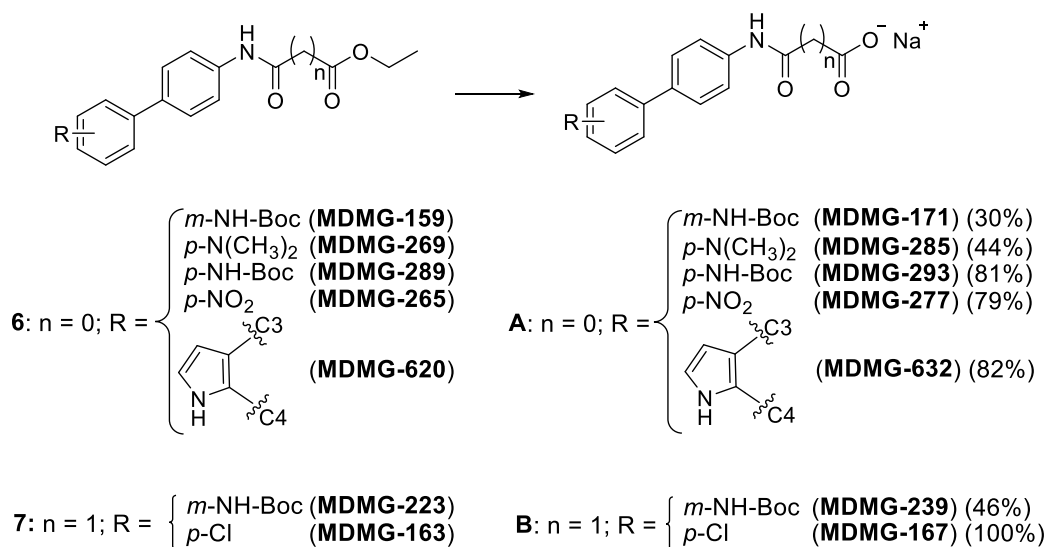


Scheme 4. Acylation of 4-phenylaniline derivatives type **3** with ethyl 2-chloro-2-oxoacetate (**4**) or ethyl 3-chloro-3-oxopropanoate (**5**) to give the corresponding ethyl 2-amino-2-oxoacetate or ethyl 3-amino-3-oxopropanoate derivatives (**6** and **7**), respectively. Reaction conditions: **3** (1 equiv), acyl chloride (2 equiv), trimethylamine (3 equiv), anhydrous tetrahydrofuran, rt, 24 h (see 5.2.1. General synthetic procedure 1). Isolated yields are shown in parenthesis.

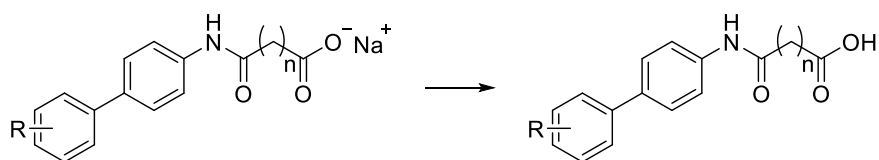


Scheme 5. Acylation of 4-phenylaniline derivatives type **3** with succinic anhydride (**8**) to give the corresponding 4-oxobutanoic acid derivatives (type **C**). Reaction conditions: **3** (1 equiv), **8** (1.1 equiv), anhydrous toluene, reflux, 24 h (see 5.2.2. General synthetic procedure 2). Isolated yields are shown in parenthesis.

Finally, the intermediate esters **6** and **7** were subjected to basic hydrolysis with NaOH to afford the final carboxylic acids type **A** and **B** as sodium carboxylates (Scheme 6). In addition, some amount of **MDMG-231**, **MDMG-171**, **MDMG-293**, and **MDMG-239**, compounds that carry a *tert*-butoxycarbonyl protective group (Boc group) on the side chain R, was subjected to deprotection with trifluoroacetic acid (TFA) to release the corresponding amino compound (Scheme 7).



Scheme 6. Reaction conditions: **6** or **7** (1 equiv), NaOH 1N (5 equiv), THF/H₂O 1/1 (10 mL/mmol ethyl ester), rt, 24 h (see 5.2.3. General synthetic procedure 3). Isolated yields are shown in parenthesis.



MDMG-171: $n = 0$; R = *m*-NH-Boc

MDMG-293: $n = 0$; R = *p*-NH-Boc

MDMG-239: $n = 1$; R = *m*-NH-Boc

MDMG-231: $n = 2$; R = *m*-NH-Boc

MDMG-191 (91%): $n = 0$; R = *m*-NH₂

MDMG-305 (100%): $n = 0$; R = *p*-NH₂

MDMG-281 (100%): $n = 1$; R = *m*-NH₂

MDMG-245 (91%): $n = 2$; R = *m*-NH₂

Scheme 7. Reaction conditions: (i) Boc-protected amino derivative (1 equiv), trifluoroacetic acid/dichloromethane (DCM) 3/7 (100 mL/mmol of Boc-protected amino derivative), rt, 3 h; (ii) HCl 5% (300 mL/mmol of Boc-protected amino derivative), rt, 3h. (see 5.2.4. General synthetic procedure 4). Isolated yields are shown in parenthesis.

3.1.1. 2-Oxoacetic acid derivatives and 3-oxopropanoic acid derivatives

3.1.1.1. 2-Oxoacetic acid derivatives

Seven compounds derived from 2-oxoacetic acid were synthesized in moderate to high overall yields (Figures 23 and 24) (for reaction yields, see 5.3.3. Synthesis of 2-oxoacetic and 3-oxopropanoic acid derivatives) and evaluated for inhibitory activity against recombinant *mGO* (colorimetric protocol) and for oxalate decreasing activity on *Agxt1^{-/-}* mouse hepatocytes (Table 2). The indole **MDMG-632** (Figure 24), carrying an electron-rich aromatic ring, proved to be the most potent *mGO*i ($IC_{50} = 7 \mu\text{M}$). However, this compound reduced oxalate production only by 15% with respect to the untreated control on *Agxt1^{-/-}* mouse hepatocytes. **MDMG-305** and **MDMG-171** (Figure 23), carrying *p*-amino and *m*-*tert*-butoxycarbonyl groups, presented moderate IC_{50} s of 18 μM against *mGO*, and reduced oxalate by 5% and 30%, respectively. Compounds **MDMG-277** and **MDMG-293**, carrying *p*-nitro and *p*-*tert*-butoxycarbonyl groups, turned out to be less potent *mGO* inhibitors, showing similar IC_{50} s of 37 and 35 μM respectively. Within this set, **MDMG-285**, carrying a *p*-dimethylamino group, was the least potent *mGO*i, inhibiting the enzyme only by 33% at 25 μM . The *p*-*tert*-butoxycarbonyl derivative **MDMG-293**, which is also the position isomer of **MDMG-171**, behaved as a moderate *mGO*i ($IC_{50} = 35 \mu\text{M}$), but showed to be the most efficient compound reducing oxalate output in the cell-based assay, showing 45% reduction of oxalate when tested at 10 μM . Deprotection of the amino group yielded compound **MDMG-305**, a more potent *mGO*i but a less efficient compound in hepatocytes. In fact, **MDMG-305**, along with **MDMG-277**, **MDMG-285**, showed almost null capacity reducing oxalate production in hepatocytes. Finally, compound **MDMG-191** was not evaluated given its high level of interference with the colorimetric method (data not shown).

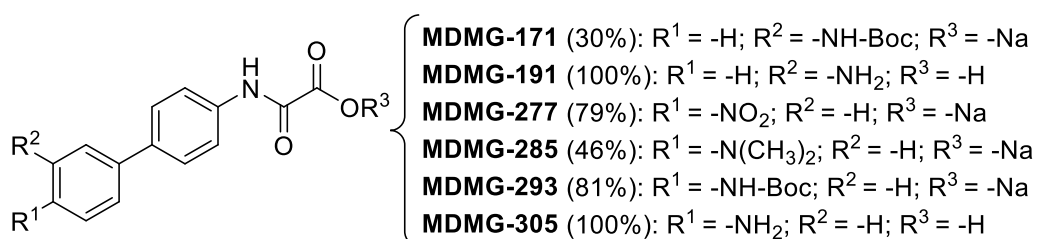


Figure 23. Structures of the 2-oxoacetic acid derivatives synthesized. Isolated yields are shown in parenthesis.

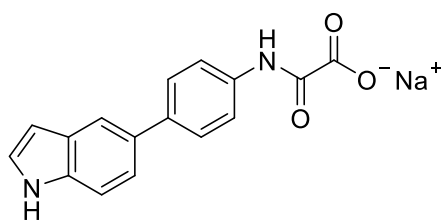
**MDMG-632 (82%)**

Figure 24. Structure of the indole **MDMG-632**. Isolated yield is shown in parenthesis.

Table 2. Biological evaluation of 2-oxoacetic acid derivatives. Biological determinations: (i) Enzymatic inhibition on purified mouse glycolate oxidase (*mGO*), at single concentration and IC_{50} calculation using the colorimetric method; (ii) Excreted oxalate in *Agxt1^{-/-}* mouse primary cultured hepatocytes, compared to control (relative oxalate).

Compound	<i>mGO</i> (%) ^a	IC_{50} ^b	R^{2c}	Relative oxalate ^d
MDMG-171	55.7 ^e	18.06 ^e	0.98	0.71 ± 0.08
MDMG-191	n/a	n/a	n/a	n/a
MDMG-277	40.9 ^e	37.74 ^e	0.94	0.92 ± 0.19
MDMG-285	33.9 ^e	n/a	n/a	0.91 ± 0.15
MDMG-293	48.4 ^e	35.22 ^e	0.93	0.55 ± 0.3
MDMG-305	66.7 ^e	18.06 ^e	0.94	0.94 ± 0.15
MDMG-632	78.2 ^e	7.53 ^e	0.95	0.86 ± 0.15

^aPercentage of inhibition of purified *mGO* with 25 μ M drug, after 1 min. ^bHalf maximal inhibitory concentration calculated in saturated conditions of glycolate (22.2 mM). ^c IC_{50} curve-fitted score. ^dOxalate output decrease tested at 24 h post-treatment with 10 μ M drug in *Agxt1^{-/-}* mouse primary hepatocytes cultured with 5 mM glycolate, in 6-well plates. Data are represented as the mean ± SD of n = 3 replicates. One-way ANOVA statistical analysis was used, and $p < 0.05$ was considered statistical significant. ^eNo SD is given. n/a: Not assessed.

3.1.1.2. 3-Oxopropanoic acid derivatives

Three compounds derived from 3-oxopropanoic acid were synthesized according to the general structure showed in Figure 25. Only compound **MDMG-239**, along with its deprotected derivative **MDMG-281**, were tested over *mGO* (Table 3). **MDMG-239**, carrying a *m-tert*-butoxycarbonyl group, was able to reduce oxalate production by 27% while being a modest *mGO* inhibitor ($IC_{50} = 24 \mu\text{M}$). Deprotection of the amino group gave rise to compound **MDMG-281**, resulting in a substantial loss of potency over *mGO* (13% *mGO* inhibition at $25 \mu\text{M}$). Compound **MDMG-167** was not evaluated given its high level of interference with the colorimetric method (data not shown).



Figure 25. Structures of the 3-oxopropanoic acid derivatives synthesized. Isolated yields are shown in parenthesis.

Table 3. Biological evaluation of 3-oxopropanoic acid derivatives. Biological determinations: (i) Enzymatic inhibition on purified mouse glycolate oxidase (*mGO*), at single concentration and IC_{50} calculation using the colorimetric method; (ii) Excreted oxalate in *Agxt1^{-/-}* mouse primary cultured hepatocytes, compared to control (relative oxalate).

Compound	<i>mGO</i> (%) ^a	IC_{50} ^b	R^{2c}	Relative oxalate ^d
MDMG-167	n/a	n/a	n/a	n/a
MDMG-239	42.9 ^e	24.36	0.84	0.73 ± 0.3
MDMG-281	13.3 ^e	n/a	n/a	n/a

^aPercentage of inhibition of purified *mGO* with $25 \mu\text{M}$ drug, after 1 min. ^bHalf maximal inhibitory concentration calculated in saturated conditions of glycolate (22.2 mM). ^c IC_{50} curve-fitted score. ^dOxalate output decrease tested at 24 h post-treatment with $10 \mu\text{M}$ drug in *Agxt1^{-/-}* mouse primary hepatocytes cultured with 5 mM glycolate, in 6-well plates. Data are represented as the mean ± SD of $n = 3$ replicates. One-way ANOVA statistical analysis was used, and $p < 0.05$ was considered statistical significant. ^eNo SD is given. n/a: Not assessed.

3.1.2. 4-Oxobutanoic acid derivatives

Finally, four compounds derived from 4-oxobutanoic acid were synthesized according to the general structure showed in Figure 26. None of these compounds showed significant *mGO* inhibitory activity, presenting percentages of inhibition ranging between 18 and 24% at 25 μM (Table 4). Given their scarce potency, neither determination of IC_{50} or assay on hepatocytes were conducted.



Figure 26. Structures of the 4-oxobutanoic acid derivatives synthesized. Isolated yields are shown in parenthesis.

Table 4. Biological evaluation of the 4-oxobutanoic acid derivatives. Biological determinations: (i) Enzymatic inhibition on purified mouse glycolate oxidase (*mGO*), at single concentration and IC_{50} calculation using the colorimetric method; (ii) Excreted oxalate in *Agxt1^{-/-}* mouse primary cultured hepatocytes, compared to control (relative oxalate).

Compound	<i>mGO</i> (%) ^a	IC_{50} ^b	R^{2c}	Relative oxalate ^d
MDMG-195	21.9 ^e	n/a	n/a	n/a
MDMG-231	18.7 ^e	n/a	n/a	n/a
MDMG-245	24.7 ^e	n/a	n/a	n/a
MDMG-257	24.7 ^e	n/a	n/a	n/a

^aPercentage of inhibition of purified *mGO* with 25 μM drug, after 1 min. ^bHalf maximal inhibitory concentration calculated in saturated conditions of glycolate (22.2 mM). ^c IC_{50} curve-fitted score. ^dOxalate output decrease tested at 24 h post-treatment with 10 μM drug in *Agxt1^{-/-}* mouse primary hepatocytes cultured with 5 mM glycolate, in 6-well plates. Data are represented as the mean \pm SD of $n = 3$ replicates. n/a: ^eNo SD is given. Not assessed.

3.1.3. Discussion

Within the oxamic acid derivatives, only the indole derivative **MDMG-632** showed a remarkable IC_{50} value below 10 μ M. Other 2-oxoacetic acid derivatives, such as **MDMG-171** and **MDMG-305**, were close in potency, but none of them presented significant oxalate reduction on hepatocytes. On the other hand, **MDMG-293**, while being a less potent *mGOi*, was the most active compound in hepatocytes within this set (45% oxalate reduction when tested at 10 μ M).

According to the results in this research, oxamic acid derivatives seemed to be the most active polar heads among the oxoalkylcarboxylic acids studied. Chain enlargement, which gave rise to the 3-oxopropanoic and 4-oxobutanoic acid derivatives, clearly worsened *mGO* inhibitory activity, especially when two methylenes were separating the carbonyl groups (4-oxobutanoic derivatives). This is in line with previous results obtained for this type of compounds, reaffirming that the introduction of one or two methylene groups between the two carbonyl groups in oxamic acid derivatives lowers the inhibitory activity over *mGO*.¹⁸² For that reason, ultimately, 3-oxopropanoic and 4-oxobutanoic derivatives were excluded from the synthesis and biological evaluation.

For all the oxamic acid derivatives, interferences with the GO inhibition and oxalate determination colorimetric assays were detected, being the results inconclusive, and therefore preventing the establishment of structure-activity relationships for these compounds. This, along with the low potency and efficacy observed for the compounds, compared to other libraries such as the salicylic derivatives, led to the abandonment of this structural family.

3.2. Salicylic acid derivatives

After excluding oxamic acid derivatives from this research, structural motifs matching the characteristics required for GO inhibitors were searched. At that time, the possibility of using the salicylic acid core as the basis for the synthesis of new molecules was contemplated, since it presents a protonated heteroatom located in β relative to an acidic function.¹⁰¹ This structural feature, which is already present in known GOi's, has proven to be beneficial for the biological activity of those compounds.^{100,101} The salicylic acid core consists of a flat electron-rich ring with a hydroxy group located in β with respect to the acidic function. The carboxy group could reproduce interactions at Arg167, Arg263 and Tyr26, and the phenolic function could act as hydrogen donor in the interaction with His260: this way, as it happens in the case of **CDST**, protonation of His260 would not be required, with the consequent energetic saving. At this point, we made preliminary docking studies that agreed with the capacity of salicylic acid to interact at *hGO* active site (Figure 27). In addition, and in support of this idea, salicylic acid core constitutes a drug-like structure and its derivatives, commonly known as salicylates, have already been used for the treatment of several diseases, as already stated.¹²³

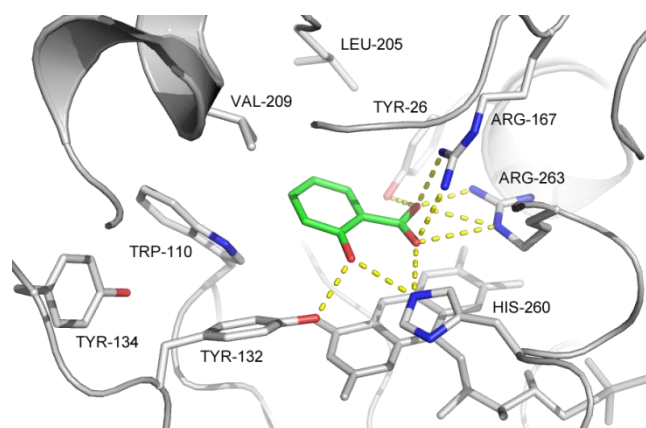


Figure 27. Docked salicylic acid inside *hGO* active site (PDBid: 2RDT).

3.2.1. Commercial salicylic acid derivatives

3.2.1.1. Results

With the aim of exploring salicylic acid derivatives as a possibility for the development of novel GOi's, we selected a set of salicylates and salicylate-related commercial compounds for a preliminary study, wherein they were evaluated for GO inhibition and for oxalate decrease in PH1 hepatocytes. These compounds were selected according to structural diversity criteria and included differently sized aliphatic, aromatic and heteroaromatic side chains, both rigid and flexible. Besides, both polar and hydrophobic functionalities were included to explore their binding mode at the access channel. Thus, this set of compounds included simple salicylic acids (**BIO-1** to **BIO-9**), benzofused derivatives (**BIO-10** to **BIO-16**), and the structurally related chloroquinoline (**BIO-17**) (Figure 28). Compound **BIO-16**, included in this first set, was not obtained commercially, but prepared in our lab.

Salicylic acid (**BIO-1**), presented a poor inhibitory effect over *mGO* (18.5% at 25 μM). Within this set of compounds, the majority of the *mGO* inhibitory activities were below 30% at 25 μM (Table 5). This is the case of halogenated derivatives (**BIO-2** and **BIO-3**), 4-aminosalicylic acid (**BIO-5**), 5-acetylsalicylic acid or mesalazine (**BIO-6**), the 5-glutamine derivative **BIO-7**, the benzofused derivatives **BIO-14** and **BIO-16**, and the chloroquinoline **BIO-17**. A slight improvement in the inhibitory activity was observed for diflunisal (**BIO-9**), bearing a 2,4-difluorophenyl group on C5, and also for the benzofused derivative **BIO-16**, which inhibited *mGO* by 26% at 25 μM . Whereas the introduction of an amine group on C4 (**BIO-5**) led to a scarce inhibitory effect over *mGO* (15% at 25 μM), the same substitution on C5, leading to 5-aminosalicylic acid (**BIO-4**), yielded higher enzymatic inhibition (72% at 25 μM , with an IC_{50} of 7.8 μM). Compound **BIO-8**, presenting a hydrophobic side chain, inhibited 82.8% *mGO* enzymatic activity at 25 μM , with an IC_{50} of 34.5 μM .

Seven benzofused salicylates (naphthyllic acids **BIO-10** to **BIO-16**) were also included in this preliminary screening, since an additional benzene ring could reinforce the binding of the molecule to the target through the establishment of additional hydrophobic interactions. The resulting increased hydrophobicity can be observed in the higher $\log P_{\text{th}}$ values predicted for these compounds (Table 5). In the simplest of these molecules, the naphthalene core only bears a bromine group (**BIO-10**), whilst more complex structures carry aromatic or heteroaromatic side chains (furan, tetrazole,

benzene or naphthalene) bonded through different electron-rich linkers (azo group, sulfur or oxygen atoms).

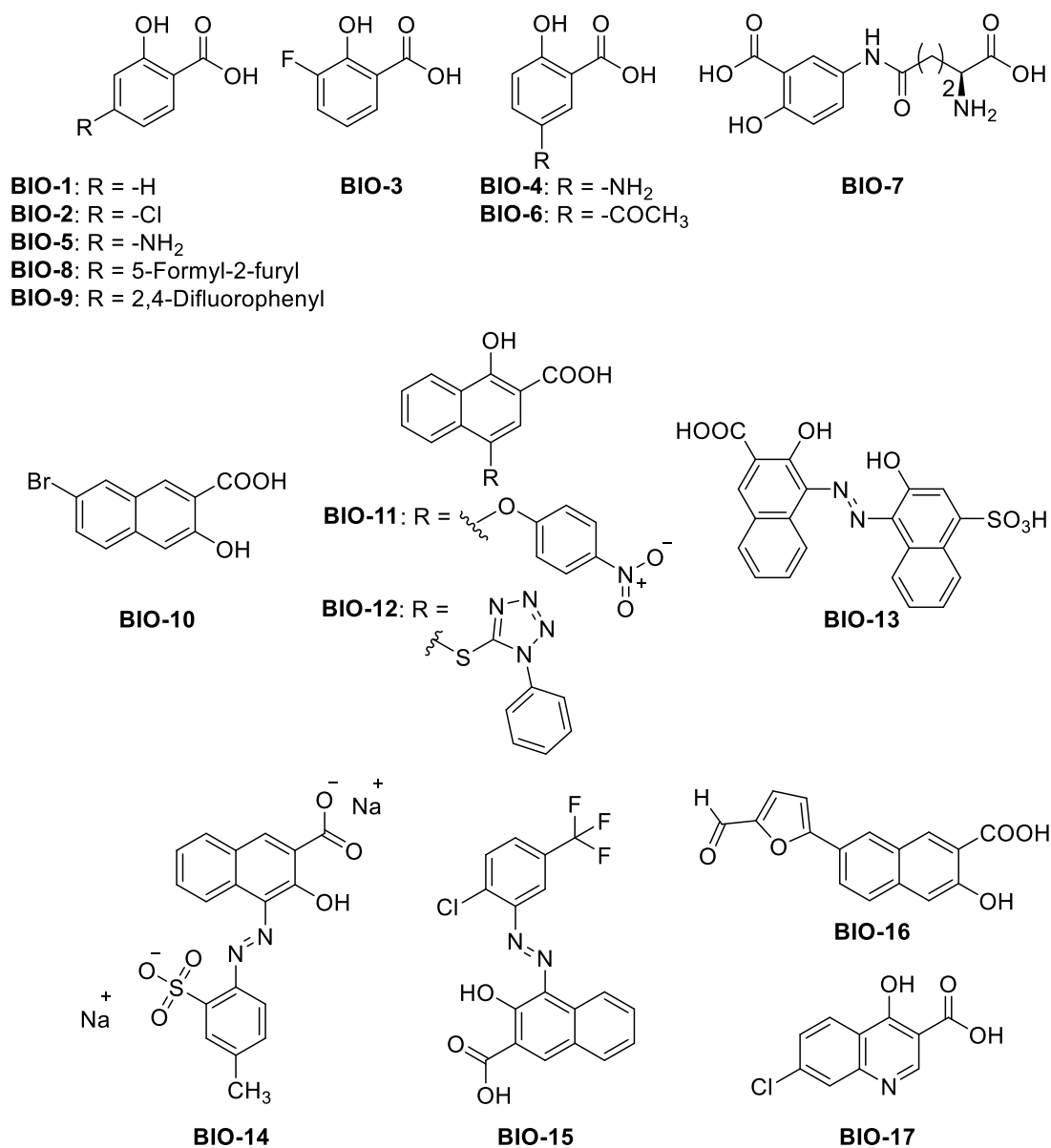


Figure 28. Structures of salicylate-related compounds selected for a preliminary screening.

Table 5. Biological data of the first set of compounds and **CCPST** and *in silico* prediction of partition coefficient ($\log P_{th}$). Biological determinations: (i) Enzymatic inhibition on purified mouse glycolate oxidase (*mGO*), at single concentration and IC_{50} calculation using the colorimetric method; (ii) Excreted oxalate in *Agxt1^{-/-}* mouse primary cultured hepatocytes, compared to control (relative oxalate).

Compound	<i>mGO</i> (%) ^a	IC_{50} (μM) ^b	R^{2c}	Relative oxalate ^d	$\log P_{th}$
CCPST	34.8 ± 4.8	43.5 ± 1.1	n/a	0.63 ± 0.16 ^e	n/a
BIO-1	18.5 ± 13.7	n/a	n/a	n/a	1.46
BIO-2	20.8 ± 4.4	n/a	n/a	n/a	1.98
BIO-3	13.5 ± 4.6	n/a	n/a	n/a	1.60
BIO-4	71.9 ± 3.2	7.8 ± 1.2	0.93	0.88 ± 0.02	0.68
BIO-5	14.9 ± 7.9	n/a	n/a	n/a	0.68
BIO-6	22.1 ± 1.0	n/a	n/a	n/a	0.77
BIO-7	7.8 ± 2.8	n/a	n/a	n/a	0.42
BIO-8	82.8 ± 5.6	34.5 ± 1.2	0.88	0.88 ± 0.18	0.29
BIO-9	27.9 ± 0.6	n/a	n/a	0.88 ± 0.08	3.42
BIO-10	42.3 ± 1.1	39.9 ± 1.1	0.94	0.99	3.25
BIO-11	96.3 ± 0.5	2.9 ± 1.1	0.97	0.77 ± 0.01	1.00
BIO-12	75.3 ± 2.6	11.1 ± 1.1	0.98	0.99 ± 0.01	5.93
BIO-13	75.1 ± 2.3	n/a	n/a	1.11 ± 0.03	4.87
BIO-14	1.5 ± 2.1	n/a	n/a	n/a	4.62
BIO-15	47.4 ± 2.3	n/a	n/a	0.91 ± 0.04	6.17
BIO-16	26.2 ± 1.6	n/a	n/a	n/a	0.72
BIO-17	24.8 ± 5.9	n/a	n/a	n/a	2.53

^aPercentage of inhibition against *mGO* with 25 μM of the drug, after 1 min. ^b IC_{50} : Calculated on mouse glycolate oxidase in saturated conditions of glycolate (22.2 mM). ^c R^2 : IC_{50} curve-fitted score. n/a: Not analyzed. ^dOxalate output tested at 24 h post-treatment with 10 μM of the drug in *Agxt1^{-/-}* mouse primary hepatocytes cultured with 5 mM glycolate, in 6-well plates. Data are represented as mean ± SD of n = 3 replicates. One-way ANOVA statistical analysis, $p < 0.05$ was considered statistically significant. ^eData at 12.5 μM in *Agxt1^{-/-}* mouse primary hepatocytes. n/a: Not assessed.

Compounds **BIO-11** and **BIO-12**, carrying ether or thioether linkers, respectively, presented good inhibition percentages on isolated *mGO* (96 and 75%, respectively) (Table 5). Compounds **BIO-13** to **BIO-15** are 4-aryloxy-3-hydroxy-2-naphthyl acids that carry rigid azo linkers: in **BIO-13** and **BIO-14**, polar sulfonic functionalities are present on the side chain, while **BIO-15** contains lipophilic halogens on it. Within this group, compound **BIO-13** inhibited 75% of *mGO* enzymatic activity at 25 μM . The activity of compounds **BIO-10** and **BIO-15** remained close to 50%, while **BIO-14** dramatically lost inhibitory activity against *mGO*. Using Suzuki–Miyaura cross-coupling, the bromine atom on the C7 of **BIO-10** was replaced with an aromatic side chain, yielding compound **BIO-16**, which presented a lower inhibitory activity. The naphthyl derivative **BIO-11** was found to be the best GOi from this set of compounds, with an

$IC_{50} = 2.9 \mu\text{M}$. It was also the most efficient hit *in vitro*, although its activity was limited to only 23% reduction of excreted oxalate at $10 \mu\text{M}$.

In silico calculations about the binding mode inside *hGO* were also made for this set of compounds. Only some representative interaction data are displayed within this text. The rest of the docking information has been arranged in figures and tables in the Appendix (section 6.1) to facilitate the reading of the text. Representative 2D-interaction diagrams for group **BIO-1** to **BIO-17** are shown in Figure 29, and 2D-interaction diagrams for the whole group **BIO-1** to **BIO-17** is shown in Figure 52 (Appendix 6.1). A summary of interactions of these compounds with the most representative aminoacids of the binding regions 1 and 2 of *hGO* is also provided (Table 23, Appendix 6.1).

In general terms, their binding modes reproduce interactions of **glyoxylate**, **CCPST** and **CDST** in the active site of *hGO*, presenting only slight differences (Table 23, Appendix 6.1). This set of compounds can be divided in two main groups: single-ring salicylic acids (**BIO-1** to **BIO-9**) and benzofused derivatives (**BIO-10** to **BIO-16**). In both sub-groups, interactions with the binding regions 1 and 2 of *hGO* were studied.

Regarding binding region 1, all these compounds interact via electrostatic and/or hydrogen bond interactions with Arg167 and Arg263 through the carboxy and hydroxy groups of the β -hydroxybenzoic fragment. Besides, single-ring salicylic acids **BIO-1** to **BIO-9** establish hydrogen bond interactions with His260 through the heteroatoms present in the salicylic acid head. However, contrary to our expectations, this interaction is established by hydrogen donation from the aminoacid, as happens with **glyoxylate** and **CCPST**. Except for **BIO-6** and **BIO-9**, all compounds establish interactions with Tyr132 by hydrophobic bonding (Table 23, Appendix 6.1).

For their part, the benzofused derivatives presented a different binding pattern in this binding region 1, except the chloroquinoline **BIO-17**, which had comparable interactions to that of single-ring salicylic acids **BIO-1** to **BIO-9** (Table 23, Appendix 6.1). Whereas interactions with Arg167 and Arg263 were kept, no interaction with His260 was observed for benzofused derivatives. Except for compound **BIO-12**, a hydrogen bond interaction with Tyr26, which had not been observed before, was established through the hydroxy and/or carboxy groups present in the salicylic acid head, acting the aminoacid as hydrogen donor. However, curiously, interaction of compound **BIO-11** with Tyr26 occurs only through the carboxy group, being the hydroxy group the one interacting with Tyr132 by hydrogen donation (Figure 29). This constitutes a remarkable fact, since compound **BIO-11** is also the most potent *mGOi*

within this set of compounds (**BIO-1** to **BIO-17**), and this interaction β -OH-Tyr132 has not been observed for the other compounds. All the compounds establish hydrophobic interactions with Tyr132, while compound **BIO-15** interacts via π - π stacking with this aminoacid (Figure 29).

In regards to the interactions in the second binding region, it is worth noting that compounds **BIO-1** to **BIO-7** and **BIO-10**, while lacking of hydrophobic tail, establish hydrophobic interactions through the salicylic acid ring. Conversely, in compound **BIO-6** this interaction occurs through its acetyl group. When a second aromatic ring (acting as side chain) is present in the molecule, interaction with Trp110 occurs through this second ring via π - π stacking for all compounds (**BIO-8**, **BIO-11** to **BIO-14**) excepting **BIO-9** and **BIO-16**, which interact through hydrophobic forces. Compound **BIO-15** constitutes the exception, presenting no interaction with that aminoacid (Figure 29). The interaction with Leu205 and Tyr208 is only established when a side chain is attached to the β -hydroxybenzoic fragment (**BIO-1** to **BIO-6** vs **BIO-7** to **BIO-16**, Table 23, Appendix 6.1.). Quinoline **BIO-17** is the only exception, interacting at Leu205 without a side chain on its structure.

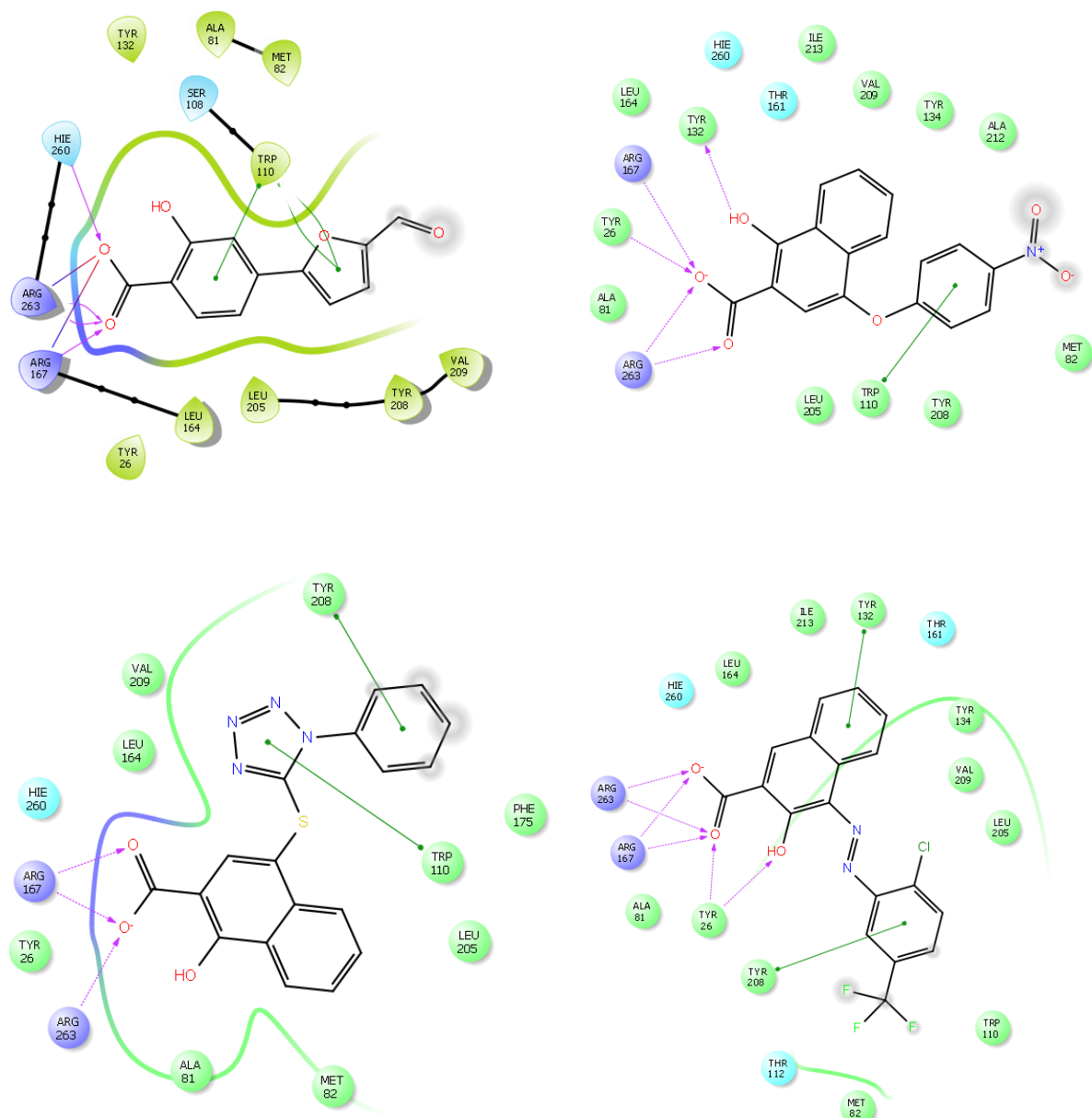


Figure 29. 2D Diagrams of interactions between compounds **BIO-8** (up, left), **BIO-11** (up, right), **BIO-12** (down, left), **BIO-15** (down, right) and human glycolate oxidase residues (purple: basic, cyan: polar uncharged, green: non-polar). Grey shadow represents interaction with solvent. Hie260: His260 protonated on N_{ϵ} [Maestro software (Schrödinger)].

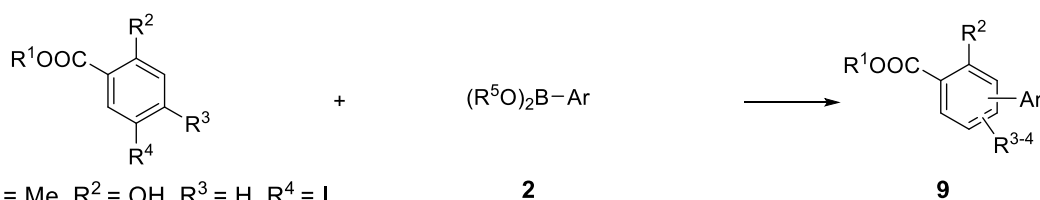
3.2.1.2. Discussion

The impact of the introduction of a fused benzene in the salicylic acid head, aiming at the establishment of novel hydrophobic interactions, has been evaluated both *in silico* and *in vitro*. As a result, prediction models showed that naphthoic derivatives could establish additional hydrophobic (**BIO-12**, **BIO-13** and **BIO-16**) and π - π stacking (**BIO-15**) interactions. In spite of this, no significant improvement of the GO inhibitory activity was observed, nor in the capacity of decreasing oxalate release. Moreover, condensed aromatic systems limit the aqueous solubility of these compounds, which would hinder their synthesis. For these reasons, from then onwards, the research was focused on the optimization of single ring salicylic acids. Information gathered from the predicted binding modes indicated that the attachment of an aromatic side chain to the salicylic acid head, either electron-poor or electron-rich, either carbocycles or heterocycles, reinforces binding to *h*GO through interactions at the binding region 2. Taking this into account, the preparation of salicylic acids bearing aromatic heterocycles and carbocycles as hydrophobic tails was planned.

3.2.2. Preliminary design, synthesis and biological evaluation of salicylic acids.

Once the salicylic acid core was established as a starting point for the synthesis of new derivatives, the synthesis of different families was addressed. Both, heterocycles and carbocycles, were attached on C4 and C5 of the salicylic acid ring, yielding heteroaryl and biphenyl derivatives, respectively. For these compounds, when necessary, we will refer to the salicylic ring as ring A and to those aromatic rings contained in the side chains as rings B, C, etc, from closest to farthest from the salicylic ring. Non-salicylic derivatives, resulting from specific structural modifications on the salicylic ring or ring A, were also prepared to determine the need for the free hydroxy and carboxy groups in the salicylic acid core.

Compound **BIO-8** (Figure 28) was taken as the reference compound to start making minor modifications to determine the role that each structural fragment plays in the biological activity of this compound. Final compounds (type **9**) were prepared following an easy one-step procedure based on Suzuki–Miyaura cross-coupling reaction (Scheme 8). Commercial halides methyl-5-iodosalicylate (**10**), 2-hydroxy-5-iodobenzoic acid (**11**) or 2-hydroxy-4-iodobenzoic acid (**12**), as well as different boronate derivatives (boronic acids and boronate esters) (**2**) were used as starting materials (Scheme 8). Three different standard methods were followed in accordance with the ease of purification and yield criteria (see 5.2.5. General synthetic procedure 5 for Suzuki–Miyaura cross-coupling). In all cases, potassium carbonate (K_2CO_3) was the selected base, and both homogeneous and heterogeneous palladium-based catalysts were used. When **10**, bearing a methyl ester, was used as the halide for Suzuki–Miyaura reaction, the basic aqueous medium, in which the Suzuki reaction was conducted, hydrolysed the ester functionality, leading to the formation of the final free carboxylic acids type **9**. In most cases, compounds were obtained in moderate to high yields (Table 6).



10: R¹ = Me, R² = OH, R³ = H, R⁴ = I

2

9

11: R¹ = H, R² = OH, R³ = H, R⁴ = I R⁵ = H: Boronic acids

12: R¹ = H, R² = OH, R³ = I, R⁴ = H R⁵ = Pinacol ester: Boronate esters

Scheme 8. Reagents and conditions (see 5.2.5. General synthetic procedure 5 for Suzuki–Miyaura cross-coupling): Method 5B: i) K₂CO₃, Pd(OAc)₂, PPh₃, DMF/H₂O (1/1), 100 °C, sealed tube; ii) HCl 10%, H₂O, 0 °C; Method 5C: i) K₂CO₃, PdEnCat[®] 30 0.4 mmol/g, EtOH/H₂O (1/1), 80 °C, sealed tube; ii) HCl 10%, H₂O, 0 °C; Method 5D: i) K₂CO₃, Pd(OAc)₂, PPh₃, DMF/H₂O (1/1), 100 °C, microwave; ii) HCl 10%, H₂O, 0 °C.

All the yields indicated in this work have been calculated after purification, considering only samples presenting an adequate purity in HPLC (more than 95%). This, along with the low scale synthesis, and the complicated purification process given the high polar nature of the final compounds, led, in some cases, to low yields.

3.2.2.1. Non-salicylic derivatives

3.2.2.1.1. Results and discussion

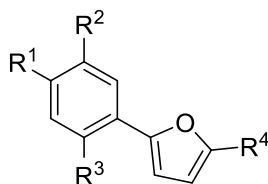
To study the influence of the salicylic acid head in the GO inhibitory activity, seven non-salicylic derivatives were synthesized (Table 6), which included the following structural modifications on the polar head:

- Elimination of the phenolic or carboxy functionalities (**MDMG-353**,¹⁸³ **MDMG-672**¹⁸⁴, **MDMG-1062**).
- Decrease or elimination of the hydrogen donor capacity at the functional group on C2 of the salicylic ring (**MDMG-451** to **MDMG-467**).
- Incapacity of ionization at physiological pH (**MDMG-357**).
- Increase in the hydrogen donor capacity on the phenolic group (**MDMG-511**).

All the compounds were synthesized following the general synthetic procedure for Suzuki-Miyaura cross-coupling indicated in Scheme 8 (see general synthetic procedures in 5.2.5). Compound **MDMG-467** was prepared by basic hydrolysis of the ester **MDMG-357** using sodium hydroxide. This hydrolysis had to be made in a different step after the coupling reaction that gave compound **MDMG-357** (Scheme 8) since, for this 2-methoxycarboxylate, ester hydrolysis did not happen under Suzuki-Miyaura conditions. This does not agree with what we had observed for the 2-hydroxycarboxylates, which hydrolyzed under Suzuki-Miyaura conditions. This

hydrolysis of 2-hydroxycarboxylates, seems to be mediated by the neighboring free hydroxy group, probably by hydrogen bridging to the basic carbonyl group. However, when a 2-alkoxybenzoate is used as starting material, this intramolecular bond does not take place, and as a result, hydrolysis needs to be carried out in a separated reaction using a stronger base.

Table 6. Structures of the non-salicylic compounds tested. In brackets, isolated yields in Suzuki-Miyaura coupling or basic hydrolysis (for **MDMG-467**).



Compound	R ¹	R ²	R ³	R ⁴
BIO-8	-COOH	-OH	-H	-CHO
MDMG-353 (42%) ^a	-H	-COOK	-H	-CHO
MDMG-672 (76%) ^b	-OH	-H	-H	-CHO
MDMG-451 (30%) ^b	-COOH	-CH ₂ OH	-H	-CHO
MDMG-467 (29%)	-COOH	-OCH ₃	-H	-CHO
MDMG-357 (57%) ^b	-COOCH ₃	-OCH ₃	-H	-CHO
MDMG-511 (48%) ^b	-COOH	-OH	-NO ₂	-H

^aSynthesized following the general synthetic procedure 5D. ^bSynthesized following the general synthetic procedure 5B. ^cSynthesized following the general synthetic procedure 5C.

As previously done, the set of non-salicylic derivatives was evaluated against *mGO* and in hyperoxaluric mouse primary hepatocytes (Table 7). Also, binding modes were predicted (Table 24 and Figure 53, Appendix 6.1) and log P_{th} values were calculated. Unfavourable negative values of log P_{th} were obtained for some compounds (Table 7).

Table 7. Biological data of non-salicylic compounds and *in silico* prediction of partition coefficient ($\log P_{th}$). Comparison with **CCPST** and **BIO-8**. Biological determinations: (i) Enzymatic inhibition on purified mouse glycolate oxidase (*mGO*) using the colorimetric method; (ii) Excreted oxalate in *Agxt1^{-/-}* mouse primary cultured hepatocytes, compared to control (relative oxalate).

Compound	<i>mGO</i> (%) ^a	Relative oxalate ^b	$\log P_{th}$
CCPST	34.8 ± 4.8	0.63 ± 0.16 ^c	n/a
BIO-8	82.8 ± 5.6	0.88 ± 0.18	0.29
MDMG-353	22.7 ± 8.7	0.86 ± 0.11	0.00
MDMG-672	24.2 ± 5.4	0.32 ± 0.06*	0.01
MDMG-451	0	0.98 ± 0.23	-0.54
MDMG-467	0	0.82 ± 0.04	-0.26
MDMG-357	17.5 ± 4.8	0.90 ± 0.10	-0.22
MDMG-511	5.9 ± 3.1	0.86 ± 0.04	-2.24

^aPercentage of inhibition of purified *mGO* with 25 μ M of the drug, after 1 min. ^bOxalate output decrease tested at 24 h post-treatment with 10 μ M of the drug in *Agxt1^{-/-}* mouse primary hepatocytes cultured with 5 mM glycolate, in 6-well plates. Data are represented as mean \pm SD of n = 3 replicates. One-way ANOVA statistical analysis, (*) $p < 0.05$ was considered statistical significant. ^cData at 12.5 μ M in *Agxt1^{-/-}* mouse primary hepatocytes. n/a: Not assessed.

When comparing the biological activities of compound **BIO-8** (83% *mGO* inhibition at 10 μ M) vs the non-salicylic derivatives, a clear worsening of *mGO* inhibitory activity can be observed (Table 7), underlining the importance of maintaining free carboxy and hydroxy groups in any derivative. The irreplaceability of the phenolic group by a benzylic hydroxy group is also evident (compound **BIO-8** vs **MDMG-451**).

It would be plausible to think, in view of the experimental data, that the β -OH group could be behaving as a hydrogen donor (compound **BIO-8** vs **MDMG-451** and **MDMG-467**). Then, **MDMG-511**, carrying a nitro electron-withdrawing group in *para* position with respect to the β -OH group, should behave as a better *mGO*i. However, the introduction of such group led to a dramatic loss of *mGO* inhibitory activity (Table 7). Unfortunately, this fall in the activity of **MDMG-511** cannot be certainly attributed to the pK_a of the β -OH, as steric factors derived from the introduction of an additional substituent on the salicylic ring (nitro group) might be involved. In fact, according to *in silico* calculations, the molecule results displaced in the active site, missing key interactions with Arg167, Arg263 and His260, which other compounds, such as **BIO-8**, **MDMG-451** and **MDMG-467**, establish through the carboxy group (Figure 30).

Regarding binding region 1, 2D-interaction diagram showed that the benzylic alcohol **MDMG-451** behaves as a hydrogen acceptor from Tyr132 (Table 24 and Figure 53, Appendix 6.1.). However, when the hydroxymethyl group of **MDMG-451** is exchanged by a methoxy group (**MDMG-467**), interactions with Tyr132 are of

hydrophobic nature and happen through the methyl group (Table 24 and Figure 53, Appendix 6.1). For compound **BIO-8** (Figure 28), binding mode predictions showed that no interaction is established through the β -OH group. Thus, its better *mGO* inhibitory activity might be due to the better accommodation of the molecule at the active site, allowed by the presence of a less bulky group in β position. Nevertheless, removing of the β -OH group (**MDMG-353**) appears to cause loss of interaction with His260 and Tyr26, which might be the reason for the absence of activity of this compound. In essence, although it could not be clarified whether the interactions established through this substituent at C2 determine the potency of the inhibitors, it does seem that a suitably sized group needs to be placed in that position.

In compounds **MDMG-672** and **MDMG-357** the carboxy group was removed or esterified, respectively. Therefore, a loss of interaction with Agr167 and Arg263 was expected. According to the predicted binding modes, both molecules result turned around, facing the furan rings toward the binding region 1 and being the polar heads oriented toward the binding region 2 (Figure 30 and Figure 53, Appendix 6.1). As a result, the formyl group in **MDMG-672** accepts hydrogen bonds from Arg167 and Arg263. Besides, both the formyl and the furan oxygen atoms interact with Tyr26 as hydrogen acceptors. While compound **MDMG-672** does not interact with His260, compound **MDMG-357**, through the formyl group, accepts hydrogen bonds both from His260 and Tyr32. However, no interaction with Arg167 and Arg263 was observed (Table 24 and Figure 53, Appendix 6.1). For both compounds, π - π stacking bonds to Trp110 were established (Table 24, Appendix 6.1).

In regards to the second binding region, non-salicylic derivatives interact with Trp110 and Tyr208, and some of them also do with Leu205 (Table 24 and Figure 53, Appendix 6.1).

Within this group of compounds, only the phenolic derivative **MDMG-672** was able to reduce the production of oxalate on *Agxt1*^{-/-} mouse primary hepatocytes (Table 7). This compound, indeed, resulted to be more effective than **CCPST**, lowering oxalate output by 68% at 10 μ M. Since **MDMG-672** is not a potent *mGOi*, other biological targets might be involved in the biological activity of this compound. The presence of interferences of **MDMG-672** with the biological methods was also discarded (see 5.6.2.4 Interference test of the cell culture assay and Tables 27 and 28 in Appendix 6.2).

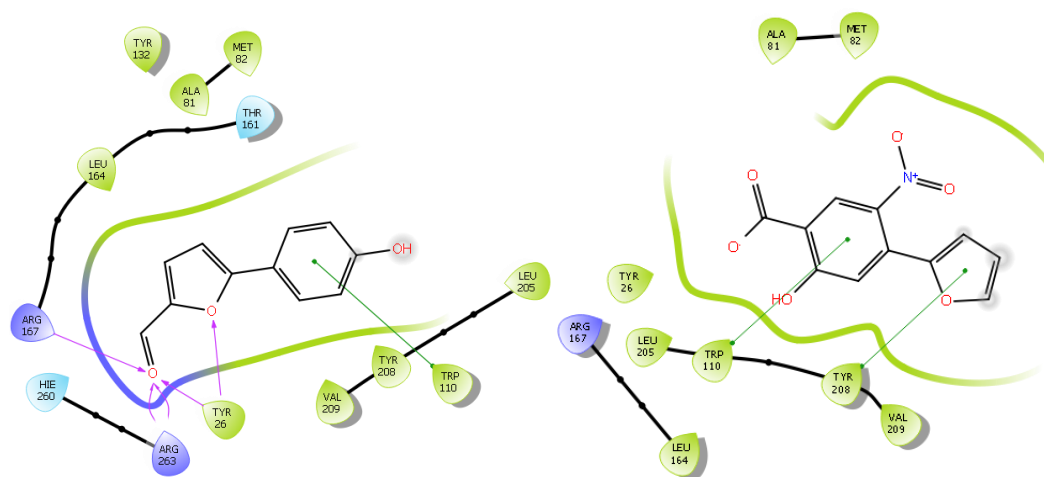


Figure 30. 2D Diagrams of interactions between compounds **MDMG-672** (left) and **MDMG-511** (right) and human glycolate oxidase residues (purple: basic, cyan: polar uncharged, green: non-polar). Grey shadow represents interaction with solvent. Hie260: His260 protonated on N_ε [Maestro software (Schrödinger)]

3.2.2.2. Heteroarylsalicylates

3.2.2.2.1. Results

Once we determined the need of maintaining the carboxy and hydroxy groups on the salicylic acid ring in order to preserve the GO inhibitory activity, we tackled the structural modulation of the side chain of compound **BIO-8** (Figure 28).

The preliminary modifications that were explored can be summarized as follows (Figure 31):

- Changes on the substitution pattern of the salicylic ring (C4 and C5 substitution).
- Modifications on the formyl group: Removal, oxidation and reduction.
- Changes on the position of the heteroatom on the side-chain heterocycle (bonding through C2' and C3').
- Isosteric replacement of the furan ring with other heterocycles (sulfur and nitrogen-containing, five and six-membered heterocycles).

Resulting of these initial modifications, 21 heteroarylsalicylates were synthesized and evaluated against recombinant *mGO* and in *Agxt1^{-/-}* mouse hepatocytes (Figure 31).

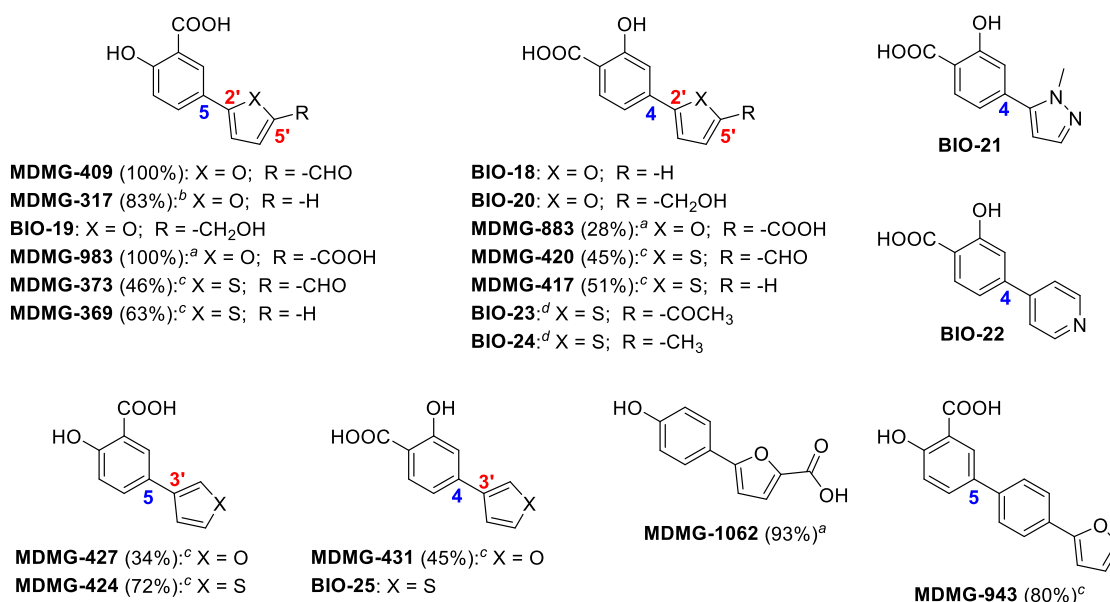


Figure 31. Structures of the heteroarylsalicylates prepared and tested. In brackets, isolated yields in Suzuki-Miyaura coupling. ^aSynthesized following the general synthetic procedure 5C. ^bSynthesized following the general synthetic procedure 5D. ^cSynthesized following the general synthetic procedure 5B. ^dObtained from commercial sources.

Suzuki-Miyaura reaction was used for the synthesis of heteroarylsalicylates following the Scheme 8. Two main catalytic systems were used, with different solvents and sources of heating. In all cases, oxygen was displaced from the reaction system by bubbling with argon in order to avoid self-coupling side reactions. In the beginning, we used our classical reaction conditions (see 5.2.5. General synthetic procedure 5 for Suzuki-Miyaura cross-coupling reaction) that included the use of soluble palladium diacetate as a catalyst and the ligand triphenylphosphine. This reaction, which could be developed using conventional or microwave heating, was conducted in dimethylformamide/water systems. In the synthesis of heteroarylsalicylates, we found that, in certain cases, these reaction conditions produced complex reaction mixtures and the purification step was complicated. This led us to the implementation of an alternative synthetic method. Thus, microencapsulated palladium acetate (PdEnCat™) was introduced as a catalyst. In this heterogeneous catalytic system, palladium is immobilized in a polyurea matrix, allowing an easy removal of the catalyst as well as its optional reuse. Besides, ligand-free reaction conditions were introduced, allowing an easier purification process. Reactions using PdEnCat™ were developed in ethanol/water mixtures. This, together with the absence of phosphine, makes this method more environmentally friendly than the previous one.^{164,165}

All the compounds were tested against recombinant *mGO* and in *Agxt1^{-/-}* mouse hepatocytes. The biological activities obtained for this family of heteroarylsalicylates are summarized in Table 8.

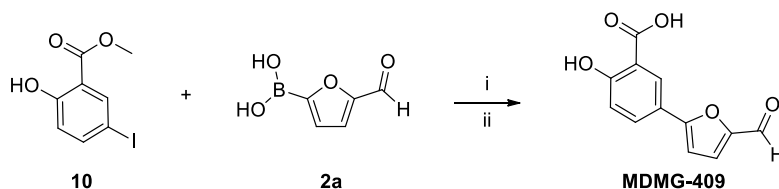
Table 8. Biological data of heteroarylsalicylates and *in silico* prediction of partition coefficient ($\log P_{th}$). Comparison with **BIO-8** and **CCPST**. Biological determinations: (i) Enzymatic inhibition on purified mouse glycolate oxidase (*mGO*), at single concentration and IC_{50} calculation using the colorimetric method; (ii) Excreted oxalate in *Agxt1^{-/-}* mouse primary hepatocytes, compared to control (relative oxalate).

Compound	<i>mGO</i> (%) ^a	IC_{50} (μM) ^b	R^{2c}	Relative oxalate ^d	$\log P_{th}$
CCPST	34.8 ± 4.8	43.5 ± 1.1	n/a	0.63 ± 0.16 ^e	n/a
BIO-8	82.8 ± 5.6	34.5 ± 1.2	0.88	0.88 ± 0.18	0.29
MDMG-317	n/r	n/r	n/r	0 ^{f,g}	-0.29
MDMG-369	30.0 ± 2.4	39.5 ± 1.1	0.91	0.82 ± 0.01	0.99
MDMG-373	52.1 ± 13.4	9.4 ± 1.3	0.87	0.93 ± 0.18	0.06
MDMG-409	42.7 ± 12.8	38.2 ± 1.2	0.81	0 ^f	2.59
MDMG-417	35.4 ± 7.2	32.5 ± 1.1	0.96	0.74 ± 0.16*	0.99
MDMG-420	28.7 ± 1.3	n/a	n/a	1.00 ± 0.20	0.06
MDMG-424	25.2 ± 5.0	n/a	n/a	0.94 ± 0.10	0.90
MDMG-427	26.6 ± 1.9	n/a	n/a	0.89 ± 0.16	0.56
MDMG-431	22.8 ± 5.6	n/a	n/a	1.02 ± 0.3	0.56
MDMG-883	0	n/a	n/a	n/a	0.13
MDMG-943	68 ^h	3.4 ± 1.08	0.96	0.95 ± 0.04	n/a
MDMG-983	0	n/a	n/a	0.68 ± 0.14*	0.13
MDMG-1062	65.1 ± 2.7	n/a	n/a	n/a	n/a
BIO-18	35.8 ± 6.9	39.3 ± 1.0	0.94	0.87 ± 0.15	0.65
BIO-19	98.0 ± 1.6	4.6 ± 1.1	0.96	0.88 ± 0.19	-0.11
BIO-20	85.7 ± 9.3	7.9 ± 1.1	0.98	0.88 ± 0.01	-0.11
BIO-21	16.2 ± 6.2	n/a	n/a	0.93 ± 0.01	0.34
BIO-22	22.7 ± 2.3	n/a	n/a	0.88 ± 0.03	2.76
BIO-23	28.1 ± 9.3	n/a	n/a	0.89 ± 0.14	1.02
BIO-24	28.7 ± 10.3	n/a	n/a	0.95 ± 0.02	1.02
BIO-25	41.4 ± 7.8	21.6 ± 1.3	0.80	0.99 ± 0.12	0.90

^aPercentage of inhibition of purified *mGO* with 25 μM , after 1 min. ^b IC_{50} : Calculated in saturated conditions of glycolate (22.2 mM). ^c R^2 : IC_{50} curve-fitted score. ^dOxalate output decrease 24 h after treatment with 10 μM of the drug in *Agxt1^{-/-}* mouse primary hepatocytes cultured with 5 mM glycolate, in 6-well plates. One-way ANOVA statistical analysis, (*) $p < 0.05$ was considered statistical significant. Data represented as mean ± SD of $n = 3$ replicates. ^eData at 12.5 μM in *Agxt1^{-/-}* mouse primary hepatocytes. ^fValues below the detection limit of the colorimetric method. ^gNo interference due to the low concentration of the drug. ^hNo SD is given. n/a: Not assessed. n/r: Not reliable data due to interference.

a. Changes on the substitution pattern of the salicylic ring (C4 and C5 substitution).

The first modification we addressed was the change of the substitution pattern of the salicylic ring in **BIO-8** (Figure 28), by shifting the formylfuran side chain from C4 to C5. The synthetic Scheme 9, led to compound **MDMG-409** (Figure 31).



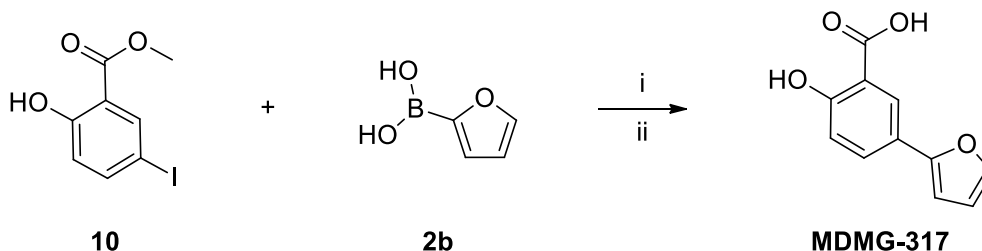
Scheme 9. Synthesis of **MDMG-409** by Suzuki-Miyaura cross-coupling. Reagents and conditions (see 5.2.5. General synthetic procedure 5C): i) K_2CO_3 , PdEnCat[®] 30 0.4 mmol/g, EtOH/H₂O 1/1, 80 °C; ii) HCl 10%, H₂O, 0 °C.

In the synthesis of **MDMG-409**, the introduction of the heterogeneous catalytic system using PdEnCat[™] resulted in an excellent quantitative yield with an adequate purity level. When comparing the biological activities for compound **MDMG-409** and compound **BIO-8**, C5/C4 isomers, a similar potency against *mGO* was observed, with IC₅₀ values of 38 μ M and 34 μ M, respectively, improving potency with respect to **CCPST**. However, when tested in cells *in vitro*, a 5-fold increase in efficacy with respect to **CCPST** was observed for compound **MDMG-409**, which showed an EC₅₀ value of 3.45 μ M (see calculation of EC₅₀ and cytotoxicity test for **MDMG-409** and **MDMG-317** in section below). Once again, as previously described for compound **MDMG-672**, a discrepancy between the enzymatic activity and phenotypic effect on cells was detected, what suggests the presence of alternative targets for these compounds. The inhibition constant (K_i) on *mGO* was calculated for compound **MDMG-409** using Cornish–Bowden and Dixon plots. The value of K_i for **MDMG-409** was 47.2 μ M and the plot indicated that the compound behaves as a competitive inhibitor (data not shown).

The interaction diagram for compound **MDMG-409** (Figure 54, Appendix 6.1) showed that the polar head interacts with Agr167, Arg263 and His260 through the carboxy and β -OH groups. Hydrophobic interactions are also established with Tyr132, Trp110, Leu205 and Tyr208 through rings A and B (salicylic ring and furan ring, respectively). Compared to compound **BIO-8**, in compound **MDMG-409** a bigger contribution of the β -OH group can be observed, since it acts as a hydrogen acceptor in the interaction with His260. When comparing with **CCPST**, the absence of interaction of **MDMG-409** with Tyr26 is the only remarkable binding difference (Table 25, Appendix 6.1).

b. Modifications on the formyl group: Removal, oxidation, reduction.

According to docking predictions, the formyl group in **MDMG-409** (Figure 54, Appendix 6.1) appears to be solvated and does not establish any interaction with the target. To study its role in the biological activity, removal, reduction and oxidation of this group were accomplished. Removal of the formyl group yielded compound **MDMG-317** (Figure 31), which was obtained by Suzuki-Miyaura reaction using the non-formylated furanboronic acid **2b** (Scheme 10).



Scheme 10. Reagents and conditions (see 5.2.5 General synthetic procedure 5D): i) K_2CO_3 , $Pd(OAc)_2$, PPh_3 , DMF/ H_2O 1/1, 100 °C, microwave; ii) HCl 10%, H_2O , 0 °C.

To our surprise, the use of PdEnCatTM that had given such good results in the synthesis of **MDMG-409**, did not result effective for the preparation of **MDMG-317**, since the starting materials remained unreacted after 24 h. Thus, the non-encapsulated palladium diacetate was used as the catalyst in the presence of the ligand triphenylphosphine and, in this case, the final product was obtained in good yield (83%) (Scheme 10).

Compound **MDMG-317**, with an $EC_{50} = 3.56 \mu M$, showed the same *in vitro* efficacy as **MDMG-409**. However, the *mGO* inhibitory activity of **MDMG-317** could not be certainly assessed as this compound interferes with the biological assays by inhibiting the horseradish peroxidase (HRP), enzyme used both in *GO*-inhibition and oxalate quantification assays (see Assay interference test in experimental section 5.6.1.1.4 and Analysis of interferences in Appendix 6.2). Accurate IC_{50} and K_i values could not be provided for this compound, since the concentration needed for such calculations exceeds the IC_{50} value of **MDMG-317** against HRP ($IC_{50} = 18 \mu M$). However, the interference is not significant at concentrations up to 5 μM , so that the EC_{50} value can be considered indicative (Table 29, Appendix 6.3).

Given the similar EC_{50} value obtained for **MDMG-409** and **MDMG-317**, the formyl group does not seem to play an important role on the oxalate decrease capacity of **MDMG-409**. The interaction profiles with *hGO* are also quite similar for both compounds, except for the richer hydrophobic interactions of **MDMG-317** (Figure 54,

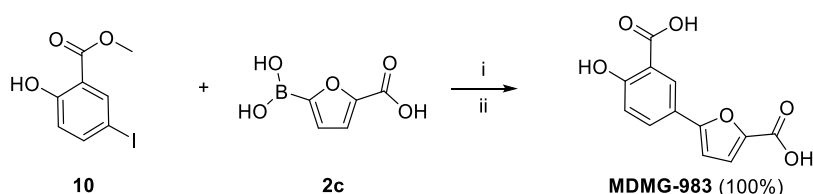
Appendix 6.1). Removing the formyl group in compound **BIO-8** led to compound **BIO-18** (Figure 31), which did not present better *mGO* inhibitory activity and resulted inactive in *Agxt1^{-/-}* mouse primary hepatocytes. When comparing the interaction profiles of **MDMG-317** and **BIO-18** (C5 and C4 isomers, respectively), again, a more extensive contribution of the β -OH group is found for the case of the C5 isomer, as previously described for the pair of C5/C4 isomers **MDMG-409/BIO-8** (Table 25 and Figure 54, Appendix 6.1). In both C5 isomers (**MDMG-409** and **MDMG-317**), the β -OH group binds to His260 acting as a hydrogen acceptor (Table 25 and Figure 54, Appendix 6.1).

In the case of compound **MDMG-409**, no enzymatic or colorimetric interferences with the biological testing were observed (see Assay interference test in experimental section 5.6.1.1.4 and Analysis of interferences in Appendix 6.2). This could be due to the smaller size of **MDMG-317** determining a lower selectivity for the compound that leads to HRP inhibition.

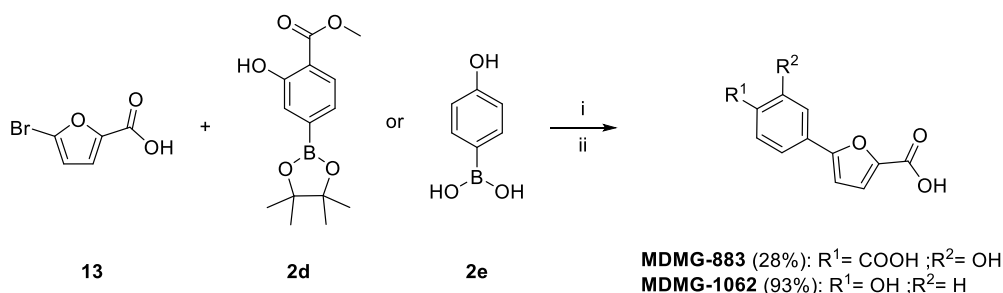
When testing compound **MDMG-409** in hyperoxaluric mouse primary hepatocytes, it could happen that this compound was metabolized into **MDMG-317** and thus, that the biological activity of **MDMG-409** was owed to this metabolite. Hence, the possible *in vitro* transformation of **MDMG-409** into **MDMG-317** needed to be discarded, and for that purpose, the metabolic profiling of both compounds was performed using mouse liver hepatocytes (see Appendix 6.3. Metabolic profiling). As a result, two main metabolites were observed for compound **MDMG-409**, corresponding to the oxidation and reduction of the formyl group (compounds **MDMG-983** and **BIO-19**, respectively) (Figure 31). These two metabolites accounted for 40.1% and 48.2% of the total metabolites after 60 min of incubation (Figure 56, Appendix 6.3.). A third metabolite meaning 11.6% was also observed after 60 min (Figures 56 and 57, Appendix 6.3). This minor metabolite, while having the same mass as **MDMG-317**, presents a different retention time in LC-MS analysis, and its origin seems to be oxidation of the formyl group plus decarboxylation on the salicylic acid ring (compound **MDMG-1062**). The samples were analyzed by LC-HRMS in negative ionization mode. Compound **MDMG-409** also showed a high intrinsic clearance with an elimination half-life of 13.3 min. For compound **MDMG-317**, a medium intrinsic clearance with an elimination half-life of 61.9 min was observed, and no metabolites were detected after 60 min of incubation (Tables 31 and 32 and Figure 58, Appendix 6.3).

The next step corresponded to the preparation of the main metabolites of compound **MDMG-409** (compounds **BIO-19** and **MDMG-983**, Figure 31) to assess their biological activity as well as their capacity to produce interferences with the biological

evaluation methods. Their C4 isomers, corresponding to the derivatives **BIO-20** and **MDMG-883** were also prepared, as well as **MDMG-1062**. The alcohols **BIO-19** and **BIO-20** were synthesized by simple reduction of the formyl group in **MDMG-409** and **BIO-8**, respectively.¹⁸⁵ The oxidized derivatives (**MDMG-983** and **MDMG-883**), as well as phenolic compound **MDMG-1062**, were synthesized via Suzuki-Miyaura cross coupling following the Schemes 11 and 12. In all cases, PdEnCatTM was used. The oxidized derivative **MDMG-983** and **MDMG-1062** were prepared in excellent yields (100% and 93%, respectively). However, **MDMG-883** was synthesized in lower yield (28%) due to its complicated purification process and the low scale synthesis determined by the limited availability of starting materials (Schemes 11 and 12).



Scheme 11. Synthesis of **MDMG-983** by Suzuki-Miyaura cross-coupling. Reagents and conditions (see 5.2.5 General synthetic procedure 5C): i) K₂CO₃, PdEnCat[®] 30 0.4 mmol/g, EtOH/H₂O 1/1, 80 °C; ii) HCl 10%, H₂O, 0 °C.



Scheme 12. Synthesis of **MDMG-883** and **MDMG-1062** by Suzuki-Miyaura cross-coupling. Reagents and conditions (see 5.2.5 General synthetic procedure 5C): i) K₂CO₃, PdEnCat[®] 30 0.4 mmol/g, EtOH/H₂O 1/1, 80 °C; ii) HCl 10%, H₂O, 0 °C.

The reduced derivatives **BIO-19** and **BIO-20** were prepared by treatment of **MDMG-409** and **BIO-8** with the reducing agent sodium borohydride. In these two compounds, potency against *mGO* was remarkably improved with respect to the formyl derivatives **MDMG-409** and **BIO-8** (IC₅₀= 4.6 and 7.9 vs 38.2 and 34.5 μM, respectively) (Table 8). No interferences could be found for these compounds, and neither relevant biological activity reducing oxalate on cells. The oxidized derivatives of **MDMG-409** and **BIO-8**, the carboxylic acids **MDMG-983** and **MDMG-883**, showed no activity as *mGO* inhibitors, and therefore interferences with HRP were also discarded. After these tests, we could confirm that the phenotypic activity of **MDMG-409** is in fact

due to this molecule itself and not to its metabolites or to misleading effects owed to interferences with the biological assay systems.

The 1,4-phenylene **MDMG-943** (Figure 31), with a rigid phenyl ring spacing the salicylic acid head and the terminal plane furan moiety, was synthesized as a benzologue of **MDMG-317**. This compound was the most potent *mGO*i within this set, with an $IC_{50} = 3 \mu M$, but unfortunately it did not show activity in hepatocytes.

c. Changes on the position of the heteroatom on the side-chain heterocycle (bonding through C2' and C3').

Changes on the position of the heteroatom on the furan attached to the salicylic ring allow the study of alternative interactions with *mGO*. In **BIO-8** (Figure 28) and its analogues **MDMG-409**, **BIO-18** and **MDMG-317** (Figure 31), the furan is attached to the salicylic head through C2'. Thus, C3' isomers of **BIO-18** and **MDMG-317**, corresponding to compounds **MDMG-431** and **MDMG-427** (Figure 31), respectively, were prepared by Suzuki–Miyaura coupling (Scheme 8). A significant decline in the *mGO* inhibitory activity was observed after this modification.

d. Isosteric replacement of the furan ring with other heterocycles (sulfur and nitrogen-containing, five and six-membered heterocycles).

Isosteric substitution of the furan ring of compounds **BIO-8** (Figure 28) and **MDMG-409** (Figure 31) was also carried out. Different nitrogen or sulfur heterocycles were introduced instead of furan, including thiophene (**MDMG-420** and **MDMG-373**), pyrazole (**BIO-21**) and pyridine (**BIO-22**), following the general procedure indicated in Scheme 8.

Compounds **MDMG-420** and **MDMG-373** are the result of an isosteric replacement of oxygen by sulfur, which changed the furan ring into thiophene, on **BIO-8** and **MDMG-409**, respectively (Figure 31). **MDMG-420** (C4 isomer) completely lost the *mGO* inhibitory activity and the efficacy on hepatocytes (Table 8). On the other hand, **MDMG-373**¹⁸⁶ (C5 isomer) resulted in a 4-fold increase of the *mGO* inhibitory activity compared to its furan-containing isoster **MDMG-409** ($IC_{50} = 9.4 \mu M$ vs $38.2 \mu M$, respectively). The same isosteric change performed on the nonformylated furan **MDMG-317** gave rise to the thiophene **MDMG-369**¹⁸⁷ (Figure 31). This compound presented a moderate activity

as GOi ($IC_{50} = 39.5 \mu\text{M}$), while its efficacy was drastically reduced if compared to **MDMG-317** (0.82 vs 0 relative oxalate) (Table 8).

Some other commercially available salicylates containing thiophene side chains were also tested. Compounds **BIO-23** and **BIO-24** contain 5'-acetyl and 5'-methylthiophenes instead of the 5'-formylthiophene present in **MDMG-420** (Figure 31). Nitrogen-based heterocycles such as pyrazole (**BIO-21**) and pyridine (**BIO-22**) were also used in substitution of the furan side-chain of **BIO-8** (Figure 31). However, none of these modifications improved the *m*GO inhibitory activity or the capacity to reduce oxalate production of **BIO-8** and **MDMG-409** (Table 8).

As previously done for the furan derivatives, the suitable orientation of the heteroatom on the side chain heterocycle was also studied in the thiophene-derived compounds. To do so, C3'-thienyl derivatives (**MDMG-424** and **BIO-25**, Figure 31) were prepared, but this modification did not improve the potency against GO (Table 8).

Regarding the $\log P_{th}$ values of heteroarylsalicylates, unfavourable negative values were only observed for compounds **MDMG-317**, **BIO-19** and **BIO-20** (Table 8).

In silico studies of the binding mode of this group of compounds revealed that key interactions are established with the binding regions 1 and 2 (Table 25, Figure 54, Appendix 6.1). In general terms, all compounds interact with Arg167, Arg263 (except compound **MDMG-373**), His260, Tyr208 and Leu205. Often, interactions with Trp110 are also established, with the exception of compounds **BIO-19**, **MDMG-369** and **MDMG-424**. The interaction with Tyr132 is less frequent, since it is not present in some 2-thienyl and 3-thienyl derivatives, in the C4/C5 isomers containing 3'-furyl side chains (**MDMG-431** and **MDMG-427**), and in the pyridinyl derivative **BIO-22**. Polar groups from the heterocycle in the side chain, such as the formyl group (**MDMG-409**, **MDMG-420**), the hydroxyl group (**BIO-19**, **BIO-20**, Figure 32) or nitrogen atoms (**BIO-21**, **BIO-22**), tend to get solvated. In compound **MDMG-883** a special binding pattern was observed: the furan ring interacts at the first binding region, while the salicylic acid ring interacts at the binding region 2.

A characteristic binding pattern was found when the C4/C5 pairs were compared (Table 25 and Figure 54 in Appendix 6.1). In the case of C5 isomers, the β -OH group interacts at His260 acting as hydrogen acceptor, reinforcing the interaction with this key aminoacid, which is also established through the carboxylate group. On the other hand, only C4 isomers establish π - π stacking interactions with Trp110, excepting the C4/C5

couple of 5-formyl-2-thienyl derivatives **MDMG-420/MDMG-373** (Figure 54, Appendix 6.1).

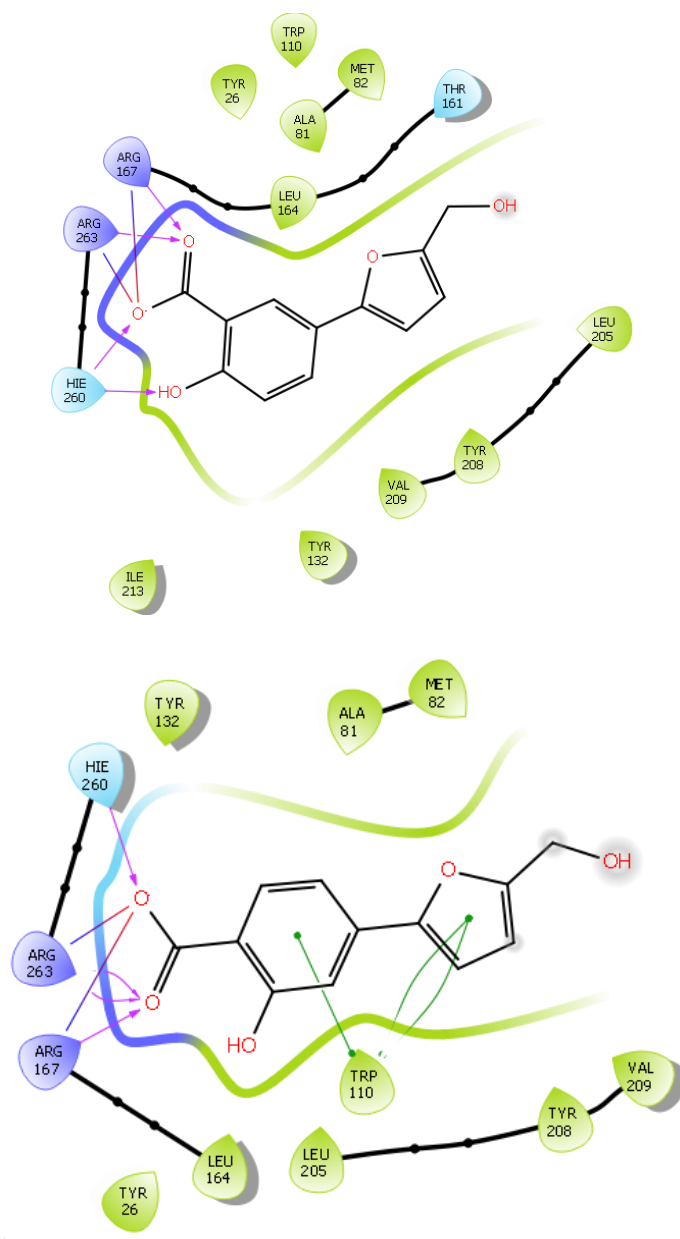


Figure 32. 2D-Diagram of interactions between the most potent *mGO* inhibitors heteroarylsalicylates, the C4/C5 isomers **BIO-19** (up) and **BIO-20** (down), and *hGO* active site residues (purple: basic, cyan: polar uncharged, green: non-polar). Grey shadow represents interaction with solvent. Hie260: His260 protonated on N_ε [Maestro software (Schrodinger)]. 2D-Interaction diagrams for the whole group in Figure 55.

3.2.2.2. Discussion

The fact that the metabolites of **MDMG-409** do not present good phenotypic activity in hyperoxaluric mouse hepatocytes, along with the absence of interferences found for these metabolites (**BIO-19** and **MDMG-983**), confirms the biological activity of the compound **MDMG-409** in cells. Thus, compound **MDMG-409**, while being a moderate *mGOi*, effectively reduces oxalate in hyperoxaluric mouse hepatocytes, and presents a notable EC_{50} value of 3.45 μ M. Its oxidized derivative **MDMG-983** shows a similar activity profile, being unable to inhibit *mGO* but reducing by 30% oxalate in the cell system. When **MDMG-409** is administered to cells, its metabolism appears to happen in favor of the oxidized derivative **MDMG-983**, causing a time-dependent loss of activity. Compounds **MDMG-409**, **MDMG-317** and **MDMG-983** share a similar activity profile: they are better reducing oxalate in hepatocytes than inhibiting *mGO*. Hence, a similar mechanism of action including alternative biological targets (different from *GO*) could be involved in the phenotypic activity of these compounds in hepatocytes.

Among the modifications performed on the side chain, only the formylthiophene derivative **MDMG-373** improved the *mGO* inhibitory activity with respect to its formylfuran isoster **MDMG-409**. The remaining sulfur derivatives could not improve the activities of their furan analogues. Regarding the cell-based assay, none of the sulfur compounds could reduce oxalate on *Agxt1*^{-/-} mouse primary hepatocytes in an efficient way. Thus, the importance of the oxygen atom on the side chain becomes evident.

With regard to the predicted binding modes, the different C4/C5 binding pattern to the enzyme did not result into considerable different potencies against *mGO* (Table 8), and a specific binding pattern could not be found for the most potent *mGOi*'s (**BIO-19**, **BIO-20**, **BIO-373** and **MDMG-943**).

Calculation of EC₅₀ and Cytotoxicity Test for MDMG-409 and MDMG-317

Given the satisfactory reduction of excreted oxalate achieved by compounds **MDMG-409** and **MDMG-317** when tested at 10 μM , their EC₅₀ values were calculated, and their cytotoxicity was also evaluated.

Compound **MDMG-409**, when tested at 6.25 μM , was able to reduce excreted oxalate levels by 67.3% after 24 h of treatment. A more efficient oxalate reduction was achieved at concentrations of 12.5 μM (105.8% and 62.3%, at 24 and 48 h of treatment, respectively) (Figure 33a). For this compound, no signs of cytotoxicity were found within the concentration range tested (Figure 33b). EC₅₀ values were calculated at each time point and resulted in 3.45 μM at 24 h, 8.36 μM at 48 h, and 11.19 μM at 72 h (Figure 34).

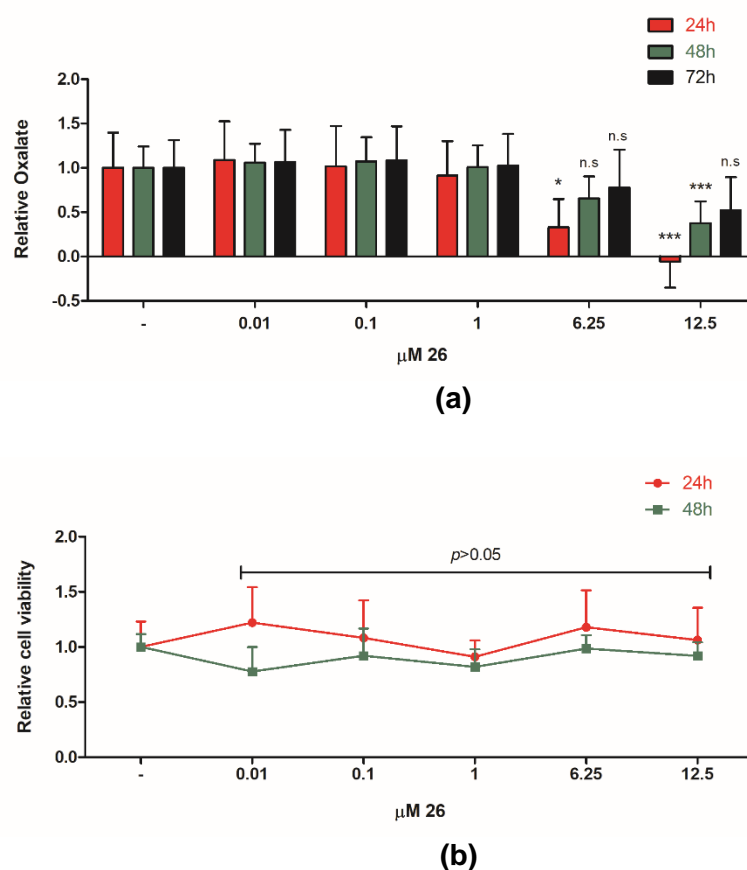


Figure 33. *Agxt1*^{-/-} mouse hepatocytes treated with **MDMG-409** (26). (a) Relative oxalate excreted after 24 h, 48 h and 72 h of treatment. (b) Cell viability within the same range of concentrations. Data are represented as mean \pm SD, from two independent experiments, with three replicates in each one. ANOVA statistical signification: (*) $p < 0.05$, (**) $p < 0.01$, (***) $p < 0.001$, NS = not significant, relative to control at each time point.

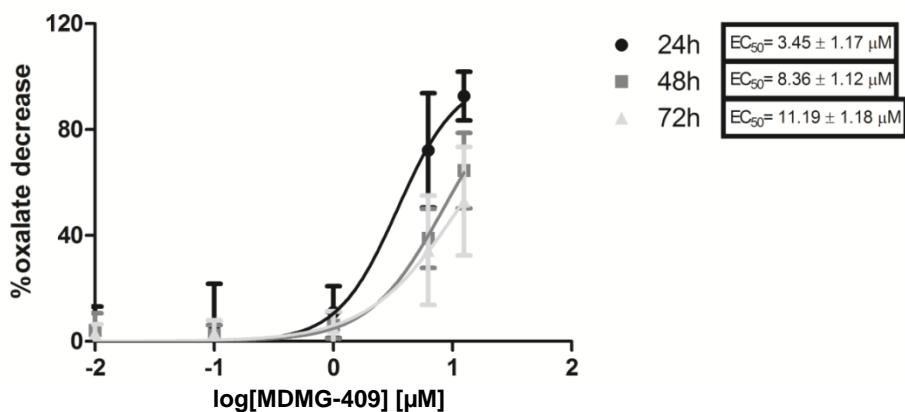
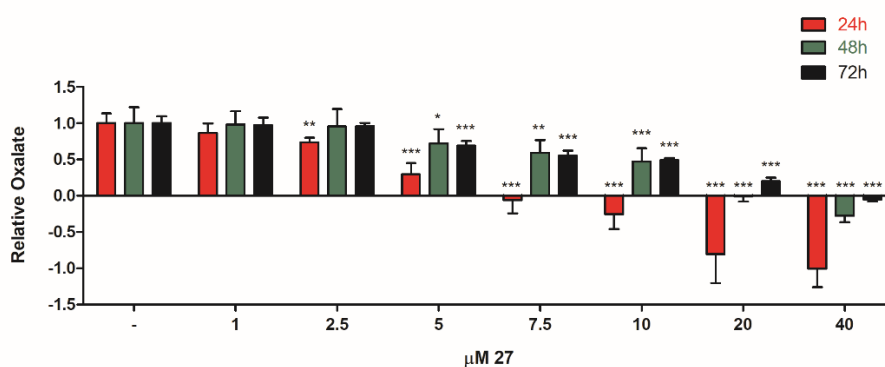
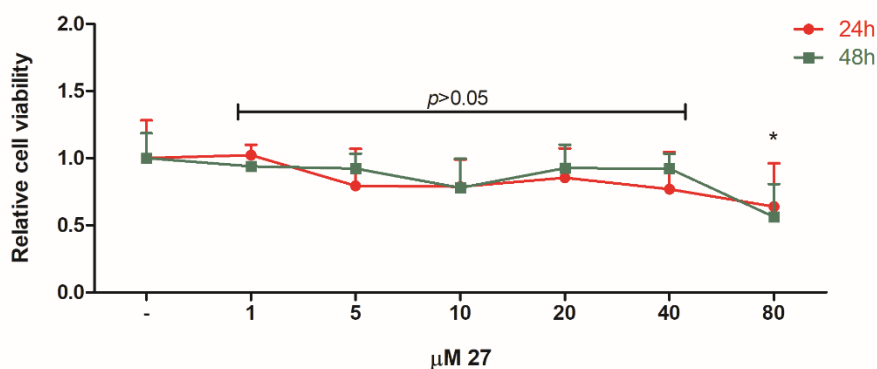


Figure 34. EC₅₀ calculation against *mGO* for compound **MDMG-409**.

The same experiments were conducted for compound **MDMG-317**. In this case, cytotoxicity was observed when concentration was exceeded from 80 µM (Figure 35b), and the calculated EC₅₀ at each time point was 3.59 µM at 24 h, 7.88 µM at 48 h, and 9.2 µM at 72 h (Figure 36).



(a)



(b)

Figure 35. *Agxt1*^{-/-} mouse hepatocytes treated with **MDMG-317** (27). (a) Relative oxalate excreted after 24 h, 48 h and 72 h of treatment. (b) Cell viability within the same range of concentrations. Data are represented as mean \pm SD, from two independent experiments, with three replicates in each one. ANOVA statistical signification: (*) $p < 0.05$, (**) $p < 0.01$, (***) $p < 0.001$, relative to control at each time point.

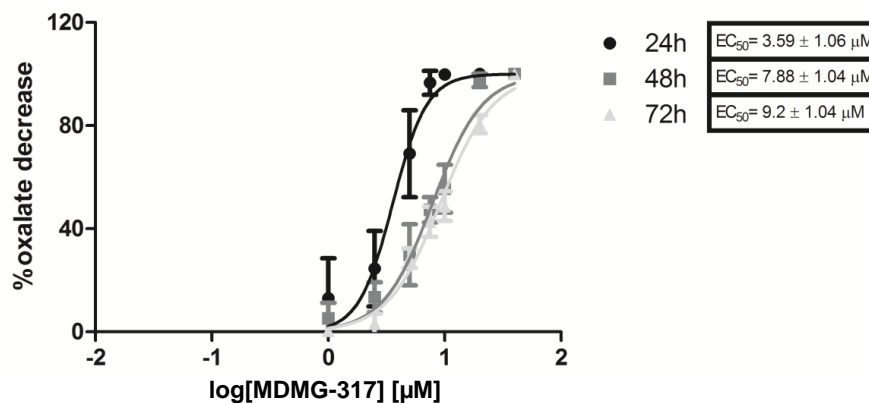


Figure 36. EC₅₀ calculation against *mGO* for compound **MDMG-317**.

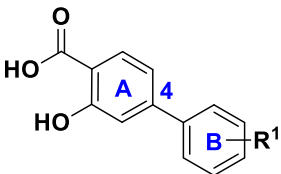
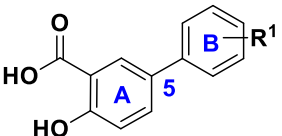
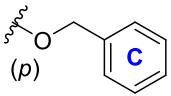
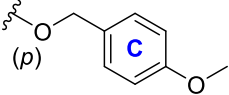
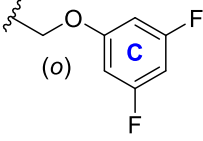
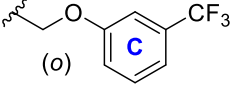
It is noteworthy that the time-dependent loss of activity of **MDMG-409** when compared to **MDMG-317** is in line with the chemical and metabolic instability previously described in the metabolic profiling of this compound.

3.2.2.3. Biphenyl or Arylsalicylate Analogues

3.2.2.3.1. Results

The family of biphenyl salicylates is included in this section in order to complete the conclusions about the biological activity of salicylic derivatives. However, the compounds belonging to this family were synthesized by different researchers belonging to our group.¹⁸⁵ Eleven biphenyl analogs were synthesized by attachment of an aromatic carbocycle (ring B), acting as the side chain, to the salicylic acid ring (ring A) by means of Suzuki-Miyaura cross-coupling (Scheme 8). The naphthoic acid **BIO-11** (Figure 28), carrying a nitrophenyl side chain and presenting an $IC_{50} = 2.9 \mu M$ against *mGO*, was used as the base for the design of this family. In the structural modulation of **BIO-11**, the naphthyl head was discarded, giving the biphenyl system of these compounds, on which ring B offers a wide variety of substitution options. The structure of these compounds resembles the one of the commercial compound **BIO-9** (Figure 28), which is also a member of this family of biphenyl salicylates.

Table 9. Structures of the prepared arylsalicylates.

R ¹		
	C4 isomers	C5 isomers
<i>p</i> -NO ₂	BIO-26	
<i>m</i> -OCH ₃	BIO-27	
<i>p</i> -OH	BIO-28	
 (<i>p</i>)	BIO-29	BIO-31
 (<i>p</i>)	BIO-30	BIO-32
 (<i>o</i>)	BIO-33	BIO-34
 (<i>o</i>)	BIO-35	BIO-36

Following the structure of compound **BIO-11** (Figure 28), which bears a *p*-nitrophenoxy side chain, arylsalicylates carrying such electron-withdrawing group (**BIO-26**) and electron-donating *m*-methoxy (**BIO-27**) and *p*-hydroxy (**BIO-28**)¹⁸⁸ groups were synthesized. In compound **BIO-26**, the presence of a *p*-nitro group increases the acidity of the carboxylic acid and the phenol. In contrast, the electron-donating *p*-hydroxy group in **BIO-28** decreases it, while the electron-donating effect of the *m*-methoxy group of **BIO-27** affects mainly to ring B. Similar IC₅₀ values, between 10 and 20 μM, were achieved for these three compounds, being that potency intermediate between the one of compounds **BIO-9**, also with an electron-withdrawing side chain, and **BIO-11** (Table 10). In the cell-based assay none of these compounds showed relevant efficacy.

In silico studies predicted that no interaction with *hGO* occurs through ring B, and the *p*-nitro, *m*-methoxy and *p*-hydroxy groups of compounds **BIO-26**, **BIO-27** and **BIO-28**, respectively, get solvated (Figure 55, Appendix 6.1). This means that the *p*-hydroxy group in **BIO-28** is not acting as a hydrogen donor, so the slightly higher potency of **BIO-28** vs **BIO-26** and **BIO-27** cannot be explained on the basis of this theory. The binding mode theoretical predictions are similar for these three compounds: the carboxylate group participates in electrostatic interactions with Arg167 and Arg263, and also acts as a hydrogen acceptor from His260 (Table 26, Appendix 6.1). Thus, the higher electron density provided by the *p*-hydroxy group in **BIO-28** could be enhancing these interactions.

With the aim of increasing π-π stacking or hydrophobic interactions at the active site access channel, a third ring (ring C) was introduced in some arylsalicylate derivatives (**BIO-29** to **BIO-36**, Table 9). Ring C was spaced from ring B through a two-atom flexible linker containing an ether oxygen, not to constrain the conformational adaptation of the molecules to the enzymatic binding sites and introducing the chance of punctual polar interactions through this heteroatom. Two different substitution patterns, *ortho* and *para*, were chosen for ring B. Ring C offers again a wide range of substitution possibilities. These three-ring compounds were prepared in a single step following the general Suzuki-Miyaura procedure (Scheme 8) starting from the corresponding halosalicylic acid and initially using commercially accessible two-ring boronic counterparts.¹⁸⁵

Table 10. Biological data of arylsalicylates **BIO-26** to **BIO-36** and *in silico* prediction of partition coefficient ($\log P_{th}$). Comparison with **BIO-9**, **BIO-11** and **CCPST**. Biological determinations: (i) Enzymatic inhibition on purified mouse glycolate oxidase (*mGO*), at single concentration and IC_{50} calculation using the colorimetric method; (ii) Excreted oxalate in *Agxt1^{-/-}* mouse primary hepatocytes, compared to control (relative oxalate).

Compound	<i>mGO</i> (%) ^a	IC_{50} (μ M) ^b	R^{2c}	Relative oxalate ^d	$\log P_{th}$
CCPST	34.8 ± 4.8	43.5 ± 1.1		0.63 ± 0.16 ^e	n/a
BIO-9	27.9 ± 0.6	n/a		0.88 ± 0.08	3.42
BIO-11	96.3 ± 0.5	2.9 ± 1.1	0.97	0.77 ± 0.01	1.00
BIO-26	41.9 ± 9.2	19.7 ± 1.2	0.87	0.91 ± 0.05	0.26
BIO-27	50.9 ± 7.3	19.5 ± 1.1	0.86	0.83 ± 0.03	2.89
BIO-28	61.3 ± 8.8	13.5 ± 1.1	0.95	0.82 ± 0.01	2.86
BIO-29	83.4 ± 8.5	10.4 ± 1.2	0.85	1.11 ± 0.18	4.67
BIO-30	65.0 ± 6.3	13.8 ± 1.2	0.89	0.90 ± 0.16	4.42
BIO-31	70.9 ± 7.8	14.8 ± 1.1	0.93	0.80 ± 0.16	4.67
BIO-32	83.8 ± 10.1	9.5 ± 1.2	0.81	1.07 ± 0.32	4.42
BIO-33	77.7 ± 7.3	8.3 ± 1.2	0.95	0.72 ± 0.16*	4.95
BIO-34	84.5 ± 4.0	5.8 ± 1.2	0.89	0.92 ± 0.08	4.95
BIO-35	98.6 ± 0.7	4.4 ± 1.2	0.95	0.62 ± 0.29*	5.52
BIO-36	96.2 ± 2.4	3.5 ± 1.2	0.86	0.68 ± 0.21*	5.52

^aPercentage of inhibition of purified *mGO* with 25 μ M, after 1 min. ^b IC_{50} : Calculated in saturated conditions of glycolate (22.2 mM). ^c R^2 : IC_{50} curve-fitted score. ^dOxalate output decrease 24 h after treatment with 10 μ M of the drug in *Agxt1^{-/-}* mouse primary hepatocytes cultured with 5 mM glycolate, in 6-well plates. Data represented as mean ± SD of n = 3 replicates. One-way ANOVA statistical analysis, (*) $p < 0.05$ was considered statistical significant. ^eData at 12.5 μ M in *Agxt1^{-/-}* mouse primary hepatocytes. n/a: Not assessed.

Compounds **BIO-29** to **BIO-32**, C4 and C5 isomers with a **para substitution pattern** on ring B, present a linear geometry. C4 isomers **BIO-29** and **BIO-30**, bearing a plain benzene and a *p*-methoxybenzene as ring C, respectively, showed similar potency as **BIO-28**. This is in line with the previous idea of an electron donating group favoring the establishment of different interactions through ring A and apparently, the introduction of ring C does not reinforce the binding to the enzyme. Regarding their C5 isomers **BIO-31** and **BIO-32**, the potency resulted equal or only slightly increased with respect to the C4 counterparts (Table 10).

Within this group, binding predictions showed that the ring C gets solvated, and therefore, the hydrophobic interactions are established through ring B (Table 9). The same C4/C5 previously reported binding pattern was fulfilled for these compounds. On one hand, C4 isomers **BIO-29** and **BIO-30** interact at Trp110 through the biphenyl core (rings A and B), while in C5 isomers **BIO-31** and **BIO-32** this interaction is lacking. On the other hand, the carboxylate and β -OH functionalities favor a more efficient interaction with His260 in C5 isomers, while C4 isomers only use the carboxy group for the interaction with this aminoacid (Figure 37 and Table 26 and Figure 55 in Appendix

6.1). IC₅₀ values between 10 and 15 μM were achieved for these compounds, although their impact on oxalate production decrease by hyperoxaluric hepatocytes was not significant (Table 10).

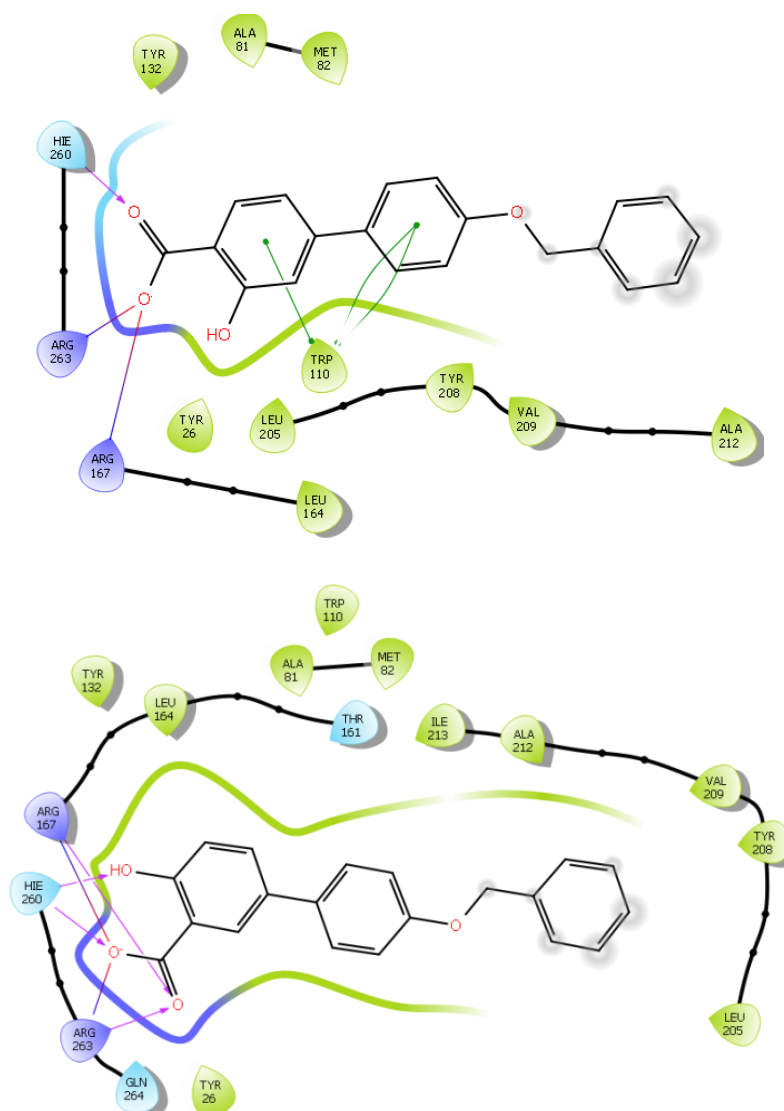


Figure 37. 2D-Diagram of interactions between the C4/C5 isomers three-ring linear arylsalicylates **BIO-29** (up) and **BIO-31** (down), and *hGO* active site residues (purple: basic, cyan: polar uncharged, green: non-polar). Grey shadow represents interaction with solvent. Hie260: His260 protonated on N_ε [Maestro software (Schrödinger)].

Compounds **BIO-33** to **BIO-36**, present an *ortho* substitution pattern on ring B, and this confers them an angled V-shaped structure. Thus, rings A and C are orientated in a *syn* disposition vs the linear disposition of compounds **BIO-29** to **BIO-32**. In compounds **BIO-33** and **BIO-34**, a π-deficient difluorophenyl moiety was introduced as ring C (Table 9). In comparison with compound **BIO-9** (Figure 28), compound **BIO-33** is nearly a benzologue carrying an extra methoxy linker, and compound **BIO-34** is the corresponding C5 isomer of **BIO-33**. These two compounds

were potent *mGOi*'s, although still less potent than compound **BIO-11** ($IC_{50} = 8.3$ and $5.8 \mu\text{M}$ for **BIO-33** and **BIO-34** vs $IC_{50} = 2.9 \mu\text{M}$ for **BIO-11**) (Tables 5 and 10).

Regarding the binding mode predictions, as happened with compound **BIO-11**, no interaction with His260 was observed for compounds **BIO-33** and **BIO-34**, and π - π stacking interactions to Trp110 are predicted to be established through the ring B of these molecules, independently of being C4 or C5 isomers (Table 26, Appendix 6.1). In the cell-based assay, compound **BIO-33** reduced oxalate approximately by 30%, while only a 10% of oxalate reduction was observed for compound **BIO-34** (Table 10).

Finally, the introduction of a trifluoromethylphenyl group on ring C gave rise to compounds **BIO-35** and **BIO-36**. The similar *ortho* substitution pattern as for compounds **BIO-33** and **BIO-34** was followed, giving π -deficient halogenated V-shaped derivatives. Within these compounds, inhibitory activity against *mGO* was remarkably improved, achieving IC_{50} values below $5 \mu\text{M}$. Besides, considerable oxalate decrease in hepatocytes was achieved, reaching almost a 40% of reduction at $10 \mu\text{M}$ (Table 10).

As previously happened in the case of compounds **BIO-33** and **BIO-34**, π - π stacking interaction with Trp110 is present both in C4 and C5 isomers (Table 26, Appendix 6.1.). Thus, compounds **BIO-35** and **BIO-36** do not comply with the previously rule for which only C4 isomers π -stack to Trp110. It is also remarkable that the C5 isomer **BIO-36** follows the previously observed trend, interacting with His260 in a more efficient manner than its C4 isomer **BIO-35**, and using for that both carboxylic and β -OH functionalities. In fact, like **CDST** and **CCPST** did, this compound interacts with all the considered amino acids located at the binding regions 1 and 2 (Figure 38).

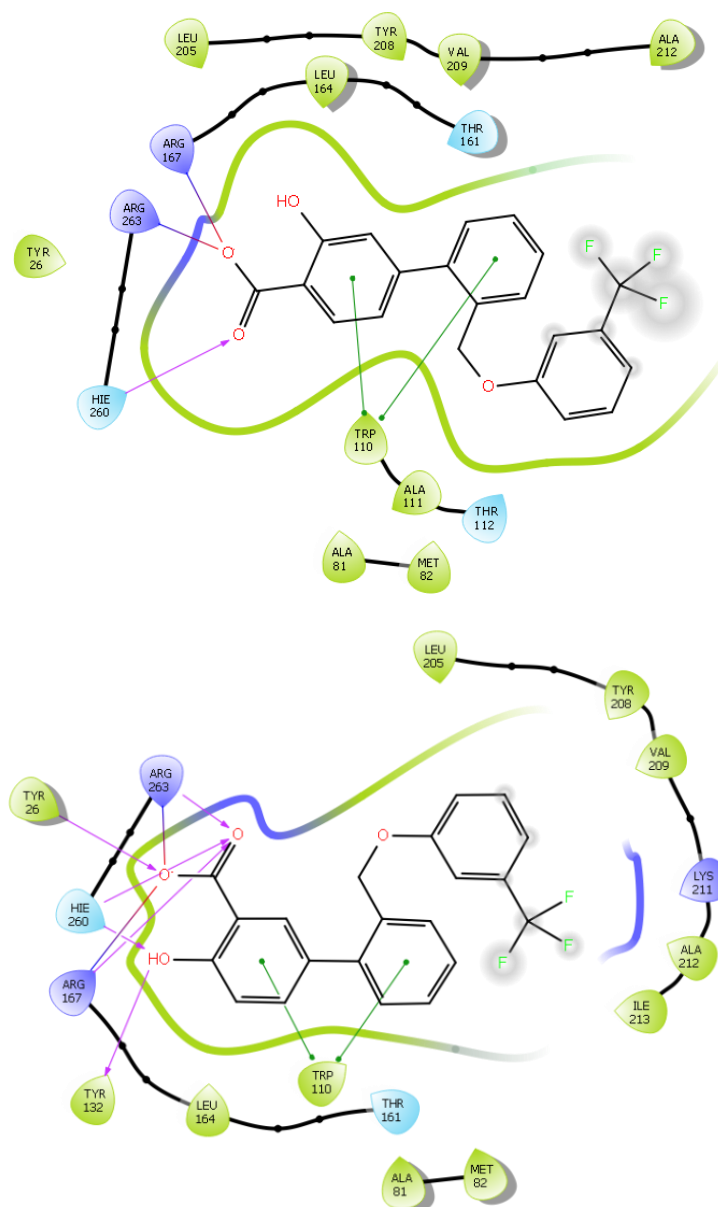


Figure 38. 2D-Diagram of interactions between the C4/C5 isomers three-ring V-shaped arylsalicylates **BIO-35** (up) and **BIO-36** (down), and *hGO* active site residues (purple: basic, cyan: polar uncharged, green: non-polar). Grey shadow represents interaction with solvent. Hie260: His260 protonated on N_ε [Maestro software (Schrödinger)].

3.2.2.3.2. Discussion

Potencies of the arylsalicylate derivatives against *mGO* ranged between 3 and 20 μM . For these compounds, a correlation between enzymatic potency and phenotypic efficacy was observed, allowing the phenotypic activity to be rationalized from *mGO* inhibition. Within this group, compounds **BIO-35** and **BIO-36** with three rings (A-C), V-shape and a trifluoromethyl substituent on ring C, proved to be the most potent *mGO*'s, as well as the most efficient agents on mouse primary hepatocytes, reducing oxalate by almost 40% at 10 μM .

With regard to the binding mode predictions for the arylsalicylates **BIO-26** to **BIO-36**, a common interaction pattern was found in most of them. In general, interactions with Arg167, Arg263 (except **BIO-34**) and His260 (except **BIO-33** and **BIO-34**) are present. Interactions with His260 are established in all cases through the carboxy group at the salicylic acid ring, and also through the β -OH group in the C5 isomers **BIO-31**, **BIO-32** and **BIO-36**. All compounds, excepting the C5 isomers **BIO-31** and **BIO-32**, interact with Trp110 establishing π - π stacking bonds. In all cases this interaction occurs through rings A and B, with only one exception: in compound **BIO-36**, it happens at rings A and C. Curiously, this is also the most potent compound, and its V-shaped structure allows a specific spatial disposition that enables this interaction (Figure 39). It is known that π - π interactions between aromatic rings with different electron densities are favored. This way, π - π interactions with the electron-rich Trp110 should be more efficiently established by π -deficient aromatic systems.¹⁸⁹ Thus, in the particular case of compound **BIO-36**, the trifluoromethyl functionality located in ring C could be enhancing this interaction. For this compound, other relevant interactions happen through the salicylic acid ring: the carboxylate group establishes electrostatic interaction with Arg167, and accepts hydrogen bonds from Arg167, Arg263, Tyr26, and His260, while the phenolic function is hydrogen acceptor with His260 and donor with Tyr132. If compared with its C4 isomer, **BIO-36** presents a more favorable ring disposition that allows the establishment of hydrophobic interactions through the linker containing ring B.

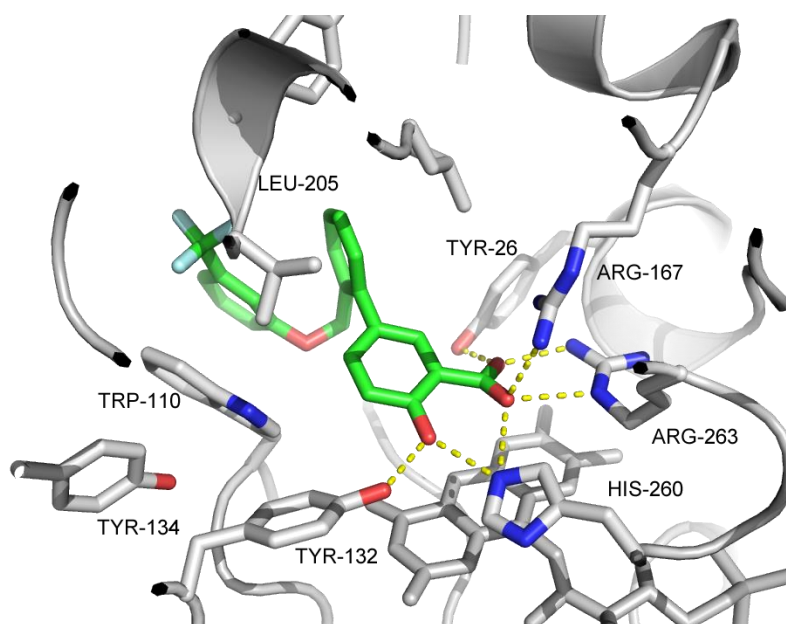


Figure 39. 3D-Diagram of interactions of **BIO-36** inside human glycolate oxidase (PDBid: 2RDT).

3.2.2.4. Discussion on the preliminary results for salicylic acid derivatives

Among all the salicylates evaluated until this point, the commercial naphthoic derivative **BIO-11** and the arylsalicylate **BIO-36** showed to be the most potent *mGOi*'s, with IC_{50} values of 2.9 and 3.5 μ M, respectively. They also presented certain efficacy reducing oxalate excretion in hepatocytes, correlating with the *mGO* inhibitory potency found. However, the most active oxalate reducing agents were the heteroarylsalicylates **MDMG-672**, **MDMG-409**, **MDMG-317** and **MDMG-983**, which in change are poor *mGOi*'s. For them, an additional mechanism of action with additional targets might be involved.

Regarding compounds **BIO-36** and **BIO-11**, the two most potent *GO* inhibitors till the moment, similar binding mode predictions have been found for them. Both present a V-shaped disposition with *syn* orientation of the aromatic rings on the polar head and the hydrophobic tail. Free rotation of the molecules is allowed through the flexible linkers, adopting the structures specific angles that enable the establishment of key interactions throughout the whole molecules. In both compounds, the β -OH group acts as hydrogen bond donor, and also π - π stacking interactions are established with Trp110. In the case of **BIO-11**, they are established through the ring B in the side chain. In **BIO-36**, they occur through rings A (salicylic acid head) and C (hydrophobic tail), thanks to the presence of the ring B acting as a flexible spacer. Ring B enables a beneficial perpendicular disposition of rings A and C, as well as a suitable distance between them that allows the simultaneous binding of those rings to the active site and the access channel (Trp110). Besides, the hydrophobic character of ring B enhances interactions with the target. One of the main differences between **BIO-36** and **BIO-11** is the binding to His260: this interaction is not present in **BIO-11**, while **BIO-36** binds this amino acid acting as hydrogen bond acceptor through the carboxylate and hydroxyl groups at the salicylic polar head. As previously reported for **CCPST** and **glyoxylate**, binding of **BIO-36** occurs after protonation of His260. This situation is thermodynamically unfavored, and explains the lower potency reported for **CCPST** in comparison with the hydrogen donor **CDST**.¹⁰⁰ Another interesting feature is the interaction with Tyr32: both **BIO-11** and **BIO-36** act as hydrogen donors through the hydroxyl group of the polar head. This interaction has not been observed in any other salicylic acid derivative, excepting compound **MDMG-451**, which binds to Tyr132 through the β -hydroxymethyl function, being the amino acid the donor part. In the case of **CDST** and **CCPST** the same interaction happens through their ring N2, which accepts hydrogen bonds.¹⁰⁰

Preliminary Structure-Activity Relationships

Once the biological activity of the first set of salicylic acid derivatives was evaluated and their binding modes were predicted, preliminary structure-activity-relationship for salicylates *mGOi*'s with oxalate decreasing activity could be provided (Figure 40).

- At the salicylic acid-based polar head, the carboxy and hydroxyl functionalities must remain free for a proper interaction with the binding region 1.
- C5 substitution pattern on the salicylic acid head is preferred over C4, since a better interaction of ring B with the binding region 2 is allowed.
- The presence of an aromatic side chain is beneficial. When an electron-deficient aromatic system is introduced in this position, interactions with Trp110 by π - π stacking are favored. Electron withdrawing substituents on an arene are preferred over the electron-poor pyridine.
- The aromatic rings constituting the polar head and the hydrophobic side chain need to be spaced by a flexible linker that allows the beneficial *syn* orientation of both rings.

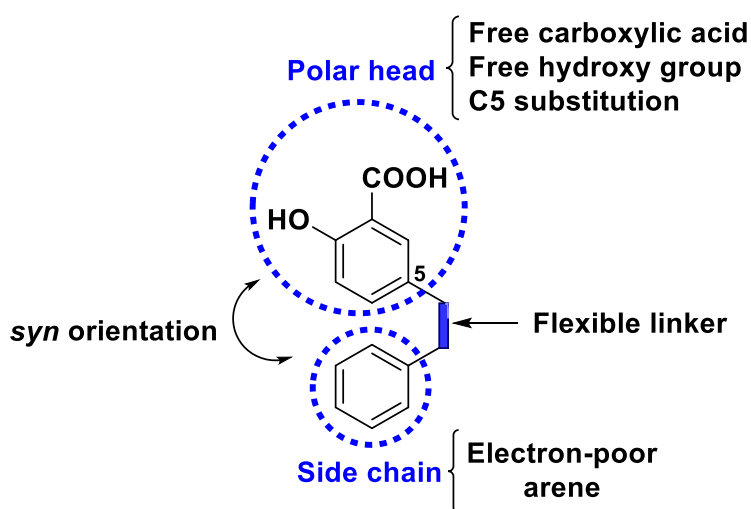


Figure 40. Summary of preliminary structure-activity relationships extracted for salicylic acid derivatives with *mGO* inhibitory activity and capacity to reduce oxalate production in hyperoxaluric mouse primary hepatocytes.

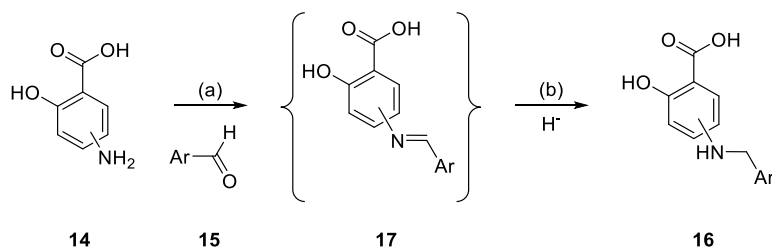
Linkers introduced so far are predicted to interact via hydrophobic forces. However, the introduction of linkers containing different heteroatoms should be considered, since additional interesting interactions, such as hydrogen bonding, could be established with the target. Thus, from this point on, the research was focused at the search of the best flexible linkers that could allow better interactions of polar head and side chain with the biological target GO, as well as possibly reinforcing the binding strength to the target with additional binding groups.

3.2.3. Salicylic acid derivatives containing two-atom nitrogen-based spacers

3.2.3.1. Results

In compounds **BIO-29** to **BIO-36**, rings A and C are spaced by ring B and a flexible two-atom linker, enabling the suitable spatial disposition of the GO-binding groups. The *ortho* substitution on the ring B confers these molecules a V-shape structure, placing rings A and C in *syn* disposition and therefore allowing the establishment of π - π stacking interactions with Trp110, a key amino acid that could be crucial for the biological activity of the compounds. When analyzing the predicted binding modes of **BIO-36** and other arylsalicylates, it was already mentioned that the introduction of different linkers should be considered, since it could lead to the establishment of novel and relevant interactions with the target.

With the aim of exploring different linker and side chain options, we selected furylsalicylate **MDMG-409** as the basis to conduct structural optimization. This compound, presenting EC_{50} at 3 μ M on oxalate decrease, as well as an easy one-pot synthesis in quantitative yield, had been previously defined as a qualifying hit for structural modulation. Sixteen structural analogs of **MDMG-409** were prepared according to the Scheme 13. The general structure of this group of compounds presents a salicylic moiety (ring A), acting as polar head, and a second aromatic ring (ring B), acting as hydrophobic side chain, separated through a linker (Figure 41). We chose to include nitrogen containing linkers because of their easy preparation by simple reductive amination, and also because the amino group confers better water solubility to the resulting molecules. Besides, the nitrogen atom could establish new polar interactions with the target. Thus, two-atom nitrogen-based linkers, both rigid and flexible, were introduced between the salicylic acid polar head and the hydrophobic side chain. Different types of terminal aryl moieties were also explored in order to verify the convenience of using electron-poor aromatic rings as side chains. When studying the binding mode and biological activity of arylsalicylates, it was noted that the presence of electron-poor aromatic rings as side chain could be enhancing the interaction with Trp110 by π - π stacking, and therefore electron-deficient aromatic systems were preferred in that position. Aiming at verifying this hypothesis, both activated and deactivated benzenes were chosen as representative aryl fragments with different electron densities, were introduced.



Scheme 13. Preparation of salicylic acid derivatives with methylamino linkers. Reaction conditions: (a) Molecular sieve (3Å), MeOH/DCM, rt. (b) i) NaBH(OAc)₃ or NaBH₄, MeOH/DCM, rt; ii) HCl (5%).

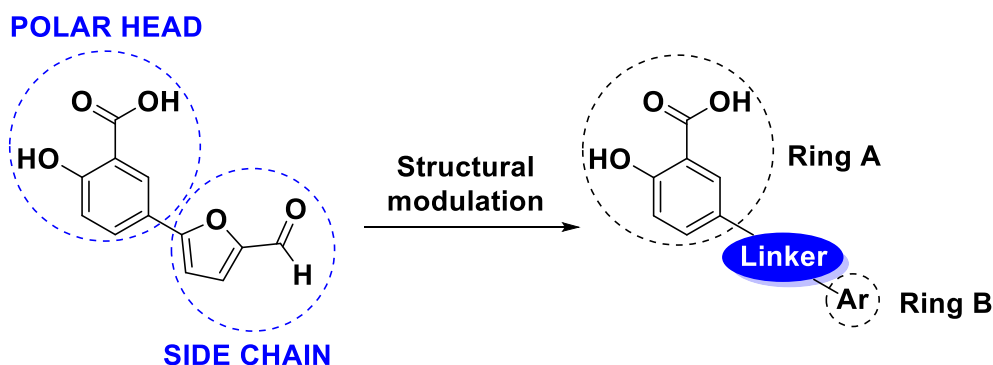


Figure 41. Structural modulation of **MDMG-409**.

First, the introduction of flexible amino linkers was explored. To that end, reductive amination using 4-amino or 5-aminosalicylic acid (**14**, Scheme 13) was carried out over different aromatic aldehydes (**15**), yielding a set of molecules holding **methylamino linkers** (**16**, Scheme 13). C5 substituted derivatives were preferably prepared, following the previously established substitution pattern for active compounds, although in some cases the corresponding C4 derivatives were also synthesized and evaluated to contrast this hypothesis within this set of compounds. The intermediate imines, which were isolated and evaluated in some cases (**17**, Scheme 13), were subjected to *in situ* reduction with sodium triacetoxyborohydride, yielding final amines in moderate to high yields.

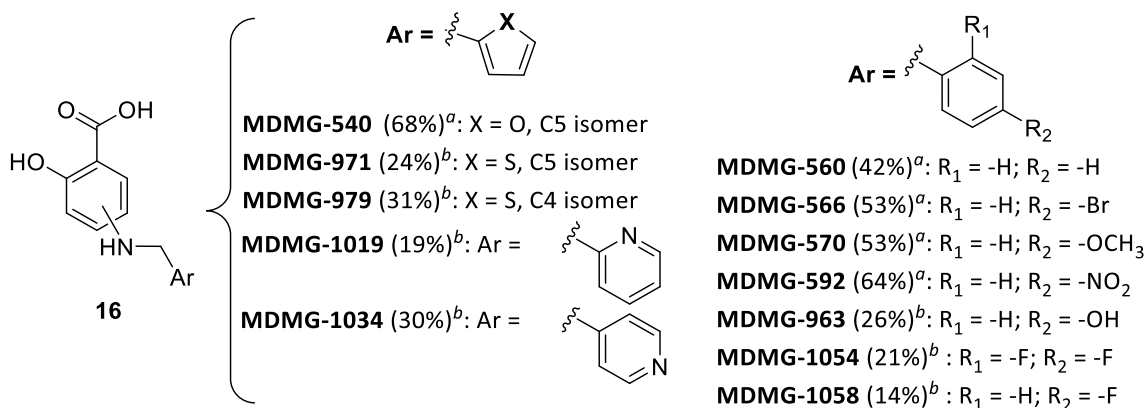


Figure 42. Structures of salicylic acid derivatives containing methylamino linkers. ^aSynthesized following the general synthetic procedure 6A (see 5.2.6. General synthetic procedure 6 for reductive amination): **14** (1 equiv), **15** (1 equiv), NaBH(OAc)₃ (2.5 equiv), DCM/MeOH, 3 h, rt; ii) 5% HCl, 0 °C. ^bSynthesized following the general synthetic procedure 6B (see 5.2.6. General synthetic procedure 6 for reductive amination): i) **14** (1.2-2 equiv), **15** (1 equiv), NaBH₄ (1.5 equiv), DCM/MeOH, 15 min, 0 °C ; ii) 5% HCl, 0 °C. Isolated yields are shown in parenthesis.

Under the reaction conditions 6A (see 5.2.6 for the general synthetic procedure 6 for reductive amination), the dialkylated product was formed in some cases (**18**, Figure 43), limiting the yields of the desired final compounds and hampering the purification process by column chromatography, given the similar mobility of both mono- and dialkylated products. To prevent this side reaction, the reaction time of step a (Scheme 13) was increased from 3 to 24 h and the amount of aldehyde limited to 1 equiv. Besides, the use of the more efficient reducing agent sodium borohydride was preferred in step b (Scheme 13), resulting in reaction conditions 6B.

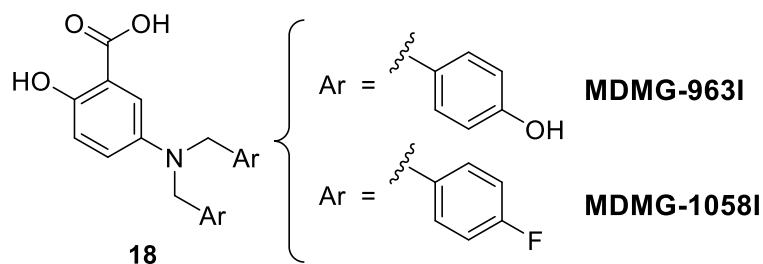


Figure 43. Structure of the dialkylation products.

A series of rigid structures with *anti* disposition of the aromatic rings were also included in this study to contrast the hypothesis about the convenience of *syn* disposition of the two aromatic groups. To that end, *trans* imines (**BIO-37** to **BIO-39**, **MDMG-574** and **MDMG-628**, Figure 44), and *trans* azoderivatives (**BIO-40** and **MDMG-**

604, Figure 45) were evaluated. Compounds obtained from commercial sources are indicated.

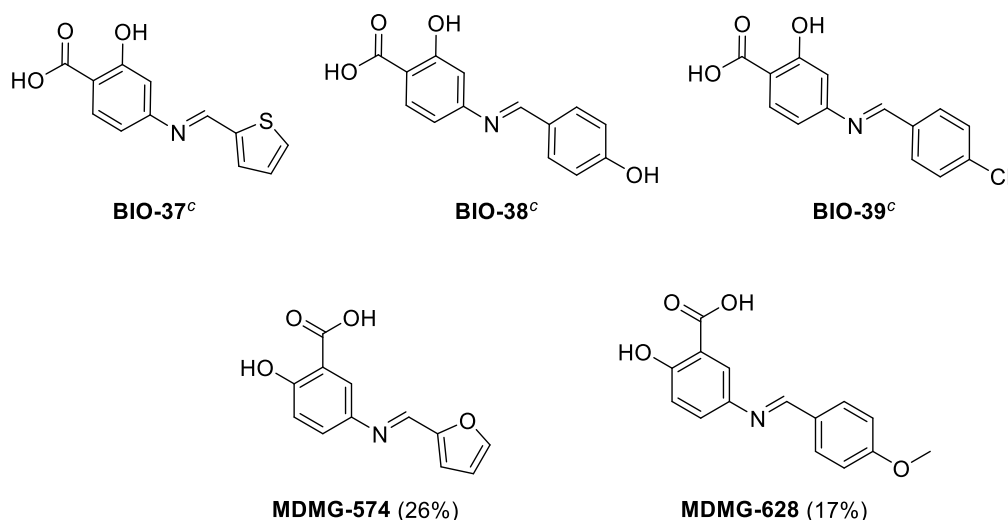
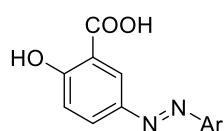


Figure 44. Structure of salicylic acid derivatives containing rigid imino linkers. Isolated yields are shown in parenthesis.^cObtained from commercial sources.



BIO-40:^a Ar = Ph

MDMG-604 (31%):^b Ar = 2-Naphthyl

Figure 45. Structure of the salicylic acid derivatives rigid azo linkers. Isolated yields are shown in parenthesis. ^aObtained from commercial sources. ^bReaction conditions for the synthesis of azo linkers by diazotisation/nucleophilic coupling: i) 2-naphthylamine (1.2 equiv), NaNO₂ (1.1 equiv), HCl, H₂O, 0 °C; ii) Salicylic acid (1 equiv), NaOH, 6h.

For this set of compounds with a two-atom nitrogen-based linker, inhibitory activities both against *hGO* and *mGO* were assessed, initially using a colorimetric protocol. In most cases, results on both enzymes were comparable. The most important differences between the potency on both enzymes were found for rigid derivatives, while flexible compounds were much more homogeneous between both isoenzymes (Tables 11 and 12).

Table 11. Biological data of salicylic acid derivatives containing flexible methylamino linkers. Comparison with **MDMG-409**. Biological determinations: (i) Enzymatic inhibition on purified mouse and human glycolate oxidase (*mGO* and *hGO*), at single concentration and IC_{50} calculation using the colorimetric method; (ii) Excreted oxalate in *Agxt1^{-/-}* mouse primary hepatocytes, compared to control (relative oxalate).

Compound	<i>mGO</i> (%) ^a	IC_{50} (μ M) ^b <i>mGO</i>	R^{2c}	<i>hGO</i> (%) ^d	IC_{50} (μ M) ^b <i>hGO</i>	R^{2c}	Relative oxalate ^e
MDMG-409	42.7 ± 12.8	38.2 ± 1.2	0.81	15 ± 3.2	n/a	n/a	0
MDMG-540	38.5 ^f	14.3 ^f	0.91	79.9 ± 0.8	12.6 ± 1.1	0.97	0.66 ± 0.02*
MDMG-560	48.5 ^f	14.4 ^f	0.97	68.4 ± 2.0	14.4 ± 1.1	0.95	0.65 ± 0.12*
MDMG-566	52.8 ^f	8.4 ^f	0.94	68.3 ± 1.1	12.4 ± 1.1	0.96	0.61 ± 0.03*
MDMG-570	38.5 ^f	25.5 ^f	0.96	62.6 ± 2.5	16.1 ± 1.1	0.97	0.67 ± 0.07
MDMG-592	62.3 ^f	14.6 ^f	0.93	79.2 ± 1.2	12.9 ± 1.1	0.94	0.42 ± 0.01*
MDMG-963	63.9 ^f	10.1 ± 1.0	0.97	72.7 ± 2.4	11.9 ± 1.1	0.95	n/a
MDMG-963I	81.4 ^f	6.1 ± 1.0	0.96	67.9 ± 0.9	10.7 ± 1.1	0.96	n/a
MDMG-971	59.1 ^f	8.6 ± 1.1	0.96	70.3 ± 1.9	11.9 ± 1.1	0.96	n/a
MDMG-979	20.0 ^f	n/a	n/a	27.5 ± 1.5	n/a	n/a	n/a
MDMG-991	53.8 ^f	9.1 ± 1.1	0.95	43.9 ± 2.1	23.2 ± 1.3	0.95	n/a
MDMG-1019	45.1 ^f	15.5 ± 1.2	0.95	50.7 ± 2.6	15.4 ± 1.1	0.95	n/a
MDMG-1034	30.1 ± 3.0	n/a	n/a	48.9 ± 2.6	42.8 ± 1.1	0.96	n/a
MDMG-1054	82.3 ± 1.6	7.5 ± 1.1	0.96	86.5 ± 0.4	8.6 ± 1.1	0.96	n/a
MDMG-1058	84.2 ± 1.4	8.6 ± 1.1	0.95	89.3 ± 0.4	10.6 ± 1.1	0.94	n/a
MDMG-1058I	96 ± 0.4	1.6 ± 1.1	0.95	84.5 ± 0.5	5.9 ± 1.1	0.96	n/a

^aPercentage of inhibition of purified *mGO* with 25 μ M, after 1 min. ^b IC_{50} : Calculated in saturated conditions of glycolate (22.2 mM). ^c R^2 : IC_{50} curve-fitted score. ^dPercentage of inhibition of purified *hGO* with 25 μ M, after 1 min. ^eOxalate output decrease 24 h after treatment with 10 μ M of the drug in *Agxt1^{-/-}* mouse primary hepatocytes cultured with 5 mM glycolate, in 6-well plates. One-way ANOVA statistical analysis, (*) $p < 0.05$ was considered statistical significant. Data represented as mean ± SD of $n = 3$ replicates. ^fNo SD is given. n/a: Not assessed.

Table 12. Biological data of salicylic acid derivatives containing rigid spacers. Comparison with **MDMG-409**. Biological determinations: (i) Enzymatic inhibition on purified mouse and human glycolate oxidase (*mGO* and *hGO*) at single concentration and IC_{50} calculation using the colorimetric method; (ii) Excreted oxalate in *Agxt1^{-/-}* mouse primary hepatocytes, compared to control (relative oxalate).

Compound	<i>mGO</i> (%) ^a	IC_{50} (μ M) ^b <i>mGO</i>	R^{2c}	<i>hGO</i> (%) ^d	IC_{50} (μ M) ^b <i>hGO</i>	R^{2c}	Relative oxalate ^e
MDMG-409	42.7 ± 12.8	38.2 ± 1.2	0.81	15 ± 3.2	n/a	n/a	0
BIO-37	88 ^f	1.8 ^f	0.94	92.4 ± 0.7	9.5 ± 1.2	0.93	0.99 ± 0.03
BIO-38	72 ^f	1.8 ^f	0.90	71.8 ± 1.1	2.4 ± 1.1	0.95	1.06 ± 0.12
BIO-39	28 ^f	n/a	n/a	73.0 ± 6.7	17.1 ± 1.1	0.96	n/a
BIO-40	28 ^f	n/a	n/a	15.0 ± 2.2	n/a	n/a	n/a
MDMG-574	4 ^f	n/a	n/a	43.6 ± 5.8	26.5 ± 1.1	0.93	n/a
MDMG-604	56 ^f	23.0 ^f	0.97	22.4 ± 0.9	n/a	n/a	1.01 ± 0.08
MDMG-628	61 ^f	8.0 ^f	0.97	75.4 ± 0.8	18.6 ± 1.1	0.96	0.97 ± 0.02

^aPercentage of inhibition of purified *mGO* with 25 μ M, after 1 min. ^b IC_{50} : Calculated in saturated conditions of glycolate (22.2 mM). ^c R^2 : IC_{50} curve-fitted score. ^dPercentage of inhibition of purified *hGO* with 25 μ M, after 1 min. ^eOxalate output decrease 24 h after treatment with 10 μ M of the drug in *Agxt1^{-/-}* mouse primary hepatocytes cultured with 5 mM glycolate, in 6-well plates. One-way ANOVA statistical analysis, $p < 0.05$ was considered statistical significant. Data represented as mean ± SD of $n = 3$ replicates. ^fNo SD is given. n/a: Not assessed.

Unfortunately, significant interferences with the GO colorimetric assay were detected for this whole set of compounds (Table 13). The nature of the interferences was then investigated. Colorimetric interferences were first discarded as we could verify that the absorbance peaks of our compounds did not match the wavelength at which the final chromophore is detected. This led us to think that the interferences caused by our compounds might be due rather to inhibition of HRP or to chemical reaction with any of the chromogenic reagents used in the method. This forced the abandonment of the colorimetric method, which had been traditionally used by our collaborators, and the implementation of a new end-point assay in our facilities using the fluorogenic reagent Amplex[®] Red, still in a HRP coupled reaction (see 5.6.1.1.3 in Experimental section).¹⁹⁰ With this new assay, the presence of certain reagents, which may be the cause of the interference, was discarded.

Table 13. Interferences of highlighted furyl salicylates containing two-atom nitrogen based linkers with the colorimetric enzymatic assay.

Compound	% Interference colorimetric assay ^a
MDMG-963	42.5 ± 0.4
MDMG-1054	60.0 ± 0.6

^aInterference with the colorimetric method measured at 25 μ M of the drug. Data represented as mean ± SD of $n = 3$ replicates.

Before proceeding with any further enzymatic determinations, the interference assay was adapted to this new evaluation method, and the percentage of interference was calculated for representative compounds. Unfortunately, even with the new method for enzymatic evaluation, interferences ranging from 30 to 60% at 20 μM persisted (Table 14). Thus, *mGO* and *hGO* inhibitory activity values obtained for these compounds using our colorimetric or fluorimetric methods cannot be considered as reliable results, and further research will be conducted in order to complete the enzymatic biological evaluation of these compounds.

Table 14. Interferences of highlighted furyl salicylates containing two-atom nitrogen based linkers with the fluorometric enzymatic assay.

Compound	% Interference fluorometric assay ^a
MDMG-540	63.1 \pm 1.0
MDMG-566	43.6 \pm 0.84
MDMG-570	46.2 \pm 0.74
MDMG-592	57.0 \pm 0.45
MDMG-963	42.6 \pm 1.2
MDMG-963-I	31.9 \pm 0.77
MDMG-971	58.6 \pm 0.28
MDMG-991	28.3 \pm 1.4
MDMG-1054	41.6 \pm 0.71
MDMG-1058	64.3 \pm 0.69
MDMG-1058I	45.0 \pm 0.23

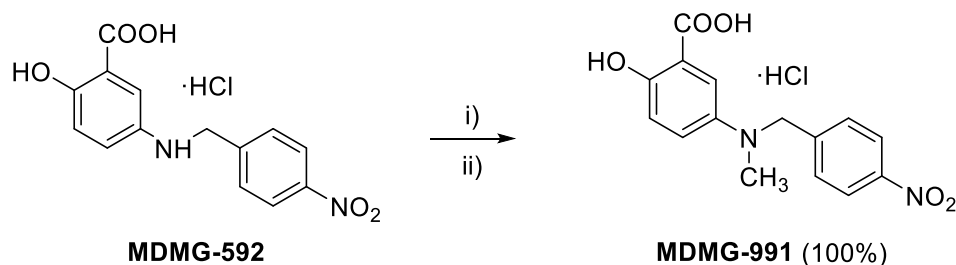
^aInterference with the fluorometric method measured at 25 μM of the drug. Data represented as mean \pm SD of n = 3 replicates.

As it was not possible to find a suitable method for the enzymatic evaluation of these compounds, the results obtained using the colorimetric method were used to roughly describe the *GO* inhibitory activity of these compounds. Conclusions must be taken carefully, due to the presence of interferences, as previously mentioned.

Regarding the **rigid derivatives**, the C4 substituted imines **BIO-37** and **BIO-38**, carrying thiophene and *p*-hydroxybenzene as terminal aryl moieties, were the best *mGO* inhibitors in this set (IC_{50} = 1.8 μM for both of them) (Table 12). The C5 substituted imine **MDMG-628**, bearing *p*-methoxybenzene as side chain, showed intermediate potency (IC_{50} = 8). The rest of imines, as well as the remaining rigid derivatives presented lower *mGO* inhibitory activities, being some of them totally unable to inhibit *mGO* at 25 μM . Among the rigid derivatives, none of these compounds resulted active lowering oxalate in the cell-based assay (Table 12). It is a general rule that, for rigid derivatives, inhibitory potency against *hGO* is lower than against *mGO* (Table 12).

In relation to the derivatives containing **flexible methylamino linkers**, the best results of potency corresponded to tertiary amines (**MDMG-963I** and **MDMG-1058I**) (dialkylation products, Figure 43). Both of them improved potency with respect to their corresponding secondary amines, especially in the case of **MDMG-1058I**, which showed the best potency within the spaced derivatives of **MDMG-409** ($IC_{50} = 1.6 \mu M$) (Table 11). This compound presents an electron-poor *p*-fluorophenyl ring B, vs the electron-rich *p*-hydroxyphenyl ring B of **MDMG-963I**. This matches the idea of electron-deficient arenes to be beneficial for a better interaction with GO. Between secondary amines (monoalkylation products, Figure 42), C5 isomers showed intermediate potency, with IC_{50} values ranging between 7 and 25 μM . Once more, the best results in term of potency against GO were obtained for compounds bearing a deactivated benzene as ring B. Concretely, secondary amines carrying halogens as deactivating groups (**MDMG-566**, **MDMG-1054** and **MDMG-1058**), showed the best potencies, with IC_{50} values ranging from 7 to 8 μM . In change, the nitro deactivating group present in **MDMG-592**, led to lower inhibitory activities, comparable to the ones of the unsubstituted benzene in **MDMG-560** ($IC_{50} = 12-14 \mu M$). Between activated benzenes, *p*-hydroxy (**MDMG-963**) is more favorable than *p*-methoxy (**MDMG-570**) (Table 11). Close in potency to halogenated benzenes, **MDMG-971**, C5 isomer with a thiophene ring B, showed a higher potency ($IC_{50} = 8 \mu M$) than its C4 counterpart **MDMG-979**, which inhibited *mGO* only by 20% at 25 μM . The secondary amines **MDMG-1019** and **MDMD-1034**, carrying pyridines as terminal aryl moieties, and **MDMG-540**, with a furan ring B, resulted, however, less potent than expected. Finally, the *p*-methoxy activated benzene **MDMG-570** resulted the least. For flexible derivatives, potencies against *mGO* and *hGO* are similar (Table 11).

With regard to the assay in *Agxt1^{-/-}* mouse hepatocytes, only the secondary amines **MDMG-540**, **MDMG-560**, **MDMG-566**, **MDMG-570** and **MDMG-592** were tested. They all were able to reduce oxalate when tested at 10 μM , showing 30-60% reduction of excreted oxalate. **MDMG-592** (*p*-nitrobenzene ring B) reduced oxalate by approximately 60%, being the most effective compound within the tested spaced derivatives. Thus, its methylated tertiary amine was prepared by simple reductive amination using formaldehyde in order to study the convenience of a secondary or tertiary amine in that position (Scheme 14). The resulting tertiary amine **MDMG-991** almost achieved a two-fold potency improvement against *mGO*, lowering the IC_{50} from 14 to 9 μM . The biological evaluation in hepatocytes of this compound and other interested spaced derivatives such as **MDMG-963I** and **MDMG-1058I** is currently ongoing.



Scheme 14. Synthesis of the tertiary amine **MDMG-991**. i) NaBH₄CN (2.6 equiv), MeOH, 30 min, 0 °C, 15 min, 0 °C; ii) 5% HCl, 0 °C. Isolated yield is shown in parenthesis.

Only preliminary *in silico* studies were conducted for selected compounds in this set: representative 2D-interaction diagrams for compounds **MDMG-540** and **MDMG-592** are shown in Figure 46. In general terms, in the binding region 1, the polar head interacts with Arg167, Arg263 and His260 through the carboxy and hydroxy groups, appearing also the interaction with Tyr132 in the case of **MDMG-592**. The flexible methylamino linker allows the desired *syn* disposition of both aromatic rings, promoting interactions between the side chains and Trp110 (second binding region). In the case of **MDMG-592**, this interaction is also established through the salicylic acid polar head.

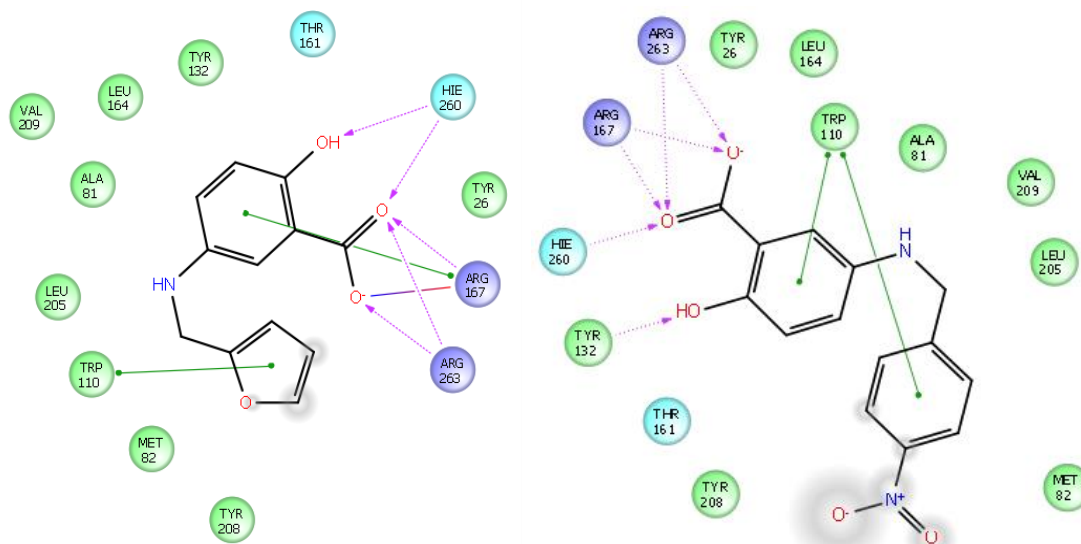


Figure 46. 2D-Diagram of interactions between compounds **MDMG-540** (left) and **MDMG-592** (right) and the enzyme *hGO* (purple: basic, cyan: polar uncharged, green: non-polar). Grey shadow represents interaction with solvent. Hie260: His260 protonated on N_ε [Maestro software (Schrödinger)].

3.2.3.2. Discussion

Within this group of spaced derivatives of compound **MDMG-409**, those with rigid imino and azo linkers resulted to be the most potent compounds against *mGO*, whilst the best efficacy on oxalate diminution was achieved with the introduction of flexible amino linkers. In most cases, potency against *mGO* was remarkably improved with respect to **MDMG-409**, and potency values over *hGO* were similar to those obtained for *mGO*. The absence of phenotypic effect in cells in the rigid imines, which behaved as potent *mGO*'s, could be due to instability issues within the cellular environment. For the rest of compounds, discrepancies between enzymatic activity and phenotypic effect are not excessive and could be due to pharmacokinetics (pass through membranes, metabolism...).

C5 isomers carrying flexible methylamino linkers led to the best results on oxalate decrease, with values ranging from 30 to 60%. Compounds **MDMG-566** and **MDMG-592**, carrying bromo and nitro substituents in *para* position, respectively, were the most efficient compounds in this term. This is coherent with the previous suggested hypothesis, in which the presence of electron-poor arenes in flexible molecules could promote π - π stacking interactions with the indole electron-rich ring of Trp110, and as result, a better oxalate lowering activity could be achieved. The preliminary docking data available for compounds **MDMG-540** and **MDMG-592**, which carry methylamino flexible linkers, corroborates this idea, predicting a *syn* disposition of the two GO-binding aromatic groups that enables interactions with key amino acids in binding regions 1 and 2.

In spite of these promising results, the interferences could not be eliminated even with the introduction of an alternative method for the enzymatic evaluation, and for that reason, the enzymatic results must be cautiously interpreted.

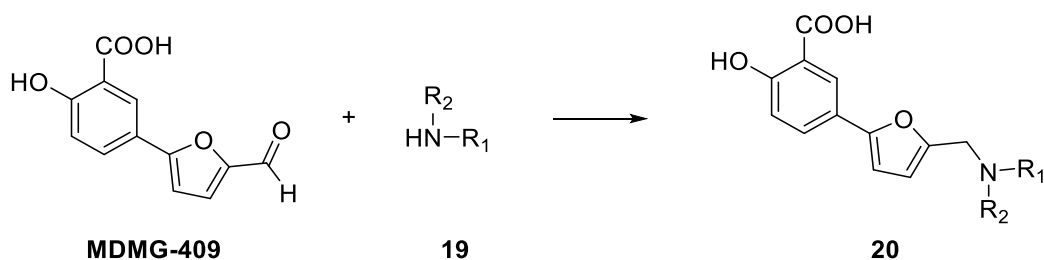
3.2.4. Chemical modifications on the formyl group of MDMG-409

Compound **MDMG-409** (Figure 31), while being an efficient agent reducing oxalate in cells, is also a moderate *mGO* inhibitor. Docking predictions for **MDMG-409**, contrary to **BIO-36** (Table 9), showed that this compound does not establish interaction with Trp110, possibly due to the lack of an aromatic ring placed at the right distance from the polar salicylic head.

After the introduction of spacers between the polar salicylic head (ring A) and the furan ring (ring B) in **MDMG-409** (family of two-atom nitrogen-based spacers), we decided to enlarge the molecule beyond the furan moiety. The formyl group in **MDMG-409** offers several possibilities of chemical modification for the attachment of new groups in order to reinforce interactions between the side chain of the molecule and the enzyme GO.

3.2.4.1. Reductive amination: Results on the synthesis of aminomethylfuryl derivatives of MDMG-409.

MDMG-409 was reacted with different primary and secondary amines by reductive amination through its terminal formyl group. As a result, a new family of 12 compounds holding a 5-aminomethyl-2-furyl flexible linker was prepared (Scheme 15).



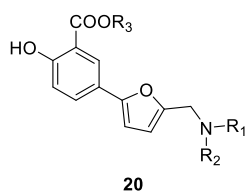
Scheme 15. Preparation of aminomethylfuryl derivatives. Reagents and conditions: i) MeOH/DCM 3/1, molecular sieves (3 Å), rt, darkness; ii) NaBH(OAc)₃, rt; iii) H₂O (see 5.2.6 General synthetic procedure 6 for reductive amination).

Primary and secondary amines (**19**) for this reaction included anilines, benzylamines, piperidin and propargylamine (Table 15). The resulting compounds (**20**, Table 15) can be then classified as aliphatic or aromatic amines, being all of them

secondary amines except **MDMG-919**, which carries a tertiary nitrogen atom in a piperidin ring. Although the main idea was the introduction of electron-poor arenes to reinforce the hydrophobic interactions with Trp110, other aryl moieties with different electron densities were used, as well as aliphatic fragments, with the goal of obtaining more solid conclusions.

Significant difficulties were found in the purification process of this set of compounds: in addition to the highly polar structure of these aminomethylfuryl derivatives, in most cases, a recurrent impurity appeared during the purification step by flash column chromatography. Some amines were detected to be unstable under the slightly acidic environment given by the silica gel used in the chromatographic purification. This challenged affording high purity compounds (of at least 95% purity on HPLC), and limited the reaction yields, which were considerably reduced in some cases. This impurity, which was later identified as a polymerization product, was formed during the flash column chromatography as a consequence of the acidic environment, although its presence was also detected after soft heating. For such unstable amines, in order to avoid polymerization, acidic silica had to be neutralized before loading the crude, by using mobile phases containing methanolic ammonia (7N) or NH_4OH (32%)/MeOH 2/100. As a result, some compounds were obtained as ammonium carboxylates after this purification step. Special care was also taken once the final compounds were purified, limiting its exposure to light and heat.

The polymerization reaction was responsible for the failure to isolate pure **MDMG-923** and **MDMG-939** (Table 15), whose presence was only detected by LC-MS. Curiously, both compounds present electron-rich anilines as side chain. Only in the case of the tertiary aliphatic amine **MDMG-919**, the polymerization process was not observed. The impurity could be finally isolated and characterized as the difurylmethane **MDMG-825** (Scheme 16). In some cases, intermediate products of this polymerization process, corresponding to the tertiary amines **MDMG-931I** and **MDMG-935I** (Figure 47), were also identified.

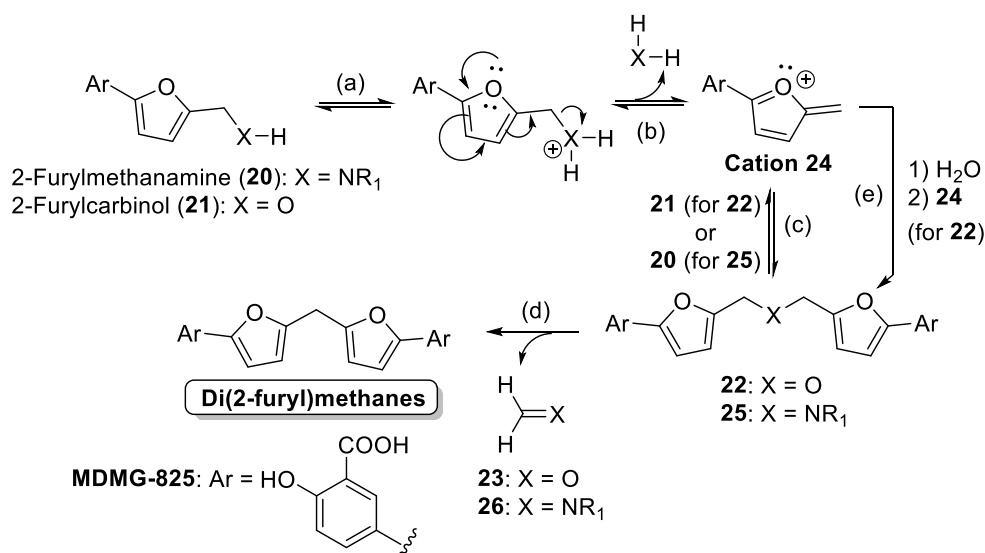
Table 15. Structures of aminomethylfuryl derivatives of the lead compound **MDMG-409**.

Compound	Starting amine (19)	R ³	
MDMG-907 (45%) ^a	19a	NH ₄	Anilines
MDMG-915 (24%) ^a	19b	NH ₄	
MDMG-923 ^b	19c	NH ₄	
MDMG-939 ^a	19d	NH ₄	
MDMG-911 (69%) ^a	19e	NH ₄	
MDMG-931P (67%) ^a	19f	NH ₄	Benzylamines
MDMG-1082 (48%) ^a	19g	NH ₄	
MDMG-1074 (52%) ^a	19h	NH ₄	
MDMG-1078 (51%) ^a	19i	NH ₄	
MDMG-927 (41%) ^a	19j	NH ₄	
MDMG-919 (59%) ^a	19k	H	Other aliphatic amines
MDMG-935P (76%) ^a	19l	NH ₄	

^aSynthesized following the general synthetic procedure 6C (see 5.2.6. General synthetic procedure 6 for reductive amination): amine (1.2 equiv), aldehyde (1 equiv), NaBH(OAc)₃ (2.5 equiv), MeOH/DCM 3/1, 3 h, rt; ii) 5% H₂O, 0 °C. ^bNot isolated because of instability issues.

The acid-catalyzed polymerization of 2-furylcarbinols (**21**, Scheme 16) to di(2-furyl)methanes has been previously described.^{191,192} First, etherification¹⁹³ between two molecules of **21** occurs in three steps (steps a-c, Scheme 16), and this is followed by decomposition of the resulting ether (**22**) into formaldehyde (**23**) and the final difurylmethane (step d, Scheme 16).¹⁹⁴ In the case of the polymerization of 2-

furylmethanamines (**20**) to di(2-furyl)methanes, corresponding to our case, only one bibliographic precedent could be found.¹⁹⁵ That process was equally explained from 2-furylmethanamine (**20**), whose amino group would be protonated and eliminated yielding cation **24** again (steps a-b), and water addition to this intermediate would yield the same ether intermediate (**22**) (step e). In our reactions, we have detected the formation of compounds type **25** (Scheme 16 and Figure 47). Tertiary amines **MDMG-931I** and **MDMG-935I** (Figure 47) were isolated as secondary products in the reaction between **MDMG-409** and the primary amines type **19**. To explain this, we suggest that compounds type **25** could be precursors for **MDMG-825**, following a nucleophilic attack of the amine type **20** on the carbocation **24** (step c). Thus, **MDMG-825** could also be formed from secondary amines type **20** (in our case, **MDMG-931** or **MDMG-935**, Table 15) following a similar mechanism as the one described for furylcarbinols, but without the need for water addition in step e. The higher electron density on the nitrogen atom of compounds type **20**, the easier this nucleophilic attack (step c) would be. This could explain why this polymerization process is mainly observed when **20** presents an activated aniline or an aliphatic amine side chain. After that, the imine fragment **26** would be eliminated from **25** and decomposed forming the starting amine type **19** (Table 15). Indeed, these starting amines type **19** (**19f** and **19I**, Table 15) were also isolated during the chromatographic process.



Scheme 16. Mechanism for the formation of difurylmethanes.

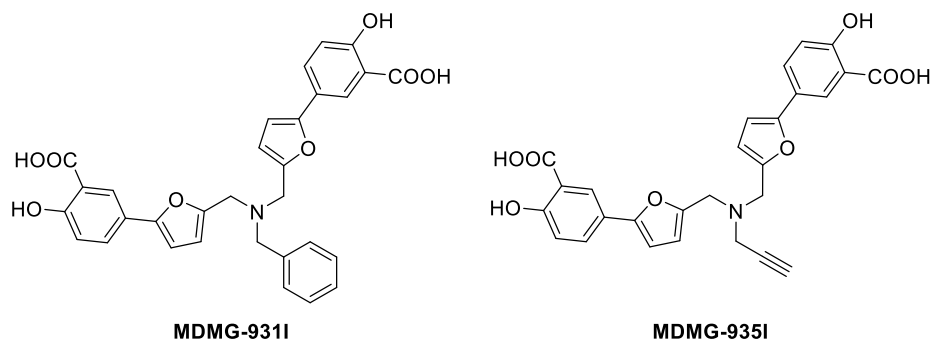


Figure 47. Structure of the tertiary amines **MDMG-9311** and **MDMG-9351**.

The synthesis of chemical probes was included as a main objective within this project. The aim of their preparation was their use in chemoproteomics experiments in order to discover additional biological targets for those compounds presenting discrepancies between enzymatic potency and phenotypic effect (i.e. **MDMG-409** and **MDMG-672**). In order to provide deeper insights into the biological mechanism of these compounds, the proteomic profiling of the selected molecules was planned. Chemoproteomics, is a technique that allows the screening on the complete proteome of the cell eliminating the risk of exclusion that screening on purified proteins involves.¹⁹⁶ This methodology uses chemical probes, which are molecules that can capture the proteins for which they have affinity. A commonly used type of molecular probe is the one called photoaffinity probe,¹⁹⁷ which includes a selectivity function, a photoreactive function and a sorting function (Figure 48). The selectivity function is the one responsible for the selective binding to the biological targets. In our case, this function would correspond structurally to the drug under study, either **MDMG-409** (for probe **MDMG-911**) or **MDMG-672** (for probe **MDMG-995**). This selectivity function is attached to a photoactivatable fragment that will, upon irradiation with a suitable wavelength, establish an irreversible bond with the biological target. Finally, the fragment called sorting function will allow the capture of the complex by reaction with a “hook” (see Appendix 6.4. International short-term stay for photoaffinity labeling experiments).

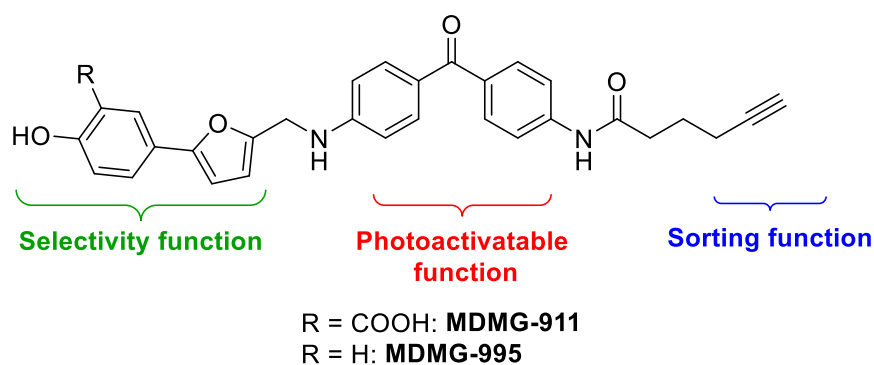


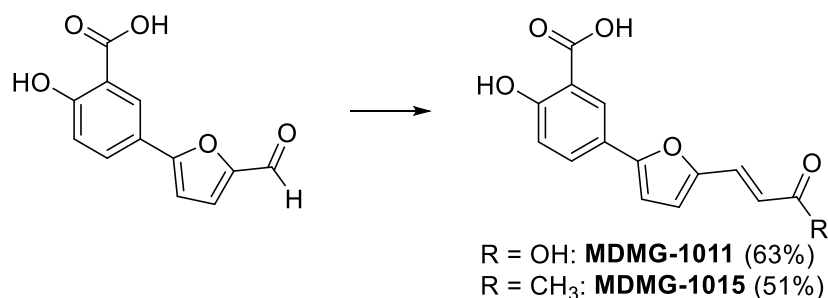
Figure 48. Structure of the photoaffinity probes **MDMG-911** and **MDMG-995**.

This way, compounds **MDMG-409** and **MDMG-672** were used as the base for the design of the probes **MDMG-911** and **MDMG-995**, which structurally belong to the aminomethylfuryl derivatives. Thus, they were also prepared by reductive amination (Scheme 15).

3.4.2.2. Aldol condensation: Results on the synthesis of α,β -unsaturated derivatives.

The formyl group on **MDMG-409** was also used as electrophile counterpart for aldol reaction. In this process, an electrophilic carbonyl group is reacted with a nucleophilic enol or enolate to give a conjugated double bond. When enolizable carbonyl compounds are used, this process allows the preparation of α,β -unsaturated carbonyl products, which in turn are versatile precursors for 1,2 or 1,4-additions of nucleophiles. In our case, these processes would be useful tools for the introduction of structural diversity on the side chain of **MDMG-409**.

To test the feasibility of the aldol reaction on our substrate **MDMG-409**, condensations with structurally simple enolizable compounds were attempted. Aldol reaction with acetic acid and acetone gave rise to the 2-carboxyvinyl derivative **MDMG-1011** and the α,β -unsaturated carbonyl **MDMG-1015**, respectively (Scheme 17).



Scheme 17. Synthesis of α,β -unsaturated derivatives from compound **MDMG-409**. Reaction conditions: For **MDMG-1011**: **MDMG-409** (1 equiv), malonic acid (1.4 equiv), piperidine (4 equiv), anhydrous pyridine, 3 h, 0°C; For **MDMG-1015**: **MDMG-409** (1 equiv), NaOH, acetone/H₂O 1/1, 10 h, rt. Yields refer to the final compounds after purification.

3.4.2.3. Results of the biological evaluation of aminomethylfuryl and α,β -unsaturated carbonyl derivatives of **MDMG-409**.

Once the compounds were prepared we proceeded to the biological evaluation of this family of compounds against *mGO*. Evaluation against *hGO* was also included to compare the results obtained in both enzymes. The colorimetric method that we had been used in previous evaluations was applied and a series of inhibition percentages and IC₅₀s were obtained (Table 16). In order to confirm the reliability of the results we did the test for interferences with the colorimetric enzymatic assay. In this test, significant deviations between 25% and 65% with respect to the control value were observed (Table 17). Again, this situation removed reliability to the biological results and forced the change of the evaluation method. The fluorometric end-point assay using the fluorogenic reagent Amplex[®] Red,¹⁹⁰ as previously done for the spaced derivatives of **MDMG-409**, was then used.

Table 16. Biological data after chemical modification of the formyl group of **MDMG-409**. Comparison with **MDMG-409**. Biological determinations: Enzymatic inhibition on purified mouse and human glycolate oxidase (*mGO* and *hGO*) at single concentration and IC_{50} calculation using the colorimetric method.

Compound	<i>mGO</i> (%) ^a	IC_{50} (μM) ^b <i>mGO</i>	R^{2c}	<i>hGO</i> (%) ^d	IC_{50} (μM) ^b <i>hGO</i>	R^{2c}
MDMG-409	42.7 ± 12.8	38.2 ± 1.2	0.81	15 ± 3.2	n/a	n/a
MDMG-907	93.8 ^e	0.97 ± 1.0	0.98	90.1 ± 1.2	3.4 ± 1.1	0.97
MDMG-911	88.2 ^e	1.3 ± 1.0	0.97	97.2 ± 0.5	4.2 ± 1.2	0.93
MDMG-915	83.0 ^e	2.6 ± 1.1	0.95	54.1 ± 0.8	10.0 ± 1.1	0.97
MDMG-919	8.8 ^e	n/a	n/a	0 ± 1.2	n/a	n/a
MDMG-927	28.2 ^e	n/a	n/a	23.3 ± 1.8	n/a	n/a
MDMG-931	28.2 ^e	n/a	n/a	28.8 ± 2.8	n/a	n/a
MDMG-931I	96.3 ^e	0.29 ± 1.0	0.98	89.3 ± 1.4	2.8 ± 1.1	0.97
MDMG-935	54.6 ^e	9.0 ± 1.1	0.96	30.7 ± 1.3	n/a	n/a
MDMG-935I	88.4 ^e	1.1 ± 1.1	0.98	75.1 ± 0.8	4.1 ± 1.0	0.98
MDMG-995	0 ^e	n/a	n/a	19.6 ± 0.8	n/a	n/a
MDMG-1011	25.1 ^e	n/a	n/a	15.5 ± 1.3	n/a	n/a
MDMG-1015	82.7 ^e	3.6 ± 1.0	0.97	55.2 ± 0.8	15.0 ± 1.1	0.96
MDMG-1074	22.3 ± 1.0	n/a	n/a	27.8 ± 1.8	n/a	n/a
MDMG-1078	29.1 ± 1.9	n/a	n/a	26.2 ± 1.6	n/a	n/a
MDMG-1082	49.4 ± 1.4	14.8 ± 1.1	0.95	47.3 ± 1.0	33.9 ± 1.5	0.94

^aPercentage of inhibition of purified *mGO* with 25 μM , after 1 min. ^b IC_{50} : Calculated in saturated conditions of glycolate (22.2 mM). ^c R^2 : IC_{50} curve-fitted score. ^dPercentage of inhibition of purified *hGO* with 25 μM , after 1 min. Data represented as mean ± SD of n = 3 replicates. ^eNo SD is given. n/a: Not assessed.

Table 17. Interferences of representative derivatives of the lead compound **MDMG-409** with the colorimetric enzymatic assay.

Compound	% Interference colorimetric assay ^a
MDMG-907	44.0 ± 0.9
MDMG-915	27.2 ± 0.4
MDMG-931I	40.8 ± 2.2
MDMG-935	30.5 ± 0.6

^aInterference with the colorimetric method measured at 25 μM of the drug. Data represented as mean ± SD of n = 3 replicates.

Before proceeding with further enzymatic assays, we tested representative compounds for possible interferences with the fluorometric method. As it can be seen (Table 18), in this case, interferences were considerably reduced if compared with the colorimetric method. Only small variations with respect to the control value, reaching a maximum of approximately 19%, were observed, contrary to what happened with the spaced derivatives of **MDMG-409**. Thus, a new method for the determination of the GO enzymatic activity was successfully implemented for this group of compounds.

Table 18. Interferences of representative derivatives of the lead compound **MDMG-409** with the fluorimetric enzymatic assay.

Compound	% Interference fluorometric assay ^a
MDMG-409	10.9 ± 2.7
MDMG-317	2.5 ± 2.2
MDMG-907	13.7 ± 1.9
MDMG-911	9.2 ± 0.2
MDMG-915	13.3 ± 2.1
MDMG-931P	0.9 ± 0.9
MDMG-931I	12.9 ± 1.9
MDMG-935P	10.7 ± 2.9
MDMG-935I	18.8 ± 1.0

^aInterference with the fluorometric method measured at 25 µM of the drug. Data represented as mean ± SD of n = 3 replicates.

Once the use of the fluorometric method had been validated for the evaluation of these compounds, the enzymatic activity against mouse and human GO enzymes was assessed. Only compounds presenting considerably high potencies in the colorimetric assay were evaluated using the new fluorometric method: IC₅₀ values against *mGO* and *hGO* were calculated (Table 19).

Table 19. Biological data of representative derivatives of the lead compound **MDMG-409**. Comparison with **MDMG-409** and **MDMG-317**. Biological determinations: (i) Enzymatic inhibition on purified mouse and human glycolate oxidase (*mGO* and *hGO*) and IC₅₀ calculation using the fluorometric method; (ii) Excreted oxalate in *Agxt1^{-/-}* mouse primary hepatocytes, compared to control (relative oxalate).

Compound	IC ₅₀ (µM) ^a <i>mGO</i>	R ^{2b}	IC ₅₀ (µM) ^a <i>hGO</i>	R ^{2b}	Relative oxalate ^c
MDMG-409	14.5 ± 1.0	0.99	36.5 ± 1.4	0.99	0
MDMG-317	7.5 ± 1.0	0.99	40.6 ± 1.5	0.99	0
MDMG-907	3.1 ± 1.0	0.99	4.2 ± 1.08	0.98	0.37 ± 0.06*
MDMG-911	1.3 ± 1.0	0.99	2.4 ± 1.0	0.99	-0.06 ± 0.09*
MDMG-915	5.4 ± 1.0	0.99	10.1 ± 1.0	0.99	-0.23 ± 0.11*
MDMG-931I	1.7 ± 1.0	0.99	1.4 ± 1.0	0.99	0.29 ± 0.11*
MDMG-935P	8.0 ± 1.0	0.99	15.3 ± 1.1	0.95	-0.08 ± 0.05*
MDMG-935I	0.8 ± 1.0	0.99	1.9 ± 1.0	0.99	0.44 ± 0.16*
MDMG-1015	0.8 ± 1.0	0.99	4.3 ± 1.0	0.99	-0.10 ± 0.06*
MDMG-1125	n/a	n/a	n/a	n/a	0.04 ± 0.12*

^aIC₅₀ values (GO inhibition data were determined by end-point fluorometric method using Amplex Red[®] and HRP: GO concentration 25 nM; glycolate concentration 180 µM). ^bR²: IC₅₀ curve-fitted score. ^cOxalate output decrease 24 h after treatment with 10 µM of the drug in *Agxt1^{-/-}* mouse primary hepatocytes cultured with 5 mM glycolate, in 6-well plates. One-way ANOVA statistical analysis, (*) *p* < 0.05 was considered statistical significant. Data represented as mean ± SD of n = 3 replicates. n/a: Not assessed.

This newly introduced method allowed the proper evaluation of **MDMG-317** (Figure 31), for which an accurate IC_{50} value could not be obtained using the colorimetric assay due to the presence of significant interferences. Evaluation of **MDMG-409** (Figure 31) was also completed, and again the good phenotypic activity (3.45 μ M) did not correlate with the moderate IC_{50} value against *mGO* (14.5 μ M).

In all cases, differences between IC_{50} values obtained for *mGO* and *hGO* were found, being potency on *hGO* between two and five times lower than the one on *mGO* in some cases (Table 19, compounds **MDMG-409**, **MDMG-911**, **MDMG-915**, **MDMG-935P**). Further research will be conducted to elucidate the reason of this difference.

Regarding *mGO* inhibition, a significant improvement in potency with respect to the lead compound **MDMG-409** was observed in all the compounds, aminomethylfuryl and α,β -unsaturated carbonyl derivatives.

Amongst the aminomethylfuryl compounds, we can distinguish between aromatic and aliphatic amines. The first group includes those compounds made by reductive amination using anilines and thus including the aniline functionality on the side chain attached to the furan ring (C5). The second group includes those compounds made by reductive amination using benzylamines, propargylamine and piperidine. Best potencies against *mGO* and *hGO* were obtained with the tertiary aliphatic amines **MDMG-931I** and **MDMG-935I**, together with the aniline **MDMG-911** (deactivated secondary aniline with a *p*-carbonyl substituent), with IC_{50} values ranging between 0.8 and 2.4 μ M (Table 19). Other deactivated secondary anilines, **MDMG-907** (*p*-bromo) and **MDMG-915** (*p*-nitro), were close in potency (IC_{50} = 3.1 and 5.4 μ M against *mGO*, respectively). The activity of compounds carrying activated anilines [**MDMG-923** (*p*-hydroxy) and **MDMG-939** (*p*-methoxy)] could not be assessed, since they were unstable. For the remaining benzylamine derivatives, all of them secondary amines, percentages of inhibition on *mGO* did not reach 30% in the colorimetric assay, so IC_{50} was not determined with the fluorometric assay. Within the rest of aliphatic amines, only the propargylamine **MDMG-935P** was worth evaluating, showing intermediate potency against *mGO* (IC_{50} = 8 μ M).

Regarding α,β -unsaturated carbonyl derivatives of **MDMG-409**, **MDMG-1011**, with an α,β -unsaturated carboxylic acid, resulted to be a poor *mGO*i (Table 16), whilst the α,β -unsaturated ketone **MDMG-1015** was a potent inhibitor against both *mGO* and *hGO* isoenzymes with IC_{50} s of 0.8 and 4.3 μ M, respectively (Table 19).

When tested in hyperoxaluric mouse hepatocytes, compounds **MDMG-911**, **MDMG-915**, **MDMG-935P**, and **MDMG-1015** reduced oxalate excretion to zero with respect to the control. Interesting values ranging between 40 and 60% on oxalate reduction were also achieved by **MDMG-907**, **MDMG-931I**, and **MDMG-935I** (Table 19).

Regarding the outstanding activity profile showed by branched tertiary aliphatic amines, we decided to test a modification on the structure of **MDMG-931I**. The structure of **MDMG-931I** was slightly simplified, following disjunctive structural modulation, by removal of one of the two salicylic heads, leading to compound **MDMG-1125** (Figure 49). Thus, the branched structure would be maintained, but a methylfuryl branch would replace the original methylfurylsalicylate fragment present in **MDMG-931I**. By removing one of the salicylic acid heads, we chased to find out whether this second salicylic fragment is or not essential for the biological activity. Besides, with this modification, both size and polarity of the molecule would be smoothed, which could result beneficial for the activity in cells. For the synthesis of this compound, reductive amination was carried out between the amine **MDMG-931P** and 2-furaldehyde following the general synthetic procedure 6C (Scheme 15). Although the GO inhibitory activity of **MDMG-1125** is still to be assessed, a significant decrease on oxalate production was observed when it was tested at 10 μM in hepatocytes (Table 19).

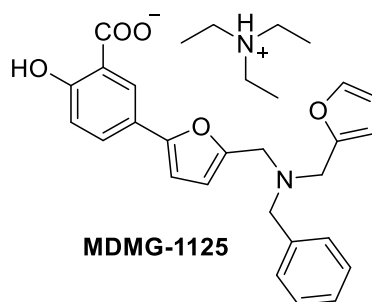


Figure 49. Structure of the tertiary amine **MDMG-1125**.

3.2.4.2. Discussion on the biological activity of aminomethylfuryl and α,β -unsaturated carbonyl derivatives of MDMG-409

Within this family, the most potent *mGOi*'s were the tertiary aliphatic amines **MDMG-931I** and **MDMG-935I**, followed by the three deactivated anilines **MDMG-907**, **MDMG-911** and **MDMG-915**. Thus, the presence of a flat aromatic ring in the side chain hanging from C5 of the furan ring seems to be beneficial for the GO inhibitory activity. The tertiary aliphatic amines have a branched structure that presents a certain similarity with the established *mGOi* **TACA** (see Figure 6 in 2.1.3.1 Biological background).

After those most potent compounds, deactivated secondary anilines **MDMG-907**, **MDMG-911** and **MDMG-915** seem to be better for GO inhibition than activated or deactivated secondary benzylamines. In the case of the secondary benzylamine derivatives, the scarce *mGO* inhibitory activity could be due to the basic nitrogen present in the molecule, which could be detrimental for biological activity. In accordance with this, the piperidine **MDMG-919** did not result a potent *mGOi* either. This observation must however be taken carefully, as, in the case of the piperidine derivative **MDMG-919**, the spatial disposition of the piperidine ring significantly differs from the one adopted by aromatic rings, and this fact could be causing steric issues that hamper the biological activity of this compound.

The main structural feature differing secondary and tertiary benzylamines is the linear or branched geometry that each of them present. This fact could be responsible for the different potency against GO of these two groups of compounds. Different binding modes to the enzyme or different binding sites inside the enzyme could be the consequence of the structural differences, as branched molecules are bulkier and more difficultly access the binding site of linear molecules. To find out whether the molecular geometry is the fact behind the different activity of secondary and tertiary benzylamines, docking and crystallographic studies are currently ongoing.

The branched tertiary amines **MDMG-931I** and **MDMG-935I**, as well as the deactivated anilines **MDMG-907**, **MDMG-911** and **MDMG-915**, which resulted to be the most potent *mGOi*'s within this set, meet the preliminary structure-activity relationship previously established for salicylates. The flexibility conferred by the presence of the aminomethylfuryl linker would allow the adoption of a V-shaped conformation with a *syn* disposition of the two aromatic moieties. This kind of disposition would enable simultaneous interaction with the active site of GO and the Trp110 located at the

access channel. In order to verify this hypothesis, *in silico* studies will be conducted with these compounds.

To proceed with a proper enzymatic evaluation of this set of compounds, a fluorometric assay needed to be introduced. Thus, the previous colorimetric assay that had led to significant interferences when key compounds were tested was replaced by this new method, which also serves as a double-check evaluation of the previous enzymatic results. This also allowed the evaluation of furylsalicylate **MDMG-317**, which had presented important interferences with the previous colorimetric method. Besides, with the implementation of the more sensitive fluorometric method, more accurate determinations were conducted: standard deviations were considerably reduced between replicates and R-squared values remarkably improved. Furthermore, a substantial reduction of the reagents and enzyme amounts led to a reduction of the cost per assay.

3.3. LDH inhibition

As mentioned above, the biological mechanism of action for some of the salicylates included in this study remains unclear. Some compounds induced a significant diminution in the oxalate production by *Agxt1^{-/-}* mouse hepatocytes in culture while having a modest effect on GO inhibition. Hence, the possibility of additional targets for these compounds was considered, and LDHA (hepatic isoenzyme) was contemplated as a plausible option. LDHA inhibition has been previously proposed as a promising target for the treatment of PH's. In fact, it has been recently published that siRNA-mediated LDHA inhibition achieve efficient oxalate reduction and prevents the deposition of calcium oxalate crystals in mice and non-human primates.¹¹⁶ Besides, the antiepileptic drug stiripentol has been newly identified as a LDHA inhibitor able to decrease urinary oxalate excretion in a PH1 patient, showing for the first time the potential of LDHA inhibition using small drugs.¹¹⁸

It is known that both GO and LDHA are able to metabolize the same substrate, glyoxylate. This way, it is logical to think that substrate analogs could be able to behave as double GO/LDHA inhibitors. Our GOi's, with a salicylic polar head, were designed to behave as substrate analogues of GO. Thus, it was contemplated that they could also be able to bind the active site of LDHA, which would lead to double GO/LDHA inhibition. Both inhibitory activities would be additive leading to an enhancement of the phenotypic effect of oxalate decrease on cellular culture.

Furthermore, LDHA inhibition would give utility to our compounds, not only for the treatment of PH1, but also for PH2 and PH3, since LDHA is involved in oxalate formation in the three types of PH.

3.3.1. Results

With the aim of exploring the *h*LDHA inhibitory activity of salicylic acid derivatives, the most potent *m*GOi's, as well as the compounds presenting discrepancy between enzymatic potency and phenotypic effect, were evaluated against *h*LDHA. Initially, a screening was performed at 10 μ M, dose at which these compounds exert their biological effect in cells. This preliminary evaluation was performed using a commercial kit (BioVision Incorporated, Milpitas, CA, USA) based on a kinetic colorimetric protocol, in which the absorbance was measured at 450 nm. As a result, significant percentages of inhibition were achieved for some compounds (Table 20).

Table 20. Percentage of inhibition against *h*LDHA of representative salicylate derivatives, determined by colorimetric assay (commercial kit). Comparison with **MDMG-409** and **MDMG-317**. Biological determinations: Enzymatic inhibition on human *h*LDHA at single concentration using the colorimetric method.

Compound	<i>h</i> LDHA (%) ^a	Compound	<i>h</i> LDHA (%) ^a
MDMG-409	60.9 \pm 9.1	MDMG-911	76.4 \pm 10.1
MDMG-317	62.2 \pm 14.1	MDMG-915	69.3 \pm 3.7
MDMG-672	17.0 \pm 20.1	MDMG-931P	78.1 \pm 10.0
MDMG-540	27.8 \pm 30.0	MDMG-931I	99.1 \pm 4.3
MDMG-566	47.5 \pm 19.3	MDMG-935P	90.1 \pm 43.3
MDMG-570	3.7 \pm 14.0	MDMG-991	64.7 \pm 23.3
MDMG-907	84.3 \pm 6.6	MDMG-995	97.5 \pm 8.6

^aPercentage of inhibition of recombinant *h*LDHA at 10 μ M of the drug. Data represented as mean \pm SD of n = 3 replicates.

Since the colorimetric kit did not allow interference quantification and its use was limited to a preliminary screening of potential inhibitors, a fluorometric protocol was implemented to completely characterize the *h*LDHA inhibitory activity of the most interesting compounds. Described colorimetric protocols to assess LDHA inhibitory activity measure NADH disappearance as it is oxidized into NAD⁺, and this process is detected through the diminution of NADH absorbance at 340 nm.¹⁹⁸ However, colorimetric interferences at such wavelength were detected for our compounds, with overlapping absorbance peaks. Thus, the implementation of a kinetic fluorometric method was preferred. In the chosen fluorometric protocol, NADH fluorescence is measured in the presence of recombinant LDH and the substrate pyruvate, at λ_{ex} 340 nm and λ_{em} 460 nm. In this method, the decrease of NADH fluorescence is monitored for 10 minutes, obtaining a negative slope, which results smoothed when a LDH inhibitor is introduced in the assay.^{199,200} Besides, by the use of this kinetic method, the determination of possible interferences can be accomplished within the same assay: the kinetic mode allows the correction of slight interferences by subtraction of the

baseline reading,^{199,200} enabling the identification of compounds interfering with NADH fluorescence.

Thus, using the fluorometric method, the most potent *mGOi*'s were again screened against *hLDHA* at 10 μM to exclude the less potent molecules (Table 21), and choose the most potent ones for IC_{50} determination. We obtained similar results with both of the evaluation methods (colorimetric and fluorometric) (Table 20 vs Table 21).

3.3.1.1. Evaluation of aminomethylfuryl derivatives and α,β -unsaturated carbonyl derivatives against *hLDH*.

a) *hLDHA* isoenzyme

Using the fluorometric evaluation method against *hLDHA*, good percentages of inhibition (Table 21) were achieved in all cases except for the secondary electron-rich benzylamines **MDMG-1074** and **MDMG-1078**, the pyridine **MDMG-927**, and the piperidine **MDMG-919** (Table 15). These compounds were therefore discarded from further analysis. IC_{50} s against *hLDHA* were determined for the rest of compounds, as well as for the lead compounds **MDMG-409** and **MDMG-317** (Figure 31), and the phenolic derivative **MDMG-672** (Table 6), given the possible existence of additional biological targets for them. Curiously, the most potent GO inhibitors presented also the best activities against *hLDHA*: the deactivated anilines **MDMG-907**, **MDMG-911** (Table 15) and the tertiary benzylamine **MDMG-931I** (Figure 47) showed IC_{50} values below 1 μM (Table 21). Notable potency against *hLDHA* was also achieved by **MDMG-915** (with *p*-nitroaniline side chain), **MDMG-931P**, **MDMG-935P** (both secondary aliphatic amines), **MDMG-935I** and **MDMG-1125** (both tertiary aliphatic amines), with IC_{50} values between 1.6 and 2 μM (Tables 15 and 21 and Figures 47 and 49). In the case of **MDMG-931P** and **MDMG-935P** (Table 15), which were modest *mGOi*'s (Tables 16 and 19), potency over *hLDHA* was considerable higher in comparison with the one over GO (Table 21). Finally, lead compounds **MDMG-409** and **MDMG-317** (Figure 31), as well as the *p*-nitro substituted benzylamine **MDMG-1082** (Table 15), showed modest *hLDHA* inhibition with IC_{50} s between 7 and 9 μM (Table 21). Though still modest, in the case of **MDMG-1082**, this inhibitory activity was also significantly higher than the one against GO (Tables 16 and 21).

Interestingly, the photoaffinity probe **MDMG-995** (Figure 48), which was totally unable to inhibit GO (Table 16), resulted a potent *h*LDHA inhibitor ($IC_{50} = 2 \mu\text{M}$), being so far the only pure LDH inhibitor among the studied compounds (Table 21).

Table 21. Biological data of the aminomethyl derivatives and α,β -unsaturated carbonyl derivatives on recombinant *h*LDHA and *h*LDHB enzymes, determined by a fluorometric assay. Comparison with **MDMG-409**, **MDMG-317** and **MDMG-672**. Biological determinations: Enzymatic inhibition on *h*LDHA and *h*LDHB at a single concentration and IC_{50} calculation using the fluorometric method.

Compound	<i>h</i> LDHA (%) ^a	IC_{50} (μM) ^b <i>h</i> LDHA	R^{2c}	<i>h</i> LDHA (%) ^d	IC_{50} (μM) ^b <i>h</i> LDHB	R^{2c}
MDMG-409	44.0 \pm 3.2	9.4 \pm 1.1	0.97	10 \pm 6.0	ND ^g	n/a
MDMG-317	29.4 \pm 7.1	6.8 \pm 1.1	0.97	0 \pm 16.5	ND ^g	n/a
MDMG-672	44.8 \pm 6.2	ND ^e	n/a	0 \pm 9.1	ND ^g	n/a
MDMG-907	89.6 \pm 2.2	0.6 \pm 1.1	0.98	93.5 \pm 5.2	1.1 \pm 1.1	0.97
MDMG-911	103.8 \pm 7.5	0.6 \pm 1.1	0.97	81.7 \pm 5.6	0.3 \pm 1.1	0.96
MDMG-915	111.7 \pm 10.4	1.7 \pm 1.1	0.98	91.4 \pm 4.3	ND ^h	n/a
MDMG-919	23.0 \pm 5.2	ND ^e	n/a	ND ^f	n/a	n/a
MDMG-927	33.7 \pm 2.7	ND ^e	n/a	ND ^f	n/a	n/a
MDMG-931P	88.8 \pm 2.5	2.2 \pm 1.1	0.97	46.5 \pm 6.0	ND ^g	n/a
MDMG-931I	95.3 \pm 6.4	0.4 \pm 1.3	0.92	84.7 \pm 8.4	0.2 \pm 1.1	0.97
MDMG-935P	116.8 \pm 7.0	2.0 \pm 1.0	0.98	29.1 \pm 6.5	ND ^g	n/a
MDMG-935I	102.1 \pm 9.2	1.6 \pm 1.1	0.97	71.1 \pm 14.7	ND ^h	n/a
MDMG-995	107.2 \pm 8.3	2.0 \pm 1.1	0.98	75.1 \pm 2.7	ND ^h	n/a
MDMG-1015	97.9 \pm 4.9	3.7 \pm 1.2	0.96	3.9 \pm 2.9	ND ^g	n/a
MDMG-1074	18.3 \pm 3.0	ND ^e	n/a	ND ^f	n/a	n/a
MDMG-1078	30.6 \pm 4.2	ND ^e	n/a	ND ^f	n/a	n/a
MDMG-1082	73.0 \pm 4.8	8.0 \pm 1.1	0.98	22.7 \pm 17.1	ND ^g	n/a
MDMG-1125	100.9 \pm 1.2	2.2 \pm 1.0	0.98	12.7 \pm 16.9	ND ^g	n/a

^aPercentage of inhibition of purified *h*LDHA at 10 μM . ^b IC_{50} (pyruvate concentration 1 mM). ^c R^2 : IC_{50} curve-fitted score. ^dPercentage of inhibition of purified *h*LDHB at 10 μM . ^eNo IC_{50} was determined as the percentage of inhibition at 10 μM was lower than 50%. ^fPercentage of inhibition of purified *h*LDHB was not assessed as the percentage of inhibition of *h*LDHA at 10 μM was lower than 50%. ^gNo IC_{50} was determined as the percentage of inhibition of *h*LDHB is low. ^hOngoing IC_{50} determination. Data represented as mean \pm SD of $n = 3$ replicates. n/a: Not assessed.

b) *h*LDHB isoenzyme

Since specific *h*LDHA inhibition would be advisable for the development of a safe treatment for PH1, IC₅₀ values against *h*LDHB (Table 21) were also calculated for the most potent *h*LDHA inhibitors in order to determine their selectivity for the hepatic isoform.

The most potent *h*LDHA inhibitors were also very potent *h*LDHB inhibitors. In the case of **MDMG-911** and **MDMG-9311**, potency against *h*LDHB resulted two-fold increased if compared to the one against *h*LDHA, with IC₅₀s of 0.3 and 0.2 μM, respectively. On the contrary, **MDMG-907** showed almost half potency for *h*LDHB (IC₅₀ = 1 μM) when compared to *h*LDHA (IC₅₀ = 0.6 μM). This difference in the activities against both isoenzymes is not enough, however, to treat **MDMG-907** as a selective *h*LDHA inhibitor.

In contrast, other more modest *h*LDHA inhibitors present a more selective activity profile, if we compare the percentages of inhibition that they exert against both *h*LDHA and *h*LDHB isoenzymes:

- At a 10 μM dose, the small compounds **MDMG-409** and **MDMG-317** produce only a 10% and a 0% inhibition of *h*LDHB vs the 44% and 29% that they produce against *h*LDHA, respectively. These compounds lack any kind of side chain beyond the furan ring attached to the salicylic head (except for a formyl group in **MDMG-409**) and present a rigid linear structure (Figure 31).
- The aliphatic amine **MDMG-935P** inhibits 100% of the *h*LDHA activity at 10 μM while it only produces a 29% of *h*LDHB inhibition at the same dose. Though it is a rough comparison, it could mean a three-fold higher potency against *h*LDHA than against *h*LDHB. **MDMG-935P** is a secondary aliphatic amine lacking aromatic side chains and presenting a propargyl rest instead (Table 15).
- Compound **MDMG-1125**, with a 12% inhibition percentage against *h*LDHB and a 100% inhibition percentage against *h*LDHA at 10 μM, presents approximately a 8/1 selectivity ratio in favour of *h*LDHA. **MDMG-1125** (Figure 49) is a tertiary benzylic amine, designed by structural simplification of **MDMG-9311**.
- Compound **MDMG-1015** presents a 24/1 selectivity ratio in favour of *h*LDHA, if we compare the 100% and the 4% inhibition percentages that it presents against *h*LDHA and *h*LDHB, respectively. This compound is a α,β-unsaturated carbonyl derivative with no aromatic side chains beyond the furan ring (Scheme 17).

3.3.1.2. Evaluation of derivatives with two-atom nitrogen-based spacers against *h*LDH.

Representative spaced derivatives of the lead compound **MDMG-409** were also evaluated against *h*LDHA. In this case, more modest inhibitory activities were observed (Table 22), and only compounds **MDMG-566**, **MDMG-991** and **MDMG-1058I** inhibited more than 50% of the enzymatic activity. Once again, compounds with electron-deficient aromatic side-chains.

Table 22. Inhibitory activities of the spaced derivatives of **MDMG-409** with methylamino linkers on recombinant *h*LDHA, determined by fluorometric assay. Comparison with **MDMG-409** and **MDMG-317**.

Compound	<i>h</i> LDHA (%) ^a	IC ₅₀ (μM) ^b <i>h</i> LDHA	R ^{2c}
MDMG-409	44.0 ± 3.2	9.4 ± 1.1	0.97
MDMG-317	29.4 ± 7.1	6.8 ± 1.1	0.97
MDMG-540	38.4 ± 8.4	ND ^d	n/a
MDMG-566	86.5 ± 4.1	12.1 ± 1.2	0.96
MDMG-570	20.2 ± 2.4	ND ^d	n/a
MDMG-592	42.5 ± 10.6	ND ^d	n/a
MDMG-963	37.4 ± 3.0	ND ^d	n/a
MDMG-963I	35.9 ± 15.0	ND ^d	n/a
MDMG-971	37.2 ± 5.7	ND ^d	n/a
MDMG-991	74.4 ± 4.3	n/a	n/a
MDMG-1054	36.6 ± 5.4	ND ^d	n/a
MDMG-1058P	16.0 ± 3.8	ND ^d	n/a
MDMG-1058I	93.9 ± 1.2	4.5 ± 1.1	0.97

^aPercentage of inhibition of purified *h*LDHA at 10 μM. ^bIC₅₀ (pyruvate concentration 1 mM). ^cR²: IC₅₀ curve-fitted score. n/a: Not assessed. Data represented as mean ± SD of n = 3 replicates. ^dNo IC₅₀ was determined as the percentage of inhibition at 10 μM was lower than 50%. n/a: Not assessed.

3.3.2. Discussion

In general, best results in term of inhibitory potency against both GO and LDH, have been obtained with those derivatives of **MDMG-409** designed by enlargement of the structure introducing side chains beyond the furan ring. Aromatic, electron-deficient side chains separated from the salicylic acid polar head by a flexible aminomethylfuryl linker were the most successful ones, giving rise to double GO/LDH inhibitors of high potency (IC_{50} s in the low micromolar range) (Figure 50). From what we have observed so far, these potent *h*LDH inhibitors present no selectivity between *h*LDHA and *h*LDHB isoenzymes.

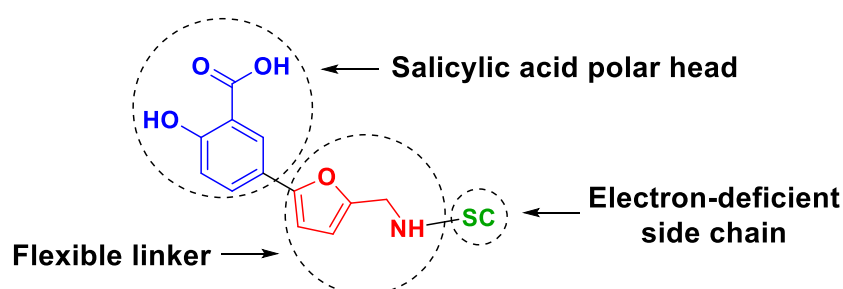


Figure 50. General structure of double GO/LDH inhibitors.

In fact, the deactivated secondary anilines **MDMG-907** and **MDMG-911**, as well as the tertiary benzylamine **MDMG-931I**, showed the best IC_{50} values against both, GO and *h*LDHA enzymes. This means that linear as well as branched structures are allowed in both enzymes. We are currently studying whether these different molecular geometries lead to different binding modes.

In this line, in the case of the lead compounds **MDMG-317** and **MDMG-409**, the absence of side chains attached to the furan ring, led to moderate IC_{50} values on GO and LDHA. In these two compounds, the moderate potency achieved against LDHA is still not sufficient to justify the phenotypic effect in culture, and therefore, they might be exerting the phenotypic effect through alternative biological targets.

If we compare the structural requirements for achieving GO and LDHA inhibition, this last enzyme allows the presence of a wider variety of substituents, not only aromatic rings, on the side chain attached to the furan ring (see general structure in Figure 50). For example, the propargylamine in **MDMG-935P** (though it is still a π -system).

In terms of *h*LDHA and *h*LDHB selectivity, it seems to be related to the presence of an aromatic side chain attached to the furan ring, on the general structure above

(Figure 50). Thus, the absence of aromatic side chains apparently means a loss of potency against *h*LDH that is more evident in the case of *h*LDHB than in the case of *h*LDHA and this way it leads to certain selectivity. However, the branched compound **MDMG-1125** presents some isoenzyme selectivity despite of holding aromatic side chains. This could support the idea of a different binding pattern for branched compounds vs linear ones that would mean as well a different selectivity mechanism.

Apart from compounds matching the general structure above (Figure 50), α,β -unsaturated carbonyl derivatives, such as **MDMG-1015**, are interesting in terms of GO and LDH inhibitory potency and selectivity between LDHA and LDHB isoenzymes. Once more, **MDMG-1015** is to some grade selective and lacks aromatic side chains beyond the furan ring.

For the first time, LDHA inhibitory activity has been attributed to salicylates, which represents an unprecedented feature for these compounds. This study supposes a step forward in understanding the biological activity of these compounds, since their mechanism of action is not fully determined so far. Furthermore, it shows the potential use of multi-target drugs for PH1 treatment, an unexplored field of research. It is well known that multi-target drugs could be more effective and safer than pure inhibitors,²⁰¹ and also present better ADME properties than genetic therapies such as siRNA.¹¹⁶ This, along with the drug-like structure and easy synthesis of our active compounds, makes them promising candidates for future drug development.

4. Conclusions/Conclusiones

4. Conclusions

1. On the basis of the structural requirements previously established for GO inhibitors, two novel families of enzymatic inhibitors have been prepared: oxamic acid derivatives and salicylic acid derivatives.

2. A total of 70 new compounds, belonging to these two new families, have been synthesized, purified and characterized, as well as evaluated against recombinant *mGO* and *hGO* enzymes and over hyperoxaluric mouse primary hepatocytes, in order to assess their efficacy on oxalate decrease.

3. Among the oxamic acid derivatives, 2-oxoacetic acid derivatives were more potent against GO than 3-oxopropanoic acid and 4-oxobutanoic acid derivatives, showing that the introduction of one or two carbon atoms spacing the carbonyl groups in the polar head worsens the biological activity of these compounds.

4. Oxamic acid derivatives, apart from presenting interferences with the colorimetric method used for their enzymatic evaluation, did not show efficacy on oxalate reduction, what led to the abandonment of this structural family.

5. Among the salicylic acid derivatives, furylsalicylates have been identified as good GO inhibitors and efficient agents reducing oxalate production in hyperoxaluric mouse primary hepatocytes, showing IC_{50} and EC_{50} values at the low micromolar range.

6. For some compounds, significant discrepancies between the GO inhibitory activity and the phenotypic effect on cells were found, and therefore the presence of off-targets was suggested for these compounds.

7. On the basis of the biological data gathered and the docking predictions, preliminary structure-activity relationships have been established for salicylates with GO inhibitory activity and capacity to reduce oxalate production in hyperoxaluric mouse primary hepatocytes.

8. The salicylic acid polar head, interacting at the binding region 1, must contain free carboxy and hydroxy functionalities, and needs to be substituted on C5.

4. Conclusions

9. The hydrophobic tail, interacting at the binding region 2, should contain electron-deficient aromatic systems or a furan ring for a better interaction with the binding region 2 residues.

10. A flexible linker should be placed spacing the polar head from the hydrophobic tail. This flexible linker allows a *syn* orientation of the rings in the polar head and the side chain, favouring the establishment of key interactions with the enzyme GO.

11. The introduction of 2-atom nitrogen-based linkers can be followed as a strategy for structural modulation of furylsalicylates. Within the spaced derivatives, C4 isomers containing rigid imino and azo linkers were the most potent compounds against GO, whilst the best efficacy on oxalate diminution was achieved with the C5 isomers carrying flexible methylamino linkers. These last ones reduced oxalate production by 30-60% when tested *in vitro* at 10 μM on *Agxt1*^{-/-} mouse hepatocytes.

12. Compounds with an aminomethylfuryl flexible linker are elongated derivatives of the lead compound **MDMG-409**. Derivatives containing anilines and aliphatic amines as side chains, showed to be potent GO inhibitors, and were also able to reduce oxalate production by 50-100% when tested *in vitro* at 10 μM on *Agxt1*^{-/-} mouse hepatocytes.

13. Within the aminomethylfuryl derivatives, side chains containing deactivated secondary anilines, as well as branched tertiary benzylamines, gave the most potent GO inhibitors, presenting IC₅₀ values between 0.8 and 5 μM .

14. The most potent aminomethylfuryl derivatives against GO were also potent compounds against LDHA, presenting remarkable IC₅₀ values between 0.6 and 1.7 μM , and in some cases, certain selectivity for the hepatic isoform. Thus, these compounds can be considered dual GO/LDH inhibitors, and constitute a promising multi-target approach for the treatment of PH1.

15. Two photoaffinity probes derived from compounds **MDMG-409** and **MDMG-672** have been successfully synthesized and will allow the implementation of a chemoproteomic study aimed at discovering additional biological targets.

4. Conclusiones

1. Tomando como base los requisitos estructurales previamente establecidos para el desarrollo de inhibidores de la enzima GO, se ha llevado a cabo preparación de dos nuevas familias de inhibidores enzimáticos: derivados de ácido oxámico y derivados de ácido salicílico.

2. Un total de 70 nuevos compuestos pertenecientes a estas dos familias han sido sintetizados, purificados y caracterizados, así como evaluados biológicamente frente a las enzimas recombinantes *mGO* y *hGO*, y sobre hepatocitos de ratón hiperoxalúrico, con objeto de medir su eficacia en la reducción de oxalato.

3. Dentro de los derivados de ácido oxámico, los compuestos derivados del ácido 2-oxoacético demostraron ser más potentes frente a GO que los derivados del ácido 3-oxopropanoico y del ácido 4-oxobutanoico, comprobándose cómo la introducción de un espaciador de uno o dos carbonos entre los grupos carbonilo de la cabeza polar repercute negativamente en la actividad biológica de estos compuestos.

4. Los derivados de ácido oxámico, además de presentar interferencias con el método colorimétrico empleado para su evaluación enzimática, no mostraron eficacia en la reducción de oxalato, lo que llevó al abandono de esta familia estructural.

5. Dentro de los derivados de ácido salicílico, los furilsalicilatos han sido identificados como potentes inhibidores GO, y como agentes eficientes en la reducción de oxalato en hepatocitos, mostrando valores de CI_{50} y CE_{50} en el rango micromolar bajo.

6. Para algunos compuestos, se han encontrado discrepancias significativas entre la actividad inhibitoria de GO y el efecto fenotípico en células, lo que ha llevado a pensar en la existencia de dianas biológicas alternativas para estos compuestos.

7. En base a los resultados biológicos obtenidos, así como a los estudios de docking realizados, se han extraído relaciones estructura actividad preliminares para salicilatos que poseen actividad moderada frente a GO y capacidad para reducir la producción de oxalato en hepatocitos de ratón hiperoxalúrico.

8. La cabeza polar de ácido salicílico, que interacciona con la región de unión 1, debe contener los grupos carboxilo e hidroxilo libres, y debe estar sustituida en el C5.

4. Conclusiones

9. La cola hidrofóbica, que interacción con la región de unión 2, debe contener sistemas aromáticos deficientes en electrones o un anillo de furano para conseguir una mejor interacción con los residuos de la región de unión 2.

10. La presencia de un espaciador flexible entre la cabeza polar y la cola hidrofóbica es beneficioso para la actividad inhibitoria de GO. Este espaciador flexible permite una orientación *syn* de los anillos de la cabeza polar y de la cadena lateral, lo que favorece el establecimiento de interacciones clave con la enzima GO.

11. La introducción de espaciadores de dos átomos conteniendo nitrógeno puede ser seguida como estrategia para la modulación estructural de los furilsalicilatos. Dentro de los derivados espaciados, los isómeros C4, portando espaciadores rígidos tipo imina y tipo azo, demostraron ser los inhibidores GO más potentes, mientras que los isómeros C5 portando espaciadores flexibles tipo metilamino, fueron los más eficaces en la reducción de oxalato. Estos últimos fueron capaces de reducir la producción de oxalato un 30-60% cuando se testaron *in vitro* a 10 μM sobre hepatocitos de ratón *Agxt1^{-/-}*.

12. Los compuestos con un espaciador flexible tipo aminometilfural son derivados elongados del compuesto líder **MDMG-409**. Los derivados con anilinas y aminas alifáticas como cadenas laterales demostraron ser los inhibidores de GO más potentes, y también fueron capaces de reducir la producción de oxalato un 50-100% cuando se testaron *in vitro* a 10 μM sobre hepatocitos de ratón *Agxt1^{-/-}*.

13. Dentro de los aminometilfural derivados, las cadenas laterales con anilinas secundarias desactivadas, así como las bencilaminas terciarias ramificadas, resultaron ser los inhibidores GO más potentes, con valores de IC_{50} comprendidos entre 0.8 y 5 μM .

14. Los aminometilfural derivados más potentes frente a GO demostraron ser también potentes inhibidores de la enzima LDHA, con destacados valores de IC_{50} comprendidos entre 0.6 y 1.7 μM , y presentando en algún caso cierta selectividad sobre a la isoenzima hepática. Así, estos compuestos, que pueden ser considerados como inhibidores dobles GO/LDH, constituyen una prometedora aproximación multi-diana para el tratamiento de HP1.

15. Se han sintetizado de forma satisfactoria dos sondas de fotoafinidad derivadas de los compuestos **MDMG-409** y **MDMG-672**, las cuales permitirán llevar a cabo un estudio de quimioproteómica encaminado al descubrimiento de dianas biológicas alternativas.

5. Experimental section

5. Experimental section

5.1. General Experimental Methods

5.1.1. Chemistry

All solvents and chemicals were used as purchased without further purification. The progress of the reactions was controlled by thin layer chromatography (TLC) on aluminum plates (Merck AL silica gel 60 F254) and detected by UV lamp (254 nm) or employing a solution of vanillin (6 g) and concentrated sulfuric acid (2.5 mL) in ethanol (250 mL) and heating. Small scale microwave-assisted synthesis was carried out in sealed vessels using a Biotage initiator microwave with automatic arm and controlled irradiation at 2.450 GHz (Biotage AB, Upsala). These parameters were established following the basic principles of microwave assisted organic synthesis. The temperature was measured with an IR sensor on the outside of the reaction vessel. Purification by flash chromatography was performed on silica gel Merck 60 (230–400 mesh ASTM). ^1H NMR and ^{13}C NMR spectra have been recorded in a two-channel 300 MHz Varian Inova Unity, a two channel 400 MHz Varian direct drive, a three-channel 500 MHz Varian direct drive and a two-channel 500 MHz Bruker Avance NEO spectrometer using CD_3OD , $(\text{CD}_3)_2\text{SO}$, $(\text{CD}_3)_2\text{CO}$, CDCl_3 , or D_2O . Chemical shifts (δ) are quoted in parts per million (ppm) and are referenced to residual H in the deuterated solvent as the internal standard. Coupling constants (J) are expressed in Hz. Splitting patterns are designated as follows: s, singlet; d, doublet; dd, double doublet; ddd, double double doublet; t, triplet; ddt, double double triplet; tt, triple triplet; q, quartet; p, pentet; m, multiplet; b, broad. High resolution mass spectra (HRMS) were recorded by time-of-flight (TOF) mass spectrometry with electrospray ionization (ESI) in positive or negative mode, using a time-of-flight apparatus with orthogonal acceleration LCT Premier. Low resolution mass spectra (LRMS) were recorded by ESI in positive or negative mode, coupled to high resolution liquid chromatography (LC–MS) in a simple quadrupole Agilent 6110 instrument equipped with a Zorbax Eclipse XDB-C18 4.6 mm \times 150 mm column. Purity of the compounds was assessed by high pressure liquid chromatography (HPLC) using an Agilent 1200 instrument with diode-array detector equipped with a Zorbax Eclipse XDB-C18 4.6 mm \times 150 mm column. Column temperature was set at 25 °C. Absorbance was measured at 214 and 254 nm. Purity of most final compounds was higher than 95% and, in every case, higher than 90%.

Melting points (mp) were taken in open capillaries on a Gallenkamp melting point apparatus and are uncorrected.

5.1.2. Biology

A Multiskan™ FC Microplate Photometer (Thermo Fisher) was used to measure absorbance and an EnSpire® Multimode Plate Reader (PerkinElmer) was used to measure absorbance and fluorescence. For the most potent GO inhibitors, colorimetric and fluorescence interference tests were performed by measuring absorbance at 515 nm and 590 nm and fluorescence with λ_{ex} 560 nm and λ_{em} 590 nm, respectively.

All the experiments related to cell culture were performed by Prof. E. Salido group (University of La Laguna), as well as most of the GO colorimetric assays. The rest of colorimetric assays both on GO and LDH, as well as the fluorometric assays on both enzymes, along with their interference tests, were performed by the doctoral candidate as part of the thesis project at the Scientific Instrumentation Center at the University of Granada (CIC).

5.1.3. HPLC Methods

5.1.3.1. HPLC methods for Purity Determination

General HPLC setup: flow 0.8 mL/min; solvent A [water (0.1% HCOOH)/acetonitrile (0.1% HCOOH)]; solvent B [acetonitrile (0.1% HCOOH) 100%].

Method 1. Detector λ = 214, 254 nm; solvent A [water (0.1% HCOOH)/acetonitrile (0.1% HCOOH) 95/5]; isocratic A 2 min + gradient A \rightarrow B 17 min + isocratic B 2 min.

Method 2. Detector λ = 214, 254 nm; solvent A [water (0.1% HCOOH)/acetonitrile (0.1% HCOOH) 90/10]; isocratic A 2 min + gradient A \rightarrow B 17 min + isocratic B 2 min.

Method 3. HPLC setup: detector λ = 214, 254 nm; solvent A [water (0.1% HCOOH)/ acetonitrile (0.1% HCOOH) 80/20]. Isocratic A 2 min + gradient A \rightarrow B 17 min + isocratic B 2 min.

Method 4. HPLC setup: detector λ = 214, 254 nm; solvent A [water (0.1% HCOOH)/acetonitrile (0.1% HCOOH) 70/30]; isocratic A 2 min + gradient A \rightarrow B 17 min + isocratic B 2 min.

Method 5. Detector $\lambda = 214, 254$ nm; solvent A [water (0.1% HCOOH)/acetonitrile (0.1% HCOOH) 60/40]; isocratic A 2 min + gradient A \rightarrow B 17 min + isocratic B 2 min.

5.1.3.2. HPLC methods for colorimetric interferences

The colorimetric interference test by HPLC was performed with compounds **MDMG-317, MDMG-409, MDMG-566, MDMG-592, MDMG-604, MDMG-672, MDMG-963, MDMG-911, MDMG-995**. HPLC setup: detector $\lambda = 515, 590$ nm; solvent A [water (0.1% HCOOH)/ acetonitrile (0.1% HCOOH) 80/20]. Isocratic A 2 min + gradient A \rightarrow B 17 min + isocratic B 2 min.

5.2. General synthetic procedures

5.2.1. General synthetic procedure 1: Aniline acylation with ethyl 2-chloro-2-oxoacetate and ethyl 3-chloro-3-oxopropanoate.

A solution of the corresponding aniline (1 equiv) in anhydrous tetrahydrofuran (THF) (10-30 mL/mmol aniline) was prepared under argon atmosphere in a round bottom flask equipped with a stirring bar. Over that solution, trimethylamine (3 equiv) and the corresponding acyl chloride (2 equiv) were slowly added (in that order), and reaction was allowed to stir at room temperature (rt) for 24 h. The mixture was then concentrated in rotavapor, and the crude residue was purified by flash column chromatography.²⁰²

5.2.2. General synthetic procedure 2: Aniline acylation with succinic anhydride.

A solution of the corresponding aniline (1 equiv) in anhydrous toluene (20-30 mL/mmol aniline) was prepared under argon atmosphere in a round bottom flask equipped with a stirring bar. Succinic anhydride (1.1 equiv) was then added at rt and the reaction was refluxed for 3 h. The mixture was then concentrated in rotavapor to reduce solvent volume and the precipitate formed was washed with toluene on a filter plate.²⁰³

5.2.3. General synthetic procedure 3: Basic hydrolysis of ethyl esters.

A solution of the corresponding ethyl ester (1 equiv) in THF/H₂O 1/1 (10 mL/mmol ethyl ester) was prepared in a round bottom flask equipped with a stirring bar and a 1N solution of sodium hydroxide (5 equiv) was added at rt. The reaction was allowed to stir at rt for 2 h. THF was then evaporated in rotavapor and the precipitate formed was washed with water on a filter plate.²⁰⁴

5.2.4. General synthetic procedure 4: Boc deprotection.

A solution of the corresponding Boc-protected amino derivative in trifluoroacetic acid/dichloromethane (DCM) 3/7 (100 mL/mmol of Boc-protected amino derivative) was prepared in a round bottom flask equipped with a stirring bar. The reaction was allowed

to stir at rt for 3 h and then HCl 5% (300 mL/mmol of Boc-protected amino derivative) was added. After that, the mixture was concentrated in rotavapor.²⁰⁵

5.2.5. General synthetic procedure 5: Suzuki–Miyaura (SM) cross-coupling.

5.2.5.1. Method A

A solution of potassium carbonate (3 equiv) in water (4 mL/mmol of halide) was prepared in a microwave vial equipped with a stirring bar. After dissolution, dimethylformamide (DMF) was added (2 mL/mmol of halide) and the mixture was degassed by bubbling with argon. Consecutively the corresponding halide (1 equiv), the boronate derivative (1.2 equiv), triphenylphosphine (15 mol%), palladium acetate (5 mol%), and DMF (2 mL/mmol of halide) were added in that sequence.²⁰⁶ The mixture was then degassed by argon bubbling during 10 min after which the vial was sealed and the reaction was set in a microwave instrument. The reaction was programmed in a microwave instrument for heating at 100/150 °C during 3 h (45 s prestirring). Then, ethyl acetate was added to the reaction crude, which was washed with water and brine. The organic layer was dried over anhydrous magnesium sulphate and evaporated in rotavapor. The final crude was purified by flash column chromatography on silica gel.

5.2.5.2. Method B

A solution of potassium carbonate (3 equiv) in water (4 mL/mmol of halide) was prepared in a glass tube equipped with a stirring bar. After dissolution, DMF was added (2 mL/mmol of halide) and the mixture was degassed by bubbling with argon. Consecutively the corresponding halide (1 equiv), the boronate derivative (1.2 equiv), triphenylphosphine (15 mol%), palladium acetate (5 mol%), and DMF (2 mL/mmol of halide) were added in that sequence.²⁰⁶ The mixture was then degassed by argon bubbling during 10 min after which the tube was sealed. The reaction was heated at 100 °C during 24 h. After this time, the reaction crude was washed with methanol (MeOH) or acetonitrile on a filter plate and the filtrate was evaporated under vacuum. The residue was dissolved in water, cooled to 0 °C, and acidified with HCl 10%. After evaporation under vacuum, the final crude was purified by flash column chromatography on silica gel.

5.2.5.3. Method C

A solution of potassium carbonate (3 equiv) in water (4 mL/mmol of halide) was prepared in a glass tube equipped with a stirring bar. After dissolution, ethanol was added (4 mL/mmol of halide) and the mixture was degassed by bubbling with argon. Consecutively, the corresponding halide (1 equiv), the boronate derivative (1.5 equiv), and PdEnCat[®] 30 (6 mol%) were added in that sequence.¹⁶⁵ The mixture was then degassed by argon bubbling during 10 min, after which the tube was sealed. The reaction was heated at 80 °C during 24 h. After this time, the reaction crude was filtered (washing with methanol) and the filtrate was evaporated in rotavapor. The residue was dissolved in water, cooled to 0 °C, and acidified with HCl 10%. After evaporation under vacuum, the final crude was purified by flash column chromatography on silica gel.

5.2.5.4. Method D

The reaction was set up as described in method B, using a microwave vial instead of a sealed tube. The reaction was programmed in a microwave instrument for heating at 100 °C during 3 h (45 s prestirring).²⁰⁶ After this time, the reaction crude was washed with methanol on a filter plate and the filtrate was evaporated under vacuum. The residue was dissolved in water, cooled to 0 °C, and acidified with HCl 10%. After evaporation under vacuum, the final crude was purified by flash column chromatography on silica gel.

5.2.6. General synthetic procedure 6: Reductive amination.

5.2.6.1. Method A

This method has been used for the preparation of compounds with amino-containing spacers.

Under argon atmosphere, 5-aminosalicylic acid (1 equiv) and the corresponding aldehyde (1 equiv) were dissolved in dry DCM/MeOH 1/1 (10-12 mL/mmol aldehyde). Activated 3Å molecular sieves were added and the mixture was stirred for 3 h at rt to form the intermediate imine. The reaction mixture was cooled to 0 °C and sodium triacetoxyborohydride (2.5 equiv) was added to carry out the *in situ* reduction to the desired amine. After 3 h, the reaction was cooled to 0 °C and quenched with HCl 5%. The mixture was filtered washing with methanol and the filtrate was concentrated in rotavapor. The crude product was purified by flash chromatography on silica gel.²⁰⁷

5.2.6.2. Method B

This method has been used for the preparation of compounds with amino-containing spacers.

Under argon atmosphere, 5-aminosalicylic acid or 4-aminosalicylic acid (1.2-2 equiv) and the corresponding aldehyde (1 equiv) were dissolved in dry DCM/MeOH 3/1 (4-10 mL/mmol aldehyde). Activated 3 Å molecular sieves were added and the mixture was stirred for 24 h at rt to form the intermediate imine. The reaction mixture was cooled to 0 °C and sodium borohydride (1 equiv.) was added to carry out the *in situ* reduction to the desired amine. After 15 min, the reaction was cooled to 0 °C and quenched with HCl 5%. The resulting mixture was filtered washing with methanol and the filtrate was concentrated in rotavapor. The crude product was purified by flash chromatography on silica gel.²⁰⁸

In some cases, the presence of the dialkylated product was observed and it was isolated during the purification step by flash chromatography.

5.2.6.3. Method C

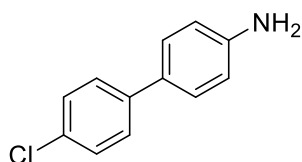
This method has been used for the preparation of compounds with amino-containing side chains.

Under argon atmosphere, the aldehyde (1 equiv) and the amine (1.2 equiv) were dissolved in dry DCM/MeOH 3/1 (8 mL/mmol of aldehyde) containing activated 3 Å molecular sieves. The mixture was stirred for 3 h at rt, protected from light, to allow the formation of the imine. Next, the reaction was cooled to 0 °C and sodium triacetoxyborohydride (2.5 equiv) was added, after which the solution was stirred for 3 h at rt. The reaction was then cooled to 0 °C and quenched with water. The mixture was filtered and the filtrate was concentrated in rotavapor. The crude product was purified by flash chromatography on silica gel to afford the desired amine.²⁰⁷

5.3. Synthesis of oxamic acid derivatives

5.3.1. Synthesis of biphenyl compounds

4'-Chlorobiphenyl-4-amine (MDMG-155)²⁰⁹



General synthetic procedure 5A. Reagents: 4-Iodoaniline (35 mg, 0.16 mmol), 4-chlorophenylboronic acid (30 mg, 0.19 mmol), PPh₃ (6.29 mg, 0.0024 mmol), Pd(OAc)₂ (1.79 mg, 0.008 mmol), K₂CO₃ (66.39 mg, 0.48 mmol), and DMF/H₂O 1/1 (2 mL) at 150 °C. Column chromatography: EtOAc/Hexane (1/4). White solid, 92% yield (30 mg, 0.147 mmol).

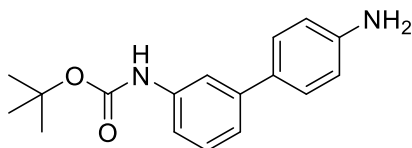
mp: 120 °C.

¹H NMR (300 MHz, CDCl₃) δ 7.45 (d, *J* = 8.5 Hz, 2H), 7.40 – 7.31 (m, 4H), 6.75 (d, *J* = 8.5 Hz, 2H).

HRMS (TOF ES⁺): *m/z* calcd for C₁₂H₁₂N (M+H)⁺ 170.0970, found 170.0974.

Experimental data agree with those reported.²⁰⁹

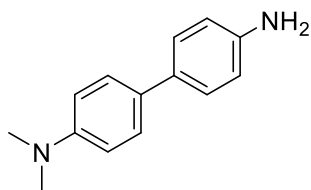
tert-Butyl *N*-(4'-aminobiphenyl-3-yl)carbamate (MDMG-151)²¹⁰



General synthetic procedure 5A. Reagents: 4-Iodoaniline (100 mg, 0.457 mmol), 3-(*N*-Boc-amino)phenylboronic acid (129.9, 0.548 mmol), PPh₃ (18.09 mg, 0.069 mmol), Pd(OAc)₂ (5.16 mg, 0.023 mmol), K₂CO₃ (189 mg, 1.367 mmol), and DMF/H₂O 1/1 (2 mL) at 100 °C. Column chromatography: EtOAc/Hexane (1/3). Brown solid, 75% yield (98 mg, 0.345 mmol).

¹H NMR (300 MHz, CDCl₃) δ 7.62 (s, 1H), 7.47 (d, *J* = 8.1 Hz, 2H), 7.41 – 7.27 (m, 3H), 6.80 (d, *J* = 8.1 Hz, 2H), 6.59 (s, 1H), 3.80 (s, 2H), 1.60 (s, 9H).

HRMS (TOF ES⁺): *m/z* calcd for C₁₇H₂₁N₂O₂ (M+H)⁺ 285.1603, found 285.1596.

***N,N*-Dimethylbiphenyl-4,4'-diamine (MDMG-235)**^{211,212}

General synthetic procedure 5A. Reagents: 4-Iodoaniline (40 mg, 0.183 mmol), potassium [4-(dimethylamino)phenyl]trifluoroborate (49.95 mg, 0.22 mmol), PPh₃ (7.08 mg, 0.027 mmol), Pd(OAc)₂ (2.02 mg, 0.009 mmol), K₂CO₃ (75.76 mg, 0.548 mmol), and DMF/H₂O 1/1 (2 mL) at 100 °C. Column chromatography: EtOAc/Hexane (1/4). Brown solid, 72% yield (28 mg, 0.132 mmol).

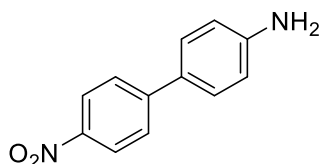
mp: 143 °C.

¹H NMR (400 MHz, CDCl₃) δ 7.41 (dd, *J* = 27.6, 8.6 Hz, 4H), 6.77 (dd, *J* = 24.8, 8.6 Hz, 4H), 3.65 (s, 2H), 2.98 (s, 6H).

¹³C NMR (101 MHz, CDCl₃) δ 149.5 (C), 144.8 (C), 132.0 (C), 129.8 (C), 127.3 (2CH), 127.1 (2CH), 115.6 (2CH), 113.1 (2CH), 40.8 (2CH₃).

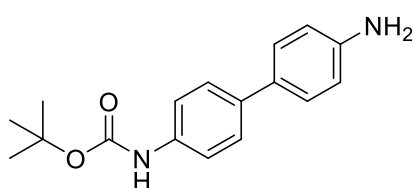
HRMS (TOF ES⁺): *m/z* calcd for C₁₄H₁₇N₂ (M+H)⁺ 213.1392, found 213.1372.

Experimental data agree with those reported.^{211,212}

4'-Nitrobiphenyl-4-amine (MDMG-253)

General synthetic procedure 5A. Reagents: 4-Iodoaniline (80 mg, 0.365 mmol), 4-nitrophenylboronic acid (73.11 mg, 0.438 mmol), PPh₃ (14.16 mg, 0.054 mmol), Pd(OAc)₂ (4.04 mg, 0.018 mmol), K₂CO₃ (151.11 mg, 1.093 mmol), and DMF/H₂O 1/1 (2 mL) at 150 °C. Column chromatography: EtOAc/Hexane (1/3 → 1/2). Orange solid, 74% yield (58 mg, 0.27 mmol).

HRMS (TOF ES⁺): *m/z* calcd for C₁₂H₁₁N₂O₂ (M-H)⁺ 215.0821, found 215.0815.

tert-Butyl N-(4'-aminobiphenyl-4-yl)carbamate (MDMG-261)²¹³

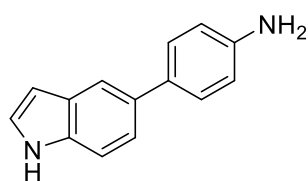
General synthetic procedure 5A. Reagents: 4-Iodoaniline (100 mg, 0.457 mmol), 4-(*N*-Boc-amino)phenylboronic acid (129.91 mg, 0.548 mmol), PPh₃ (18.09 mg, 0.069 mmol), Pd(OAc)₂ (5.13 mg, 0.023 mmol), K₂CO₃ (189.2 mg, 1.369 mmol), and DMF/H₂O 1/1 (3 mL) at 150 °C. Column chromatography: EtOAc/Hexane (1/2 → 1/1). White solid, 70% yield (91 mg, 0.320 mmol).

mp: 150 °C.

¹H NMR (300 MHz, CDCl₃) δ 7.46 (d, *J* = 8.7 Hz, 2H), 7.37 (d, *J* = 8.5 Hz, 4H), 6.74 (d, *J* = 8.5 Hz, 2H), 6.47 (s, 1H), 3.70 (s, 2H), 1.53 (s, 9H).

HRMS (TOF ES⁺): *m/z* calcd for C₁₇H₂₁N₂O₂ (M+H)⁺ 285.1603, found 285.1592.

Experimental data agree with those reported.²¹³

4-(1*H*-Indol-5-yl)aniline (MDMG-515)¹⁵²

General synthetic procedure 5A. Reagents: 4-iodoaniline (70 mg, 0.320 mmol), 5-indolylboronic acid (61.74 mg, 0.383 mmol), PPh₃ (12.57 mg, 0.048 mmol), Pd(OAc)₂ (3.59 mg, 0.016 mmol), K₂CO₃ (132.51 mg, 0.959 mmol), and DMF/H₂O 1/1 (2 mL) at 100 °C. Column chromatography: DCM/MeOH (15/1 → 9/1). Brown solid, 57% yield (38 mg, 0.182 mmol).

mp: 164 °C.

HRMS (TOF ES⁺): *m/z* calcd for C₁₄H₁₃N₂ (M+H)⁺ 209.1079, found 209.1077.

¹H NMR (400 MHz, CDCl₃) δ 8.13 (s, 1H), 7.79 (s, 1H), 7.47 (d, *J* = 8.4 Hz, 2H), 7.41 (s, 2H), 7.21 (t, *J* = 2.8 Hz, 1H), 6.78 (d, *J* = 8.4 Hz, 2H, Ar-*H*), 6.63 – 6.53 (m, 1H), 3.68 (s, 2H).

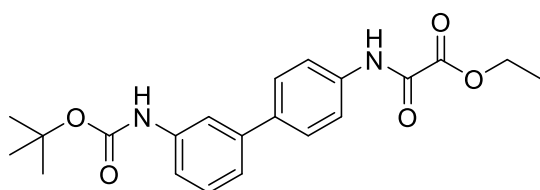
¹³C NMR (101 MHz, CDCl₃) δ 145.1 (CO), 135.0 (C), 133.6 (C), 133.3 (C), 128.5 (C), 128.3 (2CH), 124.7 (CH), 121.7 (CH), 118.5 (CH), 115.6 (2CH), 111.2 (CH), 103.0 (CH).

HPLC: (λ = 254), 100%; (λ = 214), 100%; *t_R* = 10.27 min (Method 2).

Experimental data agree with those reported.¹⁵²

5.3.2. Synthesis of ethyl 2-amino-2-oxoacetate derivatives (ethyloxamates) and ethyl 3-amino-3-oxopropanoate derivatives

Ethyl 2-{N-[3'-(*tert*-butoxycarbonylamino)biphenyl-4-yl]amino}-2-oxoacetate (MDMG-159)



General synthetic procedure 1. Reagents: **MDMG-151** (62 mg, 0.218 mmol), ethyl 2-chloro-2-oxoacetate (48.72 μ L, 0.436 mmol), Et₃N (91.16 μ L, 0.654 mmol) and anhydrous THF (5 mL). Column chromatography: EtOAc/Hexane (1/4). White solid, 69% yield (58 mg, 0.151 mmol).

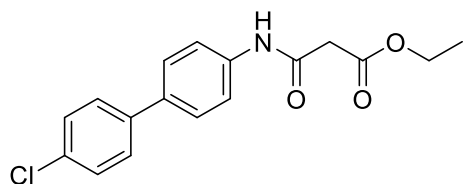
mp: 125 °C.

¹H NMR (500 MHz, CDCl₃) δ 8.95 (s, 1H), 7.73 (d, *J* = 8.6 Hz, 2H), 7.68 (s, 1H), 7.62 (d, *J* = 8.6 Hz, 2H), 7.37 (t, *J* = 7.8 Hz, 1H), 7.34 – 7.24 (m, 2H), 6.60 (s, 1H), 4.46 (q, *J* = 7.1 Hz, 2H), 1.56 (s, 9H), 1.47 (t, *J* = 7.1 Hz, 3H).

¹³C NMR (126 MHz, CDCl₃) δ 161.1 (CO), 153.9 (CO), 152.8 (CO), 141.2 (C), 139.0 (C), 138.2 (C), 135.8 (C), 129.5 (CH), 128.0 (2CH), 121.7 (CH), 120.1 (2CH), 117.6 (CH), 117.1 (CH), 80.7 (C), 63.9 (CH₂), 28.5 (3CH₃), 14.1 (CH₃).

HRMS (TOF ES⁺): *m/z* calcd for C₂₁H₂₄N₂O₅Na (M+Na)⁺ 407.1583, found 407.1575.

Ethyl 3-[N-(4'-chlorobiphenyl-4-yl)amino]-3-oxopropanoate (MDMG-163)



General synthetic procedure 1. Reagents: **MDMG-155** (30 mg, 0.147 mmol), ethyl 3-chloro-3-oxopropanoate (37.71 μ L, 0.294 mmol), Et₃N (61.59 μ L, 0.441 mmol) and anhydrous THF (5 mL). Column chromatography: EtOAc/Hexane (1/3). White solid, 66% yield (31 mg, 0.097 mmol).

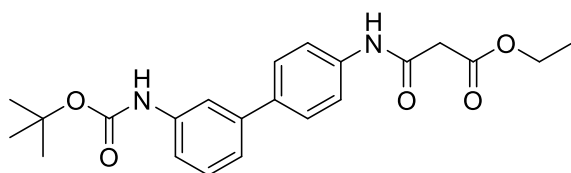
mp: 135 °C.

¹H NMR (400 MHz, CDCl₃) δ 9.33 (s, 1H), 7.64 (d, *J* = 8.6 Hz, 2H), 7.51 (dd, *J* = 11.9, 8.6 Hz, 4H), 7.39 (d, *J* = 8.5 Hz, 2H), 4.28 (q, *J* = 7.1 Hz, 2H), 3.49 (s, 2H), 1.34 (t, *J* = 7.1 Hz, 3H).

¹³C NMR (101 MHz, CDCl₃) δ 170.2 (CO), 163.0 (CO), 139.0 (C), 137.1 (C), 136.2 (C), 133.3 (C), 129.0 (2CH), 128.2 (2CH), 127.6 (2CH), 120.6 (2CH), 62.1 (CH₂), 41.5 (CH₂), 14.2 (CH₃).

HRMS (TOF ES⁺): *m/z* calcd for C₁₇H₁₇NO₃Cl (M+H)⁺ 318.0897, found 318.0890.

Ethyl 3-{*N*-[3'-(*tert*-butoxycarbonylamino)biphenyl-4-yl]amino}-3-oxopropanoate (MDMG-223)



General synthetic procedure 1.

Reagents: **MDMG-151** (98 mg, 0.344 mmol), ethyl 3-chloro-3-oxopropanoate (88.24 μL, 0.689 mmol), Et₃N (144.1 μL, 1.034 mmol) and anhydrous THF (5 mL). Column chromatography: EtOAc/Hexane (1/4). White solid, 78% yield (107 mg, 0.268 mmol).

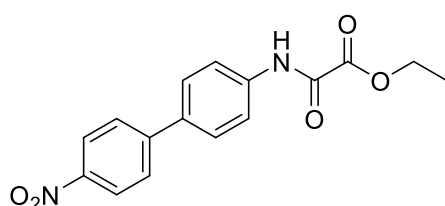
mp: Syrup.

¹H NMR (400 MHz, CDCl₃) δ 9.29 (s, 1H), 7.67 – 7.51 (m, 5H), 7.38 – 7.27 (m, 2H), 7.24 (dt, *J* = 7.0, 1.8 Hz, 1H), 6.59 (s, 1H), 4.27 (q, *J* = 7.2 Hz, 2H), 3.49 (s, 2H), 1.53 (s, 9H), 1.33 (t, *J* = 7.1 Hz, 3H).

¹³C NMR (101 MHz, CDCl₃) δ 170.1 (CO), 163.0 (CO), 152.9 (CO), 141.5 (C), 138.9 (C), 137.2 (C), 137.0 (C), 129.4 (CH), 127.8 (2CH), 121.7 (CH), 120.4 (2CH), 117.4 (CH), 117.1 (CH), 80.7 (C), 62.1 (CH₂), 41.6 (CH₂), 28.5 (3CH₃), 14.2 (CH₃).

HRMS (TOF ES⁺): *m/z* calcd for C₂₂H₂₇N₂O₅ (M+H)⁺ 399.1920, found 399.1919.

Ethyl 2-[*N*-(4'-nitrobiphenyl-4-yl)amino]-2-oxoacetate (MDMG-265)



General synthetic procedure 1. Reagents: **MDMG-253** (58 mg, 0.271 mmol), ethyl 2-chloro-2-oxoacetate (60.50 μL, 0.541 mmol), Et₃N (113.21 μL, 0.812 mmol) and anhydrous THF (5 mL).

Column chromatography: EtOAc/Hexane (1/4 → 1/2). Yellow solid, 97% yield (83 mg, 0.264 mmol).

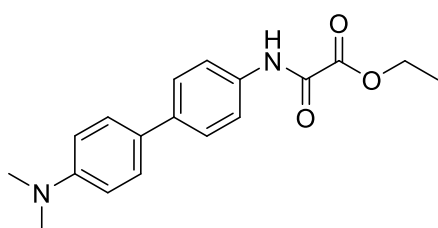
mp: 238 °C.

¹H NMR (500 MHz, CDCl₃) δ 8.99 (s, 1H), 8.30 (d, *J* = 8.8 Hz, 2H), 7.79 (d, *J* = 8.7 Hz, 2H), 7.73 (d, *J* = 8.8 Hz, 2H), 7.66 (d, *J* = 8.7 Hz, 2H), 4.45 (q, *J* = 7.2 Hz, 2H), 1.45 (t, *J* = 7.2 Hz, 3H).

¹³C NMR (126 MHz, CDCl₃) δ 160.9 (CO), 154.1 (CO), 147.2 (C), 146.6 (C), 137.1 (C), 135.8 (C), 128.4 (2CH), 127.6 (2CH), 124.3 (2CH), 120.4 (2CH), 64.1 (CH₂), 14.1 (CH₃).

HRMS (TOF ES⁻): *m/z* calcd for C₁₆H₁₃N₂O₅ (M-H)⁻ 313.0824, found 313.0834.

Ethyl 2-{*N*-[4'-(dimethylamino)biphenyl-4-yl]amino}-2-oxoacetate (MDMG-269)



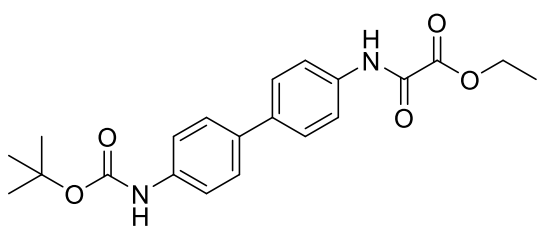
General synthetic procedure 1. Reagents: **MDMG-235** (30 mg, 0.141 mmol), ethyl 2-chloro-2-oxoacetate (31.57 μL, 0.282 mmol), Et₃N (59.08 μL, 0.424 mmol) and anhydrous THF (3 mL). Column chromatography: EtOAc/Hexane (1/3 → 1/2).

Yellow syrup, 36% yield (16 mg, 0.051 mmol).

¹H NMR (500 MHz, CDCl₃) δ 8.91 (s, 1H), 7.65 – 7.61 (m, 2H), 7.54 – 7.47 (m, 4H), 6.86 – 6.82 (m, 2H), 4.43 (q, *J* = 7.1 Hz, 2H), 3.02 (s, 10H), 1.44 (t, *J* = 7.2 Hz, 3H).

HRMS (TOF ES⁺): *m/z* calcd for C₁₈H₂₁N₂O₃ (M+H)⁺ 313.1552, found 313.1555.

Ethyl 2-{*N*-[4'-(*tert*-butoxycarbonylamino)biphenyl-4-yl]amino}-2-oxoacetate (MDMG-289)



General synthetic procedure 1. Reagents: **MDMG-261** (74 mg, 0.260 mmol), ethyl 2-chloro-2-oxoacetate (58 μL, 0.52 mmol), Et₃N (108.8 μL, 0.781 mmol) and anhydrous THF (3 mL). Column

chromatography: EtOAc/Hexane (1/3 → 1/2). Yellow solid, 94% yield (94 mg, 0.244 mmol).

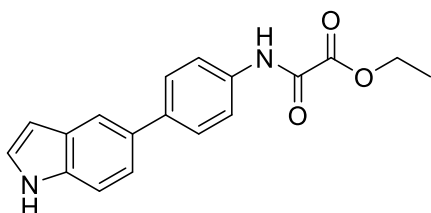
mp: >300 °C.

¹H NMR (300 MHz, CDCl₃) δ 8.94 (s, 1H), 7.69 (d, *J* = 8.6 Hz, 2H), 7.60 – 7.47 (m, 4H), 7.42 (d, *J* = 8.6 Hz, 2H), 6.60 (s, 1H), 4.43 (q, *J* = 7.2 Hz, 2H), 1.53 (s, 9H), 1.44 (t, *J* = 7.1 Hz, 3H).

HRMS (TOF ES⁻): *m/z* calcd for C₂₁H₂₃N₂O₅ (M-H)⁻ 383.1607, found 383.1605.

HPLC: (λ = 254 nm), 100%; (λ = 214 nm), 95.31%; *t_R* = 16.09 min (Method 4).

Ethyl 2-{*N*-[4-(1*H*-indol-5-yl)phenyl]amino}-2-oxoacetate (MDMG-620)



General synthetic procedure 1. Reagents: **MDMG-515** (38 mg, 0.182 mmol), ethyl chlorooxoacetate (40.77 μL, 0.365 mmol), Et₃N (76.29 μL, 0.547 mmol) and anhydrous THF (3 mL). Column chromatography: EtOAc/Hexane (1/4 → 1/2).

Yellowish solid, 90% yield (51 mg, 0.165 mmol).

mp: 174 °C.

HRMS (TOF ES⁻): *m/z* calcd for C₁₈H₁₅N₂O₃ (M-H)⁻ 307.1083, found 307.1082.

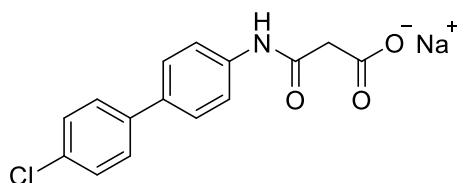
¹H NMR (400 MHz, CDCl₃) δ 8.92 (s, 1H), 8.26 (s, 1H), 7.85 (s, 1H), 7.75 – 7.63 (m, 4H), 7.48 – 7.41 (m, 2H), 7.25 (t, *J* = 2.6 Hz, 1H), 6.61 (t, *J* = 2.6 Hz, 1H), 4.44 (q, *J* = 7.1 Hz, 2H), 1.45 (t, *J* = 7.1 Hz, 3H).

¹³C NMR (101 MHz, CDCl₃) δ 161.2 (CO), 153.9 (CO), 140.0 (C), 135.5 (C), 134.8 (C), 132.5(C), 128.5 (C), 128.0 (2CH), 125.1 (CH), 121.7 (CH), 120.2 (2CH), 119.1 (CH), 111.4 (CH), 103.1 (CH), 63.8 (CH₂), 14.1 (CH₃).

HPLC: (λ = 254 nm), 93.1%; (λ = 214 nm), 93.2%; *t_R* = 13.36 min (Method 4).

5.3.3. Synthesis of 2-oxoacetic and 3-oxopropanoic acid derivatives

Sodium 3-[*N*-(4'-chlorobiphenyl-4-yl)amino]-3-oxopropanoate (MDMG-167)



General synthetic procedure 3. Reagents: **MDMG-163** (15 mg, 0.047 mmol), NaOH 1N (236 μ L, 0.2236 mmol) and THF (236 μ L). White solid, quantitative yield (14.6 mg, 0.047 mmol).

mp: 241 °C.

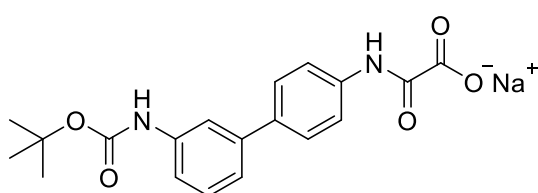
$^1\text{H NMR}$ (400 MHz, DMSO- d_6) δ 10.77 (s, 1H), 7.72 – 7.59 (m, 6H), 7.47 (d, J = 8.5 Hz, 2H), 3.29 (s, 2H).

$^{13}\text{C NMR}$ (101 MHz, DMSO- d_6) δ 169.7 (CO), 165.9 (CO), 138.8 (C), 138.5 (C), 133.5 (C), 131.8 (C), 128.8 (2CH), 128.0 (2CH), 126.9 (2CH), 119.5 (2CH), 54.9 (CH₂).

HRMS (TOF ES⁻): m/z calcd for C₁₅H₁₁NO₃Cl (M-H)⁻ 288.0427, found 288.0428.

HPLC: (λ = 254 nm), 95.17%; (λ = 214 nm), 96.25%; t_R = 12.55 min (Method 4).

Sodium 2-{*N*-[3'-(*tert*-butoxycarbonylamino)biphenyl-4-yl]amino}-2-oxoacetate (MDMG-171)



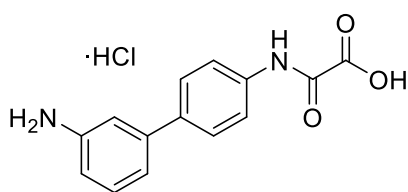
General synthetic procedure 3. Reagents: **MDMG-159** (43 mg, 0.112 mmol), NaOH 1N (559 μ L, 0.559 mmol) and THF (559 μ L). White solid, 30% yield (30 mg, 0.079 mmol).

mp: >300 °C.

$^1\text{H NMR}$ (300 MHz, DMSO- d_6) δ 10.22 (s, 1H), 9.38 (s, 1H), 7.84 (d, J = 8.0 Hz, 2H), 7.72 (s, 1H), 7.50 (d, J = 8.2 Hz, 2H), 7.44 – 7.13 (m, 3H), 1.49 (s, 9H).

HRMS (TOF ES⁻): m/z calcd for C₁₉H₁₉N₂O₅ (M-H)⁻ 355.1294, found 355.1288.

HPLC: (λ = 254), 100%; (λ = 214), 100%; t_R = 13.94 min (Method 3).

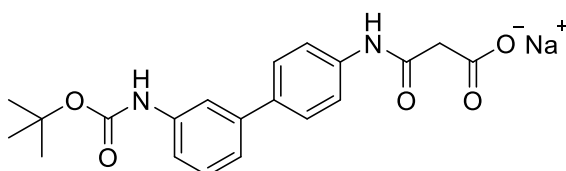
2-[N-(3'-aminobiphenyl-4-yl)amino]-2-oxoacetic acid hydrochloride (MDMG-191)

General synthetic procedure 4. Reagents: **MDMG-171** (5 mg, 0.013 mmol), TFA (1.5 mL, 0.019 mmol), DCM (4.5 mL) and HCl 6N (6.5 mL, 0.039 mmol). Brown solid, quantitative yield (3.8 mg, 0.013 mmol).

mp: >300 °C,

¹H NMR (300 MHz, CD₃OD) 7.96 – 7.55 (m, 7H), 7.37 (d, *J* = 7.4 Hz, 1H).

HRMS (TOF ES⁺): *m/z* calcd for C₁₄H₁₃N₂O₃ (M+H)⁺ 257.0926, found 257.0928.

Sodium 3-{N-[3'-(*tert*-butoxycarbonylamino)biphenyl-4-yl]amino}-3-oxopropanoate (MDMG-239)

General synthetic procedure 3. Reagents: **MDMG-223** (88 mg, 0.221 mmol), NaOH 1N (1104 μL, 1.104 mmol) and THF (1104 μL). Yellowish solid, 46%

yield (40 mg, 0.102 mmol).

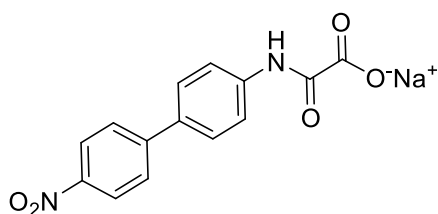
mp: >300 °C.

¹H NMR (600 MHz, CD₃OD) δ 7.66 (t, *J* = 7.2 Hz, 3H), 7.56 (d, *J* = 8.5 Hz, 2H), 7.36 (d, *J* = 7.6 Hz, 1H), 7.30 (t, *J* = 7.8 Hz, 1H), 7.24 (d, *J* = 8.2 Hz, 1H), 2.15 (s, 2H), 1.53 (s, 9H).

¹³C NMR (151 MHz, CD₃OD) δ 175.1 (CO), 170.0 (CO), 155.3 (CO), 142.5 (C), 141.0 (C), 139.2 (C), 137.9 (C), 130.1 (CH), 128.2 (2CH), 122.0 (CH), 121.3 (2CH), 118.5 (CH), 118.0 (CH), 111.4 (CH₂), 80.9 (C), 28.7 (3CH₃).

HRMS (TOF ES⁻): *m/z* calcd for C₂₀H₂₁N₂O₅ (M-H)⁻ 369.1450, found 369.1455.

HPLC: (λ = 254 nm), 96.94%; (λ = 214 nm), 96.22%, *t_R* = 14.57 min (Method 3).

Sodium 2-[N-(4'-nitrophenyl-4-yl)amino]-2-oxoacetate (MDMG-277)

mp: >300 °C

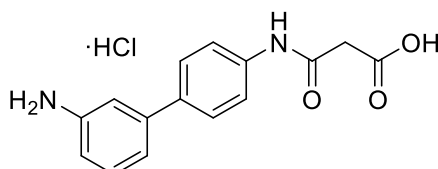
General synthetic procedure 3. Reagents: **MDMG-265** (68 mg, 0.216 mmol), NaOH 1N (1081 μ L, 1.081 mmol) and THF (1081 μ L). Yellow solid, 79% yield (53 mg, 0.172 mmol).

$^1\text{H NMR}$ (300 MHz, DMSO- d_6) δ 10.40 (s, 1H), 8.27 (d, J = 8.7 Hz, 2H), 7.95 (d, J = 8.7 Hz, 4H), 7.76 (d, J = 8.7 Hz, 2H).

$^{13}\text{C NMR}$ (126 MHz, DMSO- d_6) δ 165.1 (CO), 162.2 (CO), 146.2 (C), 146.1 (C), 139.8 (C), 132.0 (C), 127.5 (2CH), 127.1 (2CH), 124.0 (2CH), 119.6 (2CH).

HRMS (TOF ES $^-$): m/z calcd for $\text{C}_{14}\text{H}_9\text{N}_2\text{O}_5$ (M-H) $^-$ 285.0511, found 285.0501.

HPLC: (λ = 254 nm), 100%; (λ = 214 nm), 100%, t_R = 11.63 min (Method 3).

3-[N-(3'-Aminobiphenyl-4-yl)amino]-3-oxopropanoic acid hydrochloride (MDMG-281)

mg, 0.053 mmol).

mp: >300 °C,

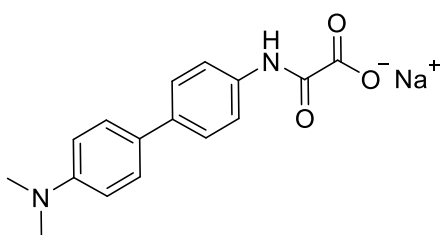
General synthetic procedure 4. Reagents: **MDMG-239** (21 mg, 0.053 mmol), TFA (6.3 mL, 0.082 mmol), DCM (14.7 mL) and HCl 6N (27.2 mL, 0.163 mmol). Yellow solid, quantitative yield (16.2

$^1\text{H NMR}$ (400 MHz, DMSO- d_6) δ 11.38 (s, 1H), 7.64 (d, J = 8.4 Hz, 2H), 7.48 (d, J = 8.6 Hz, 2H), 7.06 (t, J = 7.8 Hz, 1H), 6.81 (t, J = 1.9 Hz, 1H), 6.74 (d, J = 7.7 Hz, 1H), 6.52 (dd, J = 7.9, 1.3 Hz, 1H), 3.13 (s, 2H).

$^{13}\text{C NMR}$ (101 MHz, DMSO- d_6) δ 170.2 (CO), 167.2 (CO), 149.0 (C), 140.4 (C), 138.2 (C), 135.5 (C), 129.3 (CH), 126.6 (2CH), 119.1 (CH), 113.9 (2CH), 112.7 (CH), 111.7 (CH), 45.0 (CH $_2$).

HRMS (TOF ES $^+$): m/z calcd for $\text{C}_{15}\text{H}_{15}\text{N}_2\text{O}_3$ (M+H) $^+$ 271.1083, found 271.1088.

HPLC: (λ = 254 nm), 96.31%; (λ = 214 nm), 96.68%; t_R = 8.36 min (Method 2).

Sodium 2-{N-[4'-(dimethylamino)biphenyl-4-yl]amino}-2-oxoacetate (MDMG-285)

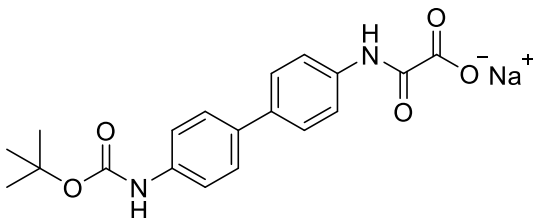
General synthetic procedure 3. Reagents: **MDMG-269** (14 mg, 0.045 mmol), NaOH 1N (224 μ L, 0.224 mmol) and THF (224 μ L). Brown solid, 44% yield (6 mg, 0.020 mmol).

mp: syrup.

$^1\text{H NMR}$ (400 MHz, DMSO- d_6) δ 10.11 (s, 1H), 7.77 (d, J = 8.6 Hz, 2H), 7.48 (dd, J = 8.6, 4.9 Hz, 4H), 6.78 (d, J = 8.8 Hz, 2H), 2.92 (s, 6H).

HRMS (TOF ES $^+$): m/z calcd for C₁₆H₁₇N₂O₃ (M+H) $^+$ 285.1239, found 285.1234.

HPLC: (λ = 254 nm), 91.93%; (λ = 214 nm), 91.25%; t_R = 8.79 min (Method 2).

Sodium 2-{N-[4'-(tert-butoxycarbonylamino)biphenyl-4-yl]amino}-2-oxoacetate (MDMG-293)

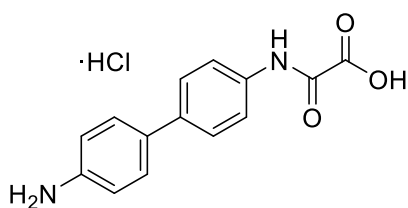
General synthetic procedure 1. Reagents: **MDMG-289** (75 mg, 0.195 mmol), NaOH 1N (975 μ L, 0.975 mmol) and THF (975 μ L). Yellow solid, 81% yield (60 mg, 0.159 mmol).

$^1\text{H NMR}$ (600 MHz, DMSO- d_6) δ = 10.23 (s, 1H), 9.40 (s, 1H), 7.83 (d, J = 8.1 Hz, 2H), 7.54 (dd, J = 15.3, 9.1 Hz, 6H), 1.48 (s, 9H).

$^{13}\text{C NMR}$ (151 MHz, DMSO- d_6) δ 164.7 (CO), 162.4 (CO), 152.7 (CO), 138.5 (C), 137.7 (C), 134.4 (C), 133.4 (C), 126.3 (2CH), 126.1 (2CH), 119.5 (2CH), 118.4 (2CH), 79.0 (C), 28.1 (3CH₃).

HRMS (TOF ES $^-$): m/z calcd for C₁₉H₁₉N₂O₅ (M-H) $^-$ 355.1294, found 355.1288.

HPLC: (λ = 254 nm), 100%; (λ = 214 nm), 99.62%, t_R = 13.52 min (Method 3).

2-[N-(4'-Aminobiphenyl-4-yl)amino]-2-oxoacetic acid hydrochloride (MDMG-305)

General synthetic procedure 4. Reagents: **MDMG-293** (45 mg, 0.118 mmol), TFA (13.5 mL, 0.175 mmol), DCM (31.5 mL) and HCl 6N (58.41 mL, 0.35 mmol). White solid, quantitative yield (34.5 mg, 0.118 mmol).

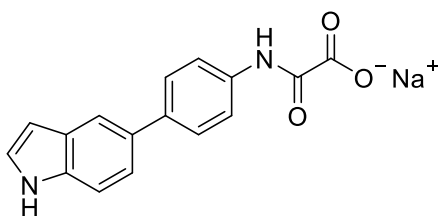
mp: >300 °C.

¹H NMR (500 MHz, DMSO-*d*₆) δ 10.83 (s, 1H), 7.87 (d, *J* = 8.7 Hz, 2H), 7.70 (dd, *J* = 32.9, 8.5 Hz, 4H), 7.42 (d, *J* = 8.0 Hz, 2H).

¹³C NMR (126 MHz, DMSO-*d*₆) δ 162.0 (CO), 156.9 (CO), 138.1 (C), 137.9 (C), 137.3 (C), 135.0 (C), 127.4 (2CH), 126.8 (2CH), 123.0 (2CH), 120.6 (2CH).

HRMS (TOF ES⁻): *m/z* calcd for C₁₄H₁₁N₂O₃ (M-H)⁻ 255.0770, found 255.0777.

HPLC: (λ = 254 nm), 100%; (λ = 214 nm), 100%; *t_R* = 11.66 min (Method 4).

Sodium 2-{N-[4-(1*H*-indol-5-yl)phenyl]amino}-2-oxoacetate (MDMG-632)

General synthetic procedure 3. Reagents: **MDMG-620** (32 mg, 0.104 mmol), NaOH 1N (519 μL, 0.519 mmol) and THF (519 μL). Column chromatography: EtOAc/CH₃CN/MeOH/H₂O (70:5:2.5:2.5 → 70:10:5:5). Yellowish solid, 82% yield (26 mg, 0.086 mmol).

mp: >300 °C.

HRMS (TOF ES⁺): *m/z* calcd for C₁₆H₁₁N₂O₃ (M+H)⁺ 279.0770, found 279.0755.

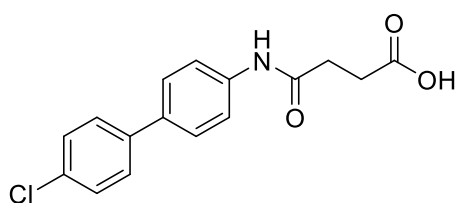
¹H NMR (400 MHz, DMSO-*d*₆) δ 11.18 (s, 1H), 10.46 (s, 1H), 7.88 (d, *J* = 8.1 Hz, 2H), 7.79 (s, 1H), 7.63 (d, *J* = 7.9 Hz, 2H), 7.44 (d, *J* = 8.5 Hz, 1H), 7.40 – 7.32 (m, 2H), 6.48 – 6.41 (m, 1H).

¹³C NMR (101 MHz, DMSO-*d*₆) δ 164.8 (CO), 135.3 (CO), 130.7 (C), 128.3 (C), 128.2 (C), 126.6 (CH), 126.5 (C), 125.9 (CH), 125.8 (C), 120.5 (CH), 120.1 (CH), 117.7 (CH), 111.7 (CH), 101.4 (CH).

HPLC: ($\lambda = 254 \text{ nm}$), 100%; ($\lambda = 214 \text{ nm}$), 100%; $t_R = 10.73 \text{ min}$ (Method 3).

5.3.4. Synthesis of 4-oxobutanoic acid derivatives from succinic anhydride

4-[*N*-(4'-Chlorobiphenyl-4-yl)amino]-4-oxobutanoic acid (MDMG-195)



General synthetic procedure 2. Reagents: **MDMG-155** (42 mg, 0.206 mmol), succinic anhydride (22.7 mg, 0.227 mmol) and anhydrous toluene (4 mL). White solid, 56% yield (35 mg, 0.115 mmol).

mp: 230 °C.

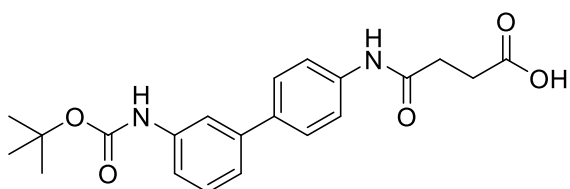
¹H NMR (400 MHz, DMSO-*d*₆) δ 12.11 (s, 1H), 10.05 (s, 1H), 7.70 – 7.55 (m, 6H), 7.46 (d, $J = 8.6 \text{ Hz}$, 2H), 2.54 (dd, $J = 15.0, 5.6 \text{ Hz}$, 4H).

¹³C NMR (101 MHz, DMSO-*d*₆) δ 173.7 (CO), 170.1 (CO), 139.0 (C), 138.5 (C), 133.1 (C), 131.7 (C), 128.7 (2CH), 127.8 (2CH), 126.8 (2CH), 119.2 (2CH), 31.0 (CH₂), 28.7 (CH₂).

HRMS (TOF ES⁻): m/z calcd for C₁₆H₁₃NO₃Cl (M-H)⁻ 302.0584, found 302.0583.

HPLC: ($\lambda = 254 \text{ nm}$): 95.72%; ($\lambda = 214 \text{ nm}$): 95.26%; $t_R = 14.78 \text{ min}$ (Method 3).

4-{*N*-[3'-(*tert*-Butoxycarbonylamino)biphenyl-4-yl]amino}-4-oxobutanoic acid (MDMG-231)



General synthetic procedure 2. Reagents: **MDMG-151** (135 mg, 0.474 mmol), succinic anhydride (52.3 mg, 0.522 mmol) and anhydrous toluene (14 mL). White solid, 87% yield (160 mg, 0.416 mmol).

mp: 171 °C.

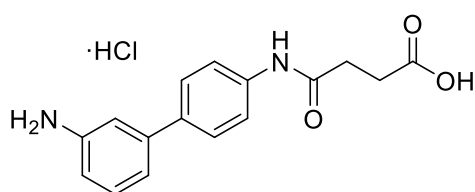
¹H NMR (400 MHz, CD₃OD) δ 7.66 (s, 1H), 7.64 – 7.52 (m, 4H), 7.34 (d, *J* = 8.1 Hz, 1H), 7.30 (t, *J* = 7.7 Hz, 1H), 7.23 (d, *J* = 7.4 Hz, 1H), 2.68 (s, 4H), 1.53 (s, 9H).

¹³C NMR (101 MHz, CD₃OD) δ 176.3 (CO), 172.8 (CO), 155.3 (CO), 142.4 (C), 141.0 (C), 139.3 (C), 137.9 (C), 130.1 (CH), 128.2 (2CH), 122.0 (CH), 121.3 (2CH), 118.4 (CH), 118.0 (CH), 80.9 (C), 32.4 (CH₂), 30.0 (CH₂), 28.7 (3CH₃).

HRMS (TOF ES⁻): *m/z* calcd for C₂₁H₂₃N₂O₅ (M-H)⁻ 383.1607, found 383.1610.

HPLC: (λ = 254), 100%; (λ = 214), 100%; *t_R* = 14.68 min (Method 3).

4-[*N*-(3'-Aminobiphenyl-4-yl)amino]-4-oxobutanoic acid hydrochloride (MDMG-245)



General synthetic procedure 2. Reagents: **MDMG-231** (25 mg, 0.064 mmol), TFA (7.5 mL, 0.019 mmol), DCM (17.5 mL) and HCl 6N (32.45 mL, 0.195 mmol). Yellow solid, quantitative yield (20.6 mg, 0.064 mmol).

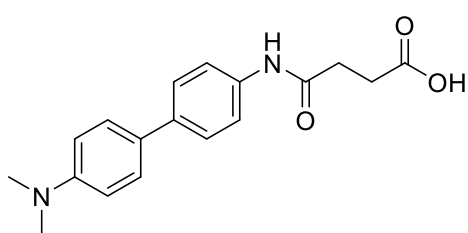
mp: >300 °C.

¹H NMR (400 MHz, CD₃OD) δ 7.89 – 7.52 (m, 13H), 7.45 (t, *J* = 8.5 Hz, 3H), 7.36 (d, *J* = 7.8 Hz, 1H), 3.67 (d, *J* = 9.7 Hz, 2H), 2.89 (s, 2H), 2.75 – 2.67 (m, *J* = 3.7 Hz, 3H), 2.60 (s, 1H).

HRMS (TOF ES⁻): *m/z* calcd for C₁₆H₁₅N₂O₃ (M-H)⁻ 283.1083, found 283.1092.

HPLC (λ = 214 nm): 23.71%, *t_R* = 9.19 min; 38.59%, *t_R* = 10.29 min. (λ = 254 nm): 51.67%, *t_R* = 9.19 min; 48.32%, *t_R* = 10.29 min (Method 2).

4-{*N*-[4'-(Dimethylamino)biphenyl-4-yl]amino}-4-oxobutanoic acid (MDMG-257)



General synthetic procedure 2. Reagents: **MDMG-241** (40 mg, 0.188 mmol), succinic anhydride (20.74 mg, 0.207 mmol) and anhydrous toluene (4 mL). White solid, 51% yield (30 mg, 0.096 mmol).

mp: >300 °C.

¹H NMR (300 MHz, DMSO-*d*₆) δ 12.06 (s, 1H), 9.92 (s, 1H), 7.82 – 7.24 (m, 8H), 6.73 (d, *J* = 8.6 Hz, 2H), 5.71 (s, 2H), 2.87 (s, 6H).

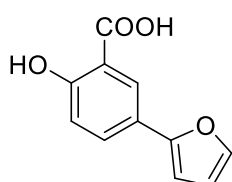
HRMS (TOF ES⁻): *m/z* calcd for C₁₈H₁₉N₂O₃ (M-H)⁻ 311.1396, found 311.1389.

HPLC: (λ = 254 nm): 84.11%; (λ = 214nm): 79.89%; *t_R* = 7.64 min (Method 3).

5.4. Synthesis of salicylic acid derivatives

5.4.1. Synthesis of non-salicylic derivatives and heteroarylsalicylates

5-(Furan-2-yl)-2-hydroxybenzoic acid (MDMG-317)¹⁸⁵



General synthetic procedure 5D. Reagents: Methyl 2-hydroxy-5-iodobenzoate (50 mg, 0.180 mmol), 2-furanboronic acid (24.2 mg, 0.216 mmol), PPh₃ (7.1 mg, 0.027 mmol), Pd(OAc)₂ (2 mg, 0.009 mmol), K₂CO₃ (74.6 mg, 0.540 mmol), H₂O/DMF 1/1 (2 mL).

Column chromatography: EtOAc/CH₃CN/MeOH/H₂O (70:2.5:1.25:1.25 → 70:10:5:5). Brown solid, 83% yield (30 mg, 0.147 mmol).

mp: > 300 °C.

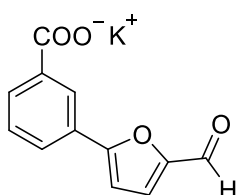
¹H NMR (400 MHz, CD₃OD) δ 8.20 (s, 1H), 7.67 (d, *J* = 7.9 Hz, 1H), 7.50-7.44 (m, 1H), 6.88 (d, *J* = 8.5 Hz, 1H), 6.58 (d, *J* = 3.3 Hz, 1H), 6.45 (dd, *J* = 3.4, 1.8 Hz, 1H).

¹³C NMR (101 MHz, CD₃OD) δ = 174.9 (CO), 162.2 (C), 155.2 (C), 142.5 (CH), 130.2 (CH), 127.1 (CH), 123.3 (C), 118.3 (C), 117.9 (CH), 112.5 (CH), 104.1 (CH).

HRMS (TOF ES⁻): *m/z* calcd for C₁₁H₇O₄ (M-H)⁻ 203.0344, found 203.0350.

HPLC (λ=214, 254 nm): 97%, *t*_R = 14.04 min (Method 3).

Potassium 3-(5-formylfuran-2-yl)benzoate (MDMG-353)¹⁸⁵



General synthetic procedure 5D. Reagents: 3-Bromobenzoic acid (50 mg, 0.249 mmol), 5-formylfuran-2-boronic acid (41.83 mg, 0.299 mmol), K₂CO₃ (103.24 mg, 0.747 mmol), PPh₃ (9.705 mg, 0.037 mmol), Pd(OAc)₂ (2.69 mg, 0.012 mmol), and DMF/H₂O 1/1

(2 mL). Column chromatography: DCM/MeOH (30:1 → 20:1). Orange solid, 42% yield (27 mg, 0.113 mmol).

mp: 266 °C.

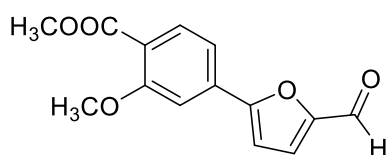
¹H NMR (400 MHz, CD₃OD) δ 9.62 (s, 1H), 8.51 (t, *J* = 1.5 Hz, 1H), 8.08 (ddt, *J* = 10.6, 7.8, 1.1 Hz, 2H), 7.60 (t, *J* = 7.8 Hz, 1H), 7.53 (d, *J* = 3.8 Hz, 1H), 7.17 (d, *J* = 3.8 Hz, 1H).

^{13}C NMR (101 MHz, CD_3OD) δ 179.3 (CHO), 169.2 (CO), 159.7 (C), 153.8 (C), 131.7 (CH), 130.8 (C), 130.4 (CH), 130.2 (CH), 127.3 (CH), 125.7 (C), 109.8 (CH), 78.9 (CH).

HRMS (TOF ES^-): m/z calcd for $\text{C}_{12}\text{H}_7\text{O}_4$ ($\text{M}-\text{H}$) $^-$ 215.0344, found 215.0354.

HPLC: ($\lambda = 214$ nm), 95.2%; ($\lambda = 254$ nm), 100% purity, $t_R = 10.72$ min (Method 3).

Methyl 4-(5-formylfuran-2-yl)-2-methoxybenzoate (MDMG-357)¹⁸⁵



General synthetic procedure 5B. Reagents: 5-Bromofurfural (60 mg, 0.343 mmol), 3-methoxy-4-methoxycarbonylphenylboronic acid (86.31 mg, 0.398 mmol), K_2CO_3 (142.2, 1.029 mmol), PPh_3 (13.37, 0.051 mmol), $\text{Pd}(\text{OAc})_2$ (3.82 mg, 0.017 mmol) and $\text{DMF}/\text{H}_2\text{O}$ 1/1 (2 mL). Column chromatography: $\text{EtOAc}/\text{hexane}$ (1:4 \rightarrow 1:2). Yellow solid, 57% yield (51 mg, 0.20 mmol).

mp: 126 °C.

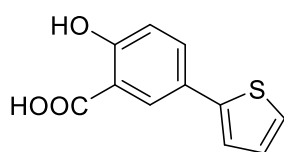
^1H NMR (400 MHz, CDCl_3) δ 9.69 (s, 1H), 7.86 (d, $J = 8.0$ Hz, 1H), 7.41 (d, $J = 1.5$ Hz, 1H), 7.39 (dd, $J = 8.0, 1.5$ Hz, 1H), 7.34 (d, $J = 3.8$ Hz, 1H), 6.94 (d, $J = 3.7$ Hz, 1H), 4.00 (s, 3H), 3.91 (s, 3H).

^{13}C NMR (101 MHz, CDCl_3) δ 177.5 (CHO), 166.1 (CO), 159.7 (CO), 158.0 (C), 152.6 (C), 133.6 (C), 132.5 (CH), 123.3 (C), 120.8 (C), 117.2 (CH), 109.5 (CH), 108.4 (CH), 56.4 (CH_3), 52.3 (CH_3).

HRMS (TOF ES^+): m/z calcd for $\text{C}_{14}\text{H}_{12}\text{O}_5\text{Na}$ ($\text{M}+\text{Na}$) $^+$ 283.0582, found 283.0591.

HPLC: ($\lambda = 254$ nm), 96.0%; ($\lambda = 214$ nm), 97.7%; $t_R = 12.97$ min (Method 3).

2-Hydroxy-5-(thien-2-yl)benzoic acid (MDMG-369)¹⁸⁵



General synthetic procedure 5B. Reagents: Methyl 2-hydroxy-5-iodobenzoate (60 mg, 0.216 mmol), thiophene-2-boronic acid (33.14 mg, 0.259 mmol), K_2CO_3 (89.56 mg, 0.648 mmol), PPh_3 (8.40 mg, 0.032 mmol), $\text{Pd}(\text{OAc})_2$ (2.47 mg, 0.011 mmol) and

DMF/H₂O 1/1 (2 mL). Column chromatography: DCM/MeOH (20:1 → 9:1) followed by EtOAc/CH₃CN/MeOH/H₂O (70:2.5:1.25:1.25 → 70:5:2.5:2.5). Yellow solid, 63% yield (30 mg, 0.136 mmol).

mp: > 300 °C.

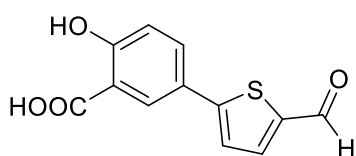
¹H NMR [400 MHz, (CD₃)₂CO] δ 8.19 (s, 1H), 7.79 (d, *J* = 6.5 Hz, 1H), 7.37 (s, 2H), 7.07 (s, 1H), 6.99 (d, *J* = 8.4 Hz, 1H).

¹³C NMR [101 MHz, (CD₃)₂CO] δ 173.1 (CO), 162.2 (C), 143.9 (C), 133.5 (CH), 129.0 (CH), 128.3 (CH), 126.6 (C), 125.1 (CH), 123.5 (CH), 118.7 (CH), 114.7 (C).

HRMS (TOF ES⁻): *m/z* calcd for C₁₁H₇O₃S (M-H)⁻ 219.0116, found 219.0100.

HPLC: (λ = 254 nm), 99.0%; (λ = 214 nm), 98.7%; *t_R* = 14.37 min (Method 3).

5-(5-Formylthien-2-yl)-2-hydroxybenzoic acid (MDMG-373)^{186,185}



General synthetic procedure 5B. Reagents: Methyl 2-hydroxy-5-iodobenzoate (60 mg, 0.216 mmol), 5-formylthiophene-2-boronic acid (40.39 mg, 0.259 mmol), K₂CO₃ (89.56 mg, 0.648 mmol), PPh₃ (8.40 mg, 0.032 mmol), Pd(OAc)₂ (2.47 mg, 0.011 mmol) and DMF/H₂O 1/1 (2 mL). Column chromatography: DCM/MeOH (15:1 → 9:1) followed by EtOAc/CH₃CN/MeOH/H₂O (70:2.5:1.25:1.25 → 70:5:2.5:2.5). Brown solid, 46% yield (25 mg, 0.101 mmol).

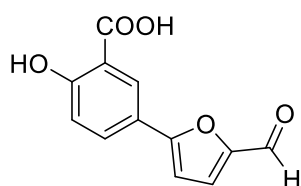
mp: > 300 °C.

¹H NMR [400 MHz, (CD₃)₂SO] δ 9.86 (s, 1H), 8.10 (d, *J* = 2.4 Hz, 1H), 7.99 (d, *J* = 4.0 Hz, 1H), 7.79 (dd, *J* = 8.6, 2.4 Hz, 1H), 7.58 (d, *J* = 4.0 Hz, 1H), 6.90 (d, *J* = 8.6 Hz, 1H).

¹³C NMR [101 MHz, (CD₃)₂SO] δ 183.6 (CO), 170.7 (C), 163.8 (C), 153.3 (C), 140.4 (C), 139.6 (CH), 131.4 (CH), 130.2 (C), 127.8 (CH), 123.5 (CH), 121.8 (C), 117.8 (CH).

HRMS (TOF ES⁻): *m/z* calcd for C₁₂H₇O₄S (M-H)⁻ 247.0065, found 247.0077.

HPLC (λ = 254 nm): 96.8%; (λ = 214 nm): 95.0%; *t_R* = 12.25 min (Method 3).

5-(5-Formylfuran-2-yl)-2-hydroxybenzoic acid (MDMG-409)^{185,183}

General synthetic procedure 5C. Reagents: Methyl 2-hydroxy-5-iodobenzoate (60 mg, 0.216 mmol), 5-formylfuran-2-boronic acid (45.32 mg, 0.324 mmol), K_2CO_3 (89.56 mg, 0.648 mmol), PdEnCat[®] 30 (32.5 mg, 0.113 mmol; 0.4 mmol/g Pd) and EtOH/H₂O 1/1 (2 mL). Column chromatography: DCM/MeOH (20:1 → 8:2). Brown solid, 100% yield (50 mg, 0.215 mmol).

mp: 232 °C.

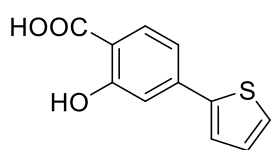
¹H NMR [400 MHz, (CD₃)₂SO] δ 9.51 (s, 1H), 8.21 (d, *J* = 2.4 Hz, 1H), 7.70 (dd, *J* = 8.5, 2.5 Hz, 1H), 7.60 (d, *J* = 3.8 Hz, 1H), 7.00 (d, *J* = 3.8 Hz, 1H), 6.76 (d, *J* = 8.6 Hz, 1H).

¹³C NMR [101 MHz, (CD₃)₂SO] δ 176.7 (CHO), 170.8 (CO), 165.5 (C), 159.8 (C), 150.8 (C), 129.2 (CH), 127.1 (CH), 120.0 (C), 117.3 (CH), 116.64, 116.62 (C, CH), 105.9 (CH).

HRMS (TOF ES⁻): calcd for C₁₂H₇O₅ (M-H)⁻ 231.0300, found; 231.0293.

HPLC: (λ = 254 nm), 100%; (λ = 214 nm), 100%; *t_R* = 11.02 min. (Method 3).

Experimental data agree with those reported.¹⁸³

2-Hydroxy-4-(thien-2-yl)benzoic acid (MDMG-417)^{185,214}

General synthetic procedure 5B. Reagents: 2-Hydroxy-4-iodobenzoic acid (70 mg, 0.265 mmol), thiophene-2-boronic acid (40.69 mg, 0.318 mmol), K_2CO_3 (109.89 mg, 0.795 mmol), PPh₃ (10.49 mg, 0.040 mmol), Pd(OAc)₂ (2.91 mg, 0.013 mmol) and DMF/H₂O 1/1 (2 mL). Column chromatography: DCM/MeOH (20:1 → 9:1). Yellow solid, 51% yield (30 mg, 0.136 mmol).

mp: 225 °C.

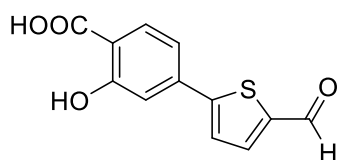
¹H NMR [400 MHz, (CD₃)₂SO] δ 7.74 (d, *J* = 8.4 Hz, 1H), 7.57 (dd, *J* = 5.1, 1.1 Hz, 1H), 7.54 (dd, *J* = 3.6, 1.1 Hz, 1H), 7.13 (dd, *J* = 5.1, 3.7 Hz, 1H), 7.05 – 6.99 (m, 2H).

¹³C NMR [101 MHz, (CD₃)₂SO] δ 171.5 (CO), 162.5 (C), 142.9 (C), 137.8 (C), 130.9 (CH), 128.5 (CH), 126.3 (CH), 124.4 (CH), 116.9 (C), 114.5 (CH), 112.5 (CH).

HRMS (TOF ES⁻): m/z calcd for C₁₁H₇O₃S (M-H)⁻ 219.0116, found 219.0105.

HPLC: (λ = 254 nm), 90.7%; (λ = 214 nm), 90.4%; t_R = 15.09 min (Method 3).

4-(5-Formylthien-2-yl)-2-hydroxybenzoic acid (MDMG-420)¹⁸⁵



General synthetic procedure 5B. Reagents: 2-Hydroxy-4-iodobenzoic acid (70 mg, 0.265 mmol), 5-formylthiophene-2-boronic acid (49.61 mg, 0.318 mmol), K₂CO₃ (109.87 mg, 0.795 mmol), PPh₃ (10.49 mg, 0.040 mmol), Pd(OAc)₂ (2.92 mg, 0.013 mmol) and DMF/H₂O 1/1 (2 mL). Column chromatography: DCM/MeOH (20:1 → 9:1). Brown solid, 45% yield (30 mg, 0.121 mmol).

mp: > 300 °C.

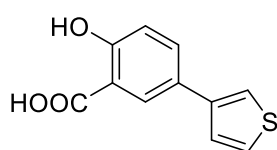
¹H NMR [400 MHz, (CD₃)₂SO] δ 9.92 (s, 1H), 8.04 (d, J = 4.0 Hz, 1H), 7.83-7.77 (m, 2H), 7.24-7.17 (m, 2H).

¹³C NMR [101 MHz, (CD₃)₂SO] δ 184.1 (CHO), 171.0 (CO), 162.4 (C), 151.7 (C), 142.4 (C), 139.0 (CH), 136.9 (C), 131.1 (CH), 126.2 (CH), 117.5 (C), 115.5 (CH), 113.6 (CH).

HRMS (TOF ES⁻): m/z calcd for C₁₂H₇O₄S (M-H)⁻ 247.0065, found 247.0060.

HPLC: (λ = 254 nm), 92.6%; (λ = 214 nm), 94.1%; t_R = 13.93 min (Method 3).

2-Hydroxy-5-(thien-3-yl)benzoic acid (MDMG-424)¹⁸⁵



General synthetic procedure 5B. Reagents: Methyl 2-hydroxy-5-iodobenzoate (70 mg, 0.252 mmol), thiophene-3-boronic acid (38.69 mg, 0.302 mmol), K₂CO₃ (104.49 mg, 0.756 mmol), PPh₃ (9.97 mg, 0.038 mmol), Pd(OAc)₂ (2.92 mg, 0.013 mmol) and DMF/H₂O 1/1 (2 mL). Column chromatography: DCM/MeOH (20:1 → 9:1) followed by EtOAc/CH₃CN/MeOH/H₂O (70:2.5:1.25:1.25 → 70:5:2.5:2.5). Brown solid, 72% yield (40 mg, 0.182 mmol).

mp: 222 °C.

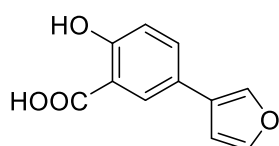
$^1\text{H NMR}$ [400 MHz, $(\text{CD}_3)_2\text{CO}$] δ 11.08 (br, s, 1H), 8.18 (d, $J = 2.4$ Hz, 1H), 7.88 (dd, $J = 8.6, 2.3$ Hz, 1H), 7.71-7.64 (m, 1H), 7.55 (dd, $J = 5.0, 2.9$ Hz, 1H), 7.52-7.46 (m, 1H), 7.01 (d, $J = 8.7$ Hz, 1H).

$^{13}\text{C NMR}$ [101 MHz, $(\text{CD}_3)_2\text{CO}$] δ 172.6 (CO), 162.1 (C), 141.7 (C), 134.7 (CH), 128.4 (CH), 128.2 (C), 127.5 (CH), 126.7 (CH), 120.4 (CH), 118.6 (CH), 113.3 (C).

HRMS (TOF ES^-): m/z calcd for $\text{C}_{11}\text{H}_7\text{O}_3\text{S}$ ($\text{M}-\text{H}$) $^-$ 219.0116, found 219.0104.

HPLC: ($\lambda = 254$ nm), 98.8%; ($\lambda = 214$ nm), 97.1%; $t_{\text{R}} = 14.64$ min (Method 2).

5-(Furan-3-yl)-2-hydroxybenzoic acid (MDMG-427)¹⁸⁵



General synthetic procedure 5B. Reagents: Methyl 2-hydroxy-5-iodobenzoate (60 mg, 0.216 mmol), furan-3-boronate pinacol ester (50.25 mg, 0.259 mmol), K_2CO_3 (89.56 mg, 0.648 mmol), PPh_3 (8.39 mg, 0.032 mmol), $\text{Pd}(\text{OAc})_2$ (2.47 mg, 0.011 mmol), and $\text{DMF}/\text{H}_2\text{O}$ 1/1 (2 mL). Column chromatography: DCM/MeOH (20:1 \rightarrow 9:1) followed by $\text{EtOAc}/\text{CH}_3\text{CN}/\text{MeOH}/\text{H}_2\text{O}$ (70:2.5:1.25:1.25 \rightarrow 70:5:2.5:2.5). Brown solid, 34% yield (15 mg, 0.073 mmol).

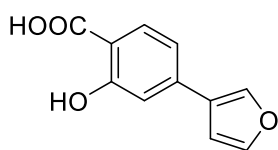
mp: >300 $^\circ\text{C}$.

$^1\text{H NMR}$ [400 MHz, $(\text{CD}_3)_2\text{SO}$] δ 7.74 (d, $J = 8.4$ Hz, 1H), 7.57 (dd, $J = 5.1, 1.1$ Hz, 1H), 7.54 (dd, $J = 3.6, 1.1$ Hz, 1H), 7.13 (dd, $J = 5.1, 3.7$ Hz, 1H), 7.03 (dd, $J = 3.3, 2.2$ Hz, 2H).

$^{13}\text{C NMR}$ [101 MHz, $(\text{CD}_3)_2\text{SO}$] δ 171.5 (CO), 162.5 (C), 142.9 (C), 137.8 (CH), 130.9 (CH), 128.5 (C), 126.3 (CH), 124.4 (CH), 116.9 (CH), 114.5 (CH), 112.5 (C).

HRMS (TOF ES^-): m/z calcd for $\text{C}_{11}\text{H}_7\text{O}_4$ ($\text{M}-\text{H}$) $^-$ 203.0344, found 203.0345.

HPLC: ($\lambda = 254$ nm), 99.8%; ($\lambda = 214$ nm), 99.6%; $t_{\text{R}} = 6.71$ min (Method 4).

4-(Furan-3-yl)-2-hydroxybenzoic acid (MDMG-431)¹⁸⁵

General synthetic procedure 5B. Reagents: 2-Hydroxy-4-iodobenzoic acid (60 mg, 0.227 mmol), furan-3-boronate pinacol ester (52.77 mg, 0.272 mmol), K_2CO_3 (94.12 mg, 0.681 mmol), PPh_3 (8.92 mg, 0.034 mmol), $Pd(OAc)_2$ (2.47 mg, 0.011 mmol) and DMF/ H_2O 1/1 (2 mL). Column chromatography: DCM/MeOH (20:1→9:1) followed by EtOAc/ CH_3CN /MeOH/ H_2O (70:2.5:1.25:1.25 → 70:5:2.5:2.5). Brown solid, 45% yield (21 mg, 0.103 mmol).

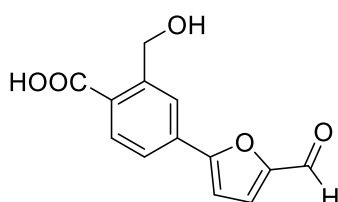
mp: >300 °C.

¹H NMR [400 MHz, $(CD_3)_2CO$] δ 8.14 (s, 1H), 7.93 (d, J = 6.8 Hz, 1H), 7.66 (s, 1H), 7.15 (d, J = 8.7 Hz, 2H), 6.93 (s, 1H).

¹³C NMR [101 MHz, $(CD_3)_2CO$] δ 167.4 (CO), 163.0 (C), 145.1 (CH), 141.3 (CH), 140.1 (C), 132.1 (CH), 126.5 (C), 117.1 (CH), 114.2 (CH), 110.8 (C), 109.4 (CH).

HRMS (TOF ES⁻): m/z calcd for $C_{11}H_7O_4$ (M-H)⁻ 203.0344, found 203.0347.

HPLC: (λ = 254 nm), 100%; (λ = 214 nm), 97.5%; t_R = 13.67 min (Method 3).

4-(5-Formylfuran-2-yl)-2-(hydroxymethyl)benzoic acid (MDMG-451)¹⁸⁵

General synthetic procedure 5B. Reagents: 4-Bromo-2-(hydroxymethyl)benzoic acid (22 mg, 0.095 mmol), 5-formyl-furan-2-boronic acid (15.95 mg, 0.114 mmol), K_2CO_3 (39.39 mg, 0.285 mmol), PPh_3 (3.67 mg, 0.014 mmol), $Pd(OAc)_2$ (1.076 mg, 0.005 mmol) and DMF/ H_2O 1/1 (2 mL). Column chromatography: DCM/MeOH (20:1 → 9:1) followed by EtOAc/ CH_3CN /MeOH/ H_2O (70:2.5:1.25:1.25 → 70:5:2.5:2.5). Brown solid, 30% yield (7 mg, 0.028 mmol).

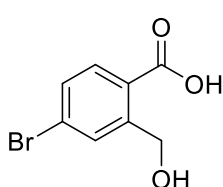
¹H NMR [300 MHz, $(CD_3)_2CO$] δ = 9.72 (s, 1H), 8.23 (s, 1H), 8.12 (d, J = 8.1 Hz, 1H), 7.87 (d, J = 8.2 Hz, 1H), 7.56 (d, J = 3.7 Hz, 1H), 7.31 (d, J = 3.6 Hz, 1H), 4.99 (s, 2H).

¹³C NMR (126 MHz, CD_3OD) δ 179.3, 159.8, 154.0, 145.5, 133.2, 132.7, 132.6, 125.2, 124.5, 112.0, 110.6, 108.6, 63.7.

HRMS (TOF ES⁻): m/z calcd for $C_{13}H_9O_5$ (M-H)⁻ 245.0450, found 245.0443.

HPLC: ($\lambda = 254$ nm), 100%; ($\lambda = 214$ nm), 96.9%; $t_R = 11.29$ min (Method 2).

4-Bromo-2-(hydroxymethyl)benzoic acid (MDMG-455)^{185,215}



In a round bottom flask equipped with a stirring bar, 5-bromophthalide (95 mg, 0.446 mmol) was refluxed in THF/aqueous NaOH 1N 1/1 (4.5 mL) for 6 h. Once the reaction finished, THF was evaporated under vacuum. The mixture was taken in water (10 mL) and it was acidified with HCl 10%. The crude after evaporation was purified by flash chromatography using DCM/MeOH (20:1 \rightarrow 9:1) followed by EtOAc/CH₃CN/MeOH/H₂O (70:10:5:5). White solid, 97% yield (100 mg, 0.45 mmol).

mp: 162-166 °C.

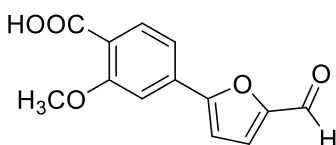
¹H NMR [400 MHz, (CD₃)₂CO] δ 7.98 (s, 1H), 7.93 (d, $J = 8.3$ Hz, 1H), 7.57 (dd, $J = 8.3, 1.9$ Hz, 1H), 4.98 (s, 2H).

¹³C NMR [101 MHz, (CD₃)₂CO] δ 167.8 (CO), 148.2 (C), 133.5 (CH), 130.9 (CH), 130.4 (CH), 127.8 (C), 127.7 (C), 62.6 (CH₂).

HRMS (TOF ES⁻): m/z calcd for C₈H₆O₃Br (M-H)⁻ 228.9500, found 228.9492.

Experimental data agree with those reported.²¹⁵

4-(5-Formylfuran-2-yl)-2-methoxybenzoic acid (MDMG-467)^{185,216}



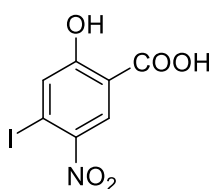
In a round bottom flask equipped with a stirring bar, compound **MDMG-357** (22 mg, 0.084 mmol) was dissolved in THF/aqueous NaOH 1N 1/1 (0.84 mL) and the mixture was stirred for 2 h at 60 °C. Once the reaction had finished, the THF was removed in rotavapor. The residue was taken in water (10 mL) and acidified with HCl 10%.²¹⁶ The resultant solid was filtered and purified by flash chromatography on silica gel using DCM/MeOH (20:1 \rightarrow 9:1) followed by EtOAc/CH₃CN/MeOH/H₂O (70:10:5:5). Orange solid, 29% yield (6 mg, 0.024 mmol).

¹H NMR [300 MHz, (CD₃)₂CO] δ 9.72 (d, $J = 2.3$ Hz, 1H), 8.05-7.95 (m, 1H), 7.67 (s, 1H), 7.64-7.55 (m, 2H), 7.37 (d, $J = 3.6$ Hz, 1H), 4.11 (d, $J = 2.2$ Hz, 3H).

HRMS (TOF ES⁻): m/z calcd for C₁₃H₉O₅ (M-H)⁻ 245.0450, found 245.0436.

HPLC: ($\lambda = 254$ nm), 98.5%; ($\lambda = 214$ nm), 96.9%; $t_R = 10.18$ min (Method 3).

2-Hydroxy-4-iodo-5-nitrobenzoic acid (MDMG-491)¹⁸⁵



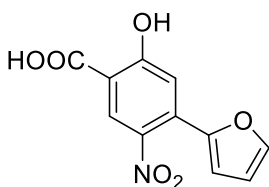
2-Hydroxy-4-iodobenzoic acid (30 mg, 0.114 mmol) was dissolved in AcOH (3 mL). The mixture was then cooled to 0 °C, and 8 μ L of HNO₃ 60% (0.114 mmol) and 12 μ L of H₂SO₄ 95–97% (0.228 mmol) were added. The reaction was allowed to stir for 48 h at rt.²¹⁷ The mixture was then concentrated in rotavapor, and the crude residue was purified by flash chromatography using EtOAc/CH₃CN/MeOH/H₂O (70:10:5:5 \rightarrow 60:10:10:10). Yellow solid, 73% yield (26 mg, 0.084 mmol).

¹H NMR [300 MHz, (CD₃)₂CO] δ 8.51 (s, 1H), 7.41 (s, 1H).

HRMS (TOF ES⁻): m/z calcd for C₇H₃NO₅I (M–H)⁻ 307.9056, found 307.9076.

HPLC: ($\lambda = 254$ nm), 93.8%; ($\lambda = 214$ nm), 93.4%, $t_R = 11.68$ min (Method 3).

4-(Furan-2-yl)-2-hydroxy-5-nitrobenzoic acid (MDMG-511)¹⁸⁵



General synthetic procedure 5B. Reagents: 2-hydroxy-4-iodo-5-nitrobenzoic acid (41 mg, 0.133 mmol), 2-furanboronic acid (31.04, 0.160 mmol), K₂CO₃ (55.15 mg, 0.399 mmol), PPh₃ (5.25 mg, 0.020 mmol), Pd(OAc)₂ (1.57mg, 0.007mmol), and DMF/H₂O 1/1 (2mL). Column chromatography: DCM/MeOH (15:1 \rightarrow 9:1) and EtOAc/CH₃CN/ MeOH/H₂O (70:5:2.5:2.5 \rightarrow 70:10:10:10). Brown solid, 48% yield (16 mg, 0.064 mmol).

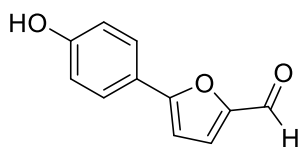
mp: 187 °C.

¹H NMR [400 MHz, (CD₃)₂CO] δ 8.40 (s, 1H), 7.63 (d, $J = 1.0$ Hz, 1H), 6.99 (s, 1H), 6.76 (d, $J = 3.2$ Hz, 1H), 6.56 (dd, $J = 3.2, 1.7$ Hz, 1H).

¹³C NMR [101 MHz, (CD₃)₂CO] δ 170.3 (CO), 166.4 (C), 150.3 (C), 144.7 (CH), 139.1 (C), 129.7 (C), 129.0 (CH), 118.9 (C), 117.5 (CH), 112.6 (CH), 110.7 (CH).

HRMS (TOF ES⁻): m/z calcd for C₁₁H₆NO₆ (M–H)⁻ 248.0195, found 248.0206.

HPLC: ($\lambda = 254$ nm), 94.0%; ($\lambda = 214$ nm), 92.1%, $t_R = 12.38$ min (Method 3).

5-(4-Hydroxyphenyl)-2-furaldehyde (MDMG-672)^{184,185}

General synthetic procedure 5B. Reagents: 4-Bromophenol (60 mg, 0.343 mmol) and 5-formylfuran-2-boronic acid (56.89 mg, 0.412 mmol), K_2CO_3 (142.22 mg, 1.029 mmol), PPh_3 (13.37 mg, 0.051 mmol), $Pd(OAc)_2$ (3.82 mg, 0.017 mmol), and DMF/ H_2O 1/1 (2 mL). Column chromatography: EtOAc/hexane (1:5 \rightarrow 1:3). Yellow solid, 76% yield (49 mg, 0.260 mmol).

mp: 170 °C.

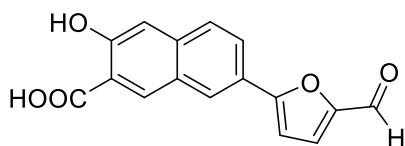
1H NMR [400 MHz, $(CD_3)_2CO$] δ 9.60 (s, 1H), 8.86 (s, 1H), 7.78–7.72 (m, 2H), 7.48 (d, J = 3.7 Hz, 1H), 6.99–6.94 (m, 3H).

^{13}C NMR [101 MHz, $(CD_3)_2CO$] δ 177.2 (CHO), 160.4 (C), 159.9 (C), 152.7 (C), 127.8 (CH), 125.3 (CH), 121.8 (C), 116.8 (CH), 106.9 (CH).

HRMS (TOF ES^-): m/z calcd for $C_{11}H_7O_3$ ($M-H$)⁻ 187.0395, found 187.0381.

HPLC (λ = 254 nm), 100%; (λ = 214 nm), 100%; t_R = 10.64 min (Method 3).

Experimental data agree with those reported.¹⁸⁴

7-(5-Formylfuran-2-yl)-3-hydroxy-2-naphthoic acid (MDMG-879)¹⁸⁵

General synthetic procedure 5B. Reagents: 7-Bromo-3-hydroxy-2-naphthoic acid (60 mg, 0.225 mmol), 5-formyl-2-furanylboronic acid (37.8 mg, 0.27 mmol), PPh_3 (8.92 mg, 0.034 mmol), $Pd(OAc)_2$ (2.47 mg, 0.011 mmol), K_2CO_3 (93.29 mg, 0.675 mmol), and DMF/ H_2O 1/1 (2 mL). Column chromatography: DCM/MeOH (20/1 \rightarrow 8/1). Brown solid, 22% yield (14 mg, 0.05 mmol).

mp: 200 °C (decomposition).

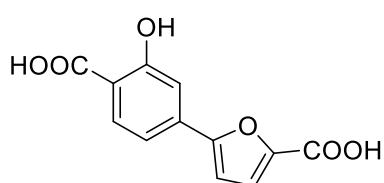
1H NMR [400 MHz, $(CD_3)_2SO$] δ 9.60 (s, 1H), 8.44 (bs, 1H), 8.32 (bs, 1H), 7.83 (d, J = 8.7 Hz, 1H), 7.72 (d, J = 8.7 Hz, 1H), 7.67 (d, J = 3.8 Hz, 1H), 7.29 (d, J = 3.8 Hz, 1H), 7.04 (bs, 1H).

^{13}C NMR [101 MHz, $(\text{CD}_3)_2\text{SO}$] δ 177.3 (CHO), 170.3 (C), 161.2 (C), 159.1 (C), 151.4 (C), 136.7 (C), 131.4 (CH), 126.4 (CH), 125.9 (CH), 125.7 (C), 125.5 (CH), 123.5 (C), 123.3 (CH), 122.1 (C), 109.2 (CH), 108.0 (CH).

HRMS (TOF ES^-): m/z calcd for $\text{C}_{16}\text{H}_9\text{O}_5$ ($\text{M}-\text{H}$) $^-$ 281.0450, found 281.0432.

HPLC: ($\lambda = 254$ nm), 99.7%; ($\lambda = 214$ nm), 100%; $t_{\text{R}} = 13.52$ min (Method 3).

4-(5-Carboxyfuran-2-yl)-2-hydroxybenzoic acid (MDMG-883)¹⁸⁵



General synthetic procedure 5C. Reagents: 5-Bromofuran-2-carboxylic acid (60 mg, 0.314 mmol), methyl 2-hydroxy-4-(4,4,5,5-tetramethyl-1,3,2-dioxaborolan-2-yl)benzoate (131 mg, 0.471 mmol), K_2CO_3 (130.19, 0.942 mmol), PdEnCat[®] 30 (47.5 mg, 0.19 mmol; 0.4 mmol/g Pd), and EtOH/ H_2O 1/1 (2 mL). The crude residue was purified by flash chromatography on silica gel using EtOAc/ CH_3CN / MeOH / H_2O (70:2.5:1.25:1.25 \rightarrow 60:10:10:10). White solid, 28% yield (22 mg, 0.089 mmol).

mp: 250–252 °C.

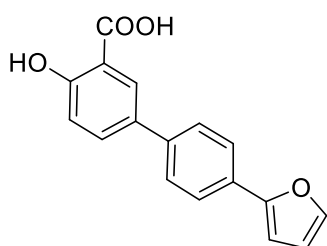
^1H NMR (400 MHz, D_2O) δ 7.89 (d, $J = 8.1$ Hz, 1H), 7.45–7.32 (m, 2H), 7.13 (d, $J = 3.6$ Hz, 1H), 7.01 (d, $J = 3.6$ Hz, 1H).

^{13}C NMR (101 MHz, D_2O) δ 175.0 (CO), 166.2 (CO), 159.9 (C), 154.1 (C), 148.7 (C), 134.5 (C), 131.0 (CH), 117.4 (C), 117.0 (CH), 115.1 (CH), 111.4 (CH), 108.9 (CH).

HRMS (TOF ES^-): m/z calcd for $\text{C}_{12}\text{H}_7\text{O}_6$ ($\text{M}-\text{H}$) $^-$ 247.0243, found 247.0256.

HPLC ($\lambda = 214$ nm), 95.5%; $t_{\text{R}} = 9.51$ min (Method 3).

5-[4-(2-Furyl)phenyl]-2-hydroxybenzoic acid (MDMG-943)



General synthetic procedure 5B. Reagents: 5-Iodosalicylic acid (70 mg, 0.265 mmol), 2-[4-(2-furyl)phenyl]-4,4,5,5-tetramethyl-1,3,2-dioxaborolan (85.95 mg, 0.318 mmol), PPh_3 (10.43 mg, 0.040 mmol), $\text{Pd}(\text{OAc})_2$ (2.97 mg, 0.013 mmol), K_2CO_3 (109.93 mg, 0.795 mmol), and DMF/ H_2O 1/1

(2 mL). Column chromatography: DCM/MeOH (20:1 → 1:1). Brown solid, 80% yield (60 mg, 0.214 mmol).

mp: 170 °C (decomposition).

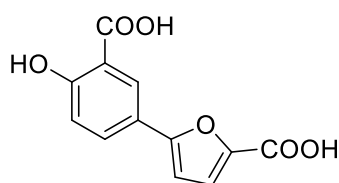
HRMS (TOF ES⁻): *m/z* calcd for C₁₇H₁₁O₄ (M-H)⁻ 279.0657, found 279.0668.

¹H NMR (400 MHz, DMSO-*d*₆) δ 8.08 (s, 1H), 7.84 (d, *J* = 8.3 Hz, 1H), 7.80 – 7.60 (m, 5H), 7.03 (d, *J* = 8.5 Hz, 1H), 6.98 (d, *J* = 2.8 Hz, 1H), 6.61 (s, 1H).

¹³C NMR (101 MHz, DMSO-*d*₆) δ 171.7 (CO), 160.8 (C), 152.7 (C), 142.9 (CH), 137.9 (C), 133.1 (CH), 130.2 (C), 128.9 (C), 127.7 (CH), 126.4 (2CH), 124.0 (2CH), 117.7 (CH), 114.2 (C), 112.1 (CH), 105.9 (CH).

HPLC: (λ = 254 nm), 92.44%; (λ = 214 nm), 95.19%; *t*_R = 16.57 min (Method 4).

5-(5-Carboxyfuran-2-yl)-2-hydroxybenzoic acid (MDMG-983)¹⁸⁵



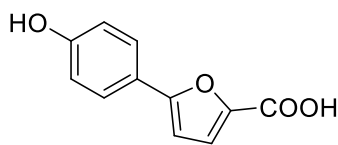
General synthetic procedure 5C. Reagents: 2-Hydroxy-5-iodobenzoic acid (15 mg, 0.057 mmol), 5-boronofuran-2-carboxylic acid (13.26 mg, 0.085 mmol), K₂CO₃ (23.63 mg, 0.171 mmol), PdEnCat[®] 30 (8.5 mg, 0.003 mmol; 0.4 mmol/g Pd), and EtOH/H₂O 1/1 (2 mL). Column chromatography: EtOAc/CH₃CN/MeOH/H₂O (70:5:2.5:2.5 → 70:10:10:10). White solid, quantitative yield (14 mg, 0.057 mmol).

¹H NMR (400 MHz, CD₃OD) δ 8.34 (s, 1H), 7.84 (d, *J* = 8.5 Hz, 1H), 7.23 (d, *J* = 3.3 Hz, 1H), 6.94 (d, *J* = 8.6 Hz, 1H), 6.76 (d, *J* = 3.3 Hz, 1H).

¹³C NMR (101 MHz, CD₃OD) δ 174.7 (CO), 163.5 (CO), 162.8 (C), 158.5 (C), 145.4 (C), 131.4 (CH), 128.2 (CH), 122.0 (C), 120.8 (CH), 118.4 (CH), 117.6 (C), 106.4 (CH).

HRMS (TOF ES⁻): *m/z* calcd for C₁₂H₇O₆ (M-H)⁻ 247.0243, found 247.0226.

HPLC: (λ = 254 nm), 100%; (λ = 214 nm), 100%; *t*_R = 10.05 min (Method 3).

5-(4-Hydroxyphenyl)furan-2-carboxylic acid (MDMG-1062)

General synthetic procedure 5C. Reagents: 5-Bromo-2-furoic acid (100 mg, 0.523 mmol), 4-hydroxyphenylboronic acid (108.33 mg, 0.785 mmol), K_2CO_3 (217.11 mg, 1.57 mmol), PdEnCat[®] 30 (77.5 mg, 0.031 mmol; 0.4 mmol/g Pd) and EtOH/H₂O 1/1 (2 mL). Column chromatography: DCM/MeOH (20:1 → 8:2). White solid, 93% yield (100 mg, 0.490 mmol).

mp: 186-188 °C.

¹H NMR (400 MHz, CD₃OD) δ 7.70 – 7.63 (m, 2H), 7.25 (d, J = 3.6 Hz, 1H), 6.89 – 6.81 (m, 2H), 6.72 (d, J = 3.6 Hz, 1H).

¹³C NMR (101 MHz, CD₃OD) δ 162.0 (CO), 159.7 (C), 144.3 (C), 127.4 (2CH), 122.6 (C), 121.4 (CH), 116.7 (2CH), 111.4 (C), 106.0 (CH).

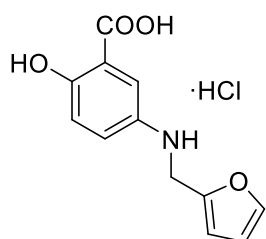
HRMS (TOF ES⁻): m/z calcd for C₁₁H₇O₄ (M-H)⁻ 203.0344, found 203.0350.

HPLC: (λ = 254 nm), 100%; (λ = 214 nm), 95.45%; t_R = 9.34 min (Method 3).

5.4.2. Synthesis of salicylic acid derivatives containing two-atom nitrogen-based spacers.

5.4.2.1. Synthesis of salicylate derivatives containing flexible methylamino linkers.

5-[(Furan-2-ylmethyl)amino]-2-hydroxybenzoic acid hydrochloride (MDMG-540)



0.222 mmol).

General synthetic procedure 6A. Reagents: 5-Aminosalicylic acid (50 mg, 0.326 mmol), 2-furaldehyde 31.37 mg, 0.326 mmol), NaBH(OAc)₃ (173 mg, 0.816 mmol) and DCM/MeOH 1:1 (4 mL). Column chromatography: EtOAc/CH₃CN/MeOH/H₂O (70:2.5:1.25:1.25 → 70:10:5:5). White solid, 68% yield (60 mg,

mp: 200 °C.

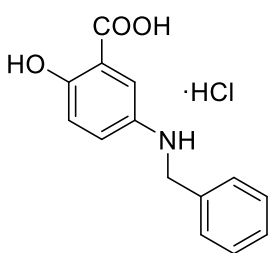
¹H NMR (400 MHz, DMSO-*d*₆) δ 7.55 (s, 1H), 7.03 (d, *J* = 2.8 Hz, 1H), 6.92 (dd, *J* = 8.8, 2.9 Hz, 1H), 6.74 (d, *J* = 8.8 Hz, 1H), 6.44 – 6.32 (m, 1H), 6.25 (d, *J* = 2.8 Hz, 1H), 4.19 (s, 2H).

¹³C NMR (101 MHz, DMSO-*d*₆) δ 172.0 (CO), 153.3 (C), 152.9 (C), 141.8 (CH), 140.9 (C), 121.8 (CH), 117.3 (CH), 112.4 (C), 111.6 (CH), 110.3 (CH), 106.8 (CH), 40.6 (CH₂).

HRMS (TOF ES⁻): *m/z* calcd for C₁₂H₁₀NO₄ (M-H)⁻ 232.0610, found 232.0604.

HPLC: (λ = 254 nm), 100%; (λ = 214 nm), 100%; *t*_R = 8.86 min (Method 2).

5-(Benzylamino)-2-hydroxybenzoic acid hydrochloride (MDMG-560)



General synthetic procedure 6A. Reagents: 5-Aminosalicylic acid (60 mg, 0.392 mmol), benzaldehyde (40 μL, 0.392 mmol), NaBH(OAc)₃ (207.59 mg, 0.979 mmol) and DCM/MeOH 1:1 (4 mL). Column chromatography: EtOAc/CH₃CN/MeOH/H₂O (70:2.5:1.25:1.25 → 70:10:5:5). White solid, 42% yield (46 mg, 0.164 mmol).

mp: 208-214 °C.

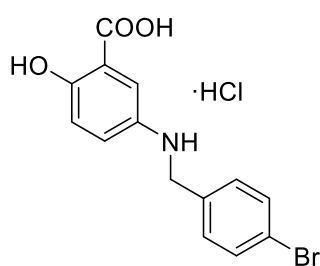
^1H NMR (400 MHz, DMSO- d_6) δ 7.33 (dt, J = 14.9, 7.4 Hz, 4H), 7.22 (t, J = 7.0 Hz, 1H), 6.96 (d, J = 2.8 Hz, 1H), 6.87 (dd, J = 8.8, 2.8 Hz, 1H), 6.72 (d, J = 8.8 Hz, 1H), 4.21 (s, 2H).

^{13}C NMR (101 MHz, DMSO- d_6) δ 172.0 (CO), 152.7 (C), 141.2 (C), 140.0 (C), 128.2 (2CH), 127.2 (2CH), 126.6 (CH), 121.8 (CH), 117.3 (CH), 112.5 (C), 111.3 (CH), 47.2 (CH₂).

HRMS (TOF ES⁻): m/z calcd for C₁₄H₁₂NO₃ (M-H)⁻ 242.0817, found 242.0813.

HPLC: (λ = 254 nm), 100%; (λ = 214 nm), 100%; t_R = 10.52 min (Method 2).

5-[(4-Bromobenzyl)amino]-2-hydroxybenzoic acid hydrochloride (MDMG-566)



General synthetic procedure 6A. Reagents: 5-Aminosalicylic acid (60 mg, 0.392 mmol), 4-bromobenzaldehyde (72.49 mg, 0.392 mmol), NaBH(OAc)₃ (207.59 mg, 0.979 mmol) and DCM/MeOH 1:1 (4 mL). Column chromatography: EtOAc/CH₃CN/MeOH/H₂O (70:2.5:1.25:1.25). White solid, 53% yield (75 mg, 0.209 mmol).

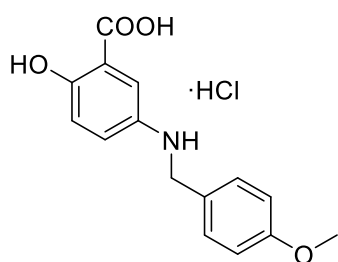
mp: 223-224 °C.

^1H NMR (400 MHz, DMSO- d_6) δ 7.50 (d, J = 8.2 Hz, 2H), 7.31 (d, J = 8.2 Hz, 2H), 6.92 (d, J = 2.8 Hz, 1H), 6.85 (dd, J = 8.8, 2.8 Hz, 1H), 6.72 (d, J = 8.8 Hz, 1H), 4.19 (s, 2H).

^{13}C NMR (101 MHz, DMSO- d_6) δ 171.9 (CO), 152.7 (C), 140.9 (C), 139.6 (C), 131.0 (2CH), 129.3 (2CH), 121.7 (CH), 119.5 (C), 117.4 (CH), 112.5 (C), 111.4 (CH), 46.5 (CH₂).

HRMS (TOF ES⁺): m/z calcd for C₁₄H₁₃NO₃Br (M+H)⁺ 322.0079, found 322.0072.

HPLC: (λ = 254 nm), 100%; (λ = 214 nm), 100%; t_R = 12.20 min (Method 3).

2-Hydroxy-5-[(4-methoxybenzyl)amino]benzoic acid hydrochloride (MDMG-570)

General synthetic procedure 6A. Reagents: 5-Aminosalicylic acid (60 mg, 0.392 mmol), 4-methoxybenzaldehyde (47.62 μ L mg, 0.392 mmol), NaBH(OAc)₃ (207.59 mg, 0.979 mmol) and DCM/MeOH 1:1 (4 mL). Column chromatography: EtOAc/CH₃CN/MeOH/H₂O 70:2.5:1.25:1.25. White solid, 53% yield (65 mg, 0.209 mmol).

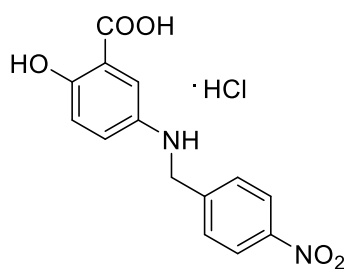
mp: 210-215 °C.

¹H NMR (400 MHz, DMSO-*d*₆) δ 7.26 (d, *J* = 8.4 Hz, 2H), 6.97 (d, *J* = 2.5 Hz, 1H), 6.92 – 6.76 (m, 3H), 6.69 (d, *J* = 8.8 Hz, 1H), 4.13 (s, 2H), 3.72 (s, 3H).

¹³C NMR (101 MHz, DMSO-*d*₆) δ 172.0 (CO), 158.0 (C), 152.8 (C), 141.0 (C), 131.7 (C), 128.4 (2CH), 121.6 (CH), 117.1 (CH), 113.6 (2CH), 113.0 (C), 111.6 (CH), 54.9 (CH₃), 46.7 (CH₂).

HRMS (TOF ES⁻): *m/z* calcd for C₁₅H₁₄NO₄ (M-H)⁻ 272.0923, found 272.0923.

HPLC: (λ = 254 nm), 100%; (λ = 214 nm), 100%; *t*_R = 10.34 min (Method 2).

2-Hydroxy-5-[(4-nitrobenzyl)amino]benzoic acid hydrochloride (MDMG-592)

General synthetic procedure 6A. Reagents: 5-Aminosalicylic acid (60 mg, 0.392 mmol), 4-nitrobenzaldehyde (59.21 mg, 0.392 mmol), NaBH(OAc)₃ (207.59 mg, 0.979 mmol) and DCM/MeOH 1:1 (4 mL). Column chromatography: EtOAc/CH₃CN/MeOH/H₂O 70:2.5:1.25:1.25. Yellow solid, 64% yield (82 mg, 0.252 mmol).

mp: 200 °C.

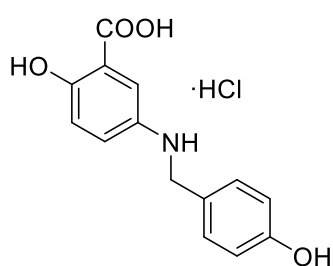
¹H NMR (500 MHz, DMSO-*d*₆) δ = 8.19 (d, *J* = 8.8 Hz, 2H), 7.61 (d, *J* = 8.8 Hz, 2H), 6.92 (d, *J* = 2.9 Hz, 1H), 6.84 (dd, *J* = 8.8, 3.0 Hz, 1H), 6.71 (d, *J* = 8.8 Hz, 1H), 4.38 (s, 2H).

¹³C NMR (126 MHz, DMSO-*d*₆) δ = 171.9 (CO), 152.9 (C), 148.9 (C), 146.3 (C), 140.6 (C), 128.0 (2CH), 123.4 (2CH), 121.4 (CH), 117.4 (CH), 113.0 (C), 111.6 (CH), 46.6 (CH₂).

HRMS (TOF ES⁻): *m/z* calcd for C₁₄H₁₁N₂O₅ (M-H)⁻ 287.0668, found 287.0673.

HPLC: (λ = 254 nm), 100%; (λ = 214 nm), 100%; *t_R* = 12.21 min (Method 3).

2-Hydroxy-5-[(4-hydroxybenzyl)amino]benzoic acid hydrochloride (MDMG-963)



General synthetic procedure 6B. Reagents: 4-Hydroxybenzaldehyde (50 mg, 0.409 mmol), 5-aminosalicylic acid (125.40 mg, 0.819 mmol), NaBH₄ (23.23 mg, 0.614 mmol) and DCM/MeOH 3:1 (4 mL). Column chromatography: EtOAc/CH₃CN/MeOH/H₂O (7:1:0.5 → 70:2:1:1). Yellowish solid, 26% yield (32 mg, 0.108 mmol).

mp: 205-207 °C.

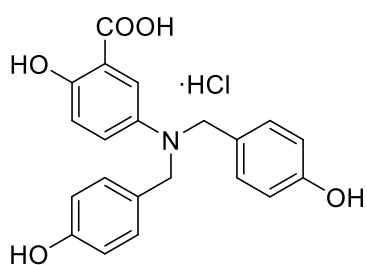
¹H NMR (400 MHz, DMSO-*d*₆) δ 9.26 (bs, 2H), 7.14 (d, *J* = 8.0 Hz, 2H), 6.97 (d, *J* = 2.9 Hz, 1H), 6.84 (dd, *J* = 8.8, 2.9 Hz, 1H), 6.74 – 6.64 (m, 3H), 4.07 (s, 2H).

¹³C NMR (101 MHz, DMSO-*d*₆) δ 172.0 (CO), 156.1 (C), 152.9 (C), 140.9 (C), 129.8 (C), 128.5 (2CH), 121.5 (CH), 117.1 (CH), 115.0 (2CH), 113.3 (C), 111.7 (CH), 47.1(CH₂).

HRMS (TOF ES⁺): *m/z* calcd for C₁₄H₁₄NO₄ (M+H)⁺ 260.0923, found 260.0907.

HPLC: (λ = 214 nm), 95.45%; (λ = 254 nm), 100%; *t_R* = 9.49 min (Method 1).

5-[*N,N*-Bis(4-hydroxybenzyl)amino]-2-hydroxybenzoic acid hydrochloride (MDMG-963I)



By-product in the synthesis of **MDMG-963**.

Column chromatography: EtOAc /CH₃CN/MeOH 7:1:0.5 → EtOAc/CH₃CN/MeOH/H₂O 70:2:1:1. Yellowish solid (20 mg, 0.050 mmol).

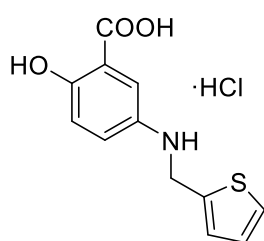
¹H NMR (300 MHz, CD₃OD) δ 7.39 (d, J = 3.0 Hz, 1H), 7.05 (d, J = 8.3 Hz, 5H), 6.72 (dd, J = 13.1, 8.7 Hz, 5H), 4.41 (s, 4H).

¹³C NMR (126 MHz, CD₃OD) 178.5, 176.2, 176.0, 167, 157.2, 131.0, 129.9, 117.2, 116.0, 104.1, 96.4, 56.0.

HRMS (TOF ES⁺): m/z calcd for C₂₁H₂₀NO₅ (M+H)⁺ 366.1341, found 366.1348.

HPLC: (λ = 254 nm), 96.92%; (λ = 214 nm), 95.00%; t_R = 10.36 min (Method 2).

2-Hydroxy-5-[*N*-(2-thienylmethyl)amino]benzoic acid hydrochloride (MDMG-971)



General synthetic procedure 6B. Reagents: 2-thiophenecarboxaldehyde (83.33 μ L, 0.892 mmol), 5-aminosalicylic acid (163.85 mg, 1.07 mmol), NaBH₄ (50.61 mg, 1.338 mmol) and DCM/MeOH 3:1 (4 mL). Column chromatography: DCM/MeOH (20:1 \rightarrow 10:1). Orange solid, 24% yield (61 mg, 0.213 mmol).

mp: 187-189 °C (decomposition).

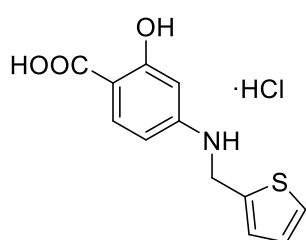
¹H NMR (400 MHz, DMSO-*d*₆) δ 7.35 (dd, J = 5.0, 1.2 Hz, 1H), 7.09 – 6.99 (m, 2H), 6.95 (dd, J = 5.0, 3.4 Hz, 1H), 6.84 (dd, J = 8.8, 2.5 Hz, 1H), 6.68 (d, J = 8.7 Hz, 1H), 4.38 (s, 2H).

¹³C NMR (101 MHz, DMSO-*d*₆) δ 172.1 (CO), 153.2 (C), 144.4 (C), 140.5 (C), 126.7 (CH), 124.5 (CH), 124.3 (CH), 121.1 (CH), 116.9 (CH), 114.0 (C), 112.3 (CH), 42.8 (CH₂).

HRMS (TOF ES⁻): m/z calcd for C₁₂H₁₀NO₃S (M-H)⁻ 248.0381, found 248.0387.

HPLC: (λ = 254 nm), 95.51%; (λ = 214 nm), 97.96%; t_R = 10.64 min (Method 2).

2-Hydroxy-4-[*N*-(2-thienylmethyl)amino]benzoic acid hydrochloride (MDMG-979)



General synthetic procedure 6B. Reagents: 2-thiophenecarboxaldehyde (83.33 μ L, 0.892 mmol), 4-aminosalicylic acid (163.85 mg, 1.07 mmol), NaBH₄ (50.61 mg, 1.338 mmol) and DCM/MeOH 1:1 (4 mL). Column

chromatography: DCM/MeOH (20:1 → 15:1). Orange solid, 31% yield (80 mg, 0.280 mmol).

mp: 154-157 °C.

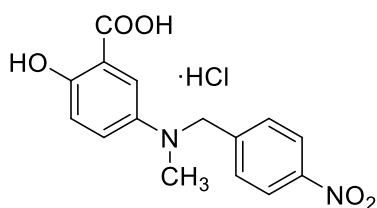
¹H NMR (500 MHz, CD₃OD) δ 7.56 (d, *J* = 8.8 Hz, 1H), 7.26 (dd, *J* = 5.1, 1.2 Hz, 1H), 7.02 (dd, *J* = 2.3, 1.1 Hz, 1H), 6.95 (dd, *J* = 5.0, 3.5 Hz, 1H), 6.20 (dd, *J* = 8.8, 2.2 Hz, 1H), 6.07 (d, *J* = 2.2 Hz, 1H), 4.52 (s, 2H).

¹³C NMR (126 MHz, CD₃OD) δ 173.7 (CO), 165.2 (C), 156.1 (C), 144.2 (C), 132.5 (CH), 127.7 (CH), 125.9 (CH), 125.3 (CH), 106.6 (CH), 102.5 (C), 98.5 (CH), 42.9 (CH₂).

HRMS (TOF ES⁻): *m/z* calcd for C₁₂H₁₀NO₃S (M-H)⁻ 248.0381, found 248.0387.

HPLC: (λ = 254 nm), 100%; (λ = 214 nm), 100%; *t_R* = 13.80 min (Method 3).

2-Hydroxy-5-[*N*-methyl-*N*-(4-nitrobenzyl)amino]benzoic acid hydrochloride (MDMG-991)



In a round bottom flask equipped with a stirring bar and under argon atmosphere, the secondary amine **MDMG-592** (30 mg, 0.092) was dissolved in MeOH, and HCHO (36.5-38% in MeOH, 8.37 μL, 0.111 mmol) was added afterwards. The reaction was refluxed for 3 h and then NaBH₃CN (15.09 mg, 0.240 mmol) was added, after which the reaction was refluxed for another 30 min to carry out the *in situ* reduction. The reaction was then cooled to 0 °C, quenched with 5% HCl and concentrated in rotavapor.²¹⁸ The crude product was purified by flash chromatography on silica gel with EtOAc/CH₃CN/MeOH/H₂O (70:2.5:1.25:1.25 → 70:5:2.5:2.5) to afford the desired compound in quantitative yield (31 mg, 0.092 mmol).

mp: 148-151 °C.

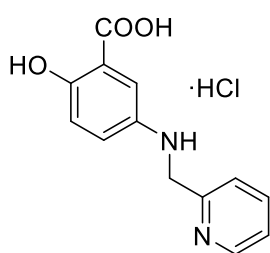
¹H NMR [400 MHz, (CD₃)₂CO] δ 6.93 – 6.85 (m, 2H), 6.21 (d, *J* = 8.7 Hz, 2H), 5.98 (d, *J* = 3.1 Hz, 1H), 5.78 (dd, *J* = 9.0, 3.1 Hz, 1H), 5.54 (d, *J* = 9.0 Hz, 1H), 3.26 (s, 2H), 1.69 (d, *J* = 4.4 Hz, 3H).

^{13}C NMR [101 MHz, $(\text{CD}_3)_2\text{CO}$] δ 154.5 (CO), 136.6 (C), 134.2 (C), 129.3 (C), 129.2 (C), 124.5 (C), 110.1 (2CH), 105.4 (2CH), 104.75 (CH), 99.5 (CH), 96.3 (CH), 39.3 (CH_2), 20.9 (CH_3).

HRMS (TOF ES^-): m/z calcd for $\text{C}_{15}\text{H}_{13}\text{N}_2\text{O}_5$ ($\text{M}-\text{H}$) $^-$ 301.0824, found 301.0814.

HPLC: ($\lambda = 254$ nm), 100%; ($\lambda = 214$ nm), 100%; $t_{\text{R}} = 11.14$ min. (Method 4).

2-Hydroxy-5-[*N*-(pyridin-2-ylmethyl)amino]benzoic acid hydrochloride (MDMG-1019)



General synthetic procedure 6B. Reagents: 2-Pyridinecarboxaldehyde (62.12 μL , 0.653 mmol), 5-aminosalicylic acid (100 mg, 0.653 mmol), NaBH_4 (37.05 mg, 0.979 mmol) and DCM/MeOH 3:1 (4 mL). Column chromatography: DCM/MeOH (20:1 \rightarrow 8:2). Yellowish solid, 18% yield (33 mg, 0.118 mmol).

mp: >300 $^\circ\text{C}$.

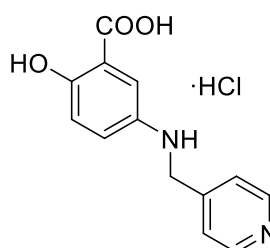
^1H NMR (400 MHz, CD_3OD) δ 8.47 (d, $J = 4.3$ Hz, 1H), 7.74 (t, $J = 7.5$ Hz, 1H), 7.46 (d, $J = 7.8$ Hz, 1H), 7.34 – 7.08 (m, 2H), 6.79 (dd, $J = 8.7, 2.0$ Hz, 1H), 6.66 (d, $J = 8.7$ Hz, 1H), 4.39 (s, 2H).

^{13}C NMR (101 MHz, CD_3OD) δ 160.9 (CO), 155.0 (C), 149.4 (CH), 141.2 (C), 138.8 (CH), 123.5 (CH), 123.4 (C), 123.2 (CH), 121.8 (CH), 118.5 (C), 117.8 (CH), 115.3 (CH), 51.0 (CH_2).

HRMS (TOF ES^+): m/z calcd for $\text{C}_{13}\text{H}_{13}\text{N}_2\text{O}_3$ ($\text{M}+\text{H}$) $^+$ 245.0926, found 245.0905.

HPLC: ($\lambda = 254$ nm), 100%; ($\lambda = 214$ nm), 99.61%; $t_{\text{R}} = 8.37$ min (Method 1).

2-Hydroxy-5-[*N*-(pyridin-4-ylmethyl)amino]benzoic acid hydrochloride (MDMG-1034)



General synthetic procedure 6B. Reagents: 4-pyridinecarboxaldehyde (123.03 μL , 1.306 mmol), 5-aminosalicylic acid (200 mg, 1.306 mmol), NaBH_4 (123.51 mg, 3.26 mmol) and DCM/MeOH 1:1 (8 mL). Column

chromatography: DCM/MeOH (20:1 → 10:1). Yellowish solid, 30% yield (110 mg, 0.392 mmol).

mp: >300 °C.

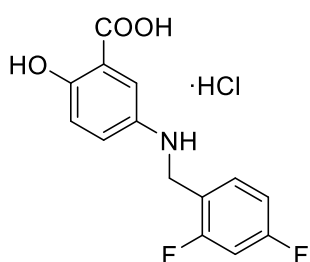
¹H NMR (400 MHz, CD₃OD) δ 8.43 (s, 2H), 7.45 (d, *J* = 4.3 Hz, 2H), 7.10 (s, 1H), 6.78 (dd, *J* = 8.7, 1.8 Hz, 1H), 6.67 (d, *J* = 8.7 Hz, 1H), 4.37 (s, 2H).

¹³C NMR (101 MHz, CD₃OD) δ 164.3(CO), 154.9 (C), 153.6 (C), 149.5 (CH), 141.4 (C), 124.1 (CH), 121.8 (CH), 118.3 (C), 117.9 (CH), 114.7 (CH), 48.4 (CH₂).

HRMS (TOF ES⁺): *m/z* calcd for C₁₃H₁₃N₂O₃ (M+H)⁺ 245.0926, found 245.0920.

HPLC: (λ = 254 nm), 100%; (λ = 214 nm), 100%; *t_R* = 7.79 min (Method 1).

5-[*N*-(2,4-Difluorobenzyl)amino]-2-hydroxybenzoic acid hydrochloride (MDMG-1054)



General synthetic procedure 6B. Reagents: 2,4-difluorobenzaldehyde (142.86 μL, 1.306 mmol), 5-aminosalicylic acid (200 mg, 1.306 mmol), NaBH₄ (98.81 mg, 2.612 mmol) and DCM/MeOH 4:1 (5 mL). Column chromatography: DCM/MeOH (20:1 → 10:1). White solid, 21% yield (90 mg, 0.285 mmol).

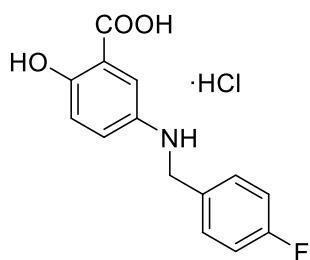
mp: 202-203 °C.

¹H NMR (400 MHz, DMSO-*d*₆) δ 7.42 (td, *J* = 8.7, 6.9 Hz, 1H), 7.21 (ddd, *J* = 10.5, 9.4, 2.6 Hz, 1H), 7.04 (tdd, *J* = 8.4, 2.5, 0.8 Hz, 1H), 6.96 (d, *J* = 2.9 Hz, 1H), 6.88 (dd, *J* = 8.8, 3.0 Hz, 1H), 6.74 (d, *J* = 8.8 Hz, 1H), 4.22 (s, 2H).

¹³C NMR (101 MHz, DMSO-*d*₆) δ 171.9 (CO), 161.9 (dd, *J*_{C-F} = 99.8, 12.3 Hz, C-F), 159.5 (dd, *J*_{C-F} = 101.5, 12.3 Hz, C-F), 152.9 (C), 140.82 (C), 130.5 (dd, *J*_{C-F} = 9.7, 6.3 Hz, CH), 122.9 (dd, *J*_{C-F} = 15.0, 3.6 Hz, C), 121.7 (CH), 117.5 (CH), 112.5 (C), 111.28 (CH), 111.24 (dd, *J*_{C-F} = 21.0, 3.6 Hz, CH), 103.6 (t, *J*_{C-F} = 25.9 Hz, CH), 40.33 (CH₂).

HRMS (TOF ES⁺): *m/z* calcd for C₁₄H₁₂NO₃F₂ (M+H)⁺ 280.0785, found 280.0769.

HPLC: (λ = 254 nm), 100%; (λ = 214 nm), 100%; *t_R* = 10.84 min (Method 3).

5-[N-(4-Fluorobenzyl)amino]-2-hydroxybenzoic acid hydrochloride (MDMG-1058P)

General synthetic procedure 6B. Reagents: 4-difluorobenzaldehyde (140.95 μL , 1.306 mmol), 5-aminosalicylic acid (200 mg, 1.306 mmol), NaBH_4 (98.81 mg, 2.612 mmol) and DCM/MeOH 4:1 (5 mL). Column chromatography: DCM/MeOH (20:1 \rightarrow 15:1). Brown solid, 14% yield (55 mg, 0.185 mmol).

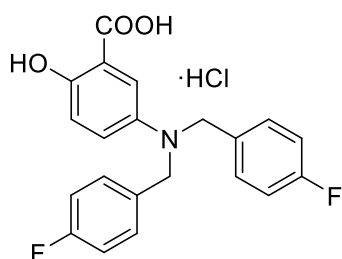
mp: 186-189 $^\circ\text{C}$.

$^1\text{H NMR}$ (400 MHz, CD_3OD) δ 7.36 (dd, $J = 8.5, 5.5$ Hz, 2H), 7.23 (s, 1H), 7.01 (t, $J = 8.8$ Hz, 2H), 6.83 (d, $J = 9.0$ Hz, 1H), 6.69 (d, $J = 8.7$ Hz, 1H), 4.24 (s, 2H).

$^{13}\text{C NMR}$ (101 MHz, CD_3OD) δ 171.1 (CO), 163.3 (d, $J_{\text{C-F}} = 243.3$ Hz, C-F), 155.5 (d, $J_{\text{C-F}} = 2.0$ Hz, C), 141.0 (C), 136.79 (C), 136.76 (C), 130.5 (d, $J_{\text{C-F}} = 8.0$ Hz, 2CH), 122.8 (CH), 117.9 (CH), 115.98 (d, $J_{\text{C-F}} = 21.6$ Hz, 2CH), 115.95 (CH), 49.70 (CH_2).

HRMS (TOF ES^+): m/z calcd for $\text{C}_{14}\text{H}_{13}\text{NO}_3\text{F}$ ($\text{M}+\text{H}$) $^+$ 262.0879, found 262.0867.

HPLC: ($\lambda = 254$ nm), 95.04%; ($\lambda = 214$ nm), 100%; $t_{\text{R}} = 11.44$ min (Method 2).

5-[N,N-Bis(4-fluorobenzyl)amino]-2-hydroxybenzoic acid hydrochloride (MDMG-1058I)

By-product in the synthesis of **MDMG-1058P**.

Column chromatography: DCM/MeOH (20:1 \rightarrow 15:1). Brown solid (8 mg, 0.004 mmol).

$^1\text{H NMR}$ (600 MHz, CD_3OD) δ 7.37 – 7.31 (d, 1H), 7.25 (dd, $J = 8.3, 5.6$ Hz, 4H), 7.06 – 6.92 (m, 5H), 6.71 (d, $J = 8.9$ Hz, 1H), 4.43 (s, 4H).

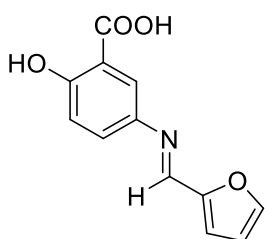
$^{13}\text{C NMR}$ (151 MHz, CD_3OD) δ 172.5 (CO), 163.3 (d, $J_{\text{C-F}} = 243.2$ Hz, C-F), 155.8 (d, $J_{\text{C-F}} = 2.1$ Hz, C), 142.8 (C), 136.08 (C), 136.06 (C), 130.3 (d, $J_{\text{C-F}} = 8.0$ Hz, 2CH), 124.5(CH), 118.2 (CH), 118.0 (CH), 115.9 (d, $J = 21.6$ Hz, 2CH), 56.2 (CH_2).

HRMS (TOF ES^+): m/z calcd for $\text{C}_{21}\text{H}_{18}\text{NO}_3\text{F}_2$ ($\text{M}+\text{H}$) $^+$ 370.1255, found 370.1235.

HPLC: ($\lambda = 254$ nm), 100%; ($\lambda = 214$ nm), 100%; $t_R = 18.83$ min (Method 2).

5.4.2.2. Synthesis of salicylate derivatives containing rigid imino and azo linkers

(*E*)-5-[*N*-(Furan-2-ylmethylidene)amino]-2-hydroxybenzoic acid (MDMG-574)



In a round bottom flask equipped with a stirring bar and under argon atmosphere, 5-aminosalicylic acid (60 mg, 0.392 mmol) and 2-furaldehyde (40 μ L, 0.470 mmol) were dissolved in dry DCM/MeOH 1:1 (6 mL). Activated 3 \AA molecular sieves were added and the mixture was stirred for 48 h at rt.²¹⁹ The crude product was filtered and the filtrate was concentrated in rotavapor and precipitated in CH_3CN to afford 24 mg of the desired compound (26% yield, 0.104 mmol).

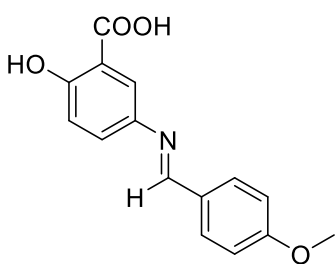
mp: > 300 $^\circ\text{C}$.

$^1\text{H NMR}$ (400 MHz, $\text{DMSO-}d_6$) δ = 8.41 (s, 1H), 7.97 – 7.58 (m, 2H), 7.18 (d, $J = 7.9$ Hz, 1H), 7.00 (d, $J = 18.9$ Hz, 1H), 6.79 – 6.42 (m, 2H).

HRMS (TOF ES^+): m/z calcd for $\text{C}_{12}\text{H}_{10}\text{NO}_4$ ($\text{M}+\text{H}$)⁺ 232.0610, found 232.0609.

HPLC: Decomposition.

(*E*)-2-Hydroxy-5-[*N*-(4-methoxybenzylidene)amino]benzoic acid (MDMG-628)²²⁰



In a round bottom flask equipped with a stirring bar and under argon atmosphere, 5-aminosalicylic acid (60 mg, 0.392 mmol) and 4-methoxybenzaldehyde (55.18 μ L, 0.47 mmol) were dissolved in dry EtOH and activated 3 \AA molecular sieves were added. The mixture was stirred for 24 h at rt and the crude product was filtered. The filtrate was concentrated in rotavapor and precipitated in CH_3CN to afford the desired compound (18 mg, 0.066 mmol 17% yield).

mp: 213 $^\circ\text{C}$.

$^1\text{H NMR}$ (500 MHz, $\text{DMSO-}d_6$) δ 8.56 (s, 1H), 7.86 (d, $J = 8.6$ Hz, 2H), 7.68 (s, 1H), 7.30 (d, $J = 8.7$ Hz, 1H), 7.05 (d, $J = 8.6$ Hz, 2H), 6.79 (d, $J = 8.6$ Hz, 1H), 3.82 (s, 3H).

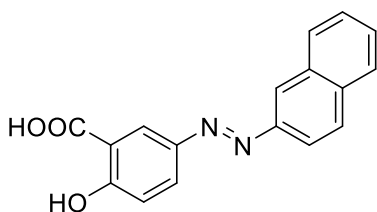
^{13}C NMR (126 MHz, DMSO- d_6) δ 172.5 (CO), 161.4 (CH), 160.8 (C), 156.4 (CH), 141.1 (C), 129.9 (2CH), 129.3 (CH), 126.5 (C), 121.8 (C), 116.7 (CH), 114.5 (C), 114.1 (2CH), 55.3 (CH₃).

HRMS (TOF ES⁻): m/z calcd for C₁₅H₁₂NO₄ (M-H)⁻ 270.0766, found 270.0773.

HPLC: Decomposition.

Experimental data agree with those reported.

5-(2-Naphthylazo)-2-hydroxybenzoic acid (MDMG-604)



Salicylic acid (50 mg, 0.362 mmol) was dissolved in 0.45 mL of NaOH 10% and added over a previously prepared solution of NaNO₂ (37.44 mg, 0.542 mmol) in 0.55 mL of H₂O. The mixture was cooled to 0 °C and added to a previously prepared solution of 2-naphthylamine (62.16 mg, 0.434 mmol) in 1 mL HCl 37%/H₂O 3:2. The mixture was allowed to stir at 0 °C for 6 h and the pH was adjusted to 6 with a saturated solution of Na₂CO₃. The crude product was purified by flash chromatography on silica gel with DCM/MeOH (100:2 → 100:20). Orange solid, 31% yield (33 mg, 0.113 mmol).

mp: > 300 °C.

^1H NMR (400 MHz, DMSO- d_6) δ 8.45 – 8.38 (m, 1H), 8.35 (d, J = 2.4 Hz, 1H), 8.16 – 8.07 (m, 1H), 8.07 – 7.93 (m, 3H), 7.86 (dd, J = 8.7, 2.5 Hz, 1H), 7.59 (p, J = 5.7 Hz, 2H), 6.79 (d, J = 8.8 Hz, 1H).

^{13}C NMR (101 MHz, DMSO- d_6) δ 170.7 (CO), 168.9 (C), 149.8 (C), 142.4 (C), 133.6 (C), 133.2 (C), 129.0 (CH), 128.9 (CH), 127.7 (CH), 127.1 (CH), 126.8 (CH), 126.4 (CH), 126.0 (CH), 125.3 (CH), 119.4 (C), 117.6 (CH), 117.0 (CH).

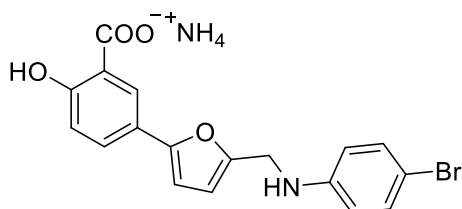
HRMS (TOF ES⁻): m/z calcd for C₁₇H₁₁N₂O₃ (M-H)⁻ 291.0770, found 291.0754.

HPLC: (λ = 254 nm), 100%; (λ = 214 nm), 100%; t_R = 16.42 min. (Method 5).

5.4.3. Synthesis of derivatives of the lead compound MDMG-409

5.4.3.1. Synthesis of aminomethylfuryl derivatives of MDMG-409.

Ammonium 5-{5-[[N-(4-bromophenyl)amino]methyl]furan-2-yl}-2-hydroxybenzoate (MDMG-907)



General synthetic procedure 6C. Reagents: **MDMG-409** (100 mg, 0.431 mmol), 4-bromoaniline (88.90 mg, 0.517 mmol), NaBH(OAc)₃ (182.56 mg, 0.861 mmol) and DCM/MeOH 3/1 (8 mL). Column chromatography:

DCM/methanolic ammonia 7N (100:1 → 100:10). Orange solid, 45% yield (80 mg, 0.197 mmol).

mp: 115-117 °C (decomposition).

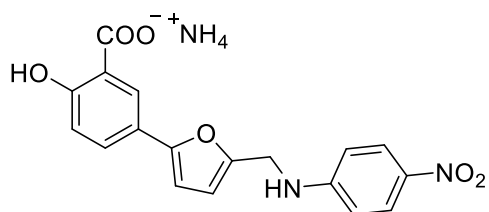
¹H NMR (400 MHz, CD₃OD) δ 8.17 (d, *J* = 1.9 Hz, 1H), 7.60 (dd, *J* = 8.5, 2.0 Hz, 1H), 7.20 (d, *J* = 8.7 Hz, 2H), 6.83 (d, *J* = 8.5 Hz, 1H), 6.64 (d, *J* = 8.7 Hz, 2H), 6.48 (d, *J* = 3.1 Hz, 1H), 6.27 (d, *J* = 3.0 Hz, 1H), 4.30 (s, 2H).

¹³C NMR (101 MHz, CD₃OD) δ 175.4 (CO), 162.1 (C), 154.6 (C), 153.0 (C), 148.9 (C), 132.6 (2CH), 129.6 (CH), 126.9 (CH), 123.1 (C), 119.2 (C), 117.7 (CH), 115.8 (2CH), 109.9 (CH), 109.4 (C), 104.6 (CH), 41.9 (CH₂).

HRMS (TOF ES⁻): *m/z* calcd for C₁₈H₁₃NO₄Br (M-H)⁻ 386.0028, found 386.0001.

HPLC: (λ = 254 nm), 98.96%; (λ = 214 nm), 97.03%; *t_R* = 16.41 min. (Method 4).

Ammonium 2-hydroxy-5-{5-[[N-(4-nitrophenyl)amino]methyl]furan-2-yl}benzoate (MDMG-915)



General synthetic procedure 6C. Reagents: **MDMG-409** (100 mg, 0.431 mmol), 4-nitroaniline (77.33 mg, 0.559 mmol), NaBH(OAc)₃ (182.56 mg, 0.861 mmol) and DCM/MeOH 3:1 (4 mL). Column chromatography:

DCM/methanolic ammonia 7N (100:1 → 100:10) (complex purification). Yellow solid, 24% yield (39 mg, 0.105 mmol).

mp: 159-161 °C.

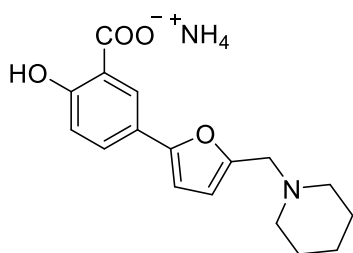
¹H NMR (400 MHz, CD₃OD) δ 8.20 (d, *J* = 2.0 Hz, 1H), 8.07 (d, *J* = 9.2 Hz, 2H), 7.62 (d, *J* = 8.5 Hz, 1H), 6.85 (d, *J* = 8.5 Hz, 1H), 6.76 (d, *J* = 9.1 Hz, 2H), 6.52 (d, *J* = 3.2 Hz, 1H), 6.36 (d, *J* = 3.2 Hz, 1H), 4.47 (s, 2H).

¹³C NMR (101 MHz, CD₃OD) δ 175.6 (CO), 162.2 (C), 155.5 (C), 155.2 (C), 151.6 (C), 138.5 (C), 129.4 (CH), 127.1 (CH), 127.0 (CH), 122.8 (C), 119.8 (C), 117.6 (CH), 112.2 (CH), 110.4 (CH), 104.5 (CH), 41.0 (CH₂).

HRMS (TOF ES⁻): *m/z* calcd for C₁₈H₁₃N₂O₆ (M-H)⁻ 353.0774, found 353.0778.

HPLC: (λ = 254 nm), 100%; (λ = 214 nm), 100%; *t_R* = 15.87 min (Method 3).

Ammonium 2-hydroxy-5-[5-(piperidin-1-ylmethyl)furan-2-yl]benzoate (MDMG-919)



General synthetic procedure 6C. Reagents: **MDMG-409** (100 mg, 0.431 mmol), piperidine (55.31 μL, 0.559 mmol), NaBH(OAc)₃ (273.83 mg, 1.292 mmol) and DCM/MeOH 3:1 (4 mL). Column chromatography: EtOAc/CH₃CN/MeOH/H₂O (70:10:5:5 → 70:10:10:10). Brownish solid, 59% yield (77 mg, 0.256 mmol).

mp: 209 °C.

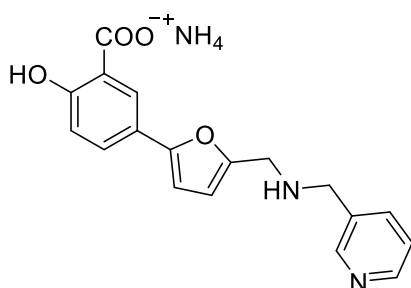
¹H NMR (400 MHz, CD₃OD) δ 8.21 (d, *J* = 2.3 Hz, 1H), 7.63 (dd, *J* = 8.5, 2.3 Hz, 1H), 6.83 (d, *J* = 8.5 Hz, 1H), 6.69 – 6.56 (m, 2H), 4.20 (s, 2H), 3.09 (s, 4H), 1.81 (p, *J* = 5.8 Hz, 4H), 1.62 (q, *J* = 5.7 Hz, 2H).

¹³C NMR (101 MHz, CD₃OD) δ 175.5 (CO), 162.9 (C), 157.5 (C), 144.8 (C), 129.6 (CH), 127.5 (CH), 121.9 (C), 120.4 (C), 117.8 (CH), 116.5 (CH), 104.9 (CH), 54.2 (CH₂), 54.0 (2CH₂), 24.7 (2CH₂), 23.1 (CH₂).

HRMS (TOF ES⁻): *m/z* calcd for C₁₇H₁₈NO₄ (M-H)⁻ 300.1236, found 300.1264.

HPLC: (λ = 254 nm), 100%; (λ = 214 nm), 97.90%; *t_R* = 10.01 min (Method 2).

Ammonium 2-hydroxy-5-{5-[[*N*-(pyridin-3-ylmethyl)amino]methyl]furan-2-yl}benzoate (MDMG-927)



General synthetic procedure 6C. Reagents: **MDMG-409** (70 mg, 0.301 mmol), 3-(aminomethyl)pyridine (40.27 μ L, 0.392 mmol), NaBH(OAc)₃ (127.79 mg, 0.603 mmol) and DCM/MeOH 3:1 (4 mL). Column chromatography: EtOAc/CH₃CN/MeOH/H₂O (70:5:2.5:2.5 \rightarrow 70:10:10:10). Pale solid, 41% yield (40 mg, 0.123 mmol).

mp: > 300 °C.

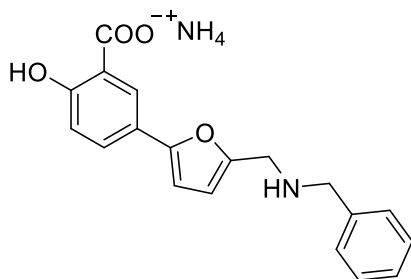
¹H NMR (400 MHz, DMSO-*d*₆) (400 MHz, DMSO-*d*₆) δ = 8.67 (s, 1H), 8.53 (d, *J* = 3.8 Hz, 1H), 8.05 (d, *J* = 2.2 Hz, 1H), 7.97 (d, *J* = 7.7 Hz, 1H), 7.54 (dd, *J* = 8.5, 2.5 Hz, 1H), 7.41 (dd, *J* = 7.8, 4.8 Hz, 1H), 6.69 (d, *J* = 8.5 Hz, 1H), 6.61 (d, *J* = 3.2 Hz, 1H), 6.56 (d, *J* = 2.7 Hz, 1H), 4.08 (d, *J* = 3.6 Hz, 4H).

¹³C NMR (101 MHz, DMSO-*d*₆) δ 171.9 (CO), 171.3 (C), 171.3 (C), 163.0 (C), 154.4 (C), 150.6 (CH), 149.2 (CH), 137.3 (CH), 127.4 (CH), 125.5 (CH), 123.4 (CH), 120.0 (C), 118.7 (C), 116.4 (CH), 112.7 (CH), 103.3 (CH), 47.6 (CH₂), 43.1 (CH₂).

HRMS (TOF ES⁻): *m/z* calcd for C₁₈H₁₅N₂O₄ (M-H⁺)⁻ 323.1032, found 323.1056.

HPLC: (λ = 254 nm), 100%; (λ = 214 nm), 92.68%; *t*_R = 8.57 min (Method 2).

Ammonium 5-[5-(benzylaminomethyl)furan-2-yl]-2-hydroxybenzoate (MDMG-931P)



General synthetic procedure 6C. Reagents: **MDMG-409** (92 mg, 0.396 mmol), benzylamine (55.19 mg, 0.515 mmol), NaBH(OAc)₃ (167.95 mg, 0.792 mmol) and DCM/MeOH 3:1 (4 mL). Column chromatography: EtOAc/CH₃CN/methanolic ammonia 7N/H₂O (70:2.5:1.25:1.25 \rightarrow 70:5:2.5:2.5).

Yellow solid, 67% yield (91 mg, 0.267 mmol).

mp: 182-185 °C.

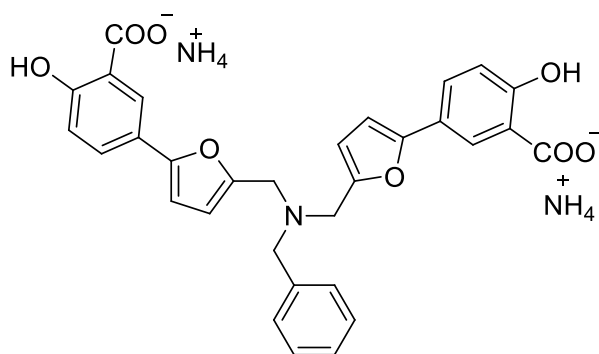
$^1\text{H NMR}$ (400 MHz, $\text{DMSO-}d_6$) δ 8.11 (s, 1H), 7.59 – 7.46 (m, 3H), 7.46 – 7.35 (m, 3H), 6.81 – 6.50 (m, 3H), 4.21 (s, 2H), 4.16 (s, 2H).

$^{13}\text{C NMR}$ (101 MHz, $\text{DMSO-}d_6$) δ 171.3 (CO), 163.2 (C), 154.9 (C), 144.7 (C), 132.7 (C), 129.8 (2CH), 128.66 (CH), 128.60 (2CH), 127.7 (CH), 125.6 (CH), 119.8 (C), 118.6 (C), 116.5 (CH), 113.6 (CH), 103.4 (CH), 49.7 (CH_2), 42.5 (CH_2).

HRMS (TOF ES^-): m/z calcd for $\text{C}_{19}\text{H}_{16}\text{NO}_4$ (M-H^+) $^-$ 322.1079, found 322.1087.

HPLC: ($\lambda = 254$ nm), 97.77%; ($\lambda = 214$ nm), 97.88%; $t_R = 8.98$ min (Method 3).

Ammonium 5,5'-{[(benzylazanediyl)bis(methylene)]bis(furan-5,2-diyl)}bis(2-hydroxybenzoate) (MDMG-931I)



Formed during the chromatographic purification of **MDMG-931**.

Brownish solid (10 mg, 0.017 mmol).

mp: 170-172 °C.

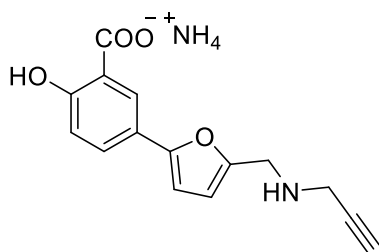
$^1\text{H NMR}$ (300 MHz, CD_3OD) δ 8.23 (d, $J = 2.2$ Hz, 2H), 7.67 (dd, $J = 8.6, 2.3$ Hz, 2H), 7.51 – 7.36 (m, 5H), 6.87 (d, $J = 8.6$ Hz, 2H), 6.59 (d, $J = 3.2$ Hz, 2H), 6.49 (d, $J = 3.2$ Hz, 2H), 3.96 (s, 4H), 3.92 (s, 2H).

$^{13}\text{C NMR}$ (126 MHz, CD_3OD) δ 175.1 (CO), 162.5 (C), 155.9 (C), 149.5 (C), 137.4 (C), 130.8 (CH), 129.9 (CH), 129.7 (CH), 129.0 (CH), 127.1 (CH), 122.8 (C), 119.1 (C), 117.9 (CH), 114.1 (CH), 104.9 (CH), 58.2 (CH_2), 52.7 (CH_2).

HRMS (TOF ES^-): m/z calcd for $\text{C}_{31}\text{H}_{24}\text{NO}_8$ (M-H^-) 538.1502, found 538.1494.

HPLC: ($\lambda = 254$ nm), 98.79%; ($\lambda = 214$ nm), 98.64%; $t_R = 12.61$ min (Method 3).

Ammonium 2-hydroxy-5-{5-[(prop-2-yn-1-ylamino)methyl]furan-2-yl}benzoate (MDMG-935P)



(100 mg, 0.347 mmol).

General synthetic procedure 6C. Reagents: **MDMG-409** (105 mg, 0.452 mmol), propargylamine (37.65 μ L, 0.588 mmol), NaBH(OAc)₃ (191.68 mg, 0.904 mmol) and DCM/MeOH 3:1 (4 mL). Column chromatography: EtOAc/CH₃CN/methanolic ammonia 7N/H₂O (70:2.5:1.25:1.25 \rightarrow 70:10:5:5). Brown solid, 76% yield

mp: 180 °C (decomposition).

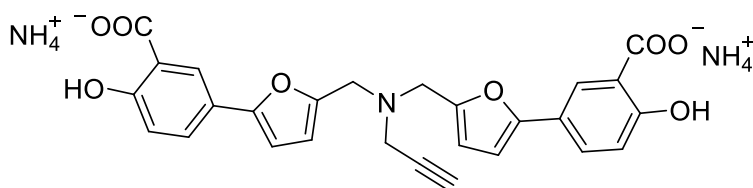
¹H NMR (300 MHz, CD₃OD) δ 8.20 (d, J = 2.3 Hz, 1H), 7.64 (dd, J = 8.6, 2.4 Hz, 1H), 6.84 (d, J = 8.7 Hz, 1H), 6.59 (s, 2H), 4.26 (s, 2H), 3.83 (d, J = 2.5 Hz, 2H), 3.11 (t, J = 2.6 Hz, 1H).

¹³C NMR (101 MHz, CD₃OD) δ 175.4 (CO), 162.9 (C), 157.2 (C), 145.7 (C), 129.8 (CH), 127.4 (CH), 122.0 (C), 119.8 (C), 117.8 (CH), 115.1 (CH), 104.9 (CH), 78.3 (C), 75.8 (CH), 43.8 (CH₂), 36.7 (CH₂).

HRMS (TOF ES⁻): m/z calcd for C₁₅H₁₂N₂O₄ (M-H)⁻ 270.0766, found 270.0757.

HPLC (λ = 254 nm), 100%; (λ = 214 nm), 99.05%; t_R = 9.66 min (Method 2).

Ammonium 5,5'-{[(prop-2-yn-1-ylazanediyl)bis(methylene)]bis(furan-5,2-diyl)}bis(2-hydroxybenzoate) (MDMG-935I)



Formed during the chromatographic purification of **MDMG-931**.

Brown solid (15 mg, 0.029 mmol).

mp: 138-140 °C (decomposition).

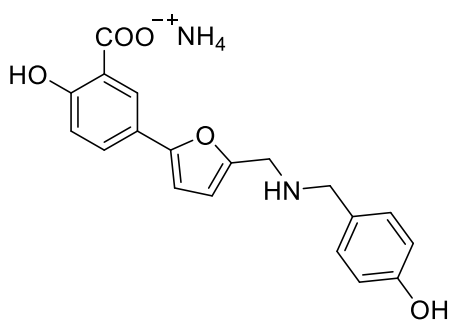
¹H NMR (300 MHz, CD₃OD) δ 8.22 (d, J = 2.3 Hz, 2H), 7.70 (dd, J = 8.6, 2.4 Hz, 2H), 6.87 (d, J = 8.7 Hz, 2H), 6.57 (d, J = 3.3 Hz, 2H), 6.44 (d, J = 3.3 Hz, 2H), 3.88 (s, 4H), 3.45 (d, J = 2.5 Hz, 2H), 2.78 (s, 1H).

^{13}C NMR (126 MHz, CD_3OD) δ 175.3, 169.3, 162.9, 157.2, 132.3, 129.7, 127.4, 122.0, 117.8, 114.8, 104.9, 78.0, 69.1, 43.9, 36.7.

HRMS (TOF ES^-): m/z calcd for $\text{C}_{27}\text{H}_{20}\text{NO}_8$ ($\text{M}-\text{H}$) $^-$ 486.1189, found 486.1193.

HPLC ($\lambda = 254$ nm), 100%; ($\lambda = 214$ nm), 95.78%; $t_{\text{R}} = 13.06$ min (Method 3).

Ammonium 2-hydroxy-5-{5-[[*N*-(4-hydroxybenzyl)amino]methyl]furan-2-yl}benzoate (MDMG-1074)



General synthetic procedure 6C. Reagents: **MDMG-409** (100, 0.431 mmol), 4-hydroxybenzylamine (68.95 mg, 0.559 mmol), $\text{NaBH}(\text{OAc})_3$ (182.56 mg, 0.861 mmol) and DCM/MeOH 3:1 (4 mL). Column chromatography: $\text{EtOAc}/\text{CH}_3\text{CN}/\text{methanolic ammonia } 7\text{N}/\text{H}_2\text{O}$ (70:2.5:1.25:1.25 \rightarrow 70:10:5:5) (complex

purification). Yellowish solid, 52% yield (80 mg, 0.224 mmol).

mp: 190 °C (decomposition).

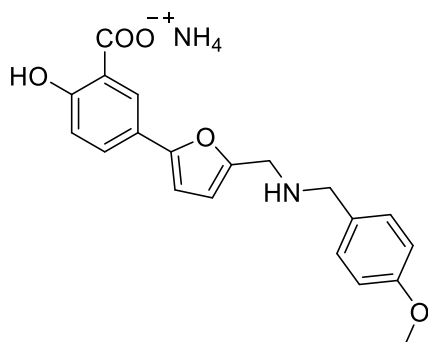
^1H NMR (400 MHz, $\text{DMSO}-d_6$) δ 9.73 (s, 1H), 8.11 (d, $J = 2.4$ Hz, 1H), 7.55 (dd, $J = 8.5, 2.3$ Hz, 1H), 7.31 (d, $J = 8.4$ Hz, 2H), 6.80 (d, $J = 8.4$ Hz, 2H), 6.70 (d, $J = 8.5$ Hz, 1H), 6.66 – 6.60 (m, 2H), 4.21 (s, 2H), 4.07 (s, 2H).

^{13}C NMR (101 MHz, $\text{DMSO}-d_6$) δ 171.1 (CO), 163.3 (C), 158.0 (C), 155.1 (C), 144.0 (C), 131.5 (2CH), 127.7 (CH), 125.6 (CH), 121.9 (C), 119.8 (C), 118.4 (C), 116.6 (CH), 115.3 (2CH), 113.9 (CH), 103.3 (CH), 49.3 (CH_2), 42.1 (CH_2).

HRMS (TOF ES^+): m/z calcd for $\text{C}_{19}\text{H}_{18}\text{NO}_5$ ($\text{M}+\text{H}$) $^+$ 340.1185, found 340.1198.

HPLC: ($\lambda = 254$ nm), 100%; ($\lambda = 214$ nm), 98.90%; $t_{\text{R}} = 10.58$ min (Method 2).

Ammonium 2-hydroxy-5-{5-[[N-(4-methoxybenzyl)amino]methyl]furan-2-yl}benzoate (MDMG-1078)



General synthetic procedure 6C. Reagents: **MDMG-409** (100, 0.431 mmol), 4-methoxybenzylamine (73.14 μ L, 0.559 mmol), NaBH(OAc)₃ (182.56 mg, 0.861 mmol) and DCM/MeOH 3:1 (4 mL). Column chromatography: EtOAc/CH₃CN/methanolic ammonia 7N/H₂O (70:2.5:1.25:1.25 \rightarrow 70:10:5:5) (complex purification). Yellowish solid, 51% yield

(82 mg, 0.221 mmol).

mp: 200-203 °C.

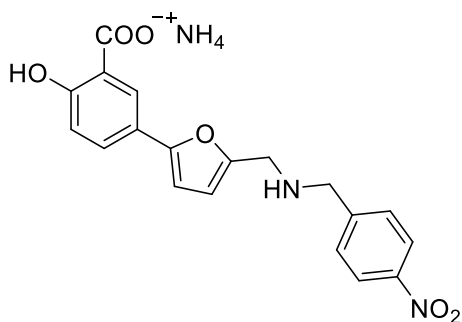
¹H NMR (600 MHz, DMSO-*d*₆) δ 9.31 (s, 1H), 8.10 (d, *J* = 2.5 Hz, 1H), 7.53 (dd, *J* = 8.4, 2.0 Hz, 1H), 7.42 (d, *J* = 8.6 Hz, 2H), 6.99 (d, *J* = 8.7 Hz, 2H), 6.68 (d, *J* = 8.5 Hz, 1H), 6.64 (d, *J* = 3.3 Hz, 1H), 6.59 (d, *J* = 3.3 Hz, 1H), 4.19 (s, 2H), 4.11 (s, 2H), 3.76 (s, 3H).

¹³C NMR (151 MHz, DMSO-*d*₆) δ 171.0 (CO), 163.5 (C), 159.6 (C), 155.1 (C), 144.3 (C), 131.4 (2CH), 127.5 (CH), 125.6 (CH), 124.2 (C), 120.1 (C), 118.2 (C), 116.5 (CH), 114.0 (2CH), 113.7 (CH), 103.2 (CH), 55.1 (CH₃), 49.2 (CH₂), 42.3 (CH₂).

HRMS (TOF ES⁺): *m/z* calcd for C₂₀H₂₀NO₅ (M+H)⁺ 354.1341, found 354.1335.

HPLC: (λ = 254 nm), 97.46%; (λ = 214 nm), 97.12%; *t*_R = 9.09 min (Method 3).

Ammonium 2-hydroxy-5-{5-[[N-(4-nitrobenzyl)amino]methyl]furan-2-yl}benzoate (MDMG-1082)



General synthetic procedure 6C. Reagents: **MDMG-409** (100 mg, 0.431 mmol), 4-nitrobenzylamine hydrochloride (105.60 mg, 0.559 mmol), NaBH(OAc)₃ (182.56 mg, 0.861 mmol) and DCM/MeOH 3:1 (4 mL). EtOAc/CH₃CN/methanolic ammonia 7N/H₂O (70:2.5:1.25:1.25 \rightarrow 70:10:5:5). Yellow solid, 48%

yield (80 mg, 0.208 mmol).

mp: 172-175 °C.

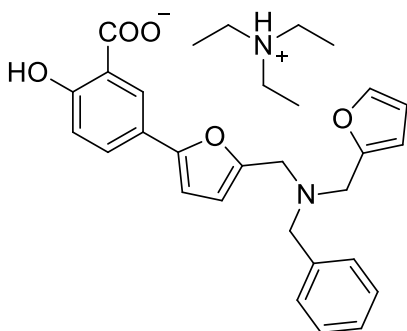
¹H NMR (400 MHz, DMSO-*d*₆) δ 8.27 (d, *J* = 8.7 Hz, 2H), 8.08 (d, *J* = 2.4 Hz, 1H), 7.75 (d, *J* = 8.7 Hz, 2H), 7.56 (dd, *J* = 8.5, 2.5 Hz, 1H), 6.72 (d, *J* = 8.5 Hz, 1H), 6.65 (d, *J* = 3.3 Hz, 1H), 6.56 (d, *J* = 3.3 Hz, 1H), 4.25 (s, 2H), 4.18 (s, 2H).

¹³C NMR (101 MHz, DMSO-*d*₆) δ 170.9, 163.2, 154.7, 151.1, 147.3, 130.7, 127.9, 125.48, 123.5, 119.2, 118.7, 116.7, 116.6, 113.0, 103.4, 49.3, 43.3.

HRMS (TOF ES⁻): *m/z* calcd for C₁₉H₁₅N₂O₆ (M-H)⁻ 367.0930, found 367.0927.

HPLC: (λ = 254 nm), 96.01%; *t_R* = 8.94 min (Method 3).

Triethylammonium 5-{5-[[*N*-benzyl-*N*-(furan-2-ylmethyl)amino]methyl]furan-2-yl}-2-hydroxybenzoate (MDMG-1125)



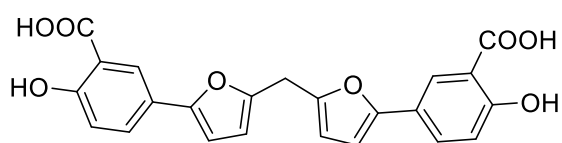
General synthetic procedure 6C. Reagents: **MDMG-931P** (30 mg, 0.088 mmol), 2-furaldehyde (10.95 μL, 0.132 mmol), NaBH(OAc)₃ (37.36 mg, 0.176 mmol) and DCM/MeOH 3:1 (1 mL). Column chromatography: EtOAc/CH₃CN/MeOH (7:1:0.5 → 7:1:1). Yellow solid, 40% yield (18 mg, 0.036 mmol).

¹H NMR (500 MHz, CD₃OD) δ 8.23 (d, *J* = 2.2 Hz, 1H), 7.67 (dd, *J* = 8.5, 2.3 Hz, 1H), 7.54 (s, 1H), 7.44 (d, *J* = 7.1 Hz, 2H), 7.37 (t, *J* = 7.5 Hz, 2H), 7.30 (t, *J* = 7.3 Hz, 1H), 6.88 (d, *J* = 8.6 Hz, 1H), 6.58 (d, *J* = 3.2 Hz, 1H), 6.43 (s, 3H), 3.85 (d, *J* = 7.7 Hz, 4H), 3.81 (s, 2H), 3.21 (q, *J* = 7.3 Hz, 8H), 1.31 (t, *J* = 7.3 Hz, 12H).

¹³C NMR (126 MHz, CD₃OD) δ 175.0 (CO), 162.4 (C), 155.6 (C), 150.1 (C), 144.0 (CH), 138.1 (C), 130.6 (CH), 130.2 (C), 130.0 (CH), 129.5 (CH), 128.8 (CH), 127.0 (CH), 122.9 (C), 118.8 (C), 117.9 (CH), 113.5 (CH), 111.46 (CH), 111.42 (CH), 104.8 (CH), 58.2 (CH₂), 50.1 (CH₂), 50.0 (CH₂), 49.71 (3CH₂), 9.21 (3CH₃).

HRMS (TOF ES⁺): *m/z* calcd for C₂₄H₂₂NO₅ (M+H)⁺ 404.1498, found 404.1504.

HPLC: (λ = 254 nm), 98.34%; (λ = 214 nm), 98.52%; *t_R* = 11.16 min (Method 3).

5,5'-[Methylenebis(furan-5,2-diyl)]bis(2-hydroxybenzoic acid) (MDMG-825)

Formed during the chromatographic purification of **MDMG-907** and **MDMG-911**.

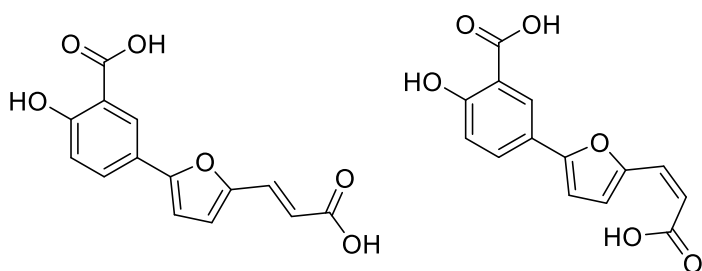
mp: 65 °C (decomposition).

¹H NMR (600 MHz, CD₃OD) δ 8.30 (s, 2H), 7.59 (dd, J = 8.6, 2.2 Hz, 2H), 6.83 (d, J = 8.5 Hz, 2H), 6.48 (d, J = 3.2 Hz, 2H), 6.20 (d, J = 3.2 Hz, 2H), 4.06 (s, 2H).

¹³C NMR (151 MHz, CD₃OD) δ 176.4 (2CO), 161.9 (2C), 154.6 (2C), 152.1 (2C), 152.08 (2C) 129.8 (2CH), 126.9 (2CH), 123.2 (2C), 117.7 (2CH), 109.2 (2CH), 104.8 (2CH), 28.2 (CH₂).

HRMS (TOF ES⁻): m/z calcd for C₂₃H₁₅O₈ (M-H⁺)⁻ 419.0767, found 419.0781.

HPLC: Decomposition.

5.4.3.2. Synthesis of α,β -unsaturated carbonyl derivatives of MDMG-409.**(*E/Z*)-5-[5-(2-Carboxyvinyl)furan-2-yl]-2-hydroxybenzoic acid (MDMG-1011)**²²¹

Under argon atmosphere, 40 mg of **MDMG-409** (0.172 mmol) were dissolved in 1 mL of anhydrous pyridine in a round bottom flask equipped with a stirring bar. Then, 25.09

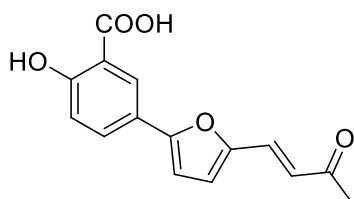
mg of malonic acid (0.241 mmol) and 68 μ L of piperidine (0.689 mmol) were added to the mixture and it was refluxed for 3 h. After that, the reaction was cooled to 0 $^{\circ}$ C, acidified with HCl 5% until pH 1 and concentrated in rotavapor. The crude product was purified by flash chromatography with DCM/MeOH (20: 1 \rightarrow 10:1). Yellow solid, 63% yield (30 mg, 0.109 mmol).

$^1\text{H NMR}$ (500 MHz, CD_3OD) δ 8.57 (s, 1H), 8.26 (dd, J = 12.6, 2.0 Hz, 2H), 7.82 (dt, J = 8.7, 2.4 Hz, 2H), 7.60 (d, J = 3.6 Hz, 1H), 7.44 (d, J = 15.6 Hz, 1H), 6.97 (t, J = 8.2 Hz, 2H), 6.85 (d, J = 12.8 Hz, 1H), 6.81 (d, J = 3.5 Hz, 1H), 6.77 (d, J = 3.6 Hz, 2H), 6.31 (d, J = 15.6 Hz, 1H), 5.74 (d, J = 12.8 Hz, 1H).

$^{13}\text{C NMR}$ (126 MHz, CD_3OD) δ 173.8, 173.7, 170.5, 169.5, 163.3, 163.1, 157.1, 155.9, 151.3, 151.1, 149.2, 139.4, 132.4, 131.9, 131.8, 130.4, 127.5, 127.4, 122.7, 122.5, 120.3, 118.9, 118.8, 118.7, 115.5, 115.0, 107.7, 107.6.

HRMS (TOF ES^-): m/z calcd for $\text{C}_{14}\text{H}_9\text{O}_6$ ($\text{M}-\text{H}$) $^-$ 273.0399, found 273.0405.

HPLC (λ = 214 nm): 66.28%, t_{R} = 11.80 min; 29.52%; t_{R} = 11.97 min. (λ = 254nm): 77.32%, t_{R} = 11.80 min; 22.67%, t_{R} = 11.97 min (Method 3).

(*E*)-2-Hydroxy-5-[5-(3-oxobut-1-en-1-yl)furan-2-yl]benzoic acid (MDMG-1015)²²²

In a round bottom flask equipped with a stirring bar, 50 mg of **MDMG-409** (0.215 mmol) were dissolved in acetone (13.62 mmol)/ H_2O 1/1 (2 mL) and the mixture was cooled to 0 $^{\circ}$ C. Next, 100 μ L of NaOH 1N were added dropwise and the reaction was stirred for 10 h at rt.

Then, the reaction was quenched with HCl 1 N until pH 1 and concentrated in rotavapor.²²³ The crude product was purified by flash chromatography with DCM/MeOH (20:1 → 15:1). Yellow solid, 51% yield (30 mg, 0.110 mmol).

mp: > 300 °C.

¹H NMR (400 MHz, CD₃OD) δ = 8.17 (d, J = 2.3 Hz, 1H), 7.95 (dd, J = 8.7, 2.4 Hz, 1H), 7.43 (d, J = 16.0 Hz, 1H), 7.10 – 7.01 (m, 3H), 6.58 (d, J = 16.0 Hz, 1H), 2.30 (s, 3H).

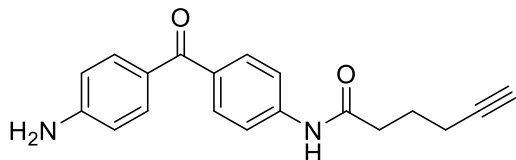
¹³C NMR (101 MHz, DMSO-*d*₆) δ = 197.2 (CO), 171.2 (CO), 161.3 (C), 154.9 (C), 149.6 (C), 131.2 (CH), 129.2 (CH), 125.7 (CH), 123.2 (CH), 120.7 (C), 119.1 (CH), 118.0 (CH), 114.2 (C), 107.8 (CH), 27.4 (CH₃).

HRMS (TOF ES⁻): m/z calcd for C₁₅H₁₁O₅ (M-H)⁻ 271.0606, found 271.0615.

HPLC: (λ = 254 nm), 95.66%; (λ = 214 nm), 97.53%; t_R = 13.26 min (Method 3).

5.5. Synthesis of chemical probes derived from MDMG-409

N-[4-(4-Aminobenzoyl)phenyl]hex-5-ynamide (MDMG-741)²²⁴



In a round bottom flask equipped with a stirring bar and under argon atmosphere, 156 μL of 5-hexynoic acid (1.413 mmol), 190.92 mg of HOBT (1.403 mmol) and 270.87 mg of EDC·HCl (1.413 mmol) were dissolved in 1 mL of anhydrous DMF and stirred at rt for 10 min. Then, in a different flask, 150 mg of 4,4'-diaminobenzophenone (0.706 mmol) were dissolved in 2.6 mL of anhydrous DMF and the first mixture was added over this one in portions along 1 h. The reaction was allowed to stir for 24 h at rt. After that time, 100 mL of EtOAc were added and the organic layer was washed with a saturated aqueous solution of NaHCO_3 (2 x 100 mL), with a 10% citric acid solution (2 x 100 mL) and finally with HCl 3N (150 mL) to remove the 4,4'-diaminobenzophenone. The organic layer was collected and neutralized at 0 $^\circ\text{C}$ with NaOH 20% in order to precipitate the final product, which was extracted with EtOAc, dried over Na_2SO_4 , filtered and concentrated in rotavapor. Yellow solid, 32% yield (71 mg, 0.232 mmol).

mp: 179-181 $^\circ\text{C}$.

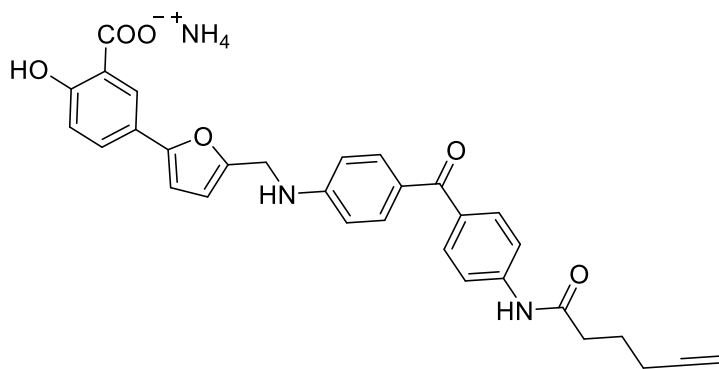
^1H NMR (400 MHz, CD_3OD) δ = 7.79 – 7.67 (m, 4H), 7.64 (d, J = 8.7 Hz, 2H), 6.72 (d, J = 8.6 Hz, 2H), 2.59 (t, J = 7.4 Hz, 2H), 2.41 – 2.25 (m, 3H), 1.94 (p, J = 7.0 Hz, 2H).

^{13}C NMR (101 MHz, CD_3OD) δ = 196.6 (CO), 174.0 (CO), 155.1 (C), 143.3 (C), 135.3 (C), 134.0 (2CH), 131.7 (2CH), 126.4 (C), 120.0 (2CH), 114.1 (2CH), 84.1 (C), 70.3 (CH), 36.6 (CH_2), 25.5 (CH_2), 18.6 (CH_2).

HRMS (TOF ES^-): m/z calcd for $\text{C}_{19}\text{H}_{19}\text{N}_2\text{O}_2$ ($\text{M}-\text{H}$) $^-$ 307.1447, found 307.1434.

HPLC: (λ = 254 nm), 100%; (λ = 214 nm), 100%; t_{R} = 12.65 min (Method 3).

Ammonium 5-{5-{{N-{4-[4-(hex-5-ynamido)benzoyl]phenyl}amino)methyl}furan-2-yl}-2-hydroxybenzoate (MDMG-911)



General synthetic procedure 6C. Reagents: **MDMG-409** (30.85 mg, 0.133 mmol), **MDMG-741** (52.92 mg, 0.172 mmol), NaBH(OAc)₃ (56.32 mg, 0.266 mmol) and DCM/MeOH 3:1 (4 mL). Column chromatography

EtOAc/CH₃CN/methanolic ammonia 7N (70:5:2.5 → 70:10:5). Orange solid, 69% yield (50 mg, 0.092 mmol).

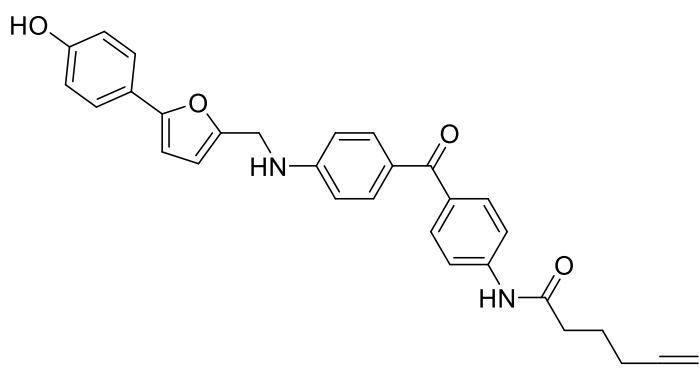
mp: 148-150 °C.

¹H NMR (400 MHz, CD₃OD) δ 8.20 (d, *J* = 2.3 Hz, 1H), 7.79 – 7.65 (m, 7H), 6.90 (d, *J* = 8.6 Hz, 1H), 6.80 (d, *J* = 8.8 Hz, 2H), 6.56 (d, *J* = 3.3 Hz, 1H), 6.37 (d, *J* = 3.3 Hz, 1H), 4.48 (s, 2H), 2.58 (t, *J* = 7.4 Hz, 2H), 2.36 – 2.27 (m, 3H), 1.93 (m, *J* = 7.0 Hz, 2H).

¹³C NMR (101 MHz, CD₃OD) δ 196.6 (CO), 174.8 (CO), 174.0 (CO), 162.2 (C), 154.5 (C), 154.3 (C), 152.6 (C), 143.3 (C), 135.3 (C), 133.9 (CH), 131.7 (CH), 130.4 (CH), 126.7 (CH), 126.4 (C), 123.3 (C), 120.0 (CH), 118.0 (CH), 117.5 (C), 112.5 (CH), 110.2 (CH), 105.0 (CH), 84.1 (C), 70.3 (CH), 41.0 (CH₂), 36.6 (CH₂), 25.5 (CH₂), 18.6 (CH₂).

HRMS (TOF ES⁻): *m/z* calcd for C₃₁H₂₅N₂O₆ (M-H)⁻ 521.1713, found 521.1703.

HPLC: (λ = 254 nm), 84.19%; (λ = 214 nm), 75.57%; *t_R* = 16.12 min (Method 3).

N-{4-[4-{N-[[5-(4-hydroxyphenyl)furan-2-yl]methyl]amino}benzoyl]phenyl}hex-5-ynamide (MDMG-995)²²⁵

In a round bottom flask equipped with a stirring bar and under argon atmosphere, the aldehyde **MDMG-672** (13.35 mg, 0.071) and the amine **MDMG-741** (18.11 mg, 0.059 mmol) were dissolved in 1.5 mL of anhydrous DCM and

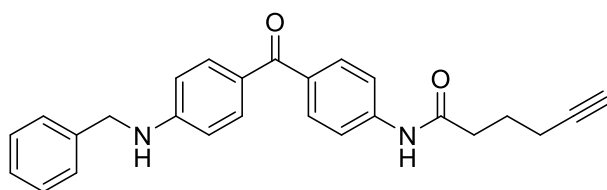
dried MgSO_4 was added to the mixture, which was refluxed for 3 h and kept overnight at rt. Then, 0.5 mL of MeOH and NaBH_3CN (7.41 mg, 0.118 mmol) were added at 0 °C and the reaction was stirred for 30 min at rt to carry out the *in situ* reduction. The mixture was then cooled to 0 °C, quenched with H_2O and concentrated in rotavapor. The crude product was purified by flash chromatography on silica gel with EtOAc/Hexane (1:5 → 2:1) containing 1% of Et_3N to afford the desired compound in 78% yield (22 mg, 0.046 mmol).

$^1\text{H NMR}$ (400 MHz, CD_3OD) δ 7.75 – 7.63 (m, 6H), 7.52 – 7.45 (m, 2H), 6.78 (ddt, J = 7.1, 5.1, 2.3 Hz, 4H), 6.46 (d, J = 3.3 Hz, 1H), 6.31 (d, J = 3.3 Hz, 1H), 4.43 (s, 2H), 2.55 (t, J = 7.5 Hz, 2H), 2.35 – 2.24 (m, 3H), 1.93 – 1.90 (m, 2H).

$^{13}\text{C NMR}$ [101 MHz, $(\text{CD}_3)_2\text{CO}$] δ 193.5 (CO), 171.7 (CO), 157.9 (C), 154.5 (C), 153.1 (C), 152.2 (C), 143.2 (C), 134.7 (C), 133.0 (CH), 131.2 (CH), 127.0 (C), 125.9 (CH), 123.7 (C), 119.0 (CH), 116.4 (CH), 112.3 (CH), 110.1 (CH), 104.5 (CH), 84.3 (C), 70.4 (CH), 40.8 (CH_2), 36.3 (CH_2), 24.9 (CH_2), 18.3 (CH_2).

HRMS (TOF ES^+): m/z calcd for $\text{C}_{30}\text{H}_{27}\text{N}_2\text{O}_4$ ($\text{M}+\text{H}$)⁺ 479.1971, found 479.1996.

HPLC; (λ = 254 nm), 99.03%; (λ = 214 nm), 97.91%; t_{R} = 14.27 min. (Method 4).

***N*-{4-[4-(Benzylamino)benzoyl]phenyl}hex-5-ynamide (MDMG-1098)**

General synthetic procedure 6C.

Reagents: Benzaldehyde (4.34 μ L, 0.043 mmol), **MDMG-741** (17 mg, 0.055 mmol), NaBH(OAc)₃ (18.09 mg, 0.085 mmol) and anhydrous

DCM/MeOH 3:1 (1 mL). Column chromatography: EtOAc /petroleum ether (1:6 \rightarrow 1:3). Yellow solid, 53% yield (9 mg, 0.023 mmol).

¹H NMR [400 MHz, (CD₃)₂CO] δ 9.42 (s, 1H), 7.78 (d, J = 8.7 Hz, 2H), 7.71 – 7.58 (m, 4H), 7.41 (d, J = 7.5 Hz, 2H), 7.34 (td, J = 6.8, 6.4, 1.6 Hz, 2H), 7.29 – 7.21 (m, 1H), 6.79 – 6.70 (m, 2H), 6.38 (t, J = 5.7 Hz, 1H), 4.48 (d, J = 5.1 Hz, 2H), 2.55 (t, J = 7.4 Hz, 2H), 2.38 (t, J = 2.7 Hz, 1H), 2.29 (td, J = 7.0, 2.7 Hz, 2H), 1.89 (p, J = 7.2 Hz, 2H).

¹³C NMR [101 MHz, (CD₃)₂CO] δ 193.4 (CO), 171.6 (CO), 153.4 (C), 143.2 (C), 140.3 (C), 134.7 (C), 133.0 (2CH), 131.2 (2CH), 129.3 (2CH), 128.1 (2CH), 127.8 (CH), 126.7 (C), 118.9 (2CH), 112.2 (2CH), 84.3 (C), 70.4 (CH), 47.5 (CH₂), 36.2 (CH₂), 24.9 (CH₂), 18.3 (CH₂).

HRMS (TOF ES⁺): m/z calcd for C₂₆H₂₅N₂O₂ (M+H)⁺ 397.1916, found 397.1947.

HPLC: (λ = 254 nm), 95.01%; (λ = 214 nm), 95.26%; t_R = 14.85 min (Method 4).

5.6. Biological evaluation of the compounds

Abstract

Enzymatic assays (*mGO*, *hGO*, LDHA and LDHB) and *in vitro* assays on hyperoxaluric mouse hepatocytes have been performed.

The synthesized compounds were initially evaluated against GO using a colorimetric assay. A preliminary screening at 22 μM was performed, and for those compounds presenting a percentage of inhibition higher than 30%, IC_{50} was calculated. Initially, these experiments were carried out on *mGO*, but later *hGO* was introduced in the assays.

However, severe interferences with the colorimetric assay were detected for some of the compounds, and this led us to the implementation of a fluorometric method to assess GO inhibition. Thus, the most potent GO inhibitors were re-evaluated using the new established protocol: in the case of compounds presenting interferences with the colorimetric assay, no interferences could be found with this new method, whilst comparable results were obtained for compounds that did not interfere with the colorimetric assay.

Those compounds presenting the best activities on GO inhibition were tested for oxalate reduction on *Agxt1^{-/-}* mouse primary hepatocytes culture: a preliminary screening at 10 μM was followed by EC_{50} for the most active compounds.

Compounds suspected to present additional biological targets were tested for lactate dehydrogenase A inhibition (LDHA). Initially, a screening at 10 μM was performed for the most interesting compounds using a commercial kit based in a colorimetric assay.

For those compounds presenting the highest percentages of inhibition of LDHA at 10 μM , IC_{50} values were calculated for such enzyme with a fluorometric assay. Finally, the most potent LDHA inhibitors were tested for LDHB inhibition in order to study their selectivity.

5.6.1. Enzymatic assays

5.6.1.1. Glycolate oxidase

5.6.1.1.1. Glycolate oxidase production

Both *mGO* and *hGO* were produced and purified prior to their use in the enzymatic assay. Initially, GO was produced (following method A) by the research group of Prof. E. Salido (University of La Laguna), but later on, they kindly provided us with the transformed *E.coli* bacteria for *mGO* and *hGO* production. In this way, and in collaboration with Dr. A. Pey (University of Granada), we were able to produce both enzymes (following method B) and to perform the enzymatic assays in our facilities.

Method A for GO production (University of La Laguna).⁸⁰ BL21 (DE3) *E.coli* transformed with recombinant pET-15b expression vector carrying the coding sequence of mouse *Hao1* cDNA and an *N*-terminal His-tag was grown in the presence of 0.1 mg/mL ampicillin in LB medium. Once the optical density value of the culture reached 0.6-0.8 at 600 nm, the expression was induced with the addition of 0.5 mM isopropyl β -D-thiogalactopyranoside (IPTG, AppliChem), followed by incubation for 5 h at 25 °C. Then, bacteria were split in 50 mL aliquots, centrifuged at 4500 g for 10 min at 4 °C (Hettich ROTINA 420 centrifuge) and resuspended in 0.9% NaCl. After that, bacteria were centrifuged in the same conditions, the pellet was washed again with 0.9% NaCl and re-centrifuged. Finally, pellets were frozen at -80 °C until further use.

When required, pellets were resuspended in cold lysis buffer (20 mM NaH₂PO₄, 500 mM NaCl, 5 mM imidazole, 50 μ M FMN, pH 7.5) in the presence of 1 mM PMSF (protease inhibitor), 0.1% Triton X-100 and 0.2 mg/mL lysozyme and were sonicated (ultrasonic processor UP100H Hielscher). The samples were then centrifuged at 4800 g for 10 minutes at 4 °C (Kubota 1700 centrifuge) and the supernatant was loaded into a Ni-NTA agarose column (Qiagen) to purify the His-tagged recombinant mouse glycolate oxidase. In order to enable the interaction between the 6 histidines and the nickel-charged affinity resin, the column was incubated for 30 min at 4 °C while rotating. After that, this Pre-column fraction was eluted and the column was washed with two bed volumes of lysis buffer containing 20 mM imidazole to remove unbound proteins (wash fraction). Finally, GO was eluted from the column with the addition of the elution buffer (20 mM NaH₂PO₄, 500 mM NaCl, 300 mM imidazole, pH 7.5) in four consecutive portions of 350 μ L (F1), 1000 μ L (F2), 500 μ L (F3) and 500 μ L (F4). The eluted fraction F2 was introduced in a dialysis membrane and dialyzed overnight at 4 °C against dialysis buffer (20 mM NaH₂PO₄, 500 mM NaCl, pH 7.5). The protein

concentration was measured using the bicinchoninic acid assay and *mGO* was kept at 4 °C protected from light. When necessary, the enzyme was obtained in glycerol, what allowed its easier storage at -20 °C and manipulation. To this end, the dialysis buffer used contained 20% glycerol in it (20 mM NaH₂PO₄, 500 mM NaCl, 20% glycerol, pH 7.5).

For the obtention of *hGO* the same procedure was repeated using the recombinant pET-15b expression vector carrying the coding sequence of human *Hao1* cDNA.

Method B for GO production (University of Granada). BL21 (DE3) *E.coli* transformed with recombinant pET-15b expression vector carrying the coding sequence of mouse *Hao1* cDNA and an *N*-terminal His-tag was grown in the presence of 0.1 mg/mL ampicillin in LB medium for 3 h at 37 °C. The expression was induced with the addition of 0.5 mM IPTG (isopropyl β-D-thiogalactopyranoside), followed by incubation for 5 h at 25 °C. Bacteria were split in aliquots, centrifuged at 4500 g for 10 min at 4 °C (Kokusan H-251 centrifuge) and resuspended in phosphate-buffered saline (20 mM NaH₂PO₄, 500 mM NaCl, pH 7.5). After that, bacteria were re-centrifuged (Hettich Universal 320R centrifuge) at 2800 g for 10 min at 4 °C and the pellets were frozen at -80 °C overnight.

The following day cells were thawed, resuspended in cold lysis buffer (20 mM NaH₂PO₄, 500 mM NaCl, 20 mM imidazole, 50 μM FMN, pH 7.5) in the presence of PMSF (protease inhibitor) and sonicated. The samples were then centrifuged at 15000 rpm for 10 minutes at 4 °C and the enzyme contained within the supernatant was purified by immobilized metal affinity chromatography (IMAC). To this end, the soluble fraction was loaded into a His GraviTrap™ column (GE-Heathcare) in order to bind the His-tagged protein to the Ni Sepharose® stationary phase. This fraction (pre-column fraction) was then eluted and the column was washed with three bed volumes of lysis-binding-wash buffer to remove unbound proteins (wash fraction). Then, elution buffer (20 mM NaH₂PO₄, 500 mM NaCl, 300 mM imidazole, pH 7.5) was added to the column and GO was eluted in two fractions of 500 μl (F1) and 2500 μL (F2). F2 was subjected to buffer exchange using a PD-10 desalting column containing Sephadex™ G-25 resin (GE-Heathcare). For that, 2500 μL corresponding to F2 were loaded into the column and eluted in 3.2 mL of working buffer (20 mM NaH₂PO₄, 500 mM NaCl, pH 7.5).

Finally, the protein concentration was measured spectrophotometrically according to the extinction molar coefficient of $\epsilon_{280} = 48\,000\text{ M}^{-1}\text{ cm}^{-1}$ corresponding to the primary sequence of the enzyme.

The enzyme was split in aliquots, preserved in liquid nitrogen and stored at -80 °C.

For the obtention of *hGO* the same procedure was repeated using the recombinant pET-15b expression vector carrying the coding sequence of human *Hao1* cDNA.

5.6.1.1.2. Glycolate oxidase colorimetric assay

General information

Inhibitory activity of the compounds against purified *mGO* and *hGO* was determined in the presence of glycolate as substrate. The addition of the corresponding chromogen (whether sulfonated-DCIP or DCHBS) and 4-aminoantipyrine, in a coupled horseradish peroxidase (HRP) reaction using the hydrogen peroxide released in the enzymatic reaction, yields a quinoneimine dye whose absorbance is spectrophotometrically measured.⁹⁸

The enzymatic assay was performed on 96-well plates and all experiments were conducted in triplicates. Two different chromophores were employed due to availability issues: sulfonated-DCIP (dichloroindophenol) and DCHBS (Sodium 3,5-dichloro-2-hydroxybenzenesulfonate). Trinder buffer, containing 4-aminoantipyrine 4.9 mM, was used in the assay. The absorbance was measured using a Multiskan™ FC Microplate Photometer (ThermoFisher). Phosphate buffer 50 mM (pH 7) was used and the final volume in each well was set to 225 µL. Compounds were dissolved in DMSO as 10 mM stock solutions and if necessary, intermediate stocks were prepared. The concentration of DMSO was kept at a maximum of 2.2%. A dilution of GO in phosphate buffer is prepared at 0.1-0.6 µg/µL in each experiment in order to adjust the absorbance to the linear range.

Detailed procedure

To determine the percentage of inhibition of GO at a single dose (22 µM), a 1 mM intermediate stock in DMSO was prepared for each compound and 5 µL from it were added to the corresponding well over 35 µL of phosphate buffer (final DMSO concentration of 2.2%). To assess the IC₅₀ values, the compounds in the appropriate DMSO stock were added to the plate and diluted in phosphate buffer with 8-point 1:2 or 1:3 serial dilutions (final DMSO concentration of 2.2%).

Simultaneously, a standard curve using growing amounts of diluted GO at 0.1-0.6 $\mu\text{g}/\mu\text{L}$ (0, 5, 10, 15, 20, 30 μL) and phosphate buffer was built, reaching 50 μL of final volume in each well.

After that, 10 μL of GO were added to the wells where the compounds are tested and the plate was left to incubate for 5 min at rt to allow the interaction between the compound and the enzyme. Then, 125 μL of glycolate buffer (40 mM in H_2O) were added to each well (final concentration 22 mM) and the plate was incubated for 1 min at 37 °C. Finally, a mix containing 50 μL of HRP in Trinder buffer (1 mg HRP/mL Trinder buffer) and the chromogen (30 μL of 120 mM chromogen in $\text{H}_2\text{O}/\text{mL}$ Trinder buffer) were added into each well, and after the incubation for 1 min at rt the absorbance was measured at the suitable wavelength for each chromophore (515 nm for sulfonated DCIP and 493 nm for DCHBS). Finally, enzymatic activity was calculated from the extinction molar coefficients of the chromophores ($\epsilon = 21 \text{ mM}^{-1} \text{ cm}^{-1}$ for sulfonated- DCIP and $\epsilon_{515} = 26 \text{ mM}^{-1} \text{ cm}^{-1}$ for DCHBS)²²⁶ using the Lambert-Beer equation in MS Excel software. The percentage of inhibition was determined for each concentration and the IC_{50} value was calculated using GraphPad Prism 6 software.

5.6.1.1.3. Glycolate oxidase fluorometric assay

General information

Due to the interferences found for several compounds when the colorimetric assay was used, a new method for the evaluation of the final compounds against GO was introduced. IC_{50} values were only calculated for the most potent compounds.

Following previous established protocols, a method based on the H_2O_2 detection with the use of Amplex[®] Red reagent was implemented.⁸²

In this method, the H_2O_2 released in the GO reaction in the presence of 180 μM glycolate as substrate is used by HRP to oxidize Amplex[®] Red reagent to the fluorophore resorufin. Its fluorescence was measured in an EnSpire[®] Multimode Plate Reader (PerkinElmer) with λ_{ex} 560 nm and λ_{em} 590 nm.

The assay was performed on black opaque 96-well microplates (OptiPlate, PerkinElmer). Phosphate buffer 50 mM (pH 7) was used in the assay and the final volume was set to 200 μL in each well. Compounds were dissolved in DMSO as 5-50 mM stock solutions. Amplex[®] Red reagent was dissolved in DMSO as 10 mM stock

solution, and the final concentration in the assay was set at 50 μM . The concentration of DMSO was kept at a maximum of 1.5%. A 500 nM dilution of GO in phosphate buffer was prepared for every assay and the final enzyme concentration was set to 25 nM.

Controls for the establishment of the 0% and 100% enzymatic activity were introduced in the assay. In the case of the 0% control, H_2O was added instead of substrate, whilst for the 100% control no inhibitor was added. For both of them, 1.5% of DMSO was kept.

Detailed procedure

To assess the IC_{50} values, the compounds in the appropriate DMSO stock were added to the plate and diluted in phosphate buffer with 8-point or 1:3 serial dilutions (final DMSO concentration of 1.5%), so that the final volume after the serial dilutions was 40 μL . After that, 10 μL of 500 nM GO were added into each well (final concentration 25 nM) and the plate was left to incubate for 10 min at rt. Then, 50 μL of 720 μM glycolate buffer (final concentration 180 μM) were added and the plate was incubated at rt for 10 min. After that time, 100 μL of 100 μM Amplex[®] Red (final concentration 50 μM) containing 5 units of HRP were added per well and the plate was incubated protected from light for 10 min. Finally, the fluorescence was read with λ_{ex} 560 nm and λ_{em} 590 nm.

The percentage of inhibition was determined for each concentration using MS Excel software and the IC_{50} value was calculated using GraphPad Prism 6 software.

5.6.1.1.4. Interference tests in the GO enzymatic assay

Those compounds presenting the best activities in the GO enzymatic assay and in the oxalate determination assay were tested for possible interference with the different biological assays.

Test for colorimetric interferences. Selected compounds were analyzed by HPLC to detect possible absorbance at the wavelengths used in the biological assays. For that, compounds **MDMG-317**, **MDMG-409**, **MDMG-566**, **MDMG-592**, **MDMG-604**, **MDMG-672**, **MDMG-963**, **MDMG-911** and **MDMG-995** (0.1 mg) were dissolved in a water/acetonitrile 80/20 mixture (1 mL), filtered, and transferred into separate HPLC vials. The resulting solutions were injected in HPLC and analyzed

for absorbance at 515 and 590 nm (see 5.1.3. General experimental methods for HPLC setup). No absorbance could be observed for any of the tested compounds at those wavelengths.

Test for interferences by HRP inhibition (colorimetric assay). A standard curve was built using 0, 5, 10, 15, 20, and 30 μL of a solution of H_2O_2 (1:10000) and measuring absorbance at 493 nm after 1 min in the presence of HRP, sulfonated-DCIP or DCHBS, and 4-aminoantipyrine, using the same conditions as for GO enzymatic assay. For the construction of the standard curve, the process was carried out in duplicate. The interference detection assay was performed by measuring HRP reaction in the absence of GO and glycolate, using 10 μL of H_2O_2 (1:10000) as substrate and 5 μL of a stock solution (1 mM) of the tested compound (**MDMG-317**, **MDMG-409**, **MDMG-915**, **MDMG-931I**, **MDMG-935P**, **MDMG-943**, **MDMG-963**, **MDMG-991**, **MDMG-1015**, **MDMG-1054**, **MDMG-1062**) in DMSO (final concentration of the tested compound = 22.2 μM). Absorbance was measured at 493 nm after 1 min. The process was carried out in duplicate. Diminution of the standard absorbance, indicating HRP inhibition, was observed for compounds **MDMG-931I**, **MDMG-935P**, **MDMG-963**, **MDMG-991**, **MDMG-1054**, **MDMG-1062**.

Test for Interferences by HRP Inhibition (fluorometric assay). Compounds **MDMG-317**, **MDMG-409**, **MDMG-540**, **MDMG-566**, **MDMG-570**, **MDMG-592**, **MDMG-943**, **MDMG-963**, **MDMG-963I**, **MDMG-907**, **MDMG-911**, **MDMG-915**, **MDMG-931P**, **MDMG-931I**, **MDMG-935P**, **MDMG-935I**, **MDMG-971**, **MDMG-991**, **MDMG-995**, **MDMG-1015**, **MDMG-1054**, **MDMG-1058P**, **MDMG-1058I** and **MDMG-1062** were tested for interferences with the fluorometric assay.

A standard curve using 0, 5, 10, 15, 20, 30, 40 and 50 μL of a solution of H_2O_2 (1:100000) was built to establish the linear range. DMSO (2 μL) were added to each well of the curve and the volume was completed up to 50 μL with phosphate buffer. In parallel, 2 μL of 2 mM stocks in DMSO of the tested compounds were dissolved in 33 μL of phosphate buffer and 15 μL of the same solution of H_2O_2 . A control for the establishment of the 100% enzymatic activity was included in the assay by introducing 3 replicates of the point 4 of the standard curve (2 μL of DMSO, 15 μL of H_2O_2 and 33 μL of phosphate buffer). Then, 50 μL of H_2O were added instead of glycolate to each well. After that, 100 μL of 100 μM Amplex[®] Red (final concentration 50 μM) containing 5 units of HRP were added per well and the fluorescence was immediately read with

λ_{ex} 560 nm and λ_{em} 590 nm. The concentration of DMSO was kept at 1.5% in a final volume of 200 μL in all wells. Diminution of the standard absorbance, indicating HRP inhibition, was observed for compounds **MDMG-540**, **MDMG-566**, **MDMG-570**, **MDMG-592**, **MDMG-963**, **MDMG-963I**, **MDMG-971**, **MDMG-991**, **MDMG-1054**, **MDMG-1058P**, **MDMG-1058I** and **MDMG-1062**.

5.6.1.2. LDH enzymatic assay

5.6.1.2.1. LDH enzymatic assay (absorbance assay)

LDHA inhibitory activity of the compounds was initially determined by using a commercial colorimetric assay kit (BioVision Incorporated, Milpitas, CA, USA) following the manufacturer's instructions. With this method, only the percentages of inhibition of LDHA at 10 μM (using MS Excel software) were calculated for the most interesting compounds.

5.6.1.2.2. LDH enzymatic assay (fluorometric assay)

General information

Recombinant human LDHA and LDHB with an *N*-terminal His-tag were acquired from Novusbio. Recombinant *h*LDHA, corresponding to the amino acids 1-332 of *h*LDHA, presented a specific activity of 443 units/mg (in which one unit converts 1.0 μmole of pyruvate to L-lactate per minute at pH 7.5 at 37°C) and a concentration of 0.5 mg/mL, determined by Bradford assay (221 units/mL). Recombinant *h*LDHB, corresponding to the amino acids 1-334 of *h*LDHB, presented a specific activity of 760 units/mg and a concentration of 1 mg/mL (845 units/mL).

The LDH activity was assessed with a method based on the monitoring of the descent of the β -NADH fluorescence as the enzyme catalyzes the reduction of pyruvate into lactate and β -NADH is oxidized to β -NAD⁺.^{199,200}

The enzymatic assay was performed on black opaque 96-well microplates (OptiPlate, PerkinElmer). The fluorescence of β -NADH was measured in an EnSpire[®] Multimode Plate Reader (PerkinElmer) with λ_{ex} 340 nm and λ_{em} 460 nm. 50 mM phosphate buffer pH 7 was used in the assay and the final volume in each well was set

to 200 μL . The concentration of DMSO was kept at a maximum of 2.5%. For each type of sample triplicates were introduced in the assay.

Controls for the establishment of the 0% and 100% enzymatic activity were introduced in the assay. In the case of the 0% control, phosphate buffer was added instead of substrate, whilst for the 100% control, no inhibitor was added. For both of them, the same concentration of DMSO as for the wells where the compounds were tested was added.

Detailed procedure

Compounds were dissolved in DMSO as 5-50 mM stock solutions. To determine the percentage of inhibition of LDH at a single dose (10 μM), a 400 μM intermediate stock in DMSO was prepared for each compound and 5 μL from it were added to the corresponding well over 35 μL of phosphate buffer (final DMSO concentration of 2.5%). Sodium oxamate was introduced as positive control and tested at 1.25 mM in each assay: 5 μL of 50 mM stock in DMSO were added to the positive control well. To assess the IC_{50} values, compounds in the appropriate DMSO stock were added to the plate and diluted in phosphate buffer with 8-point 1:3 serial dilutions (final DMSO concentration of 2%). In all cases, the volume in each well was 40 μL after this step.

For both enzymes, an intermediate stock with 0.3 units/mL was prepared in phosphate buffer. β -NADH was dissolved in phosphate buffer as 600 μM stock solution. A mix containing 10 μL of 0.3 units/mL LDH and 50 μL of 600 μM β -NADH was prepared per well and the 60 μL were added by columns using a multichannel pipette (final concentration 0.015 units/mL for LDH and 150 μM for β -NADH in the final volume of 200 μL /well).

The decrease in the fluorescence was monitored for 10 min at rt (10 measures, one every 60 s) and the baseline was established in order to correct possible interferences of the compounds in the fluorescence.

Subsequently, 100 μL of a 2 mM stock solution of pyruvic acid in phosphate buffer were added into each well (final concentration of pyruvate 1 mM).

The decrease of β -NADH fluorescence was monitored for 10 min at rt (10 measures, one every 60 s) and the slope for each well was calculated during the 10 min linear timeframe. The percentage of inhibition for each dose was obtained by

comparison between the average slope of each compound and the 100% enzymatic activity control.

The percentage of inhibition was determined for each concentration using MS Excel software and the IC₅₀ value was calculated using GraphPad Prism 6 software.

5.6.2. Cell culture assay

5.6.2.1. *Agxt1*^{-/-} primary hepatocytes isolation and culture

Hepatocytes were isolated by *in situ* collagenase perfusion method²²⁷ from male C57BL/6 *Agxt1*^{-/-} mice liver. Culture of primary hepatocytes was performed as described previously.⁸⁰ Briefly, 3.0x10⁵ cells/well were cultured in 6-well plates with Williams E medium supplemented with 5% fetal bovine serum, 2 mM L-glutamine, 100 U/mL penicillin, 100 µg/mL streptomycin, 2.2 mUI/mL insulin and 0.3 µg/mL hydrocortisone. After 5 h, the medium was changed to Williams E complete medium (Biochrom, Cambridge, U.K.) without serum and cells were treated with compounds in the presence of 5 mM glycolate. Culture medium was harvested at 24 h after treatment for oxalate quantification on secondary assays, and also at 48 and 72 h for full dose-response curves.

5.6.2.2. Cell viability and cytotoxicity

96-Well plates were seeded with 1.0x10⁴ cells/well and treated with the same concentrations of compounds as in 6-well plates. At each time point, 20 µL of Cell Titer 96® Aqueous One Solution Reagent (Promega, Madison, WI) was added to the medium, incubated 2 h at 37 °C 5% CO₂ and spectrophotometrically measured at 493 nm.

5.6.2.3. Oxalate determination

Determination of oxalate excreted to the medium was measured by the oxalate oxidase assay using a commercial kit (Trinity Biotech, Co Wicklow, Ireland), following manufacturer's instructions. The method involves oxidation of oxalate (1 equiv) by oxalate oxidase with formation of H₂O₂ (1 equiv) and subsequent utilization of the generated H₂O₂ for the formation of a dye (absorbance at 595 nm) in a HRP catalyzed reaction with the substrates 3-methyl-2-benzothiazolinone hydrazone (MBTH) and 3-(dimethylamino) benzoic acid (DMAB).

5.6.2.4. Interference test of the cell culture assay

Detection of interferences with the oxalate determination test. The most active compounds decreasing oxalate production (**MDMG-672**, **MDMG-409**, and **MDMG-317**) were subjected to determination of interferences with the commercial kit. A standard absorbance vs oxalate curve was built using the commercial kit for oxalate determination and growing amounts of oxalate (0, 0.5, 1, 2, 4, and 5 nmol). The same culture medium used in the cellular assay was used here as a solvent. The average absorbance was calculated from triplicate experiments. The interference detection assay was performed by construction of an absorbance vs oxalate curve for each tested compounds at 10 μM in the cell-culture medium. Deviations from the standard curve were only observed for compound **MDMG-317**, agreeing with the HRP inhibition capacity found for this compound in the former experiment (see Appendix 6.2).

Calculation of EC_{50} against oxalate detection commercial kit for compound MDMG-317.

A value of EC_{50} was calculated for compound **MDMG-317** against the mixture of enzymes contained in the commercial kit for oxalate determination (oxalate oxidase and HRP), with 5 nmol of the substrate oxalate, the highest point on the standard curve, dissolved in culture media. The standard curve was built using the commercial kit, by measuring absorbance at 595 nm in the presence of 0, 0.5, 1, 2, 4, 5 nmol of oxalate and in the absence of **MDMG-317** ($R^2 = 0.9948$). The EC_{50} value was calculated by measuring absorbance in mixtures containing different concentrations of **MDMG-317** (0, 1, 2.5, 5, 7.5, 10, 20, and 40 μM), 5 nmol oxalate in culture media, and the components of the commercial kit. EC_{50} for compound **MDMG-317** was determined to be 18 μM (see Appendix 6.2).

5.7. In silico studies

In silico studies were performed by Dr. Miguel X. Fernandes at Instituto Universitario de Bio-Orgánica “Antonio González” (IUBO-AG), at University of La Laguna (Spain).

Interactions of GO with the compounds were analyzed by computational docking using Maestro software (Schrödinger). Crystallographic structure of *h*GO was obtained from Protein Data Bank (PDB code 2RDT). Protein structure was energetically minimized using OPAL3 force field, and a maximum rmsd of 0.3 Å from crystallographic positions was selected. Grid generation for ligand binding was established around the volume where CDST was co-crystallized with *h*GO; exclusion volumes were not established and rotation of hydroxyl and thiol groups of serine, threonine, tyrosine, and cysteine was blocked. Ligand structures were drawn in HyperChem (Hypercube Inc.) software, and their energy was minimized using OPAL3 force field. Molecules geometry was optimized using the Polak–Ribiere conjugated gradient algorithm, with an atomic gradient convergence of $\text{rms} < 0.01 \text{ kcal}/(\text{Å mol})$. The energy of the interaction was defined by the equation $\Delta G_{\text{bind}} = \Delta G_{\text{electrostatic}} + \Delta G_{\text{vdW}} \sim \alpha \Delta G_{\text{electrostatic}} + \beta \Delta G_{\text{vdW}}$. β scaling factor of nonpolar interactions was set on 0.8, with a partial charge limit of 0.15. Standard precision method was configured for docking calculations, allowing total flexibility of the ligands. Nonplanar conformations of amides were penalized, as well as low probability tautomers. Their docking score values were penalized using Epik algorithm. Postdocking energy minimization was also performed. 2D diagrams were obtained from Maestro software (Schrödinger). 3D illustrations of *h*GO and ligands were performed using Pymol software, and polar interactions were analyzed.

5.8. Statistical analysis

Descriptive data are expressed as the mean \pm SD and plotted in GraphPad Prism 5 software. Nonlinear regression analysis was used for dose–response curve fitting of logarithm of inhibitor concentration vs normalized enzymatic activity to calculate IC₅₀ values, generating also the proper curve. One-way ANOVA test was used for comparison between independent groups. Tukey's range test was chosen as post hoc analysis. All data were analyzed using SPSS version 19 statistical package. A *p*-value of <0.05 was considered significant.

6. Appendices

6. Appendices

6.1. In silico predictions

Table 23. Summary of interactions of compounds **BIO-1-BIO-17** with the most representative aminoacids of the binding regions 1 and 2 of human glycolate oxidase (hGO). Data were obtained using hGO crystallographic active site structure (PDB ID: 2rdt). Interactions were obtained using Maestro software (Schrödinger). Comparison with glyoxylate, CDST and CCPST crystallographic data.

Compound	Arg167	Arg263	Tyr26	His260	Tyr132	Trp110	Leu205	Tyr208
Glyoxylate	E _{COO⁻}	H _{Arg→COO⁻}	H _{Tyr→COO⁻}	H _{His→CO}	X	X	X	X
CDST	E _{COO⁻}	H _{Arg→COO⁻}	H _{Tyr→COO⁻}	H _{N3→His}	H _{Tyr→N2}	Hy	Hy	Hy
CCPST	E _{COO⁻}	H _{Arg→COO⁻}	H _{Tyr→COO⁻}	H _{His→N3}	H _{Tyr→N2}	π-π	π-π	Hy
BIO-1	E _{COO⁻} H _{Arg→COO⁻}	E _{COO⁻}	X	H _{His→COO⁻} H _{His→β-OH}	Hy	Hy (ring A)	X	X
BIO-2 (C4)	E _{COO⁻} H _{Arg→COO⁻}	E _{COO⁻} H _{Arg→COO⁻}	X	H _{His→COO⁻}	Hy	Hy (ring A)	X	X
BIO-3 (C3)	E _{COO⁻} H _{Arg→COO⁻}	E _{COO⁻} H _{Arg→COO⁻}	X	H _{His→COO⁻} H _{His→β-OH}	Hy	Hy (ring A)	X	X
BIO-4 (C5)	E _{COO⁻} H _{Arg→COO⁻}	E _{COO⁻} H _{Arg→COO⁻}	X	H _{His→COO⁻} H _{His→β-OH}	Hy	Hy (ring A)	X	X
BIO-5 (C4)	E _{COO⁻} H _{Arg→COO⁻}	E _{COO⁻} H _{Arg→COO⁻}	X	H _{His→COO⁻} H _{His→β-OH}	Hy	Hy (ring A)	X	X
BIO-6 (C5)	E _{COO⁻} H _{Arg→COO⁻}	E _{COO⁻} H _{Arg→COO⁻}	H _{Tyr→COO⁻}	H _{His→COO⁻} H _{His→β-OH}	X	Hy	X	X
BIO-7 (C5)	E _{COO⁻} H _{Arg→COO⁻}	E _{COO⁻} H _{Arg→COO⁻}	Hy (ring A)	H _{His→COO⁻} H _{His→β-OH}	Hy (ring A)	Hy (ring A)	Hy	Hy
BIO-8 (C4)	E _{COO⁻} H _{Arg→COO⁻}	E _{COO⁻} H _{Arg→COO⁻}	X	H _{His→COO⁻}	Hy (ring A)	π-π _{ringA} π-π _{ringB}	Hy (ring A)	Hy (ring B)
BIO-9 (C5)	E _{COO⁻} H _{Arg→COO⁻}	E _{COO⁻} H _{Arg→COO⁻}	X	H _{His→COO⁻} H _{His→β-OH}	X	Hy (ring B)	Hy (ring A)	Hy (ring B)
BIO-10	E _{COO⁻} H _{Arg→COO⁻}	E _{COO⁻}	H _{Tyr→COO⁻}	H _{His→COO⁻}	Hy (ring A)	Hy (ring A)	Hy (ring A)	Hy (ring A)
BIO-11	H _{Arg→COO⁻}	H _{Arg→COO⁻} H _{Arg→COO⁻}	H _{Tyr→COO⁻}	X	H _{β-OH→Tyr}	π-π _{ringB}	X	X
BIO-12	H _{Arg→COO⁻} H _{Arg→COO⁻}	H _{Arg→COO⁻}	X	X	X	π-π _{ringB}	X	π-π _{ringC}
BIO-13	E _{COO⁻} H _{Arg→COO⁻}	H _{Arg→COO⁻} H _{Arg→COO⁻}	H _{Tyr→COO⁻} H _{Tyr→β-OH}	X	Hy (ring A)	π-π _{ringB}	Hy (ring B)	π-π _{ringB}
BIO-14	H _{Arg→COO⁻} H _{Arg→COO⁻}	H _{Arg→COO⁻} H _{Arg→COO⁻}	H _{Tyr→β-OH}	X	X	π-π _{ringB}	Hy (ring B)	π-π _{ringB}

Table 23 (continuation).

BIO-15	H _{Arg→COO⁻} H _{Arg→COO⁻}	H _{Arg→COO⁻} H _{Arg→COO⁻}	H _{Tyr→COO⁻} H _{Tyr→β-OH}	X	π-π _{ringA}	X	Hy (ring B)	π-π _{ringB}
BIO-16	E _{COO⁻} H _{Arg→β-OH}	E _{COO⁻}	H _{Tyr→COO⁻}	X	Hy	Hy (ring B)	Hy (ring B)	Hy (ring B)
BIO-17	E _{COO⁻} H _{Arg→COO⁻}	E _{COO⁻} H _{Arg→COO⁻}	X	H _{His→COO⁻}	Hy	X	Hy (ring A)	X

E: Electrostatic interaction (subindex indicates the group of the drug involved in the interaction). H: Hydrogen bond (subindex arrows indicate the direction of the hydrogen cession). π-π: Stacking interaction (subindex indicates the group of the drug involved in the interaction). Hy: Hydrophobic interaction (in brackets the group of the drug involved in the interaction). X: No interaction. Ring A: Polar head ring. Ring B, ring C: Side chain rings. Shadowed: Characteristic binding features of salicylic acids (green), naphthyllic acids (grey) and compound **BIO-11** (pink).

Table 24. Summary of interactions of the non-salicylic compounds with the most representative aminoacids of the binding regions 1 and 2 of human glycolate oxidase (*hGO*). Data were obtained using *hGO* crystallographic active site structure (PDBID:2rdt). Interactions were obtained using Maestro software (Schrödinger). Comparison with **BIO-8** and **glyoxylate**, **CDST** and **CCPST** crystallographic data.¹⁰⁰

Compound	Arg167	Arg263	Tyr26	His260	Tyr132	Trp110	Leu205	Tyr208
Glyoxylate	E _{COO⁻}	H _{Arg→COO⁻}	H _{Tyr→COO⁻}	H _{His→CO}	X	X	X	X
CDST	E _{COO⁻}	H _{Arg→COO⁻}	H _{Tyr→COO⁻}	H _{N3→His}	H _{Tyr→N2}	Hy	Hy	Hy
CCPST	E _{COO⁻}	H _{Arg→COO⁻}	H _{Tyr→COO⁻}	H _{His→N3}	H _{Tyr→N2}	π-π	π-π	Hy
BIO-8 (C4)	E _{COO⁻} H _{Arg→COO⁻}	E _{COO⁻} H _{Arg→COO⁻}	X	H _{His→COO⁻}	Hy (ringA)	π-π _{ringA} π-π _{ringB}	Hy (ringA)	Hy (ringB)
MDMG-353	E _{COO⁻} H _{Arg→COO⁻}	E _{COO⁻} H _{Arg→COO⁻}	X	X	X	Hy (ringA)	Hy (ringA)	Hy (ringB)
MDMG-672	H _{Arg→CHO}	H _{Arg→CHO} H _{Arg→CHO}	H _{Tyr→CHO} H _{Tyr→O- furan}	X	X	π-π _{ringA}	X	Hy (ringA)
MDMG-451 (C4)	E _{COO⁻} H _{Arg→COO⁻}	E _{COO⁻}	X	H _{His→COO⁻}	H _{Tyr→OHbn}	Hy (ringA)	Hy	Hy
MDMG-467 (C4)	E _{COO⁻} H _{Arg→COO⁻}	H _{Arg→COO⁻}	X	H _{His→COO⁻}	Hy (Me)	π-π _{ringA} π-π _{ringB}	Hy (ringB)	Hy (ringA)
MDMG-357 (C4)	X	X	X	H _{His→CHO}	H _{Tyr→CHO}	π-π _{ringA}	Hy (ringB)	Hy (ringA)
MDMG-511 (C4)	X	X	Hy (ringA)	X	X	π-π _{ringA}	Hy (ringA)	π- π _{ringB}

E: Electrostatic interaction (subindex indicates the group of the drug involved in the interaction). H: Hydrogen bond (subindex arrows indicate the direction of the hydrogen cession). π-π: Stacking interaction (subindex indicates the group of the drug involved in the interaction). Hy: Hydrophobic interaction (in brackets the group of the drug involved in the interaction). X: No interaction. Ring A: Polar head ring. Ring B, ring C: Side chain rings. Bn: Benzyl. Me: Methyl.

Table 25. Summary of interactions of heteroarylsalicylates, with the most representative aminoacids of the binding regions 1 and 2 of human glycolate oxidase (*hGO*). Data were obtained using *hGO* crystallographic active site structure (PDBID:2rdt). Interactions were obtained using Maestro software (Schrödinger). Comparison with **glyoxylate**, **CDST** and **CCPST** crystallographic data.¹⁰⁰

Compound	Arg167	Arg263	Tyr26	His260	Tyr132	Trp110	Leu205	Tyr208
Glyoxylate	E _{COO⁻}	H _{Arg→COO⁻}	H _{Tyr→COO⁻}	H _{His→CO}	X	X	X	X
CDST	E _{COO⁻}	H _{Arg→COO⁻}	H _{Tyr→COO⁻}	H _{N3→His}	H _{Tyr→N2}	Hy	Hy	Hy
CCPST	E _{COO⁻}	H _{Arg→COO⁻}	H _{Tyr→COO⁻}	H _{His→N3}	H _{Tyr→N2}	π-π	π-π	Hy
BIO-8 (C4)	E _{COO⁻} H _{Arg→COO⁻}	E _{COO⁻} H _{Arg→COO⁻}	X	H _{His→COO⁻}	Hy (ringA)	π-π _{ringA} π-π _{ringB}	Hy (ringA)	Hy (ringB)
MDMG-409 (C5)	H _{Arg→COO⁻} H _{Arg→COO⁻}	H _{Arg→COO⁻} H _{Arg→COO⁻}	H _{Tyr→COO⁻}	H _{His→COO⁻} H _{His→β-OH}	Hy (ringA)	Hy (ringB)	Hy (ringB)	Hy (ringB)
MDMG-317 (C5)	E _{COO⁻} H _{Arg→COO⁻}	H _{Arg→COO⁻} H _{Arg→COO⁻}	H _{Tyr→COO⁻}	H _{His→COO⁻} H _{His→β-OH}	Hy (ringA)	Hy (ringB)	Hy (ringB)	Hy (ringB)
BIO-18 (C4)	E _{COO⁻} H _{Arg→COO⁻}	E _{COO⁻} H _{Arg→COO⁻}	X	H _{His→COO⁻}	Hy (ringA)	π-π _{ringA}	X	Hy (ringB)
BIO-19 (C5)	E _{COO⁻} H _{Arg→COO⁻}	E _{COO⁻} H _{Arg→COO⁻}	X	H _{His→COO⁻} H _{His→β-OH}	Hy (ringA)	X	Hy (ringB)	Hy (ringB)
BIO-20 (C4)	E _{COO⁻} H _{Arg→COO⁻}	E _{COO⁻} H _{Arg→COO⁻}	X	H _{His→COO⁻}	X	π-π _{ringA} π-π _{ringB}	Hy (ringA)	Hy (ringB)
MDMG-983 (C5)	E _{COO⁻}	H _{Arg→COO⁻} H _{Arg→COO⁻}	H _{Tyr→COO⁻}	H _{His→COO⁻}	Hy (ringA)	Hy (furan)	Hy (furan)	Hy (furan)
MDMG-883 (C4)	H _{Arg→COO⁻} (furan) H _{Arg→COO⁻} (furan)	H _{Arg→COO⁻} (furoic) H _{Arg→COO⁻} (furoic)	H _{Tyr→COO⁻} (furoic) H _{Tyr→O-} furan	H _{His→COO⁻} (furan)	Hy (ringB)	π-π _{ringB}	Hy (ringA)	Hy (ringA)
MDMG-431 (C4)	E _{COO⁻}	E _{COO⁻}	X	H _{His→COO⁻}	X	π-π _{ringA}	Hy (ringB)	Hy (ringB)
MDMG-427 (C5)	E _{COO⁻} H _{Arg→COO⁻}	E _{COO⁻} H _{Arg→COO⁻}	X	H _{His→COO⁻} H _{His→β-OH}	X	π-π _{ringB}	X	X
MDMG-420 (C4)	E _{COO⁻} H _{Arg→COO⁻}	H _{Arg→COO⁻} H _{Arg→COO⁻}	Hy (ringA)	H _{His→COO⁻}	Hy (ringA)	π-π _{ringA} π-π _{ringB}	Hy (ringA)	Hy (ringB)
MDMG-373 (C5)	X	X	Hy (ringA)	H _{His→COO⁻}	H _{Tyr→COO⁻}	H _{Trp→COO⁻} π-π _{ringA} π-π _{ringB}	Hy (ringA)	Hy (ringB)
MDMG-417 (C4)	E _{COO⁻}	E _{COO⁻}	X	H _{His→COO⁻}	X	π-π _{ringA} π-π _{ringB}	Hy (ringB)	Hy (ringB)
MDMG-369 (C5)	E _{COO⁻} H _{Arg→COO⁻}	E _{COO⁻} H _{Arg→COO⁻}	X	H _{His→COO⁻} H _{His→β-OH}	Hy (ringA)	X	Hy (ringB)	Hy (ringB)

Table 25 (continuation).

BIO-25 (C4)	E_{COO^-} $H_{Arg \rightarrow COO^-}$	E_{COO^-} $H_{Arg \rightarrow COO^-}$	X	$H_{His \rightarrow COO^-}$	Hy (ringA)	$\pi\text{-}\pi_{ringA}$	X	Hy (ringB)
MDMG-424 (C5)	E_{COO^-} $H_{Arg \rightarrow COO^-}$	E_{COO^-} $H_{Arg \rightarrow COO^-}$	X	$H_{His \rightarrow COO^-}$ $H_{His \rightarrow \beta-OH}$	X	X	X	Hy (ringB)
BIO-23 (C4)	E_{COO^-} $H_{Arg \rightarrow COO^-}$	E_{COO^-} $H_{Arg \rightarrow COO^-}$	Hy (ringA)	$H_{His \rightarrow COO^-}$	X	$\pi\text{-}\pi_{ringA}$ $\pi\text{-}\pi_{ringB}$	Hy (ringA)	Hy (ringB)
BIO-24 (C4)	E_{COO^-} $H_{Arg \rightarrow COO^-}$	E_{COO^-} $H_{Arg \rightarrow COO^-}$	X	$H_{His \rightarrow COO^-}$	X	$\pi\text{-}\pi_{ringA}$ $\pi\text{-}\pi_{ringB}$	Hy (ringA)	Hy (ringB)
BIO-21 (C4)	E_{COO^-} $H_{Arg \rightarrow COO^-}$	E_{COO^-}	$H_{\beta-OH}$ $\rightarrow Tyr$	$H_{His \rightarrow COO^-}$	$H_{Tyr \rightarrow COO^-}$	$\pi\text{-}\pi_{ringA}$	Hy (ringB)	Hy (ringB)
BIO-22 (C4)	E_{COO^-}	E_{COO^-}	X	$H_{His \rightarrow COO^-}$	X	$\pi\text{-}\pi_{ringA}$ $\pi\text{-}\pi_{ringB}$	Hy (ringB)	Hy (ringB)

E: Electrostatic interaction (subindex indicates the group of the drug involved in the interaction). H: Hydrogen bond (subindex arrows indicate the direction of the hydrogen cession). $\pi\text{-}\pi$: Stacking interaction (subindex indicates the group of the drug involved in the interaction). Hy: Hydrophobic interaction (in brackets the group of the drug involved in the interaction). X: No interaction. Ring A: Polar head ring. Ring B: Side chain ring. Shaded: Specific binding features of C4 (grey) and C5 (green) isomers and compounds **MDMG-373** and **BIO-21** (pink).

Table 26. Summary of interactions of **BIO-9**, **BIO-11**, and the arylsalicylates **BIO-26** to **BIO-36**, with the most representative aminoacids of the binding regions 1 and 2 of human glycolate oxidase (*hGO*). Data were obtained using *hGO* crystallographic active site structure (PDBID:2rdt). Interactions were obtained using Maestro software (Schrödinger). Comparison with glyoxylate, CDST and CCPST crystallographic data.¹⁰⁰

Compound	Arg167	Arg263	Tyr26	His260	Tyr132	Trp110	Leu205	Tyr208
Glyoxylate	E _{COO⁻}	H _{Arg→COO⁻}	H _{Tyr→COO⁻}	H _{His→CO}	X	X	X	X
CDST	E _{COO⁻}	H _{Arg→COO⁻}	H _{Tyr→COO⁻}	H _{N3→His}	H _{Tyr→N2}	Hy	Hy	Hy
CCPST	E _{COO⁻}	H _{Arg→COO⁻}	H _{Tyr→COO⁻}	H _{His→N3}	H _{Tyr→N2}	π-π	π-π	Hy
BIO-9 (C5)	E _{COO⁻} H _{Arg→COO⁻}	E _{COO⁻} H _{Arg→COO⁻}	X	H _{His→COO⁻} H _{His→β-OH}	X	Hy	Hy	Hy
BIO-11	H _{Arg→COO⁻}	H _{Arg→COO⁻} H _{Arg→COO⁻}	H _{Tyr→COO⁻}	X	H _{β-OH→Tyr}	π-π _{ringB}	X	X
BIO-26 (C4)	E _{COO⁻}	E _{COO⁻}	X	H _{His→COO⁻}	X	π-π _{ringA} π-π _{ringB}	Hy (ringB)	Hy (ringB)
BIO-27 (C4)	E _{COO⁻}	E _{COO⁻}	Hy (ringA)	H _{His→COO⁻}	Hy (ringA)	π-π _{ringA} π-π _{ringB}	Hy (ringB)	Hy (ringB)
BIO-28 (C4)	E _{COO⁻}	E _{COO⁻}	X	H _{His→COO⁻}	X	π-π _{ringA} π-π _{ringB}	Hy (ringB)	Hy (ringB)
BIO-29 (C4)	E _{COO⁻}	E _{COO⁻}	Hy (ringA)	H _{His→COO⁻}	X	π-π _{ringA} π-π _{ringB}	Hy (ringA)	Hy (ringB)
BIO-30 (C4)	E _{COO⁻}	E _{COO⁻}	Hy (ringA)	H _{His→COO⁻}	X	π-π _{ringA} π-π _{ringB}	Hy (ringB-C)	Hy (ringB-C)
BIO-31 (C5)	E _{COO⁻} H _{Arg→COO⁻}	E _{COO⁻} H _{Arg→COO⁻}	Hy	H _{His→COO⁻} H _{His→β-OH}	Hy	X	X	X
BIO-32 (C5)	E _{COO⁻} H _{Arg→COO⁻}	E _{COO⁻} H _{Arg→COO⁻}	X	H _{His→COO⁻} H _{His→β-OH}	Hy (ringA)	X	X	X
BIO-33 (C4)	E _{COO⁻} H _{Arg→COO⁻}	H _{Arg→COO⁻}	X	X	X	π-π _{ringB}	X	Hy (ringB)
BIO-34 (C5)	X	X	H _{β-OH→Tyr}	X	H _{Tyr→COO⁻}	π-π _{ringB} H _{Trp→COO⁻}	X	X
BIO-35 (C4)	E _{COO⁻}	E _{COO⁻}	X	H _{His→COO⁻}	X	π-π _{ringA} π-π _{ringB}	X	X
BIO-36 (C5)	E _{COO⁻} H _{Arg→COO⁻}	H _{Arg→COO⁻} H _{Arg→COO⁻}	H _{Tyr→COO⁻}	H _{His→COO⁻} H _{His→β-OH}	H _{β-OH→Tyr}	π-π _{ringA} π-π _{ringC}	Hy (ringB)	Hy (ringB)

E: Electrostatic interaction (subindex indicates the group of the drug involved in the interaction). H: Hydrogen bond (subindex arrows indicate the direction of the hydrogen cession). π-π: Stacking interaction (subindex indicates the group of the drug involved in the interaction). Hy: Hydrophobic interaction (in brackets the group of the drug involved in the interaction). X: No interaction. Ring A: Polar head ring. Ring B, ring C: Side chain rings. Shadowed: Noteworthy binding features.

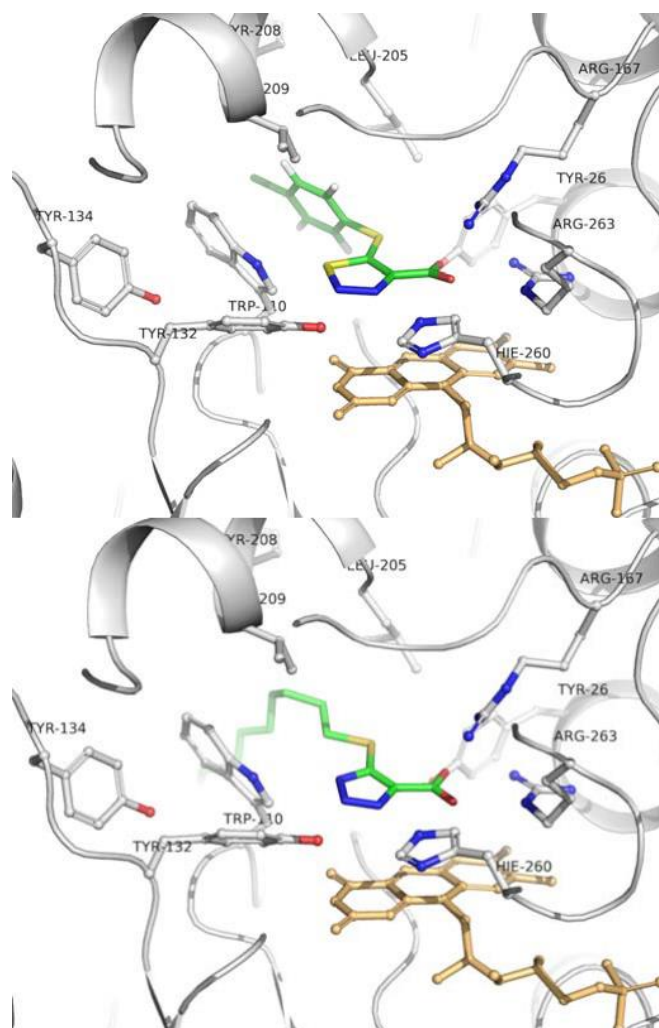


Figure 51. 3D-Representation of docked **CCPST** (up) and **CDST** (down) inside human glycolate oxidase activesite. Data were obtained using *hGO* crystallographic active site structure (PDBID:2rdt). Interactions were obtained using Maestro software (Schrödinger).

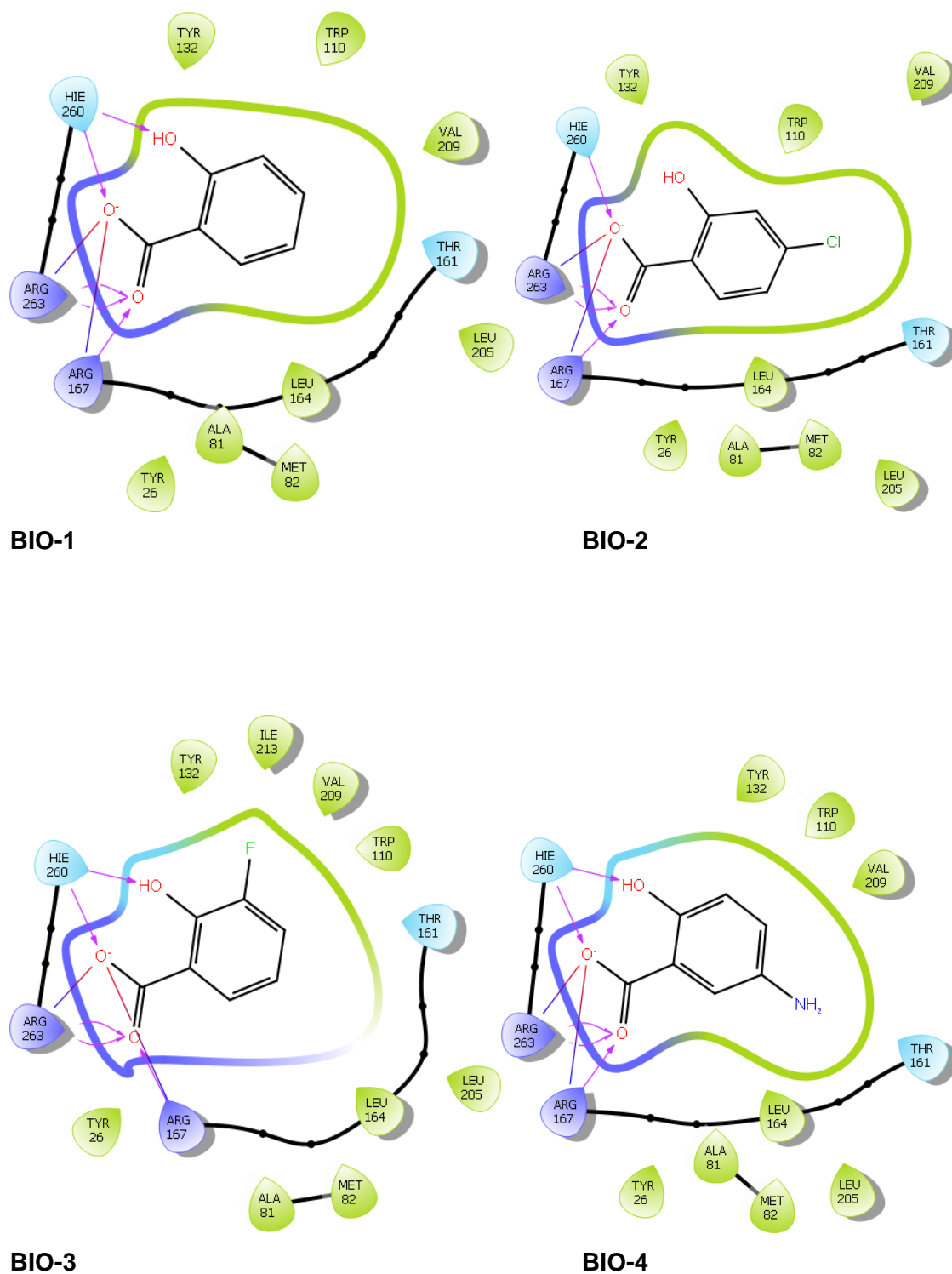


Figure 52. 2D Diagrams of interactions between compounds **BIO-1** to **BIO-17** and human glycolate oxidase residues (purple: basic, cyan: polar uncharged, green: non-polar). Grey shadow represents interaction with solvent. Hie260: His260 protonated on N ϵ [Maestro software (Schrödinger)].

Figure 52 (continuation).

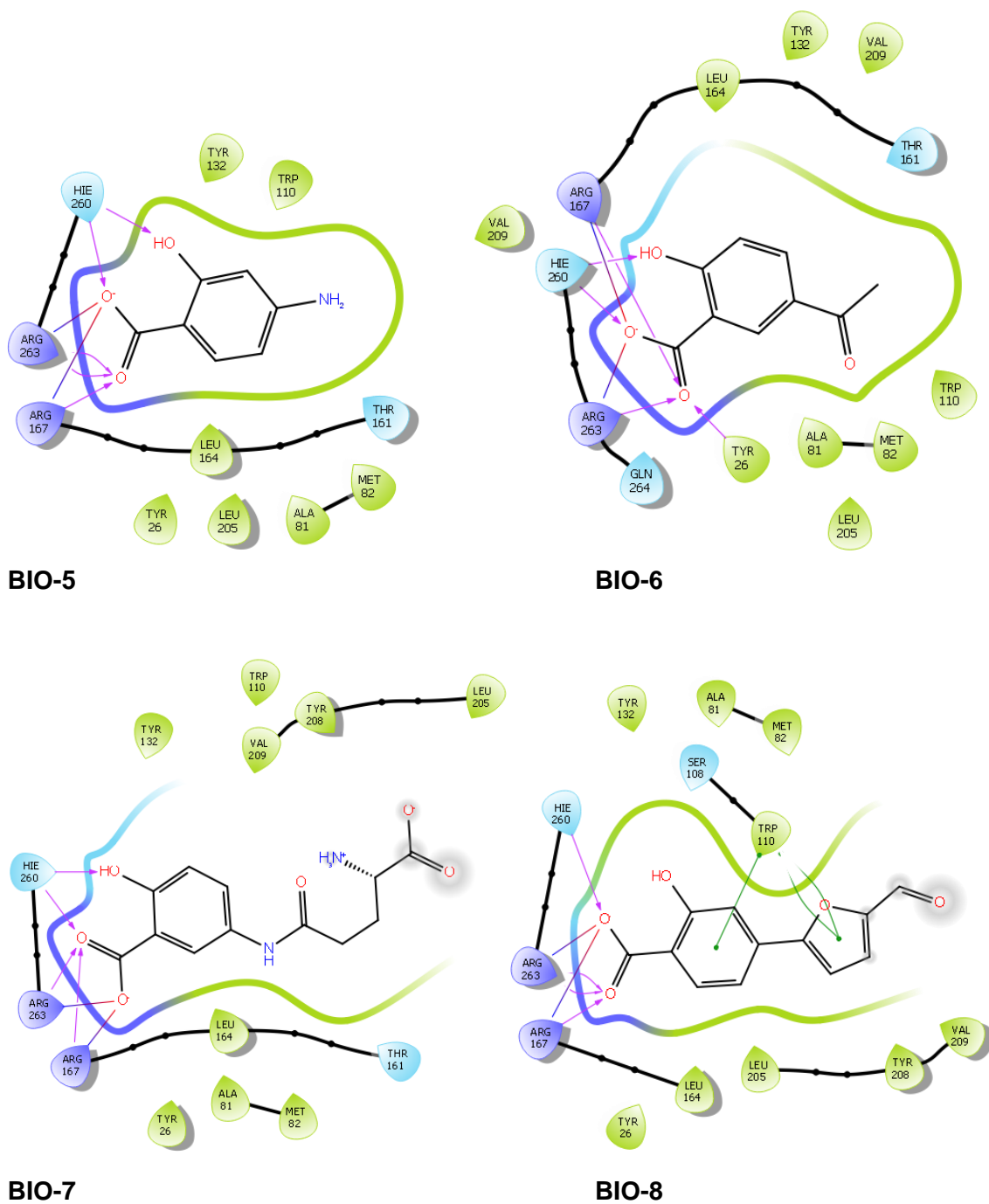


Figure 52 (continuation).

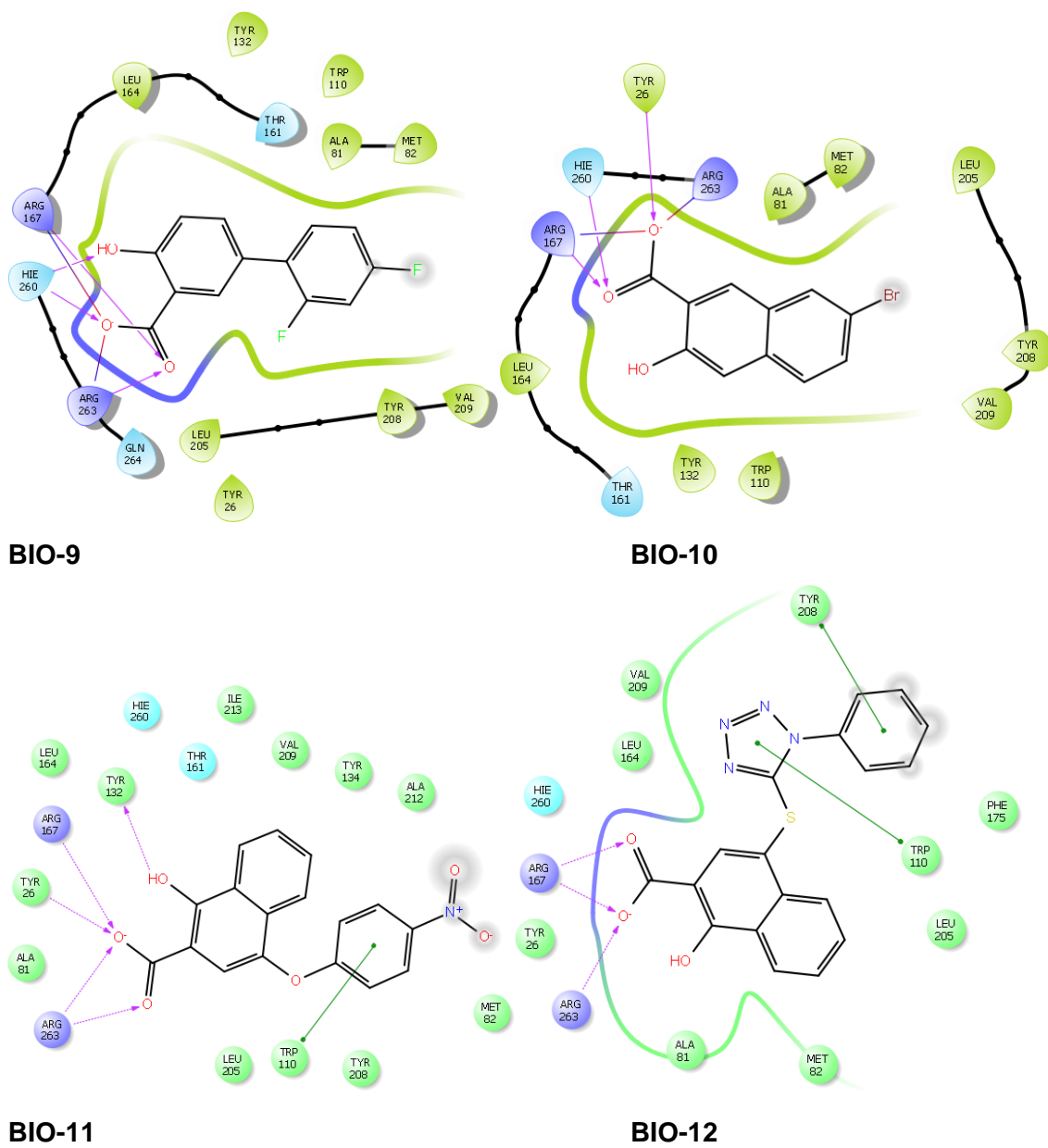
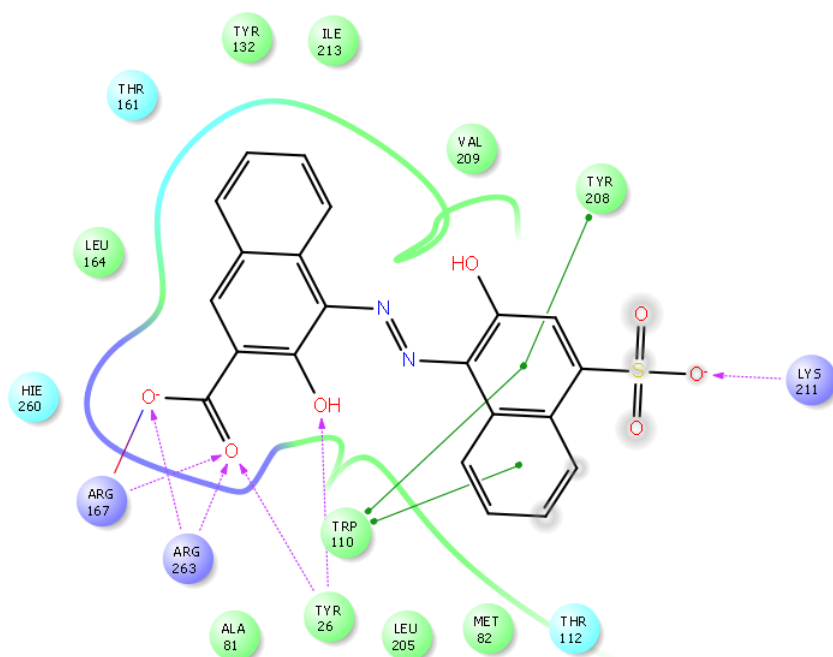
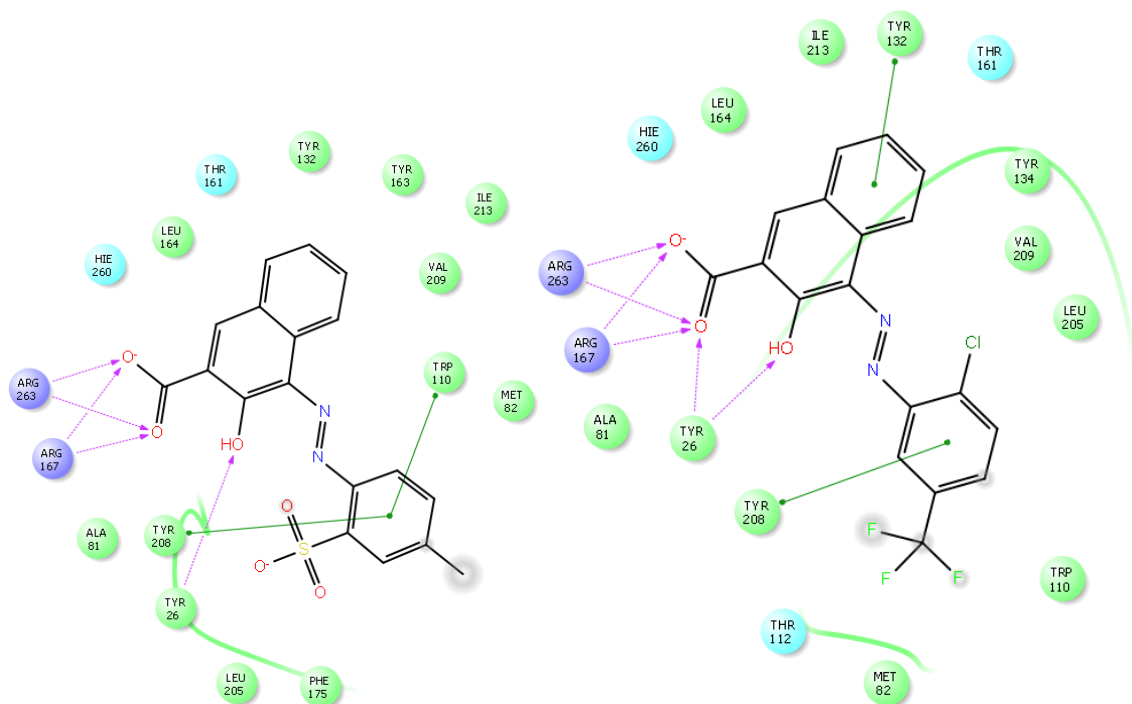


Figure 52 (continuation).



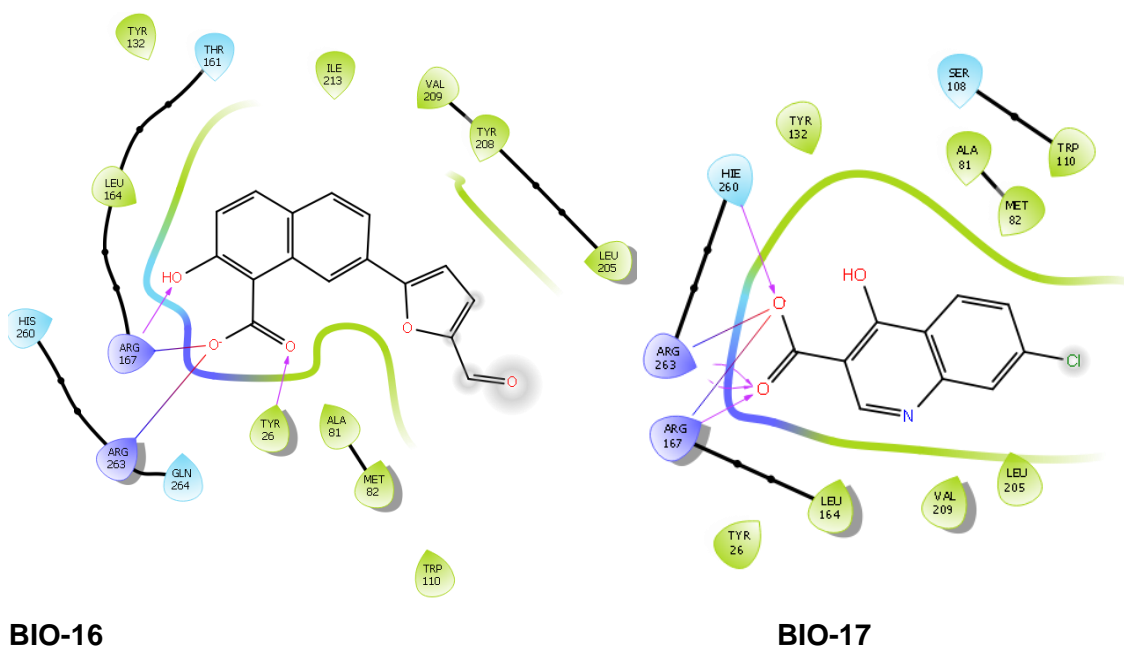
BIO-13



BIO-14

BIO-15

Figure 52 (continuation).



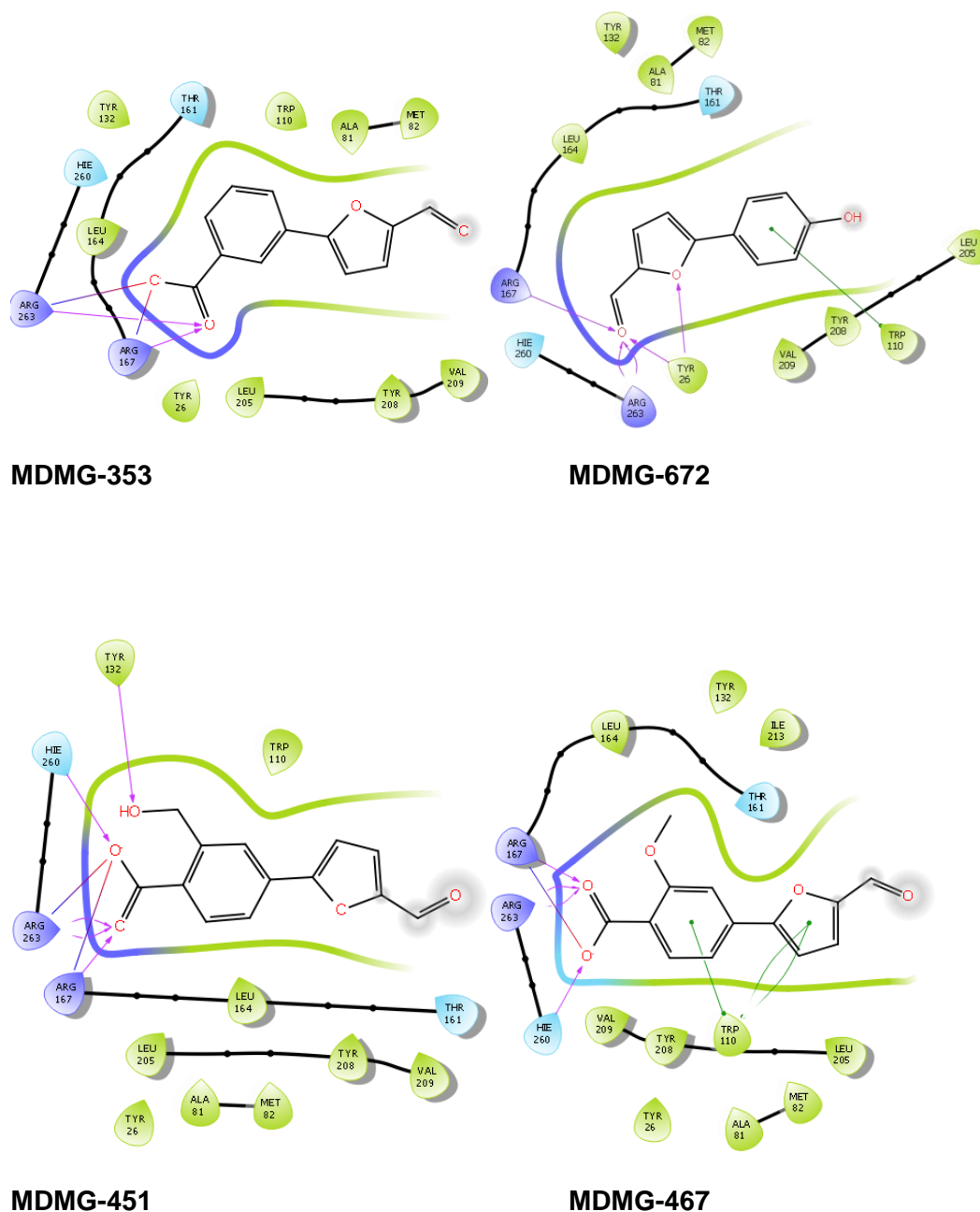
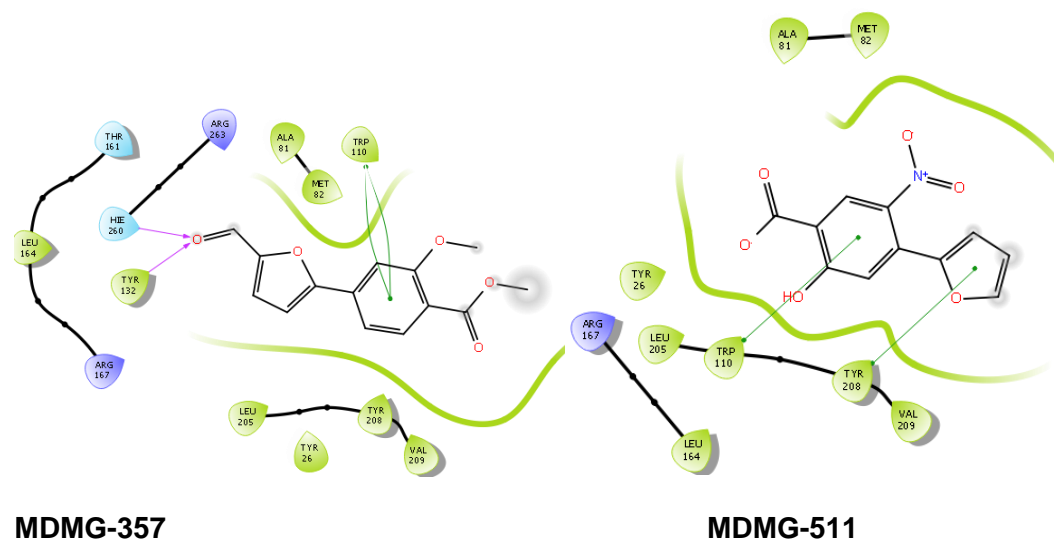


Figure 53. 2D Diagrams of interactions between compounds non-salicylic derivatives and **MDMG-511** and human glycolate oxidase residues (purple: basic, cyan: polar uncharged, green: non-polar). Grey shadow represents interaction with solvent. Hie260: His260 protonated on N_{ϵ} [Maestro software (Schrödinger)].

Figure 53 (continuation).



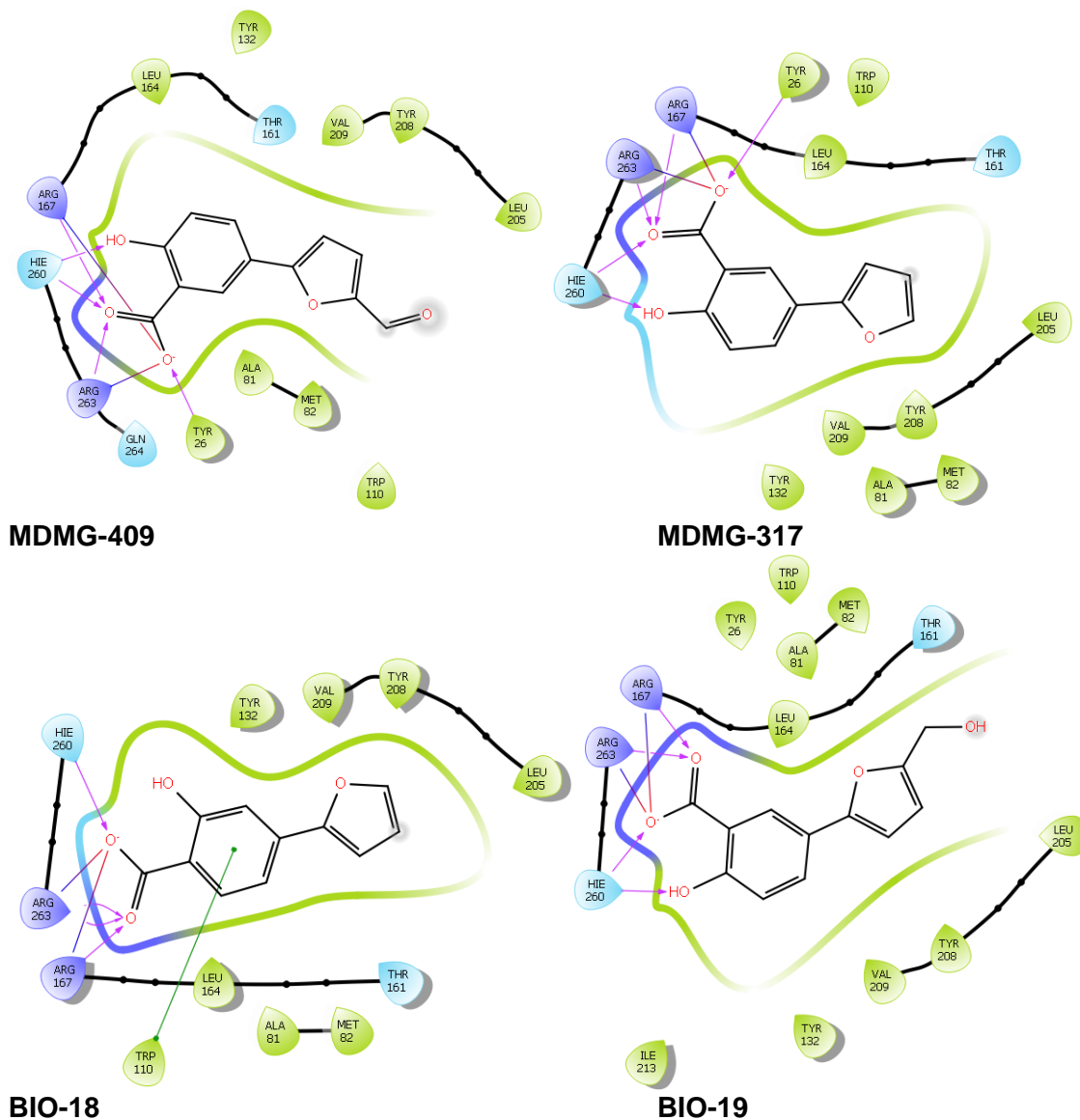


Figure 54. 2D Diagrams of interactions between heteroaryl derivatives and human glycolate oxidase residues (purple: basic, cyan: polar uncharged, green: non-polar). Grey shadow represents interaction with solvent. Hie260: His260 protonated on N_ε [Maestro software (Schrödinger)].

Figure 54 (continuation).

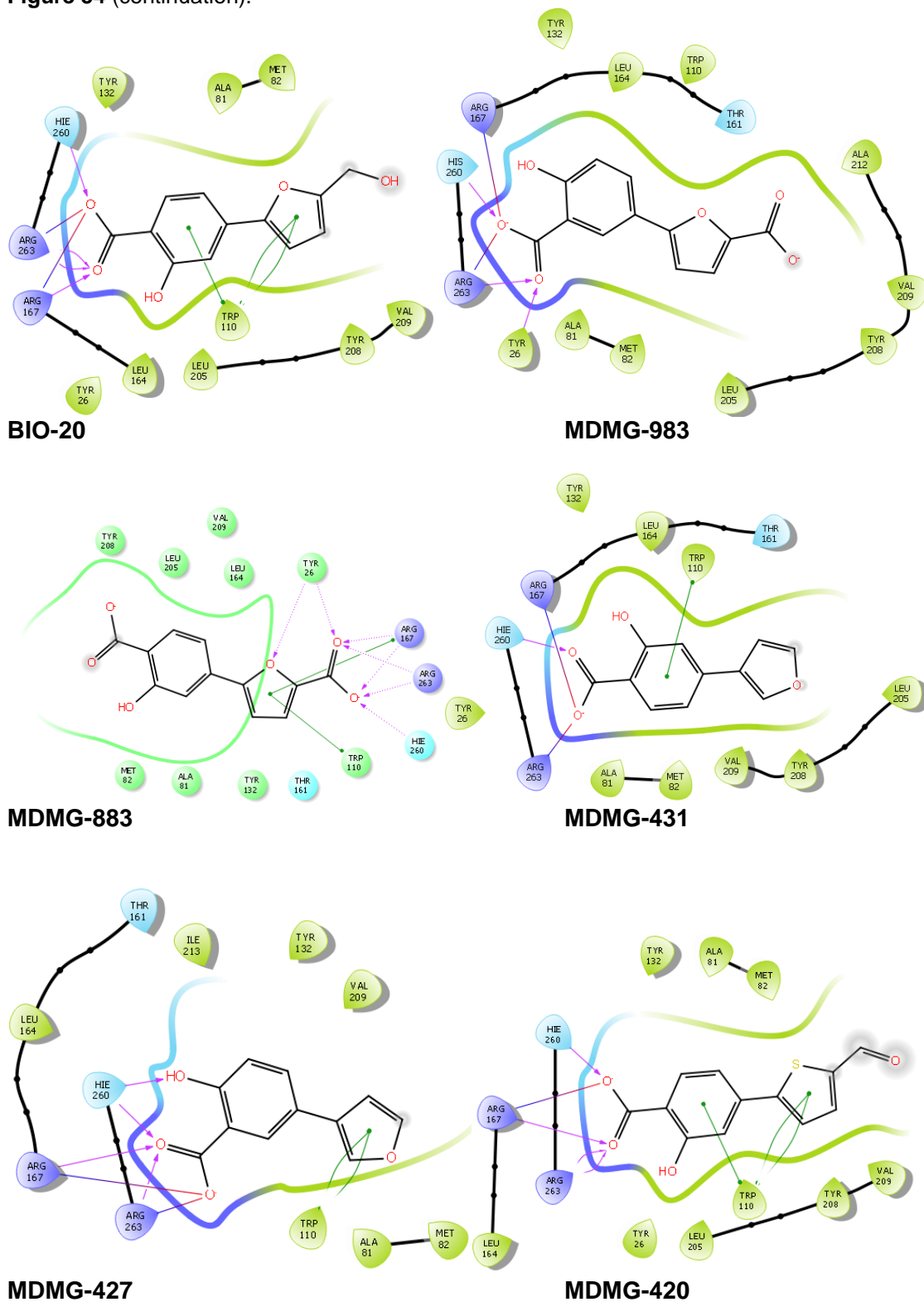


Figure 54 (continuation).

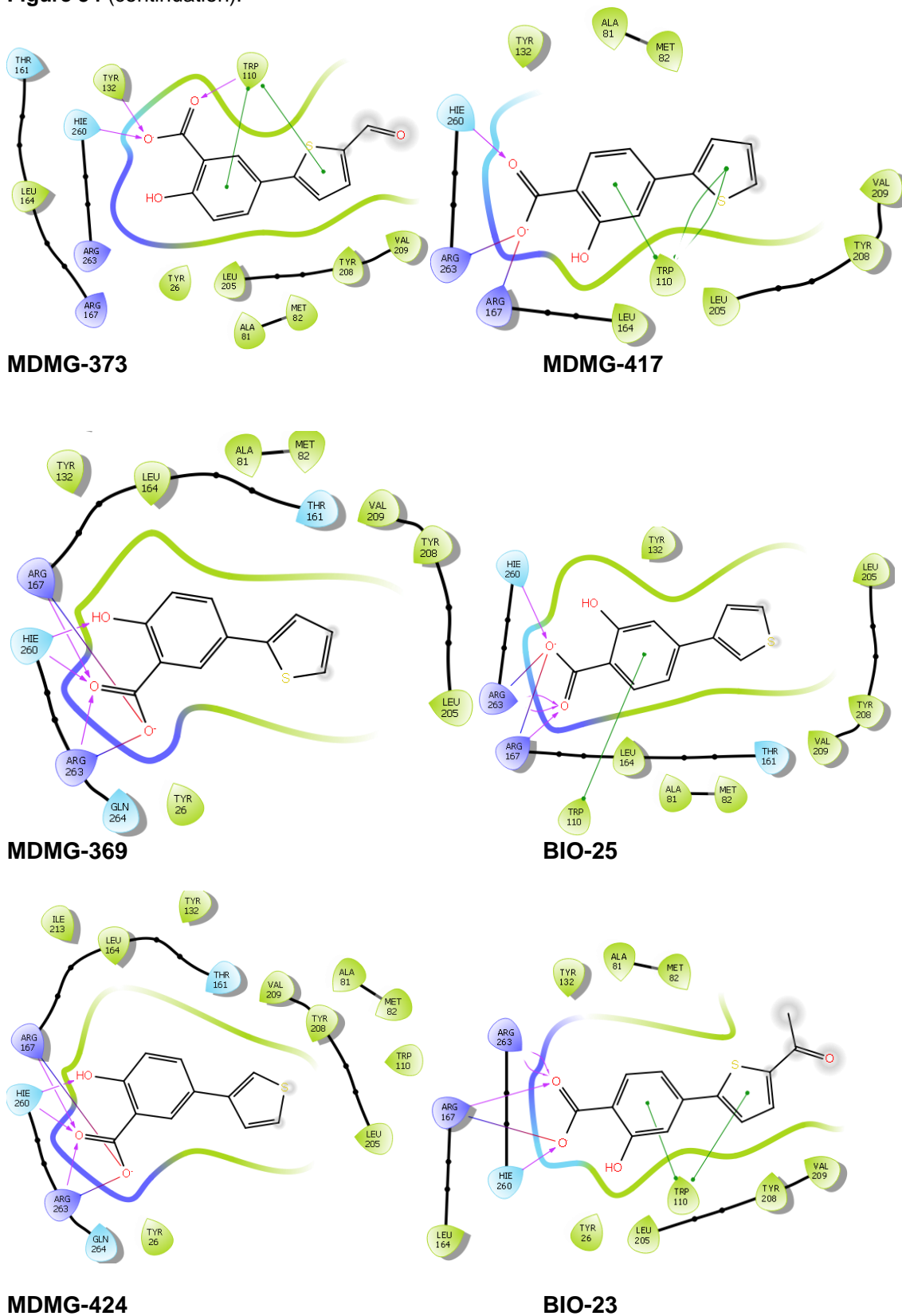
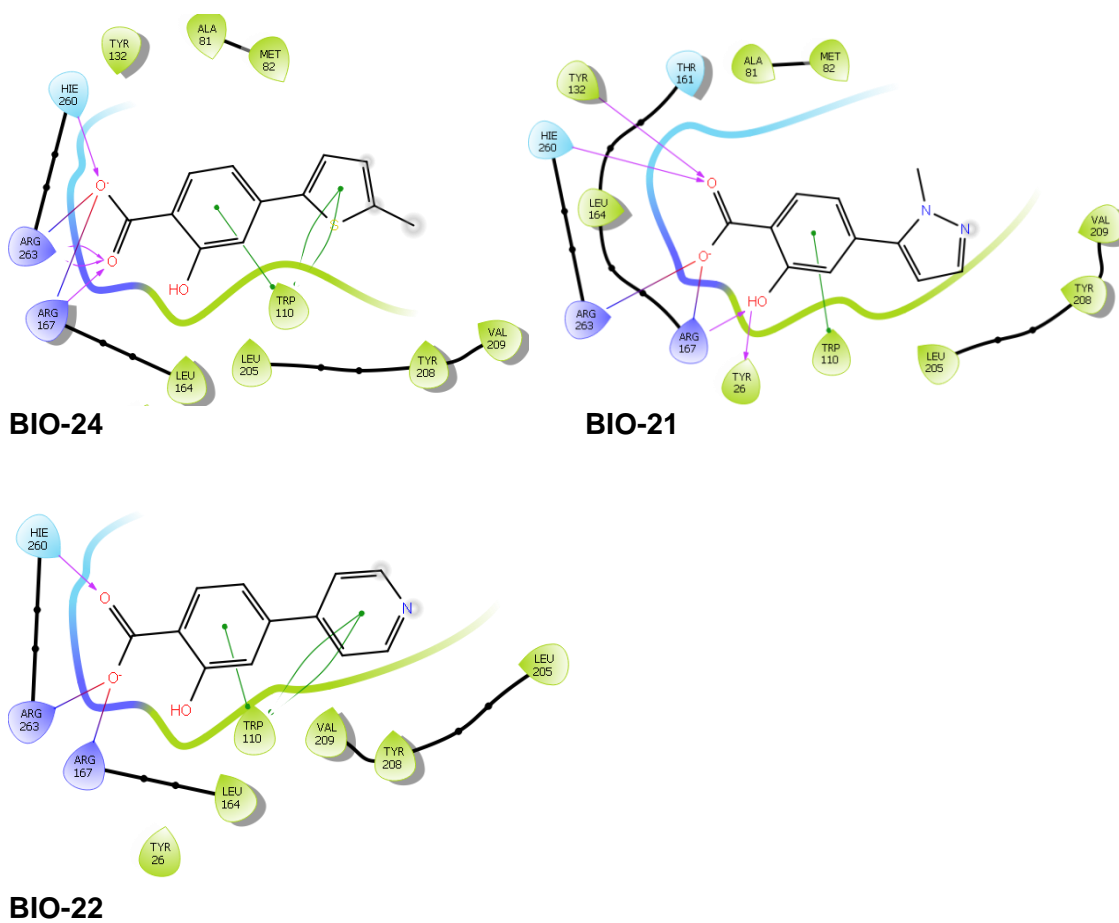


Figure 54 (continuation).



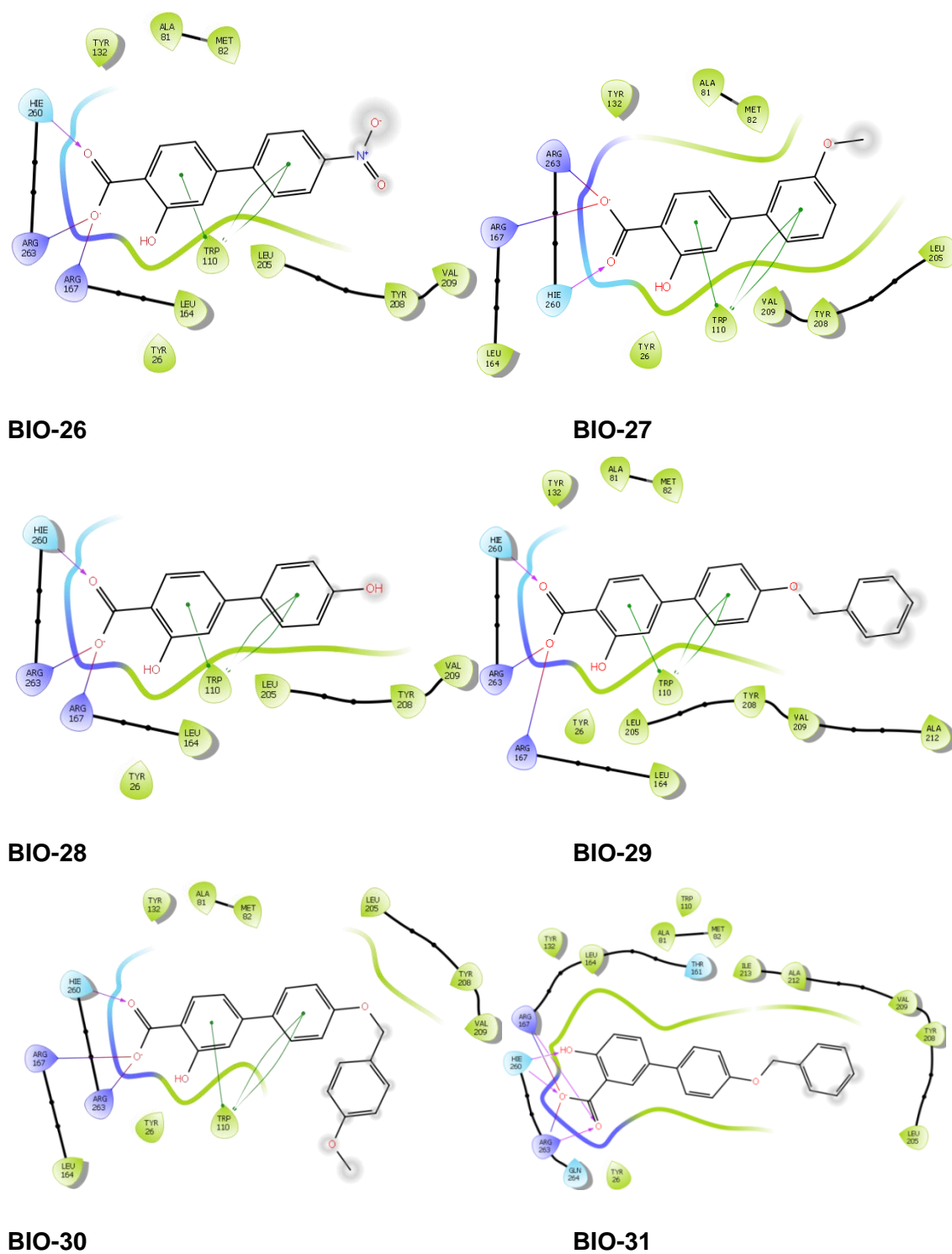
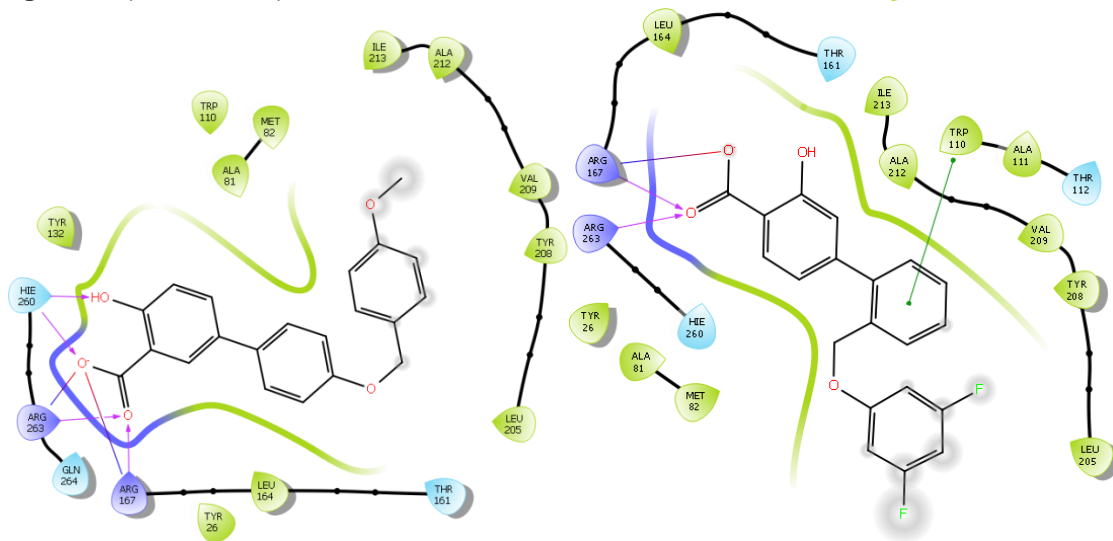


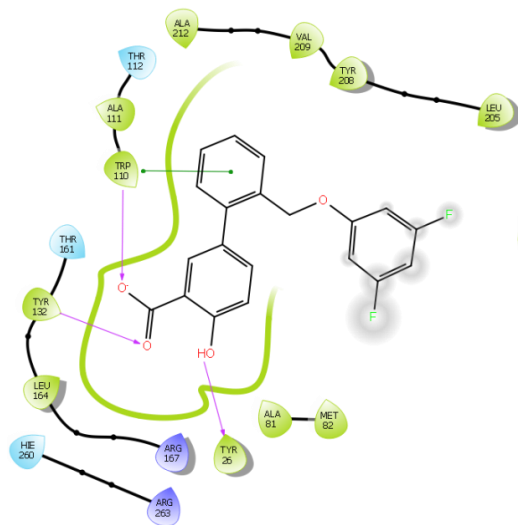
Figure 55. 2D Diagrams of interactions between compounds **BIO-45** to **BIO-55** and human glycolate oxidase residues (purple: basic, cyan: polar uncharged, green: non-polar). Grey shadow represents interaction with solvent. Hie260: His260 protonated on N_ε [Maestro software (Schrödinger)].

Figure 55 (continuation).

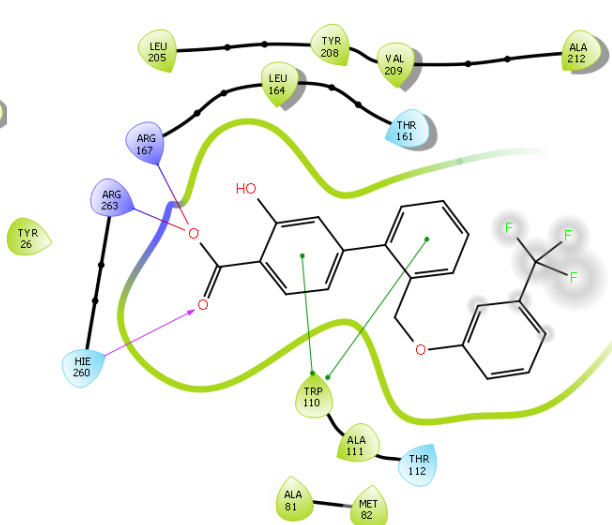


BIO-32

BIO-33

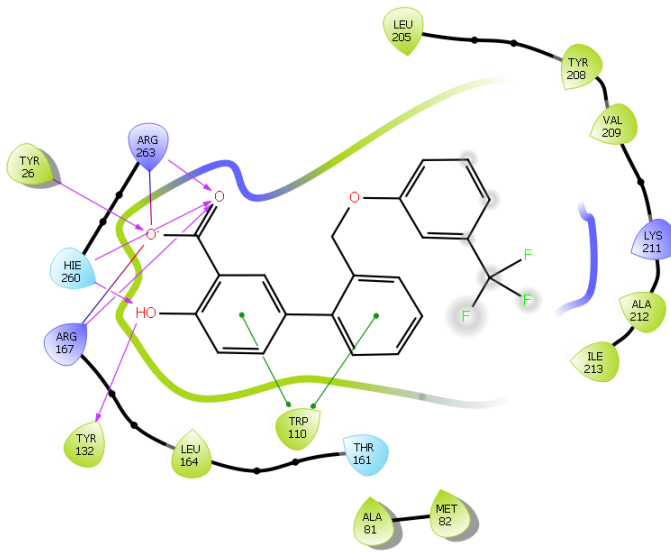


BIO-34



BIO-35

Figure 55 (continuation).



BIO-36

6.2. Analysis of interferences

Table 27. Potential HRP inhibition in the *mGO* colorimetric enzymatic assay (measured in absence of *mGO* and glycolate and in presence of H₂O₂ as substrate).

Compound	μM inhibitor	μg GO	μL H ₂ O ₂	U (nmol/min)	% inhibition
MDMG-409	100	0	10	3.745	-0.14
MDMG-317	100	0	10	3.268	12.61
MDMG-672	100	0	10	3.713	0.72
BIO-34	100	0	10	3.782	-1.15
BIO-35	100	0	10	3.911	-4.58
BIO-36	100	0	10	3.900	-4.30

Table 28. Analysis of interference in the oxalate determination assay. Potential oxalate oxidase or HRP inhibition in the oxalate detection assay were measured by diminution of absorbance at 595 nm. Inhibitors were tested at a final concentration of 10 μM. In the graphic, the y-axis represents the absorbance correspondent to the colorimetric oxalate oxidase/HRP catalyzed reaction. No significant deviation was observed for compounds **MDMG-409** (26) and **MDMG-672** (21) vs the standard. Standard: Absence of drug.

Experiment	nmoles Oxalate	Standard	MDMG-409 (26)	MDMG-317 (27)	MDMG-672 (21)
1	0	0.061	0.071	0.053	0.063
	0.5	0.118	0.121	0.064	0.123
	1	0.175	0.167	0.073	0.168
	2	0.267	0.126	0.168	0.246
	4	0.455	0.435	0.310	0.415
	5	0.545	0.532	0.442	0.493
2	0	0.068	0.067	0.054	0.067
	0.5	0.124	0.131	0.065	0.125
	1	0.182	0.174	0.075	0.169
	2	0.262	0.270	0.161	0.256
	4	0.424	0.441	0.294	0.431
	5	0.515	0.515	0.334	0.522

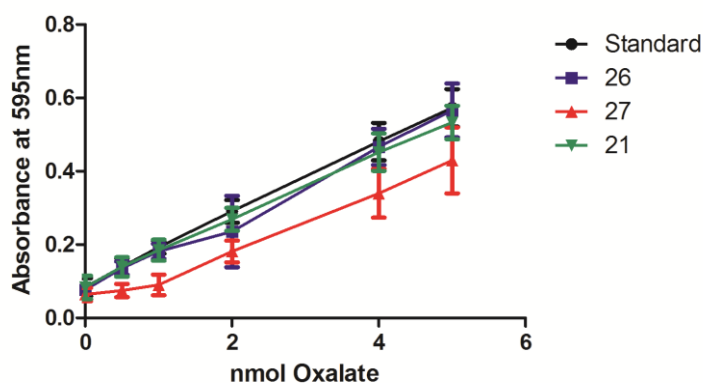


Table 29. Determination of IC_{50} for compound **MDMG-317** (27) against the oxalate determination kit containing oxalate oxidase and HRP.

nmol oxalate	μM MDMG-317 (27)	Mean calculated nmol oxalate	SD
5	0	5.0342	0.0000
5	1	4.7463	0.1198
5	2.5	4.5148	0.1916
5	5	4.2551	0.1437
5	7.5	3.9559	0.0399
5	10	3.5889	0.1437
5	20	2.7307	0.1597
5	40	0.7603	0.0080

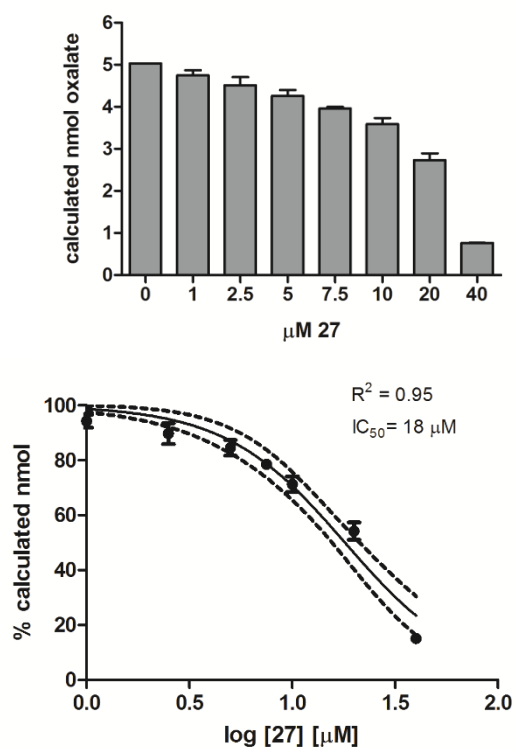


Table 30. Determination of interferences of compounds **BIO-19** and **BIO-20** in the oxalate detection assay.

Experiment	nmoles Oxalate	Standard	BIO-19	BIO-20
1	0	0.094	0.092	
	0.5	0.147	0.156	
	1	0.206	0.205	
	2	0.325	0.311	
	4	0.539	0.523	
	5	0.622	0.650	
2	0	0.086		0.085
	0.5	0.150		0.149
	1	0.155		0.213
	2	0.313		0.267
	4	0.535		0.488
	5	0.633		0.615

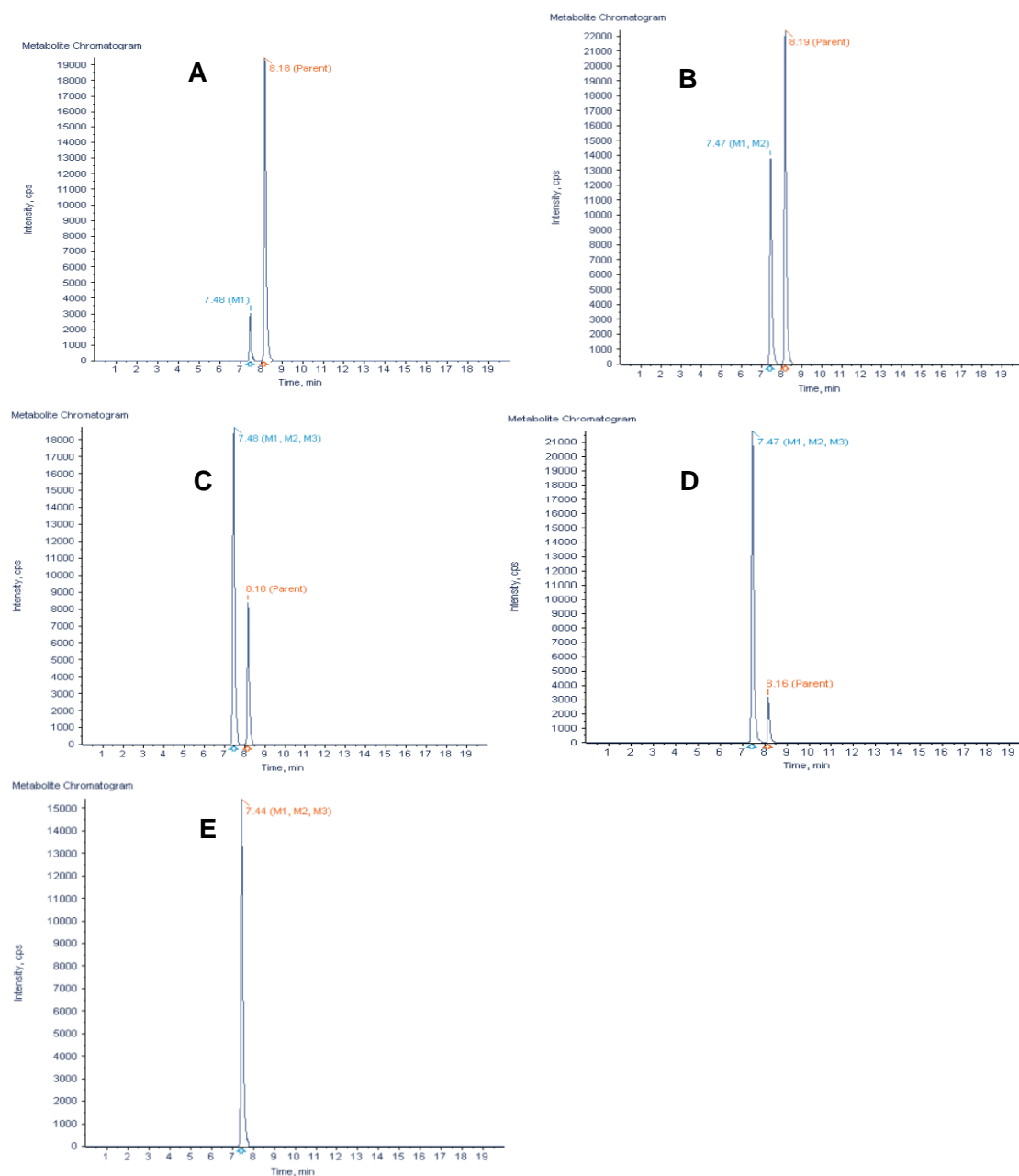
6.3. Metabolic profiling

Table 31. Metabolic stability of **MDMG-409**: Percentage of **MDMG-409** remaining at each incubation time.

With NADPH	
Time (min)	% Compound remaining
0	100.00 ± 2.7
5	67.2 ± 19.6
15	48.4 ± 10.9
30	19.2 ± 3.3
45	9.9 ± 2.1
60	3.9 ± 0.4
Without NADPH	
0	134.0 ± 13.3
60	90.2 ± 8.3

Table 32. Metabolic stability of **MDMG-317**: Percentage of **MDMG-317** remaining at each incubation time.

With NADPH	
Time (min)	% Compound remaining
0	100.00 ± 9.9
5	94.9 ± 16.1
15	85.6 ± 14.4
30	80.7 ± 9.2
60	50.8 ± 12.6
Without NADPH	
0	93.9 ± 9.9
60	89.1 ± 18.4



Peak ID	Name	Formula	<i>m/z</i>	ppm	R.T. (min)	Peak area	Area (%)	Score (%)
M2	Oxidation	C ₁₂ H ₈ O ₅	247.0256	3.3	7.44	5.36E+04	48.2	78.4
M1	Hydrogenation	C ₁₂ H ₁₀ O ₅	233.0465	3.9	7.46	4.46E+04	40.1	73.7
M3	Loss of CO	C ₁₁ H ₈ O ₄	203.0357	3.4	7.42	1.29E+04	11.6	72.9

Figure 56. Metabolite chromatograms of **MDMG-409** at 5, 15, 30, 45 and 60 min (from A to E). Table: Potential Metabolites of **MDMG-409** in mouse liver microsomes incubations at 60 min. RT: Retention time.

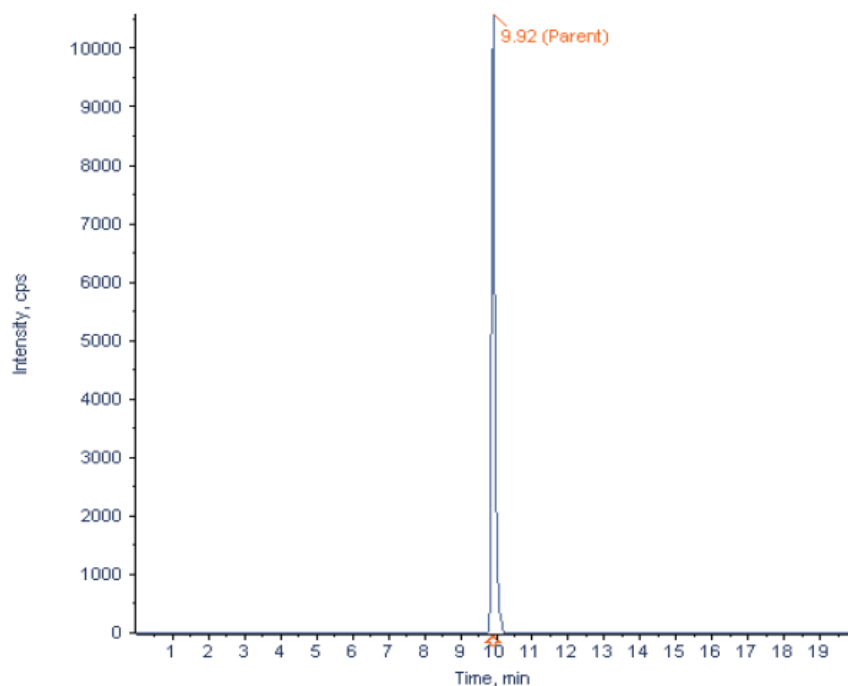


Figure 57. Chromatogram of compound **MDMG-1062**.

a)

$$t_{1/2} \text{ (min)} = 0.693/k$$

k = Slope of the natural log of the percent remaining vs time.

b)

$$CL_{\text{int H}} = \frac{\ln 2}{t_{1/2} \text{ (min)}} * \frac{\text{volume incubation (mL)}}{\text{microsomal protein (mg)}} * 45(\text{MPPGL}) \frac{2 \text{ g mouse liver}}{0.025 \text{ kg mouse body weight}}$$

CL_{int} : mL/min/mg microsomal protein

MPPGL: mg of microsomal protein per gram of liver

Figure 58. Equations for the calculation of half-life ($t_{1/2}$) (a) and intrinsic clearance (CL_{int}) (b) of compounds **MDMG-409** and **MDMG-317**.

6.4. International short-term stay

Photoaffinity labeling experiments with a THC-based probe performed on neuronal cells to identify off-target proteins of THC (tetrahydrocannabinol).

As previously mentioned in 3.2.4.1, within this project, a chemoproteomic study was planned after the appearance of some discording results, which suggest that a multi-target mechanism could be involved in the biological activity of some of our compounds. In fact, the off-target effect for GO inhibitors has been previously considered in the **CCPST** study.⁸⁰ Thus, I have developed two photoaffinity probes (**MDMG-911** and **MDMG-995**, Figure 48), which should be tested in hyperoxaluric mouse hepatocytes to study their proteomic profile.

In order to gain expertise in this technique, an international short-term stay was planned at Prof. M. van der Stelt group (Leiden, The Netherlands). Since it would be difficult to carry the *Agxt1*^{-/-} hepatocytes on which the photoaffinity probes should be tested, joining a chemoproteomics ongoing project seemed the best option. The recent publications of Prof. M. van der Stelt show his expertise in applying chemoproteomics to identify all the protein targets of a certain molecule.^{228–230} As a result of such investigations, they designed a THC-based probe aimed at studying off-target proteins of THC, due to the persisting biological effects of THC found in mice that lack of CB₁ receptor. This fact suggests additional proteins target of THC, a comparable situation to our discording results in PH1. Hence, we proposed a work plan in which chemoproteomics would be applied to find out off-target proteins of THC.

6.4.1. Background

During this short-term stay at Leiden University, a work plan consisting of photoaffinity labeling experiments with a THC-based probe was designed (Figure 59). The novel THC-like photoaffinity labeling (PAL) probe **GIA213** previously synthesized was used as a chemical tool to perform the PAL experiments of this project. This Δ^8 -THC-derived probe has a high affinity for both the CB₁ and CB₂ receptors ($K_i = 6.84 \pm 0.71$ nM and 4.69 ± 1.8 nM respectively), and was therefore successfully designed as a true pharmacological analog of Δ^8 -THC. Its structure contains the functional group diazirine as photoreactive function and a terminal alkyne as sorting function (“click”-handle).

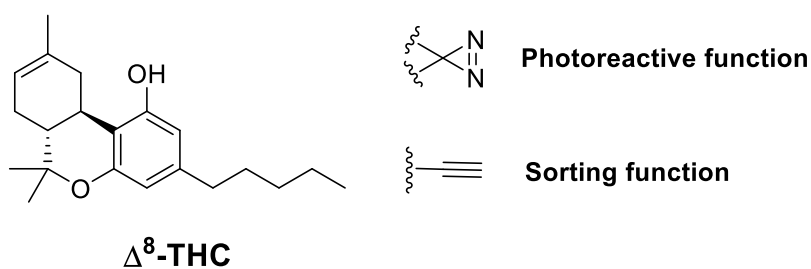


Figure 59. Structure of the Δ^8 -THC-derived photoaffinity probe.

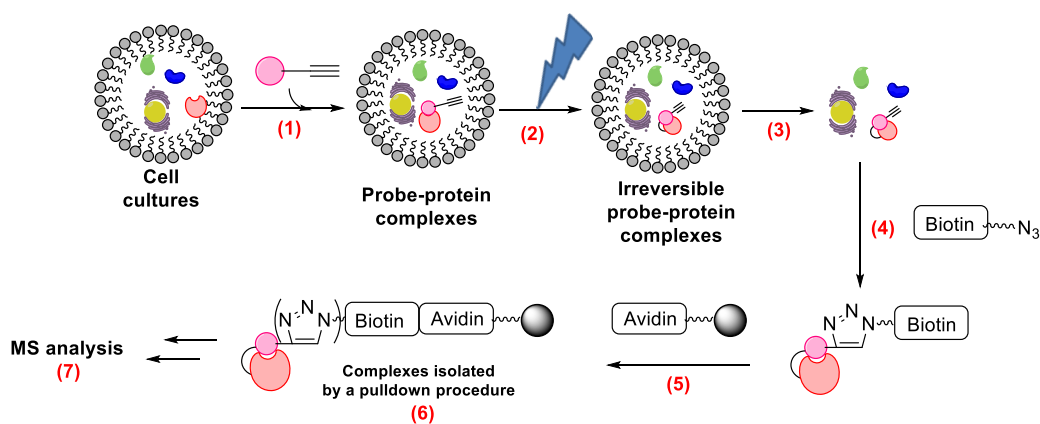
6.4.2. Objectives

In order to identify possible off-targets of THC, photoaffinity labeling experiments were performed on neuronal cells with the Δ^8 -THC-derived probe. The main objectives included:

1. Learning in culture handling
2. Incubation with the THC-based probe, irradiation for the probe-protein complex formation.
3. Isolation of the labeled complexes by a pulldown procedure using avidin beads.
4. Mass Spectrometry (MS) analysis and interpretation of results.

6.4.3. Methodology

A work plan following the Scheme 18 was established to complete the stated objectives.



Scheme 18. Representation of the process for protein capture by chemical probes.

Neuro2a cells were grown to confluency in 10 cm dishes at 37°C under a humidified 5% CO₂ atmosphere. The culture medium consisted of DMEM (Dulbecco's Modified Eagle Medium) supplemented with 10% New Born Calf Serum, 1% Glutamax and 0.2% Penicillin/Streptomycin (P/S).

For every type of sample, duplicates were included in each experiment. Both negative controls and competition samples were included to assess probe binding to target proteins:

- Negative controls: untreated controls (treated with DMSO instead of the probe) and non-irradiated controls were used to discard unspecific binding.
- Competition samples: cells were pre-treated with probe competitors Δ^8 -THC and Δ^9 -THC (cannabinoid receptors ligands) before probe treatment to evaluate comparative binding between probe and THC. With this competition samples, the grade of inhibition of the probe-protein binding by THC was measured.

Cell treatment (Step 1, Scheme 18): After growing cells to confluency, the medium was removed and each plate was washed two times with 6 ml PBS. After that, 3 mL of buffer A (PBS containing 1mM CaCl₂ and 1 mM MgCl₂) were added to each plate. Buffer A was removed from the plate.

- **Pre-treatment:** competition samples were treated with 2997 μ L of competitor solution (Δ^8 -THC or Δ^9 -THC, stock solution 10 mM in DMSO) 10 μ M in buffer A. Non-competition samples were treated with 2997 μ L of a solution containing same % of DMSO. Cells were incubated at 37 °C for 30 minutes in the dark.
- **Treatment:** 3 μ L of the probe GIA213 (stock solution 10 mM in DMSO, final concentration 10 μ M) were added to the treated samples. The same amount of DMSO was added to untreated samples and cells were incubated at 37 °C for 30 minutes in the dark.

Irradiation (Step 2, Scheme 18): probe solution was removed from cells and 1.5 mL of buffer A were added to plates. Plates were then irradiated for 5 min at 4 °C in the CaproBox™ preset on 350 nm. After that, cells were scraped of the plate and transferred to 2 mL Eppendorf tubes. Samples were centrifuged for 10 min at 1200 g at 4°C. The supernatant was then removed and 250 μ L of buffer B (50mM HEPES) were added.

Cell lysate (Step 3, Scheme 18): Cells were destroyed with a Heidolph Silent Crusher instrument (20 seconds on 25.000 rpm) and sonicated (10 times x 2.5 seconds with intervals of 0.5 seconds). Membranes were separated from cytosol by high speed centrifugation (1.5 hour, 30100 g, 4°C) and samples were frozen overnight at -80°C. To the membrane fraction or the whole lysate (when the step of cytosol/membranes separation is omitted), 2 µL of 10% SDS were added and the samples were sonicated (10 times x 0.5 seconds with intervals of 0.5 seconds).

Click reaction (Step 4, Scheme 18): 25 µL of lysate were transferred to a different eppendorf to perform **Cy5-N₃ click reaction**. Click mix for 2.5 µL: 1.25 µL CuSO₄ (25 mM in Milli-Q), 0.75 µL NaAsc (250 mM in Milli-Q), 0.25 µL THPTA (25 mM in DMSO), 0.25 µL Cy5-N₃ (0.9 mM in DMSO). Reaction Steps:

- 2.5 µL of Cy5-N₃ containing click mix were added to each sample and samples were incubated for 1 hour in the dark at room temperature.
- 9.2 µL of 4x SDS-PAGE sample buffer were added to each sample and samples were incubated at room temperature for 30 minutes.
- Samples were frozen at -20°C until further use.
- Protein concentrations of the rest of cell lysate were determined using the BSA protein assay on a microplate reader. Sample volumes were adjusted to 400 µL with buffer B after protein quantification.

Click chemistry was performed over the remaining lysates using **biotin-alkyl-N₃**. Click mix for 43.7 µL: 21.85 µL CuSO₄ (25 mM in Milli-Q), 13.1471 µL NaAsc (250 mM in Milli-Q), 4.37 µL THPTA (25 mM in DMSO), 4.37 µL biotin-alkyl-N₃ (2.25 mM in DMSO). Reaction Steps:

- 43.73 µL of biotin-alkyl-N₃ containing click mix were added to each sample.
- Samples were incubated for 1 hour in the dark at room temperature.

MeOH/CHCl₃ precipitation: Labeled proteins were precipitated by adding 666 µL of MeOH, 166 µL of CHCl₃ and 300 µL of Milli-Q, in that order. Samples were then centrifuged at 20238 g for 10 minutes and supernatants were discarded. 600 µL of MeOH were added to each pellet, and pellets were resuspended by sonication (6 times x 0.5 seconds with intervals of 0.5 seconds). Finally, supernatants were discarded.

Denaturation, reduction and alkylation: Samples were resuspended in 500 µL of freshly prepared 1% SDS with ammonium bicarbonate (NH₄HCO₃) and incubated for 15 minutes at room temperature. 5 µL of dithiothreitol (DTT, 1M solution in Milli-Q) were added and samples were incubated at 65 °C for 15 minutes while shaking at 700

rpm. Samples were cooled to room temperature (5-10 minutes). 40 μL of IAA (iodoacetamide 0.5 M in Milli-Q) were added and samples were incubated for 30 minutes at room temperature in the dark. Finally, 140 μL of 10% SDS were added to each sample.

Washing of beads: 50 μL of avidin beads for each sample were removed from a 50% slurry and washed with 6 mL of PBS for 3 times in a 15 mL ube (washing steps were performed by pelleting beads at 2000 g for 2 minutes and removing supernatant). Beads were resuspended in 6 mL PBS.

Pulldown and washing (Step 5, Scheme 18): Samples were transferred to the beads and incubated for 2 hours at room temperature while rotating. After incubation, beads were washed with 6 mL 0.5% SDS in PBS once and then with 6 mL of PBS for 3 times (each washing step was performed by pelleting beads at 2000 g for 2 minutes and removing supernatant).

On-bead digestion: Samples were incubated with 250 μL of on-bead digestion buffer containing trypsin or chymotrypsin in low-binding Eppendorf tubes. On-bead digestion buffer (3 mL recipe): 300 μL of 1 M Tris, 300 μL of 1 M NaCl, 3 μL of 1 M CaCl_2 , 60 μL of acetonitrile, 3 μL of 0.5 $\mu\text{g}/\mu\text{L}$ trypsin and 2334 μL Milli-Q. Samples were then shaken vigorously (1000 rpm) at 37°C (for trypsin) or 25°C (for chymotrypsin) overnight. After spinning down briefly, samples were quenched with 12.5 μL of formic acid and beads were removed with a biospin column by centrifugation at 600 g for 2 minutes in 2 mL Eppendorf tubes. The stage tips were prepared with 2 layers of C18 column material, and were desalted, washed, loaded and eluted.

LCMS samples preparation: Samples were completely evaporated in Speedvac at 45 °C. 50 μL of LCMS solution were added to each sample. LCMS solution (2 mL recipe): 1900 μL of Milli-Q, 60 μL of acetonitrile, 2 μL of formic acid, 40 μL of yeast enolase stock (final concentrations 3% acetonitrile, 0.1% formic acid and 20 fmol/ μL enolase).

MS analysis (Step 6, Scheme 18): Samples were measured with a Synapt G2-Si instrument and the data were processed with the commercial software Progenesis.

6.4.4. Results and discussion

The cited protocol was carried out 4 times, with duplicates, over Neuro2a cultures using GIA213 probe and competitors at 10 μM . After the MS measurement and Progenesis processing, data were analyzed to identify target proteins for the probe. The data analysis included:

- Deleting of proteins with 0 unique peptides and peptide count below 2.
- Calculation of the average normalized abundance for the treated, untreated and non-irradiated samples. With these values, ratios treated/untreated and treated/non-irradiated were calculated and ratios over 2 were selected as significant.
- Over the selected proteins, the average normalized abundance was calculated for the competition samples and treated samples. Ratios competitor Δ^8 -THC/treated and competitor Δ^9 -THC/treated were calculated. The lowest values in this ratios show higher inhibition of the probe-protein binding by THC. For each protein, error of ratio and t-test were calculated, and proteins with values below 0.05 in t-test were selected as significant.
- The target proteins obtained in the four experiments were compared and some overlaps were detected. However, these overlaps were not as significant as expected. Thus, new experiments were designed introducing some changes in the protocol
- Probe concentration was reduced to 1 μM keeping competitor concentration in 10 μM in order to identify high affinity targets for the probe. To ensure that the probe is active at 1 μM , a PAL experiment with different probe concentrations (0 μM , 1 μM , 3 μM , and 10 μM), in absence of competitors and with UV irradiation was performed on Neuro2a cells. Samples were treated with the Cy5- N_3 containing click mix and SDS-PAGE was carried out. Thereby, activity of the probe at 1 μM was confirmed.
- The cytosol/membrane separation step was removed to reduce variability in the experiment. If an interesting target protein was found in the future, this step could be included again to identify the location of such protein.
- Triplicates instead of duplicates were introduced in every experiment to obtain
- Due to the normalization of the negative control done by the MS software (increasing the signals for untreated and non-irradiated samples), negative controls may not reflect accurate information. Thus, apart from reprocessing data, a possible option was processing negative controls separately and use

the proteins identified in these samples as an exclusion list for the positive controls. For this reason, the next experiments were carried out without the mentioned negative controls.

- As significant result could not be obtained from the SDS-PAGE, this step was removed from the protocol.
- The same experiment including the cited changes was performed 3 times over Neuro2a cells and the samples were measured by MS.

This work contributed to a previously started research developed by other members of the group, and as a result, an article was published.²³¹ The PAL experiments performed over Neuro2A cells, revealed around 150 protein targets. When the competition experiment was carried out, four putative protein targets were identified for Δ^8 -THC (Reep5, Mtch2, and Gnb1) and one for Δ^9 -THC (Cox4i1), which are involved in energy metabolism, apoptosis or DNA maintenance. Thus, this supposes a step forward in understanding the proteomic profile of THC, which could help to the development of novel treatments based on THC.

6.5. Rights and permissions



Copyright Clearance Center



Home

Create Account

Help

LIVE CHAT



ACS Publications
Most Trusted. Most Cited. Most Read.

Title: Salicylic Acid Derivatives Inhibit Oxalate Production in Mouse Hepatocytes with Primary Hyperoxaluria Type 1

Author: María Dolores Moya-Garzón, Cristina Martín Higuera, Pablo Peñalver, et al

Publication: Journal of Medicinal Chemistry

Publisher: American Chemical Society

Date: Aug 1, 2018

Copyright © 2018, American Chemical Society

LOGIN

If you're a copyright.com user, you can login to RightsLink using your copyright.com credentials.

Already a [RightsLink](#) user or want to [learn more?](#)

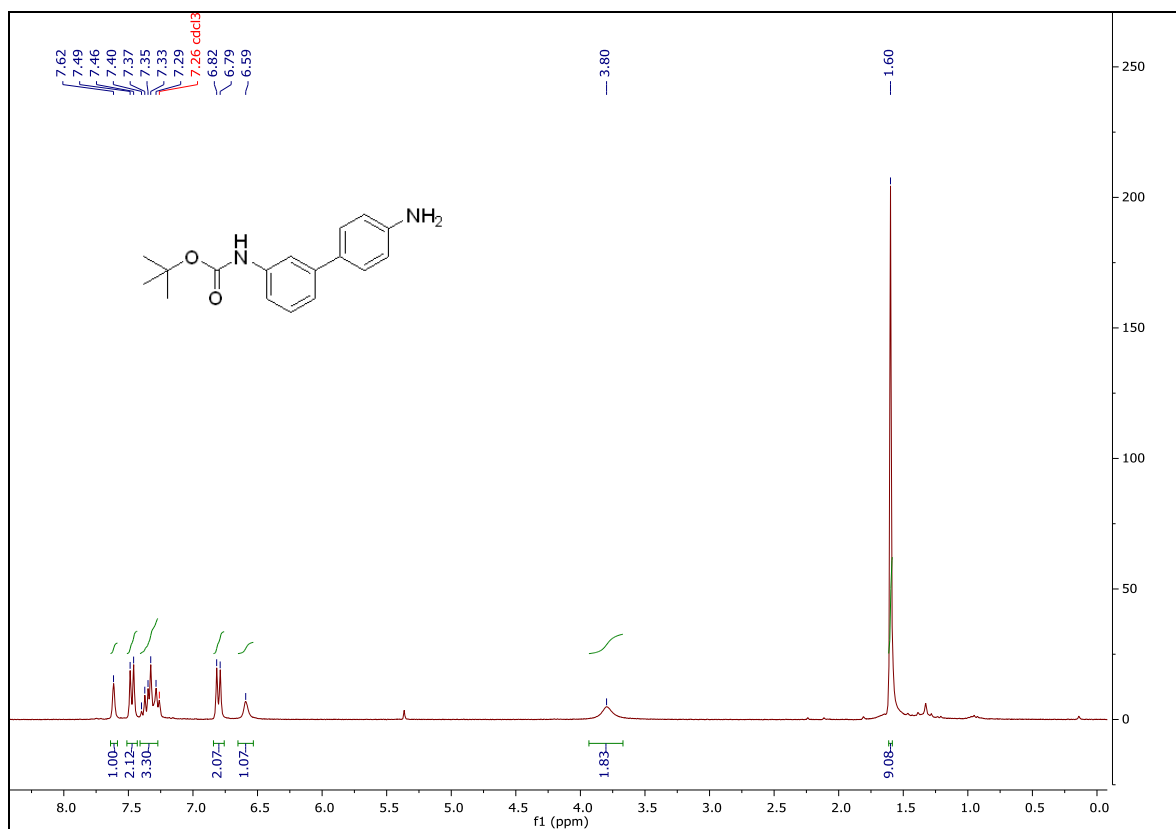
PERMISSION/LICENSE IS GRANTED FOR YOUR ORDER AT NO CHARGE

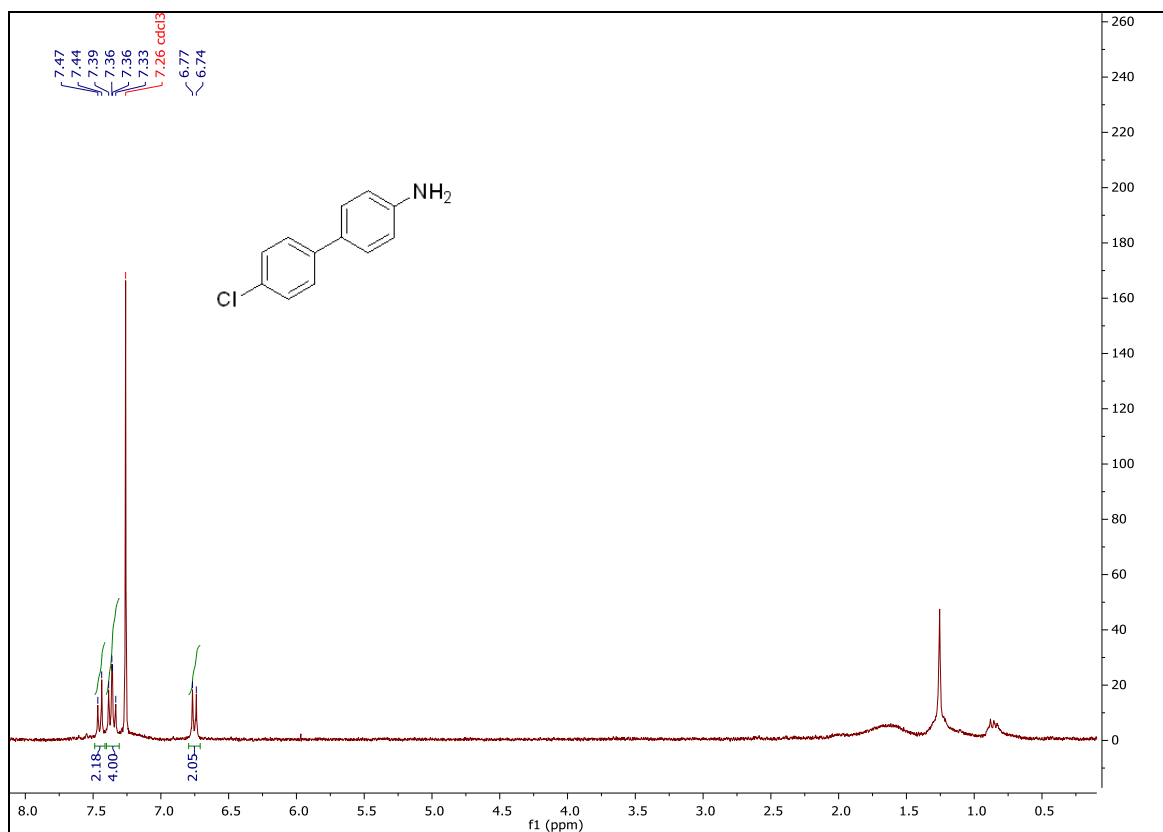
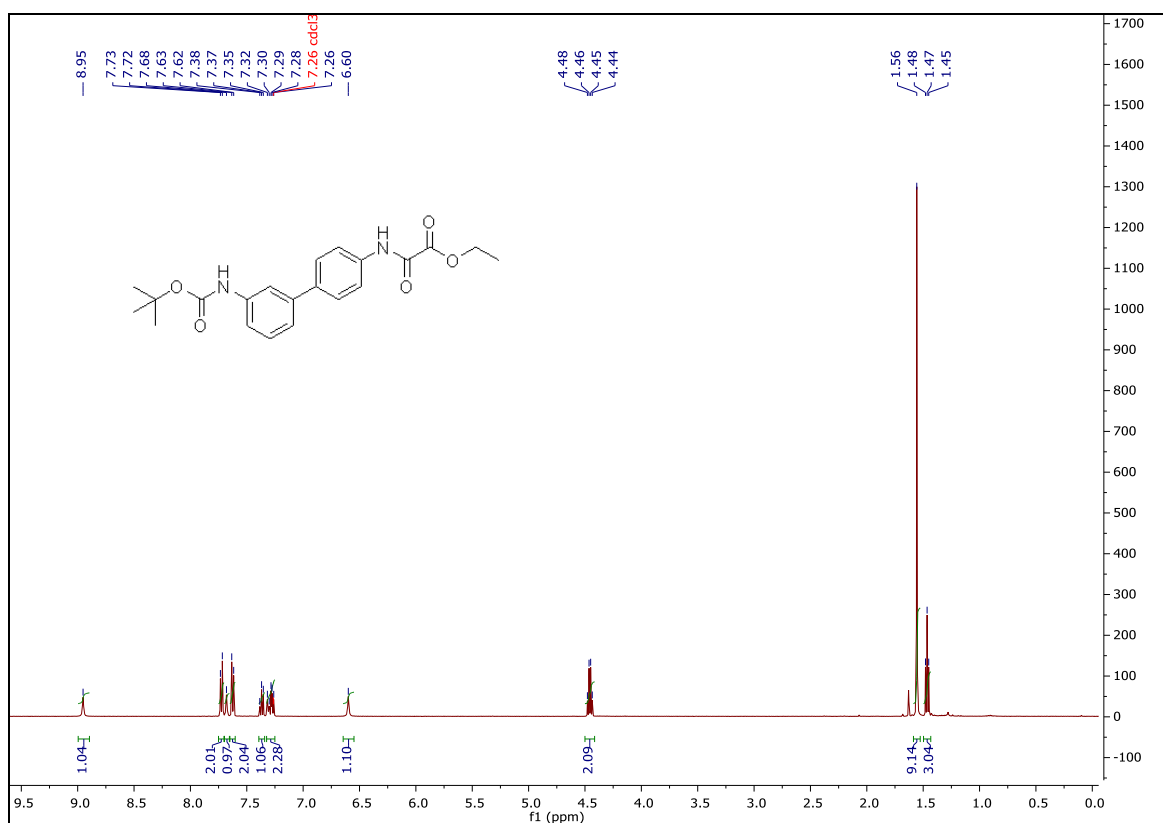
This type of permission/license, instead of the standard Terms & Conditions, is sent to you because no fee is being charged for your order. Please note the following:

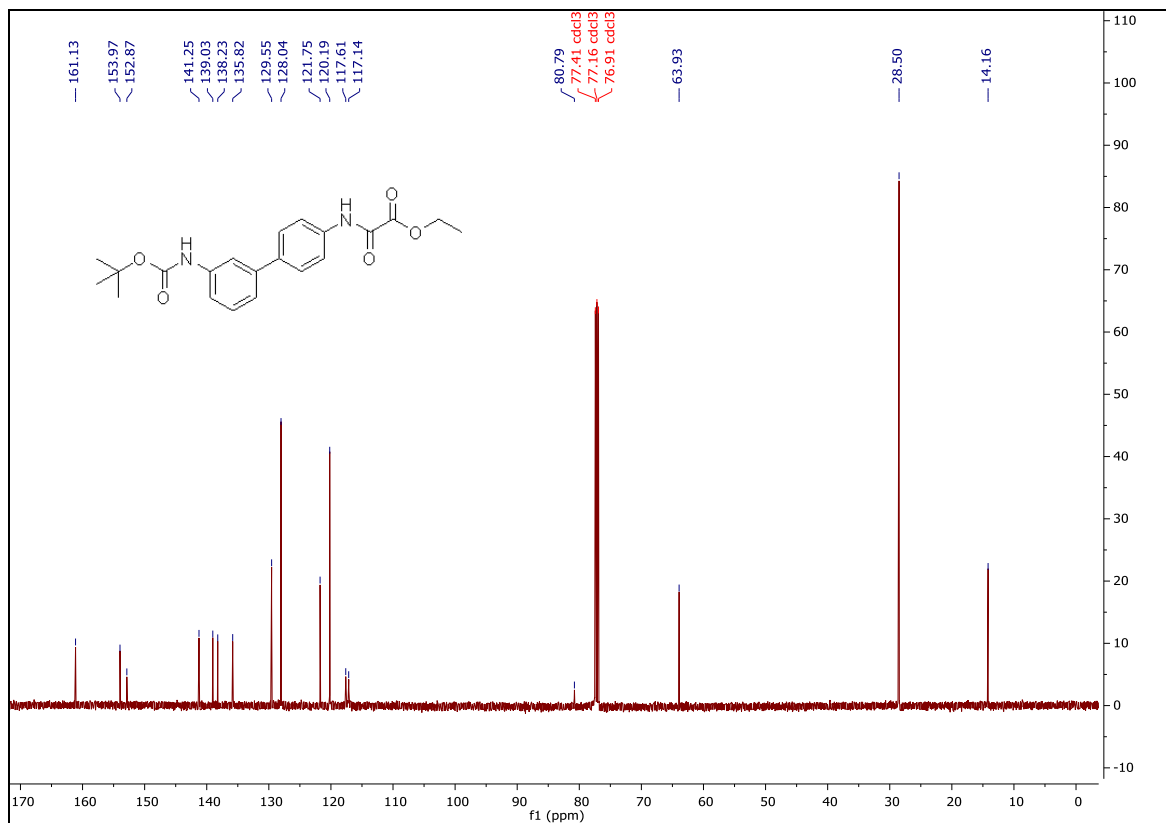
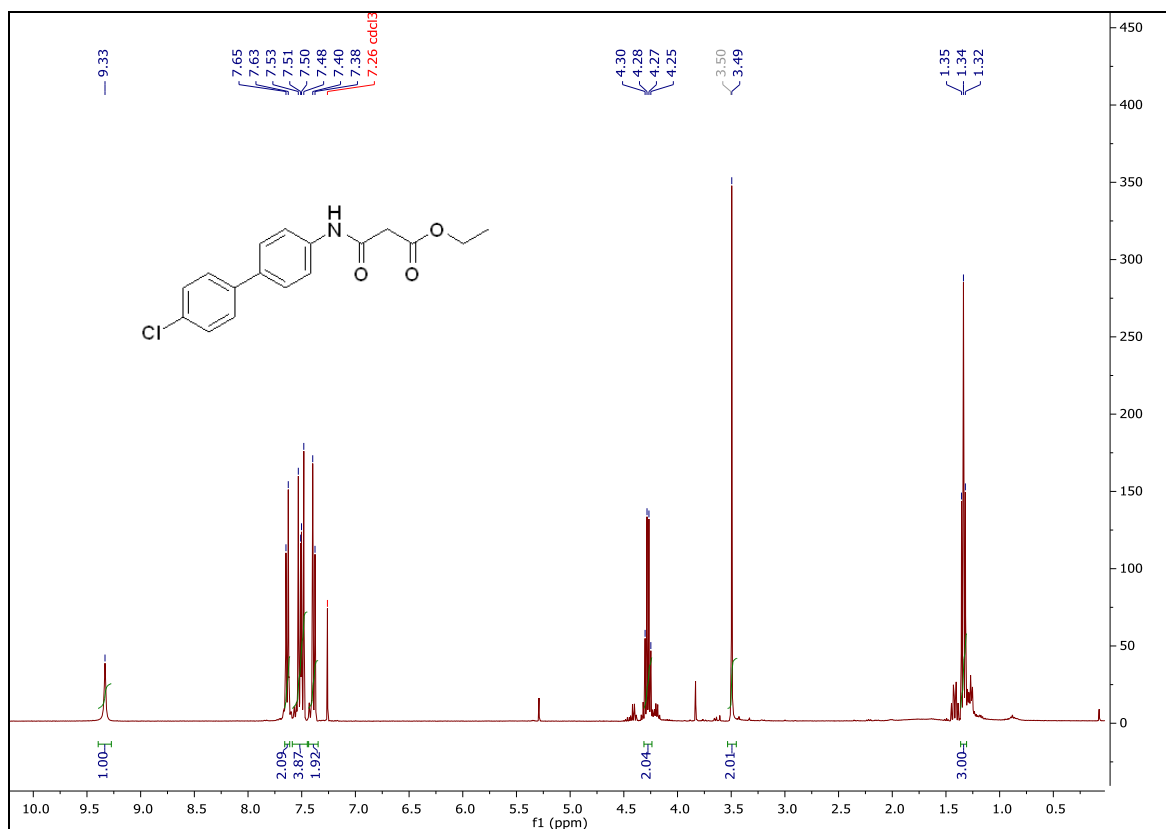
- Permission is granted for your request in both print and electronic formats, and translations.
- If figures and/or tables were requested, they may be adapted or used in part.
- Please print this page for your records and send a copy of it to your publisher/graduate school.
- Appropriate credit for the requested material should be given as follows: "Reprinted (adapted) with permission from (COMPLETE REFERENCE CITATION). Copyright (YEAR) American Chemical Society." Insert appropriate information in place of the capitalized words.
- One-time permission is granted only for the use specified in your request. No additional uses are granted (such as derivative works or other editions). For any other uses, please submit a new request.

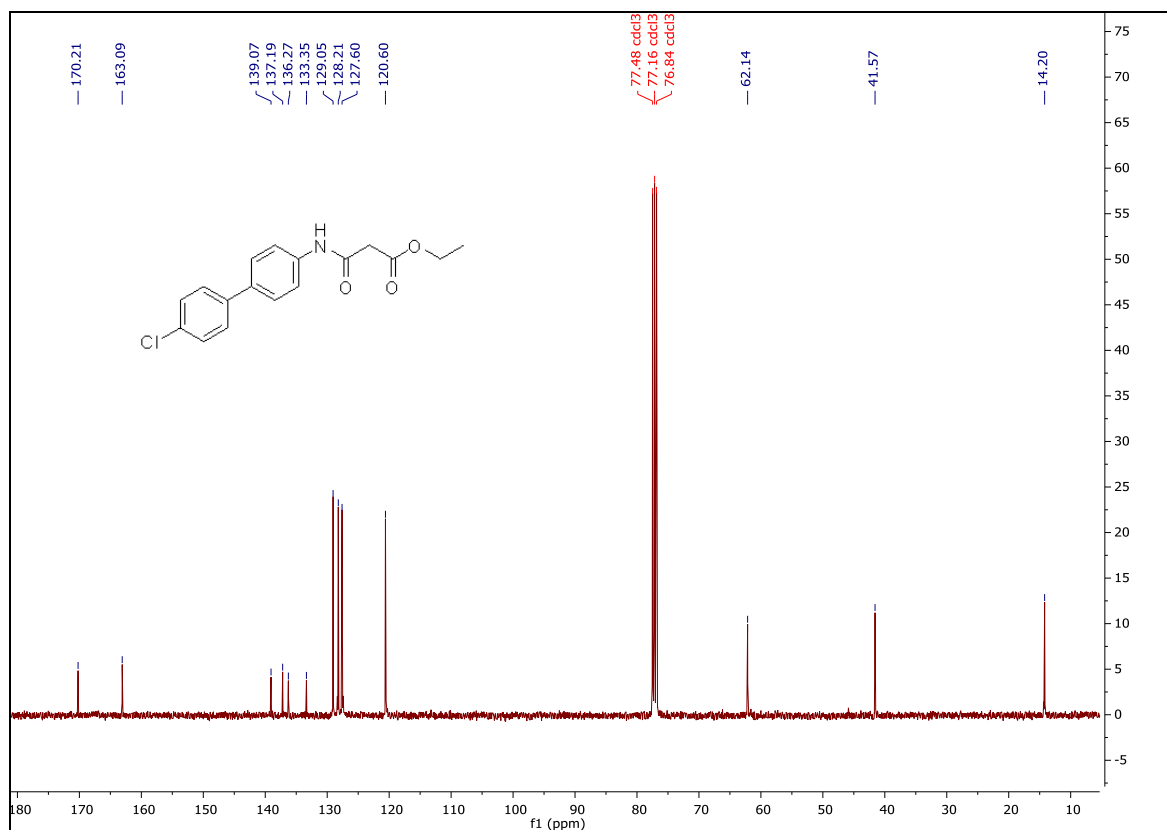
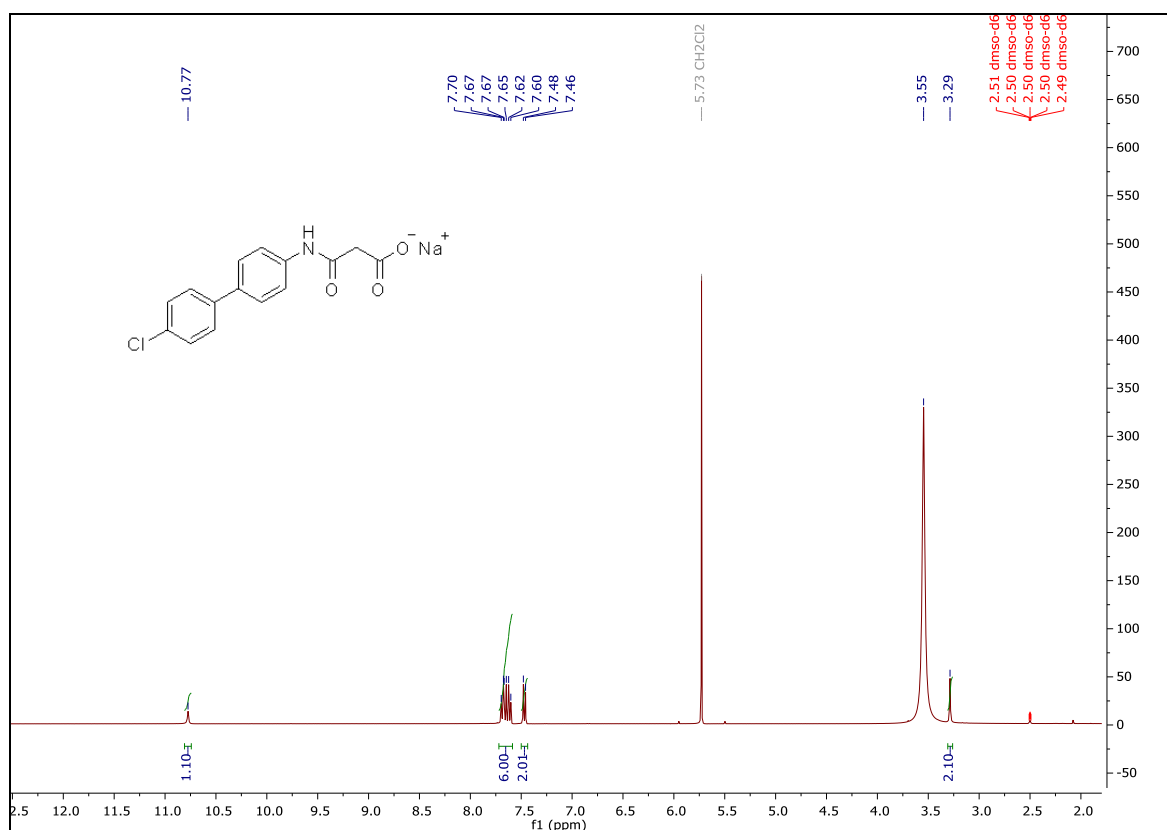
6.6. NMR Spectra

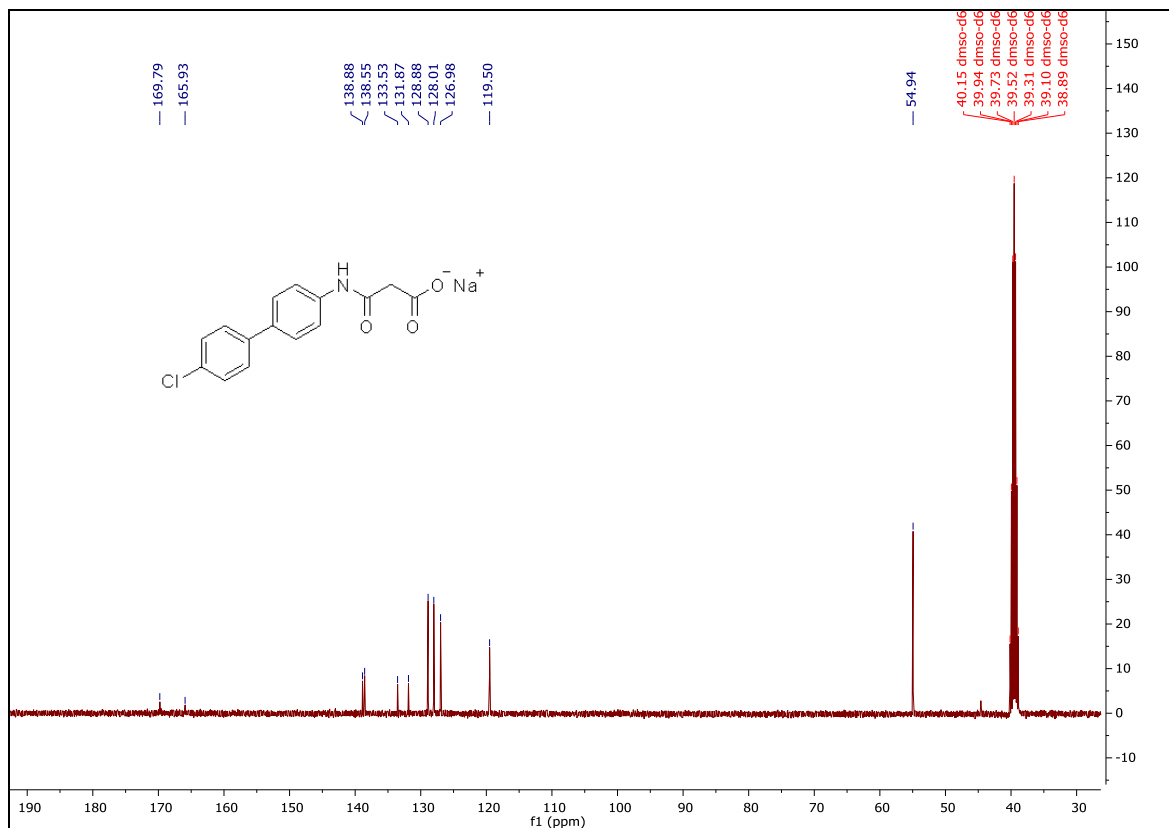
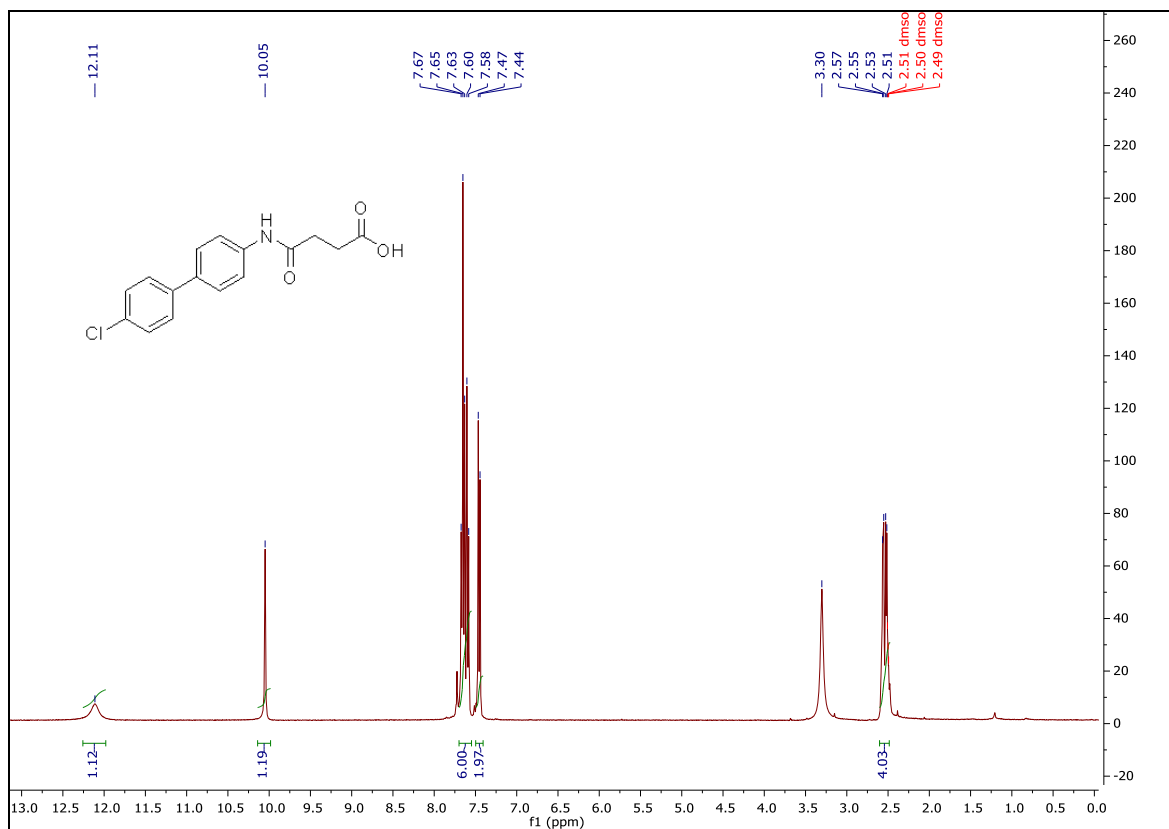
^1H spectrum of **MDMG-151**

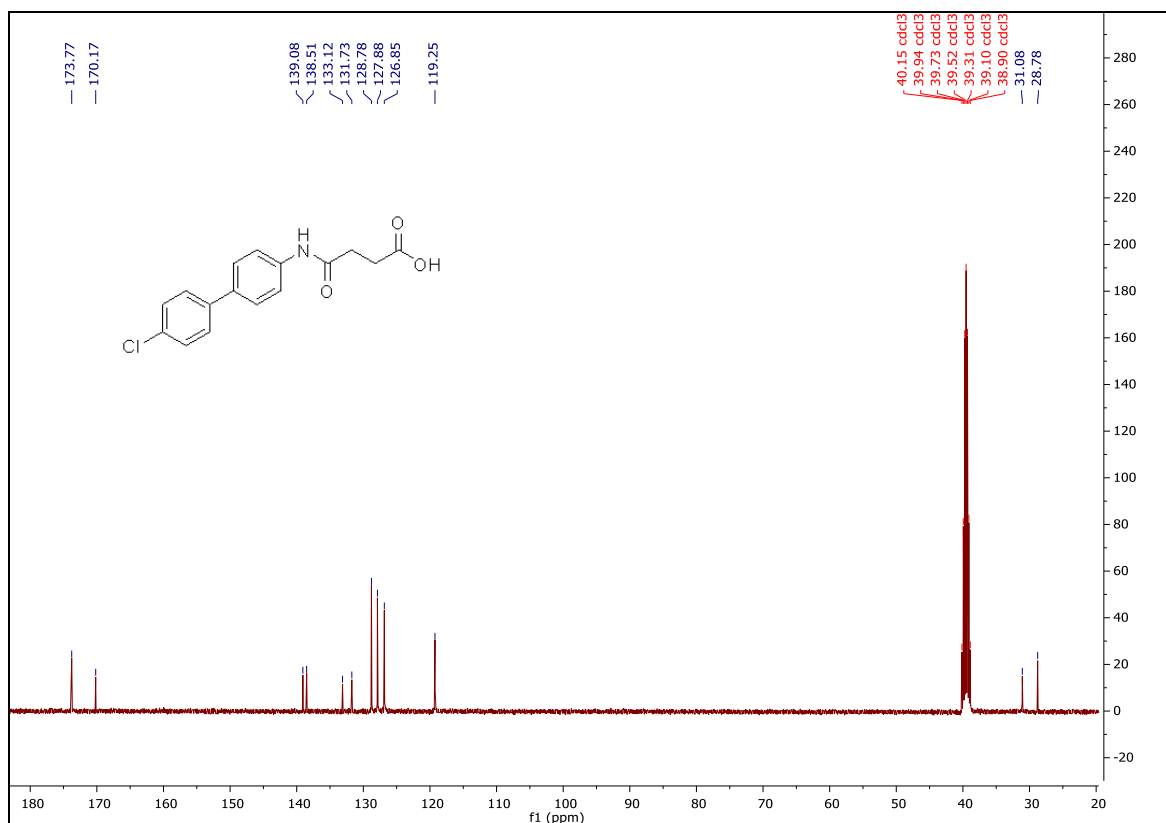
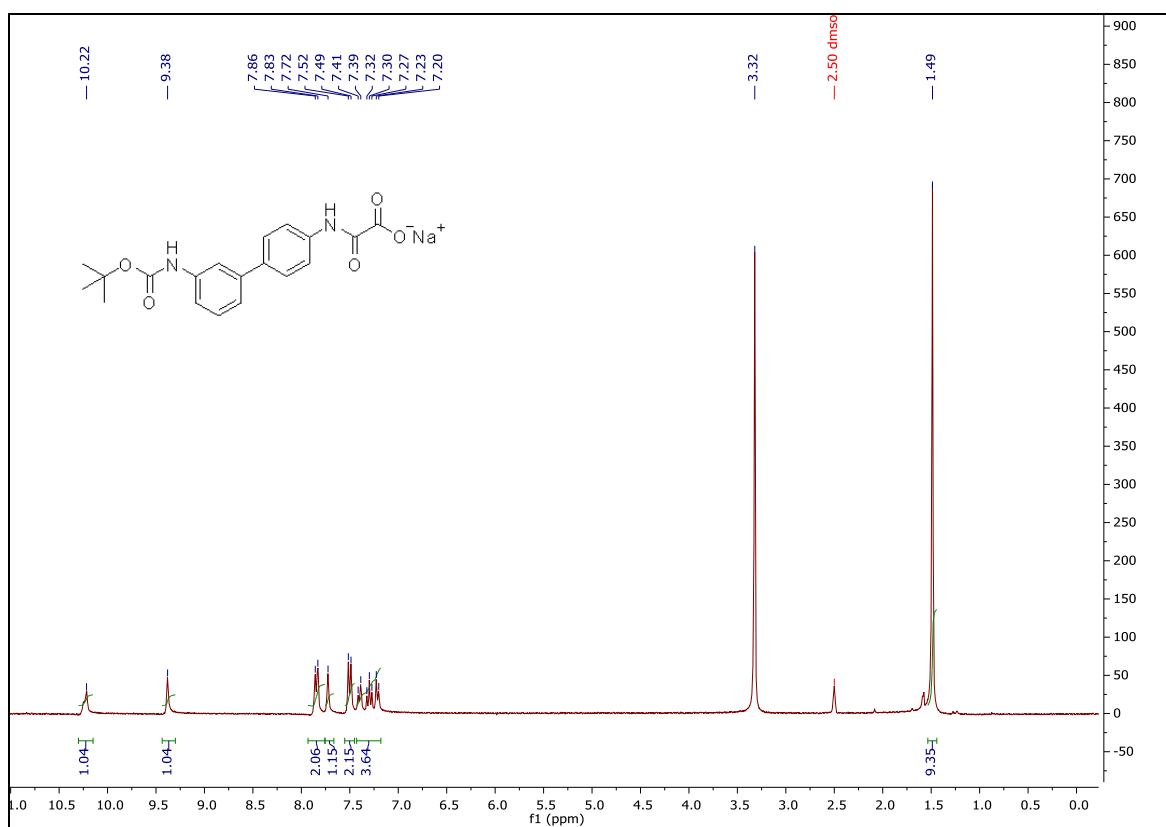


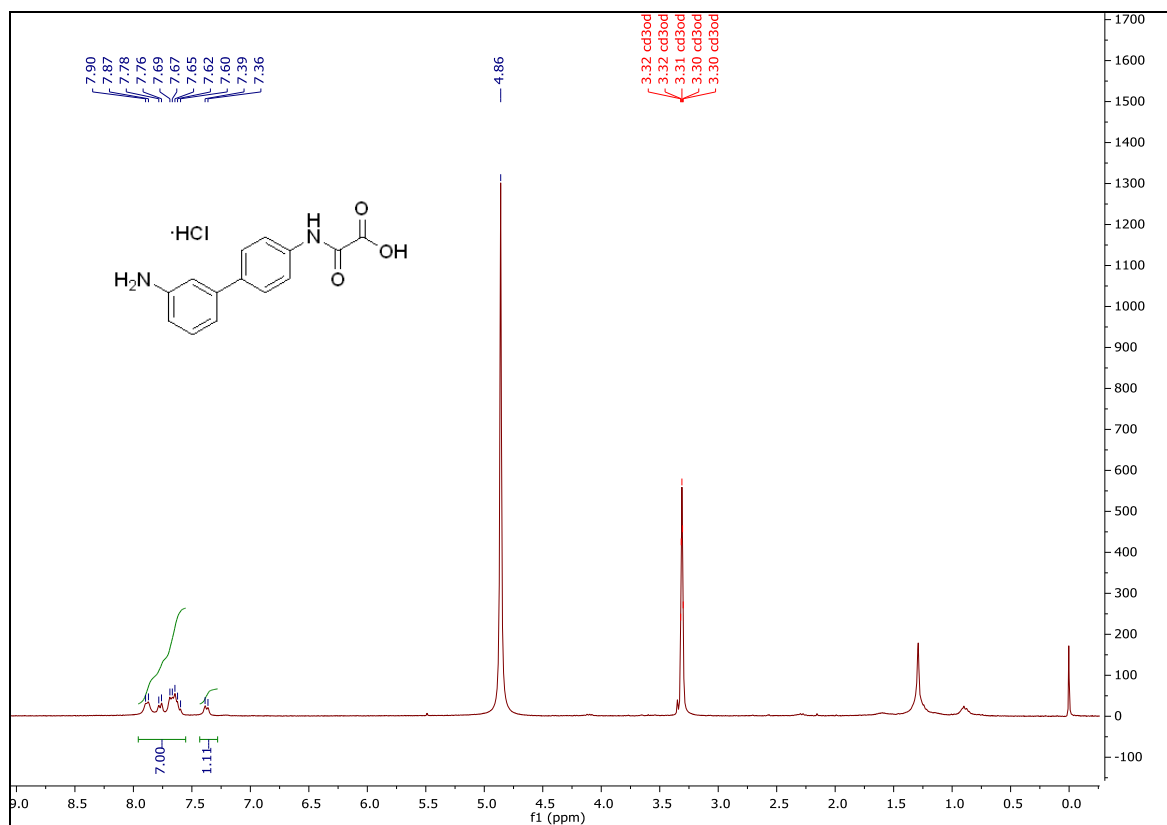
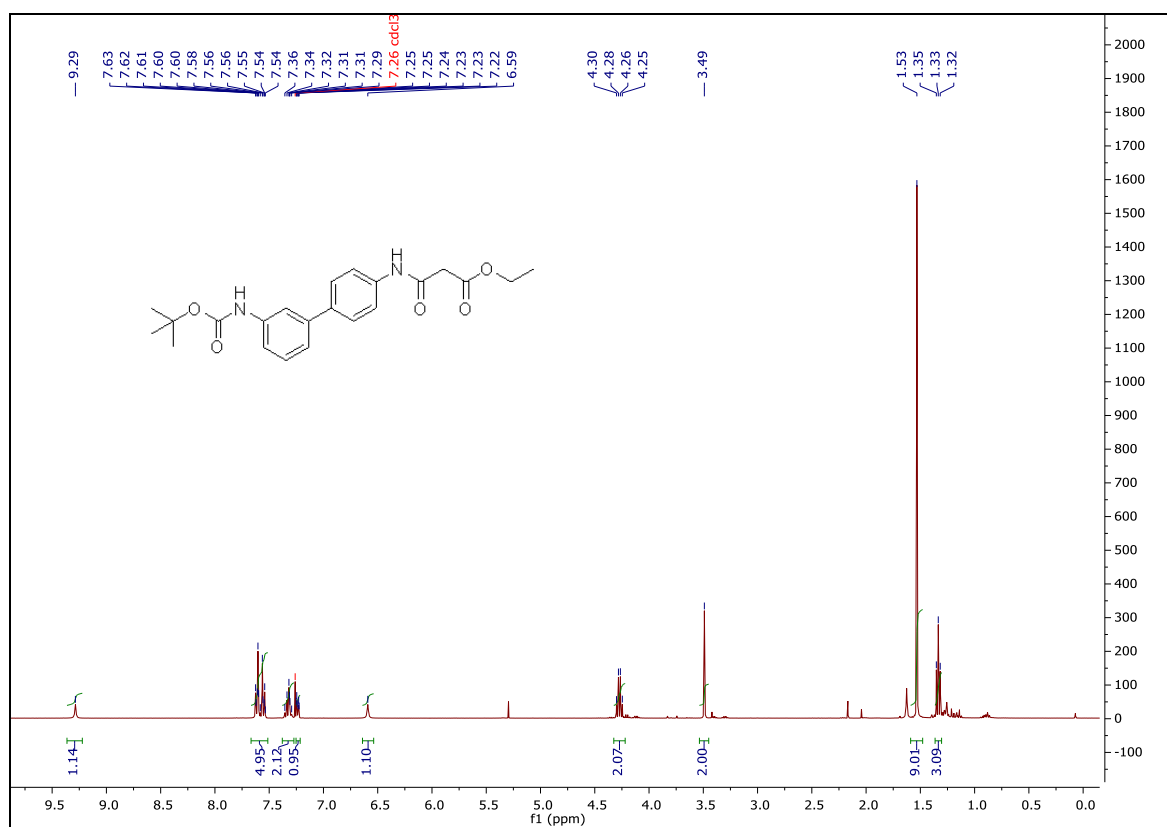
¹H spectrum of MDMG-155¹H spectrum of MDMG-159

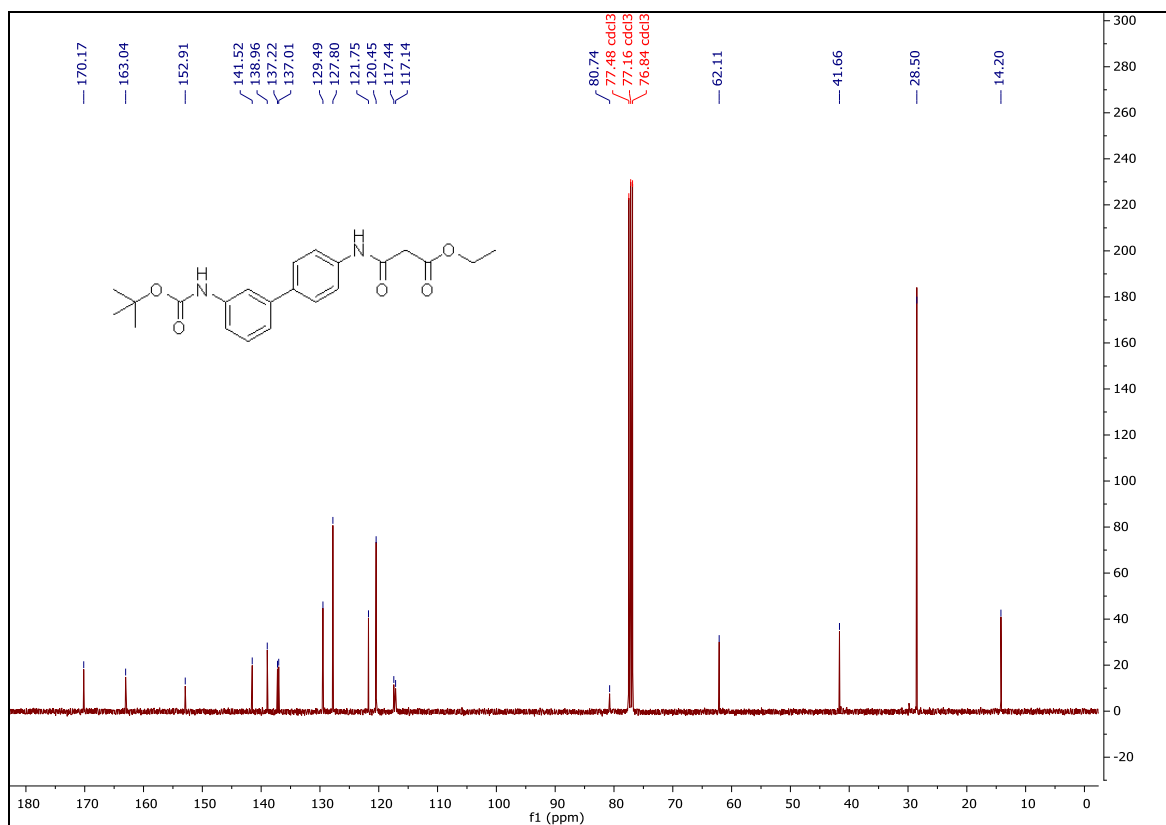
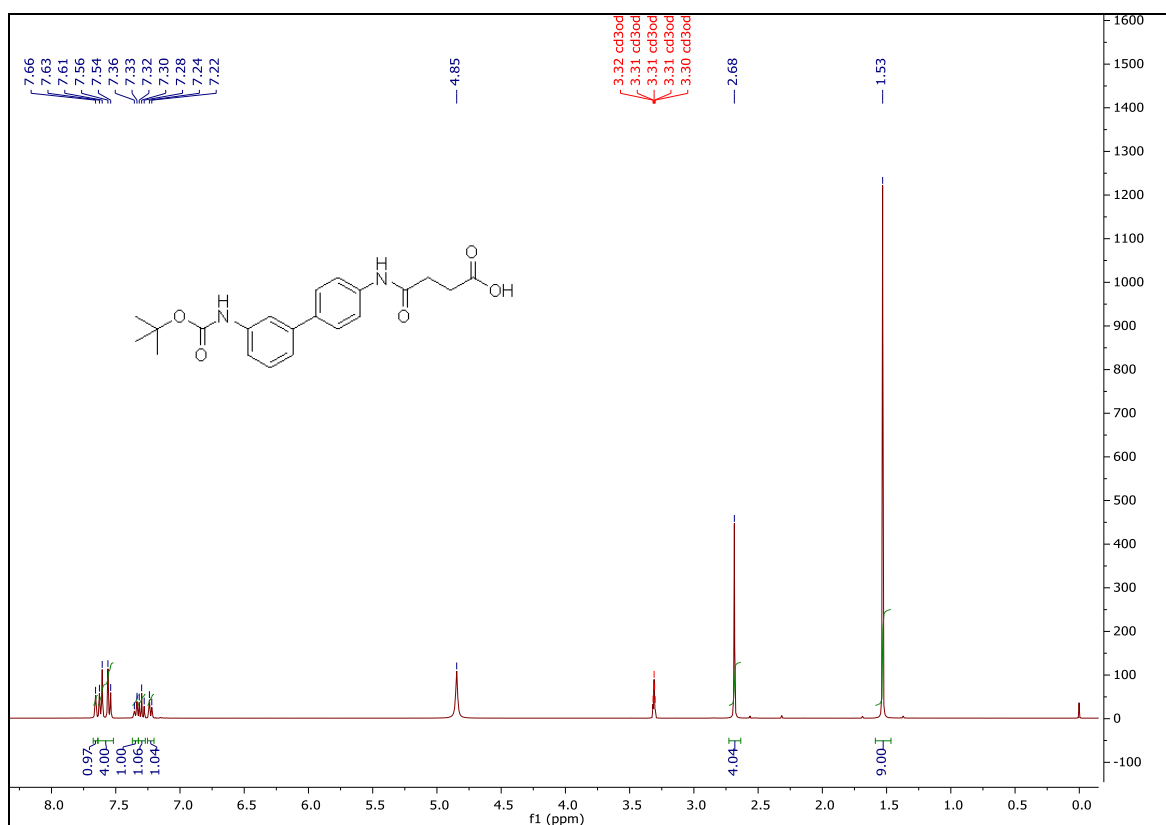
¹³C spectrum of **MDMG-159**¹H spectrum of **MDMG-163**

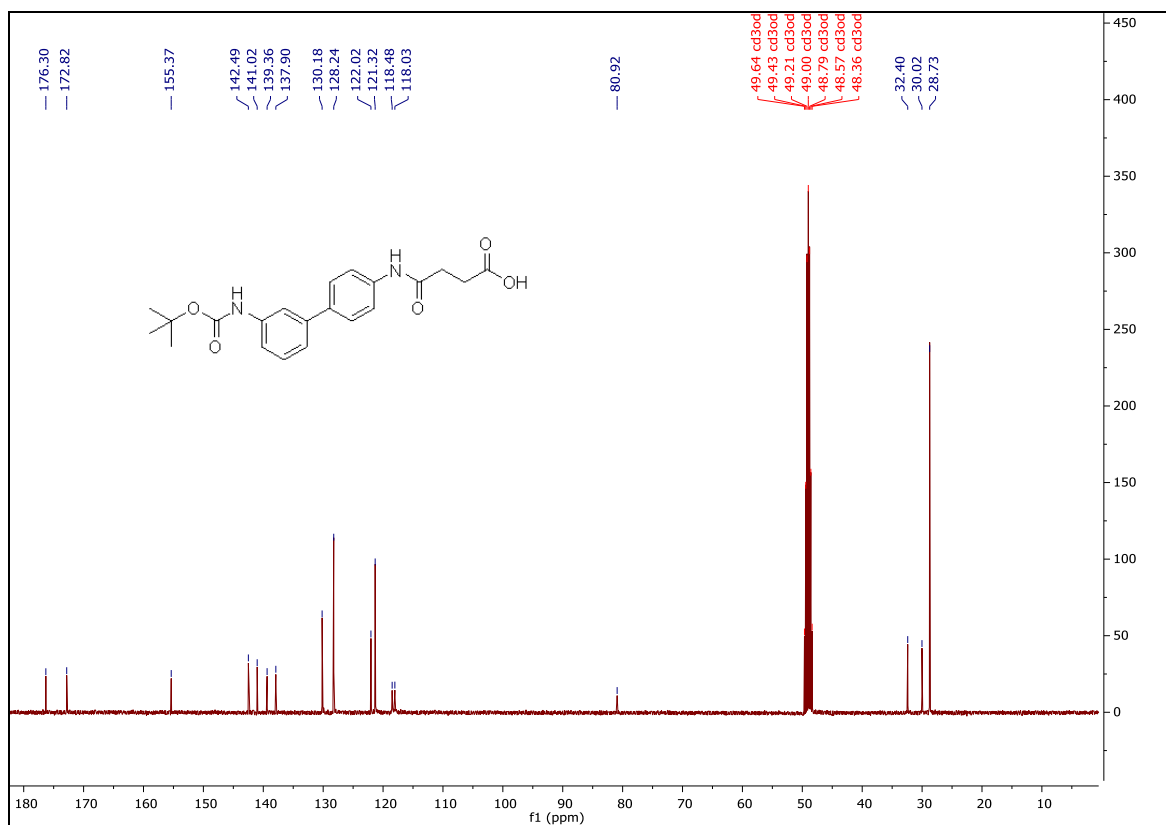
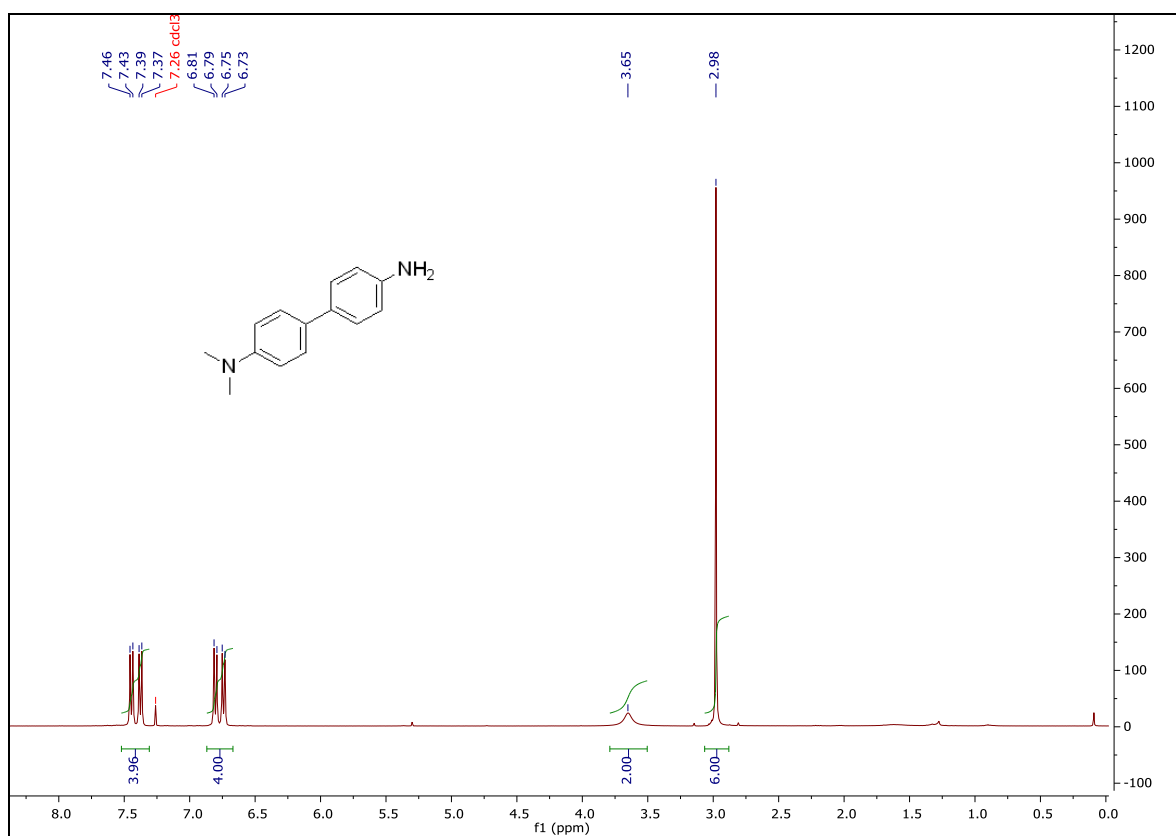
¹³C spectrum of **MDMG-163**¹H spectrum of **MDMG-167**

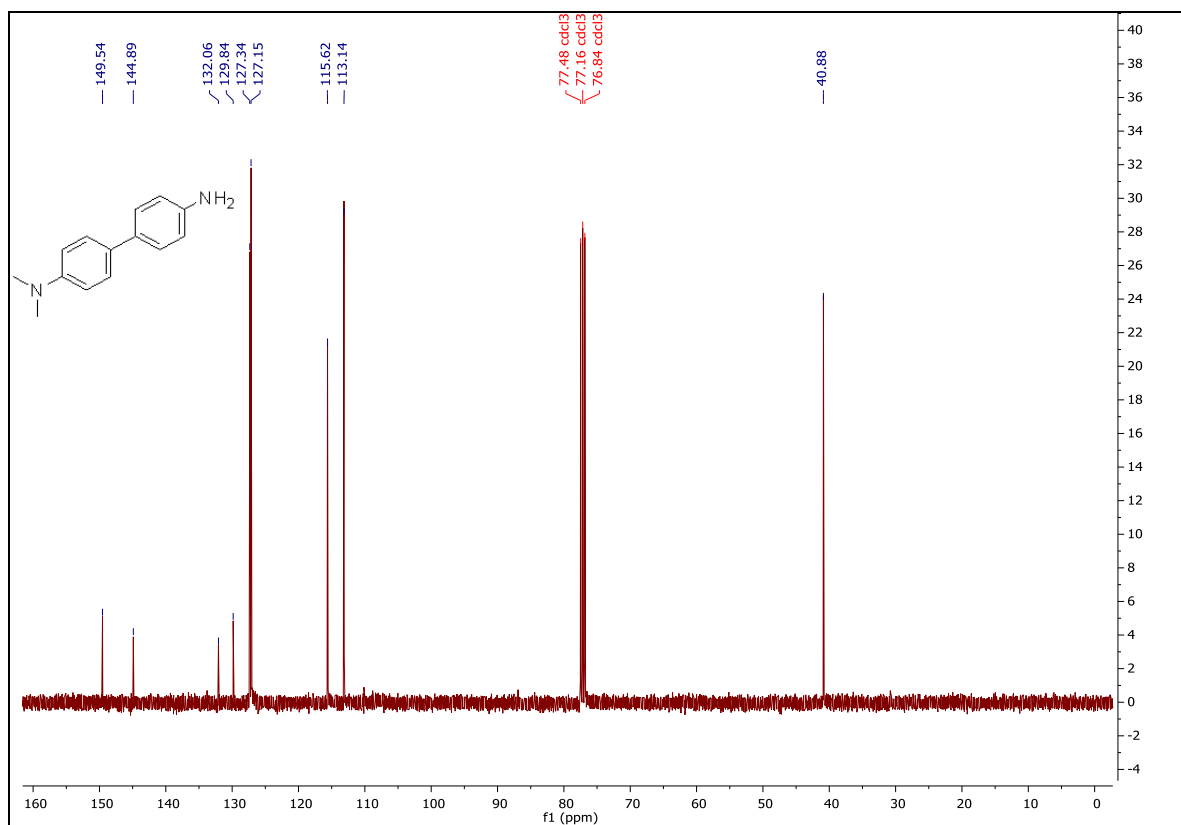
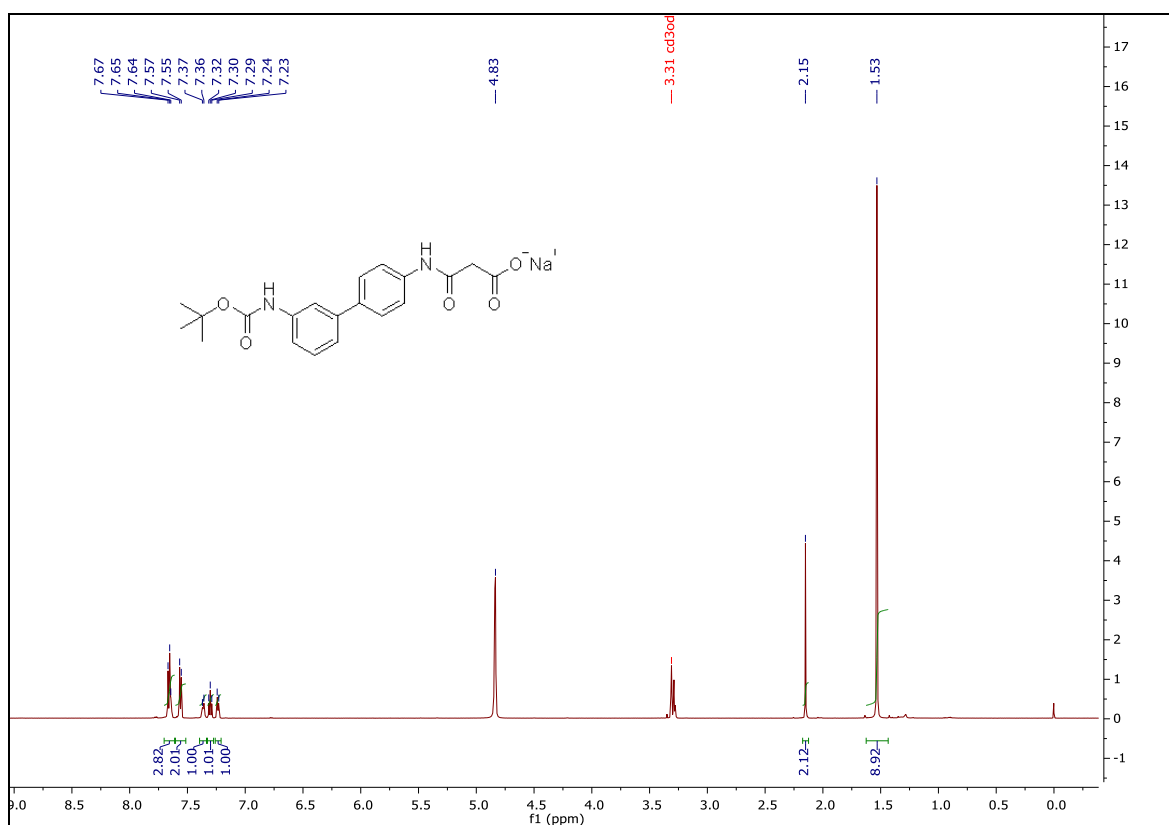
¹³C spectrum of **MDMG-167**¹H spectrum of **MDMG-195**

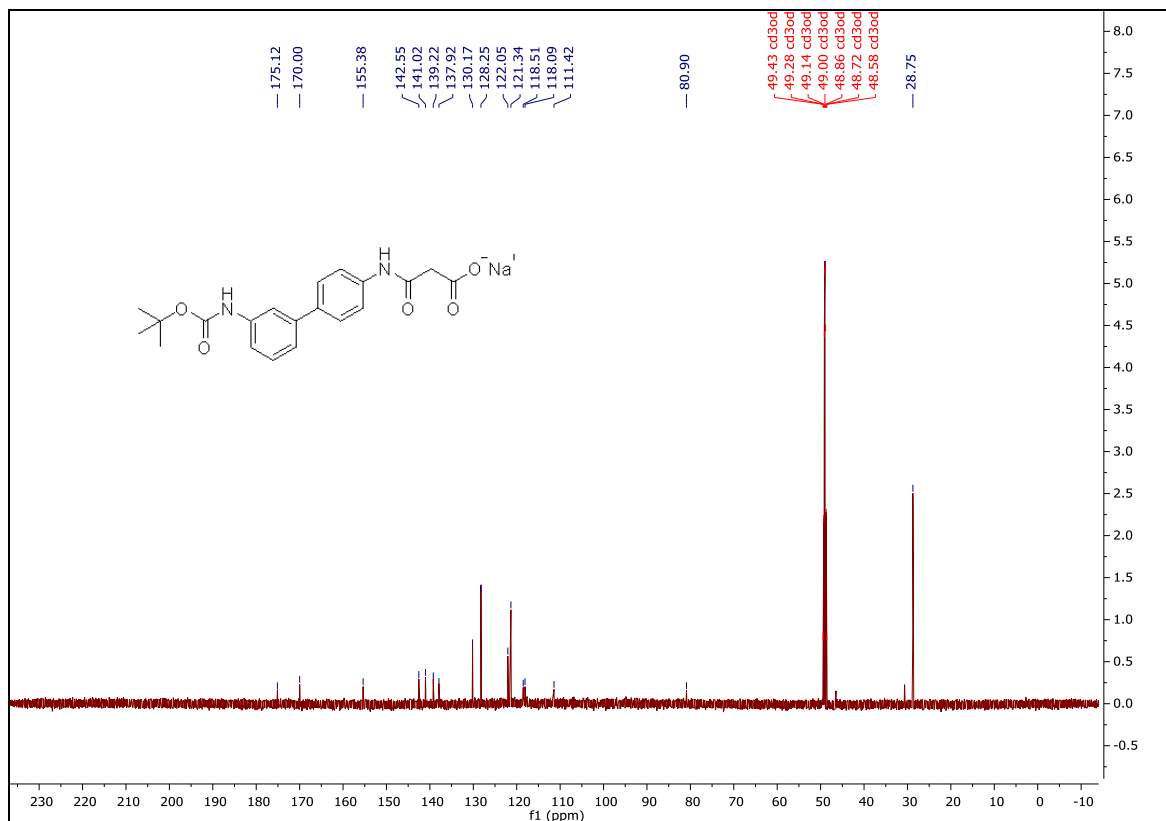
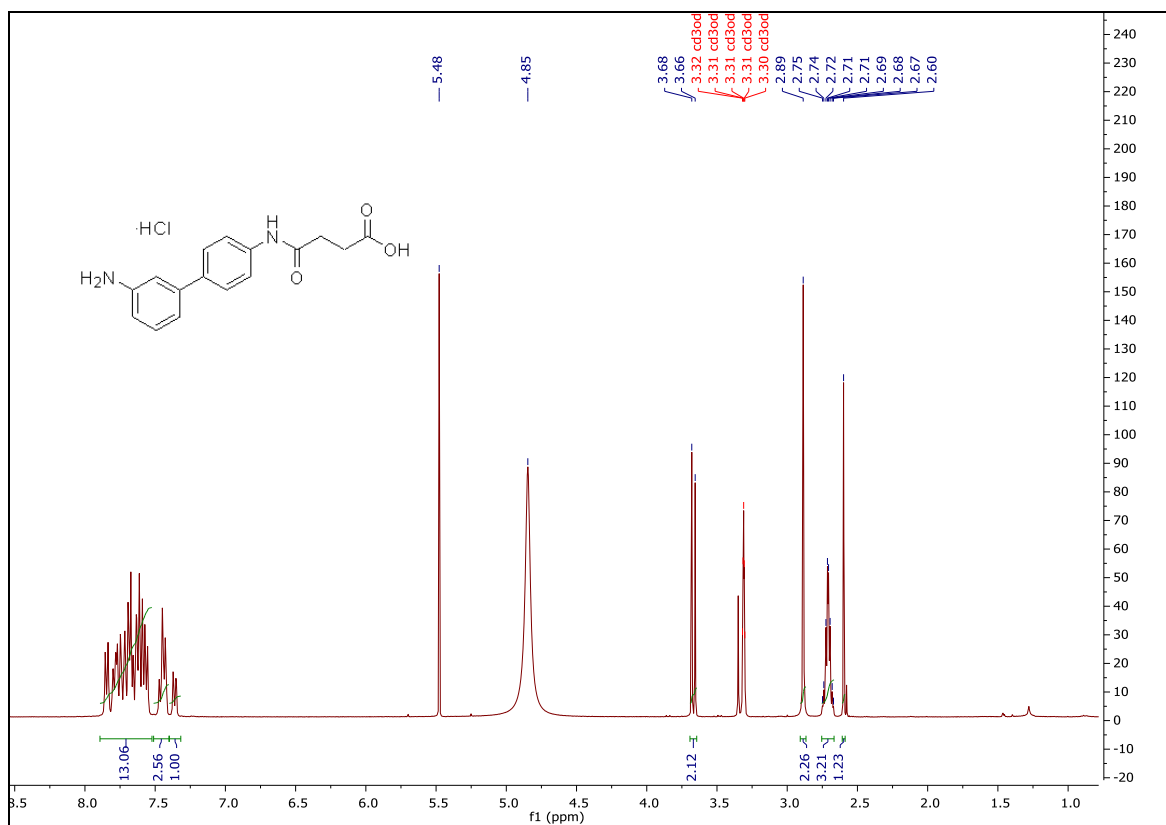
¹³C spectrum of **MDMG-195**¹H spectrum of **MDMG-171**

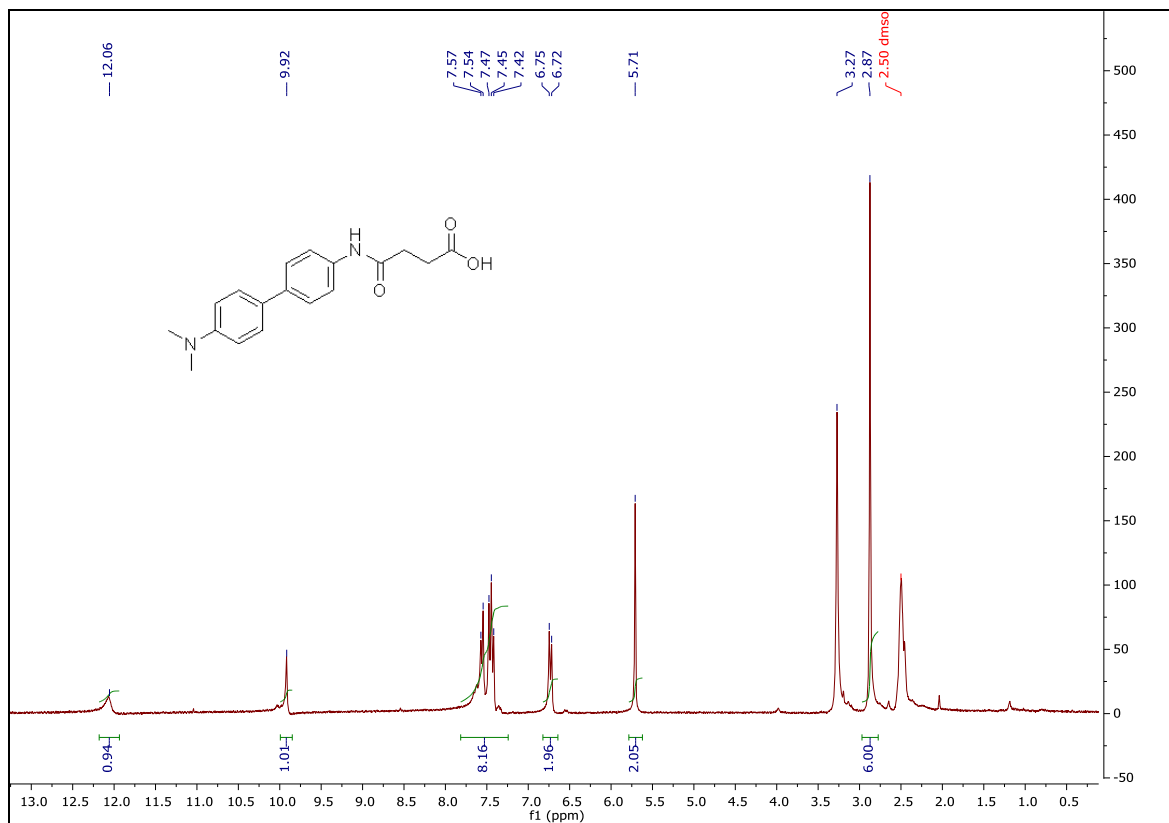
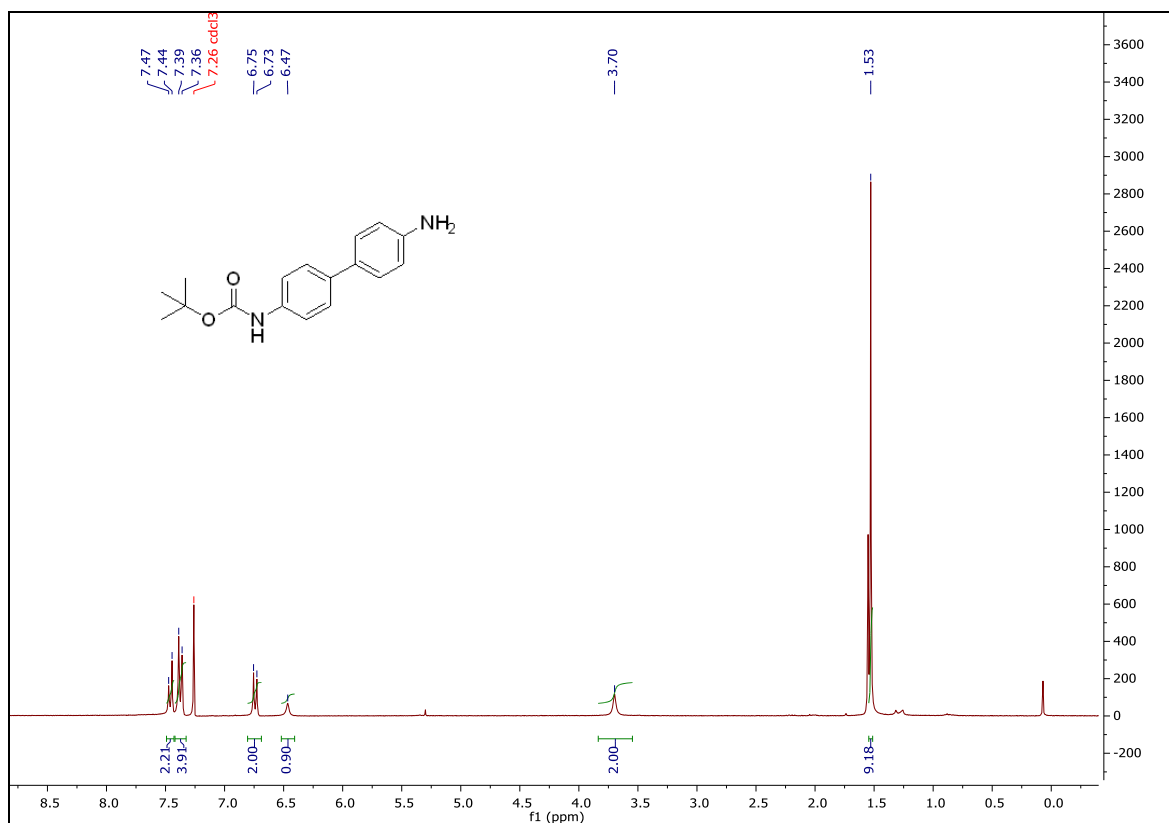
¹H spectrum of **MDMG-191**¹H spectrum of **MDMG-223**

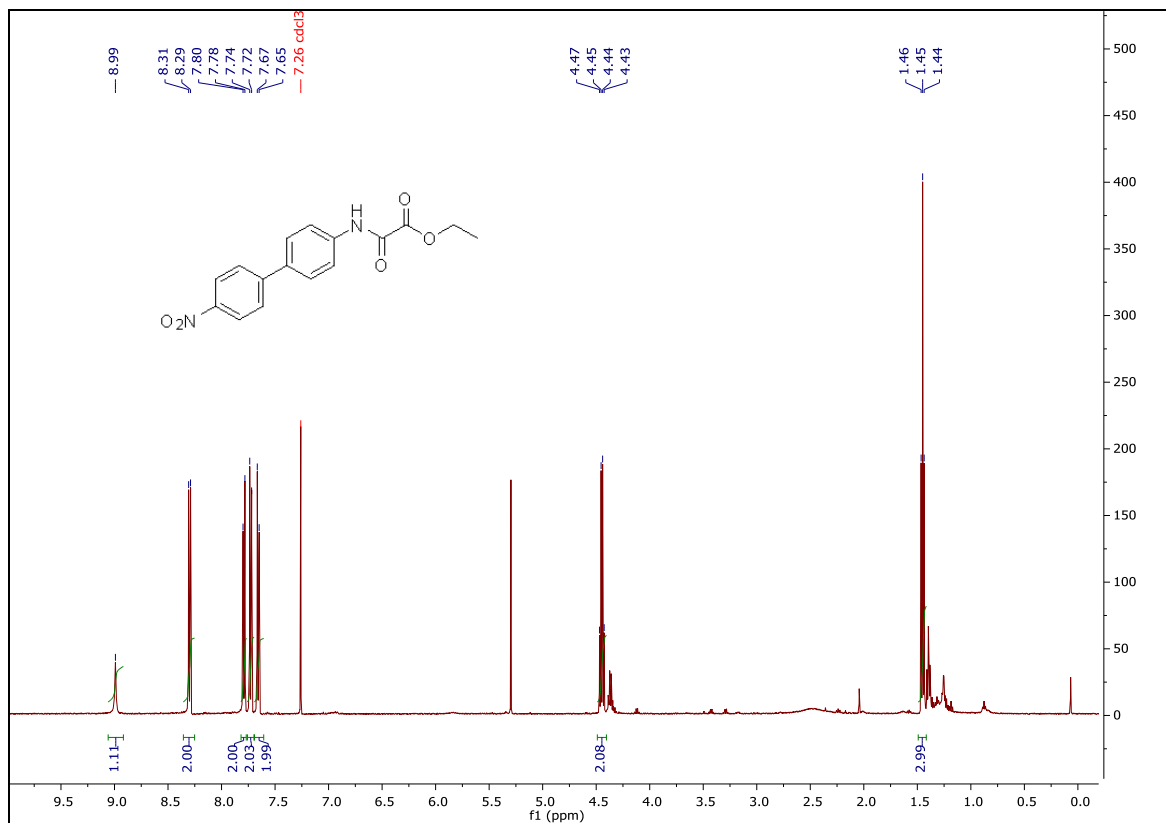
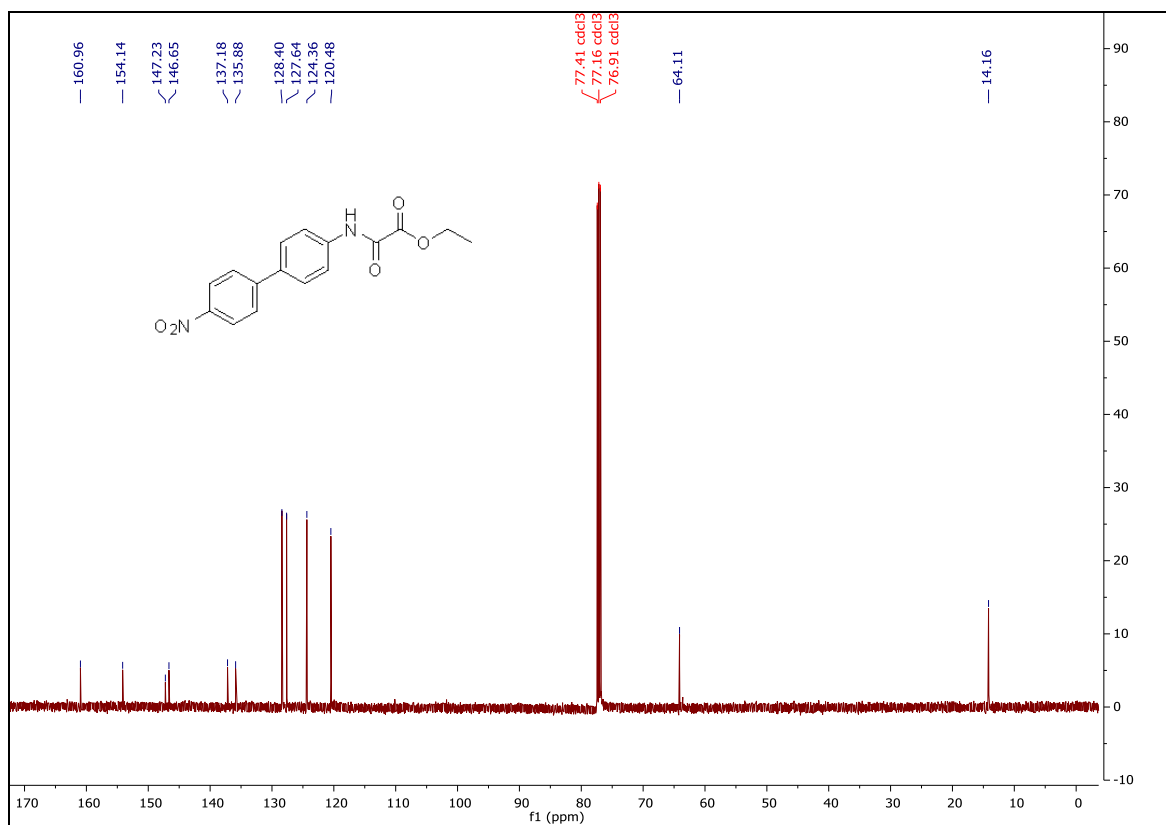
¹³C spectrum of **MDMG-223**¹H spectrum of **MDMG-231**

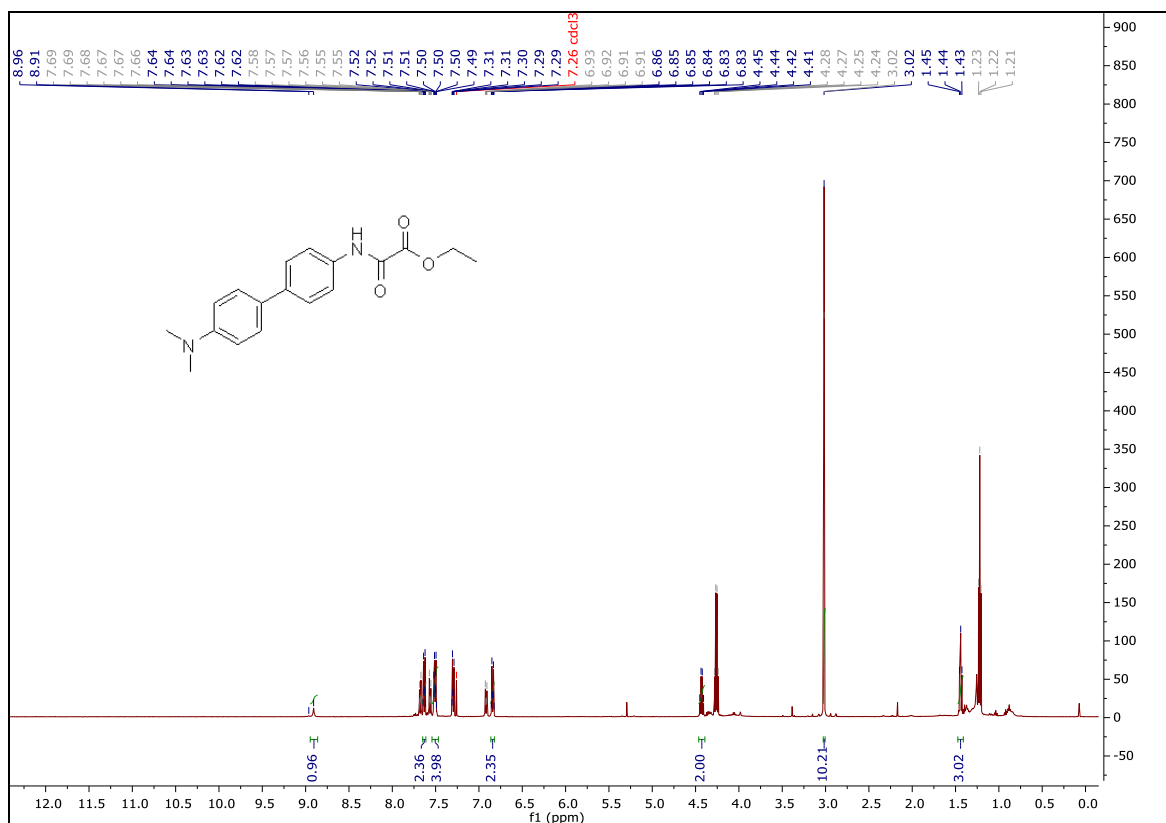
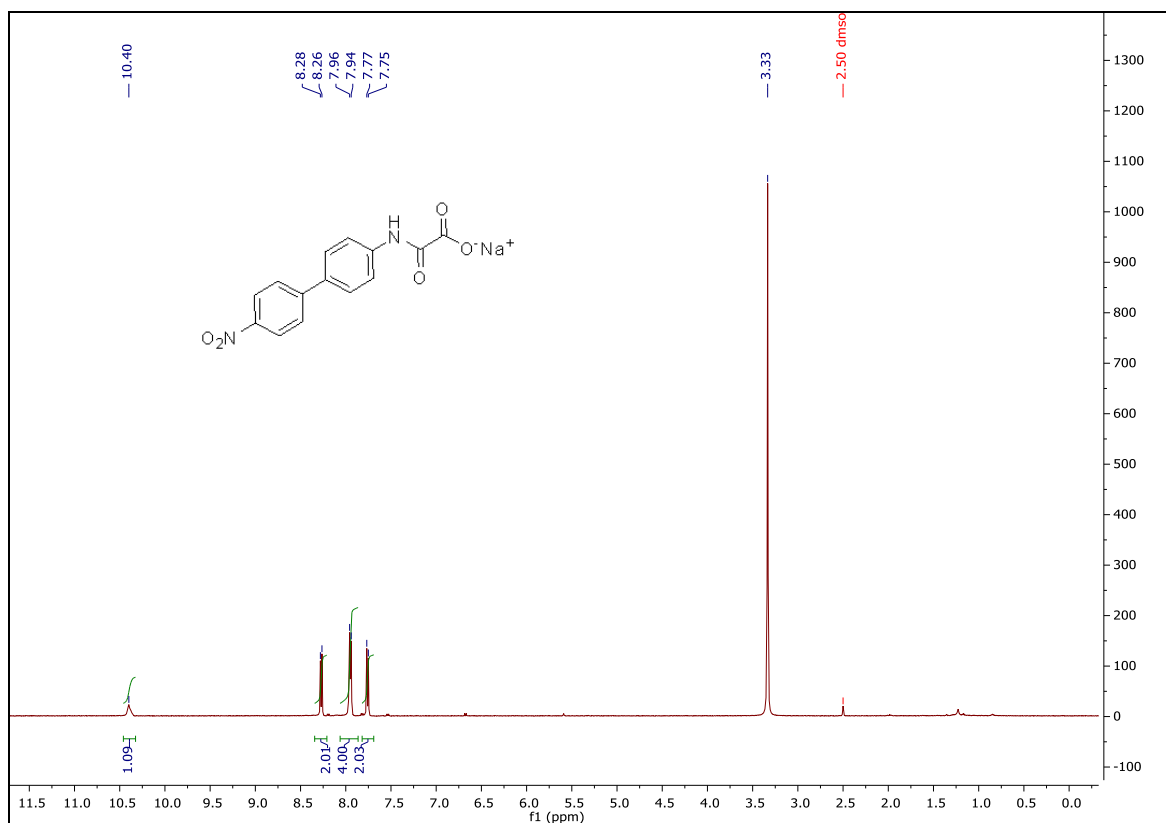
¹³C spectrum of **MDMG-231**¹H spectrum of **MDMG-235**

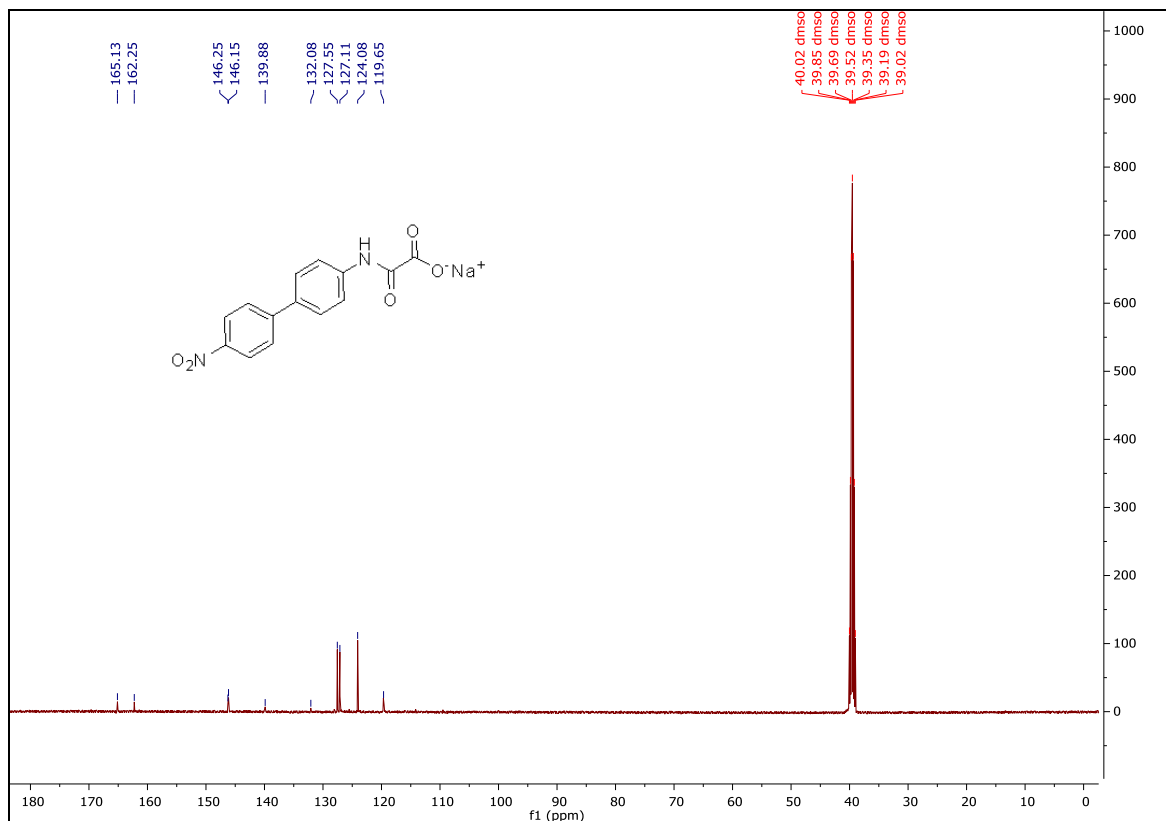
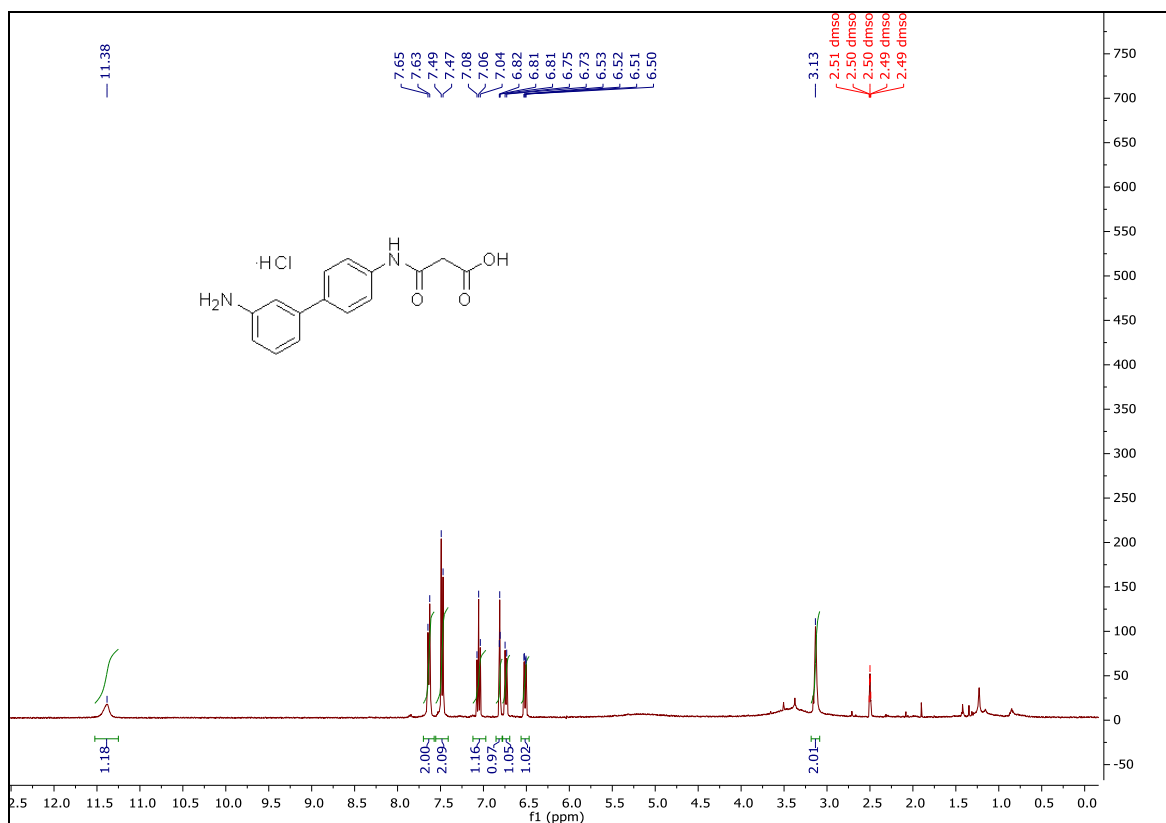
¹³C spectrum of MDMG-235¹H spectrum of MDMG-239

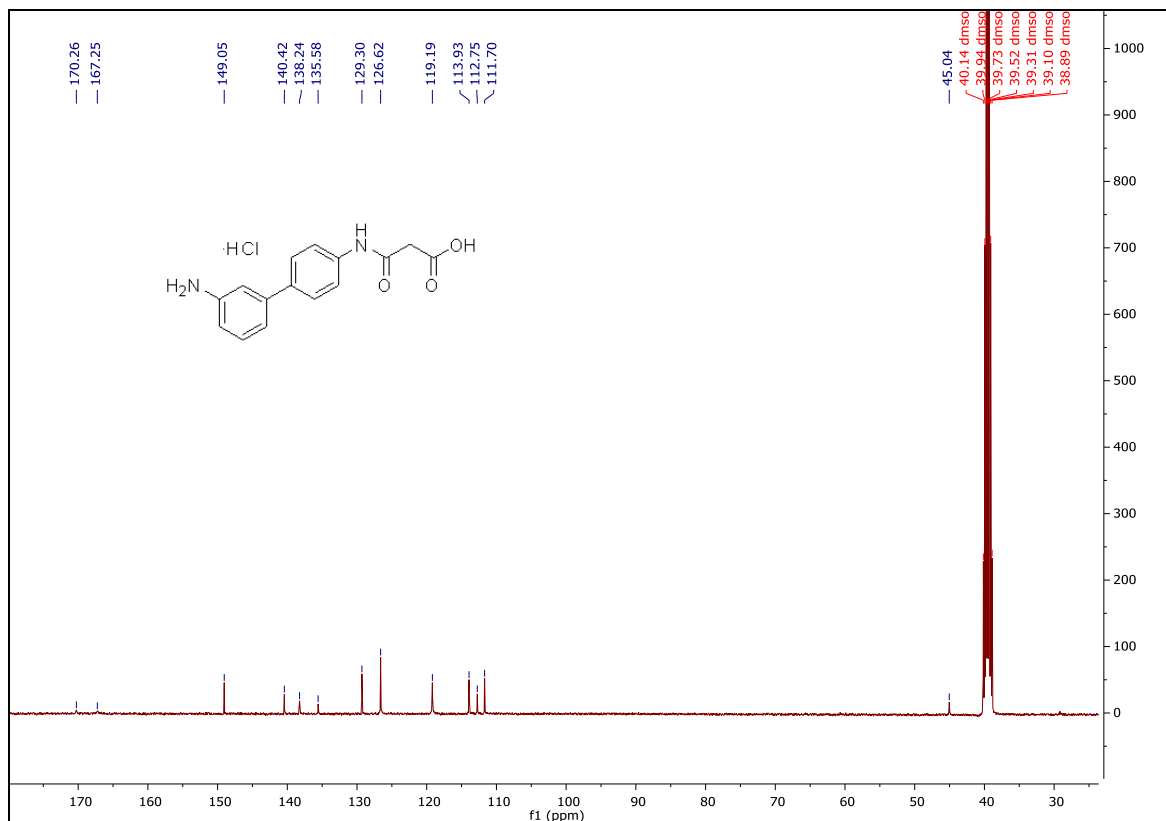
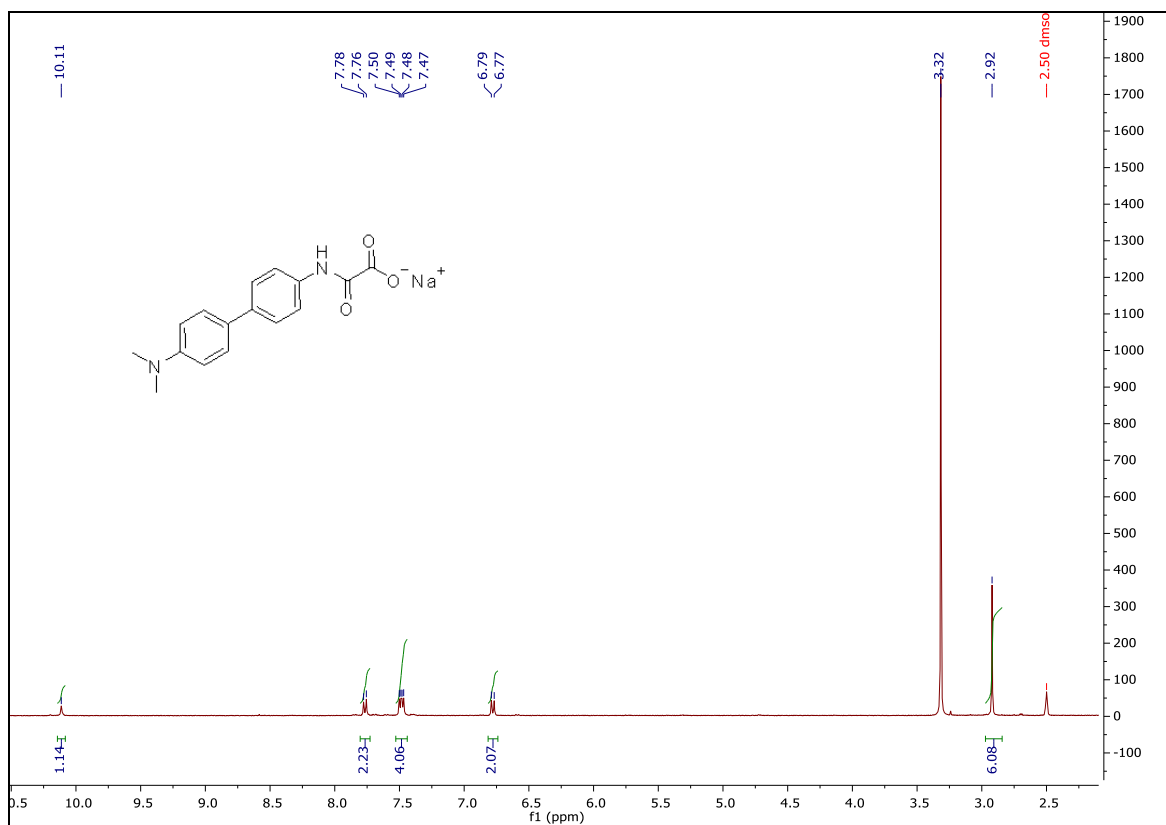
¹³C spectrum of **MDMG-239**¹H spectrum of **MDMG-245**

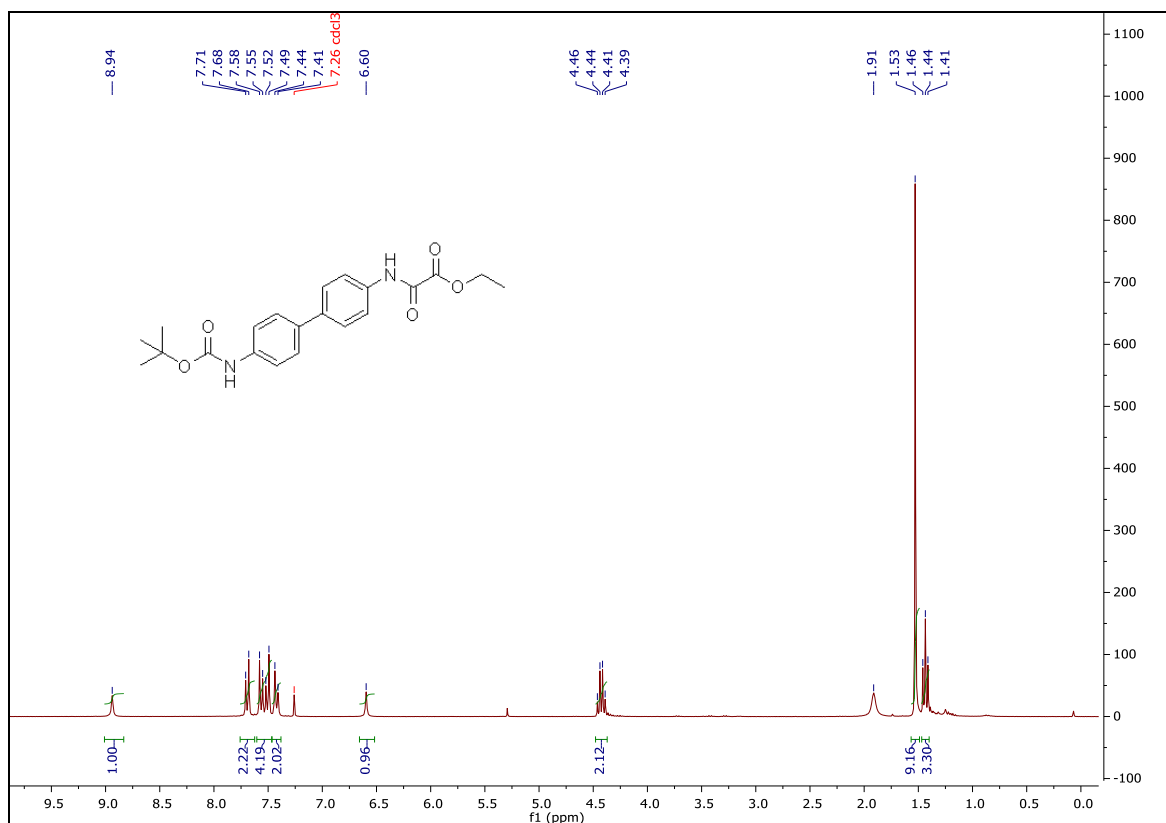
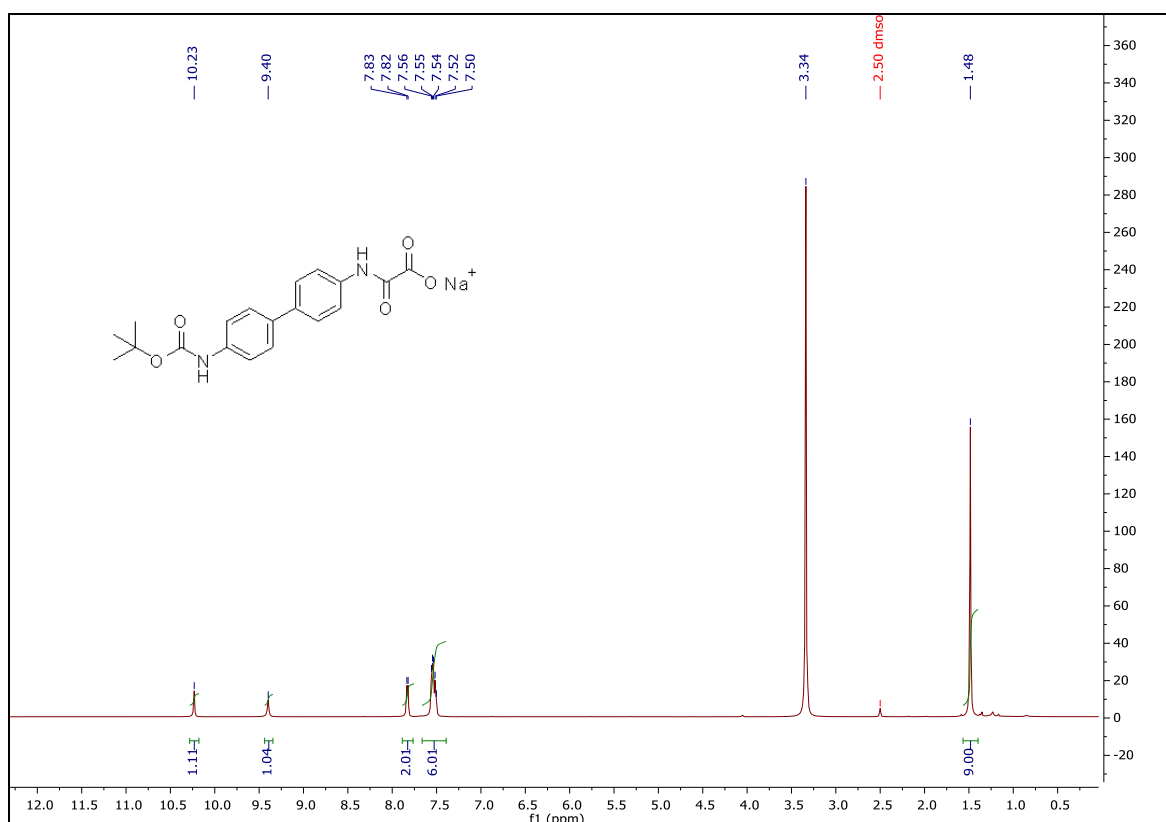
¹H spectrum of **MDMG-257**¹H spectrum of **MDMG-261**

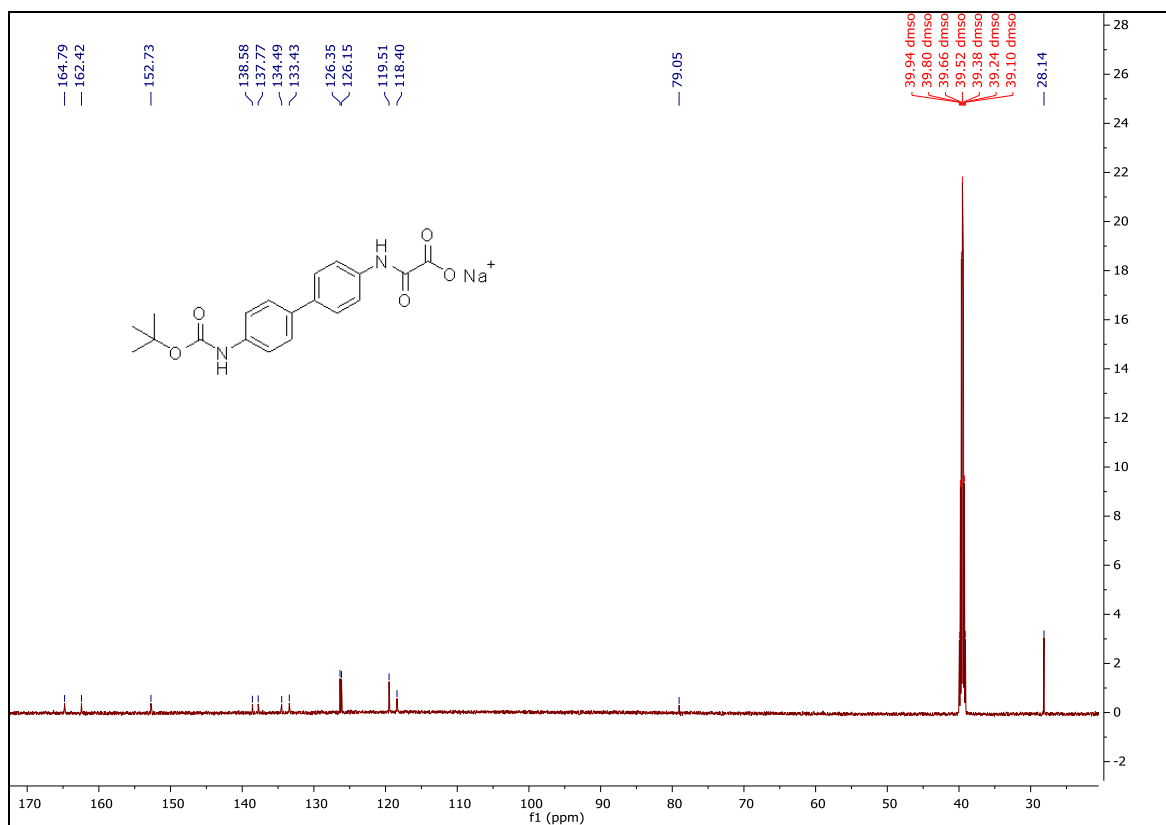
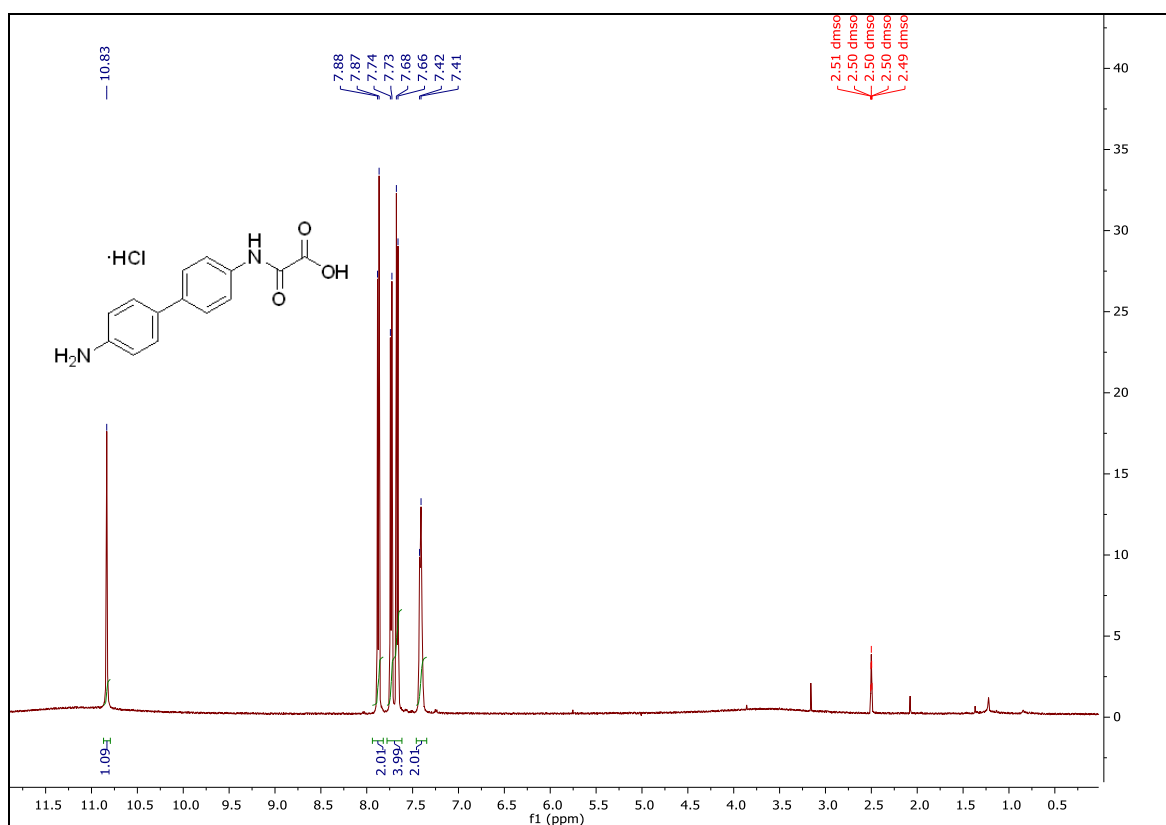
¹H spectrum of **MDMG-265**¹³C spectrum of **MDMG-265**

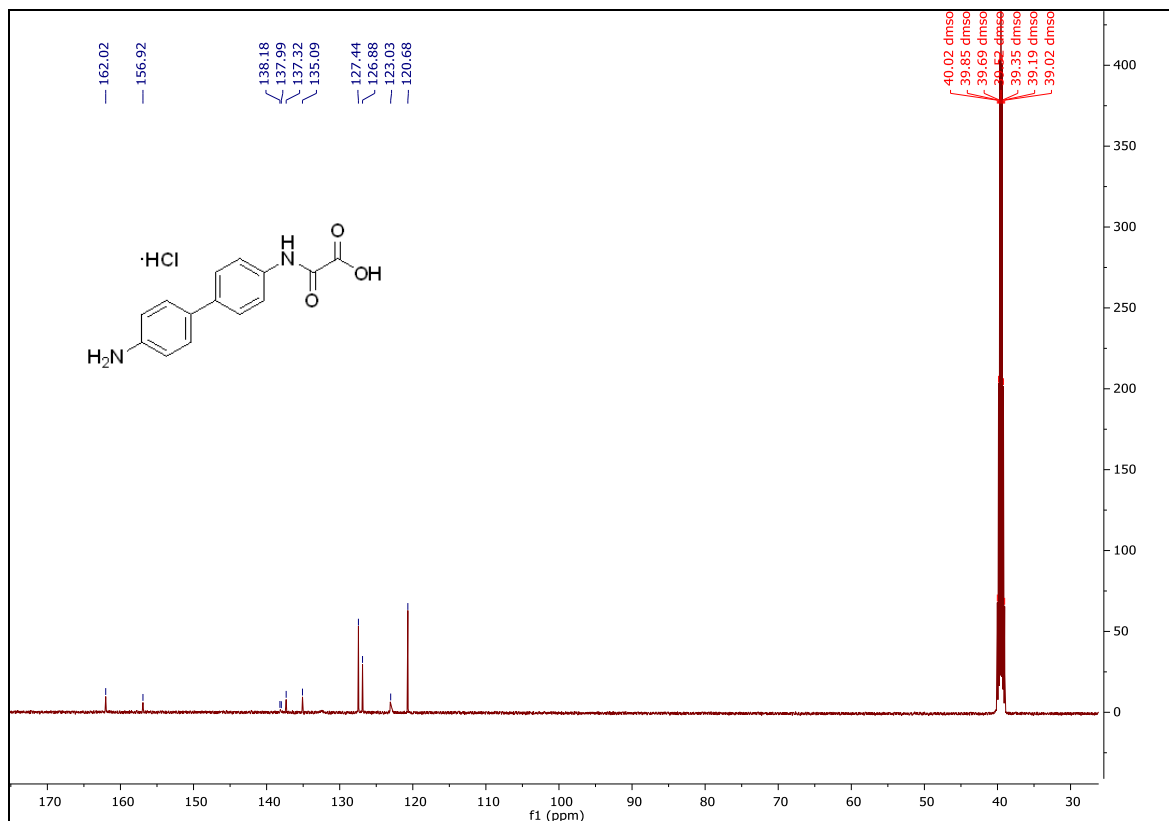
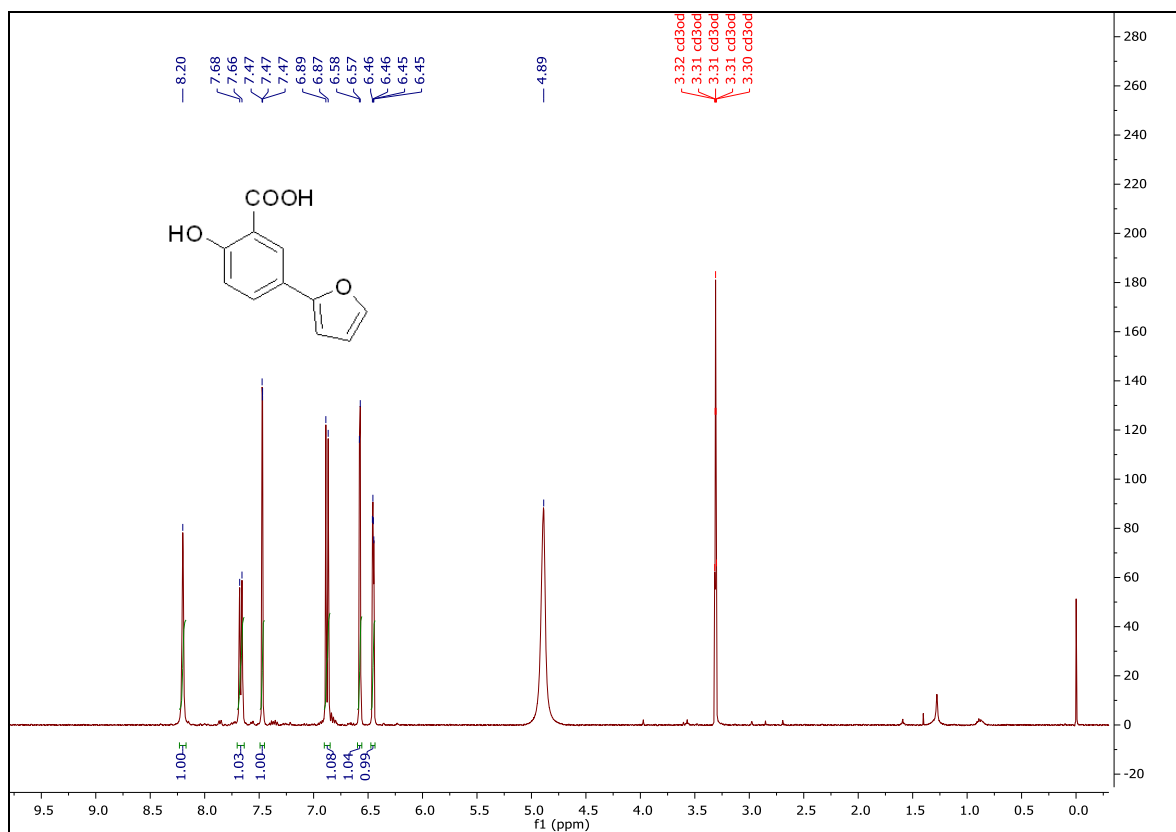
¹H spectrum of **MDMG-269**¹H spectrum of **MDMG-277**

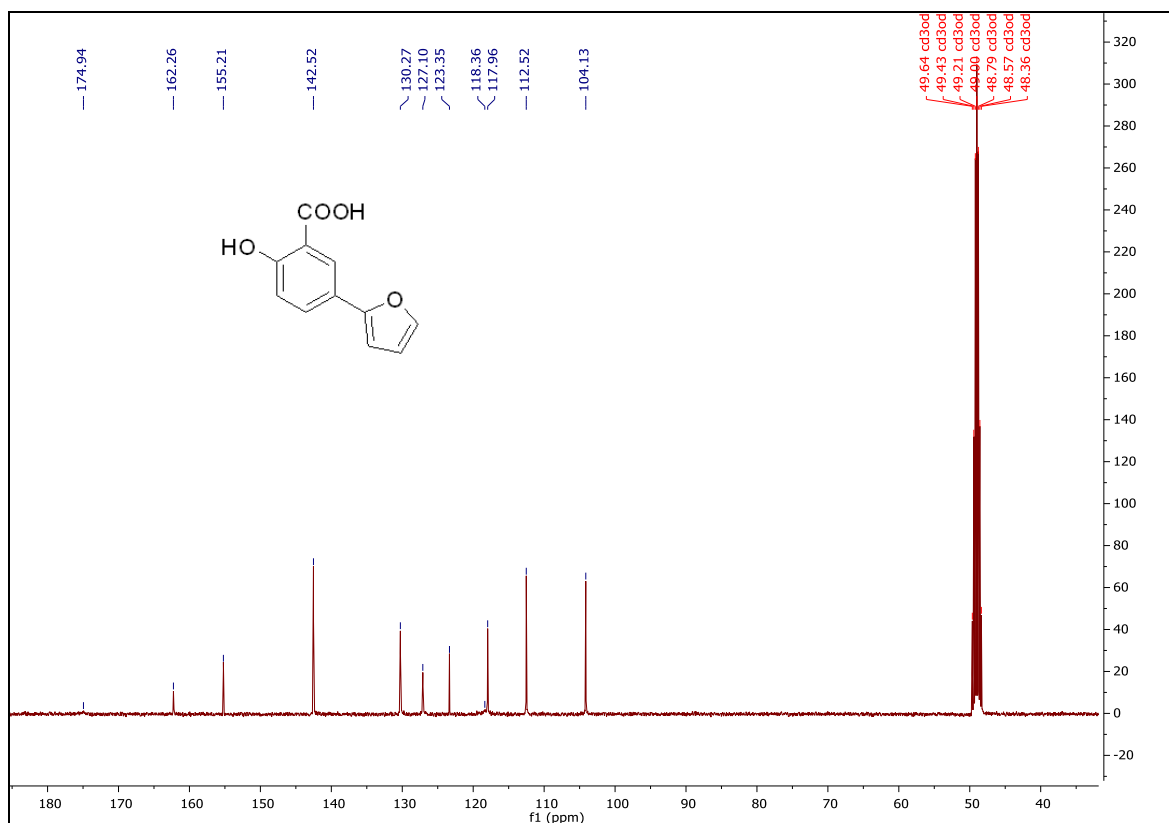
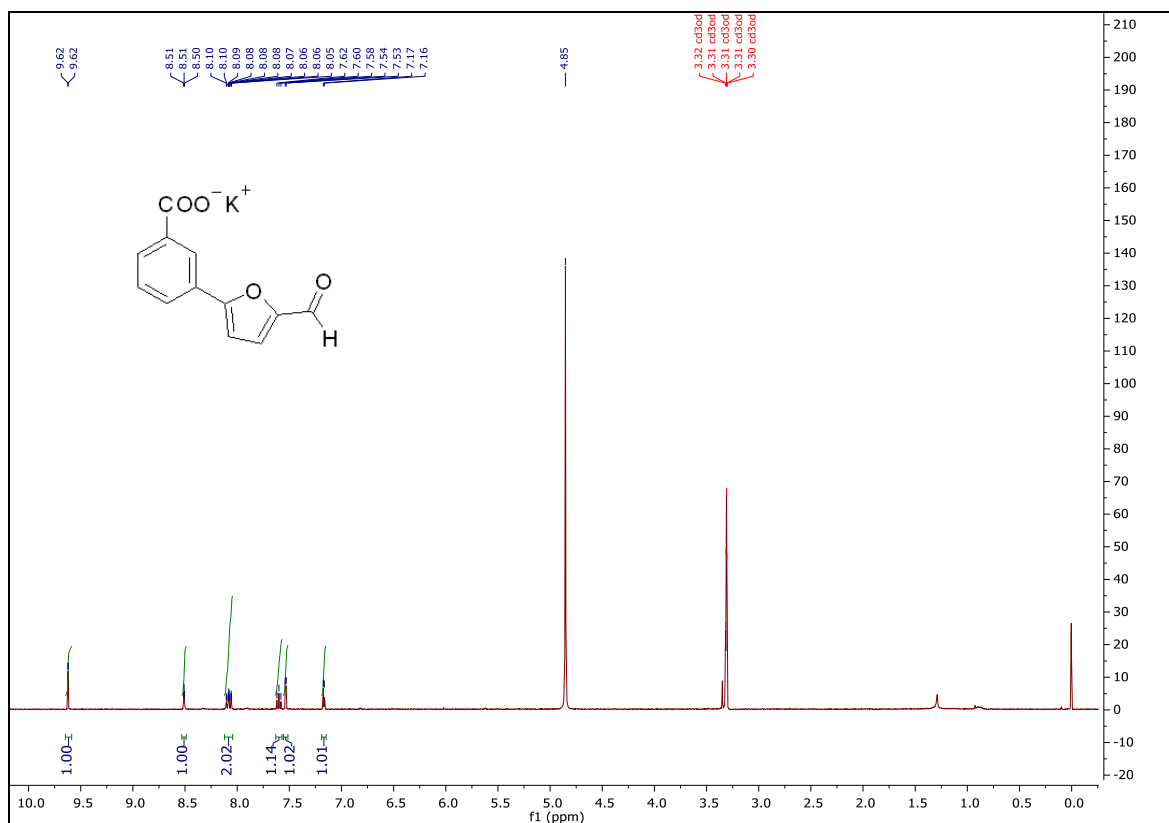
¹³C spectrum of **MDMG-277**¹H spectrum of **MDMG-281**

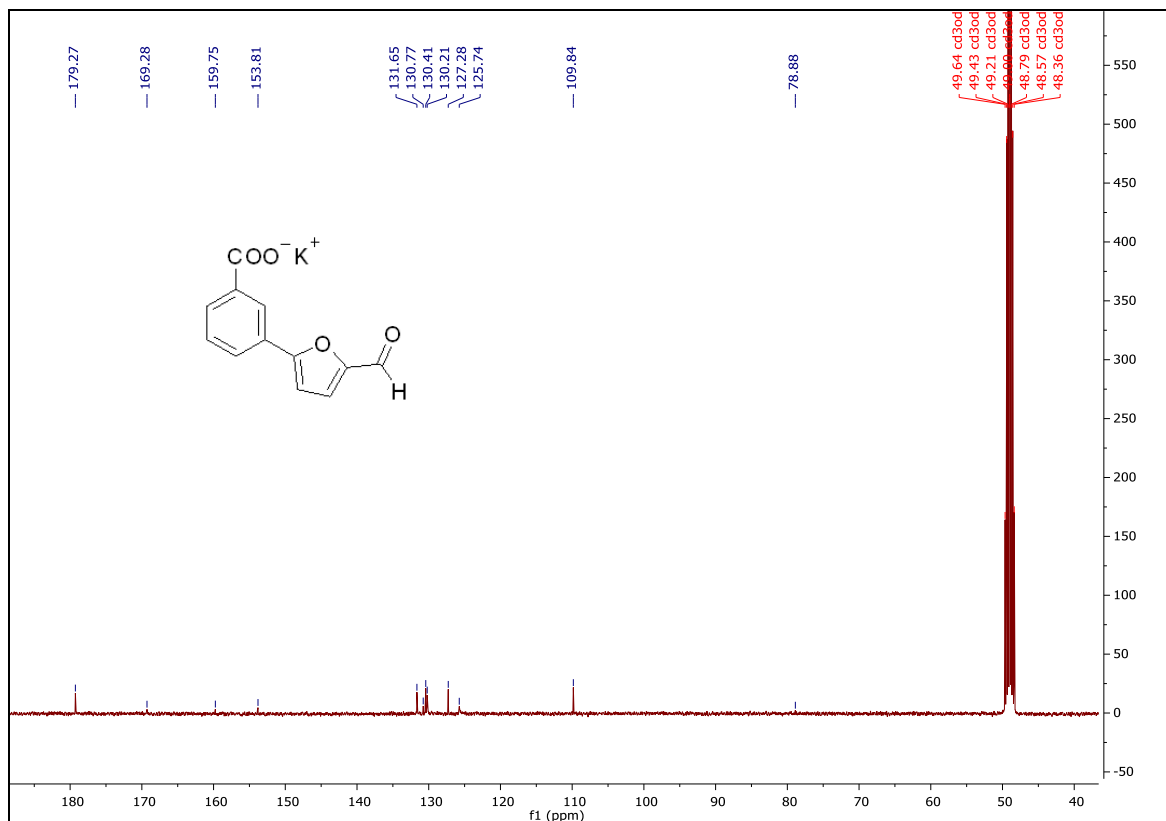
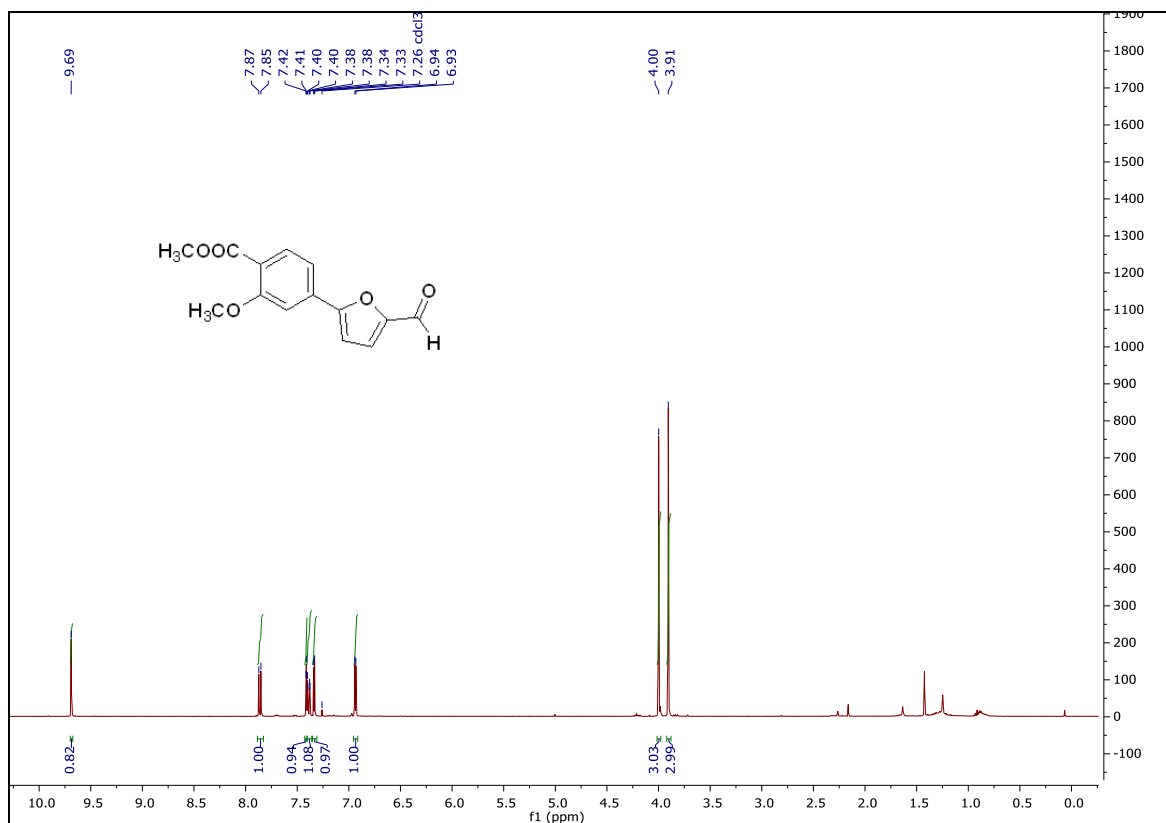
^{13}C spectrum of **MDMG-281** ^1H spectrum of **MDMG-285**

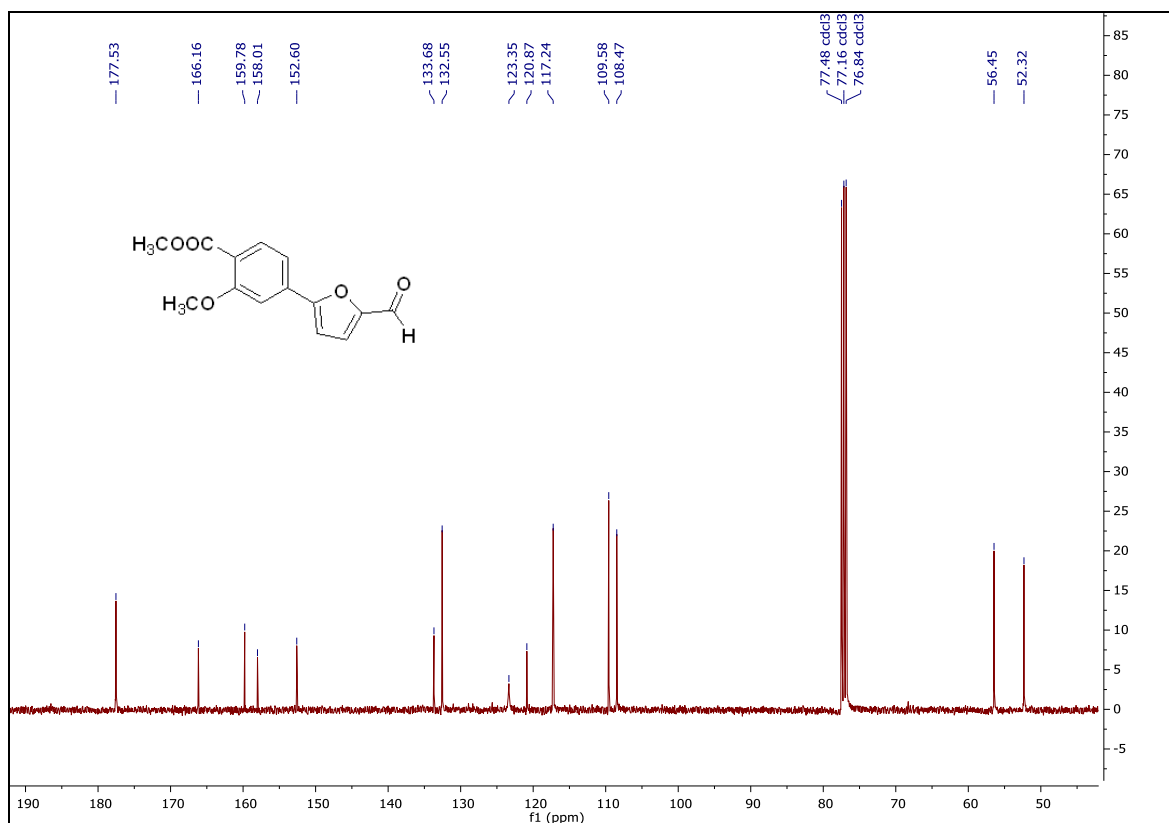
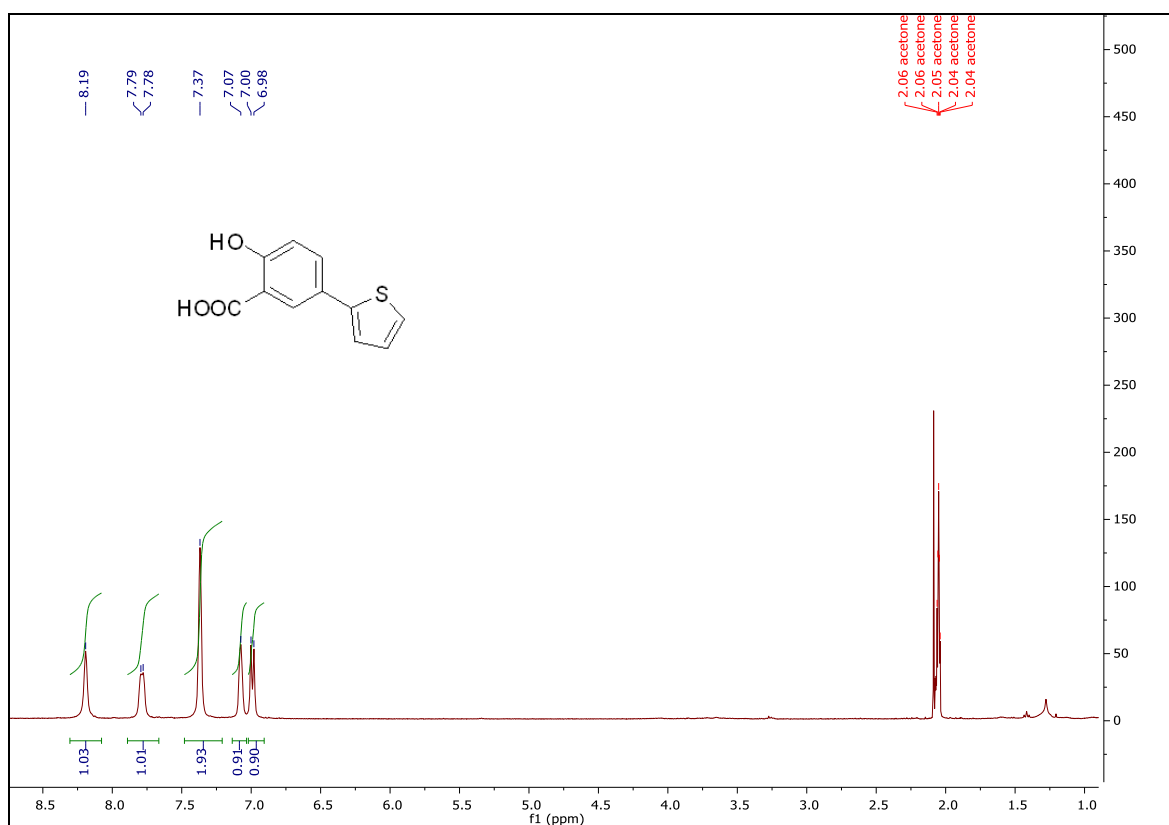
¹H spectrum of **MDMG-289**¹H spectrum of **MDMG-293**

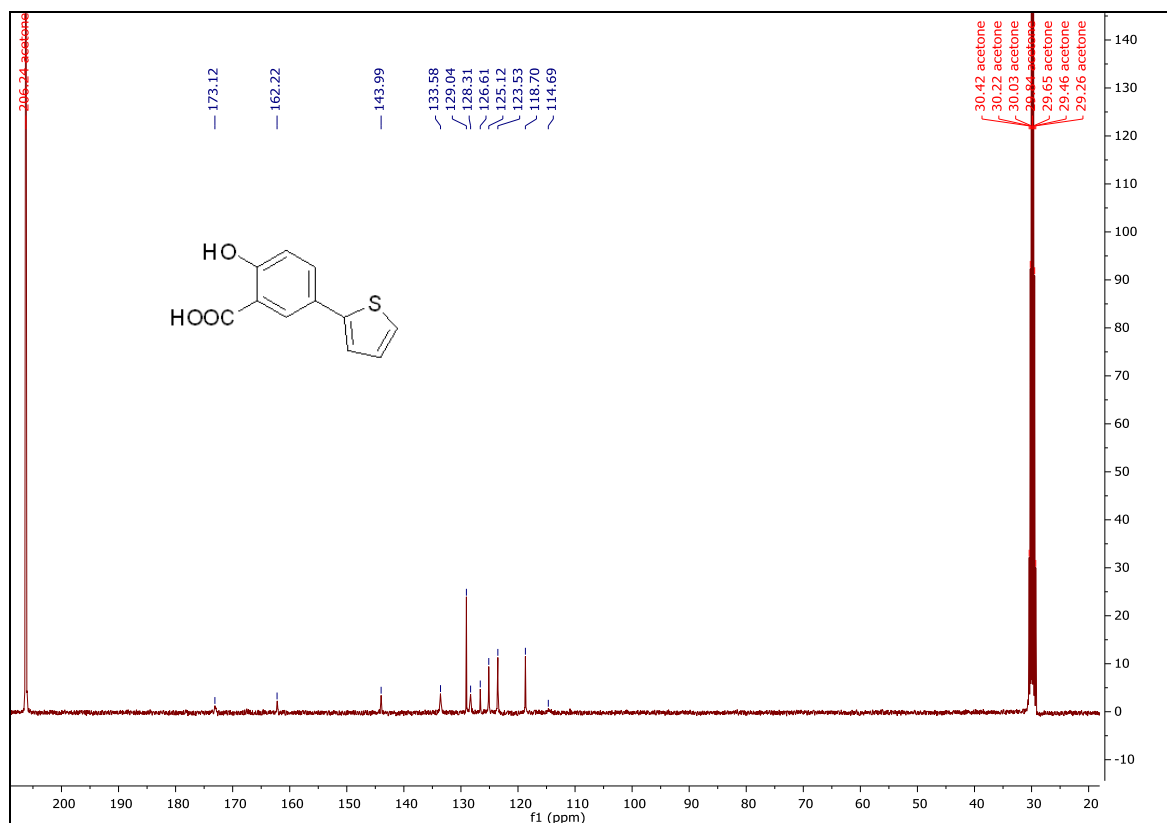
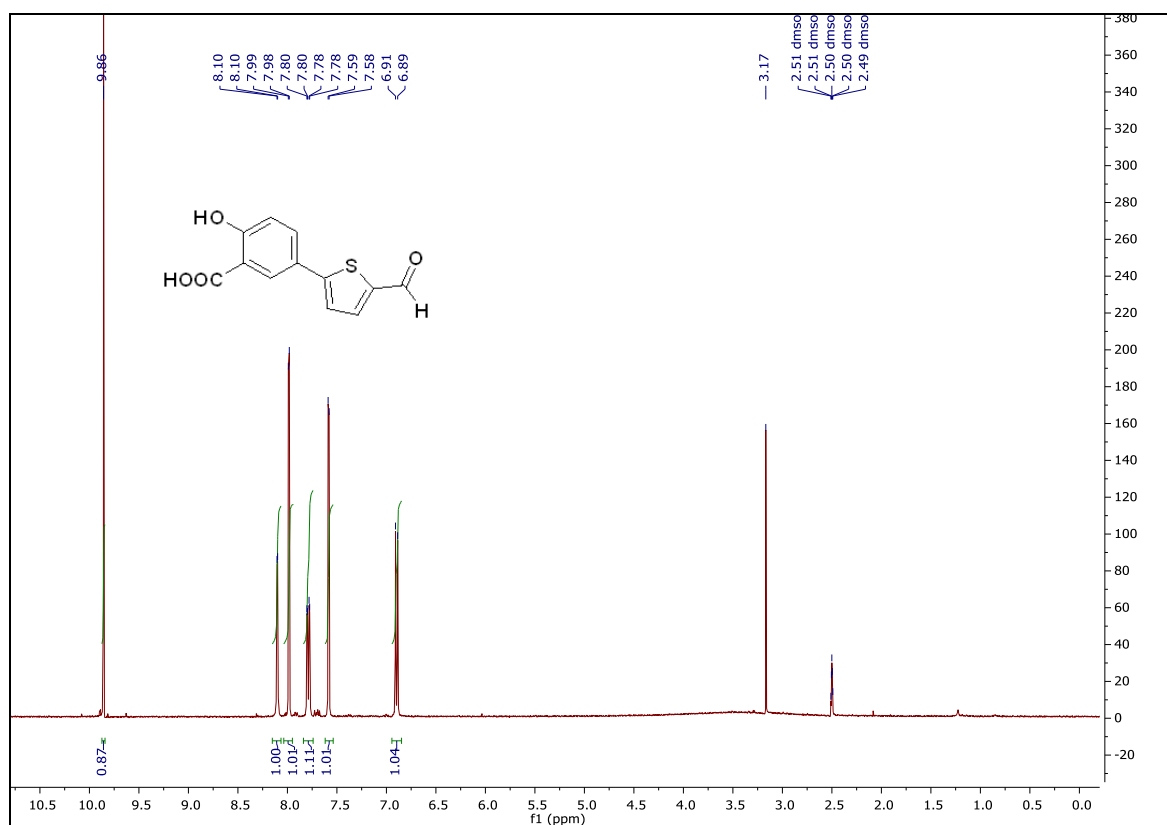
¹³C spectrum of **MDMG-293**¹H spectrum of **MDMG-305**

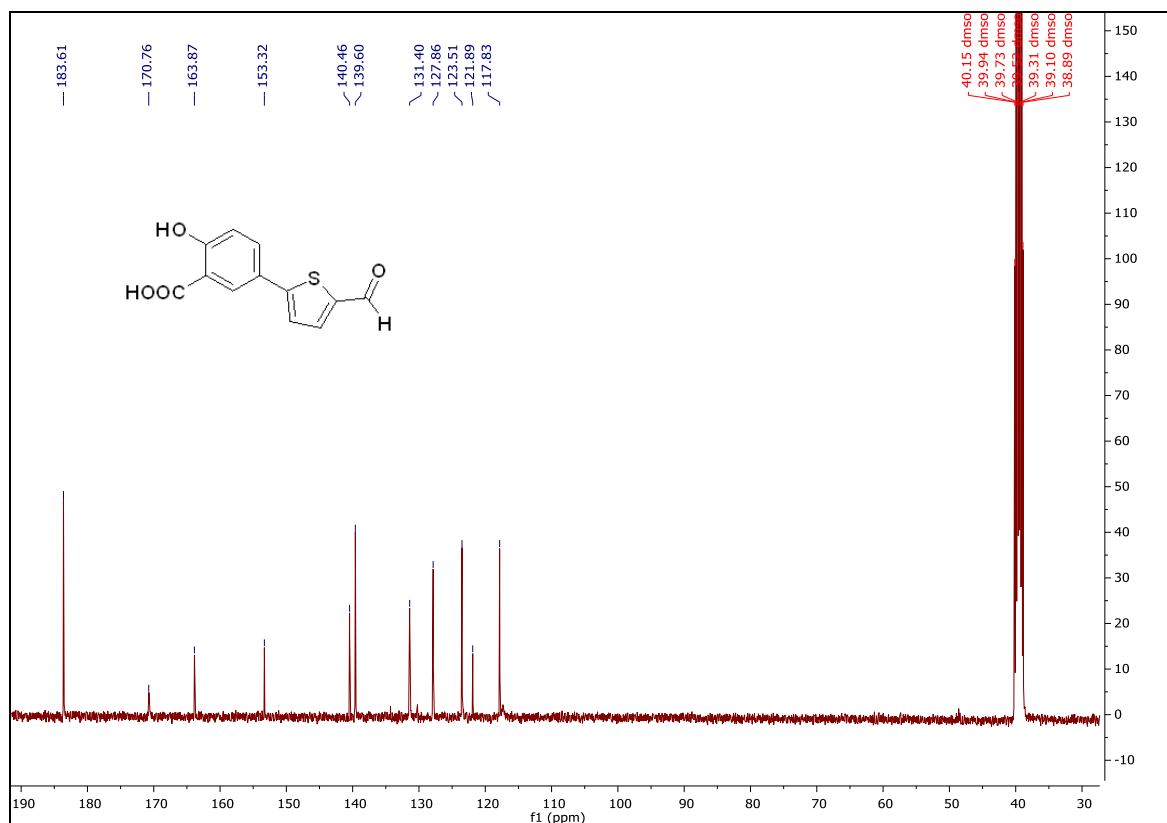
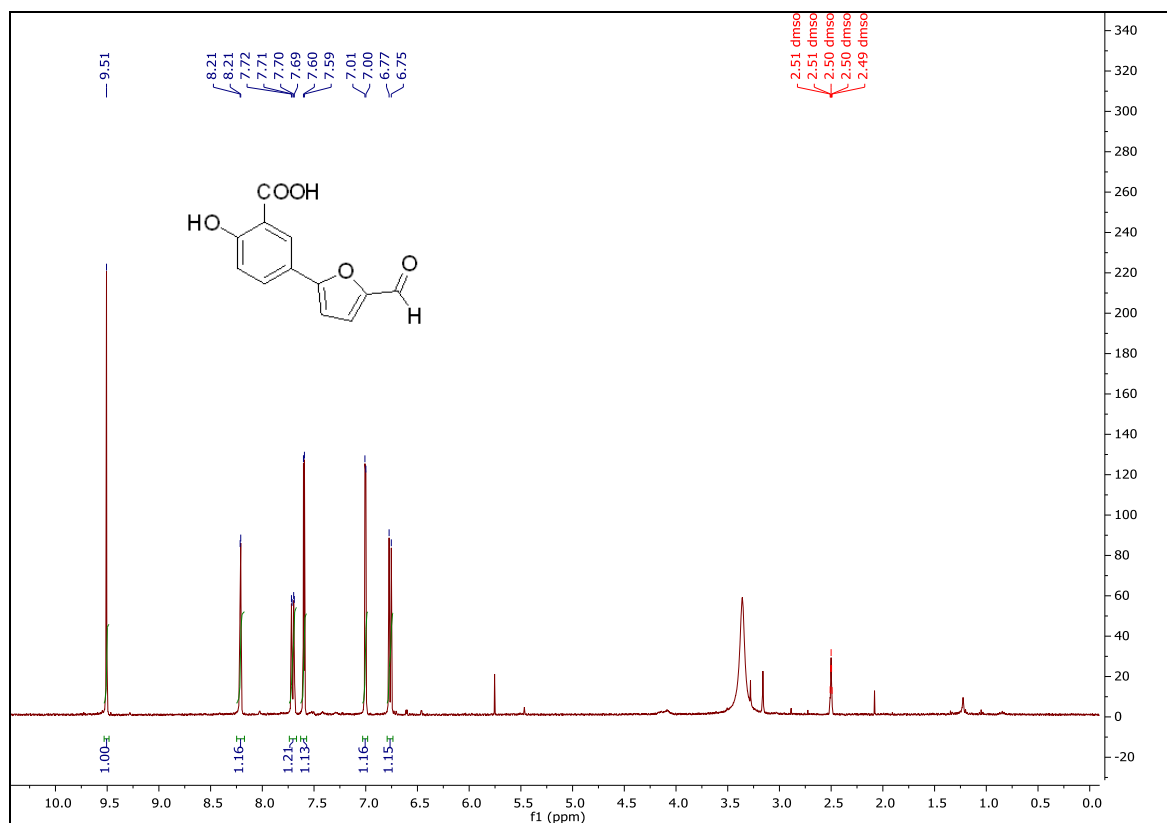
^{13}C spectrum of **MDMG-305** ^1H spectrum of **MDMG-317**

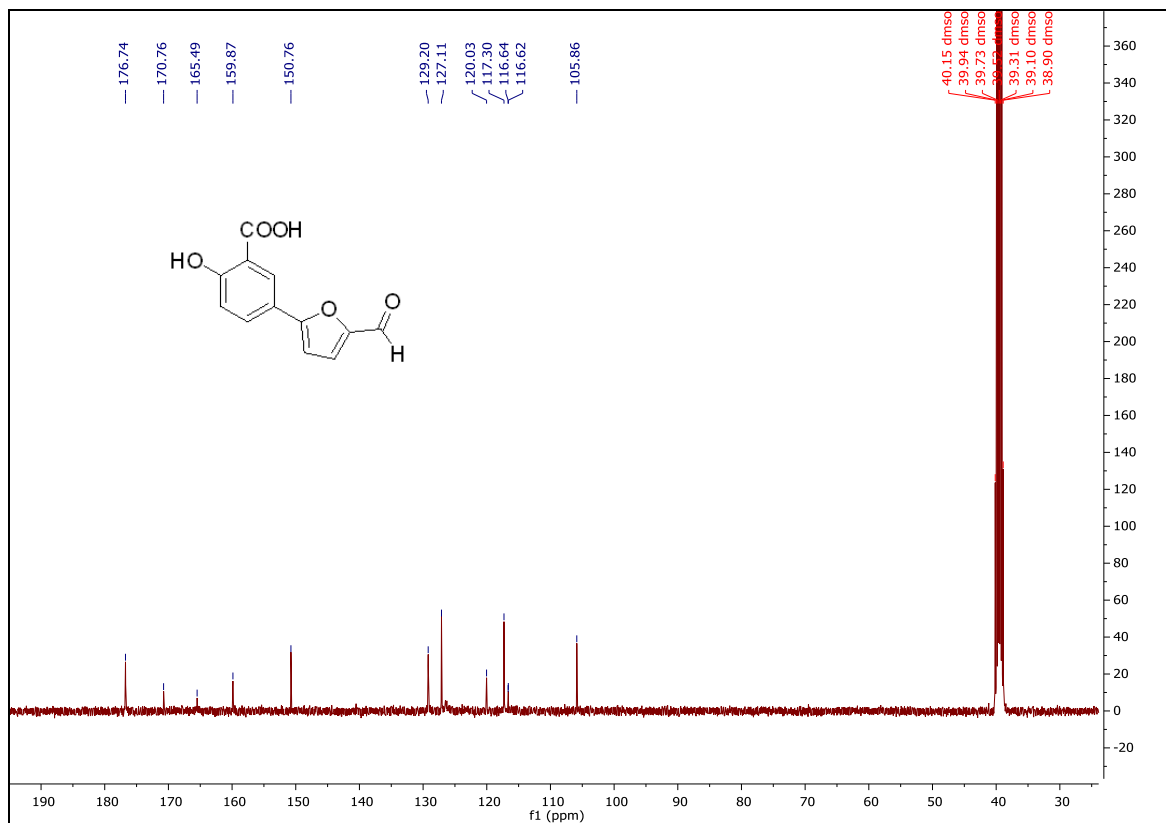
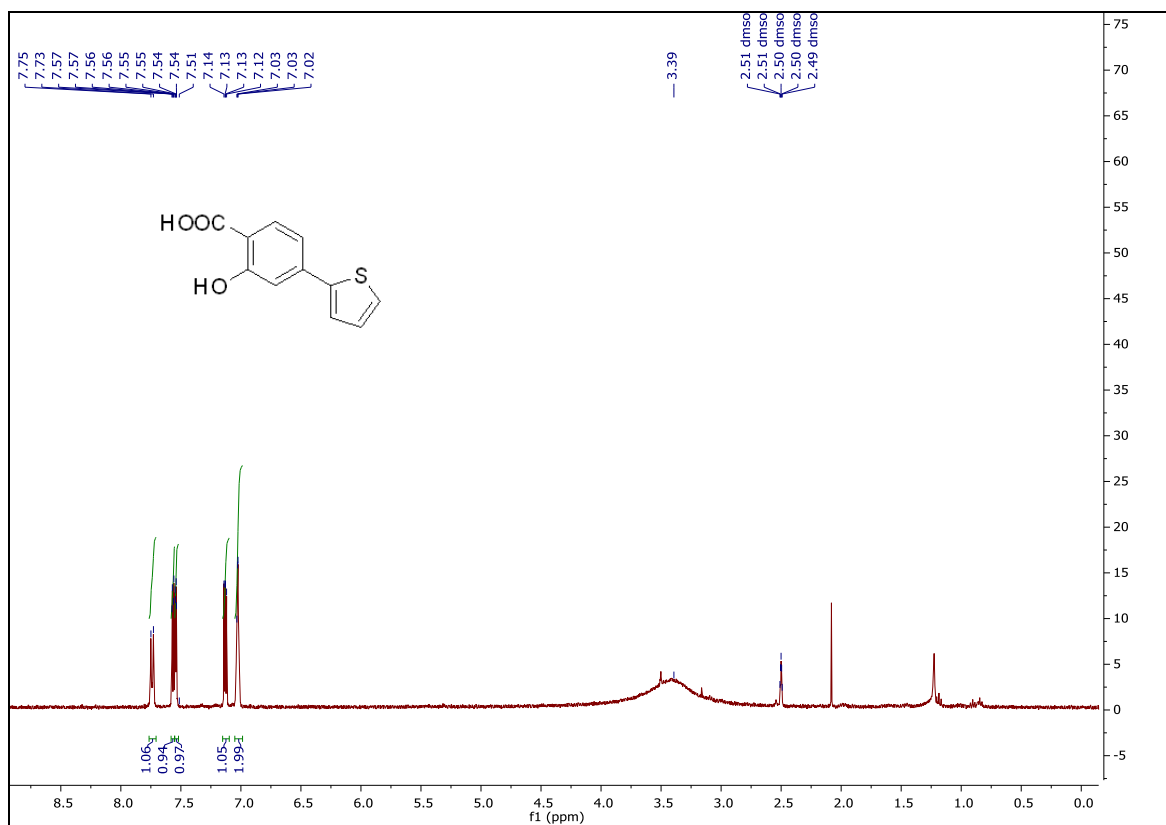
¹³C spectrum of **MDMG-317**¹H spectrum of **MDMG-353**

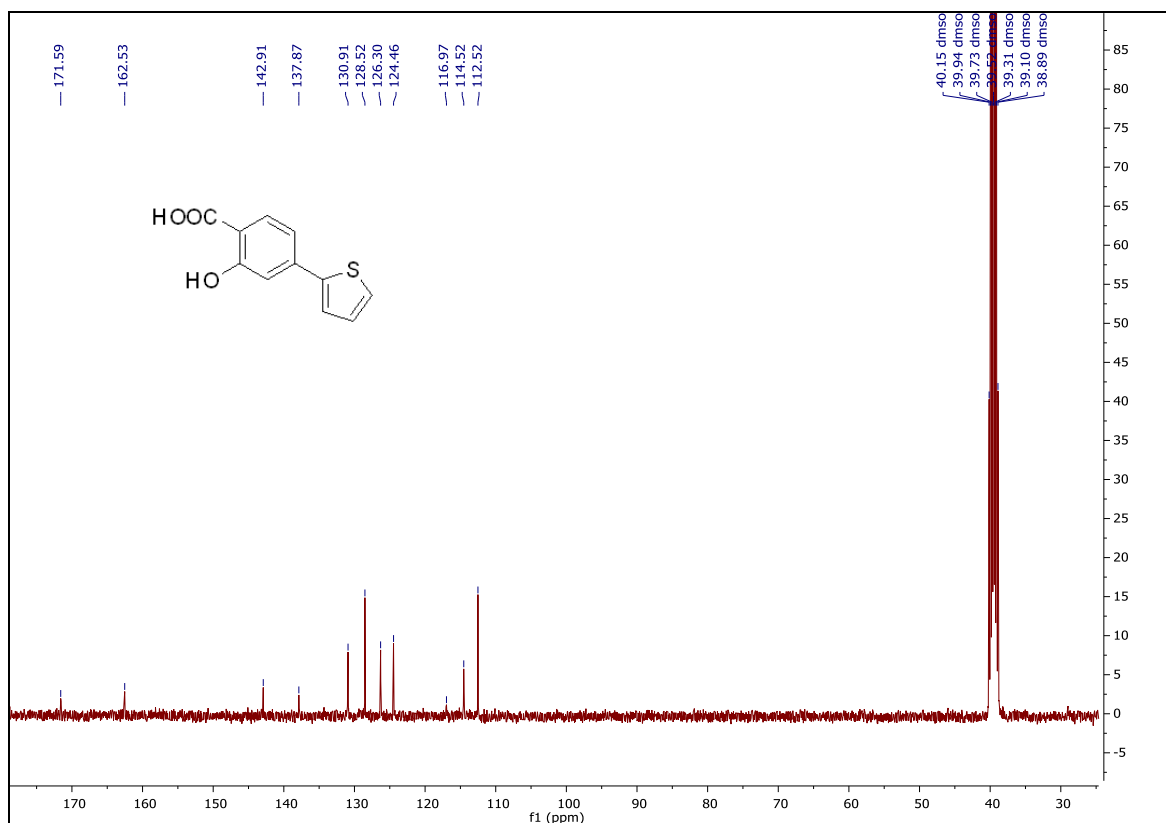
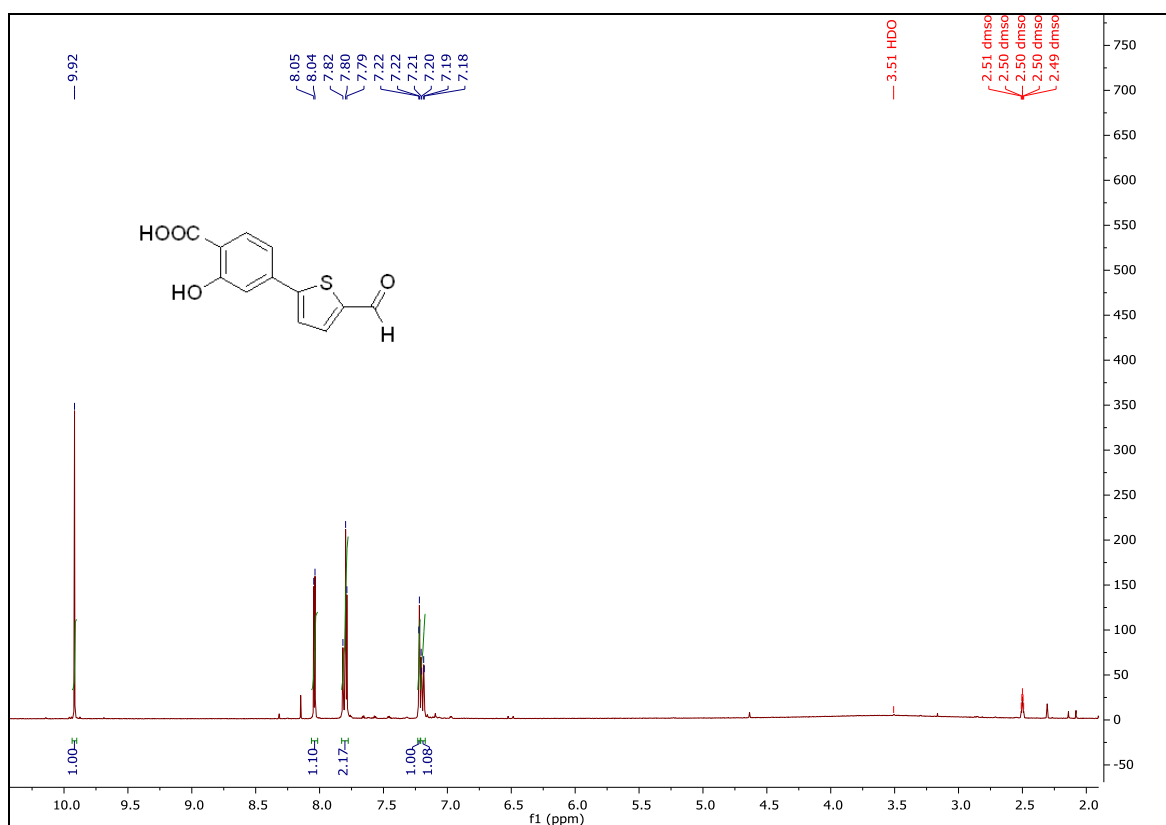
¹³C spectrum of **MDMG-353**¹H spectrum of **MDMG-357**

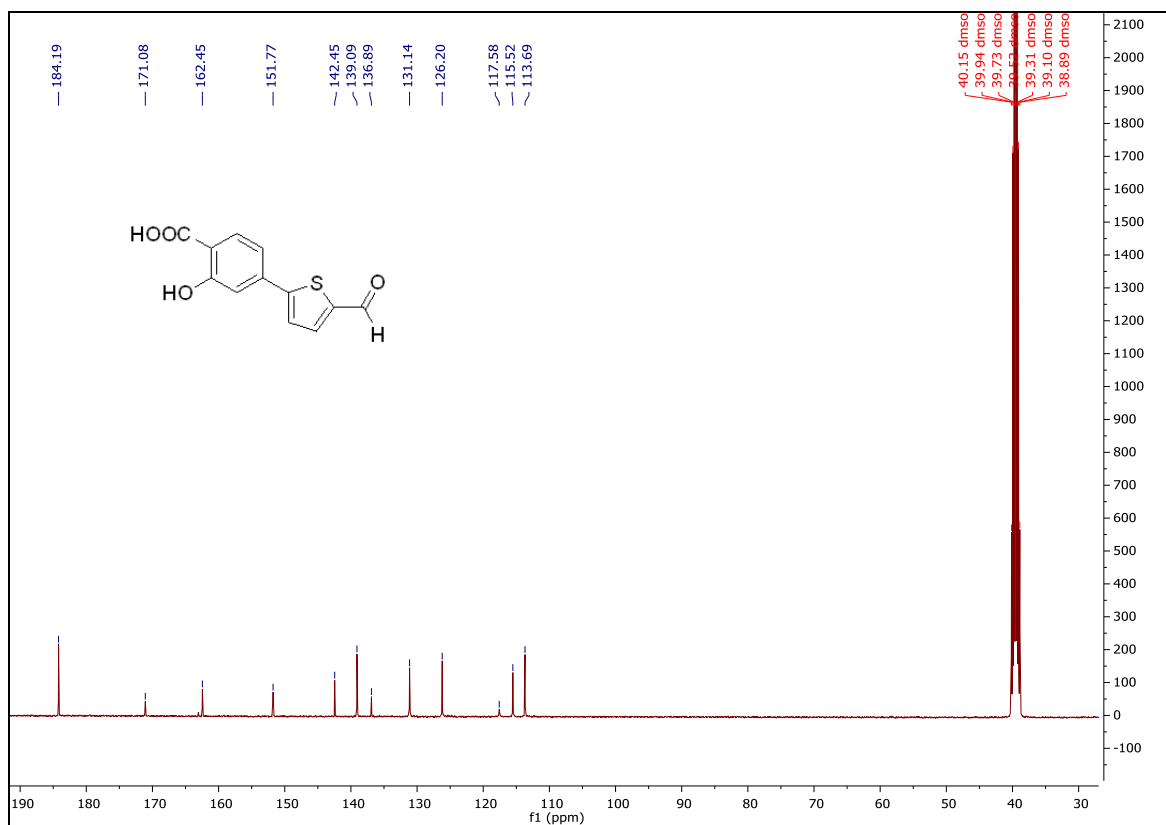
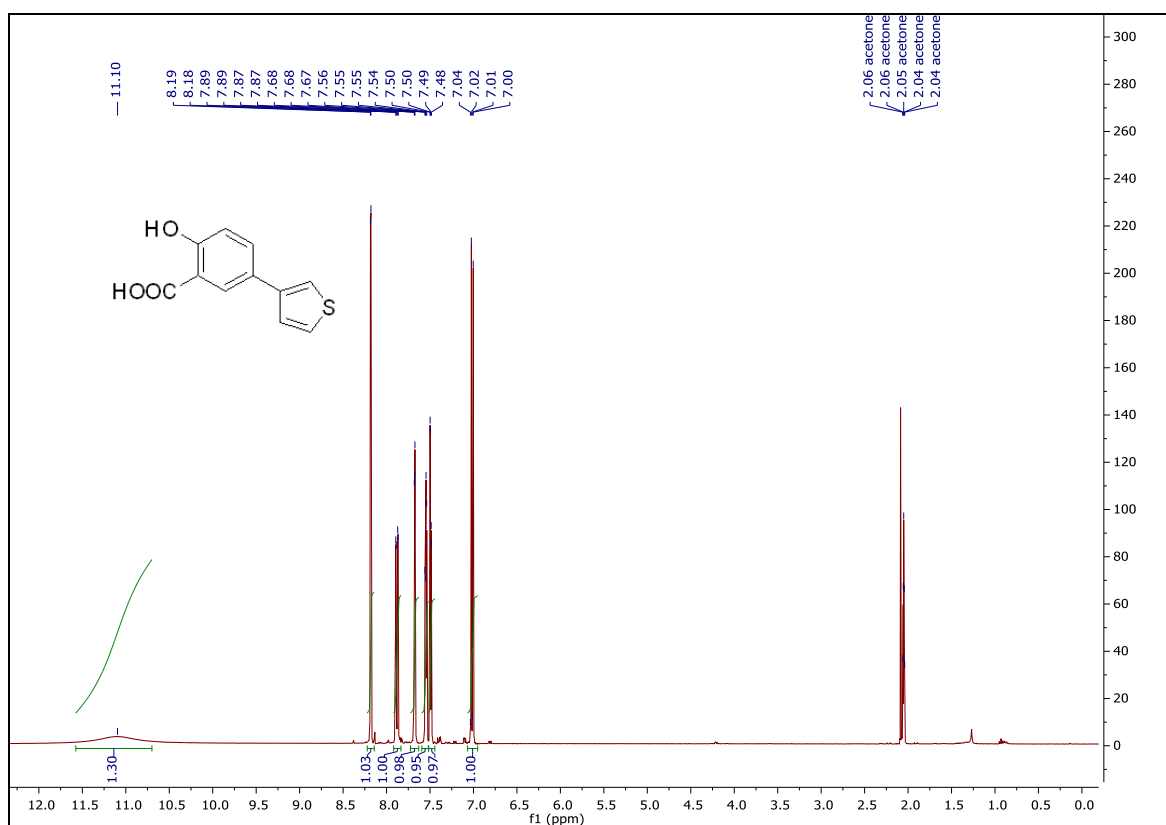
^{13}C spectrum of **MDMG-357** ^1H spectrum of **MDMG-369**

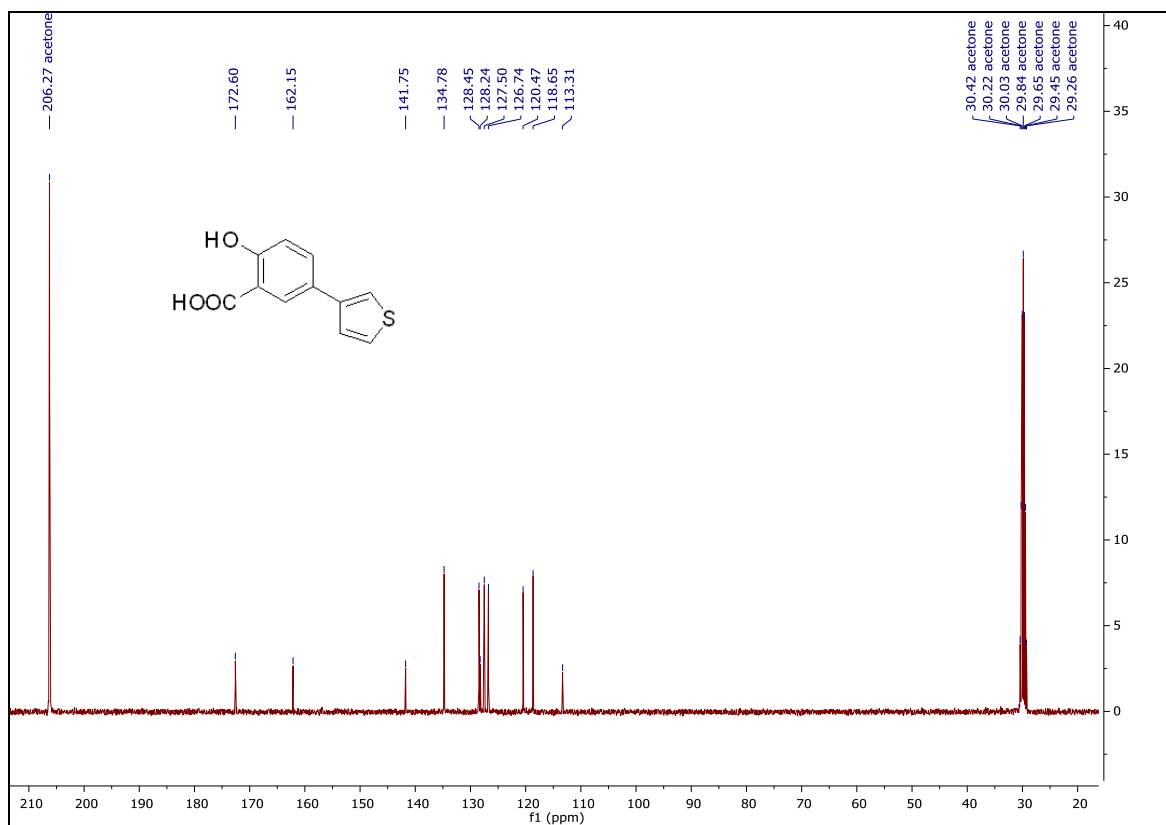
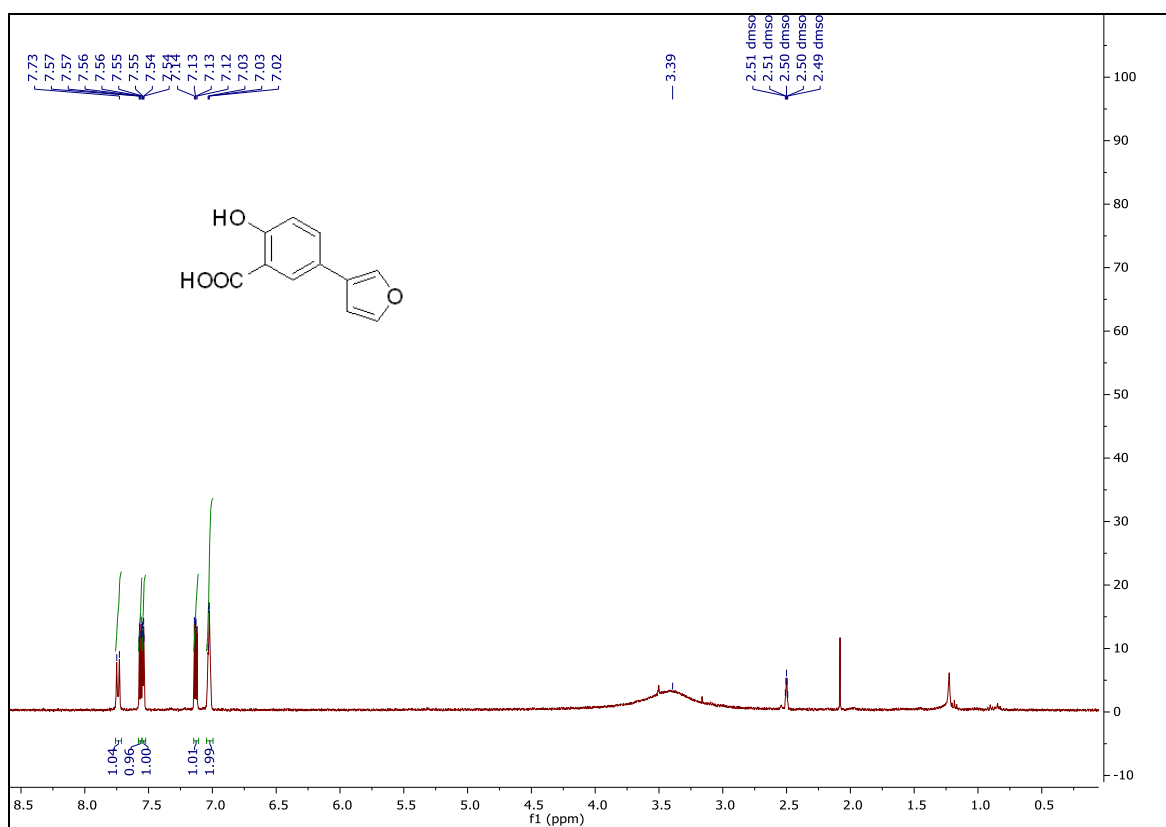
^{13}C spectrum of **MDMG-369** ^1H spectrum of **MDMG-373**

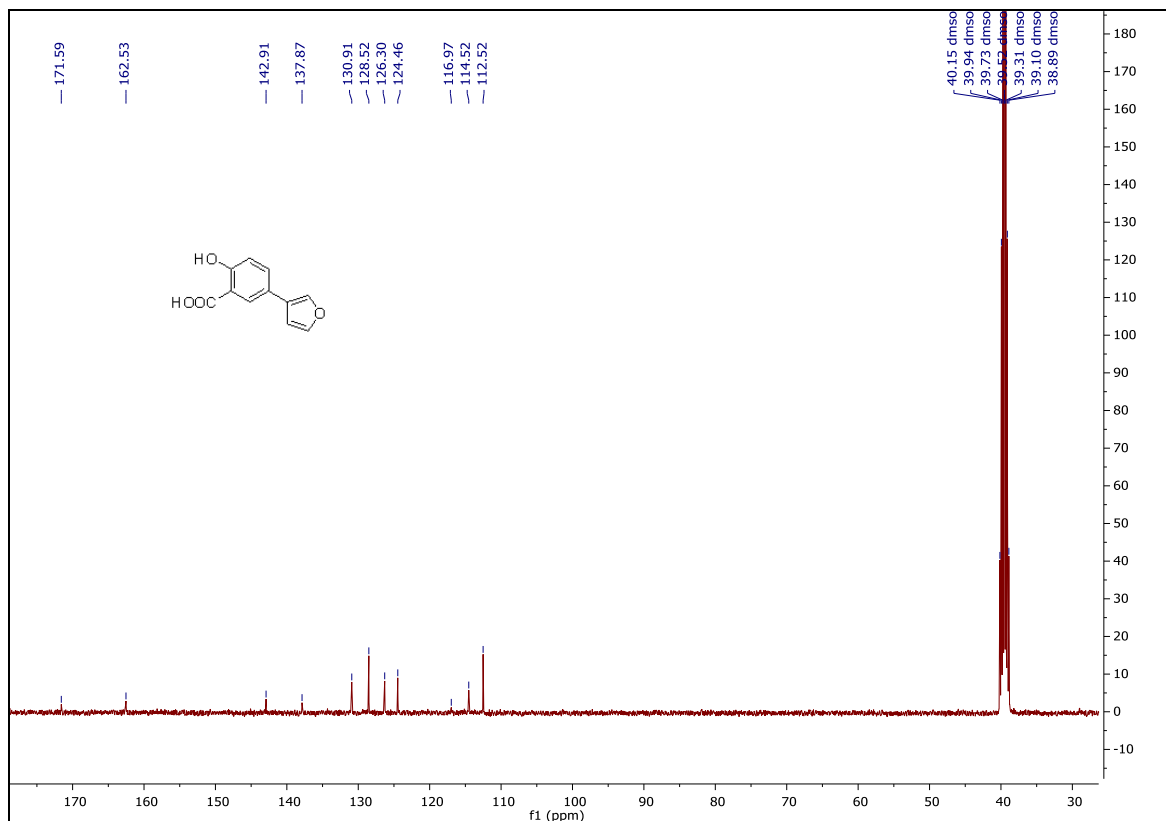
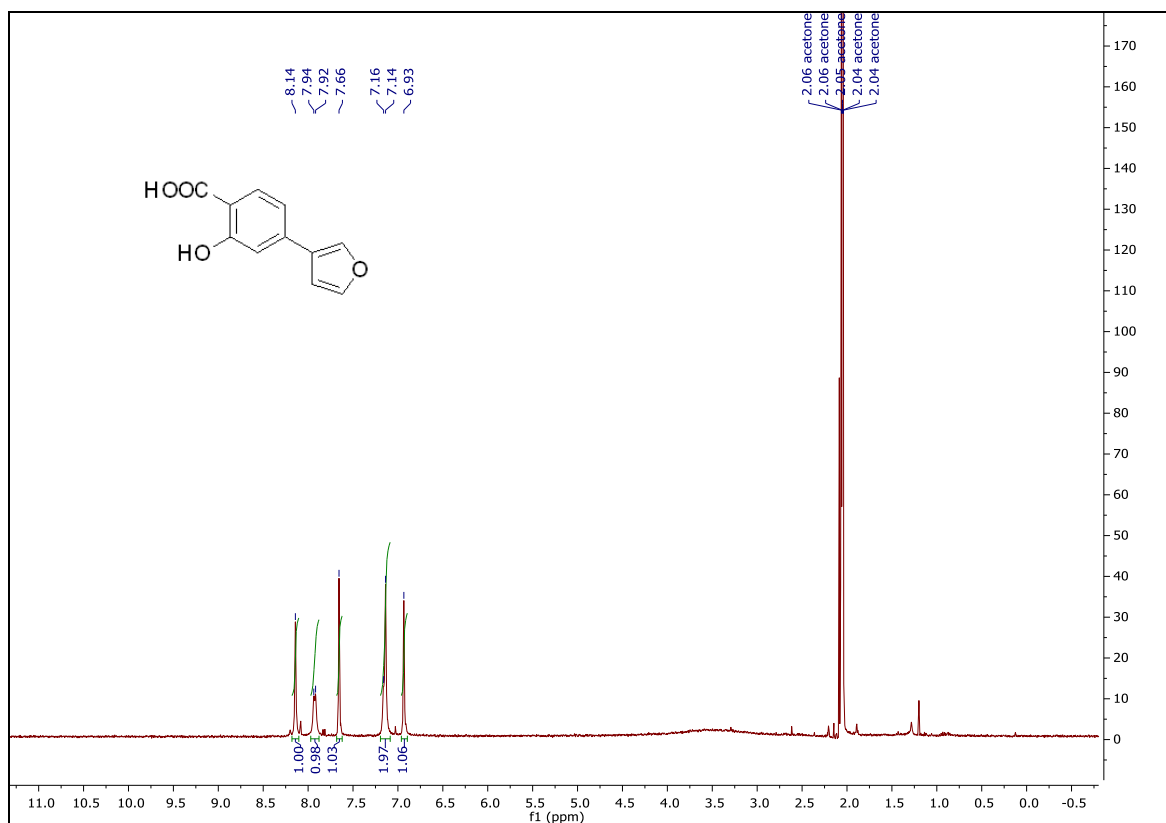
^{13}C spectrum of **MDMG-373** ^1H spectrum of **MDMG-409**

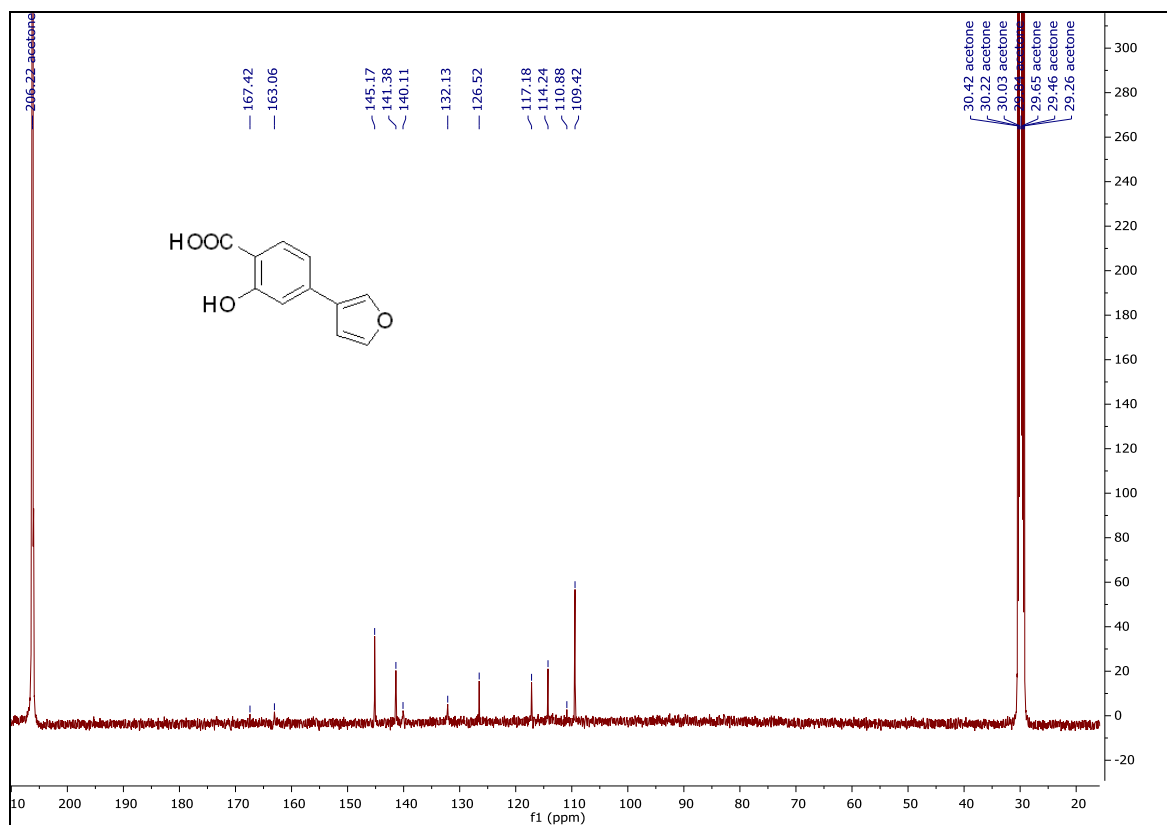
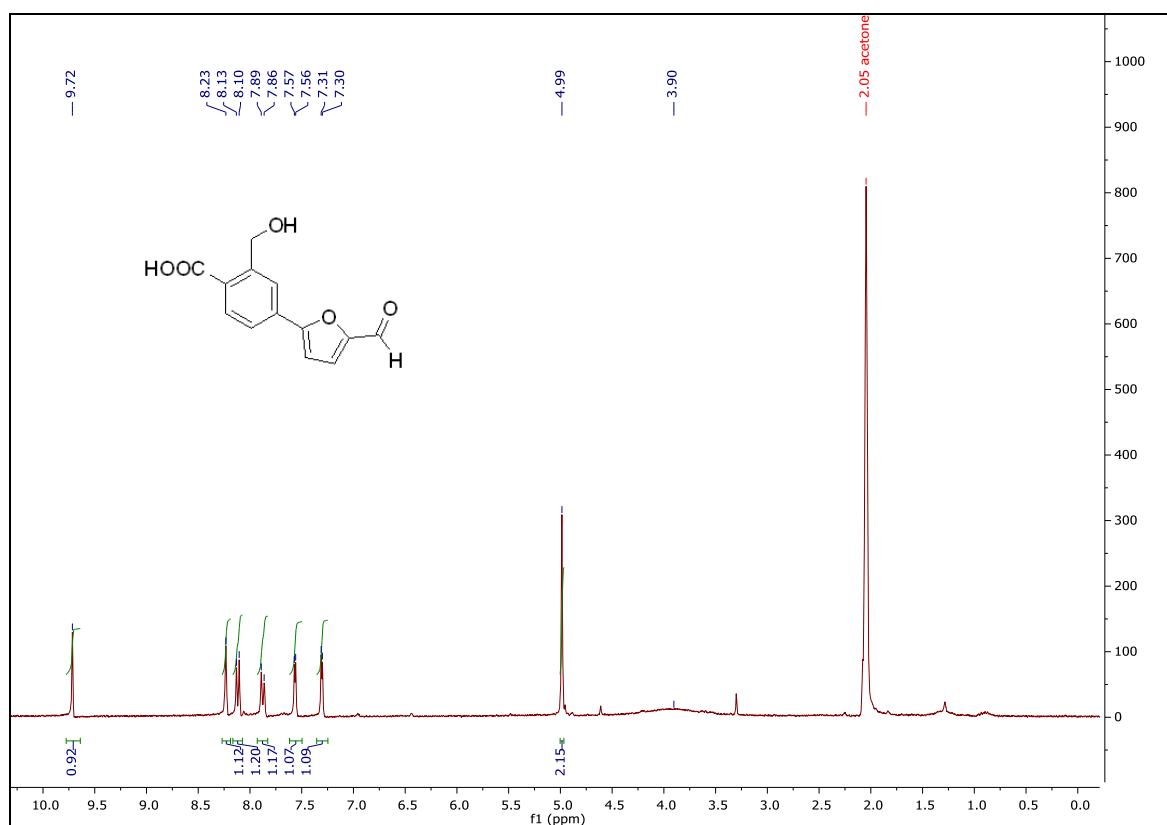
¹³C spectrum of MDMG-409¹H spectrum of MDMG-417

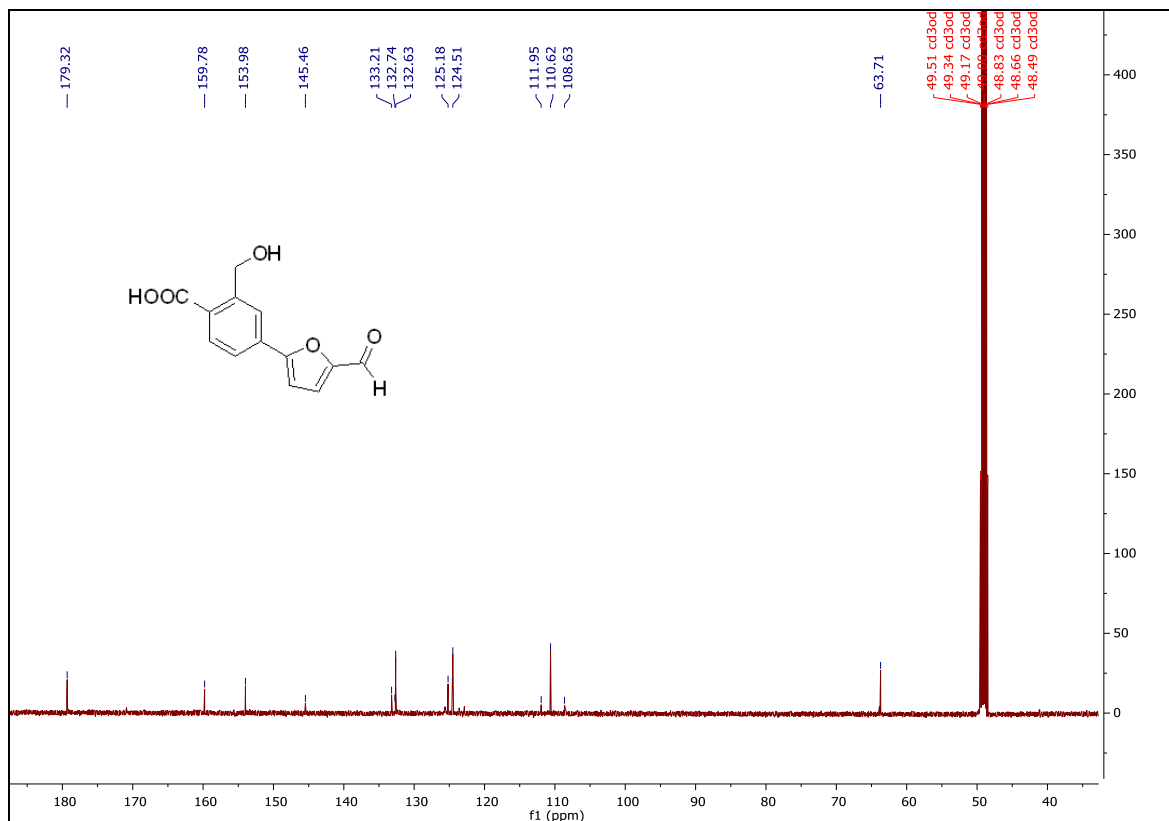
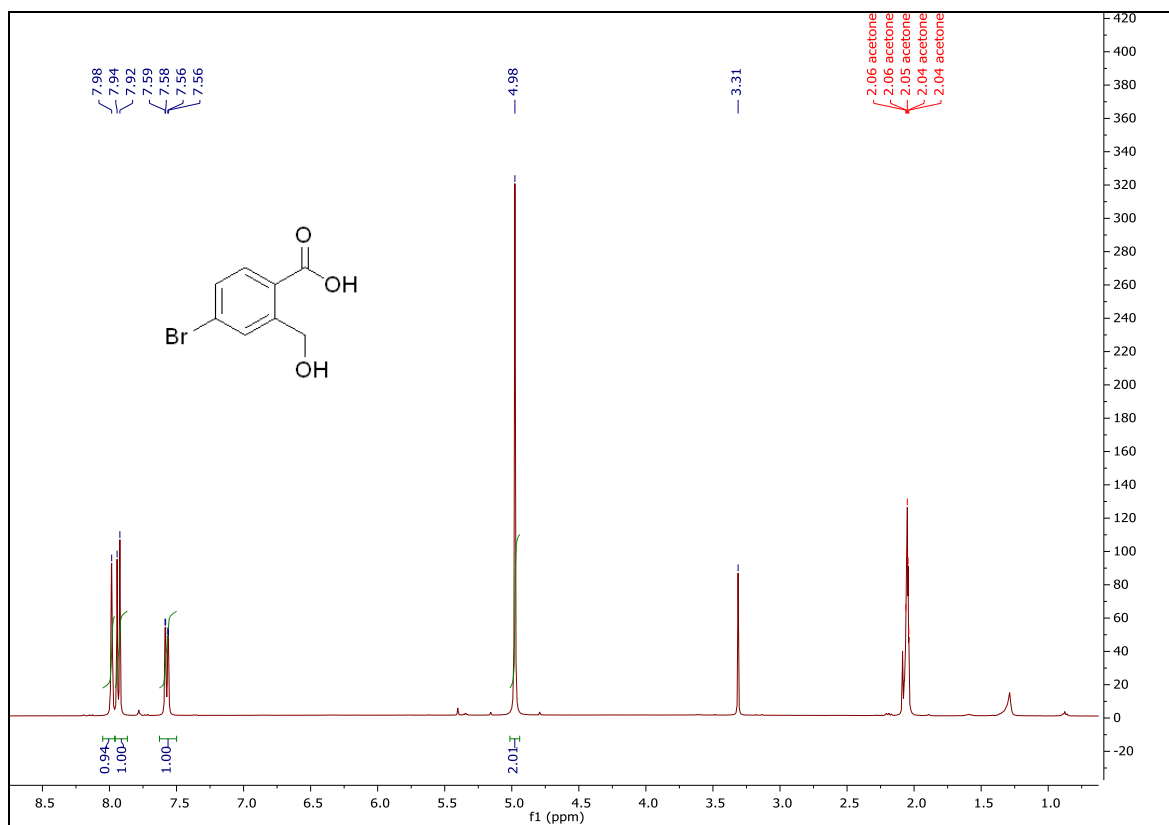
^{13}C spectrum of **MDMG-417** ^1H spectrum of **MDMG-420**

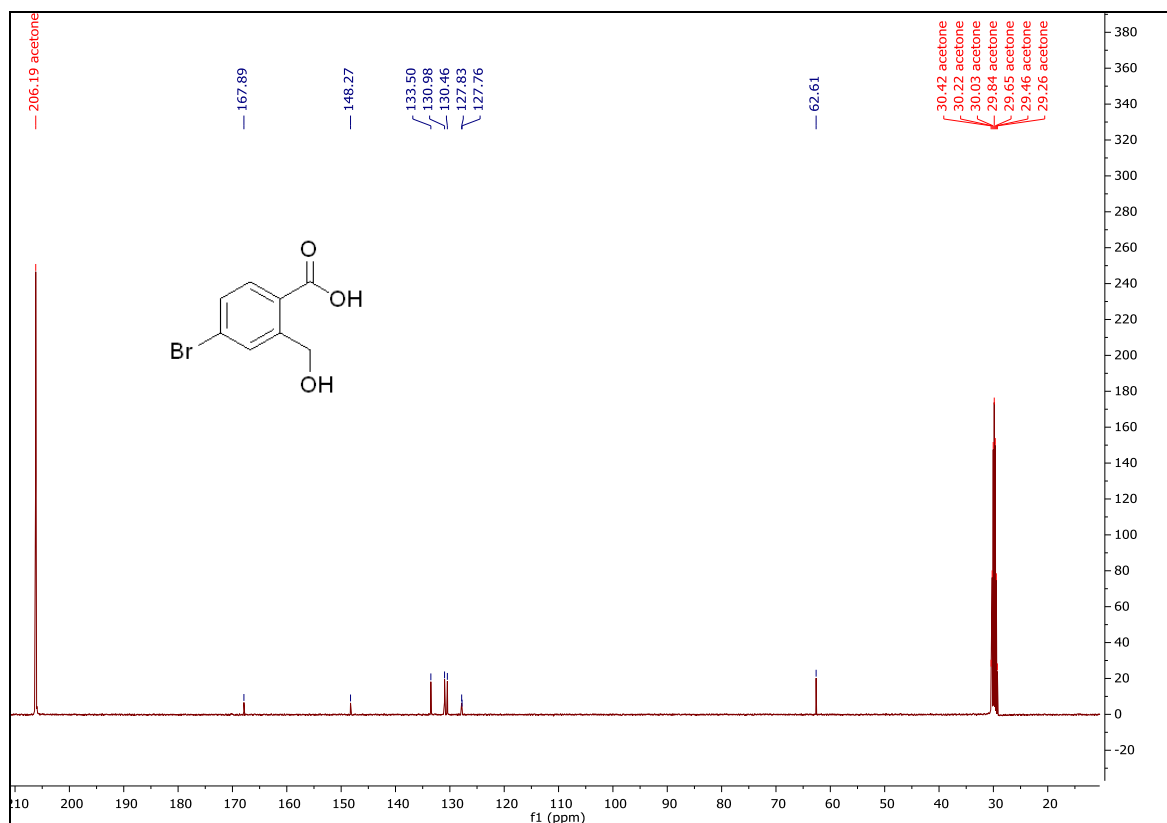
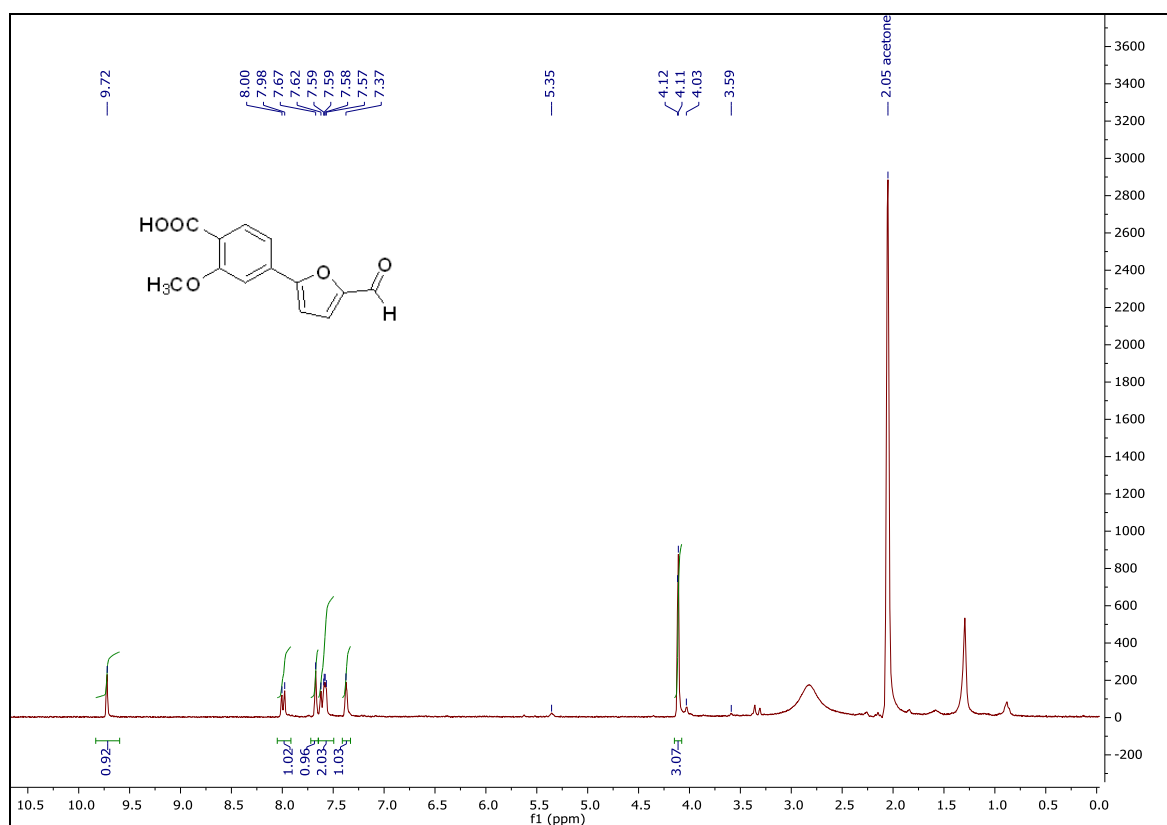
^{13}C spectrum of **MDMG-420** ^1H spectrum of **MDMG-424**

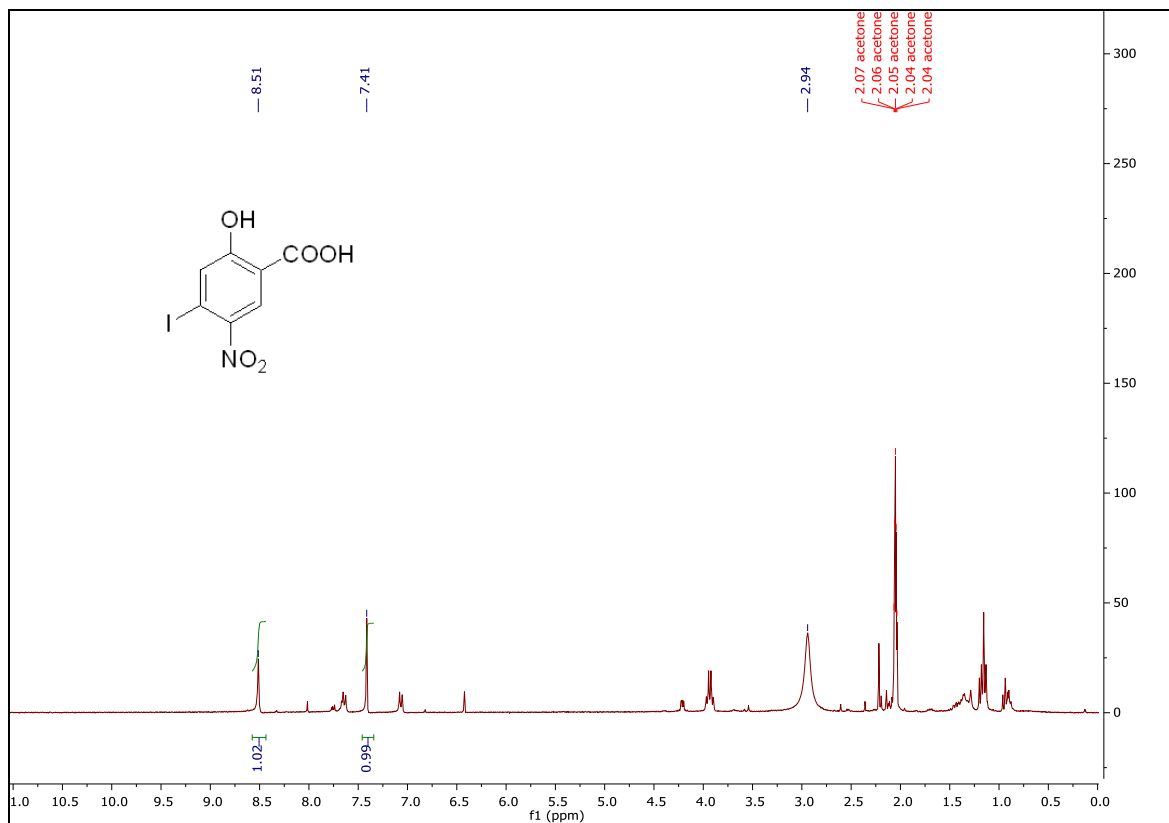
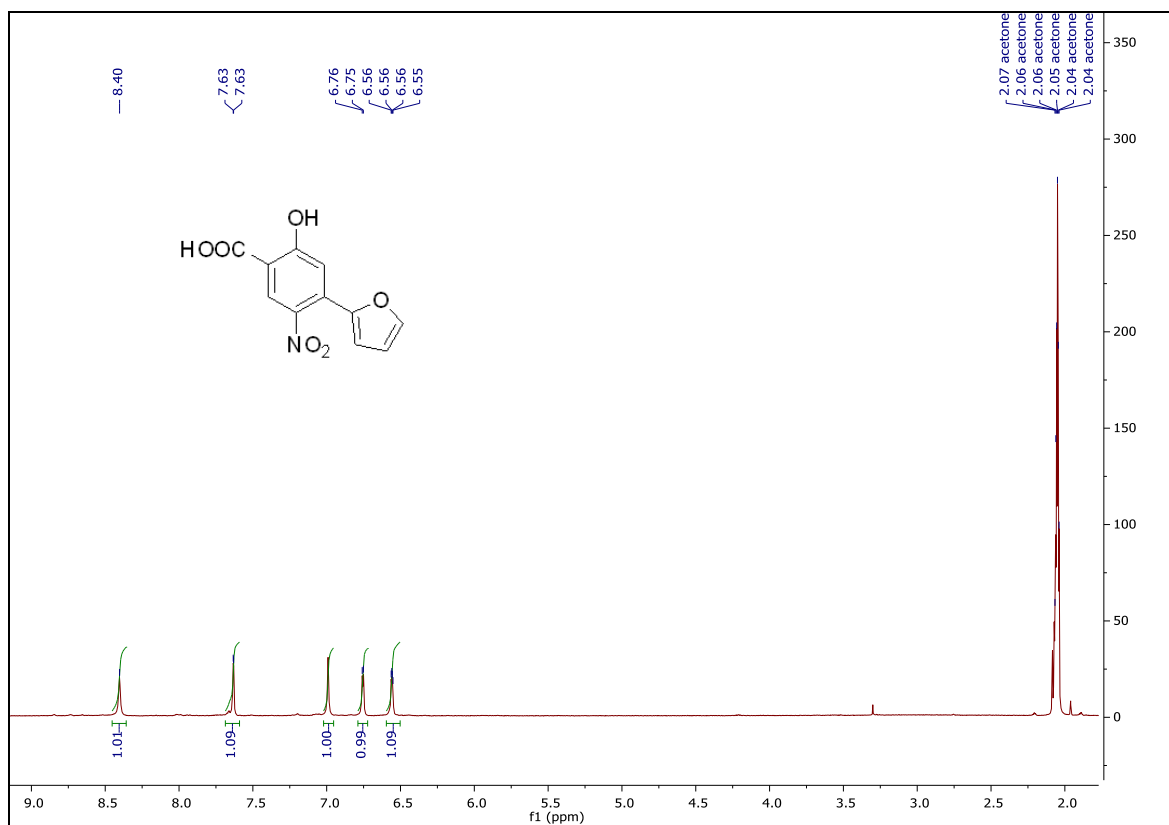
^{13}C spectrum of **MDMG-424** ^1H spectrum of **MDMG-427**

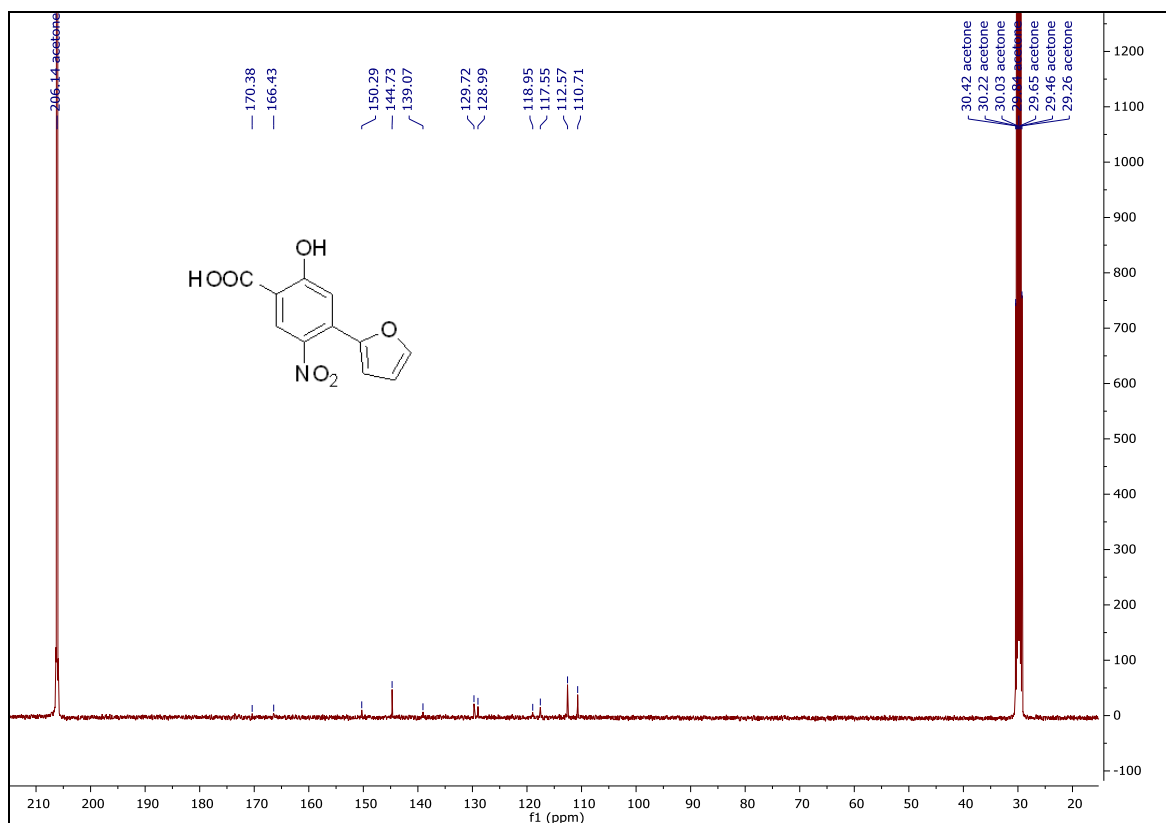
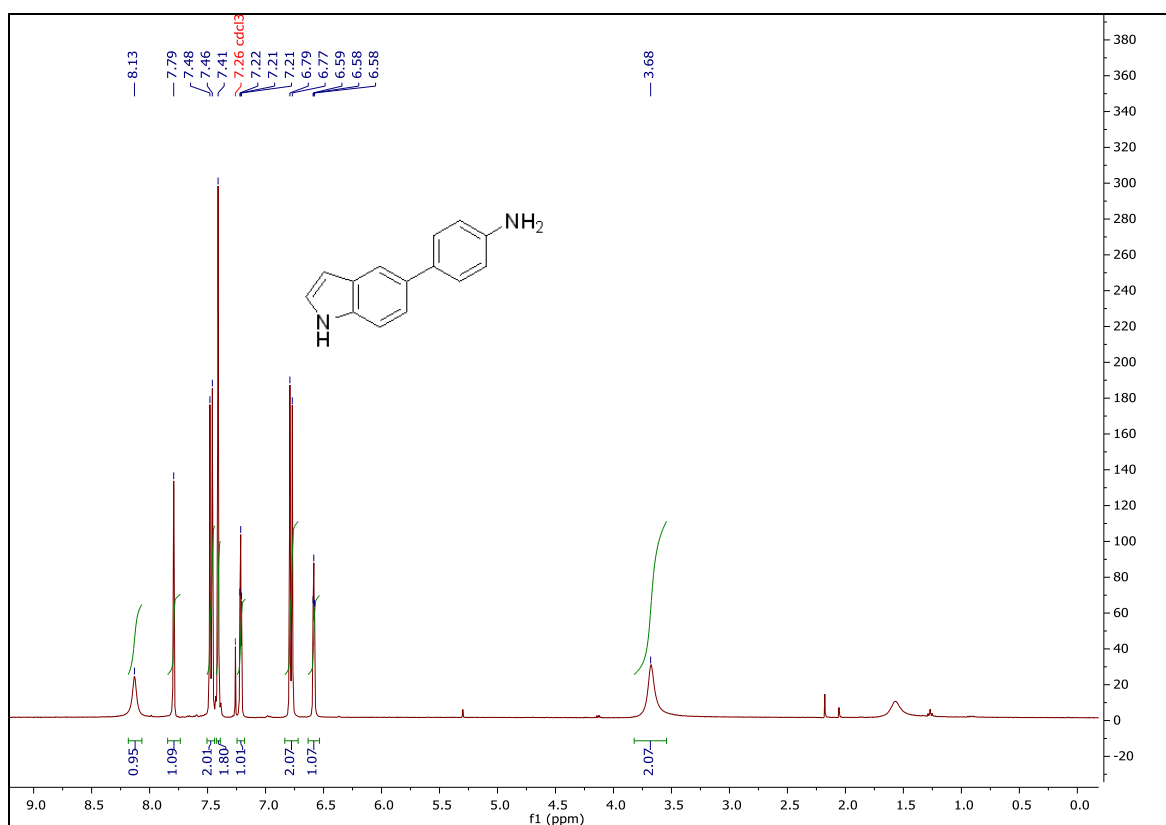
^{13}C spectrum of **MDMG-427** ^1H spectrum of **MDMG-431**

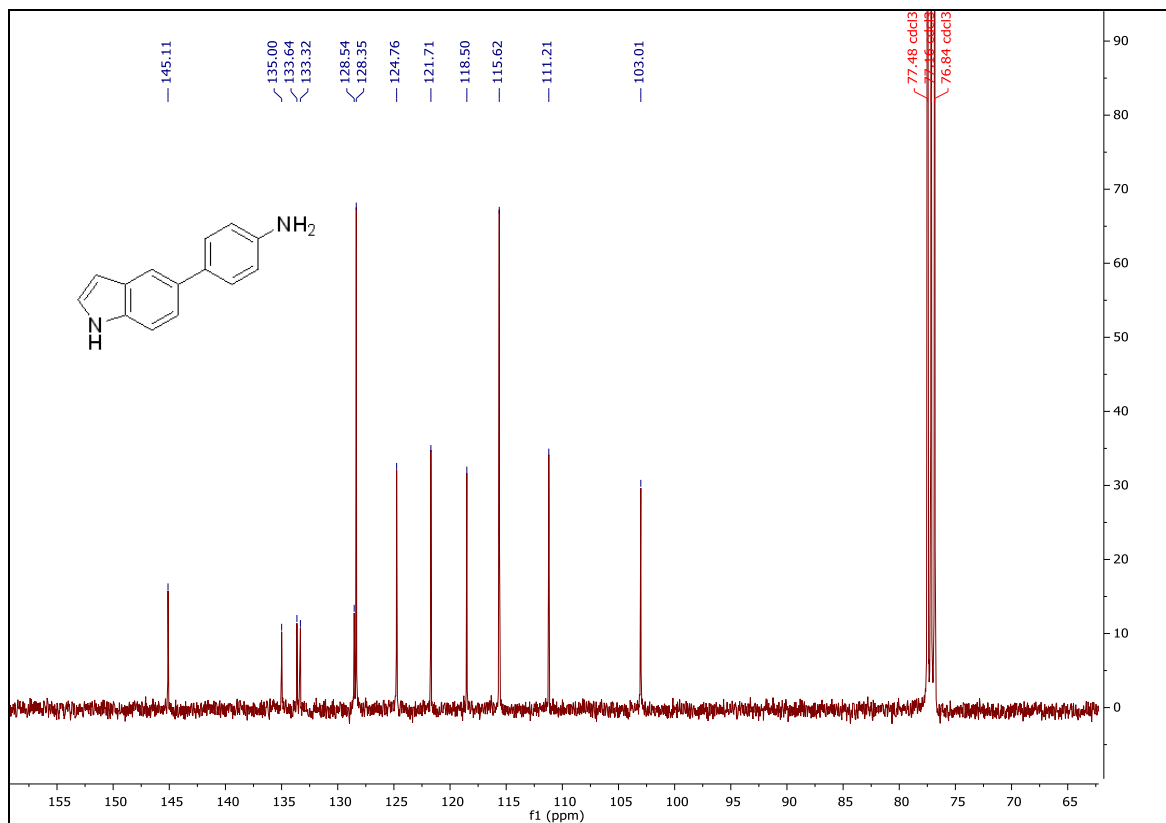
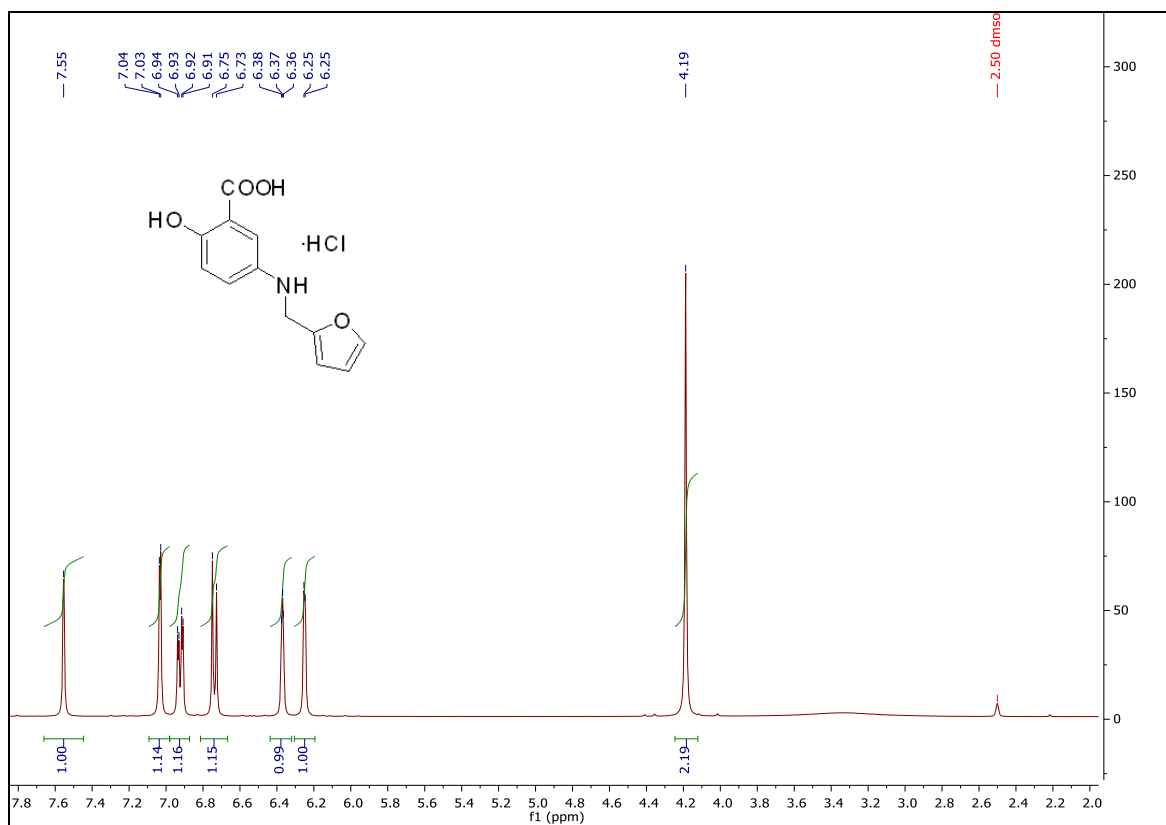
^{13}C spectrum of **MDMG-431** ^1H spectrum of **MDMG-451**

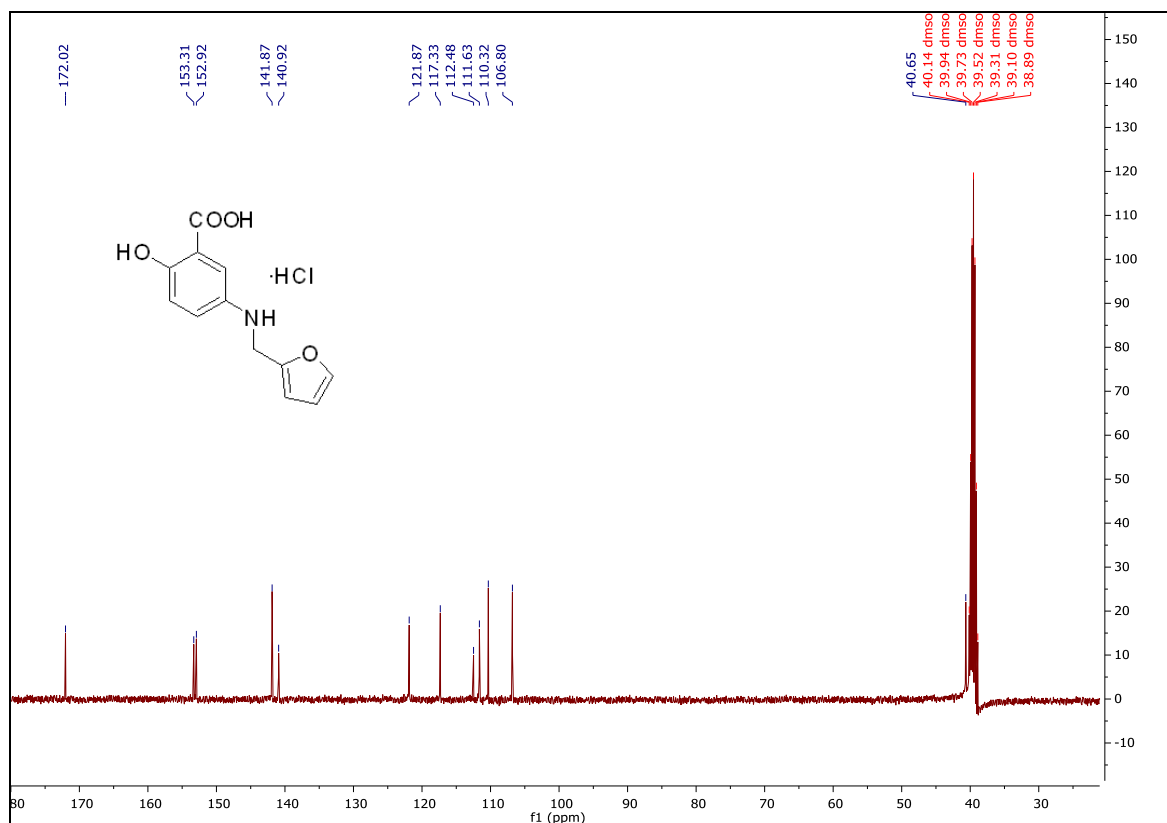
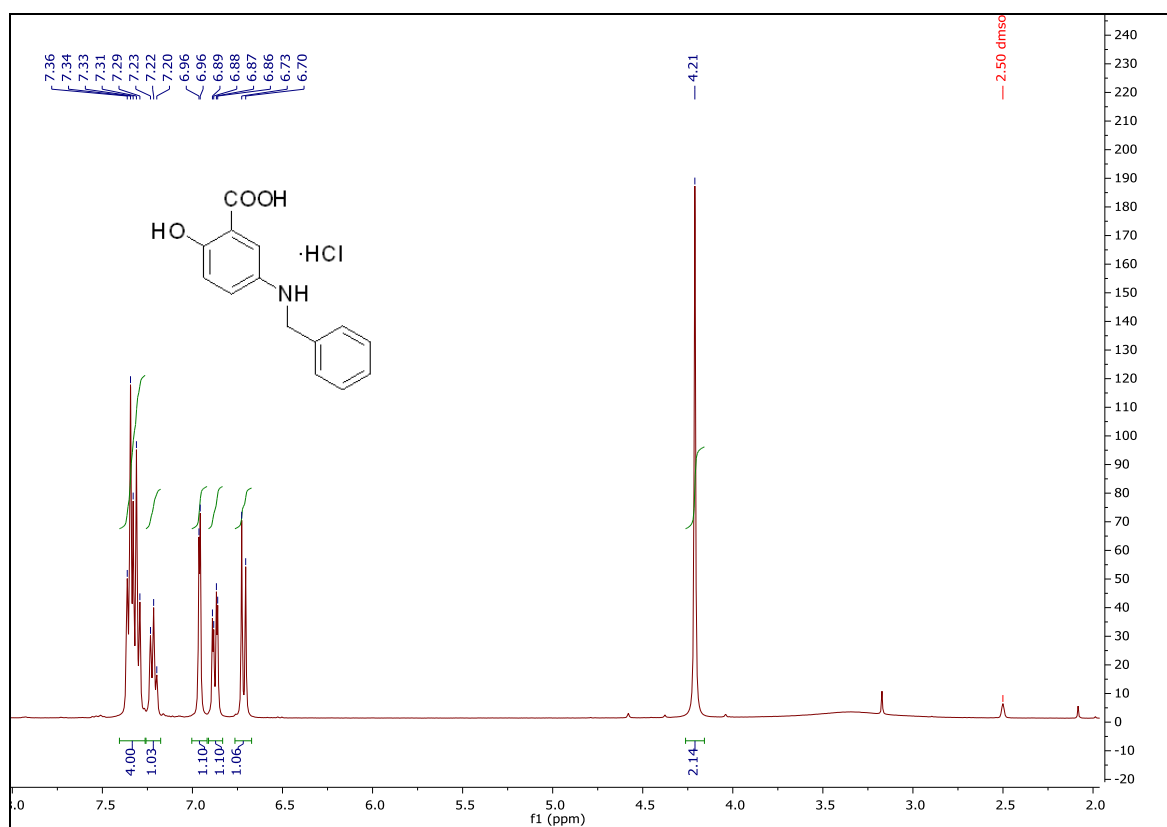
^{13}C spectrum of **MDMG-451** ^1H spectrum of **MDMG-455**

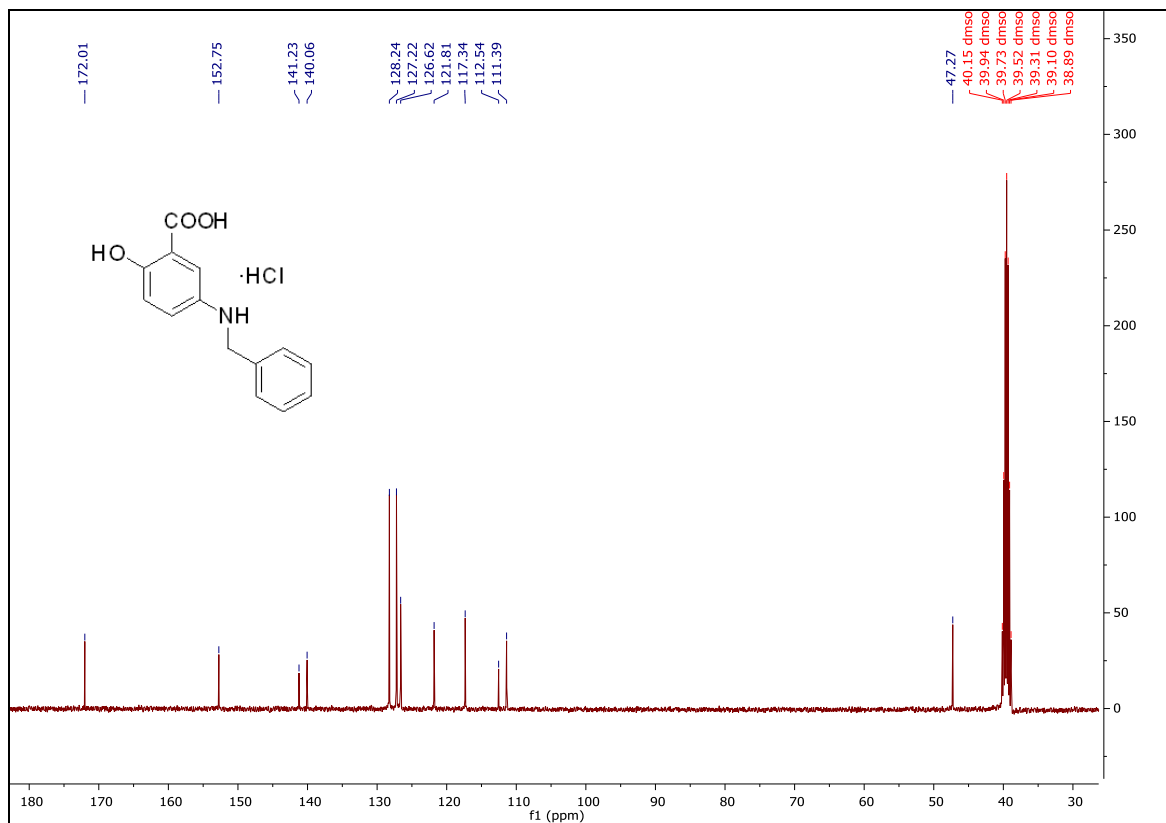
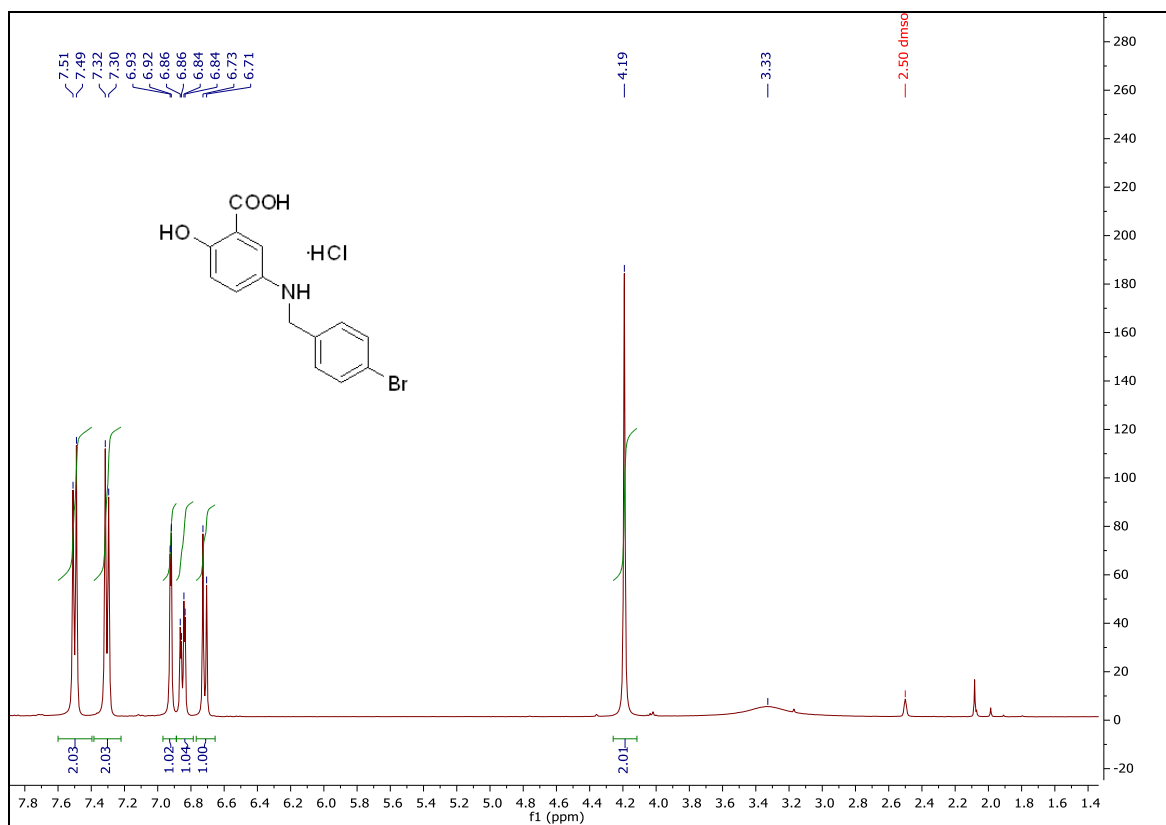
^{13}C spectrum of **MDMG-455** ^1H spectrum of **MDMG-467**

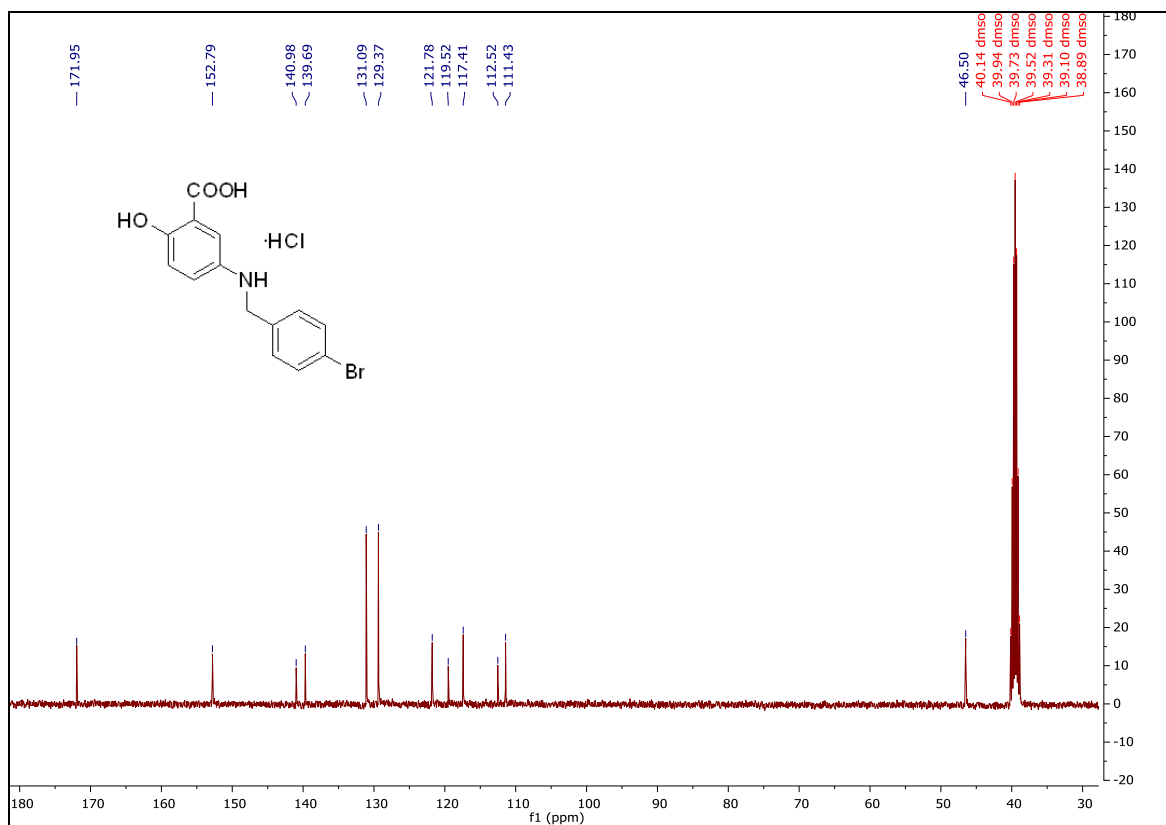
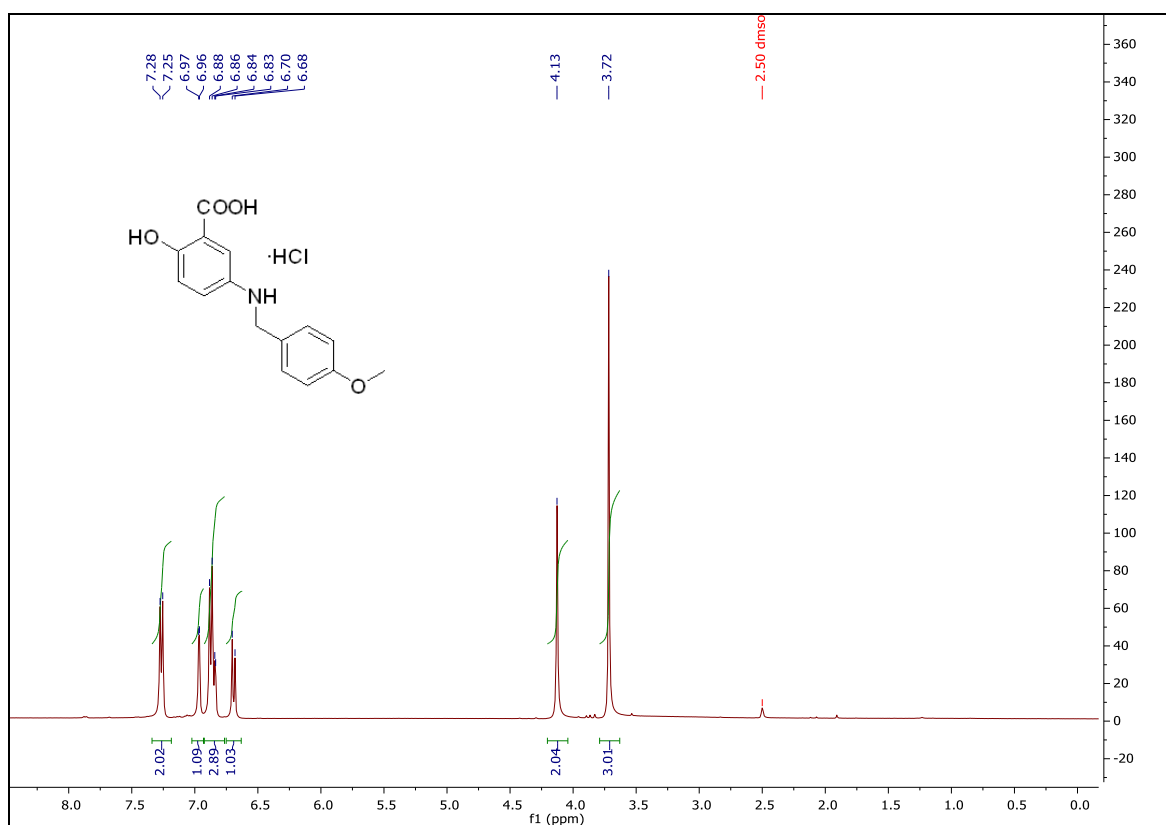
¹H spectrum of **MDMG-491**¹H spectrum of **MDMG-511**

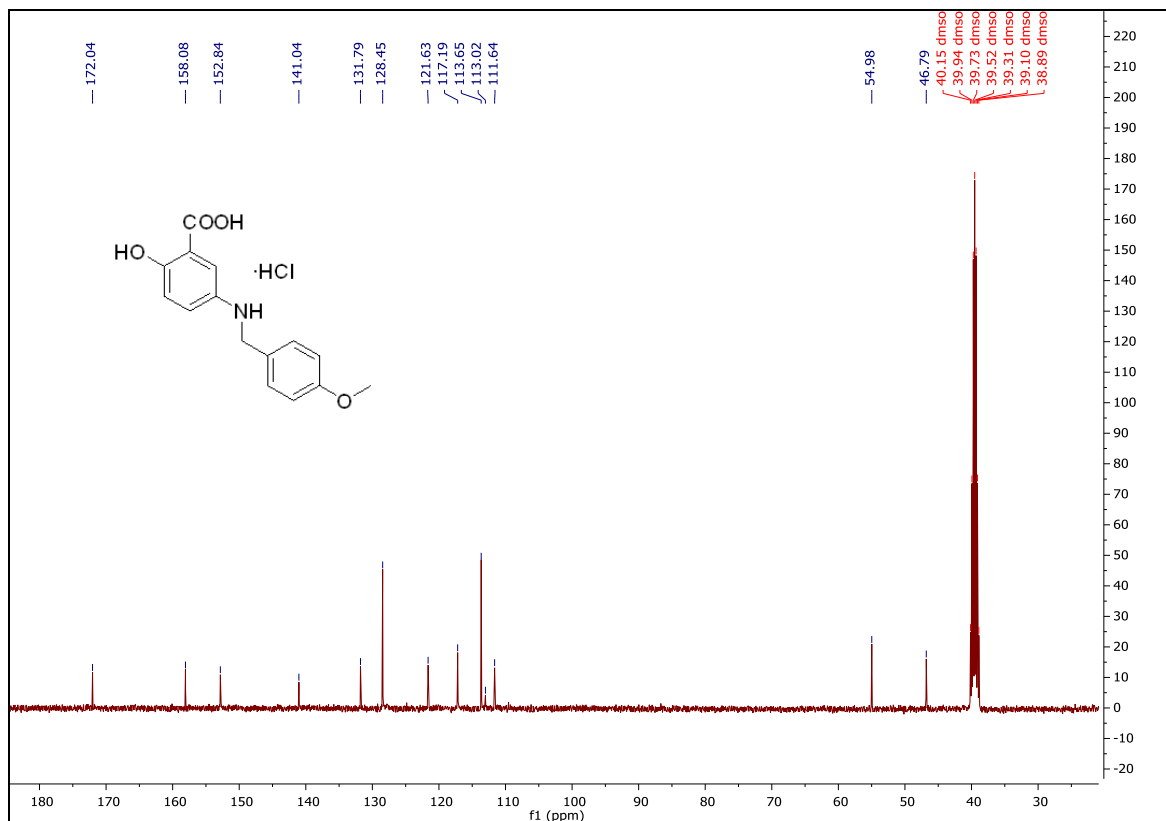
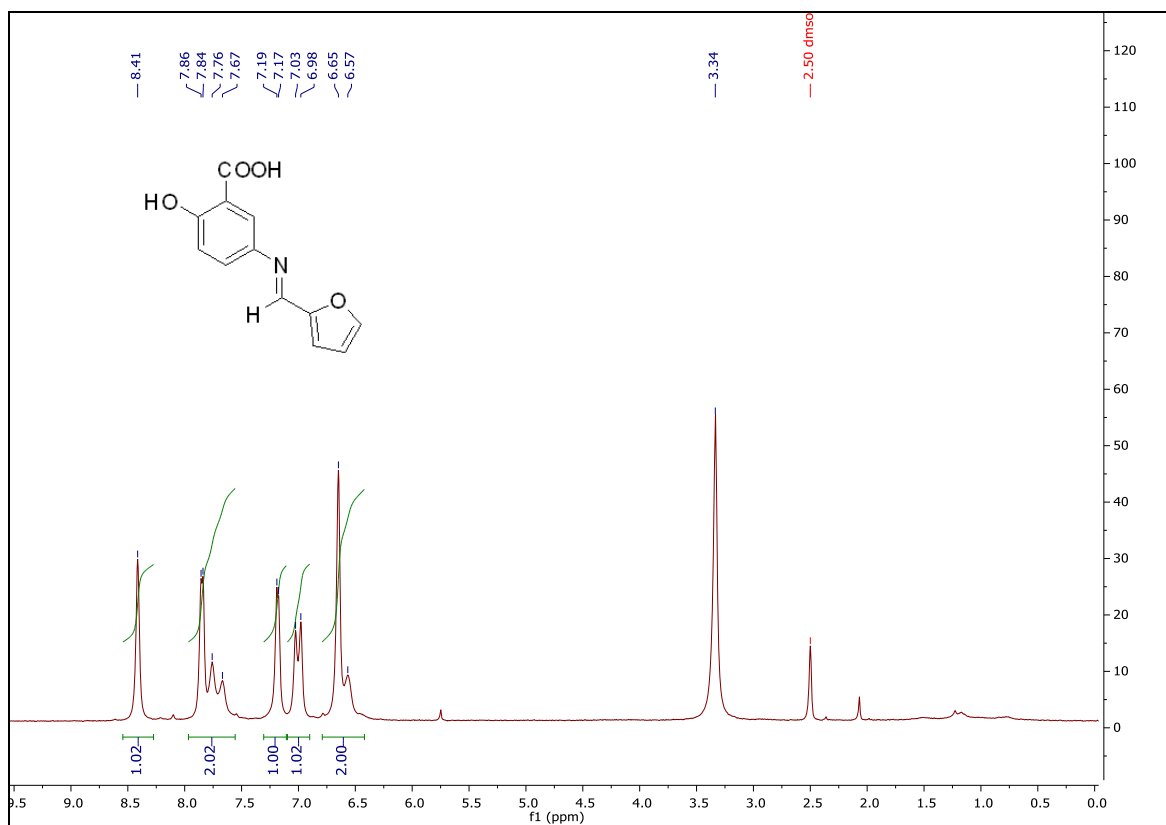
^{13}C spectrum of **MDMG-511** ^1H spectrum of **MDMG-515**

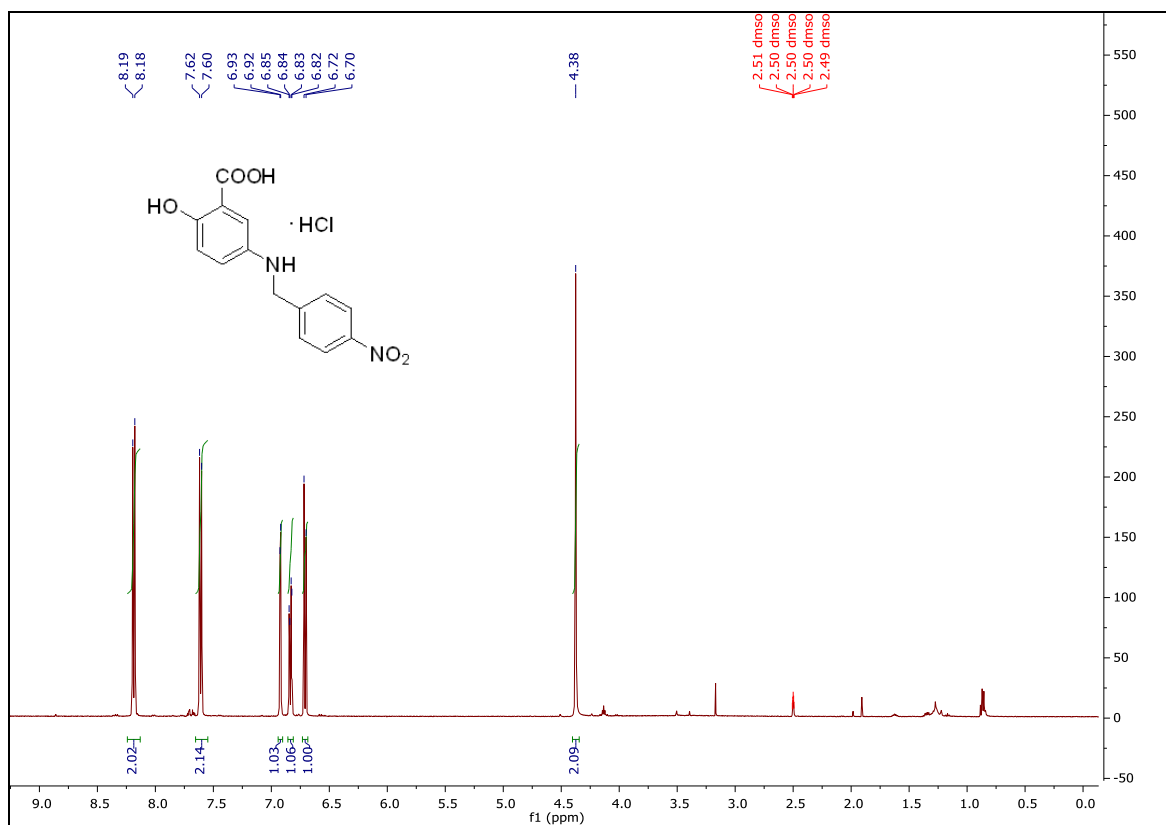
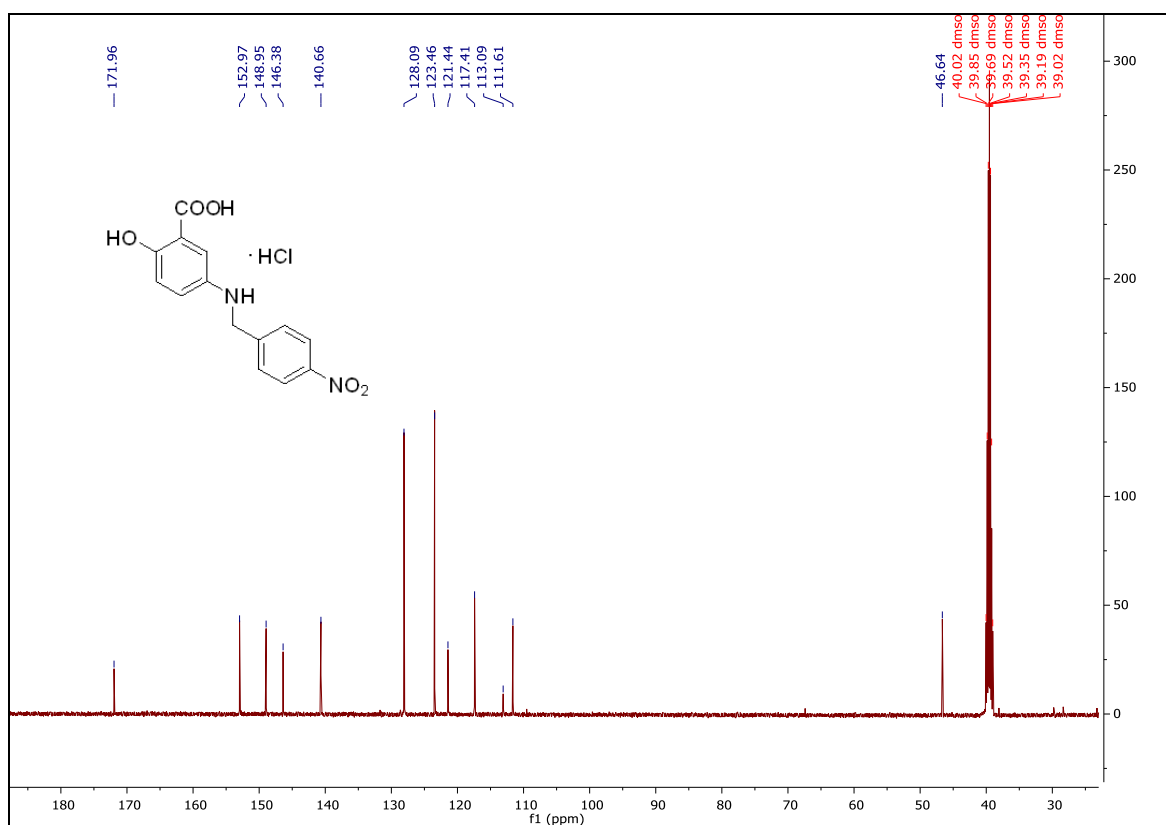
¹³C spectrum of **MDMG-515**¹H spectrum of **MDMG-540**

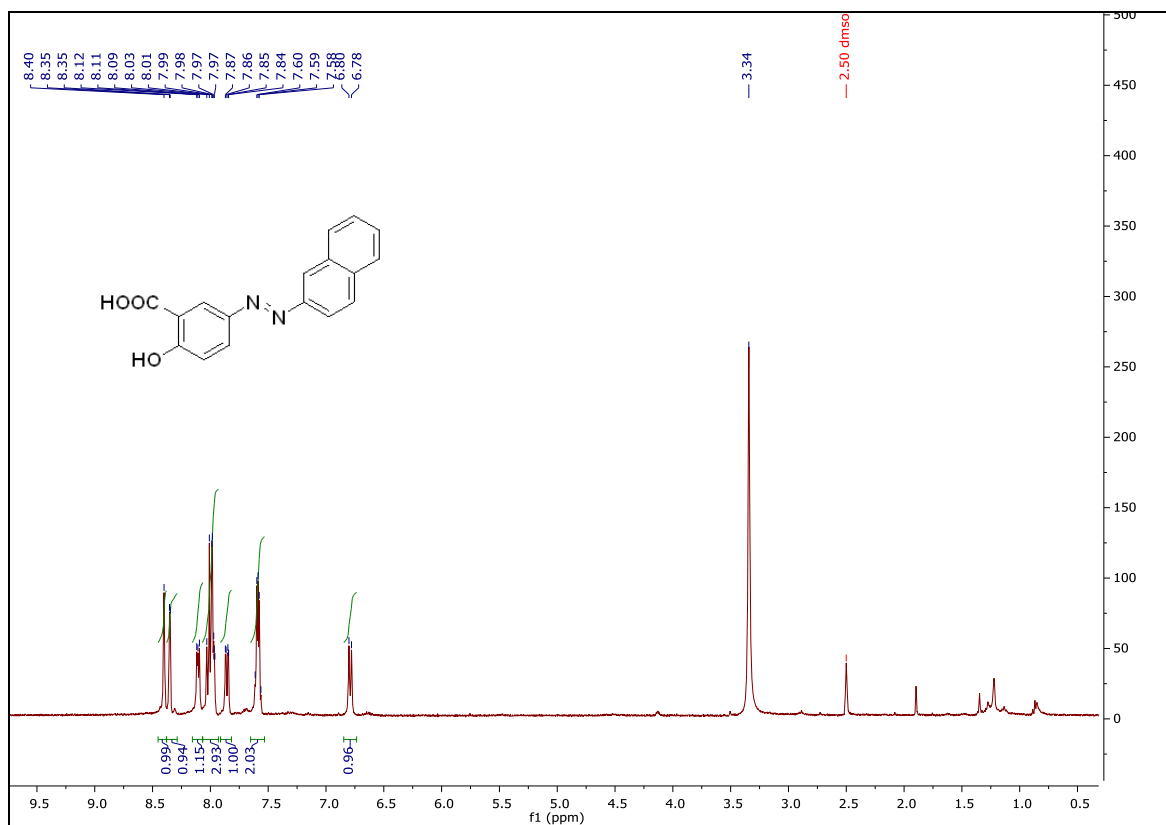
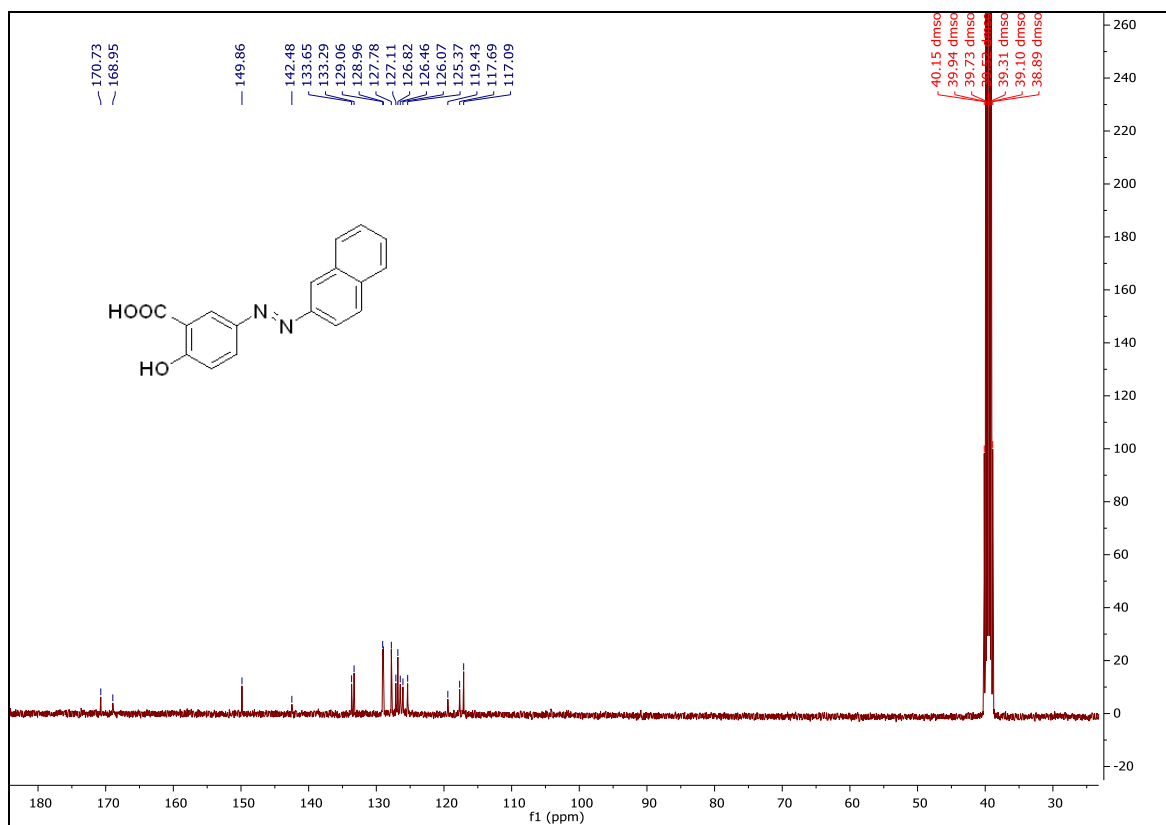
^{13}C spectrum of **MDMG-540** ^1H spectrum of **MDMG-560**

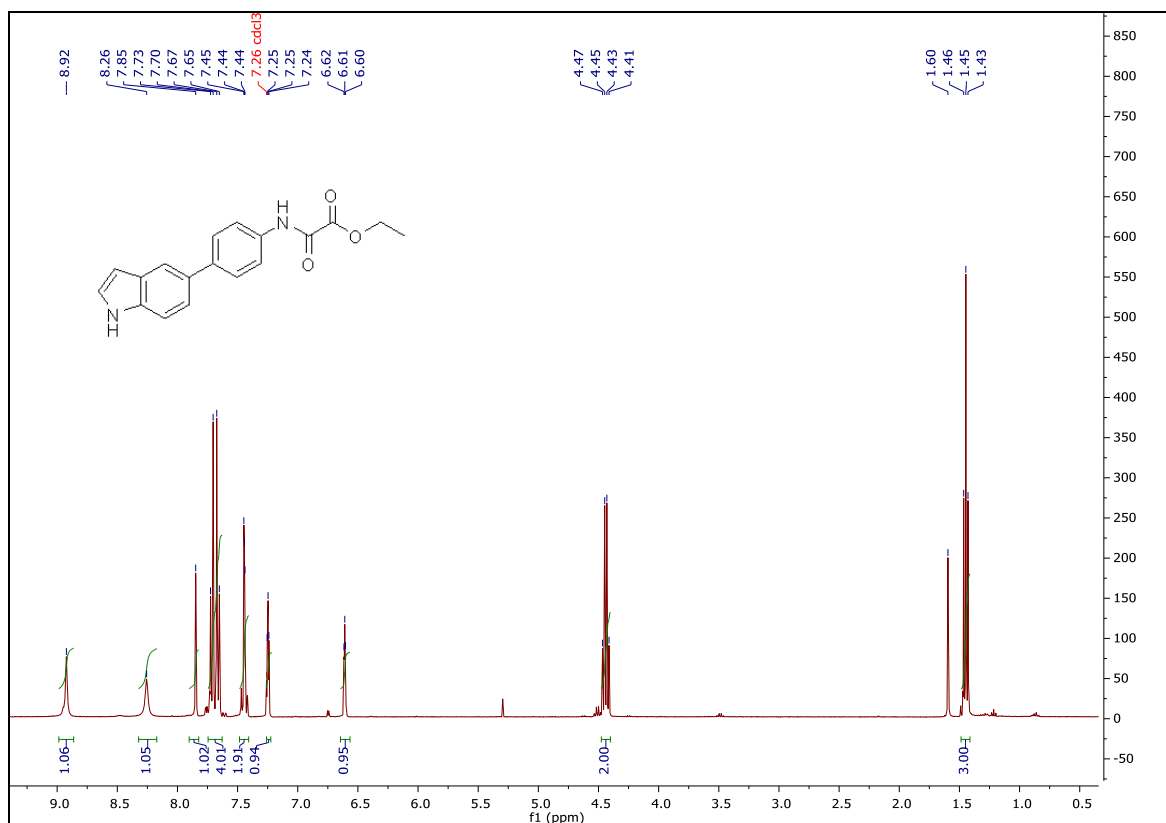
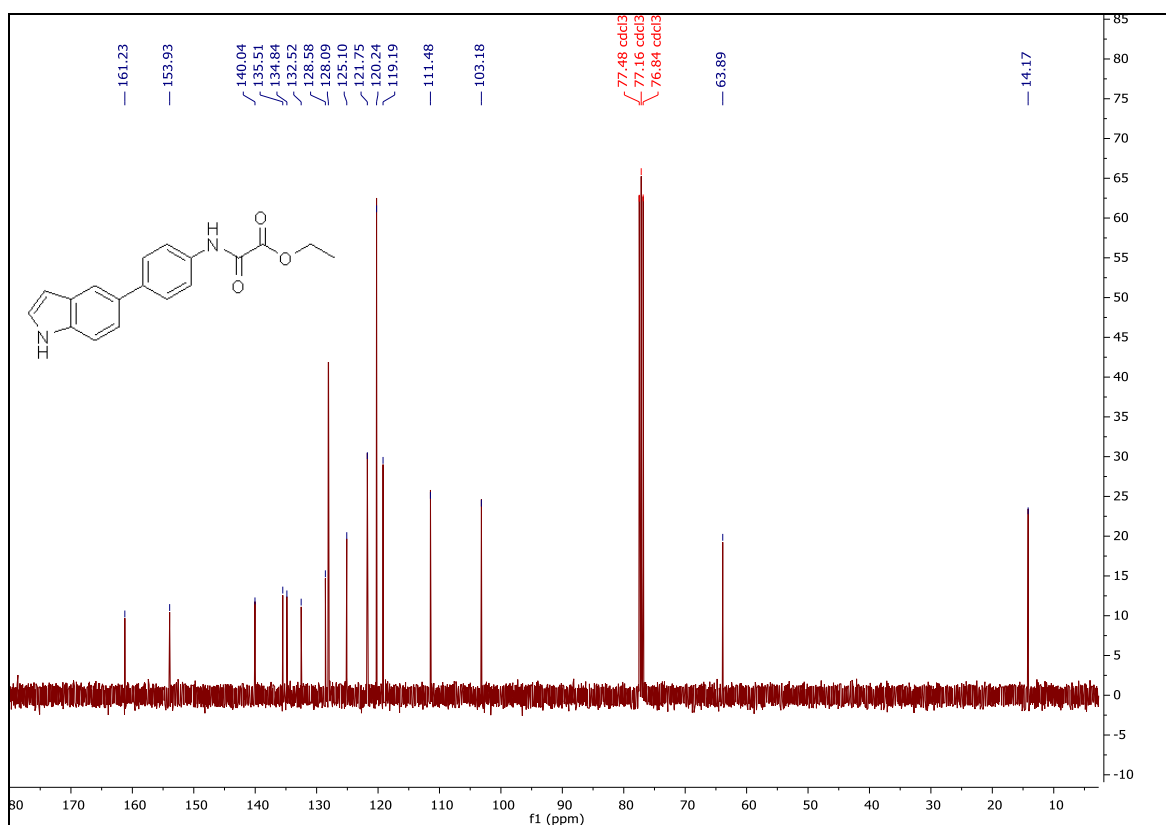
^{13}C spectrum of **MDMG-560** ^1H spectrum of **MDMG-566**

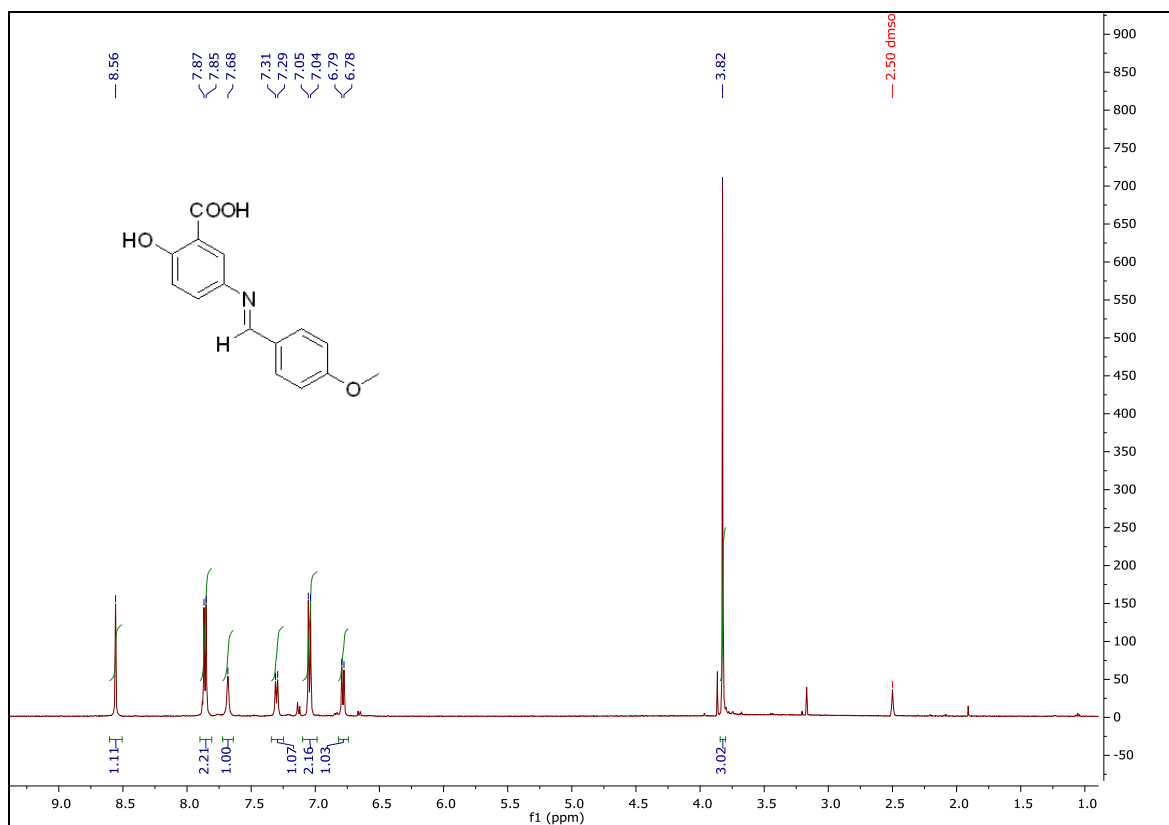
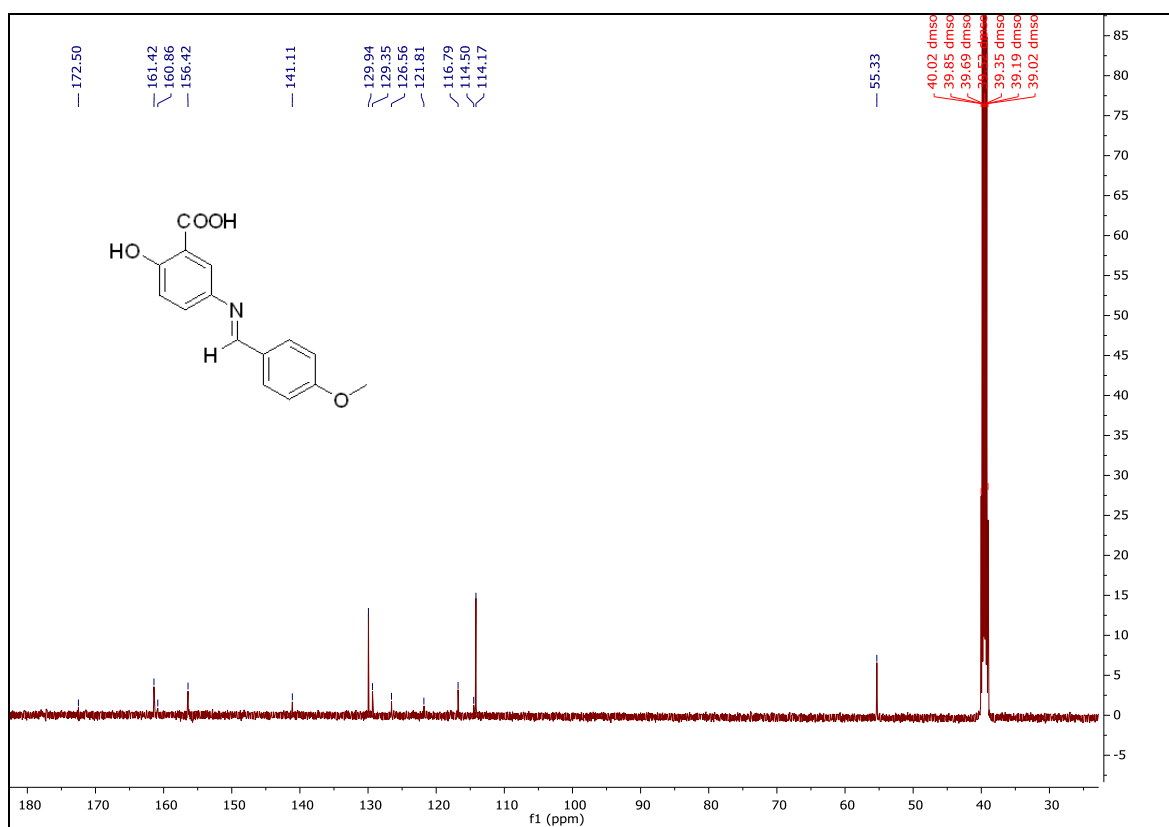
^{13}C spectrum of **MDMG-566** ^1H spectrum of **MDMG-570**

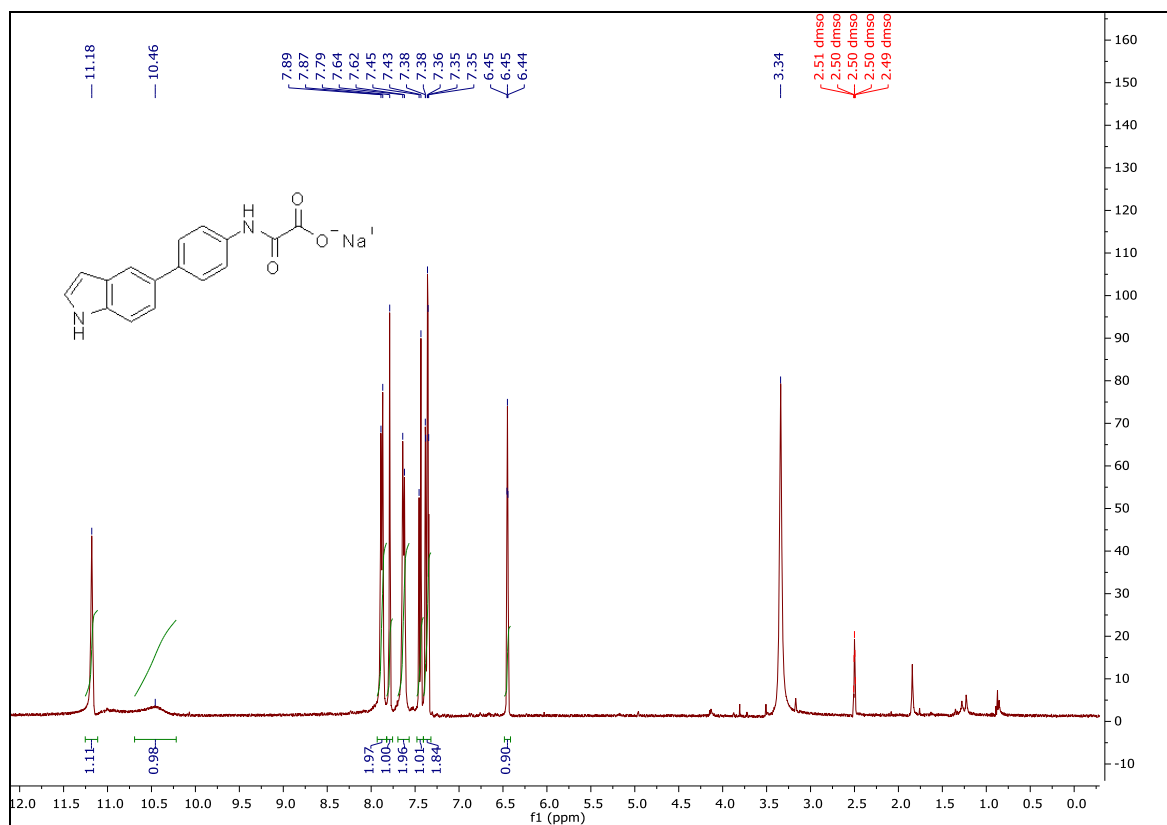
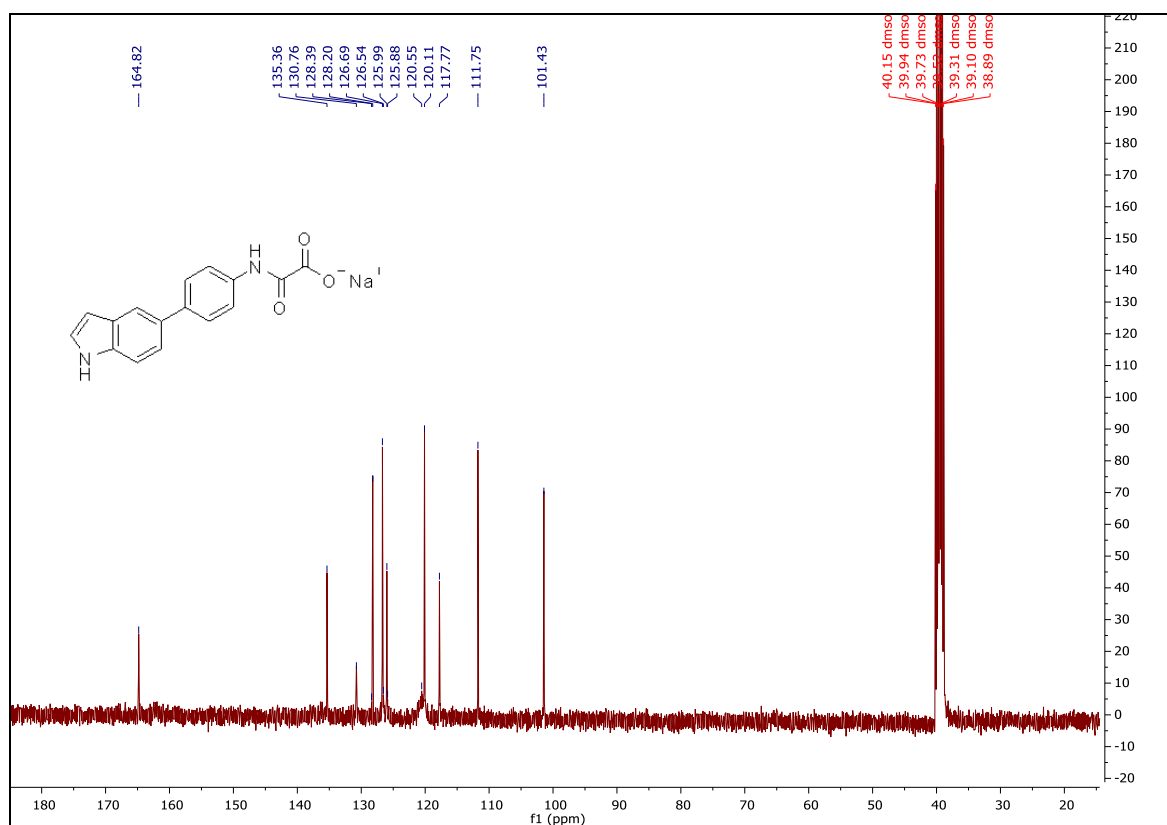
^{13}C spectrum of **MDMG-570** ^1H spectrum of **MDMG-574**

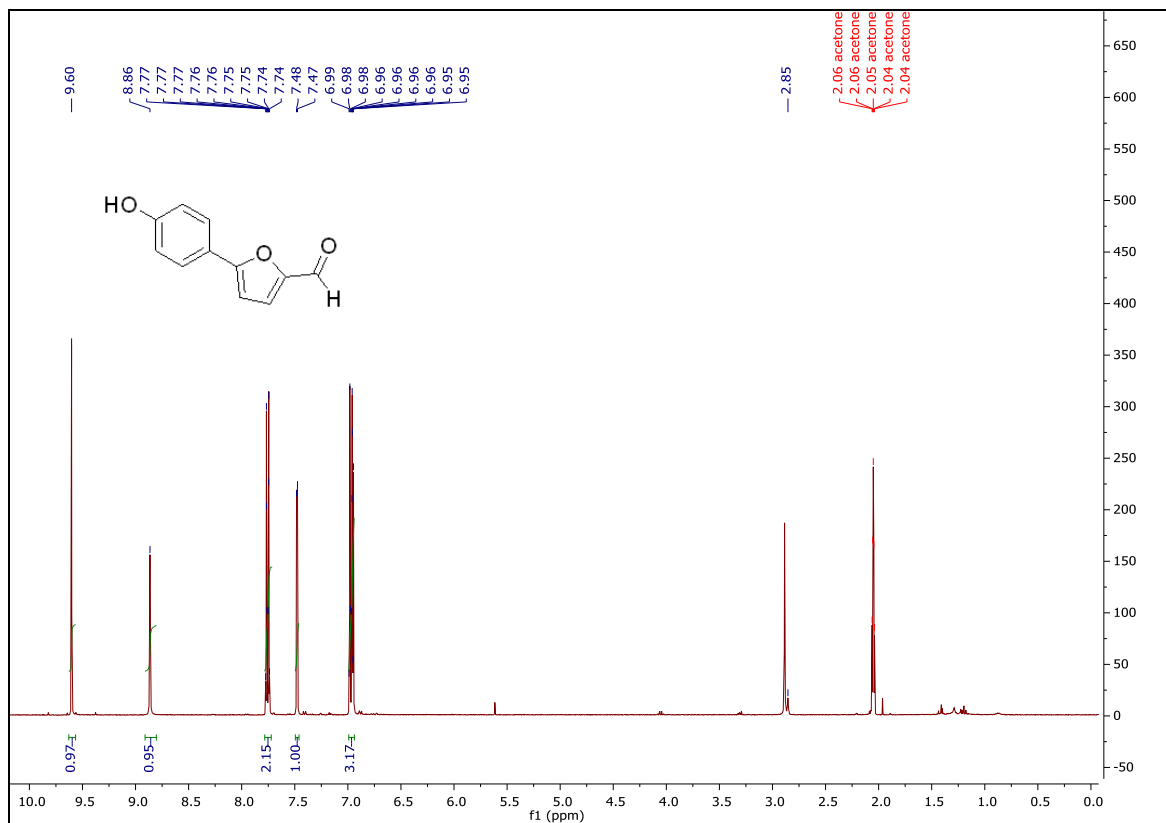
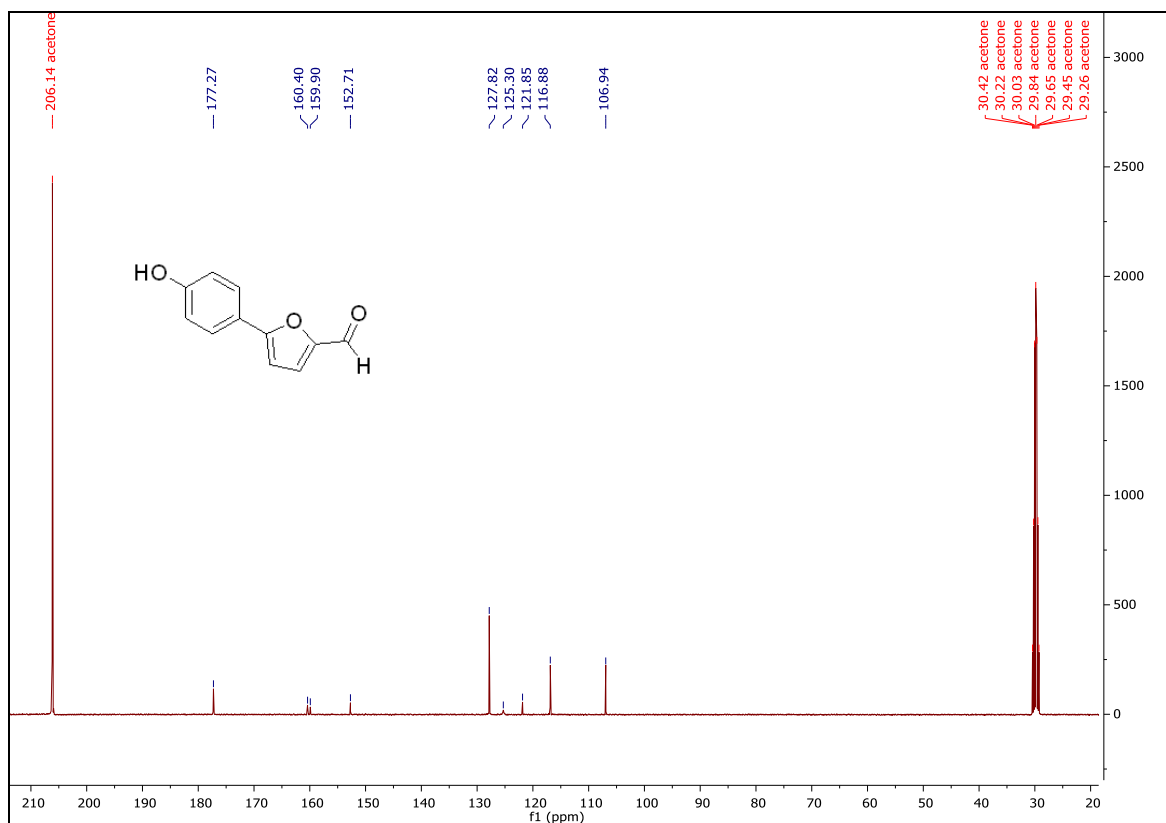
¹H spectrum of **MDMG-592**¹³C spectrum of **MDMG-592**

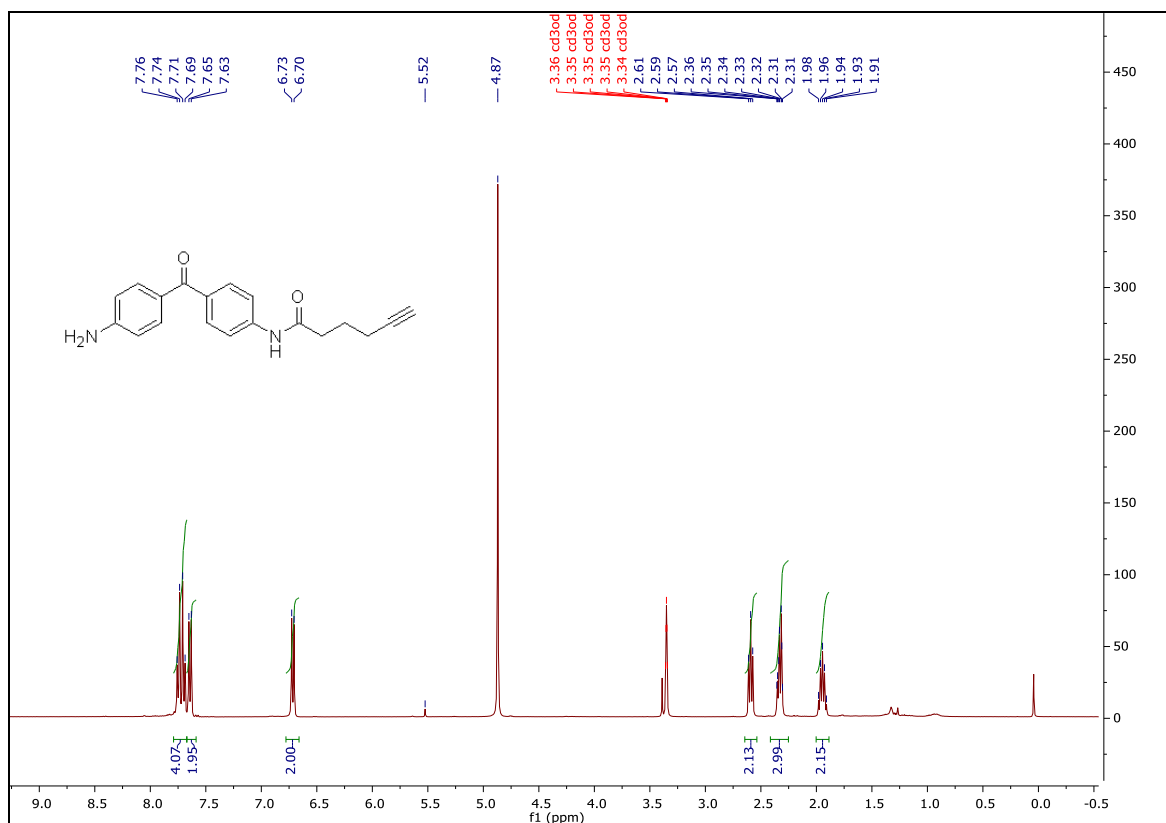
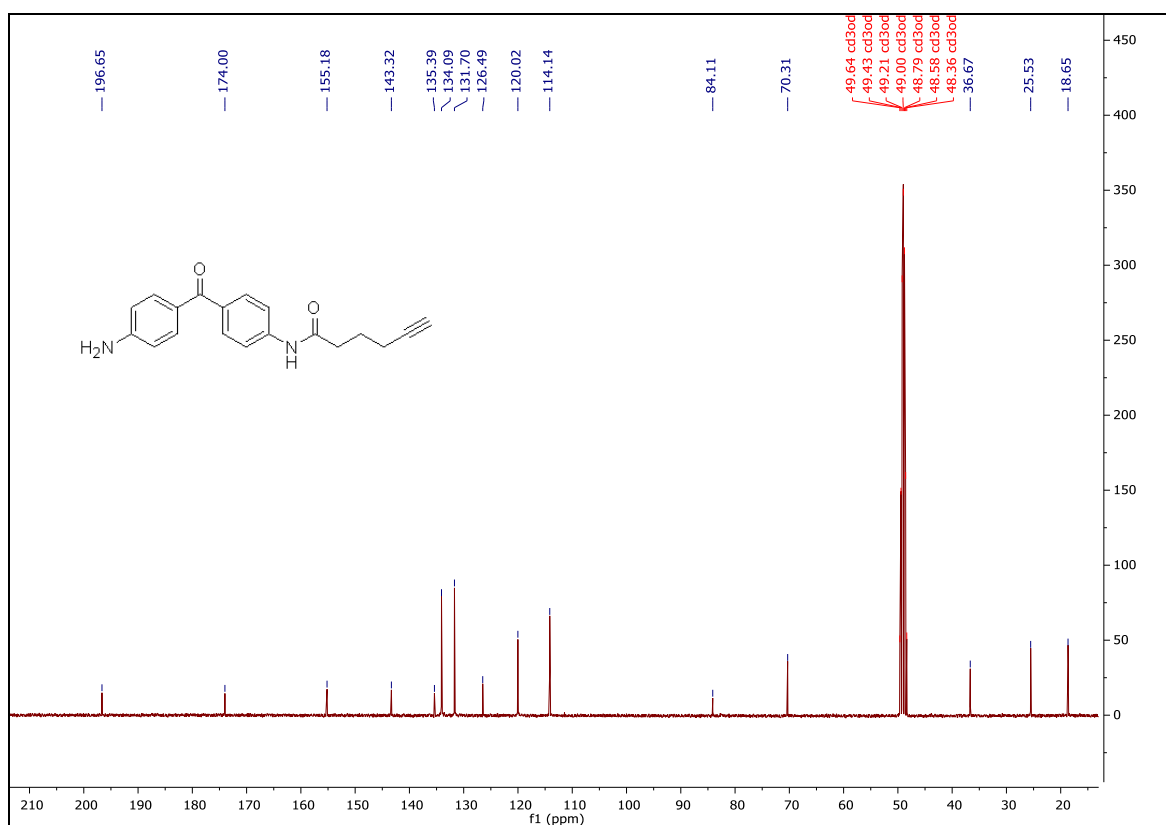
¹H spectrum of **MDMG-604**¹³C spectrum of **MDMG-604**

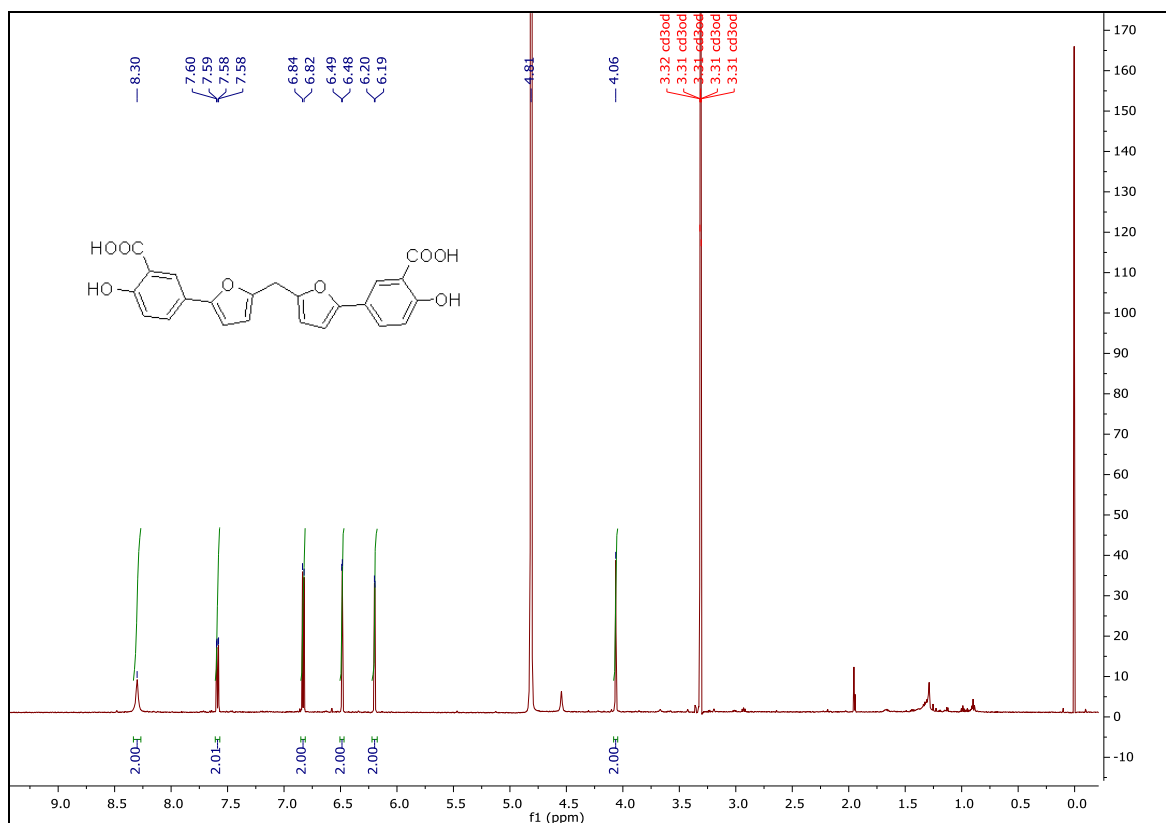
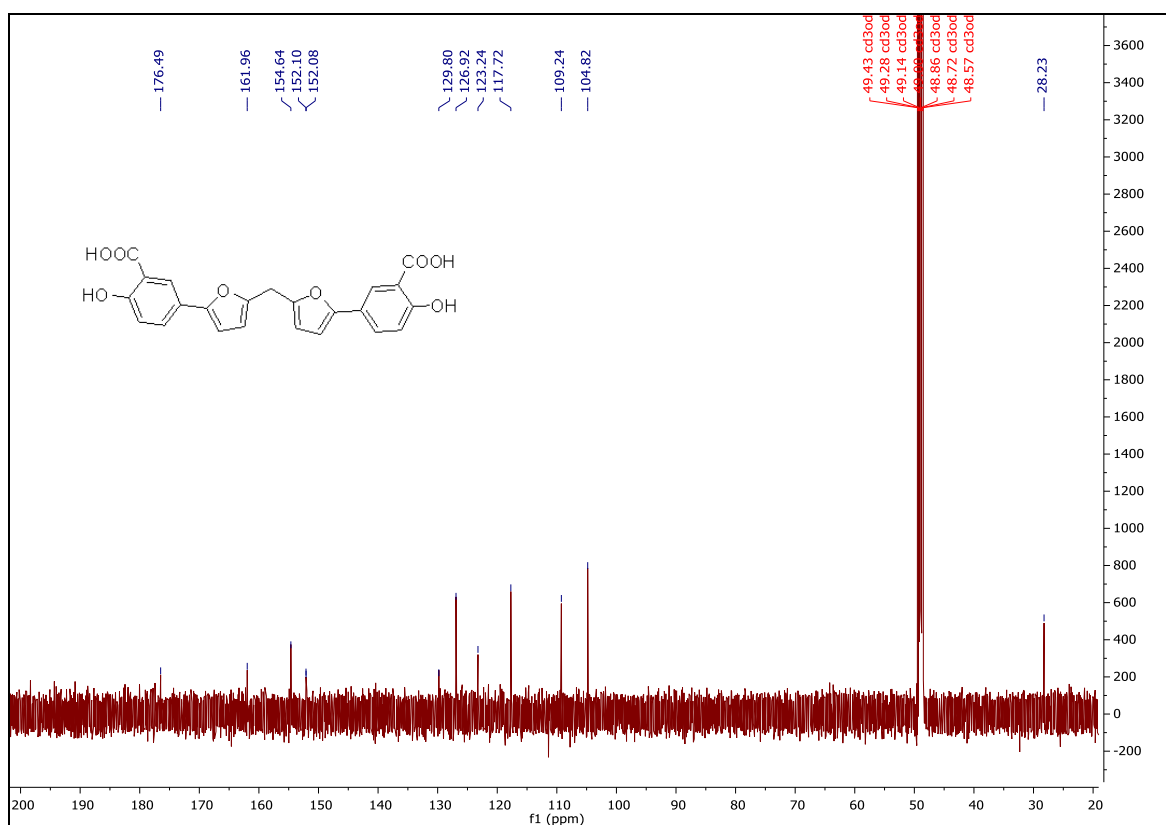
¹H spectrum of MDMG-620¹³C spectrum of MDMG-620

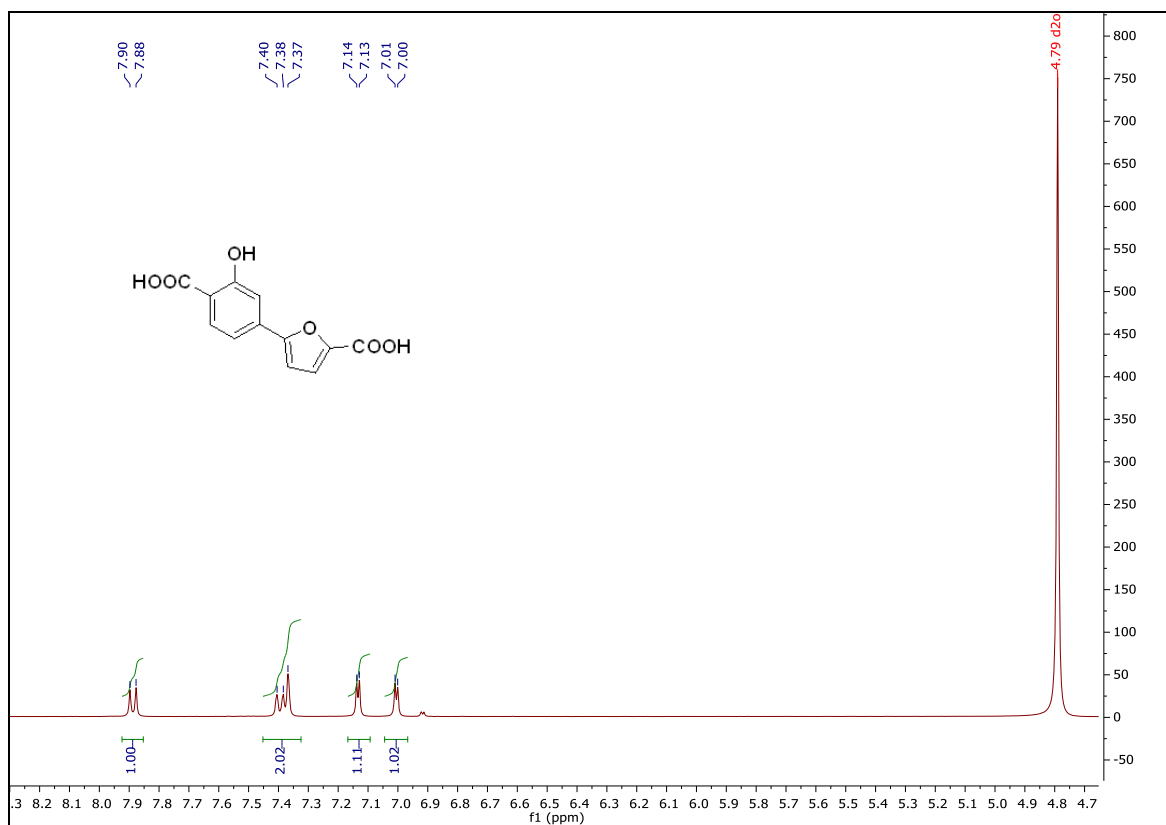
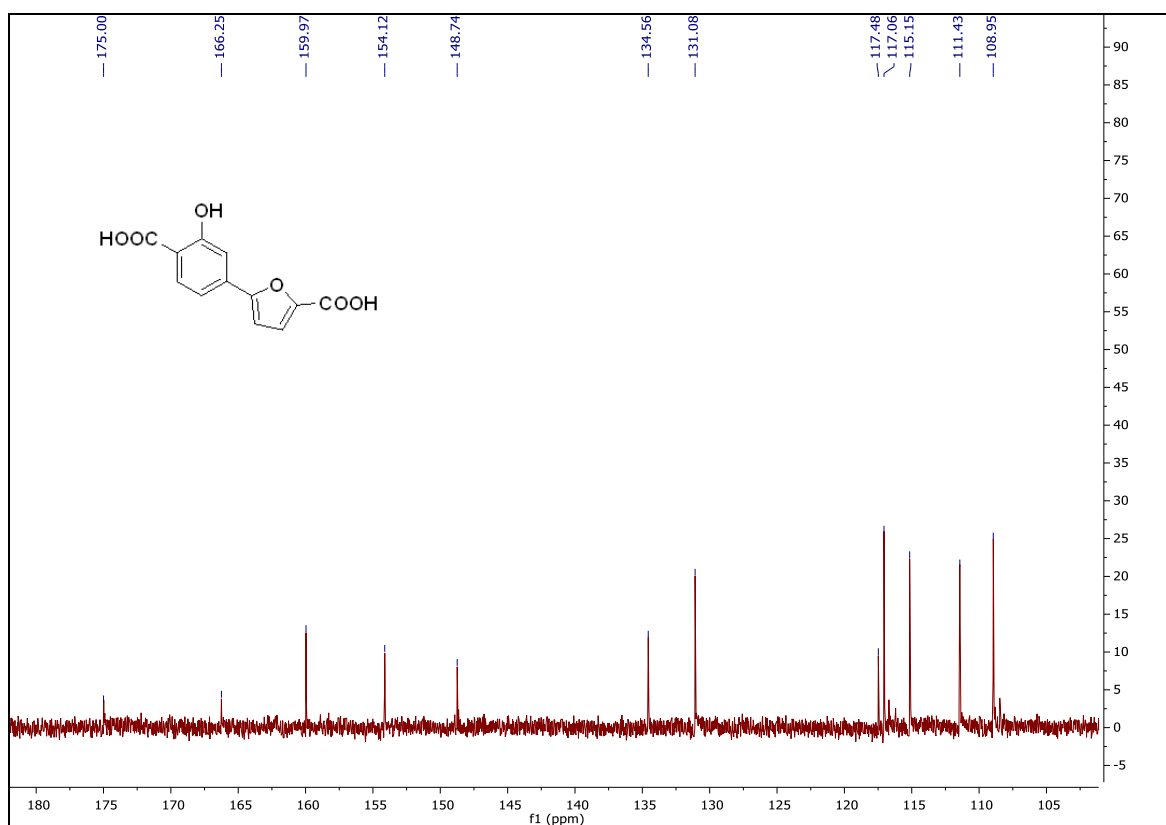
¹H spectrum of **MDMG-628**¹³C spectrum of **MDMG-628**

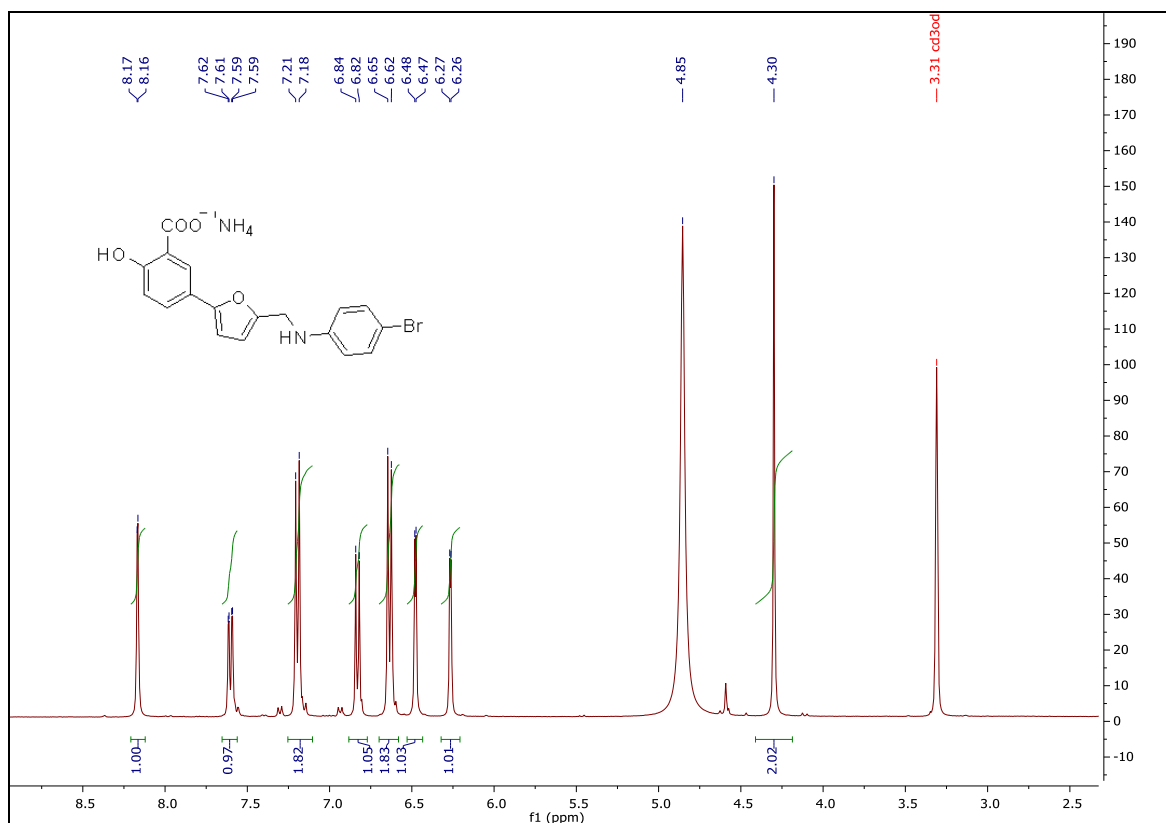
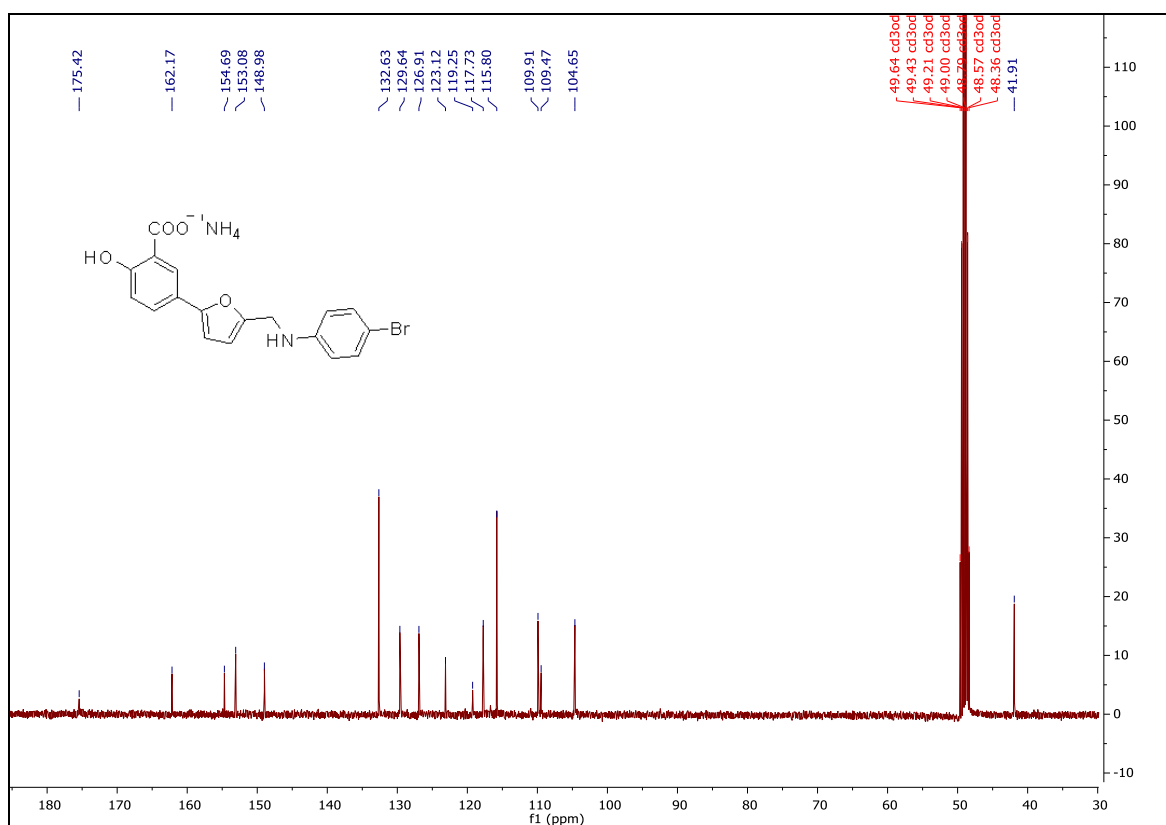
¹H spectrum of **MDMG-632**¹³C spectrum of **MDMG-632**

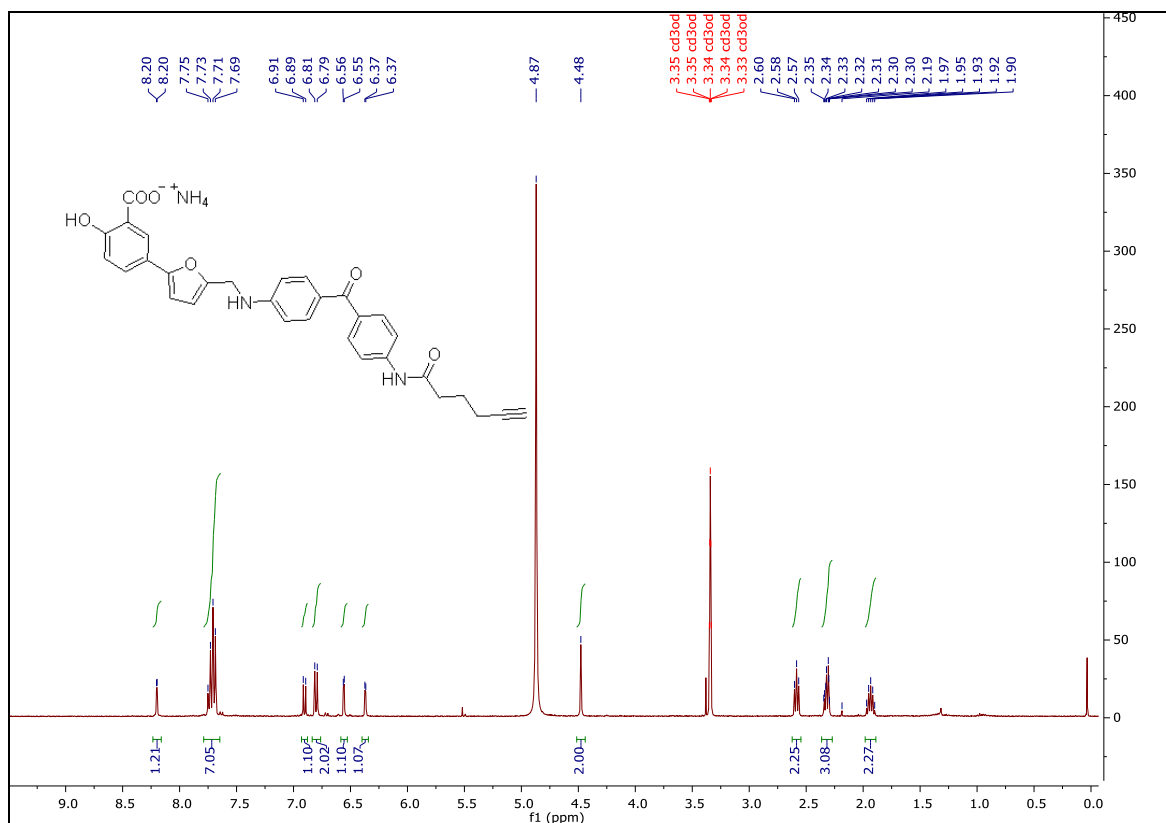
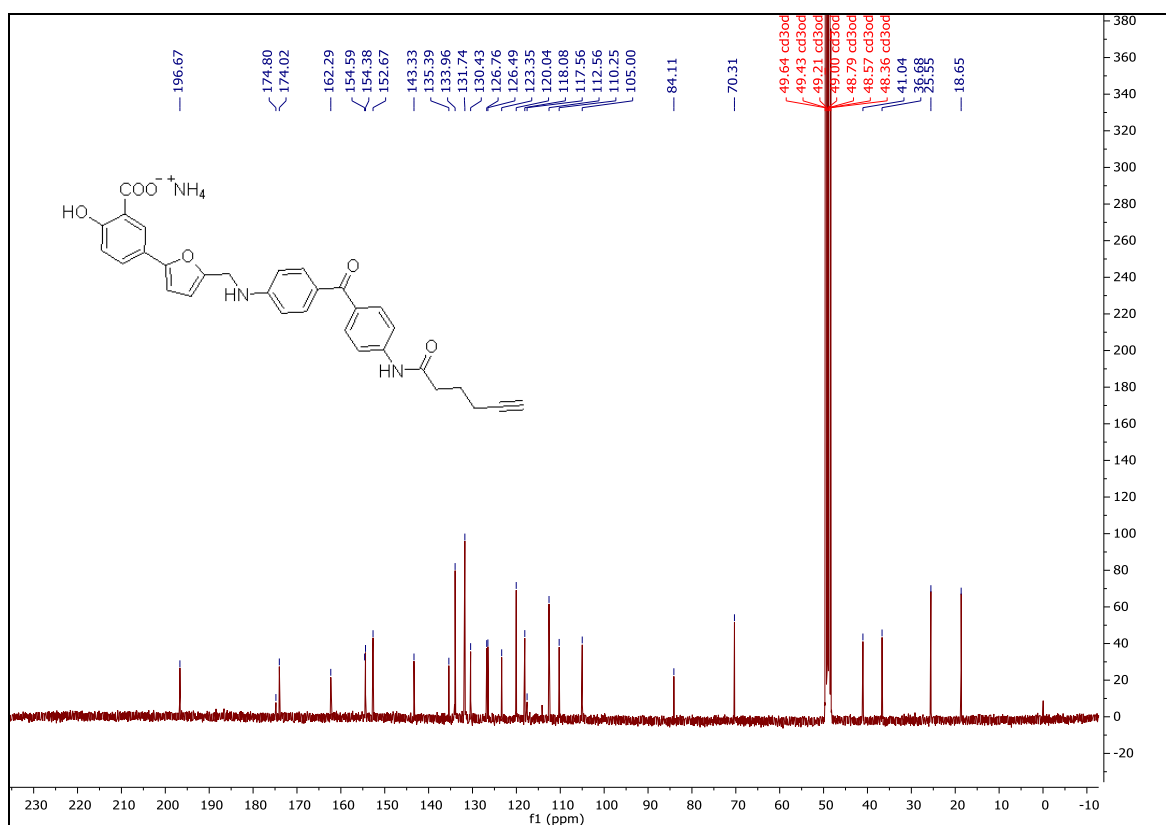
¹H spectrum of **MDMG-672**¹³C spectrum of **MDMG-672**

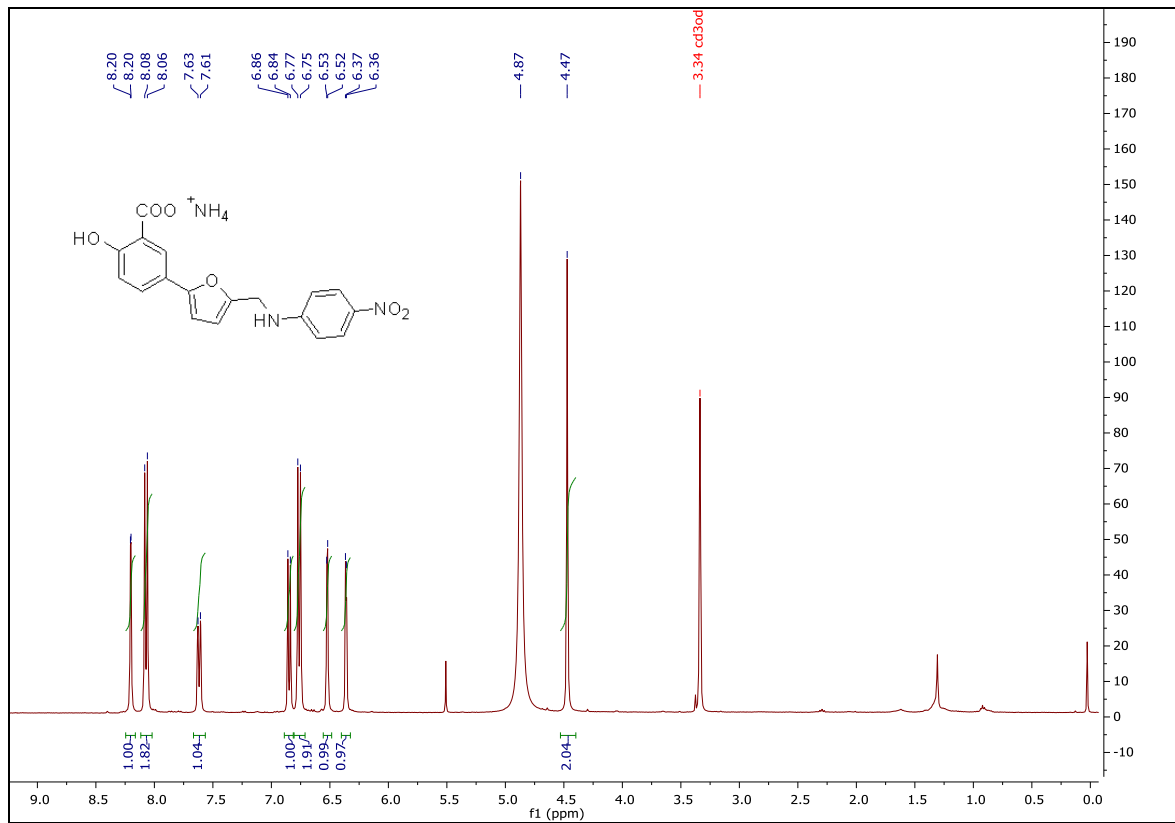
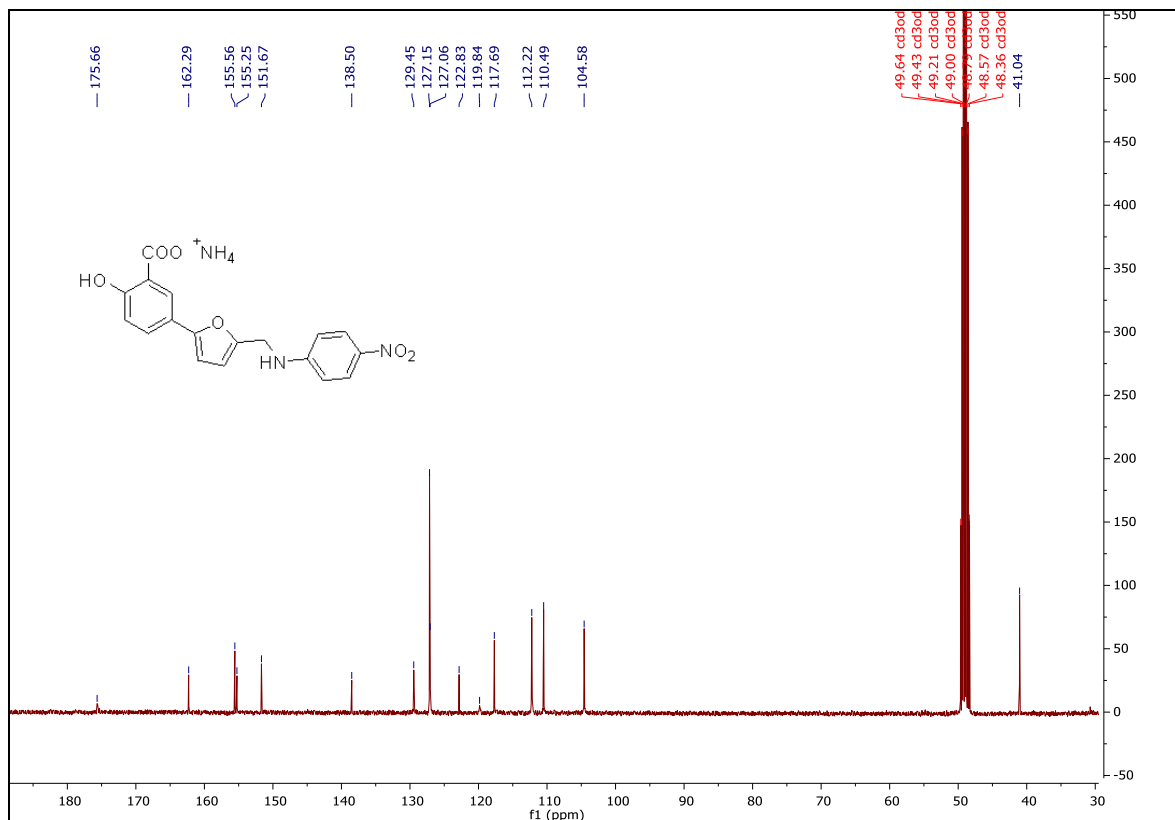
¹H spectrum of **MDMG-741**¹³C spectrum of **MDMG-741**

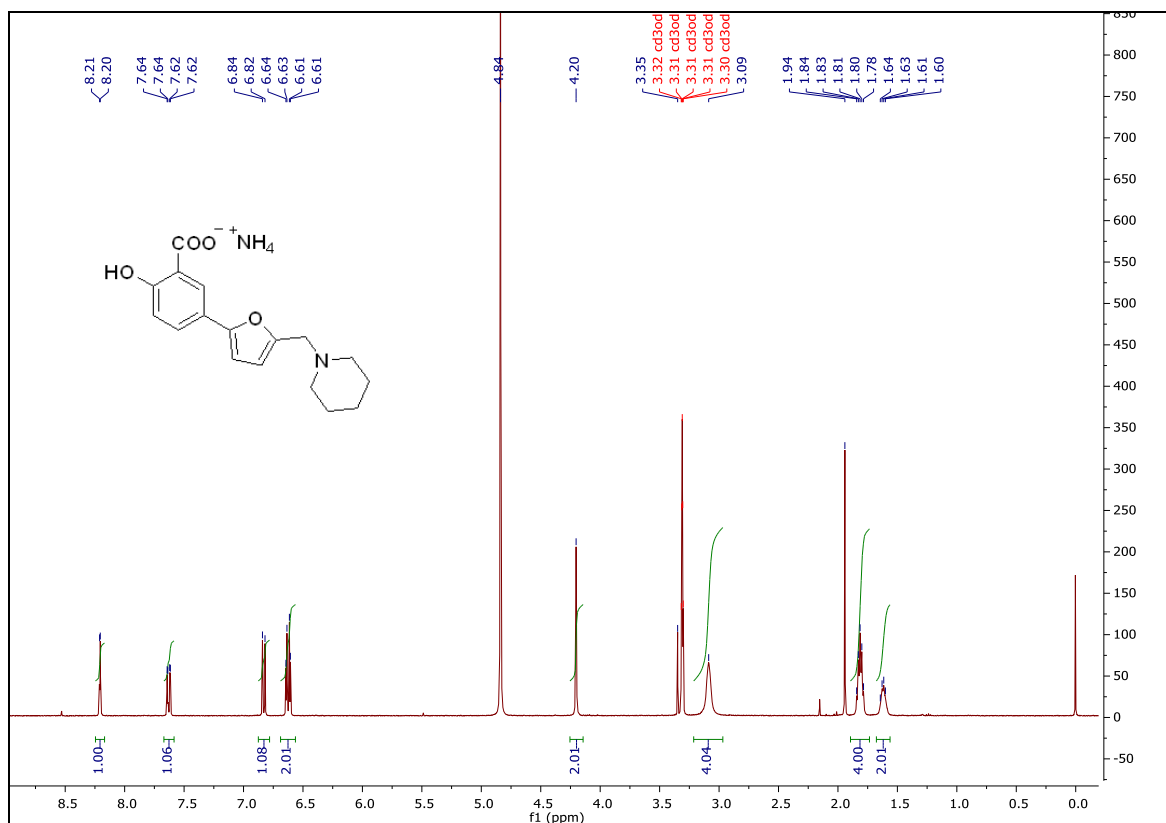
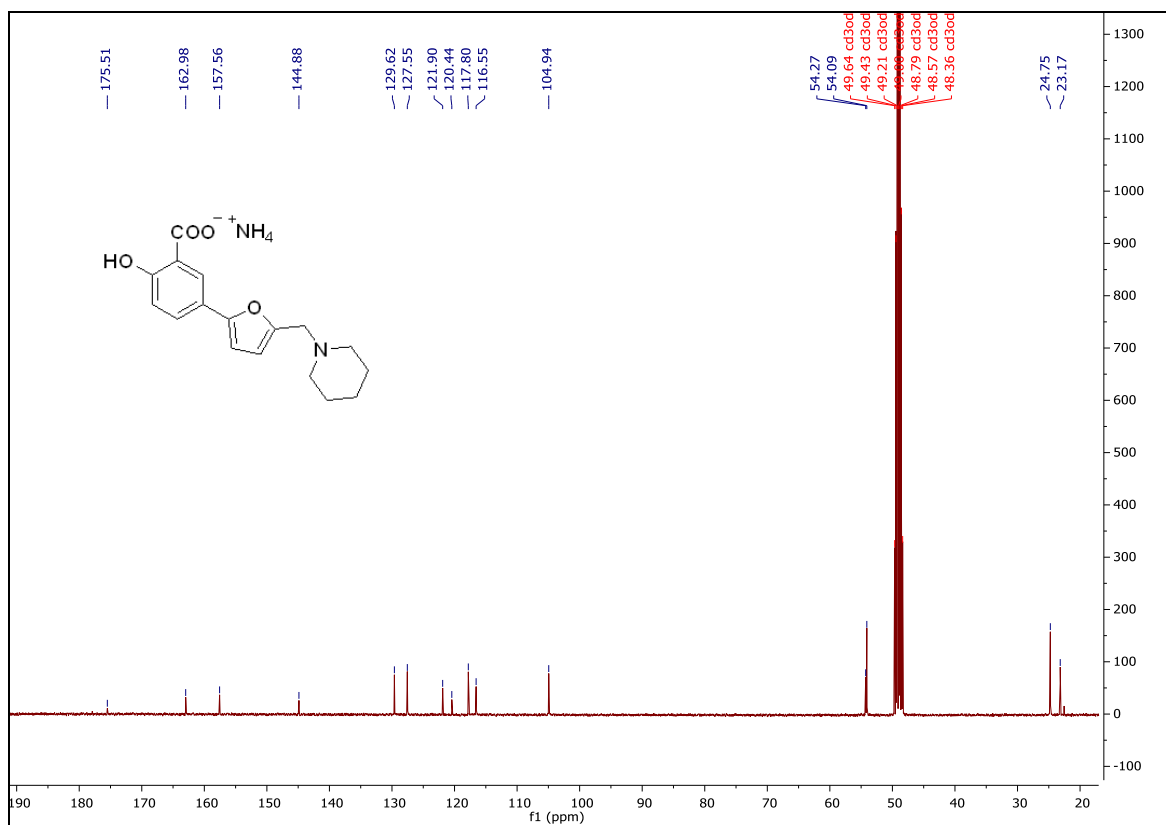
¹H spectrum of **MDMG-825**¹³C spectrum of **MDMG-825**

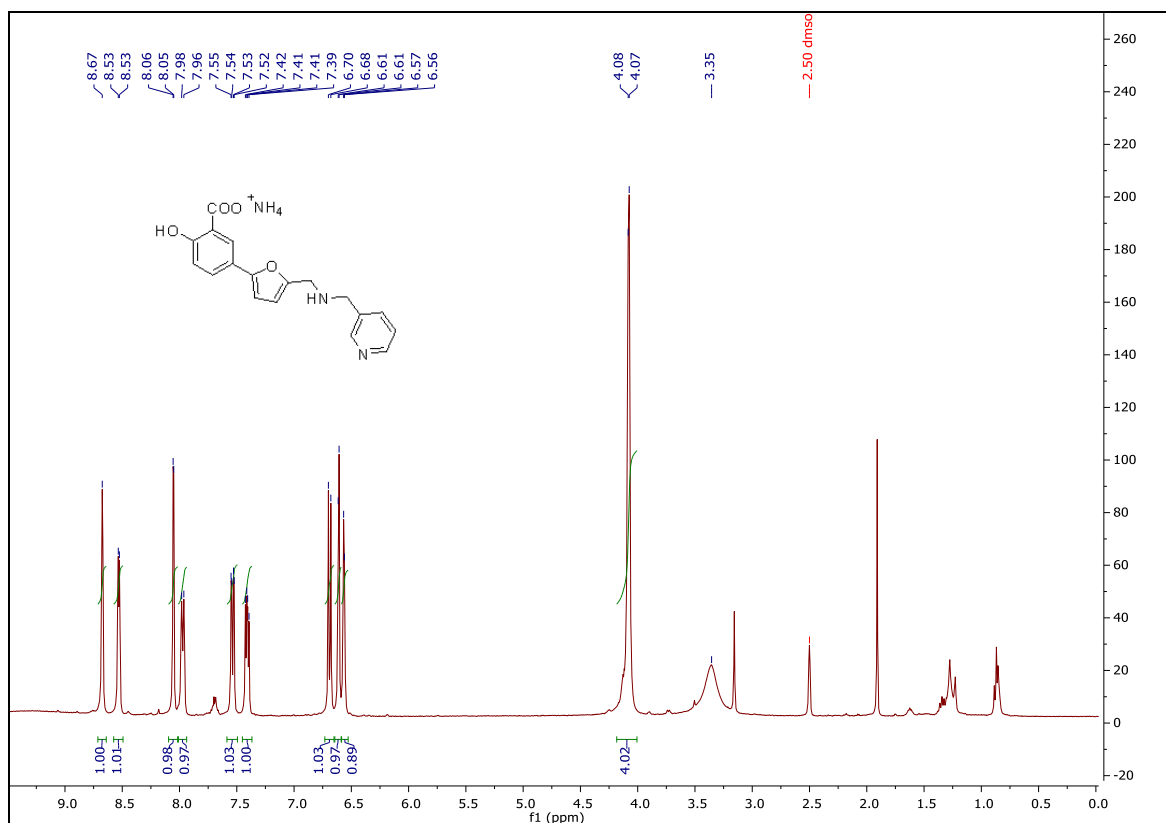
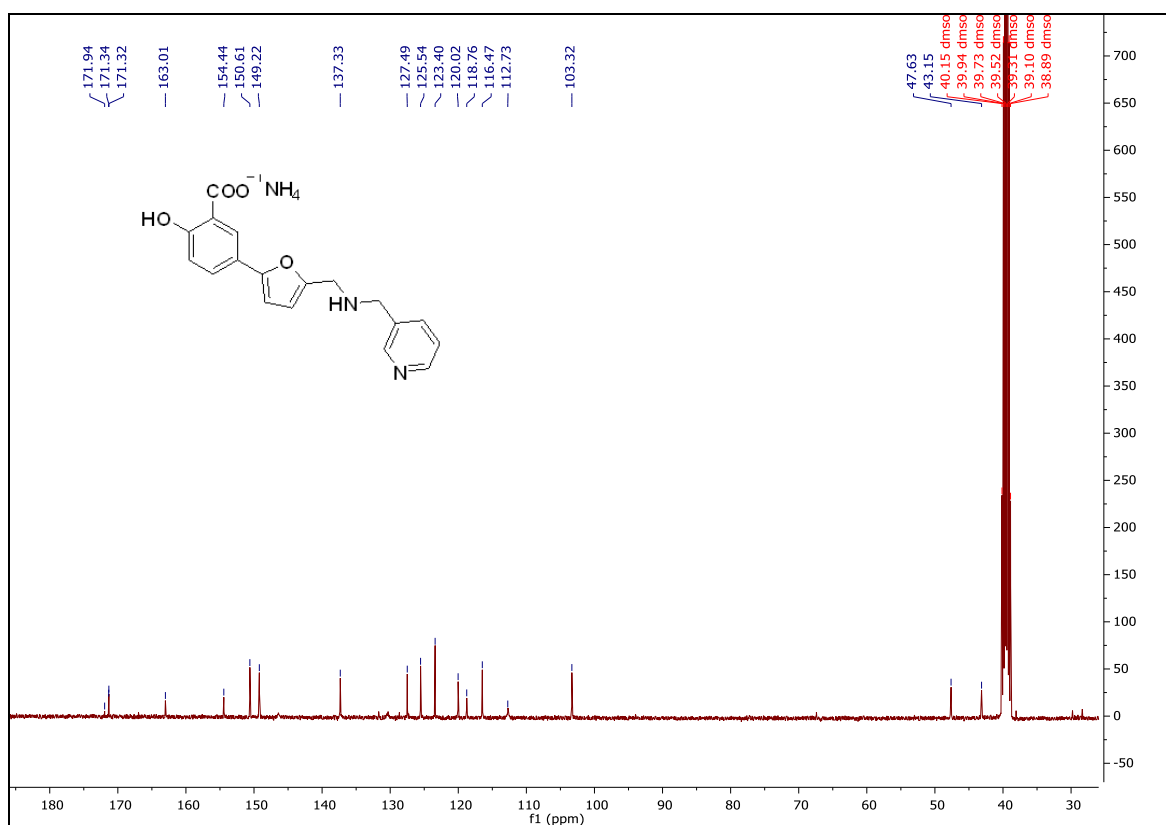
¹H spectrum of **MDMG-883**¹³C spectrum of **MDMG-883**

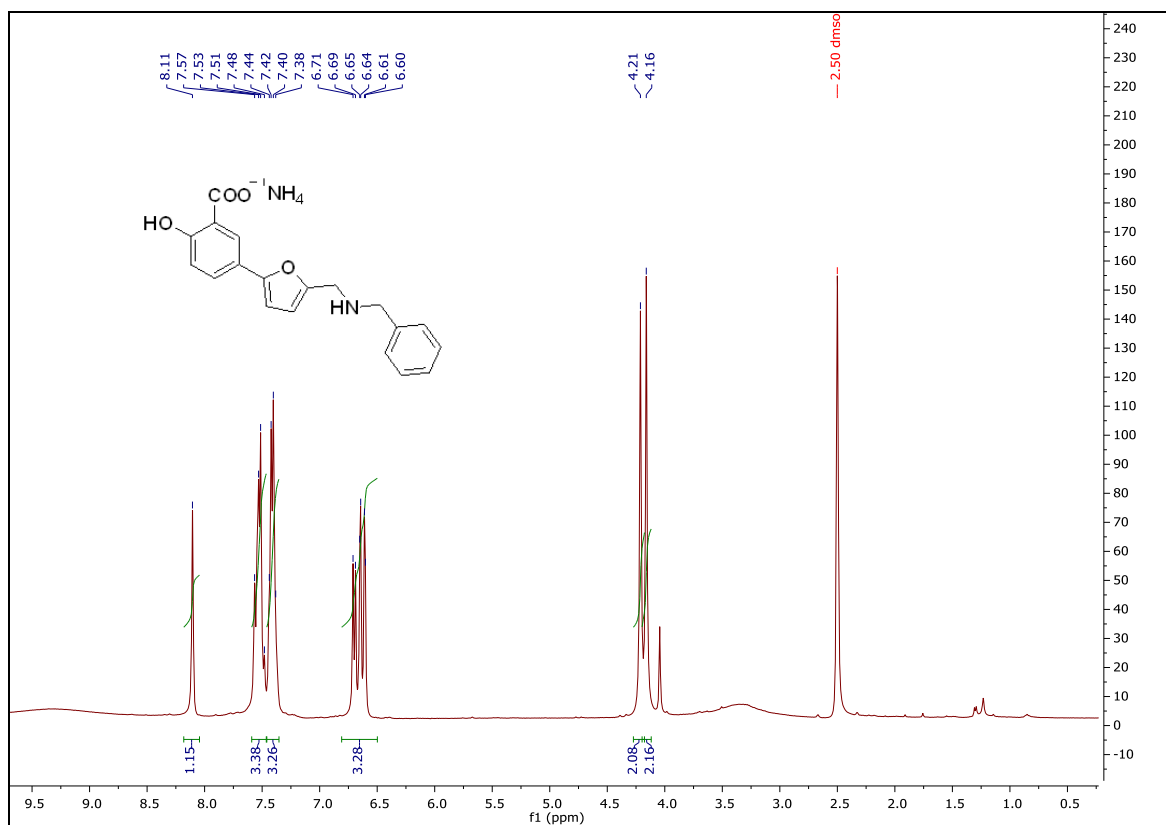
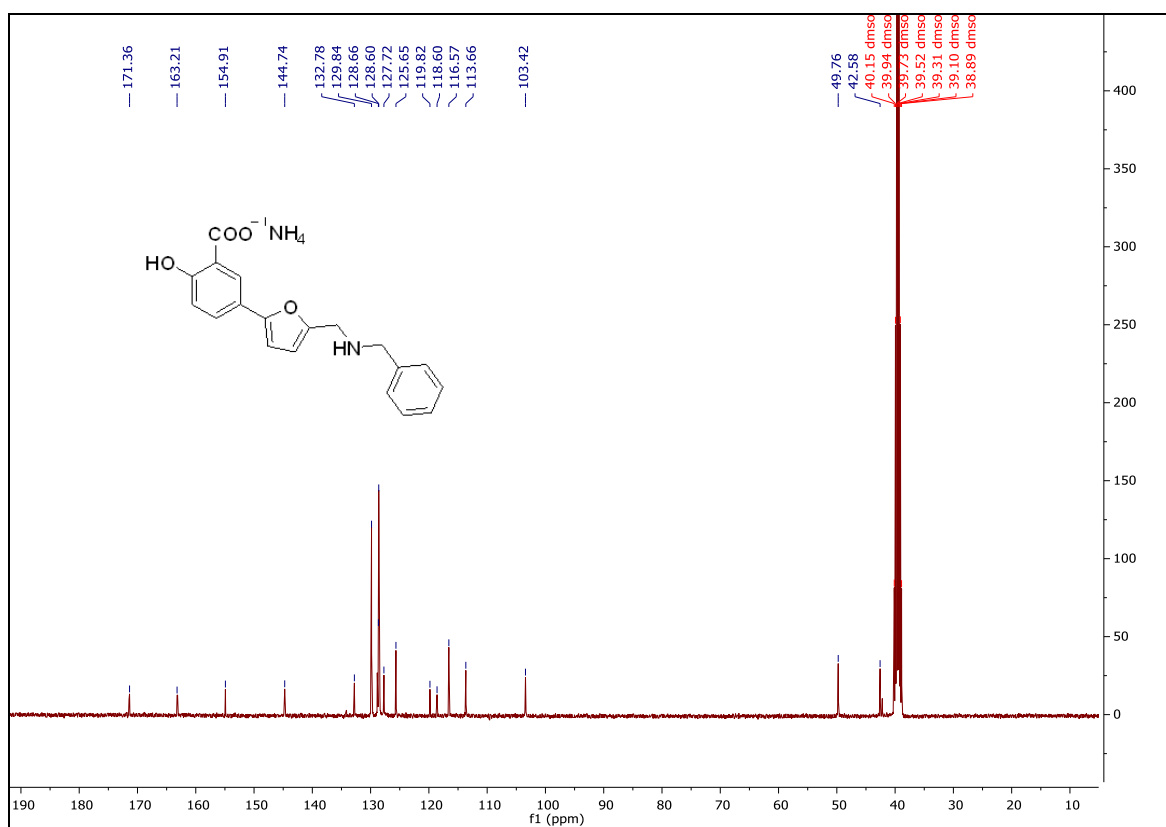
¹H spectrum of **MDMG-907**¹³C spectrum of **MDMG-907**

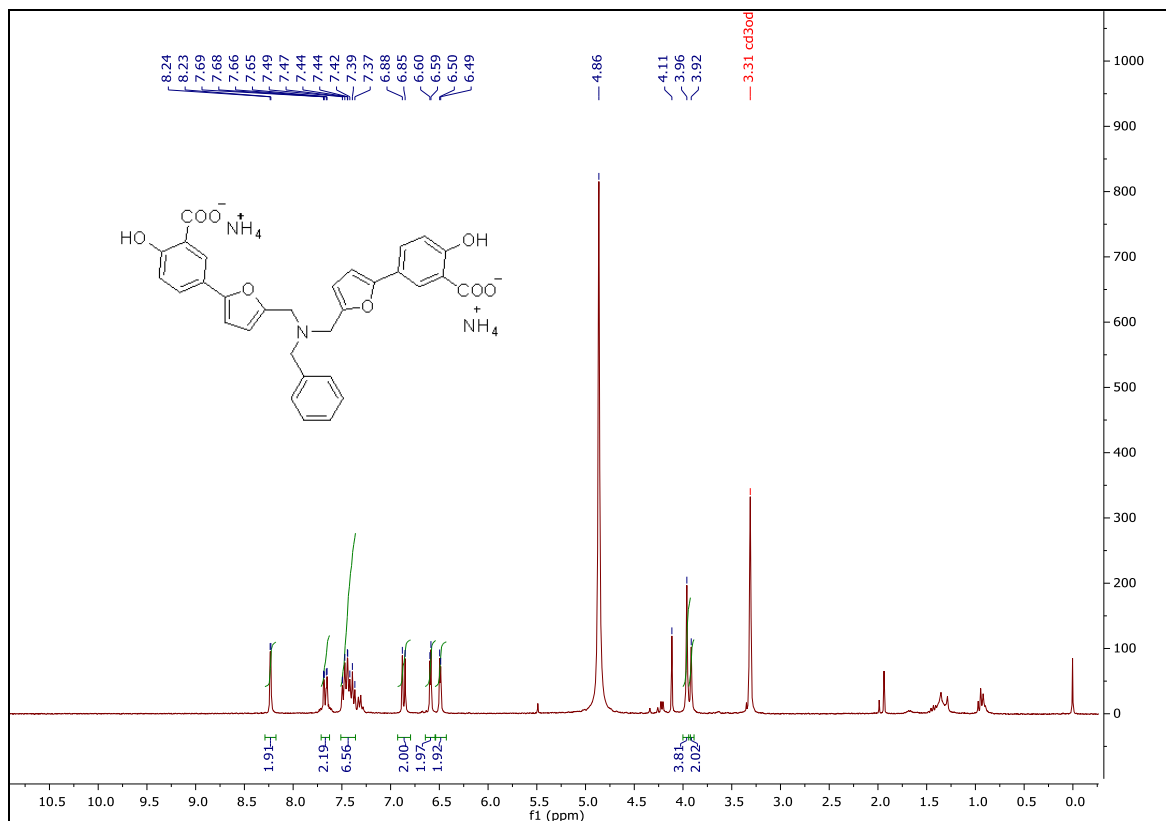
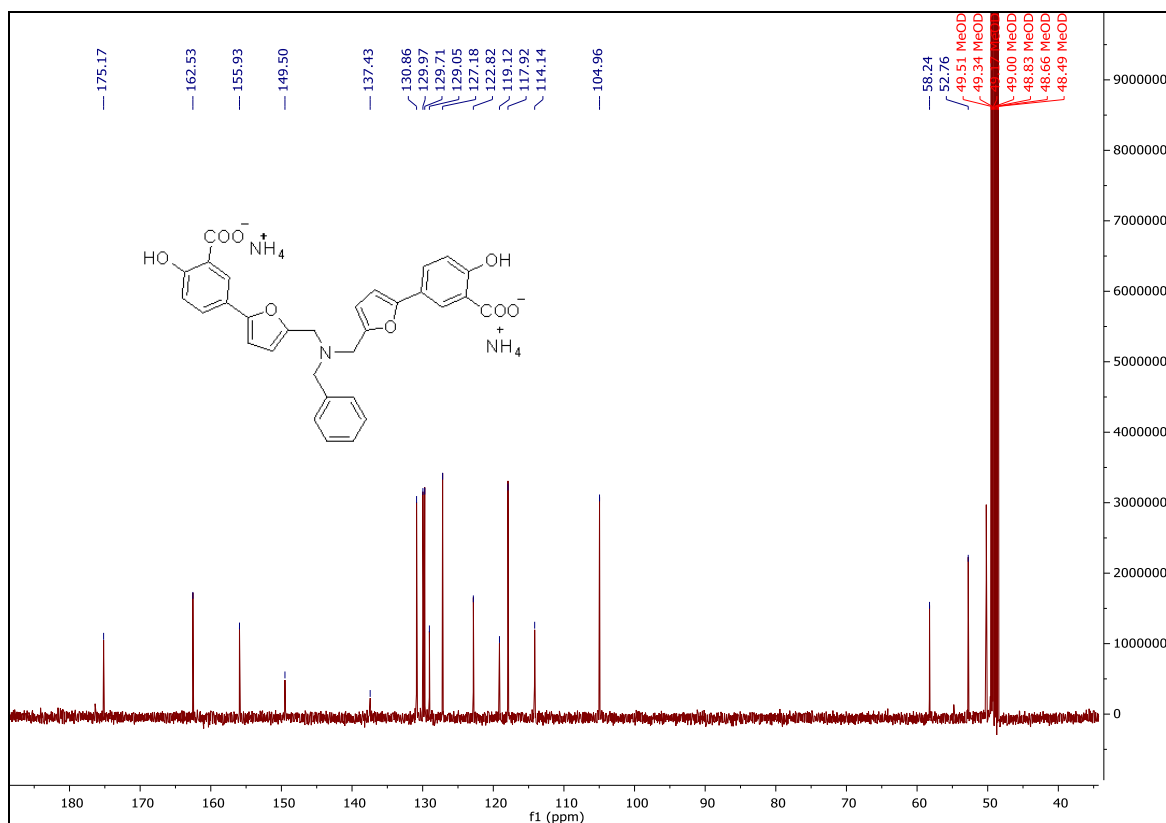
¹H spectrum of MDMG-911¹³C spectrum of MDMG-911

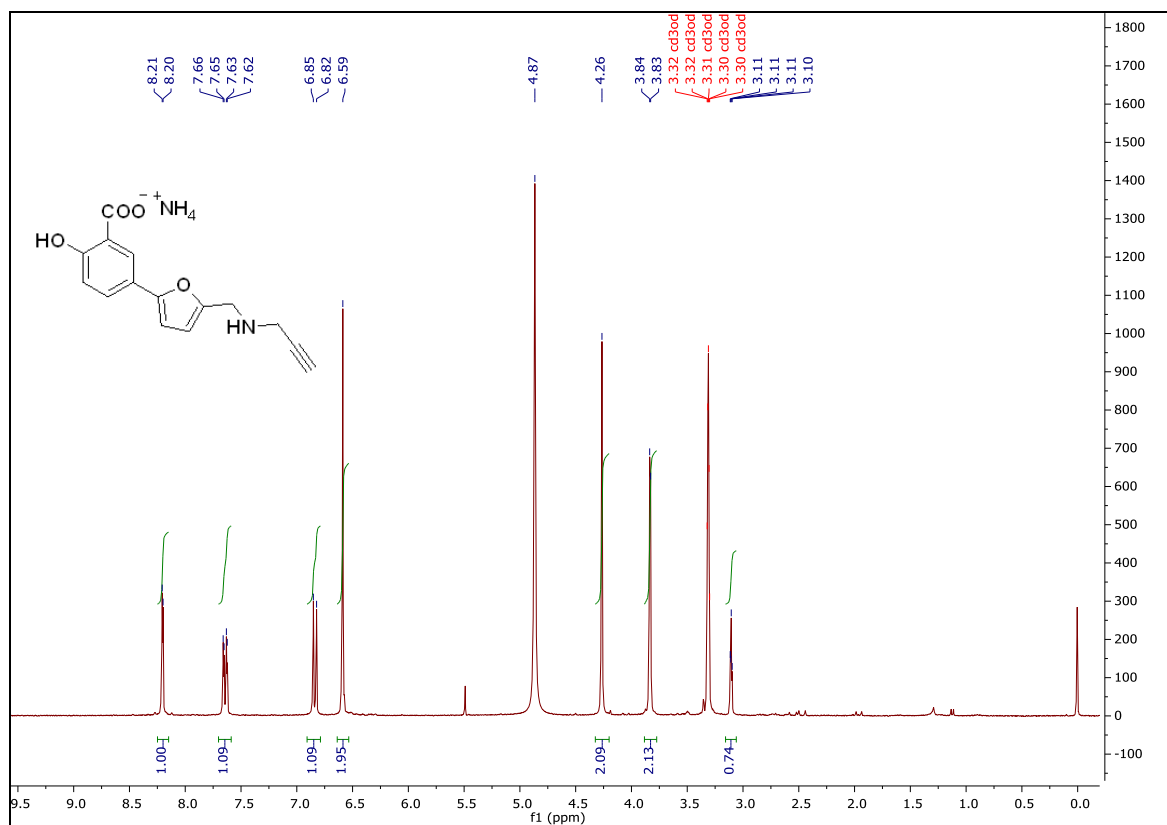
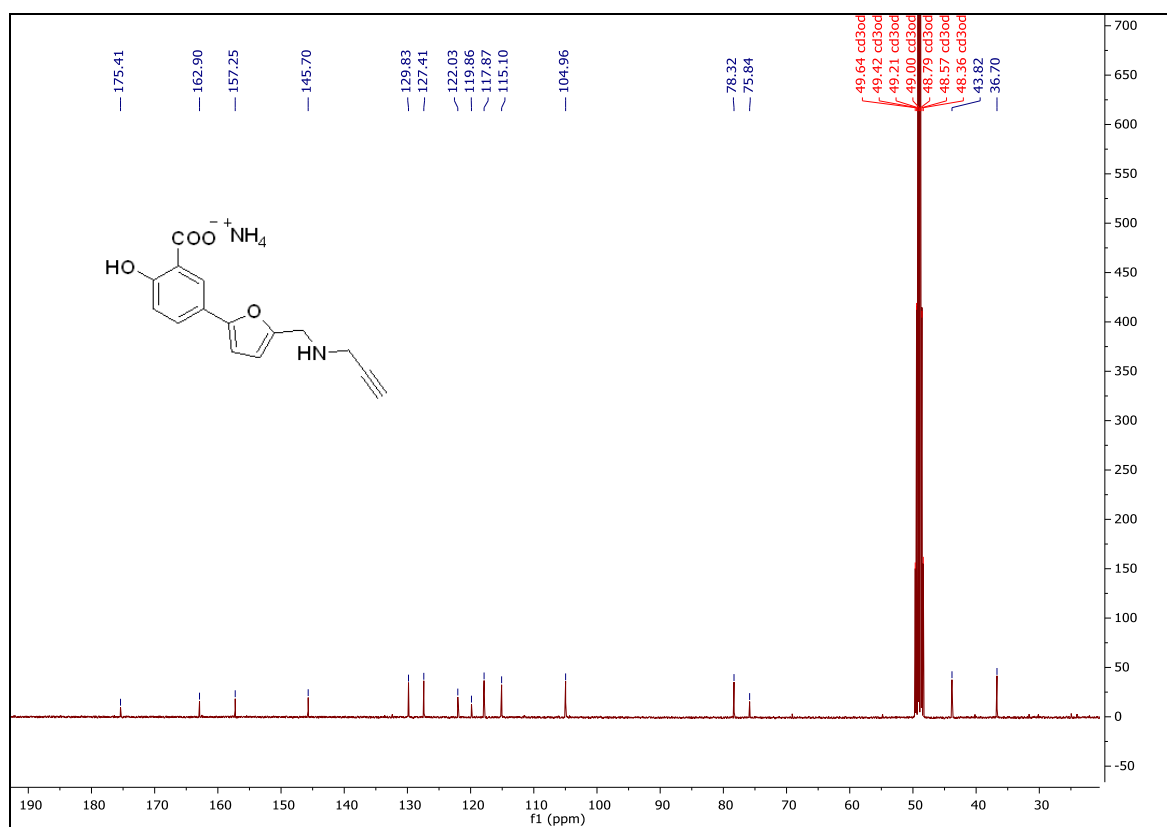
¹H spectrum of MDMG-915¹³C spectrum of MDMG-915

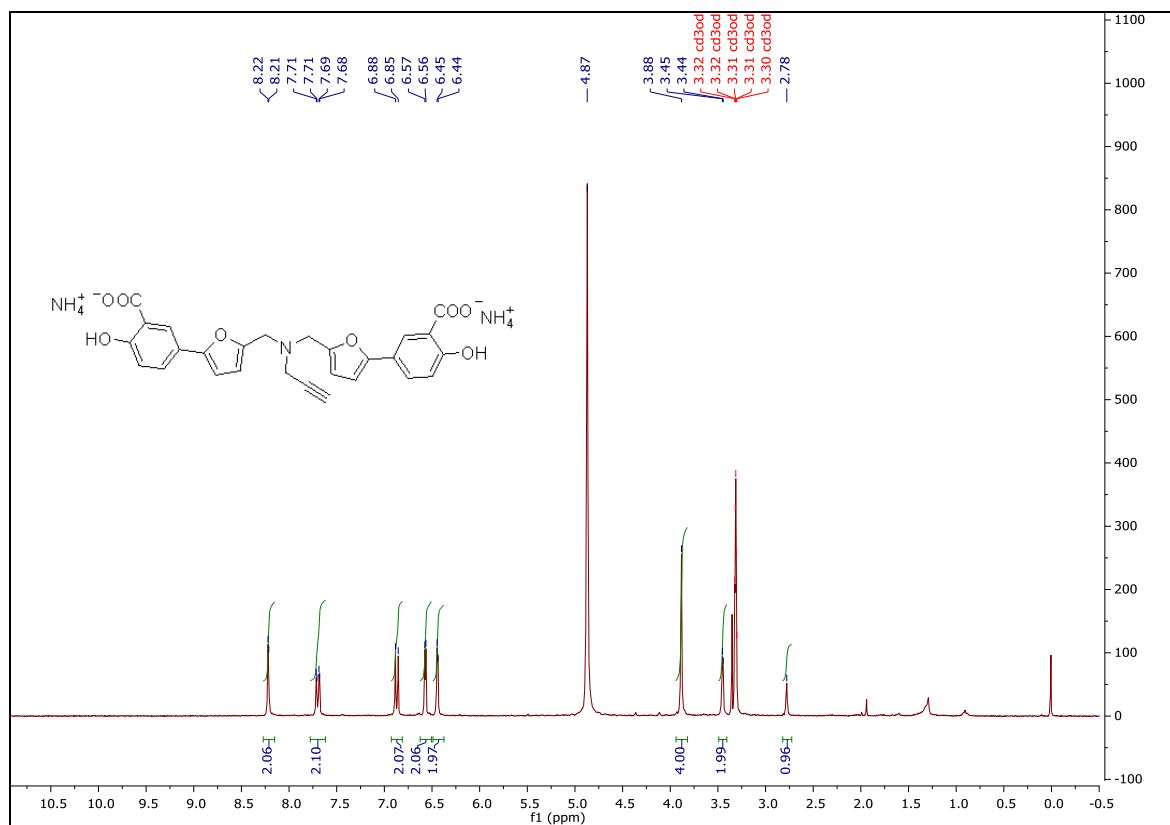
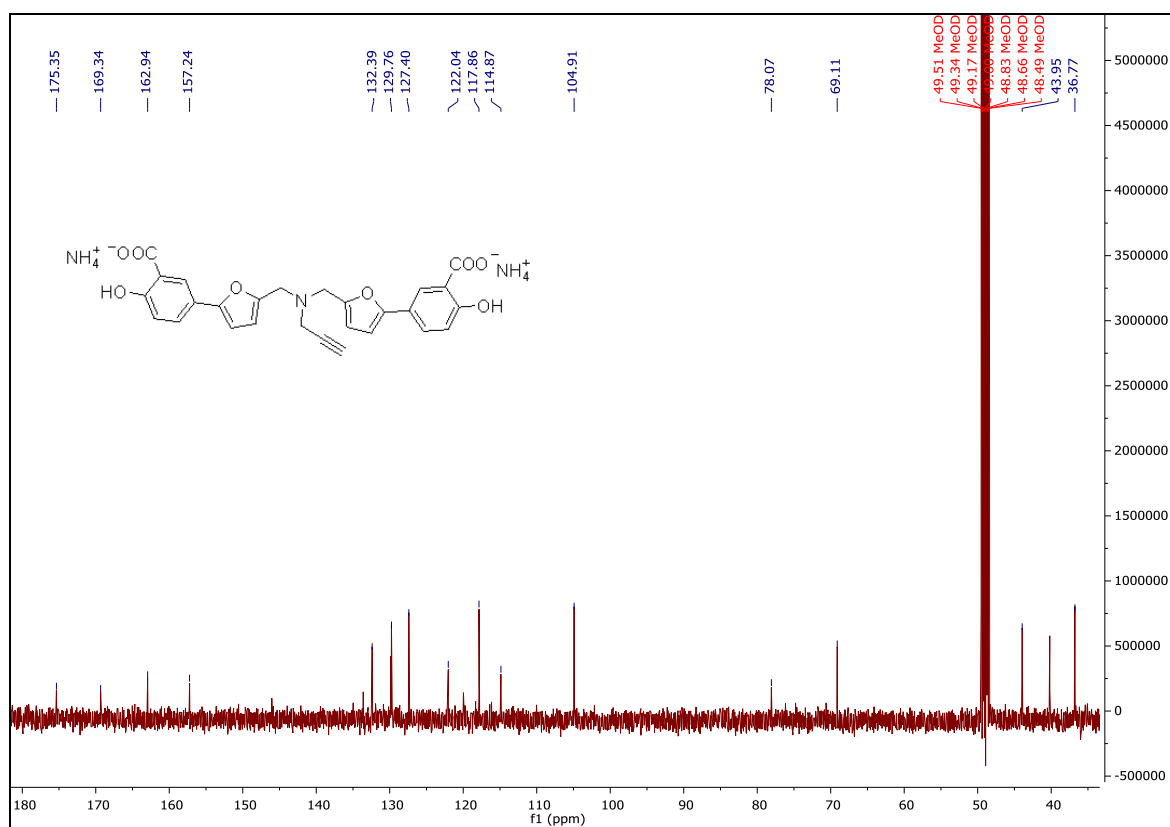
¹H spectrum of MDMG-919¹³C spectrum of MDMG-919

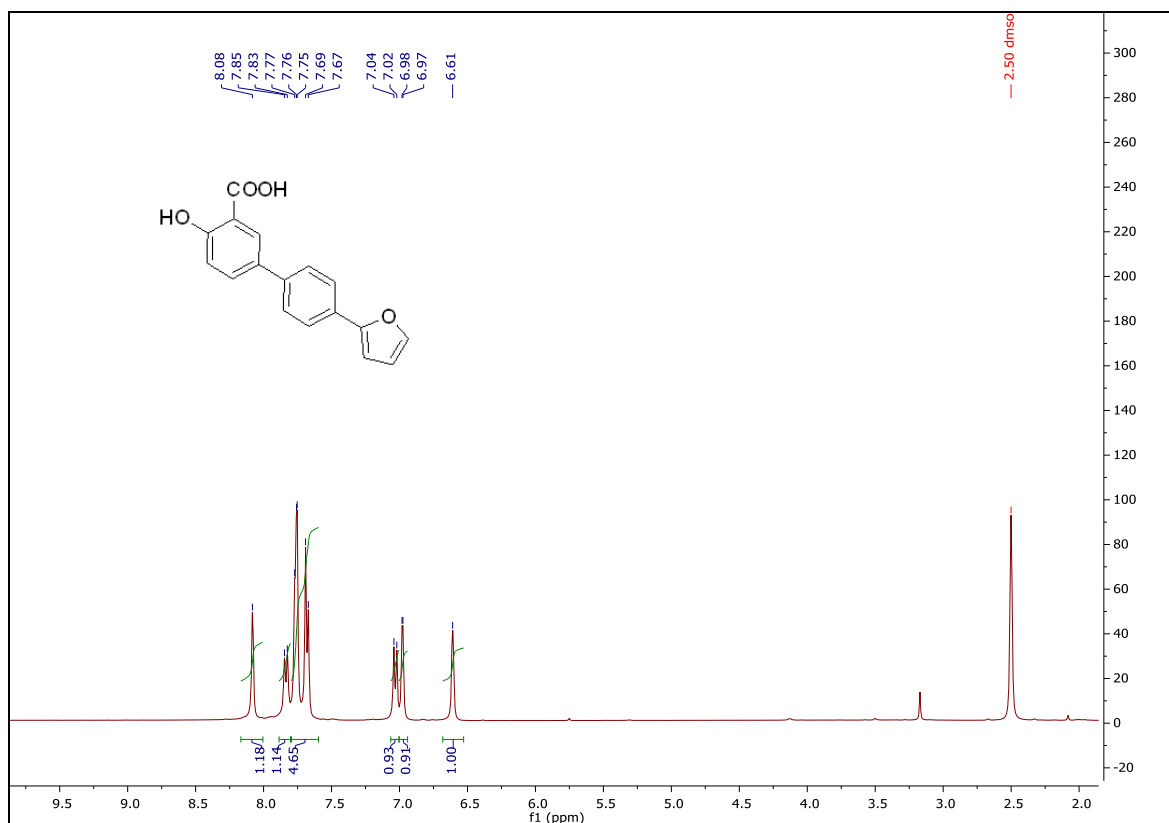
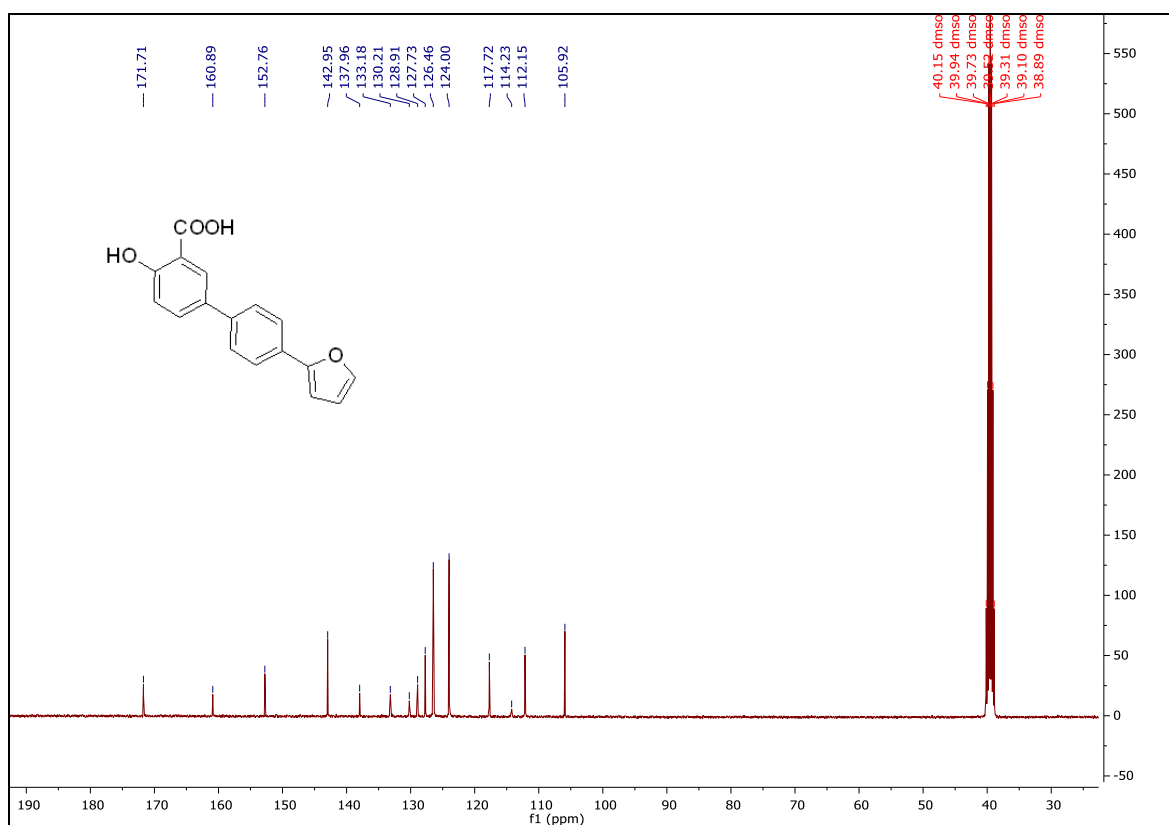
¹H spectrum of **MDMG-927**¹³C spectrum of **MDMG-927**

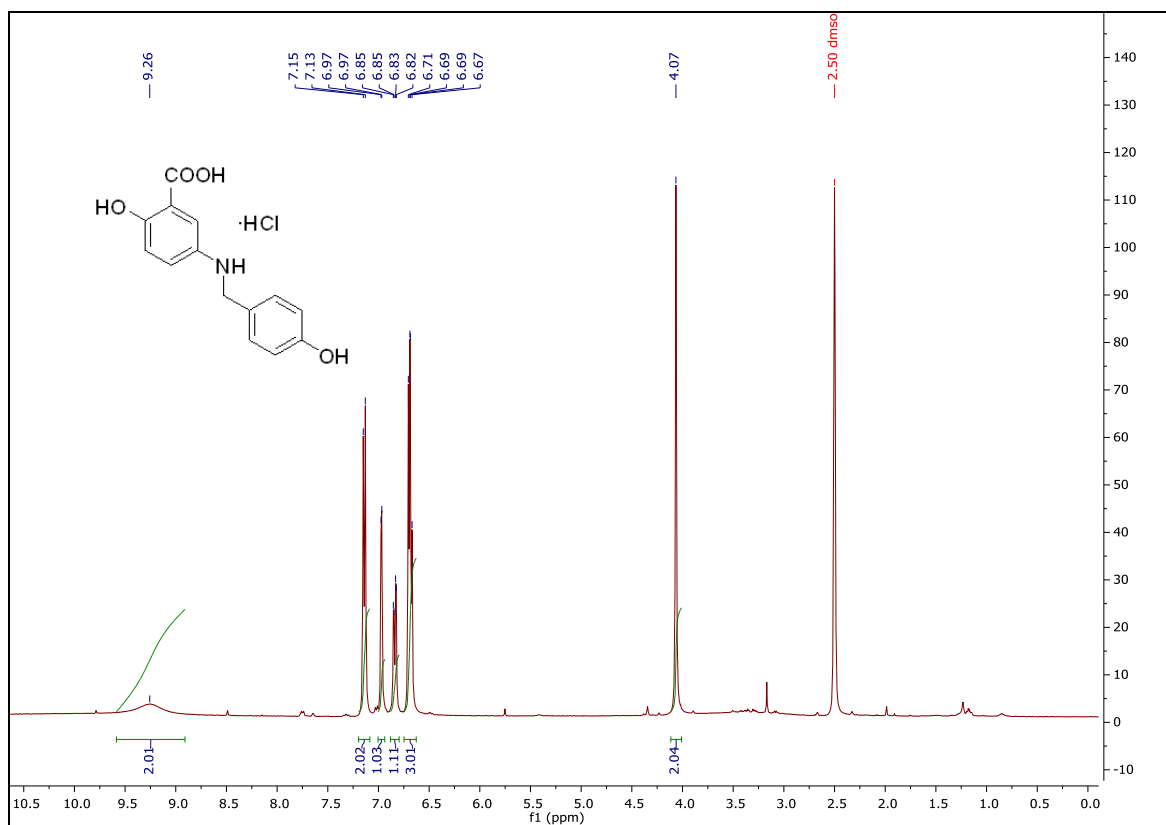
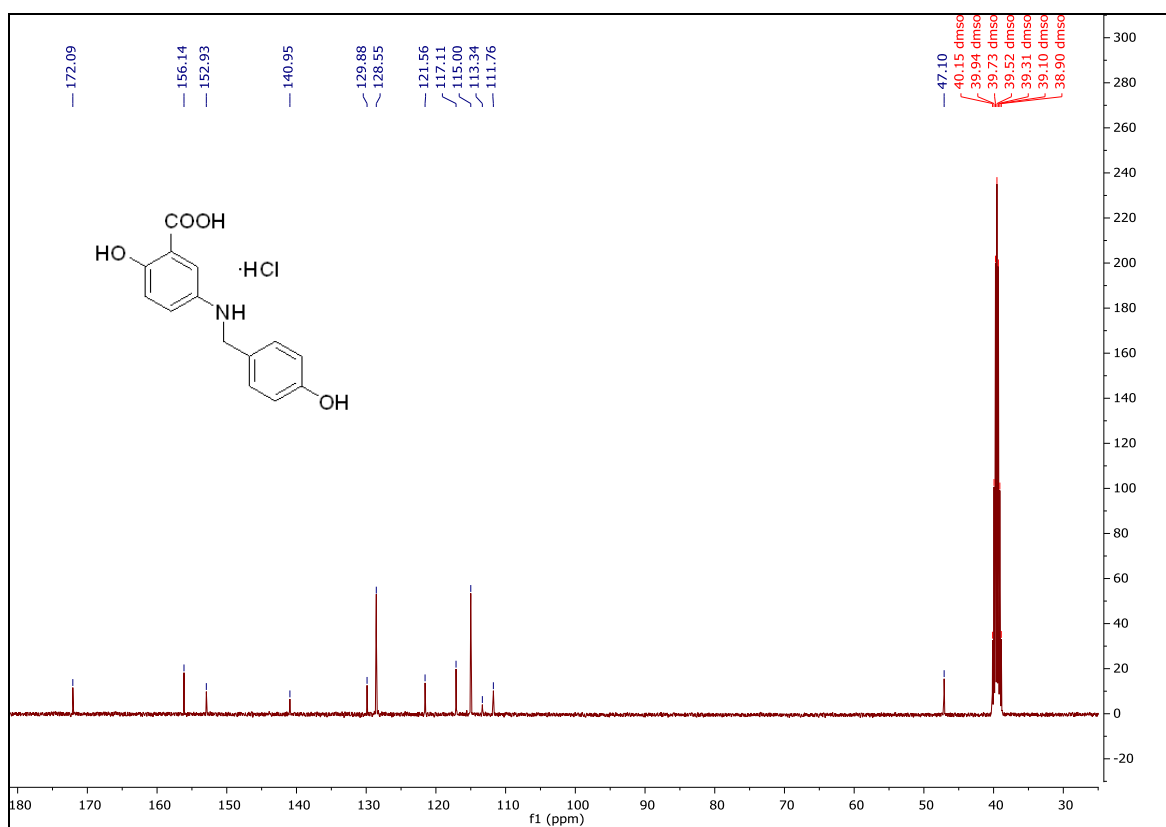
¹H spectrum of MDMG-931P¹³C spectrum of MDMG-931P

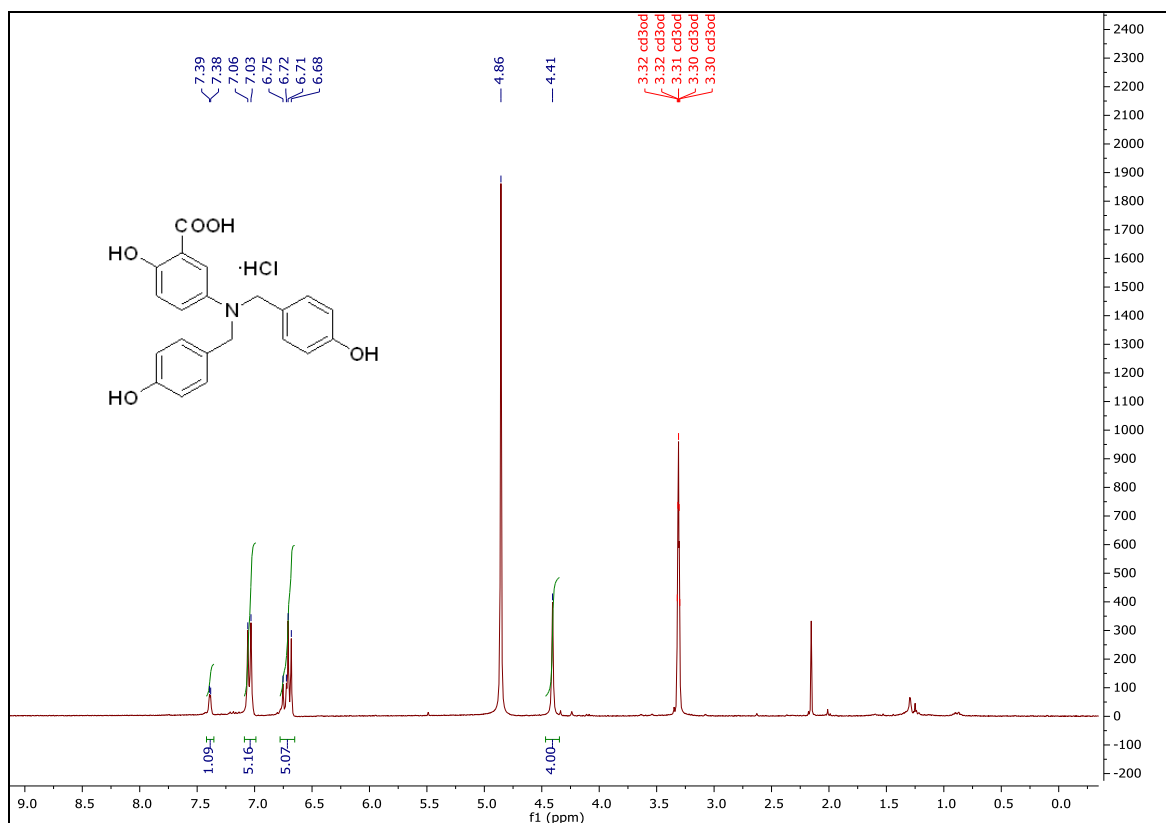
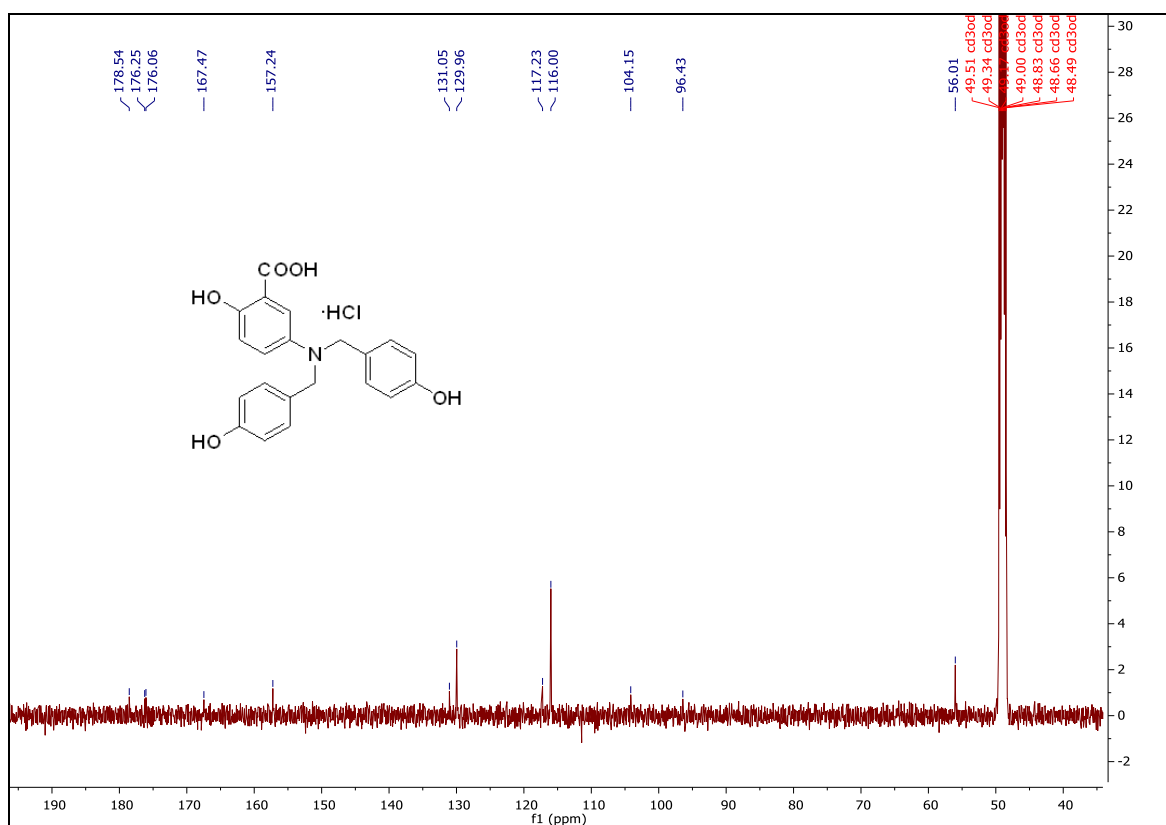
¹³C spectrum of MDMG-931I¹³C spectrum of MDMG-931I

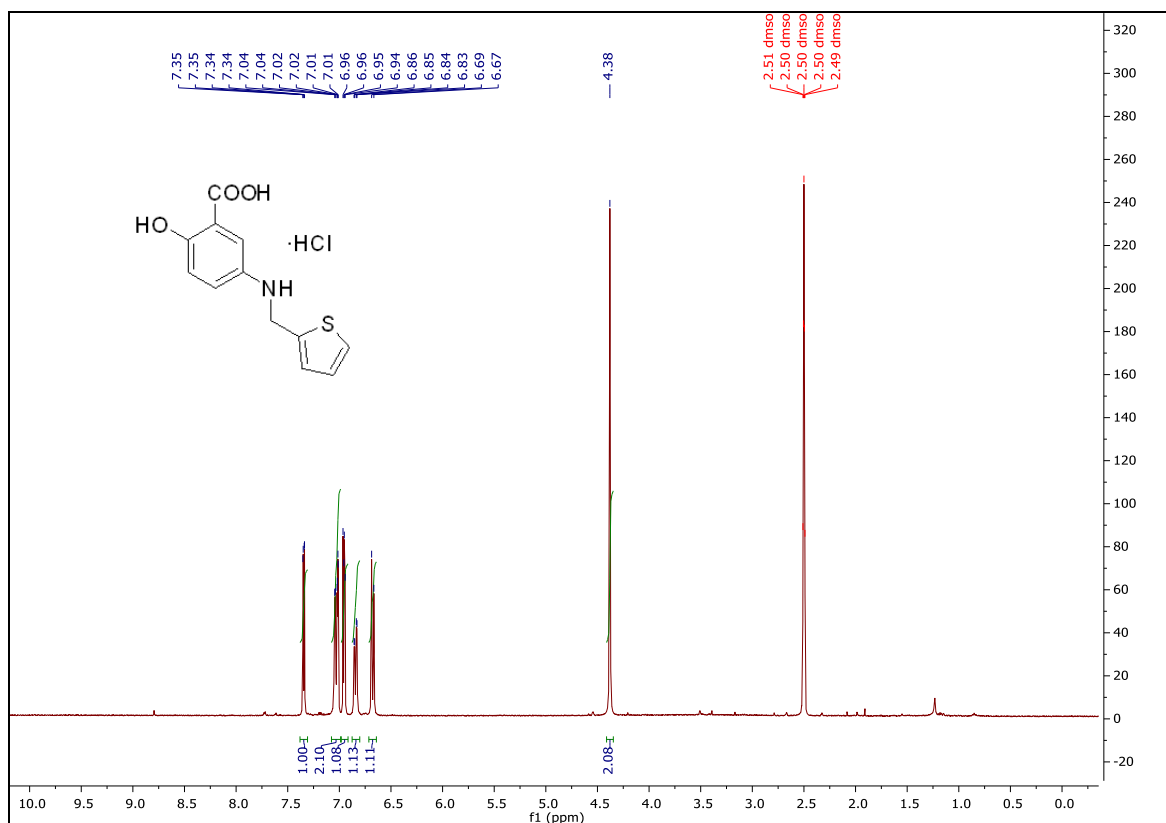
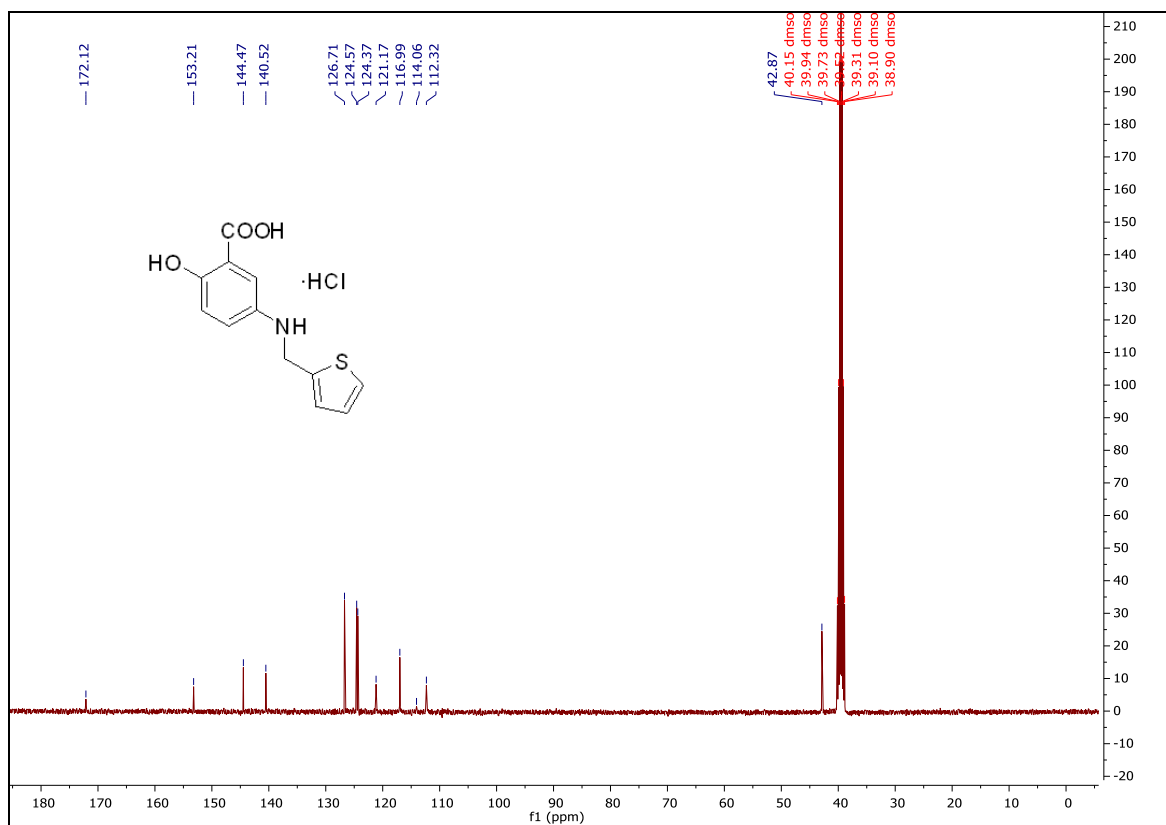
¹H spectrum of **MDMG-935P**¹³C spectrum of **MDMG-935P**

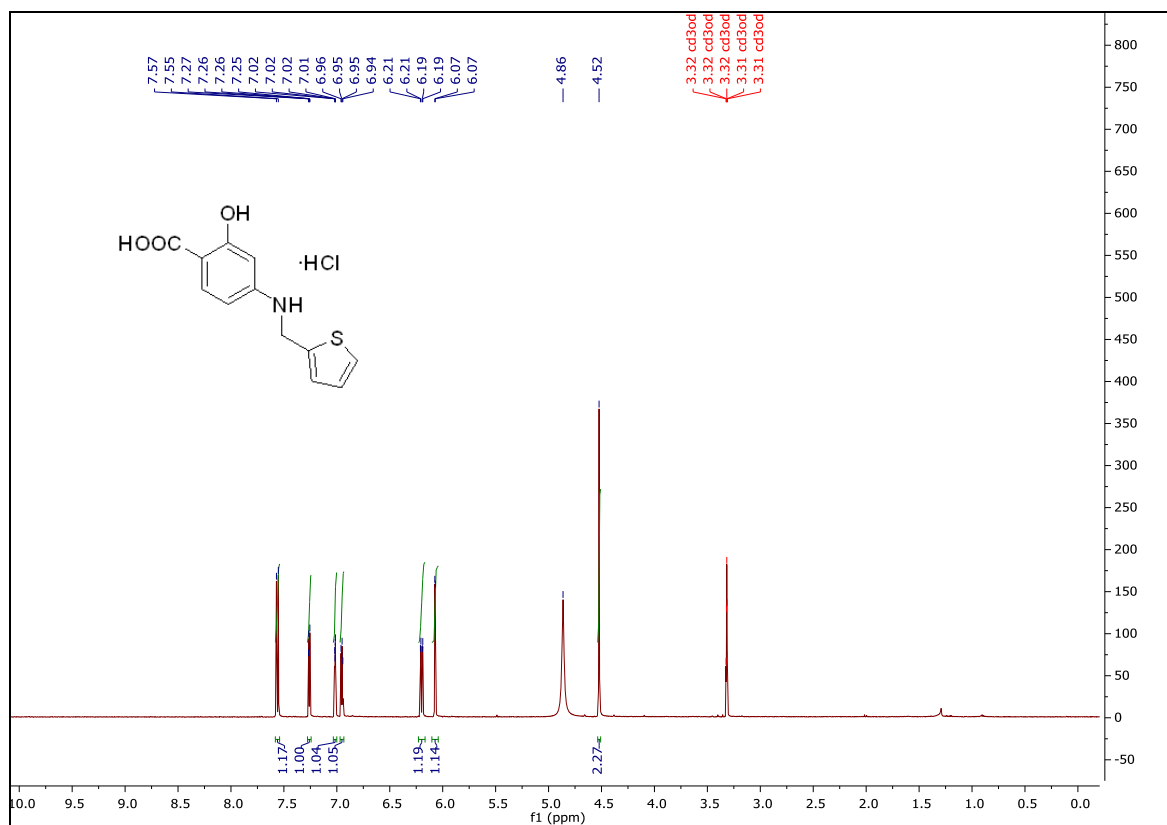
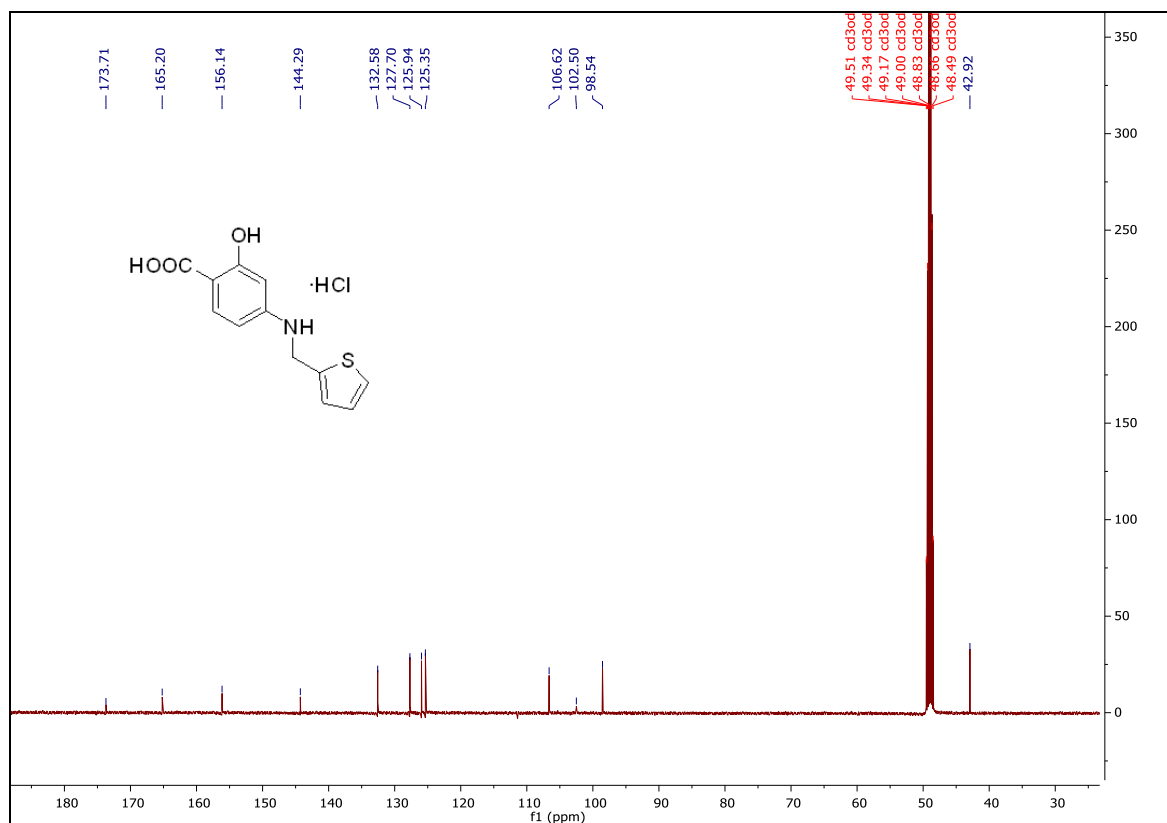
¹H spectrum of **MDMG-935I**¹³C spectrum of **MDMG-935I**

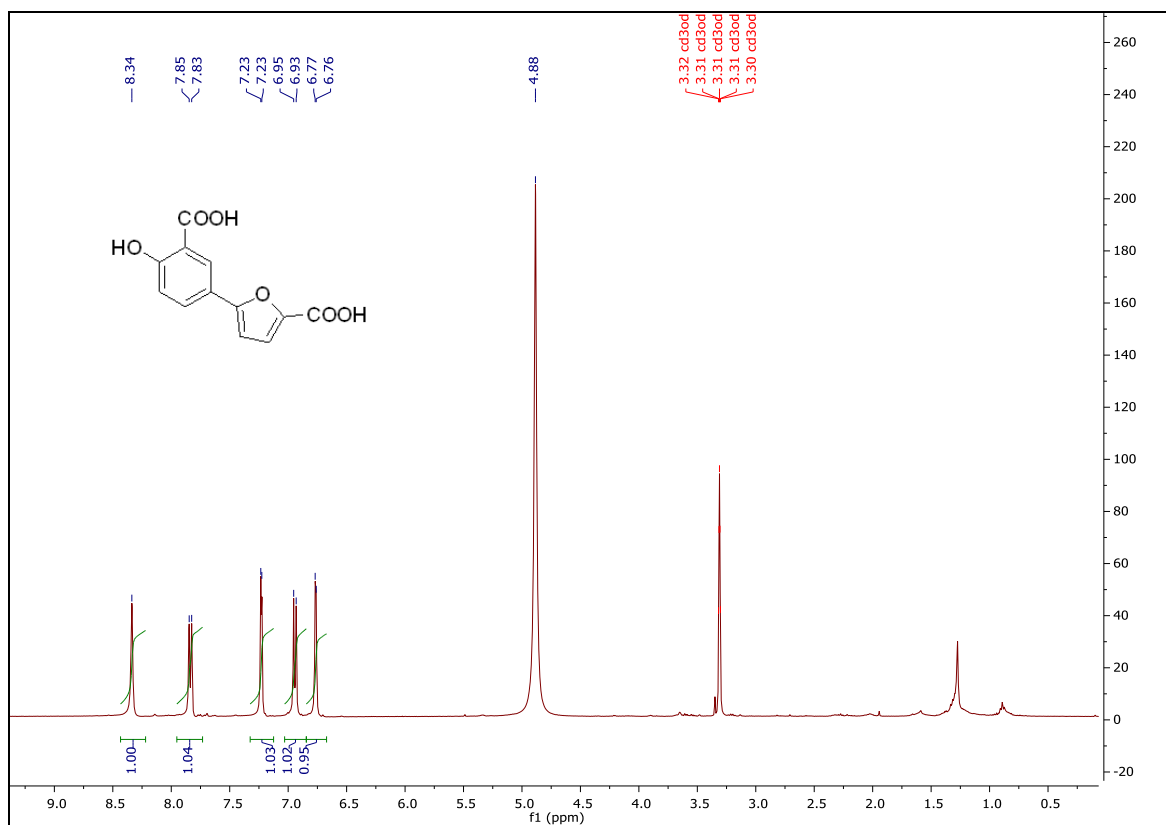
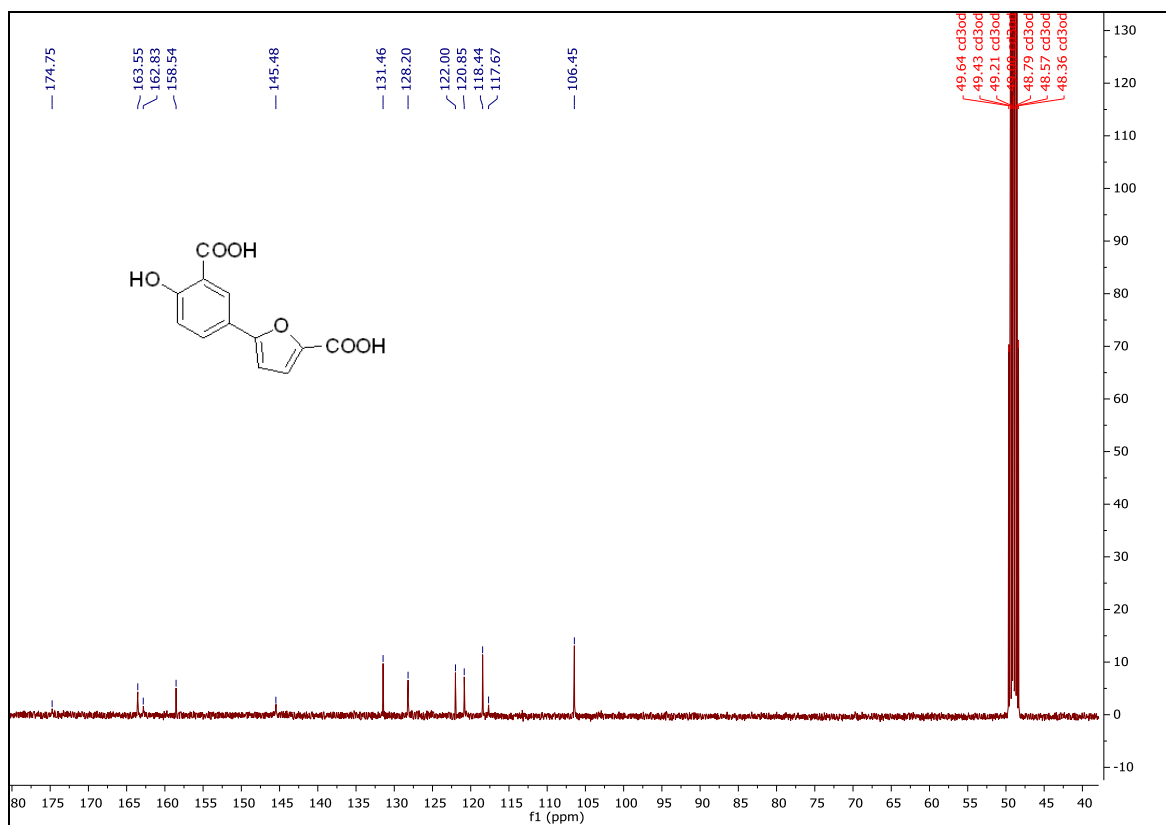
¹H spectrum of **MDMG-943**¹³C spectrum of **MDMG-943**

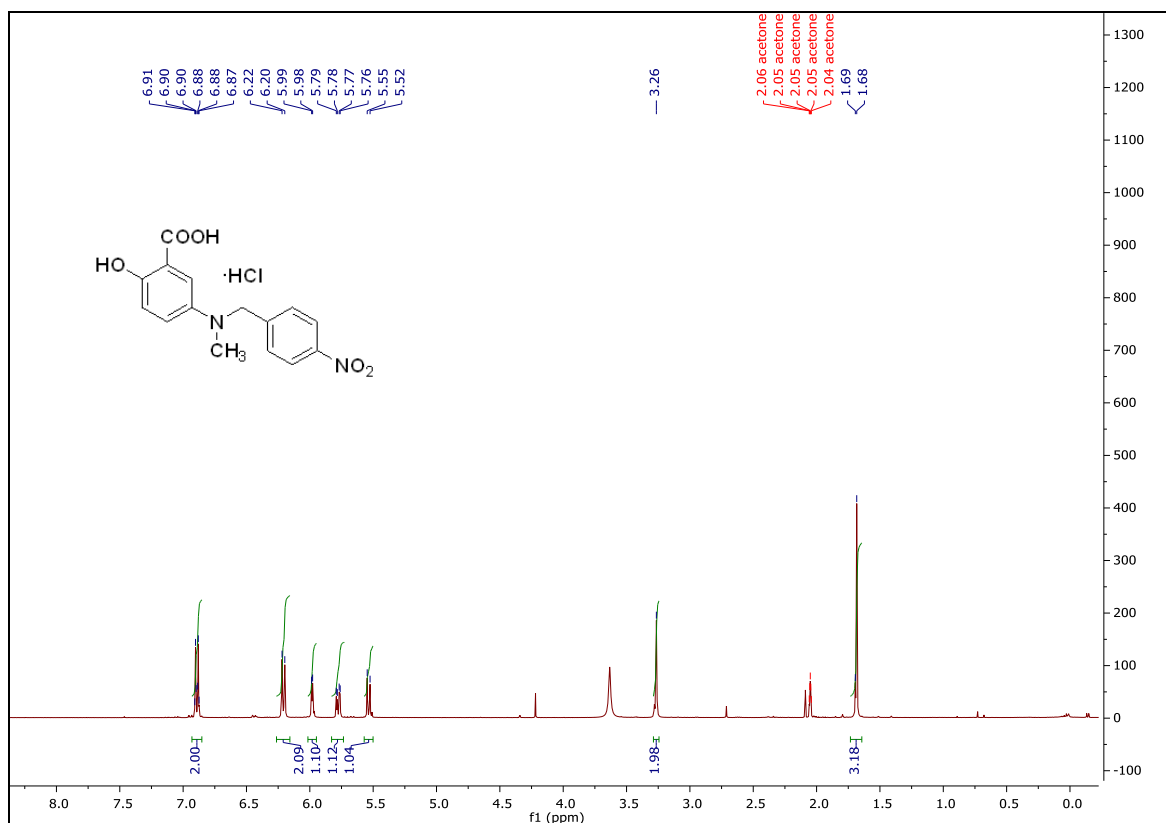
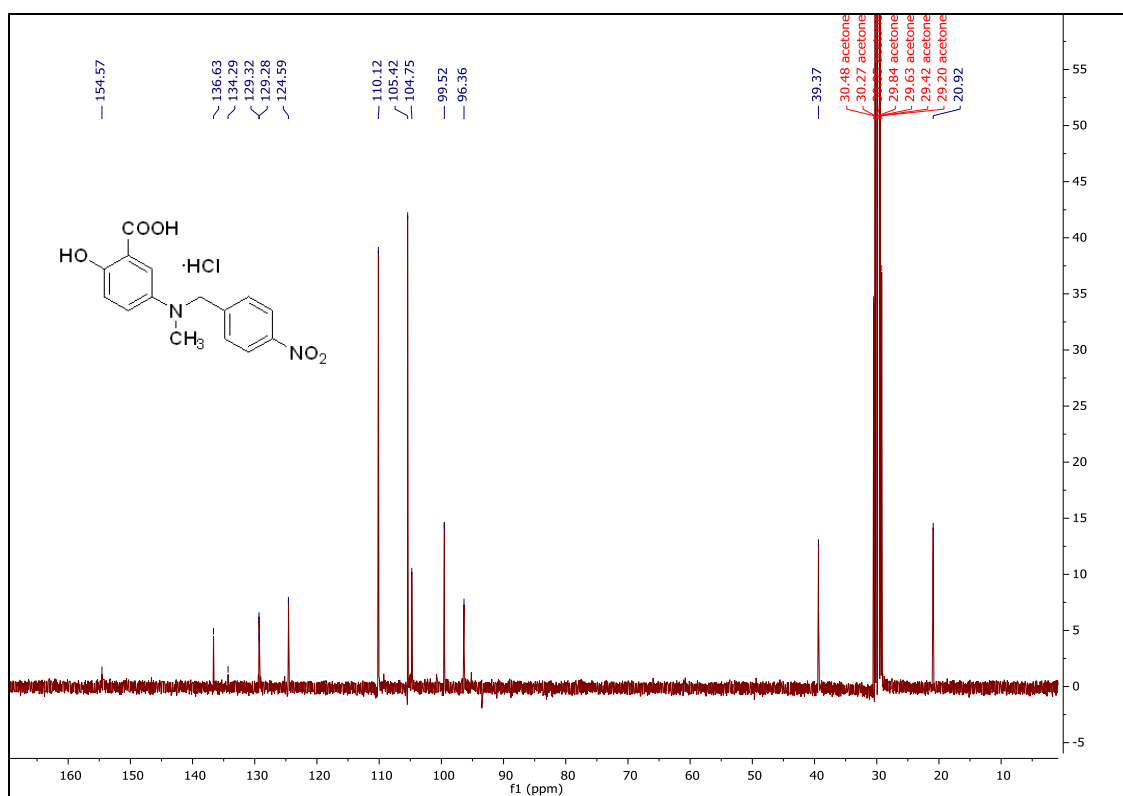
¹H spectrum of **MDMG-963**¹³C spectrum of **MDMG-963**

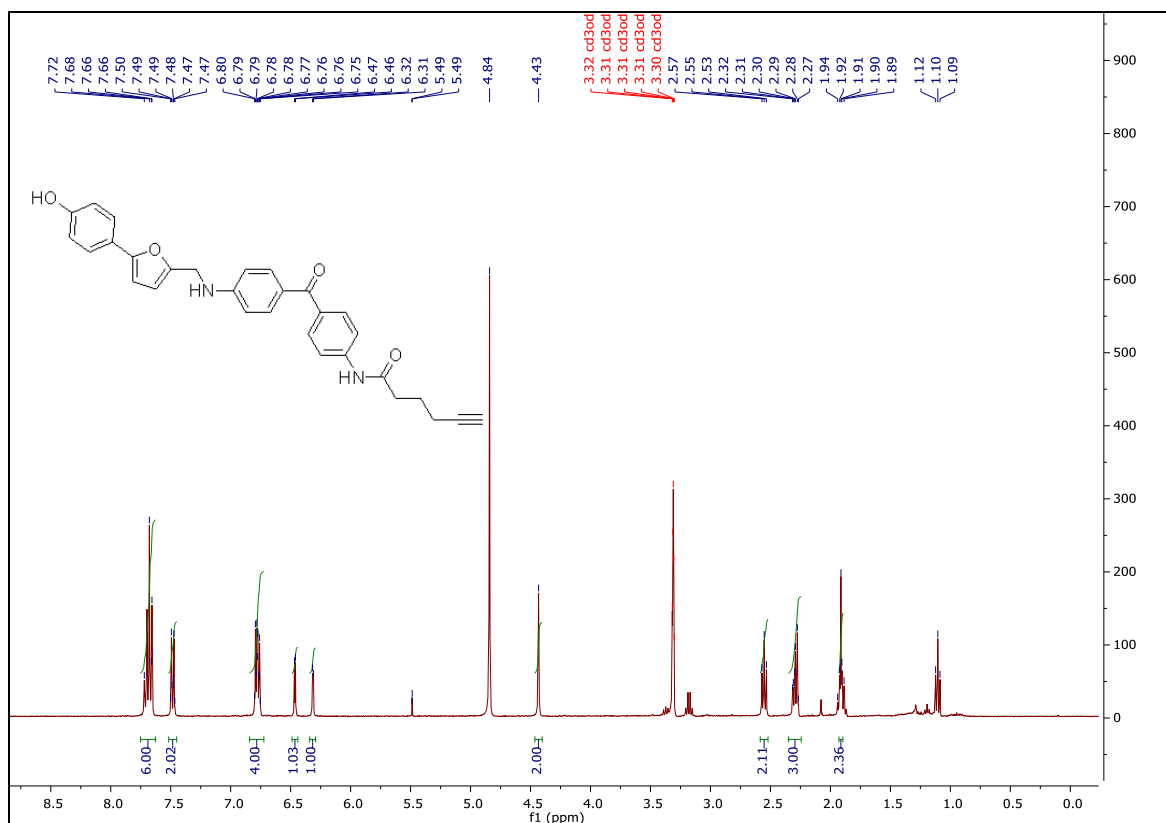
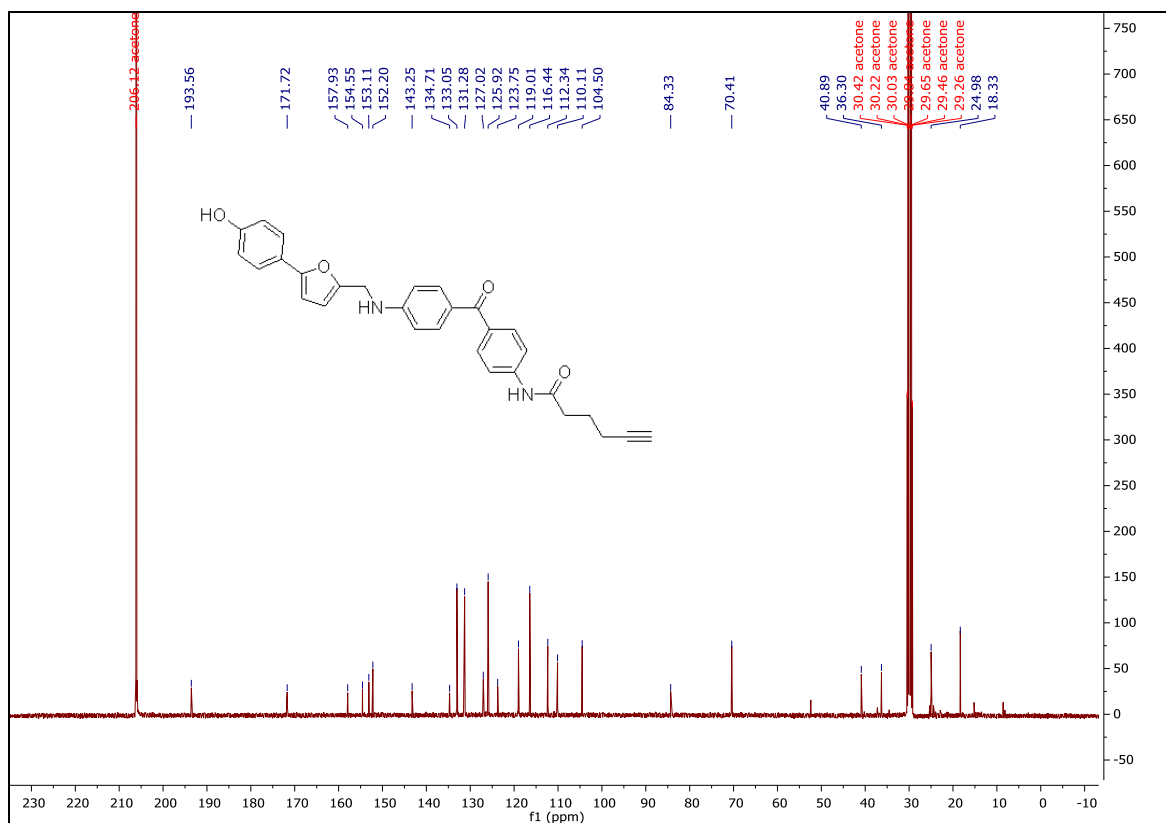
¹H spectrum of **MDMG-963I**¹³C spectrum of **MDMG-963I**

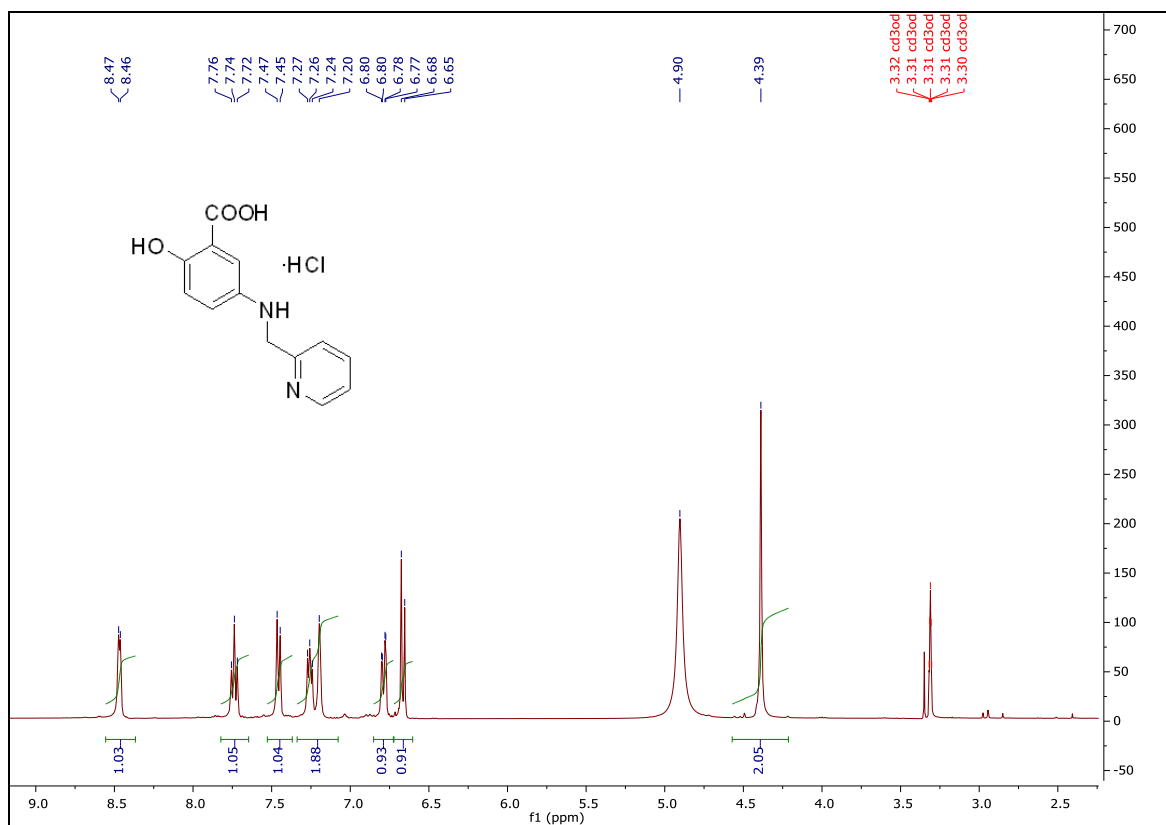
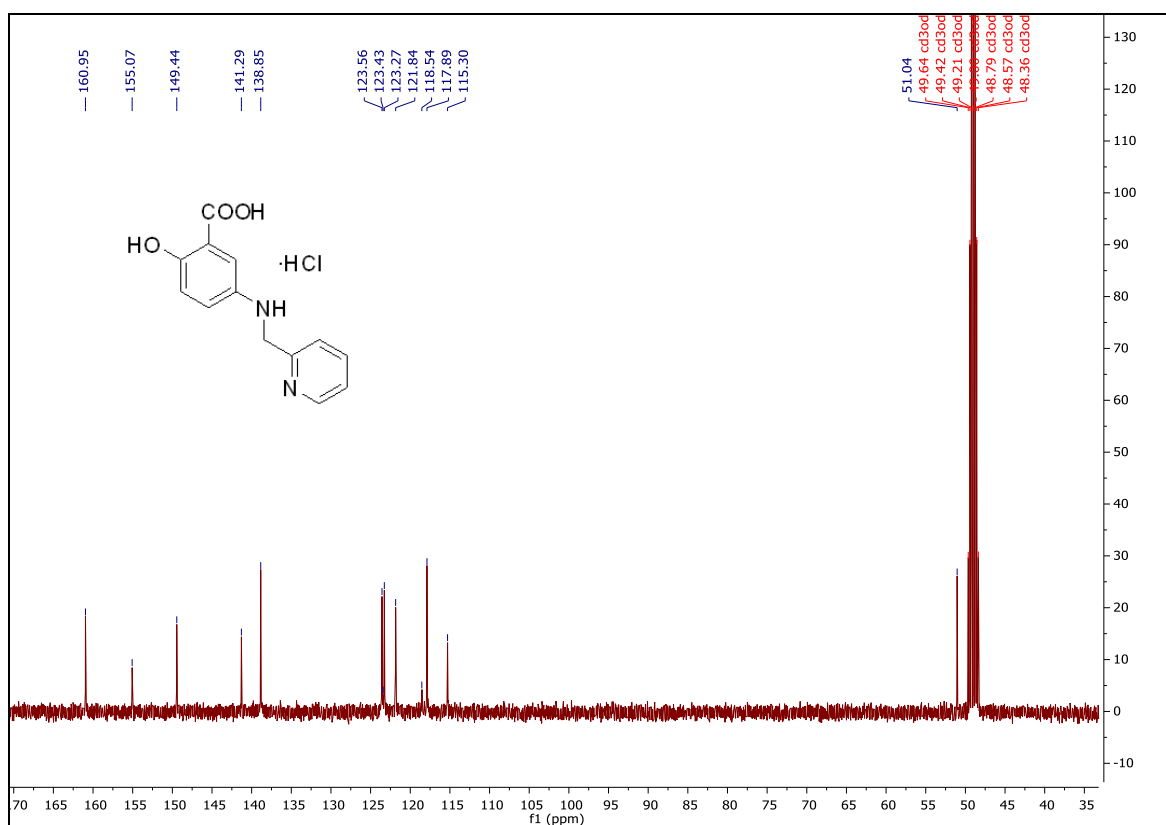
¹H spectrum of **MDMG-971**¹³C spectrum of **MDMG-971**

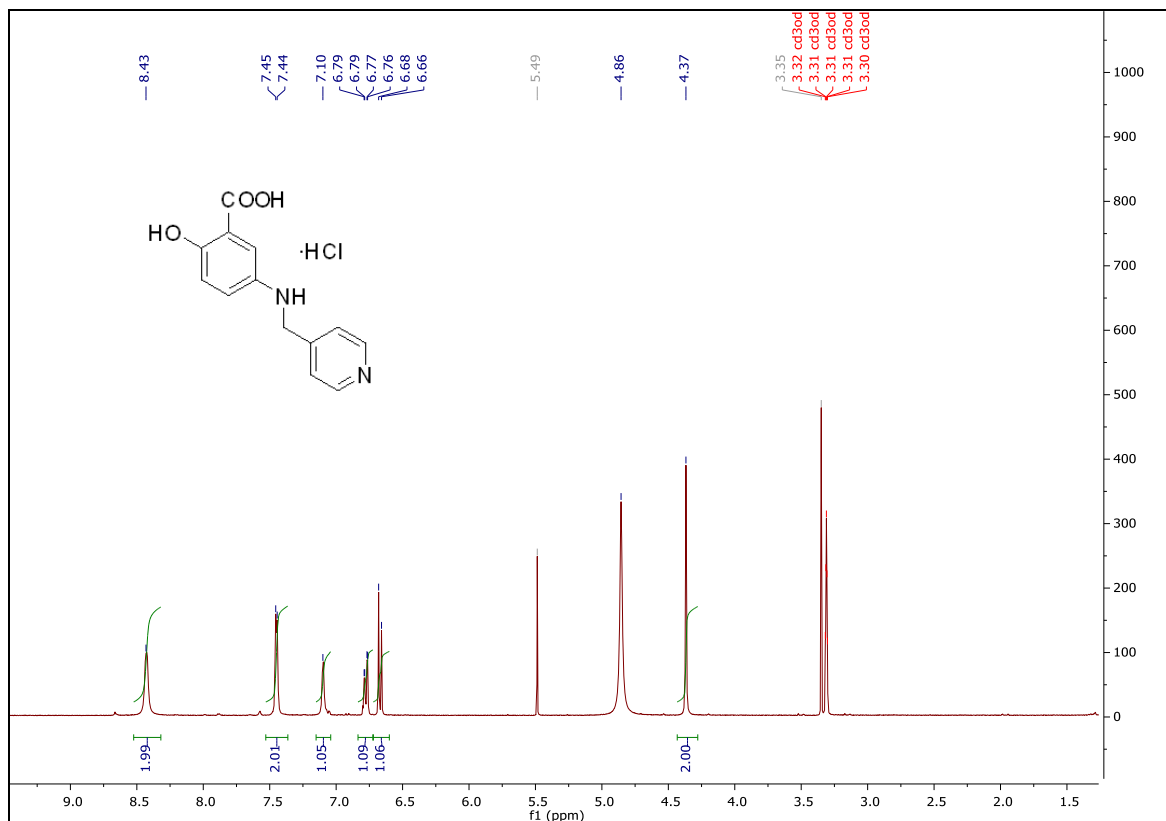
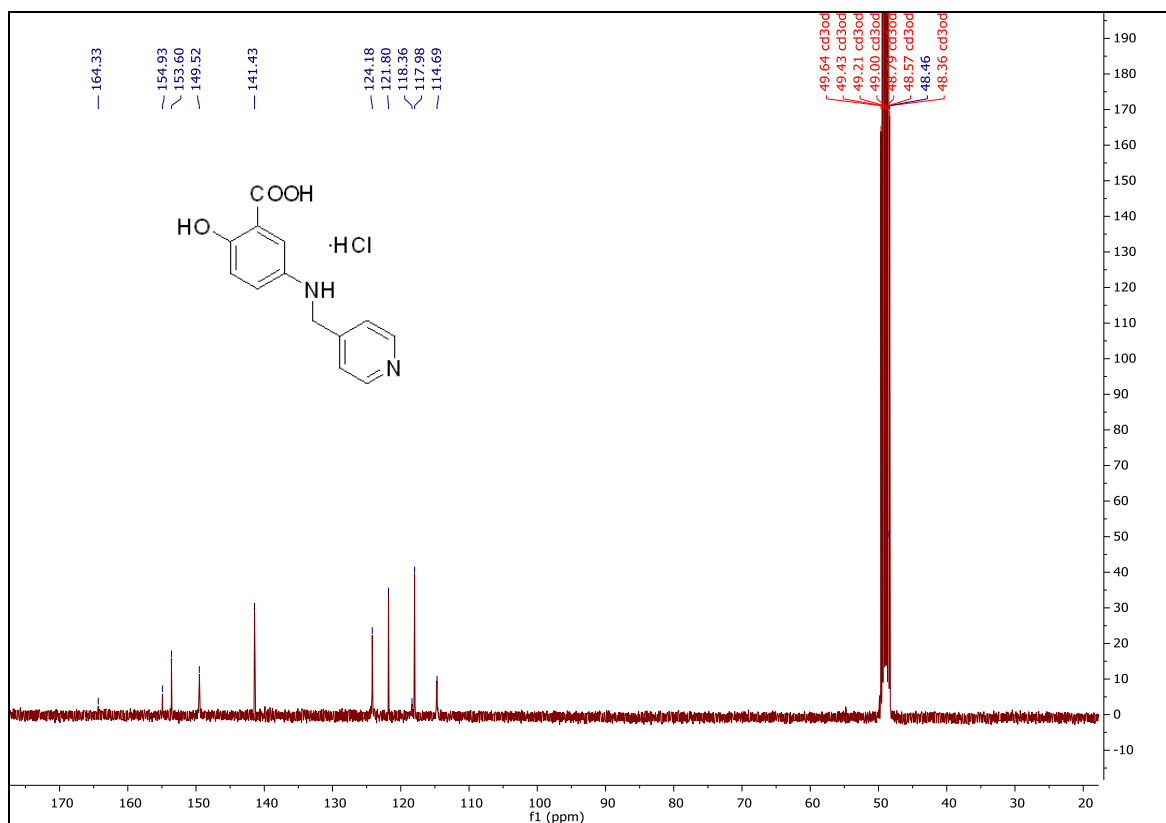
¹H spectrum of **MDMG-979**¹³C spectrum of **MDMG-979**

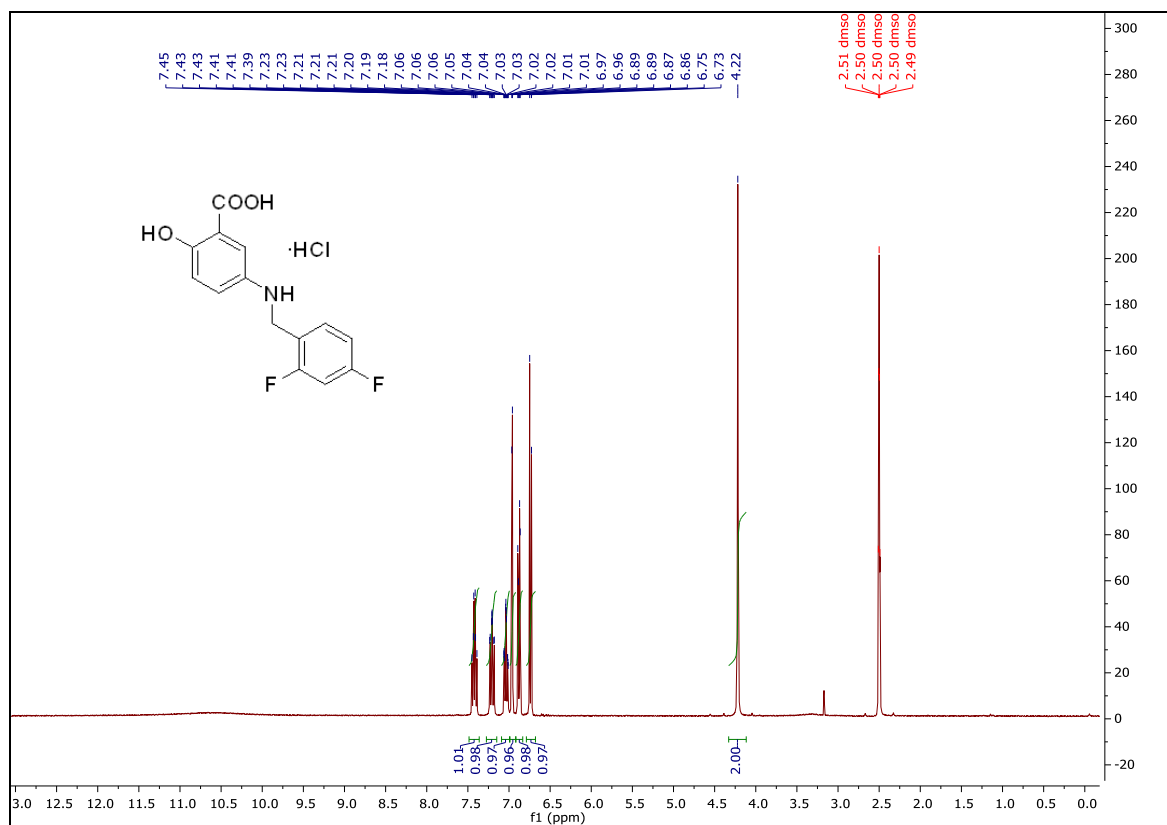
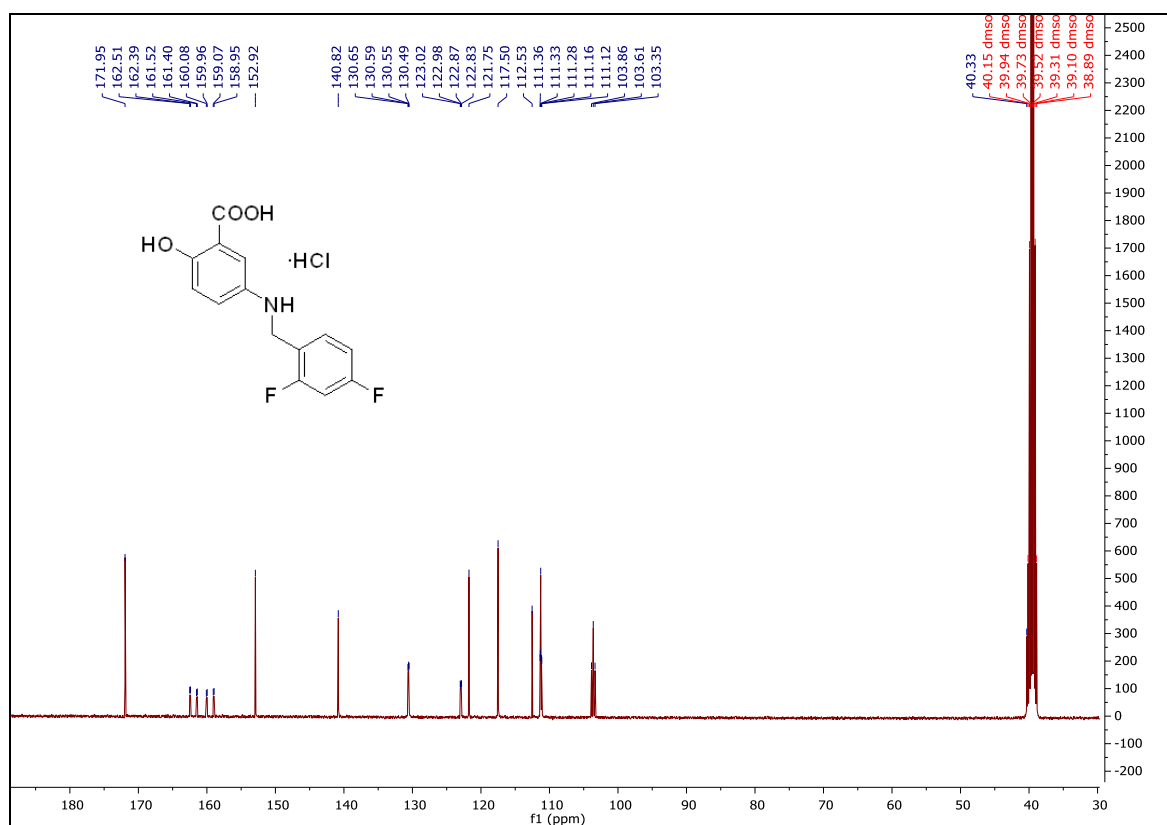
¹H spectrum of **MDMG-983**¹³C spectrum of **MDMG-983**

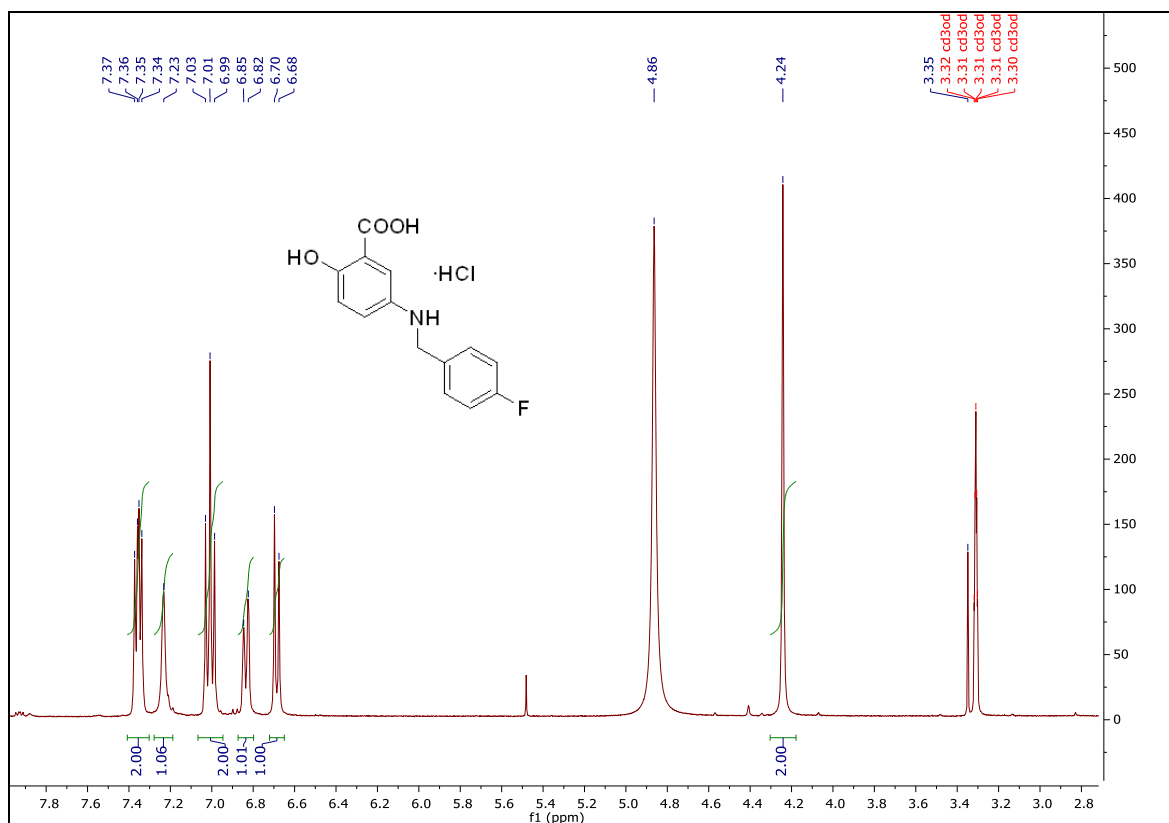
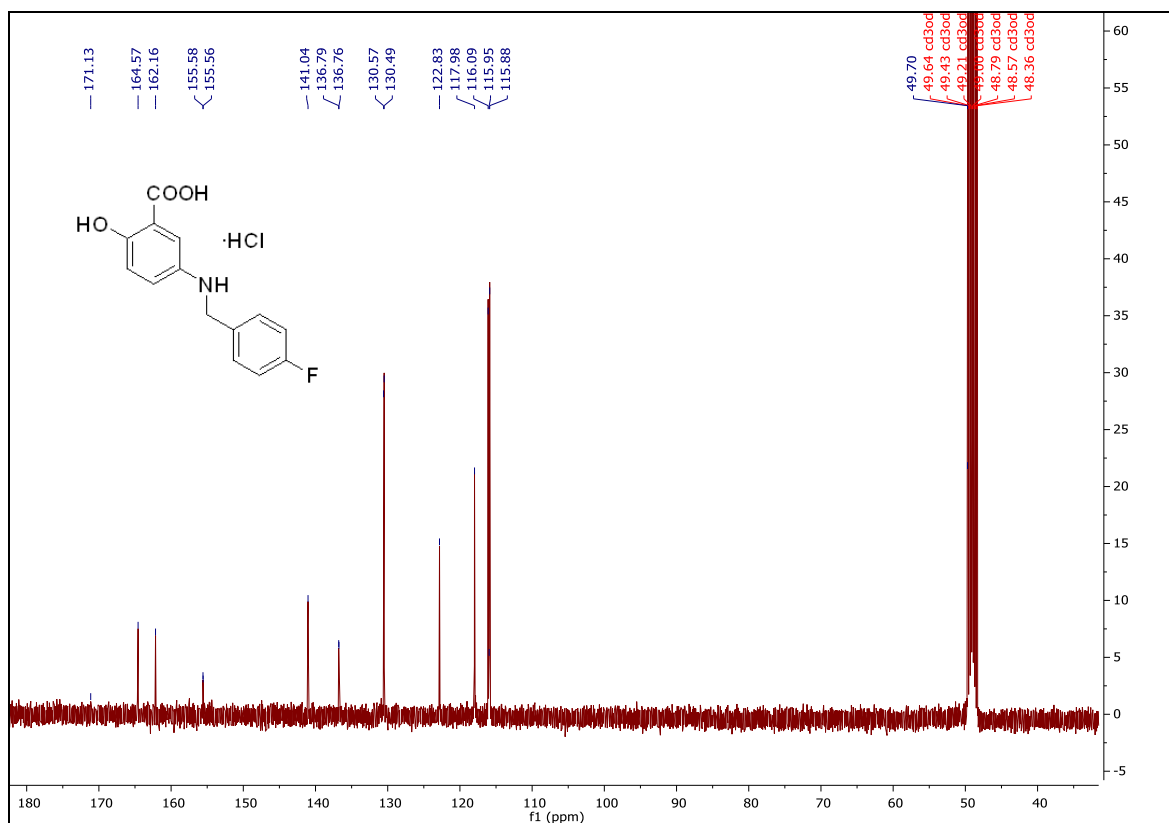
¹H spectrum of **MDMG-991**¹³C spectrum of **MDMG-991**

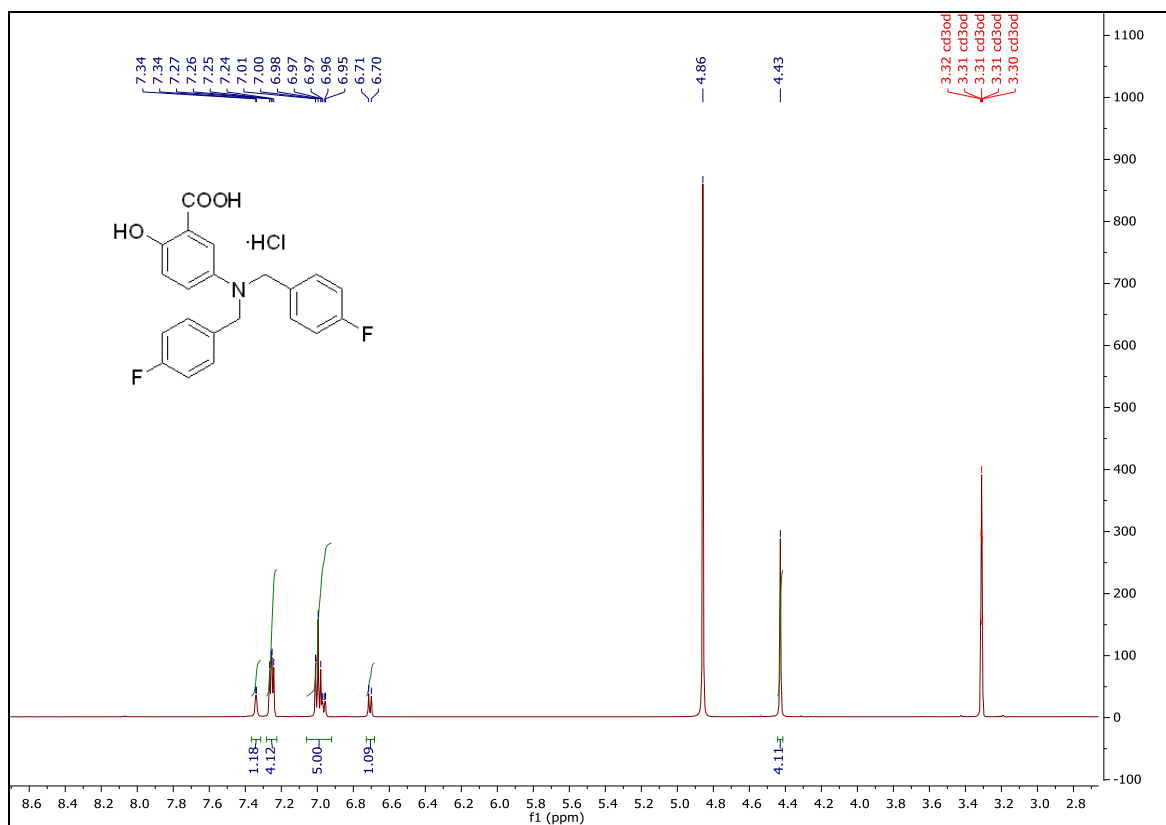
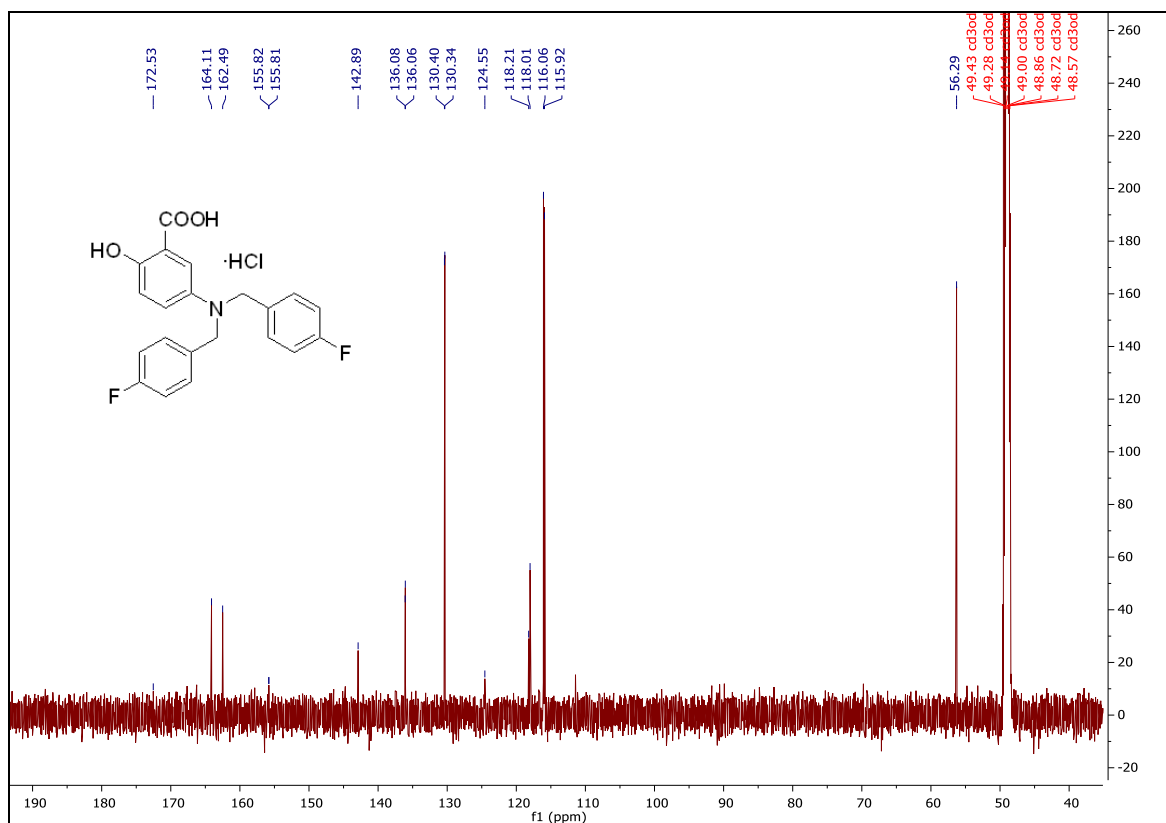
¹H spectrum of MDMG-995¹³C spectrum of MDMG-995

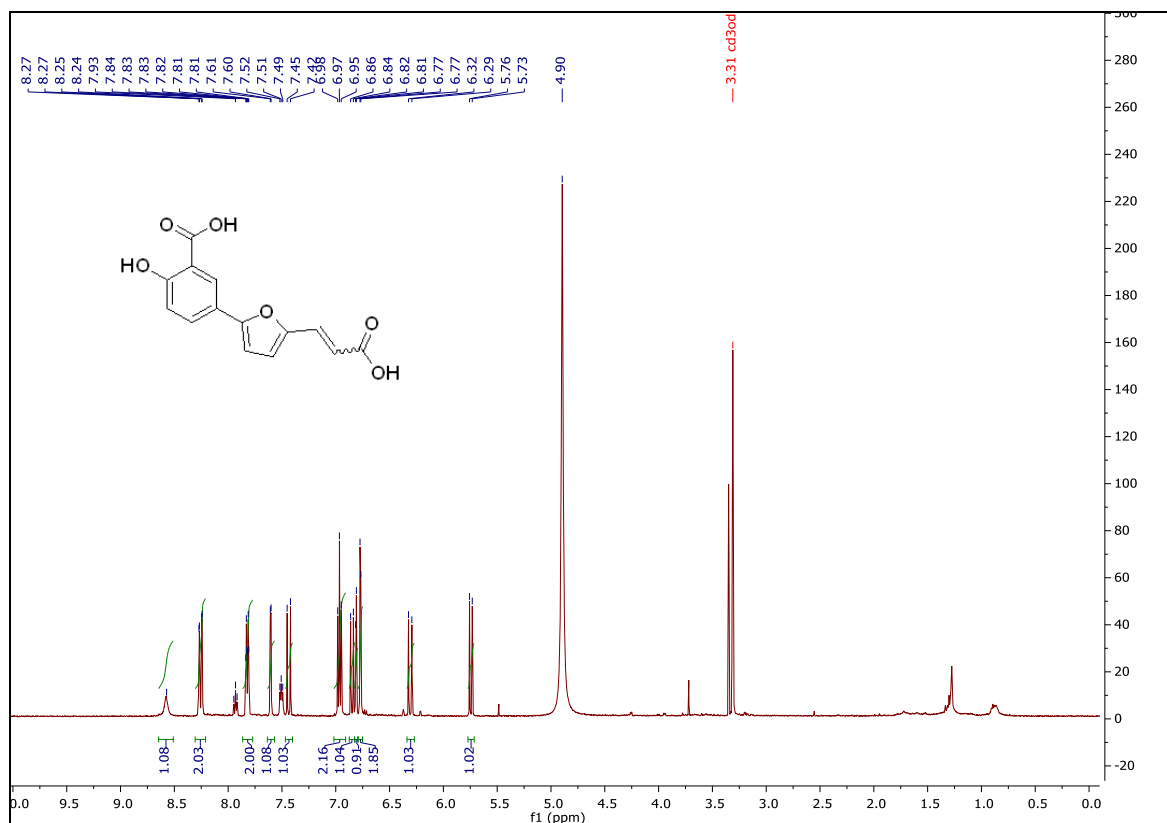
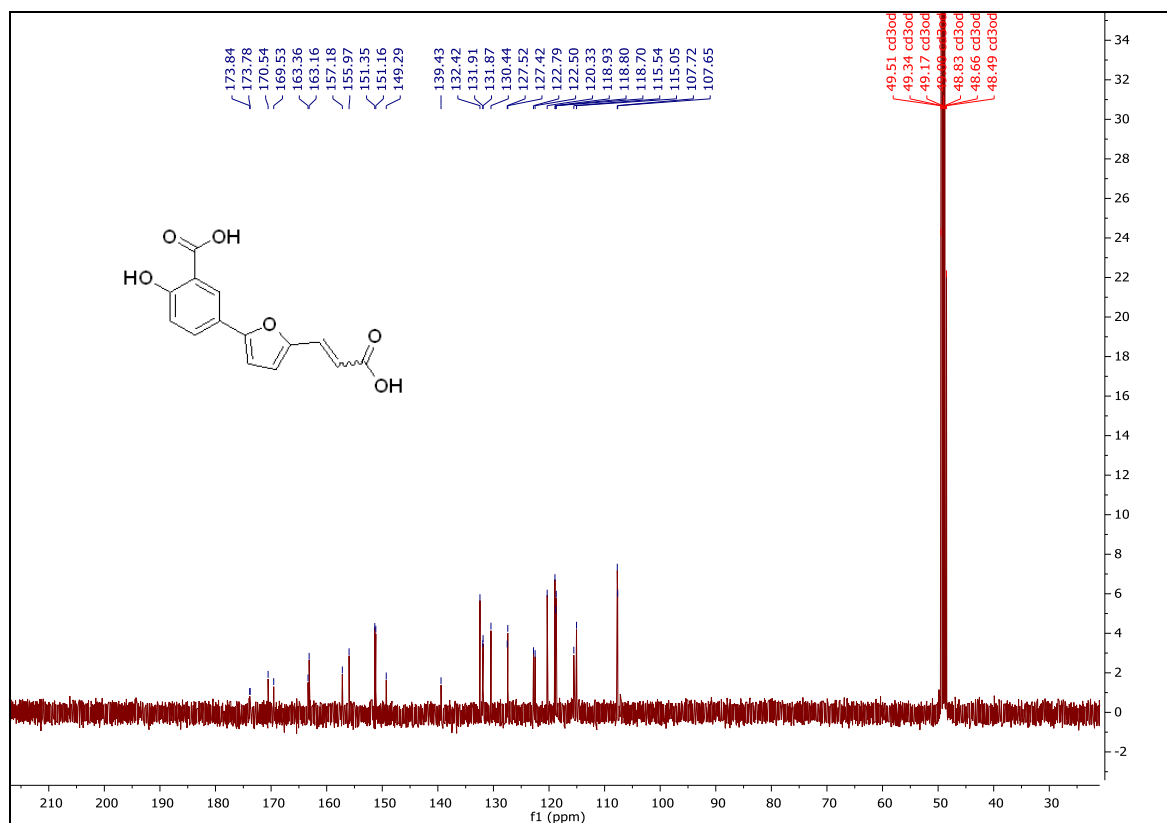
¹H spectrum of **MDMG-1019**¹³C spectrum of **MDMG-1019**

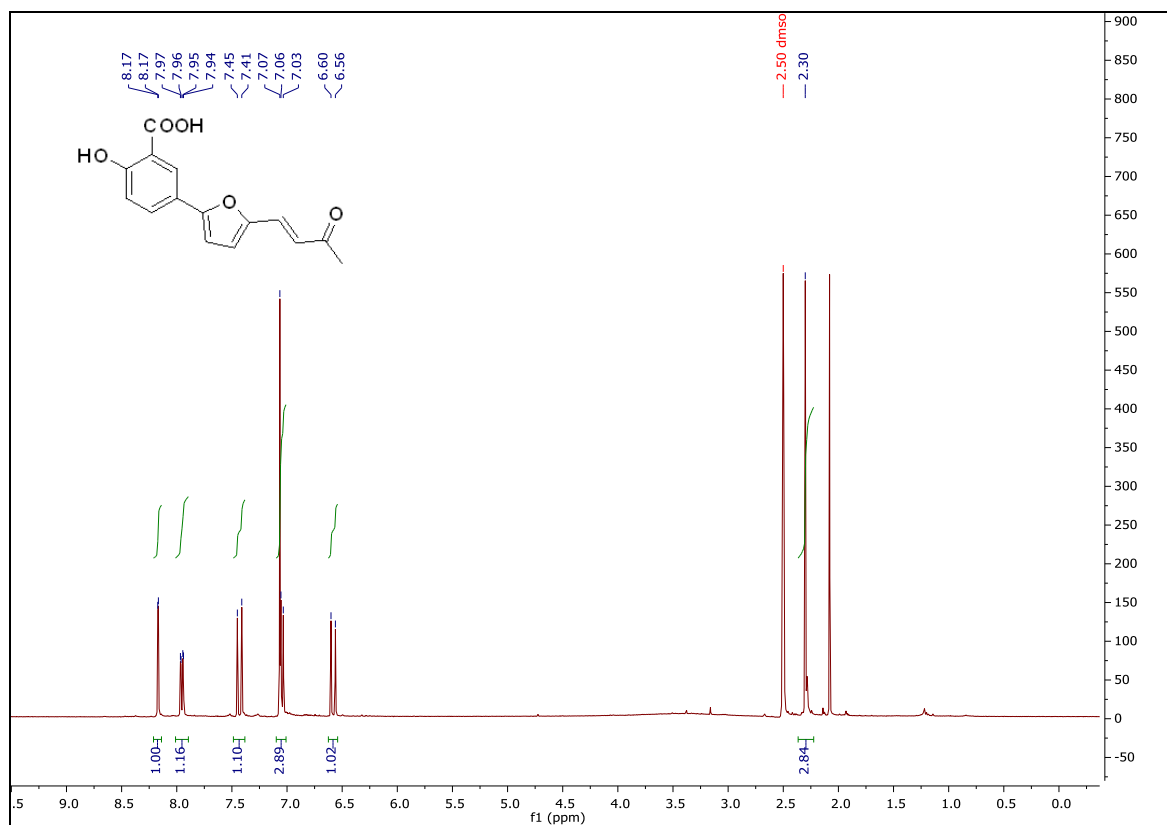
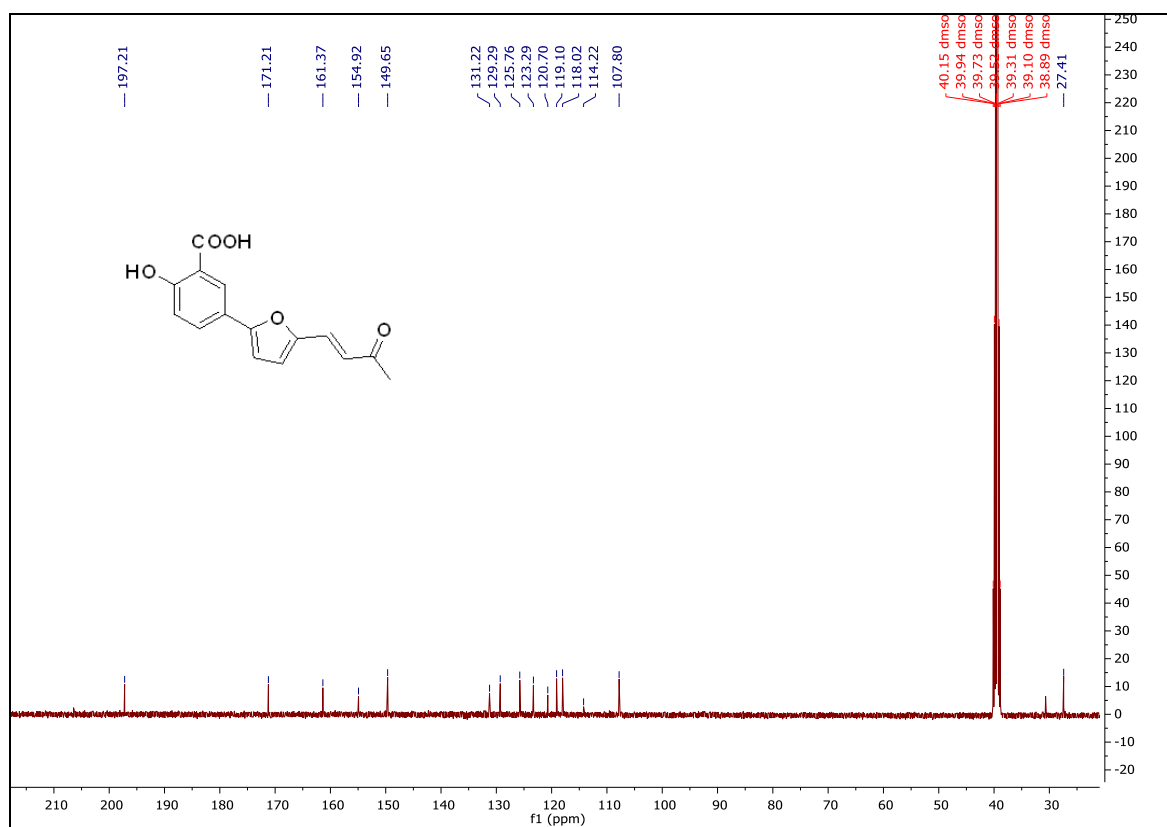
¹H spectrum of **MDMG-1034**¹³C spectrum of **MDMG-1034**

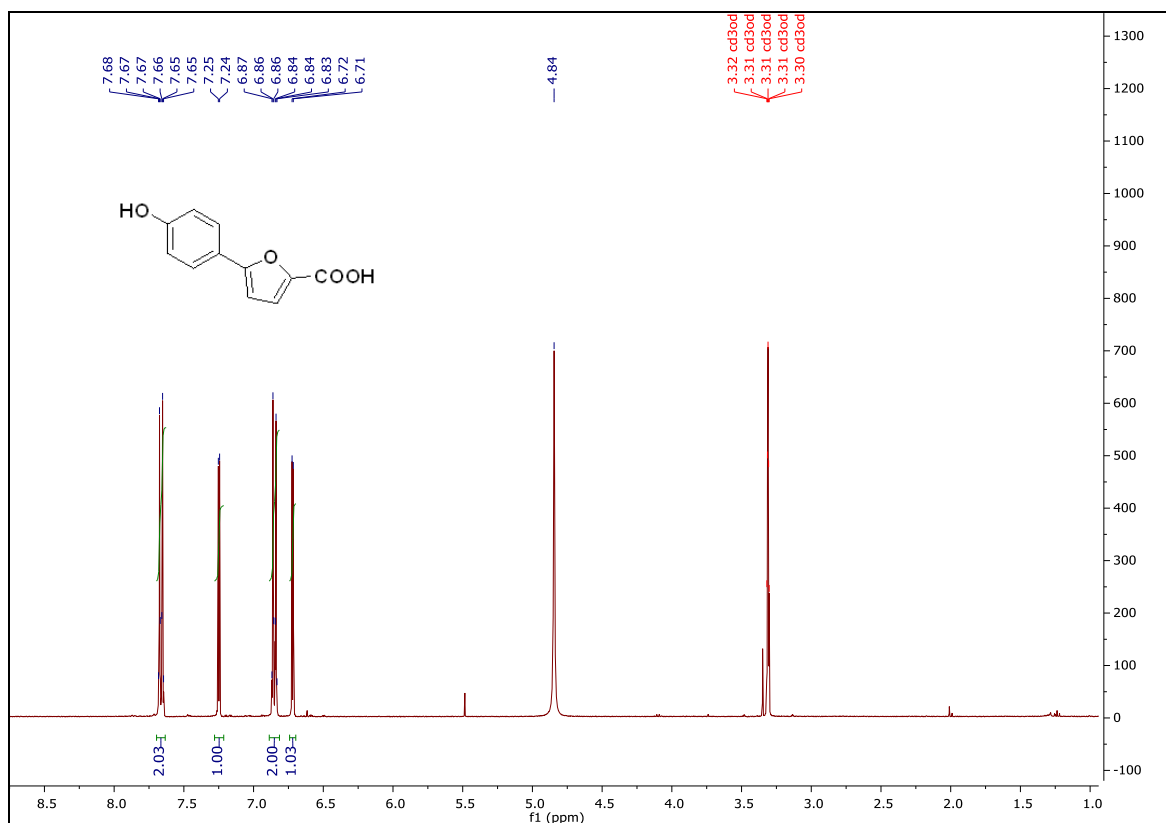
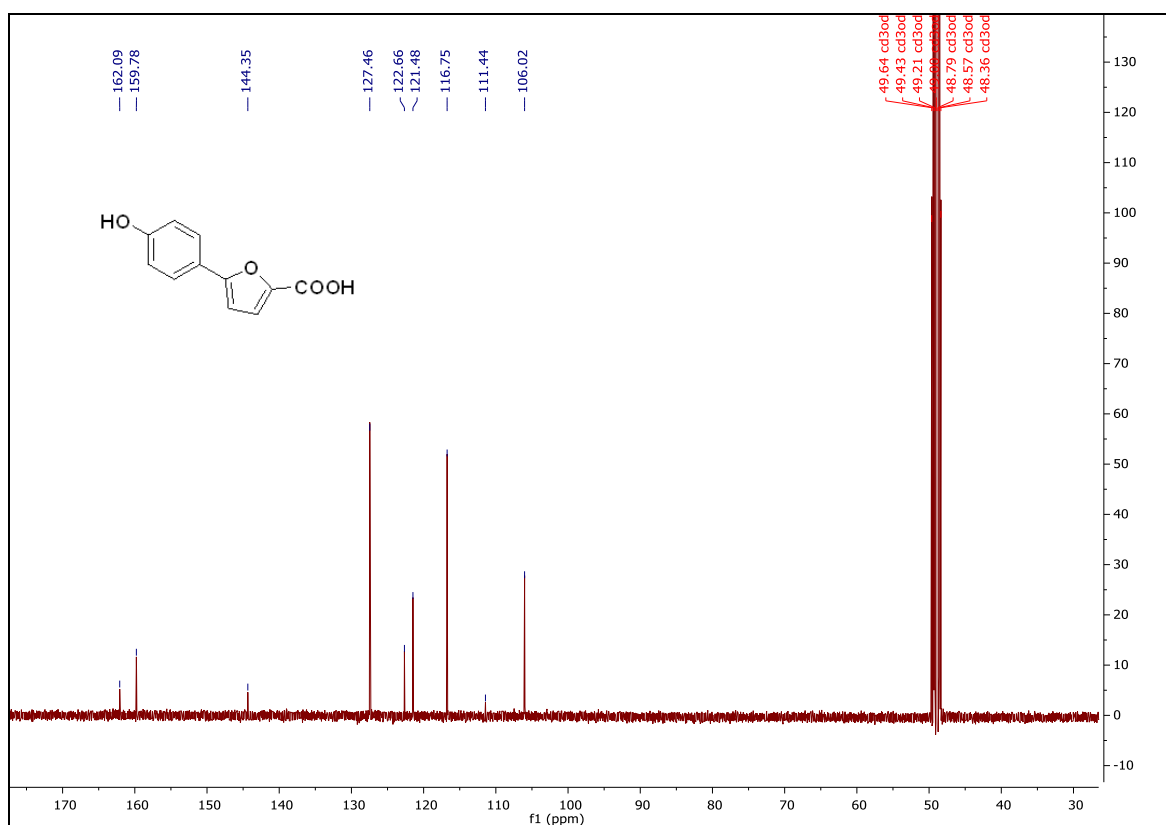
¹H spectrum of **MDMG-1054**¹³C spectrum of **MDMG-1054**

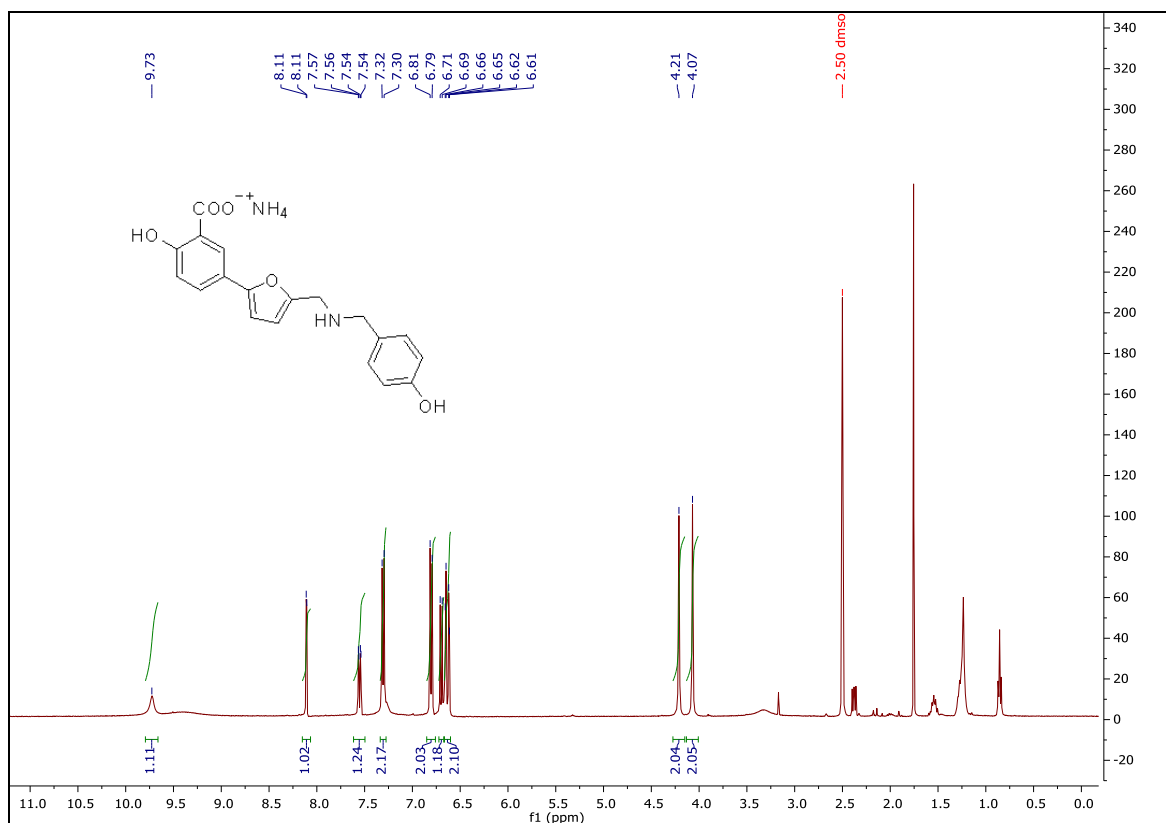
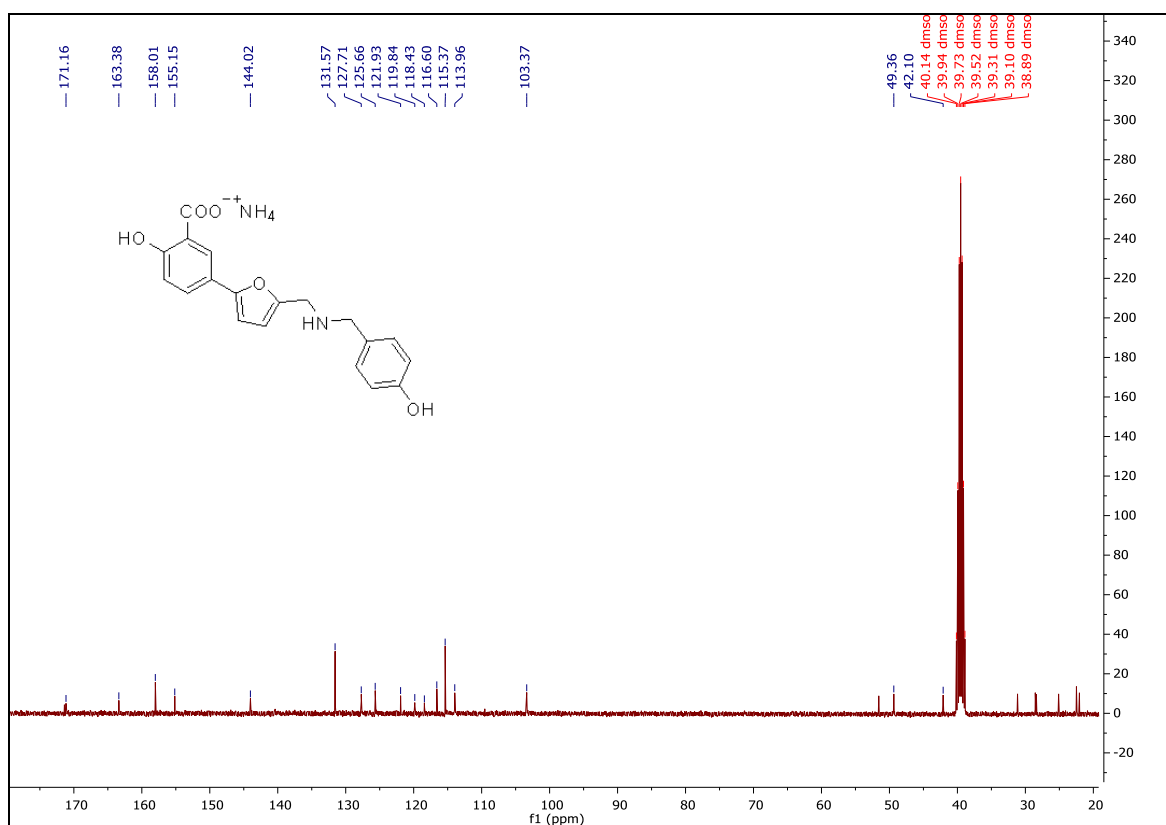
¹H spectrum of **MDMG-1058P**¹³C spectrum of **MDMG-1058P**

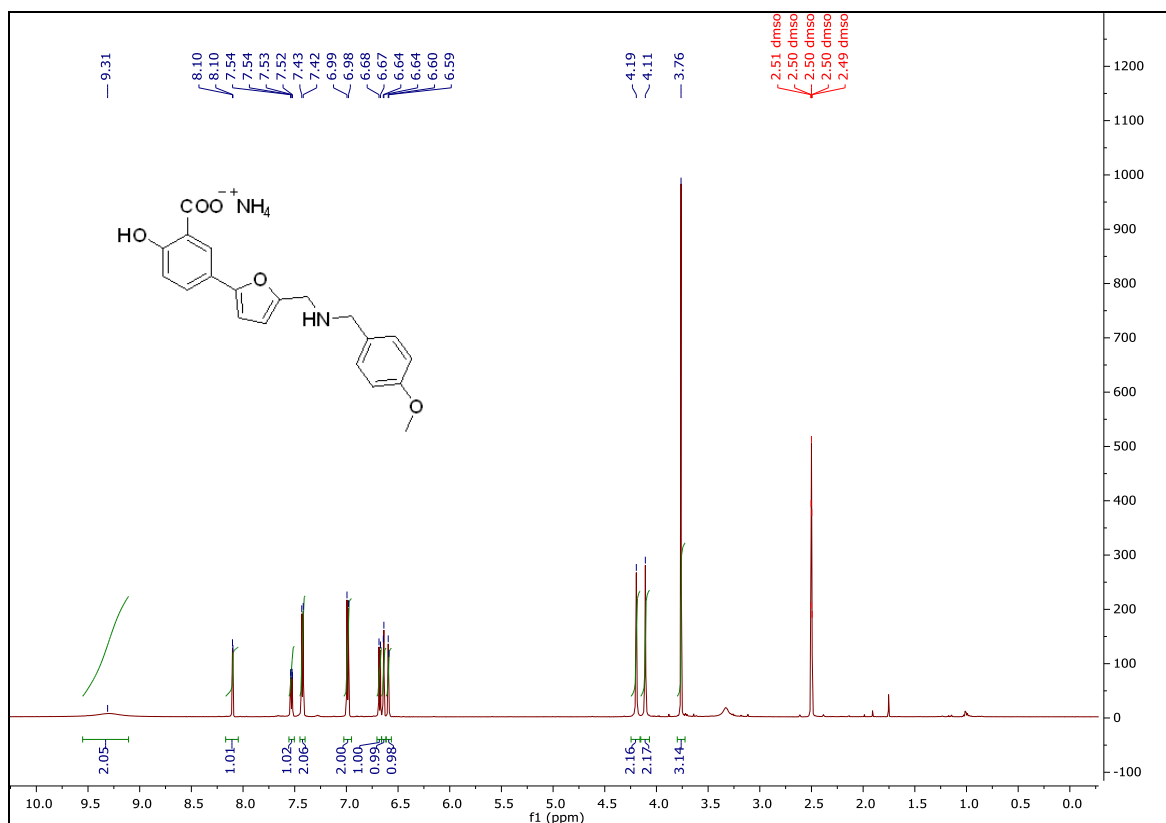
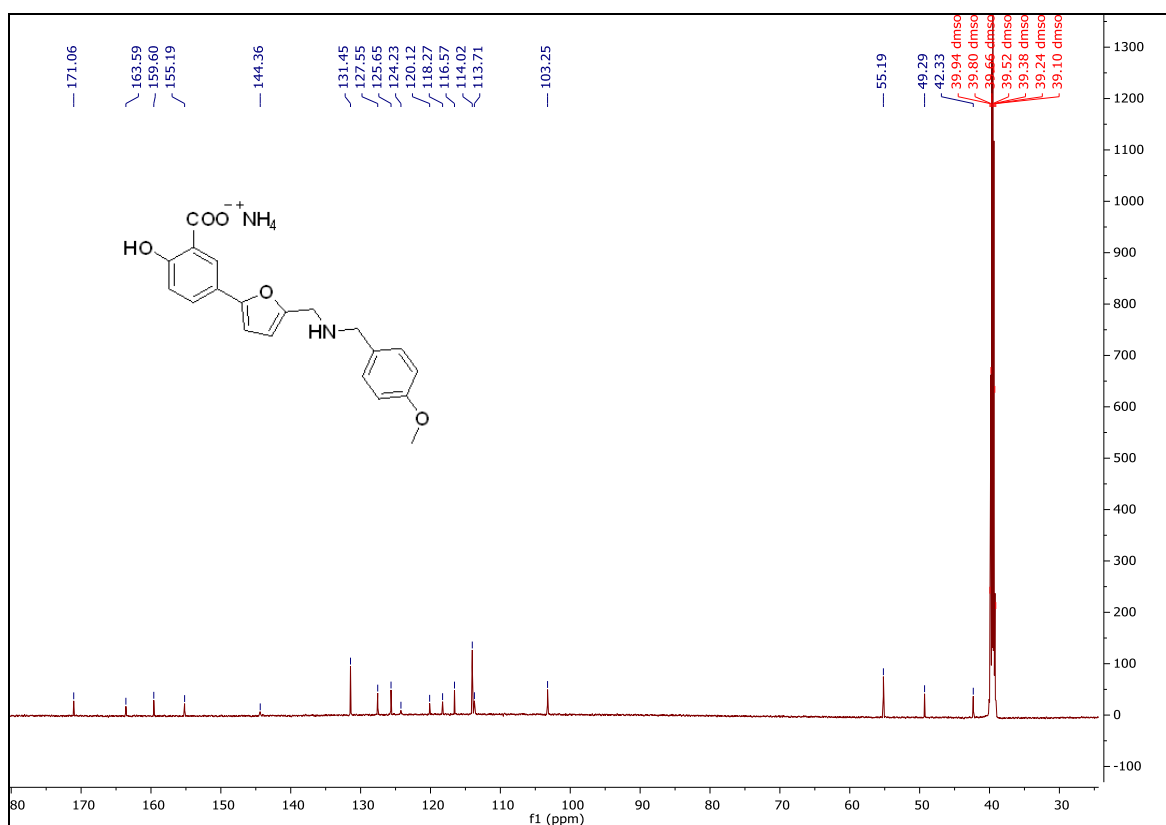
¹H spectrum of **MDMG-1058I**¹³C spectrum of **MDMG-1058I**

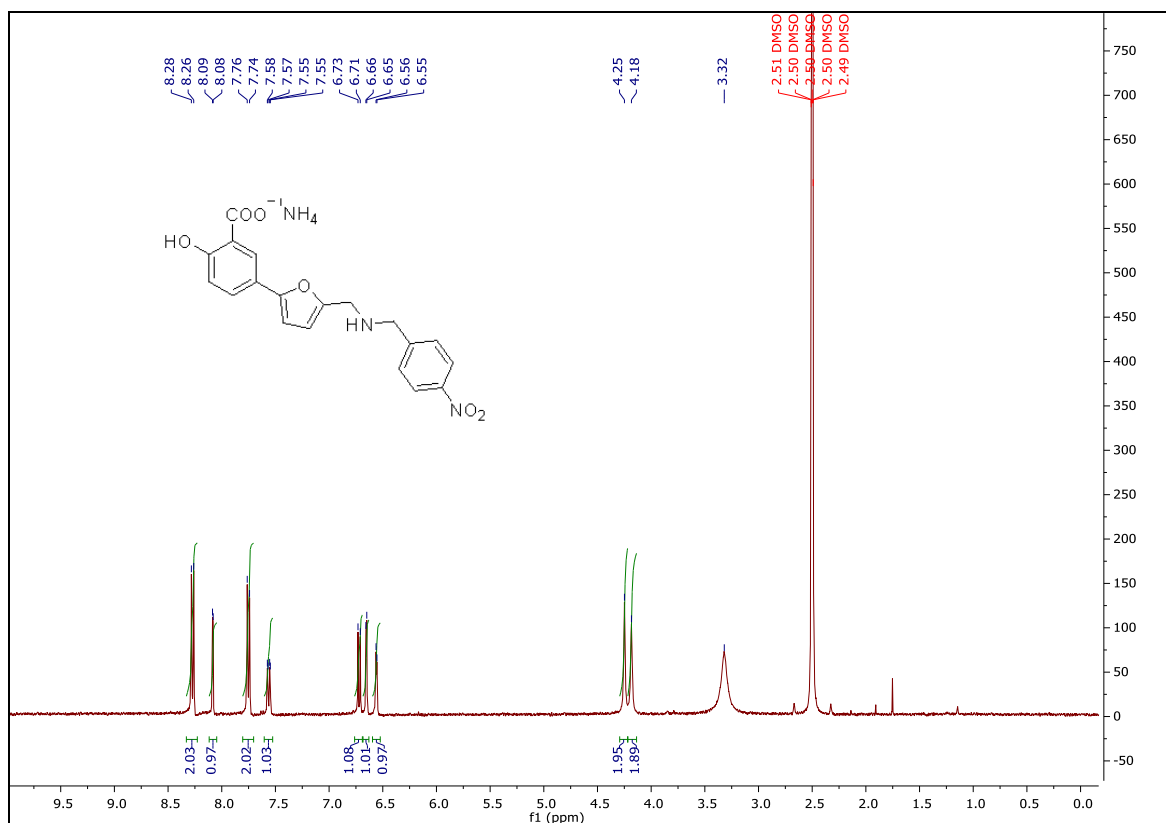
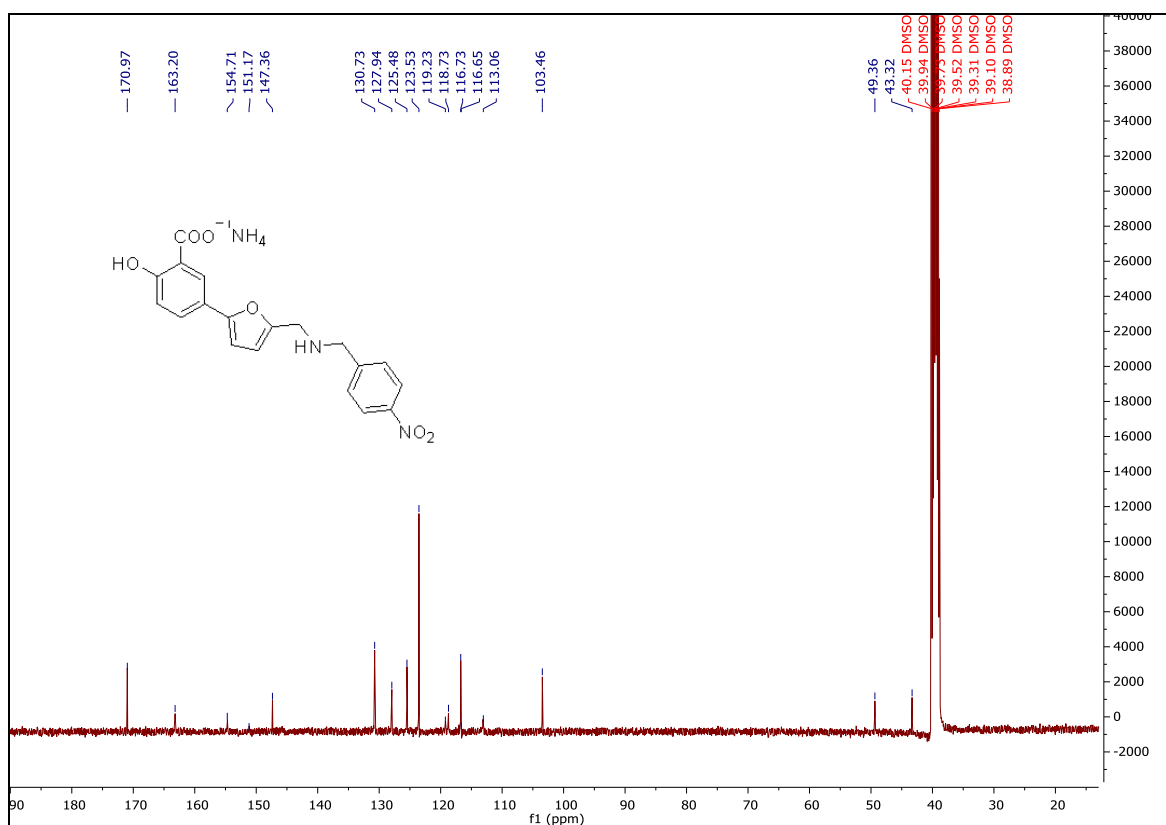
¹H spectrum of **MDMG-1011**¹³C spectrum of **MDMG-1011**

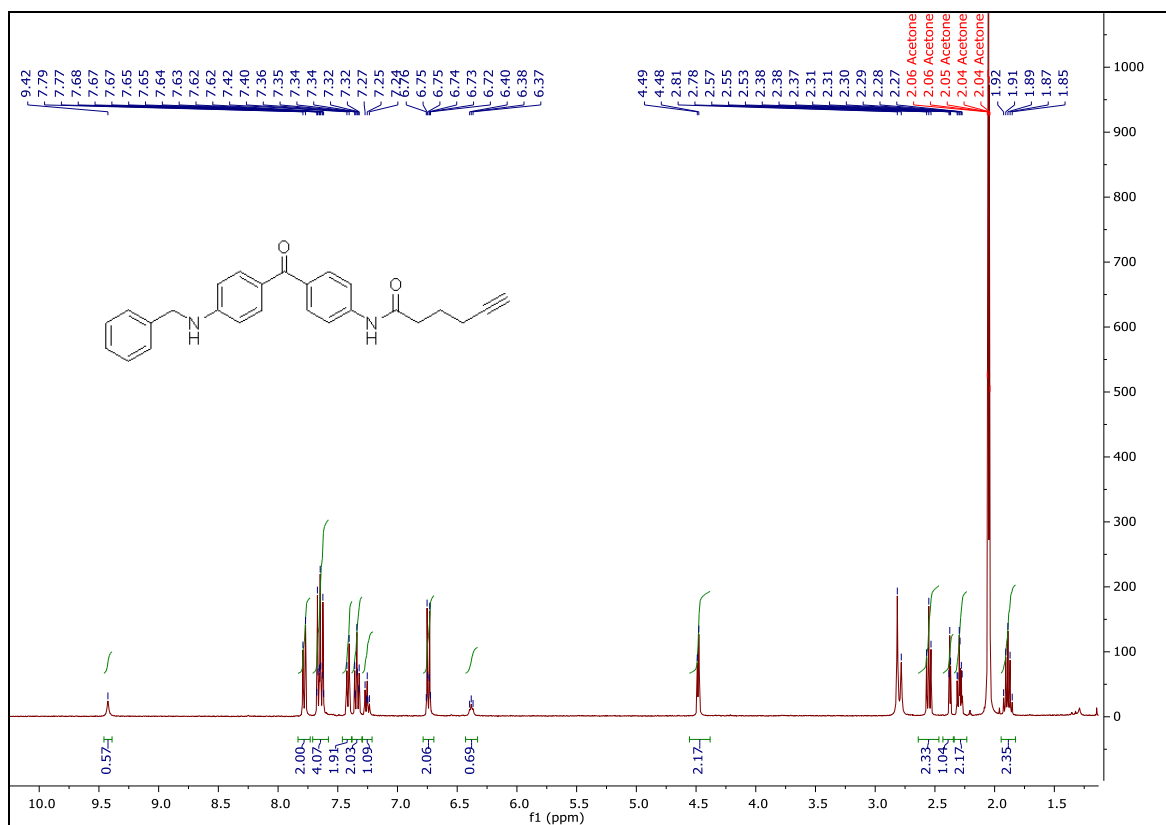
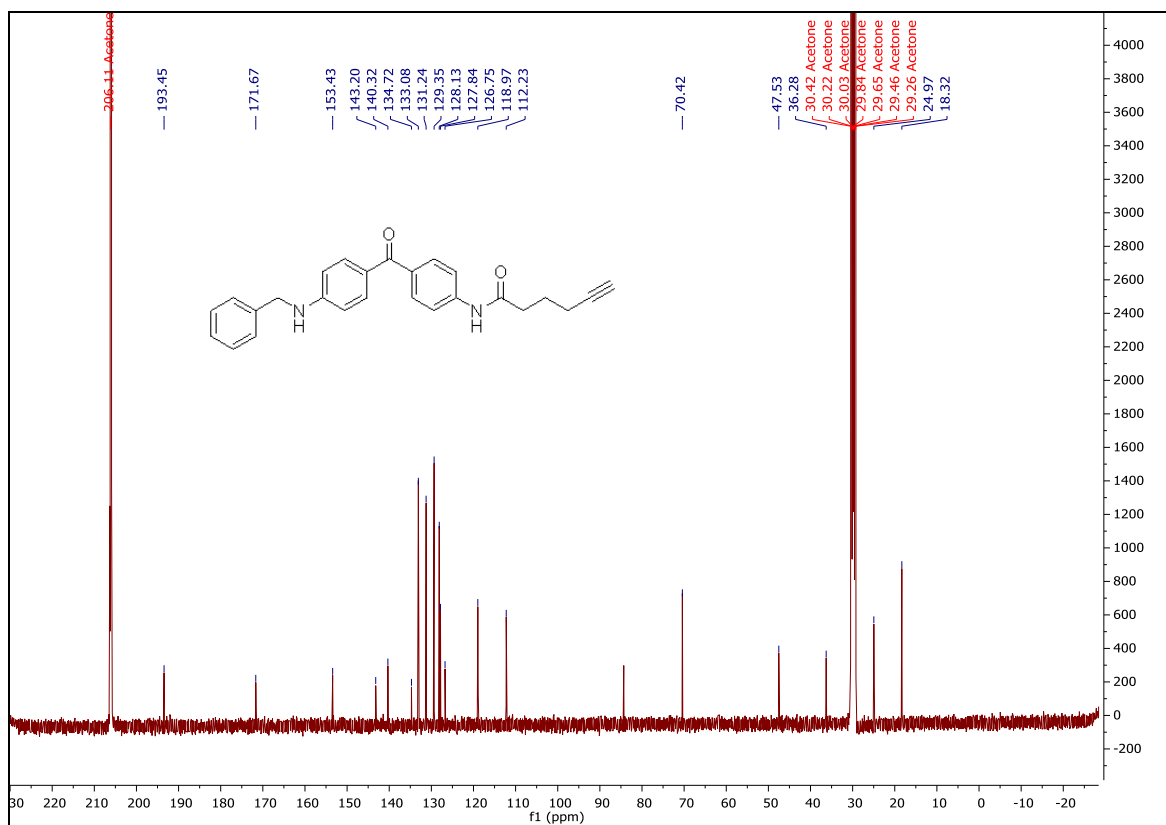
¹H spectrum of **MDMG-1015**¹³C spectrum of **MDMG-1015**

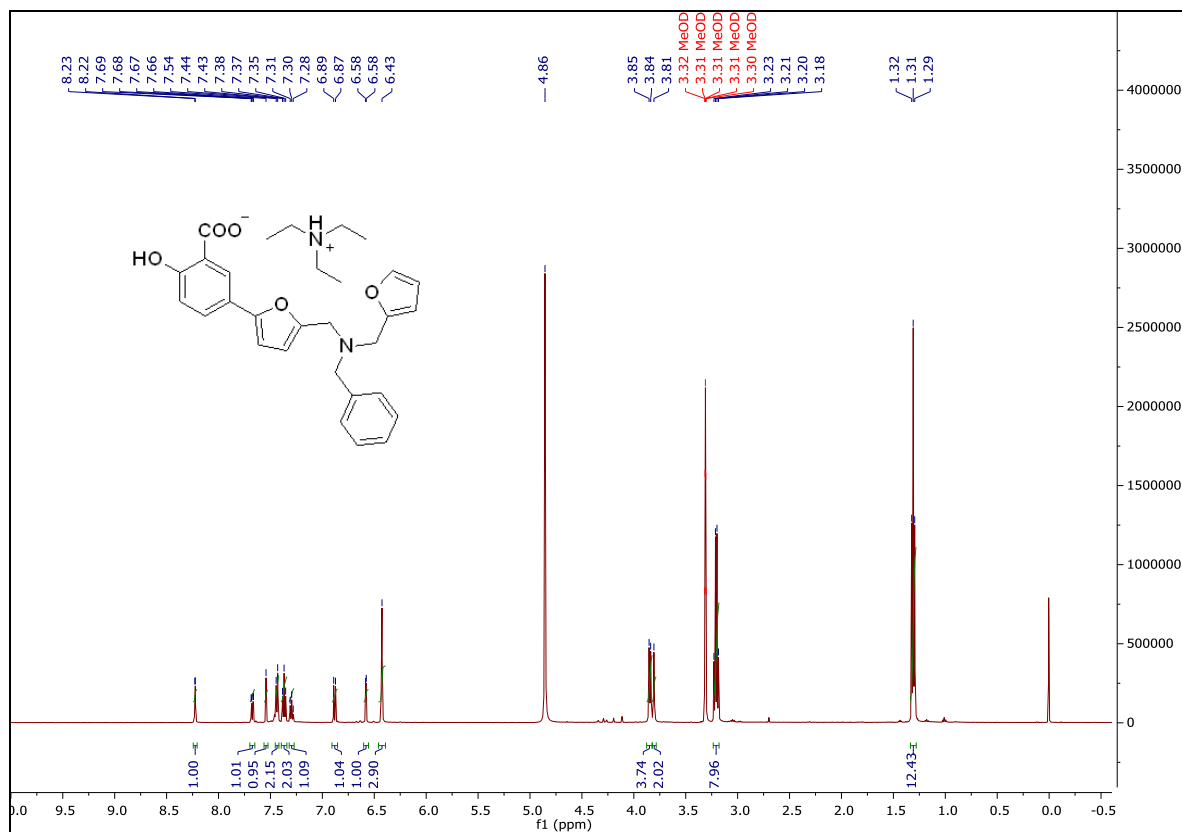
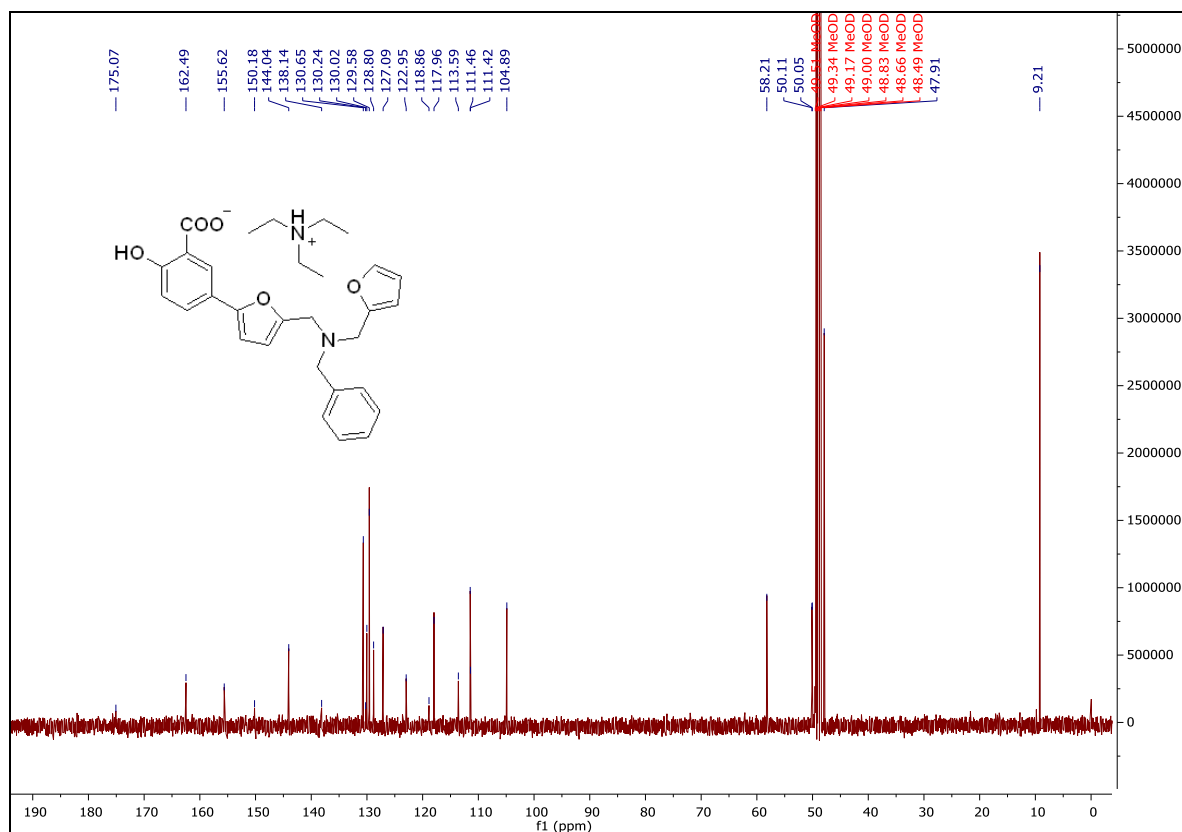
¹H spectrum of **MDMG-1062**¹³C spectrum of **MDMG-1062**

¹H spectrum of **MDMG-1074**¹³C spectrum of **MDMG-1074**

¹H spectrum of **MDMG-1078**¹³C spectrum of **MDMG-1078**

¹H spectrum of **MDMG-1082**¹³C spectrum of **MDMG-1082**

¹H spectrum of **MDMG-1098**¹³C spectrum of **MDMG-1098**

¹H spectrum of **MDMG-1125**¹³C spectrum of **MDMG-1125**

7. Bibliography

7. Bibliography

- [1] Lepoutre. Calculs Multiples Chez Un Enfant: Infiltration Du Parenchyme Rénal Par Des Dépôts Cristallins. **1925**, 20, 424.
- [2] Archer, H. E.; Dormer, A. E.; Scowen, E. F.; Watts, R. W. E. Primary Hyperoxaluria. *The Lancet* **1957**, 270 (6990), 320–322.
- [3] Sikora, P.; von Unruh, G. E.; Beck, B.; Feldkötter, M.; Zajączkowska, M.; Hesse, A.; Hoppe, B. [13C2]Oxalate Absorption in Children with Idiopathic Calcium Oxalate Urolithiasis or Primary Hyperoxaluria. *Kidney Int.* **2008**, 73 (10), 1181–1186.
- [4] Danpure, C. J.; Rumsby, G. Molecular Aetiology of Primary Hyperoxaluria and Its Implications for Clinical Management. *Expert Rev. Mol. Med.* **2004**, 6 (1), 1–16.
- [5] Harambat, J.; Fargue, S.; Bacchetta, J.; Acquaviva, C.; Cochat, P. Primary Hyperoxaluria. *Int. J. Nephrol.* **2011**, 2011.
- [6] Hoppe, B.; Beck, B. B.; Milliner, D. S. The Primary Hyperoxalurias. *Kidney Int.* **2009**, 75 (12), 1264–1271.
- [7] Cochat, P.; Rumsby, G. Primary Hyperoxaluria. *N. Engl. J. Med.* **2013**, 369 (7), 649–658.
- [8] Salido, E.; Pey, A. L.; Rodriguez, R.; Lorenzo, V. Primary Hyperoxalurias: Disorders of Glyoxylate Detoxification. *Biochim. Biophys. Acta BBA - Mol. Basis Dis.* **2012**, 1822 (9), 1453–1464.
- [9] Danpure, C. J.; Jennings, P. R. Peroxisomal Alanine:Glyoxylate Aminotransferase Deficiency in Primary Hyperoxaluria Type I. *FEBS Lett.* **1986**, 201 (1), 20–34.
- [10] Cellini, B.; Bertoldi, M.; Montioli, R.; Paiardini, A.; Borri Voltattorni, C. Human Wild-Type Alanine:Glyoxylate Aminotransferase and Its Naturally Occurring G82E Variant: Functional Properties and Physiological Implications. *Biochem. J.* **2007**, 408 (1), 39–50.
- [11] Poore, R. E.; Hurst, C. H.; Assimos, D. G.; Holmes, R. P. Pathways of Hepatic Oxalate Synthesis and Their Regulation. *Am. J. Physiol.-Cell Physiol.* **1997**, 272 (1), 289–294.
- [12] Primary hyperoxaluria mutation database
<https://www.uclh.nhs.uk/OurServices/ServiceA-Z/PATH/PATHBIOMED/CBIO/Pages/Phmdatabase.aspx>.
- [13] Danpure, C. J.; Jennings, P. R.; Fryer, P.; Purdue, P. E.; Allsop, J. Primary Hyperoxaluria Type 1: Genotypic and Phenotypic Heterogeneity. *J. Inher. Metab. Dis.* **1994**, 17 (4), 487–499.
- [14] Danpure, C. J.; Birdsey, G. M.; Rumsby, G.; Lumb, M. J.; Purdue, P. E.; Allsop, J. Molecular Characterization and Clinical Use of a Polymorphic Tandem Repeat in an Intron of the Human Alanine:Glyoxylate Aminotransferase Gene. *Hum. Genet.* **1994**, 94 (1), 55–64.
- [15] Purdue, P. E.; Takada, Y.; Danpure, C. J. Identification of Mutations Associated with Peroxisome-to-Mitochondrion Mistargeting of Alanine/Glyoxylate Aminotransferase in Primary Hyperoxaluria Type 1. *J. Cell Biol.* **1990**, 111 (6), 2341–2351.
- [16] Takada, Y.; Kaneko, N.; Esumi, H.; Purdue, P. E.; Danpure, C. J. Human Peroxisomal L-Alanine: Glyoxylate Aminotransferase. Evolutionary Loss of a Mitochondrial Targeting Signal by Point Mutation of the Initiation Codon. *Biochem. J.* **1990**, 268 (2), 517–520.

7. Bibliography

- [17] Danpure, C. J.; Lumb, M. J.; Birdsey, G. M.; Zhang, X. Alanine:Glyoxylate Aminotransferase Peroxisome-to-Mitochondrion Mistargeting in Human Hereditary Kidney Stone Disease. *Biochim. Biophys. Acta BBA - Proteins Proteomics* **2003**, *1647* (1), 70–75.
- [18] Hopp, K.; Cogal, A. G.; Bergstralh, E. J.; Seide, B. M.; Olson, J. B.; Meek, A. M.; Lieske, J. C.; Milliner, D. S.; Harris, P. C. Phenotype-Genotype Correlations and Estimated Carrier Frequencies of Primary Hyperoxaluria. *J. Am. Soc. Nephrol.* **2015**, *26* (10), 2559–2570.
- [19] Cochat, P.; Deloraine, A.; Rotily, M.; Olive, F.; Liponski, I.; Deries, N. Epidemiology of Primary Hyperoxaluria Type 1. Société de Néphrologie and the Société de Néphrologie Pédiatrique. *Nephrol. Dial. Transplant. Off. Publ. Eur. Dial. Transpl. Assoc. - Eur. Ren. Assoc.* **1995**, *10 Suppl 8*, 3–7.
- [20] van Woerden, C. S.; Groothoff, J. W.; Wanders, R. J. A.; Davin, J.-C.; Wijburg, F. A. Primary Hyperoxaluria Type 1 in The Netherlands: Prevalence and Outcome. *Nephrol. Dial. Transplant. Off. Publ. Eur. Dial. Transpl. Assoc. - Eur. Ren. Assoc.* **2003**, *18* (2), 273–279.
- [21] Lorenzo, V.; Alvarez, A.; Torres, A.; Torregrosa, V.; Hernández, D.; Salido, E. Presentation and Role of Transplantation in Adult Patients with Type 1 Primary Hyperoxaluria and the I244T AGXT Mutation: Single-Center Experience. *Kidney Int.* **2006**, *70* (6), 1115–1119.
- [22] Santana, A.; Salido, E.; Torres, A.; Shapiro, L. J. Primary Hyperoxaluria Type 1 in the Canary Islands: A Conformational Disease Due to I244T Mutation in the P11L-Containing Alanine:Glyoxylate Aminotransferase. *Proc. Natl. Acad. Sci.* **2003**, *100* (12), 7277–7282.
- [23] Al-Eisa, A. A.; Samhan, M.; Naseef, M. End-Stage Renal Disease in Kuwaiti Children: An 8-Year Experience. *Transplant. Proc.* **2004**, *36* (6), 1788–1791.
- [24] Kamoun, A.; Lakhoua, R. End-Stage Renal Disease of the Tunisian Child: Epidemiology, Etiologies, and Outcome. *Pediatr. Nephrol. Berl. Ger.* **1996**, *10* (4), 479–482.
- [25] Williams, H. E.; Smith, L. H. L-Glyceric Aciduria. *N. Engl. J. Med.* **1968**, *278* (5), 233–239.
- [26] Seargeant, L. E.; deGroot, G. W.; Dilling, L. A.; Mallory, C. J.; Haworth, J. C. Primary Oxaluria Type 2 (L-Glyceric Aciduria): A Rare Cause of Nephrolithiasis in Children. *J. Pediatr.* **1991**, *118* (6), 912–914.
- [27] Cramer, S. D.; Ferree, P. M.; Lin, K.; Milliner, D. S.; Holmes, R. P. The Gene Encoding Hydroxypyruvate Reductase (GRHPR) Is Mutated in Patients with Primary Hyperoxaluria Type II. *Hum. Mol. Genet.* **1999**, *8* (11), 2063–2069.
- [28] Rumsby, G.; Cregeen, D. P. Identification and Expression of a cDNA for Human Hydroxypyruvate/Glyoxylate Reductase. *Biochim. Biophys. Acta BBA - Gene Struct. Expr.* **1999**, *1446* (3), 383–388.
- [29] Rumsby, G.; Sharma, A.; Cregeen, D. P.; Solomon, L. R. Primary Hyperoxaluria Type 2 without L-Glyceric Aciduria: Is the Disease Under-diagnosed? *Nephrol. Dial. Transplant.* **2001**, *16* (8), 1697–1699.
- [30] Behnam, J. T.; Williams, E. L.; Brink, S.; Rumsby, G.; Danpure, C. J. Reconstruction of Human Hepatocyte Glyoxylate Metabolic Pathways in Stably Transformed Chinese-Hamster Ovary Cells. *Biochem. J.* **2006**, *394* (2), 409–416.
- [31] Bhat, S.; Williams, E. L.; Rumsby, G. Tissue Differences in the Expression of Mutations and Polymorphisms in the GRHPR Gene and Implications for Diagnosis of Primary Hyperoxaluria Type 2. *Clin. Chem.* **2005**, *51* (12), 2423–2425.
- [32] Sas, D. J.; Harris, P. C.; Milliner, D. S. Recent Advances in the Identification and Management of Inherited Hyperoxalurias. *Urolithiasis* **2019**, *47* (1), 79–89.

- [33] Milliner, D. S.; Wilson, D. M.; Smith, L. H. Phenotypic Expression of Primary Hyperoxaluria: Comparative Features of Types I and II. *Kidney Int.* **2001**, *59* (1), 31–36.
- [34] Booth, M. P. S.; Conners, R.; Rumsby, G.; Brady, R. L. Structural Basis of Substrate Specificity in Human Glyoxylate Reductase/Hydroxypyruvate Reductase. *J. Mol. Biol.* **2006**, *360* (1), 178–189.
- [35] Belostotsky, R.; Seboun, E.; Idelson, G. H.; Milliner, D. S.; Becker-Cohen, R.; Rinat, C.; Monico, C. G.; Feinstein, S.; Ben-Shalom, E.; Magen, D.; et al. Mutations in DHPSL Are Responsible For Primary Hyperoxaluria Type III. *Am. J. Hum. Genet.* **2010**, *87* (3), 392–399.
- [36] Riedel, T. J.; Johnson, L. C.; Knight, J.; Hantgan, R. R.; Holmes, R. P.; Lowther, W. T. Structural and Biochemical Studies of Human 4-Hydroxy-2-Oxoglutarate Aldolase: Implications for Hydroxyproline Metabolism in Primary Hyperoxaluria. *PLOS ONE* **2011**, *6* (10), e26021.
- [37] Monico, C. G.; Rossetti, S.; Belostotsky, R.; Cogal, A. G.; Herges, R. M.; Seide, B. M.; Olson, J. B.; Bergstrahl, E. J.; Williams, H. J.; Haley, W. E.; et al. Primary Hyperoxaluria Type III Gene HOGA1 (Formerly DHPSL) as a Possible Risk Factor for Idiopathic Calcium Oxalate Urolithiasis. *Clin. J. Am. Soc. Nephrol.* **2011**, *6* (9), 2289–2295.
- [38] Riedel, T. J.; Knight, J.; Murray, M. S.; Milliner, D. S.; Holmes, R. P.; Lowther, W. T. 4-Hydroxy-2-Oxoglutarate Aldolase Inactivity in Primary Hyperoxaluria Type 3 and Glyoxylate Reductase Inhibition. *Biochim. Biophys. Acta* **2012**, *1822* (10), 1544–1552.
- [39] Li, X.; Knight, J.; Todd Lowther, W.; Holmes, R. P. Hydroxyproline Metabolism in a Mouse Model of Primary Hyperoxaluria Type 3. *Biochim. Biophys. Acta BBA - Mol. Basis Dis.* **2015**, *1852* (12), 2700–2705.
- [40] Hoppe, B.; Leumann, E.; von Unruh, G.; Laube, N.; Hesse, A. Diagnostic and Therapeutic Approaches in Patients with Secondary Hyperoxaluria. *Front. Biosci. J. Virtual Libr.* **2003**, *8*, 437–443.
- [41] Schork, N. J. Personalized Medicine: Time for One-Person Trials. *Nat. News* **2015**, *520*, 609–611.
- [42] Cellini, B. Treatment Options in Primary Hyperoxaluria Type I. *Expert Opin. Orphan Drugs* **2017**, *5* (4), 309–319.
- [43] Cochat, P.; Hulton, S.-A.; Acquaviva, C.; Danpure, C. J.; Daudon, M.; De Marchi, M.; Fargue, S.; Groothoff, J.; Harambat, J.; Hoppe, B.; et al. Primary Hyperoxaluria Type 1: Indications for Screening and Guidance for Diagnosis and Treatment. *Nephrol. Dial. Transplant. Off. Publ. Eur. Dial. Transpl. Assoc. - Eur. Ren. Assoc.* **2012**, *27* (5), 1729–1736.
- [44] Mandrile, G.; van Woerden, C. S.; Berchiolla, P.; Beck, B. B.; Acquaviva Bourdain, C.; Hulton, S.-A.; Rumsby, G. Data from a Large European Study Indicate That the Outcome of Primary Hyperoxaluria Type 1 Correlates with the AGXT Mutation Type. *Kidney Int.* **2014**, *86* (6), 1197–1204.
- [45] Li, X.; Knight, J.; Fargue, S.; Buchalski, B.; Guan, Z.; Inscho, E. W.; Liebow, A.; Fitzgerald, K.; Querbes, W.; Todd Lowther, W.; et al. Metabolism of ¹³C₅-Hydroxyproline in Mouse Models of Primary Hyperoxaluria and Its Inhibition by RNAi Therapeutics Targeting Liver Glycolate Oxidase and Hydroxyproline Dehydrogenase. *Biochim. Biophys. Acta BBA - Mol. Basis Dis.* **2016**, *1862* (2), 233–239.
- [46] Hatch, M.; Freel, R. W. The Roles and Mechanisms of Intestinal Oxalate Transport in Oxalate Homeostasis. *Semin. Nephrol.* **2008**, *28* (2), 143–151.
- [47] Hatch, M.; Freel, R. W. A Human Strain of Oxalobacter (HC-1) Promotes Enteric Oxalate Secretion in the Small Intestine of Mice and Reduces Urinary Oxalate Excretion. *Urolithiasis* **2013**, *41* (5), 379–384.
- [48] Hatch, M.; Gjymishka, A.; Salido, E. C.; Allison, M. J.; Freel, R. W. Enteric Oxalate Elimination Is Induced and Oxalate Is Normalized in a Mouse Model of

- Primary Hyperoxaluria Following Intestinal Colonization with Oxalobacter. *Am. J. Physiol. Gastrointest. Liver Physiol.* **2011**, 300 (3), G461-469.
- [49] Hoppe, B.; Groothoff, J. W.; Hulton, S.-A.; Cochat, P.; Niaudet, P.; Kemper, M. J.; Deschênes, G.; Unwin, R.; Milliner, D. Efficacy and Safety of Oxalobacter Formigenes to Reduce Urinary Oxalate in Primary Hyperoxaluria. *Nephrol. Dial. Transplant.* **2011**, 26 (11), 3609–3615.
- [50] Hoppe, B.; Niaudet, P.; Salomon, R.; Harambat, J.; Hulton, S.-A.; Van't Hoff, W.; Moochhala, S. H.; Deschênes, G.; Lindner, E.; Sjögren, A.; et al. A Randomised Phase I/II Trial to Evaluate the Efficacy and Safety of Orally Administered Oxalobacter Formigenes to Treat Primary Hyperoxaluria. *Pediatr. Nephrol.* **2017**, 32 (5), 781–790.
- [51] Milliner, D.; Hoppe, B.; Groothoff, J. A Randomised Phase II/III Study to Evaluate the Efficacy and Safety of Orally Administered Oxalobacter Formigenes to Treat Primary Hyperoxaluria. *Urolithiasis* **2018**, 46 (4), 313–323.
- [52] Grujic, D.; Salido, E. C.; Shenoy, B. C.; Langman, C. B.; McGrath, M. E.; Patel, R. J.; Rashid, A.; Mandapati, S.; Jung, C. W.; Margolin, A. L. Hyperoxaluria Is Reduced and Nephrocalcinosis Prevented with an Oxalate-Degrading Enzyme in Mice with Hyperoxaluria. *Am. J. Nephrol.* **2009**, 29 (2), 86–93.
- [53] Van Woerden, C. S.; Groothoff, J. W.; Wijburg, F. A.; Annink, C.; Wanders, R. J. A.; Waterham, H. R. Clinical Implications of Mutation Analysis in Primary Hyperoxaluria Type 1. *Kidney Int.* **2004**, 66 (2), 746–752.
- [54] Skolarikos, A.; Alivizatos, G.; de la Rosette, J. Extracorporeal Shock Wave Lithotripsy 25 Years Later: Complications and Their Prevention. *Eur. Urol.* **2006**, 50 (5), 981–990.
- [55] Straub, M.; Gschwend, J.; Zorn, C. Pediatric Urolithiasis: The Current Surgical Management. *Pediatr. Nephrol. Berl. Ger.* **2010**, 25 (7), 1239–1244.
- [56] Monico, C. G.; Rossetti, S.; Olson, J. B.; Milliner, D. S. Pyridoxine Effect in Type I Primary Hyperoxaluria Is Associated with the Most Common Mutant Allele. *Kidney Int.* **2005**, 67 (5), 1704–1709.
- [57] Jamieson, N. V. A 20-Year Experience of Combined Liver/Kidney Transplantation for Primary Hyperoxaluria (PH1): The European PH1 Transplant Registry Experience 1984–2004. *Am. J. Nephrol.* **2005**, 25 (3), 282–289.
- [58] Summitt, C. B.; Johnson, L. C.; Jönsson, T. J.; Parsonage, D.; Holmes, R. P.; Lowther, W. T. Proline Dehydrogenase 2 (PRODH2) Is a Hydroxyproline Dehydrogenase (HYPDH) and Molecular Target for Treating Primary Hyperoxaluria. *Biochem. J.* **2015**, 466 (2), 273–281.
- [59] Salido, E.; Rodriguez-Pena, M.; Santana, A.; Beattie, S. G.; Petry, H.; Torres, A. Phenotypic Correction of a Mouse Model for Primary Hyperoxaluria with Adeno-Associated Virus Gene Transfer. *Mol. Ther.* **2011**, 19 (5), 870–875.
- [60] Castello, R.; Borzone, R.; D'Aria, S.; Annunziata, P.; Piccolo, P.; Brunetti-Pierri, N. Helper-Dependent Adenoviral Vectors for Liver-Directed Gene Therapy of Primary Hyperoxaluria Type 1. *Gene Ther.* **2016**, 23 (2), 129–134.
- [61] Hoppe, B. An Update on Primary Hyperoxaluria. *Nat. Rev. Nephrol.* **2012**, 8 (8), 467–475.
- [62] Beck, B. B.; Habbig, S.; Dittrich, K.; Stippel, D.; Kaul, I.; Koerber, F.; Goebel, H.; Salido, E. C.; Kemper, M.; Meyburg, J.; et al. Liver Cell Transplantation in Severe Infantile Oxalosis—A Potential Bridging Procedure to Orthotopic Liver Transplantation? *Nephrol. Dial. Transplant.* **2012**, 27 (7), 2984–2989.
- [63] Martin-Higueras, C.; Torres, A.; Salido, E. Molecular Therapy of Primary Hyperoxaluria. *J. Inherit. Metab. Dis.* **2017**, 40 (4), 481–489.
- [64] Zapata-Linares, N.; Rodriguez, S.; Salido, E.; Abizanda, G.; Iglesias, E.; Prosper, F.; Gonzalez-Aseguinolaza, G.; Rodriguez-Madoz, J. R. Generation and Characterization of Human iPSC Lines Derived from a Primary Hyperoxaluria Type I Patient with p.I244T Mutation. *Stem Cell Res.* **2016**, 16 (1), 116–119.

- [65] Guha, C.; Yamanouchi, K.; Jiang, J.; Wang, X.; Chowdhury, N. R.; Santana, A.; Shapiro, L. J.; Salido, E.; Roy-Chowdhury, J. Feasibility of Hepatocyte Transplantation-Based Therapies for Primary Hyperoxalurias. *Am. J. Nephrol.* **2005**, *25* (2), 161–170.
- [66] Jiang, J.; Salido, E.; Guha, C.; Wang, X.; Moitra, R.; Liu, L.; Roy-Chowdhury, J.; Roy-Chowdhury, N. Correction of Hyperoxaluria by Liver Repopulation with Hepatocytes in a Mouse Model of Primary Hyperoxaluria Type-1. *Transplantation* **2008**, *85* (9), 1253–1260.
- [67] Ringe, D.; Petsko, G. A. Q&A: What Are Pharmacological Chaperones and Why Are They Interesting? *J. Biol.* **2009**, *8* (9), 80.
- [68] Cellini, B.; Montioli, R.; Oppici, E.; Astegno, A.; Voltattorni, C. B. The Chaperone Role of the Pyridoxal 5'-Phosphate and Its Implications for Rare Diseases Involving B6-Dependent Enzymes. *Clin. Biochem.* **2014**, *47* (3), 158–165.
- [69] Fargue, S.; Rumsby, G.; Danpure, C. J. Multiple Mechanisms of Action of Pyridoxine in Primary Hyperoxaluria Type 1. *Biochim. Biophys. Acta* **2013**, *1832* (10), 1776–1783.
- [70] Oppici, E.; Fargue, S.; Reid, E. S.; Mills, P. B.; Clayton, P. T.; Danpure, C. J.; Cellini, B. Pyridoxamine and Pyridoxal Are More Effective than Pyridoxine in Rescuing Folding-Defective Variants of Human Alanine:Glyoxylate Aminotransferase Causing Primary Hyperoxaluria Type I. *Hum. Mol. Genet.* **2015**, *24* (19), 5500–5511.
- [71] Oppici, E.; Montioli, R.; Dindo, M.; Maccari, L.; Porcari, V.; Lorenzetto, A.; Chellini, S.; Voltattorni, C. B.; Cellini, B. The Chaperoning Activity of Amino-Oxyacetic Acid on Folding-Defective Variants of Human Alanine:Glyoxylate Aminotransferase Causing Primary Hyperoxaluria Type I. *ACS Chem. Biol.* **2015**, *10* (10), 2227–2236.
- [72] Miyata, N.; Steffen, J.; Johnson, M. E.; Fargue, S.; Danpure, C. J.; Koehler, C. M. Pharmacologic Rescue of an Enzyme-Trafficking Defect in Primary Hyperoxaluria 1. *Proc. Natl. Acad. Sci.* **2014**, *111* (40), 14406–14411.
- [73] Madoux, F.; Janovick, J. A.; Smithson, D.; Fargue, S.; Danpure, C. J.; Scampavia, L.; Chen, Y.-T.; Spicer, T. P.; Conn, P. M. Development of a Phenotypic High-Content Assay to Identify Pharmacoperone Drugs for the Treatment of Primary Hyperoxaluria Type 1 by High-Throughput Screening. *ASSAY Drug Dev. Technol.* **2015**, *13* (1), 16–24.
- [74] Al Hafid, N.; Christodoulou, J. Phenylketonuria: A Review of Current and Future Treatments. *Transl. Pediatr.* **2015**, *4* (4), 304–317–317.
- [75] Lachmann, R. Enzyme Replacement Therapy for Lysosomal Storage Diseases. *Curr. Opin. Pediatr.* **2011**, *23* (6), 588–593.
- [76] Roncador, A.; Oppici, E.; Talelli, M.; Pariente, A. N.; Donini, M.; Dusi, S.; Voltattorni, C. B.; Vicent, M. J.; Cellini, B. Use of Polymer Conjugates for the Intraperoxisomal Delivery of Engineered Human Alanine:Glyoxylate Aminotransferase as a Protein Therapy for Primary Hyperoxaluria Type I. *Nanomedicine Nanotechnol. Biol. Med.* **2017**, *13* (3), 897–907.
- [77] Mesa-Torres, N.; Yunta, C.; Fabelo-Rosa, I.; Gonzalez-Rubio, J. M.; Sánchez-Ruiz, J. M.; Salido, E.; Albert, A.; Pey, A. L. The Consensus-Based Approach for Gene/Enzyme Replacement Therapies and Crystallization Strategies: The Case of Human Alanine-Glyoxylate Aminotransferase. *Biochem. J.* **2014**, *462* (3), 453–463.
- [78] Kukreja, A.; Lasaro, M.; Cobaugh, C.; Forbes, C.; Tang, J.-P.; Gao, X.; Martin-Higueras, C.; Pey, A. L.; Salido, E.; Sobolov, S.; et al. Systemic Alanine Glyoxylate Aminotransferase mRNA Improves Glyoxylate Metabolism in a Mouse Model of Primary Hyperoxaluria Type 1. *Nucleic Acid Ther.* **2019**, *29* (2), 104–113.

7. Bibliography

- [79] Smid, B. E.; Aerts, J. M. F. G.; Boot, R. G.; Linthorst, G. E.; Hollak, C. E. M. Pharmacological Small Molecules for the Treatment of Lysosomal Storage Disorders. *Expert Opin. Investig. Drugs* **2010**, *19* (11), 1367–1379.
- [80] Martin-Higueras, C.; Luis-Lima, S.; Salido, E. Glycolate Oxidase Is a Safe and Efficient Target for Substrate Reduction Therapy in a Mouse Model of Primary Hyperoxaluria Type I. *Mol. Ther. J. Am. Soc. Gene Ther.* **2016**, *24* (4), 719–725.
- [81] Frishberg, Y.; Zeharia, A.; Lyakhovetsky, R.; Bargal, R.; Belostotsky, R. Mutations in HAO1 Encoding Glycolate Oxidase Cause Isolated Glycolic Aciduria. *J. Med. Genet.* **2014**, *51* (8), 526–529.
- [82] Wang, M.; Xu, M.; Long, Y.; Fargue, S.; Southall, N.; Hu, X.; McKew, J. C.; Danpure, C. J.; Zheng, W. High Throughput Cell-Based Assay for Identification of Glycolate Oxidase Inhibitors as a Potential Treatment for Primary Hyperoxaluria Type 1. *Sci. Rep.* **2016**, *6*, 34060.
- [83] Pelkonen, R.; Kivirikko, K. I. Hydroxyprolinemia* an Apparently Harmless Familial Metabolic Disorder. *N. Engl. J. Med.* **1970**, *283* (9), 451–456.
- [84] Staufner, C.; Haack, T. B.; Feyh, P.; Gramer, G.; Raga, D. E.; Terrile, C.; Sauer, S.; Okun, J. G.; Fang-Hoffmann, J.; Mayatepek, E.; et al. Genetic Cause and Prevalence of Hydroxyprolinemia. *J. Inherit. Metab. Dis.* **2016**, *39* (5), 625–632.
- [85] Lowther, W. T.; Holmes, R. P. Hypdh Inhibitors and Methods of Use for the Treatment of Kidney Stones. WO2016123012A1, August 4, **2016**.
- [86] Brown, B. D.; Dudek, H. T. Methods and Compositions for the Specific Inhibition of Glycolate Oxidase (*Hao1*) by Double-Stranded Rna. WO2015100436A1, July 2, **2015**.
- [87] Dutta, C.; Avitahl-Curtis, N.; Pursell, N.; Larsson Cohen, M.; Holmes, B.; Diwanji, R.; Zhou, W.; Apponi, L.; Koser, M.; Ying, B.; et al. Inhibition of Glycolate Oxidase With Dicer-Substrate siRNA Reduces Calcium Oxalate Deposition in a Mouse Model of Primary Hyperoxaluria Type 1. *Mol. Ther. J. Am. Soc. Gene Ther.* **2016**, *24* (4), 770–778.
- [88] Liebow, A.; Li, X.; Racie, T.; Hettinger, J.; Bettencourt, B. R.; Najafian, N.; Haslett, P.; Fitzgerald, K.; Holmes, R. P.; Erbe, D.; et al. An Investigational RNAi Therapeutic Targeting Glycolate Oxidase Reduces Oxalate Production in Models of Primary Hyperoxaluria. *J. Am. Soc. Nephrol. JASN* **2017**, *28* (2), 494–503.
- [89] Querbes, W.; Fitzgerald, K.; Bettencourt, B.; Liebow, A.; Erbe, D. Compositions and Methods for Inhibition of *Hao1* (Hydroxyacid Oxidase 1 (Glycolate Oxidase)) Gene Expression. WO/2016/057893, April 15, **2016**.
- [90] Hinkle, G. Polynucleotide Agents Targeting Hydroxyacid Oxidase (Glycolate Oxidase, *Hao1*) and Methods of Use Thereof. WO2016205323A8, February 16, **2017**.
- [91] Zabaleta, N.; Barberia, M.; Martin-Higueras, C.; Zapata-Linares, N.; Betancor, I.; Rodriguez, S.; Martinez-Turrillas, R.; Torella, L.; Vales, A.; Olagüe, C.; et al. CRISPR/Cas9-Mediated Glycolate Oxidase Disruption Is an Efficacious and Safe Treatment for Primary Hyperoxaluria Type I. *Nat. Commun.* **2018**, *9* (1), 5454.
- [92] Murray, M. S.; Holmes, R. P.; Lowther, W. T. Active Site and Loop 4 Movements within Human Glycolate Oxidase: Implications for Substrate Specificity and Drug Design. *Biochemistry* **2008**, *47* (8), 2439–2449.
- [93] Pennati, A.; Gadda, G. Involvement of Ionizable Groups in Catalysis of Human Liver Glycolate Oxidase. *J. Biol. Chem.* **2009**, *284* (45), 31214–31222.
- [94] Stenberg, K.; Lindqvist, Y. Three-Dimensional Structures of Glycolate Oxidase with Bound Active-Site Inhibitors. *Protein Sci.* **1997**, *6* (5), 1009–1015.
- [95] Zelitch, I.; Ochoa, S. Oxidation and Reduction of Glycolic and Glyoxylic Acids in Plants I. Glycolic and Oxidase. *J. Biol. Chem.* **1953**, *201* (2), 707–718.
- [96] Lindqvist, Y.; Brändén, C. I. Preliminary Crystallographic Data for Glycolate Oxidase from Spinach. *J. Biol. Chem.* **1979**, *254* (15), 7403–7404.

- [97] Williams, E.; Cregeen, D.; Rumsby, G. Identification and Expression of a cDNA for Human Glycolate Oxidase. *Biochim. Biophys. Acta BBA - Gene Struct. Expr.* **2000**, *1493* (1), 246–248.
- [98] Vignaud, C.; Pietrancosta, N.; Williams, E. L.; Rumsby, G.; Lederer, F. Purification and Characterization of Recombinant Human Liver Glycolate Oxidase. *Arch. Biochem. Biophys.* **2007**, *465* (2), 410–416.
- [99] Frederick, E. W.; Rabkin, M. T.; Richie, R. H.; Smith, L. H. Studies on Primary Hyperoxaluria. *N. Engl. J. Med.* **1963**, *269* (16), 821–829.
- [100] Bourhis, J.-M.; Vignaud, C.; Pietrancosta, N.; Guéritte, F.; Guénard, D.; Lederer, F.; Lindqvist, Y. Structure of Human Glycolate Oxidase in Complex with the Inhibitor 4-Carboxy-5-[(4-Chlorophenyl)Sulfanyl]-1,2,3-Thiadiazole. *Acta Crystallograph. Sect. F Struct. Biol. Cryst. Commun.* **2009**, *65* (12), 1246–1253.
- [101] Chen, Z.; Vignaud, C.; Jaafar, A.; Lévy, B.; Guéritte, F.; Guénard, D.; Lederer, F.; Mathews, F. S. High Resolution Crystal Structure of Rat Long Chain Hydroxy Acid Oxidase in Complex with the Inhibitor 4-Carboxy-5-[(4-Chlorophenyl)Sulfanyl]-1,2, -Thiadiazole. Implications for Inhibitor Specificity and Drug Design. *Biochimie* **2012**, *94* (5), 1172–1179.
- [102] Kameda, K.; Yanagawa, M.; Kawamura, J. Effects of D,L-2-Hydroxy-3-Butynoic Acid, an Inhibitor of Glycolate Oxidase, on Oxalogenesis from Glycolate *in Vivo*. *Biomed. Res.* **2000**, *21*, 139–144.
- [103] Randall, W. C.; Streeter, K. B.; Cresson, E. L.; Schwam, H.; Michelson, S. R.; Anderson, P. S.; Cragoe, E. J.; Williams, H. W. R.; Eichler, E.; Rooney, C. S. Quantitative Structure-Activity Relationships Involving the Inhibition of Glycolic Acid Oxidase by Derivatives of Glycolic and Glyoxylic Acids. *J. Med. Chem.* **1979**, *22* (6), 608–614.
- [104] Schwam, H.; Michelson, S.; Randall, W. C.; Sondey, J. M.; Hirschmann, R. Purification and Characterization of Human Liver Glycolate Oxidase. Molecular Weight, Subunit, and Kinetic Properties. *Biochemistry* **1979**, *18* (13), 2828–2833.
- [105] Williams, H. W. R.; Eichler, E.; Randall, W. C.; Rooney, C. S.; Cragoe, E. J.; Streeter, K. B.; Schwam, H.; Michelson, S. R.; Patchett, A. A.; Taub, D. Inhibitors of Glycolic Acid Oxidase. 4-Substituted-2,4-Dioxobutanoic Acid Derivatives. *J. Med. Chem.* **1983**, *26* (8), 1196–1200.
- [106] Dawson, D. M.; Goodfriend, T. L.; Kaplan, N. O.; Kaplan, N. O. Lactic Dehydrogenases: Functions of the Two Types. *Science* **1964**, *143* (3609), 929–933.
- [107] Read, J. A.; Winter, V. J.; Eszes, C. M.; Sessions, R. B.; Brady, R. L. Structural Basis for Altered Activity of M- and H-Isozyme Forms of Human Lactate Dehydrogenase. *Proteins Struct. Funct. Bioinforma.* **2001**, *43* (2), 175–185.
- [108] Rani, R.; Kumar, V. Recent Update on Human Lactate Dehydrogenase Enzyme 5 (HLDH5) Inhibitors: A Promising Approach for Cancer Chemotherapy. *J. Med. Chem.* **2016**, *59* (2), 487–496.
- [109] Warburg, O. On the Origin of Cancer Cells. *Science* **1956**, *123* (3191), 309–314.
- [110] Granchi, C.; Roy, S.; Giacomelli, C.; Macchia, M.; Tuccinardi, T.; Martinelli, A.; Lanza, M.; Betti, L.; Giannaccini, G.; Lucacchini, A.; et al. Discovery of *N*-Hydroxyindole-Based Inhibitors of Human Lactate Dehydrogenase Isoform A (LDH-A) as Starvation Agents against Cancer Cells. *J. Med. Chem.* **2011**, *54* (6), 1599–1612.
- [111] Doherty, J. R.; Cleveland, J. L. Targeting Lactate Metabolism for Cancer Therapeutics. *J. Clin. Invest.* **2013**, *123* (9), 3685–3692.
- [112] Kanno, T.; Sudo, K.; Maekawa, M.; Nishimura, Y.; Ukita, M.; Fukutake, K. Lactate Dehydrogenase M-Subunit Deficiency: A New Type of Hereditary Exertional Myopathy. *Clin. Chim. Acta* **1988**, *173* (1), 89–98.
- [113] Maekawa, M.; Sudo, K.; Kanno, T.; Li, S. S.-L. Molecular Characterization of Genetic Mutation in Human Lactate Dehydrogenase-A (M) Deficiency. *Biochem. Biophys. Res. Commun.* **1990**, *168* (2), 677–682.

7. Bibliography

- [114] Choi, S.; Beeler, A. B.; Pradhan, A.; Watkins, E. B.; Rimoldi, J. M.; Tekwani, B.; Avery, M. A. Generation of Oxamic Acid Libraries: Antimalarials and Inhibitors of Plasmodium Falciparum Lactate Dehydrogenase. *J. Comb. Chem.* **2007**, *9* (2), 292–300.
- [115] Shi, Y.; Pinto, B. M. Human Lactate Dehydrogenase A Inhibitors: A Molecular Dynamics Investigation. *PLOS ONE* **2014**, *9* (1), e86365.
- [116] Lai, C.; Pursell, N.; Gierut, J.; Saxena, U.; Zhou, W.; Dills, M.; Diwanji, R.; Dutta, C.; Koser, M.; Nazef, N.; et al. Specific Inhibition of Hepatic Lactate Dehydrogenase Reduces Oxalate Production in Mouse Models of Primary Hyperoxaluria. *Mol. Ther.* **2018**, *26* (8), 1983–1995.
- [117] Wood, K. D.; Holmes, R. P.; Erbe, D.; Liebow, A.; Fargue, S.; Knight, J. Reduction in Urinary Oxalate Excretion in Mouse Models of Primary Hyperoxaluria by RNA Interference Inhibition of Liver Lactate Dehydrogenase Activity. *Biochim. Biophys. Acta BBA - Mol. Basis Dis.* **2019**.
- [118] Dudal, M. L.; Huguet, L.; Perez, J.; Vandermeersch, S.; Boudierlique, E.; Tang, E.; Martori, C.; Chemaly, N.; Nabbout, R.; Haymann, J.-P.; et al. Stiripentol Protects against Calcium Oxalate Nephrolithiasis and Ethylene Glycol Poisoning. *J. Clin. Invest.* **2019**, *129* (6).
- [119] Sada, N.; Lee, S.; Katsu, T.; Otsuki, T.; Inoue, T. Targeting LDH Enzymes with a Stiripentol Analog to Treat Epilepsy. *Science* **2015**, *347* (6228), 1362–1367.
- [120] Raskin, I.; Ehmann, A.; Melander, W. R.; Meeuse, B. J. D. Salicylic Acid: A Natural Inducer of Heat Production in Arum Lilies. *Science* **1987**, *237* (4822), 1601–1602.
- [121] Malamy, J.; Carr, J. P.; Klessig, D. F.; Raskin, I. Salicylic Acid: A Likely Endogenous Signal in the Resistance Response of Tobacco to Viral Infection. *Science* **1990**, *250* (4983), 1002–1004.
- [122] Métraux, J. P.; Signer, H.; Ryals, J.; Ward, E.; Wyss-Benz, M.; Gaudin, J.; Raschdorf, K.; Schmid, E.; Blum, W.; Inverardi, B. Increase in Salicylic Acid at the Onset of Systemic Acquired Resistance in Cucumber. *Science* **1990**, *250* (4983), 1004–1006.
- [123] Klessig, D. F.; Tian, M.; Choi, H. W. Multiple Targets of Salicylic Acid and Its Derivatives in Plants and Animals. *Front. Immunol.* **2016**, *7*.
- [124] Ekinci, D.; Şentürk, M.; Küfrevioğlu, Ö. İ. Salicylic Acid Derivatives: Synthesis, Features and Usage as Therapeutic Tools. *Expert Opin. Ther. Pat.* **2011**, *21* (12), 1831–1841.
- [125] Mitchell, A. G.; Broadhead, J. F. Hydrolysis of Solubilized Aspirin. *J. Pharm. Sci.* **1967**, *56* (10), 1261–1266.
- [126] Proost, J. H.; Van Imhoff, G. W.; Wesseling, H. Plasma Levels of Acetylsalicylic Acid and Salicylic Acid after Oral Ingestion of Plain and Buffered Acetylsalicylic Acid in Relation to Bleeding Time and Thrombocyte Function. *Pharm. Weekbl.* **1983**, *5* (1), 22–27.
- [127] Vane, J. R. Inhibition of Prostaglandin Synthesis as a Mechanism of Action for Aspirin-like Drugs. *Nature. New Biol.* **1971**, *231* (25), 232–235.
- [128] Mitchell, J. A.; Saunders, M.; Barnes, P. J.; Newton, R.; Belvisi, M. G. Sodium Salicylate Inhibits Cyclo-Oxygenase-2 Activity Independently of Transcription Factor (Nuclear Factor KB) Activation: Role of Arachidonic Acid. *Mol. Pharmacol.* **1997**, *51* (6), 907–912.
- [129] Mitchell, J. A.; Warner, T. D. Cyclo-Oxygenase-2: Pharmacology, Physiology, Biochemistry and Relevance to NSAID Therapy. *Br. J. Pharmacol.* **1999**, *128* (6), 1121–1132.
- [130] Chandrasekharan, N. V.; Dai, H.; Roos, K. L. T.; Evanson, N. K.; Tomsik, J.; Elton, T. S.; Simmons, D. L. COX-3, a Cyclooxygenase-1 Variant Inhibited by Acetaminophen and Other Analgesic/Antipyretic Drugs: Cloning, Structure, and Expression. *Proc. Natl. Acad. Sci. U. S. A.* **2002**, *99* (21), 13926–13931.

- [131] Smith, M. J. H.; Ford-Hutchinson, A. W.; Elliott, P. N. C. Prostaglandins and the Anti-Inflammatory Activities of Aspirin and Sodium Salicylate. *J. Pharm. Pharmacol.* **1975**, *27* (7), 473–478.
- [132] Mitchell, J. A.; Akarasereenont, P.; Thiemermann, C.; Vane, J. R. Selectivity of Nonsteroidal Antiinflammatory Drugs as Inhibitors of Constitutive and Inducible Cyclooxygenase. *Proc Natl Acad Sci USA* **1993**, *90* (24), 11693–11697.
- [133] Giuliano, F.; Mitchell, J. A.; Warner, T. D. Sodium Salicylate Inhibits Prostaglandin Formation without Affecting the Induction of Cyclooxygenase-2 by Bacterial Lipopolysaccharide *in Vivo*. *J. Pharmacol. Exp. Ther.* **2001**, *299* (3), 894–900.
- [134] Kopp, E.; Ghosh, S. Inhibition of NF-Kappa B by Sodium Salicylate and Aspirin. *Science* **1994**, *265* (5174), 956–959.
- [135] Chemler, S. R.; Trauner, D.; Danishefsky, S. J. The B-Alkyl Suzuki-Miyaura Cross-Coupling Reaction: Development, Mechanistic Study, and Applications in Natural Product Synthesis. *Angew. Chem. Int. Ed Engl.* **2001**, *40* (24), 4544–4568.
- [136] Hassan, J.; Sévignon, M.; Gozzi, C.; Schulz, E.; Lemaire, M. Aryl-Aryl Bond Formation One Century after the Discovery of the Ullmann Reaction. *Chem. Rev.* **2002**, *102* (5), 1359–1470.
- [137] Hooshmand, S. E.; Heidari, B.; Sedghi, R.; Varma, R. S. Recent Advances in the Suzuki–Miyaura Cross-Coupling Reaction Using Efficient Catalysts in Eco-Friendly Media. *Green Chem.* **2019**, *21* (3), 381–405.
- [138] Littke, A. F.; Fu, G. C. Palladium-Catalyzed Coupling Reactions of Aryl Chlorides. *Angew. Chem. Int. Ed.* **2002**, *41* (22), 4176–4211.
- [139] Lloyd-Williams, P.; Giralt, E. Atropisomerism, Biphenyls and the Suzuki Coupling: Peptide Antibiotics. *Chem. Soc. Rev.* **2001**, *30* (3), 145–157.
- [140] Miyaura, Norio.; Suzuki, Akira. Palladium-Catalyzed Cross-Coupling Reactions of Organoboron Compounds. *Chem. Rev.* **1995**, *95* (7), 2457–2483.
- [141] Nicolaou, K. C.; Bulger, P. G.; Sarlah, D. Palladium-Catalyzed Cross-Coupling Reactions in Total Synthesis. *Angew. Chem. Int. Ed.* **2005**, *44* (29), 4442–4489.
- [142] Phan, N. T. S.; Van Der Sluys, M.; Jones, C. W. On the Nature of the Active Species in Palladium Catalyzed Mizoroki–Heck and Suzuki–Miyaura Couplings – Homogeneous or Heterogeneous Catalysis, A Critical Review. *Adv. Synth. Catal.* **2006**, *348* (6), 609–679.
- [143] Rocard, L.; Hudhomme, P. Recent Developments in the Suzuki–Miyaura Reaction Using Nitroarenes as Electrophilic Coupling Reagents. *Catalysts* **2019**, *9* (3), 213.
- [144] Sellars, J. D.; Steel, P. G. Transition Metal-Catalysed Cross-Coupling Reactions of P-Activated Enols. *Chem. Soc. Rev.* **2011**, *40* (10), 5170–5180.
- [145] Miyaura, N.; Yamada, K.; Suzuki, A. A New Stereospecific Cross-Coupling by the Palladium-Catalyzed Reaction of 1-Alkenylboranes with 1-Alkenyl or 1-Alkynyl Halides. *Tetrahedron Lett.* **1979**, *20* (36), 3437–3440.
- [146] Suzuki, A. Cross-Coupling Reactions Of Organoboranes: An Easy Way To Construct C-C Bonds (Nobel Lecture). *Angew. Chem. Int. Ed.* **2011**, *50* (30), 6722–6737.
- [147] Miyaura, N.; Suzuki, A. Stereoselective Synthesis of Arylated (*E*)-Alkenes by the Reaction of Alk-1-Enylboranes with Aryl Halides in the Presence of Palladium Catalyst. *J. Chem. Soc. Chem. Commun.* **1979**, (19), 866–867.
- [148] Miyaura, N.; Yanagi, T.; Suzuki, A. The Palladium-Catalyzed Cross-Coupling Reaction of Phenylboronic Acid with Haloarenes in the Presence of Bases. *Synth. Commun.* **1981**, *11* (7), 513–519.
- [149] Suzuki, A. Synthetic Studies via the Cross-Coupling Reaction of Organoboron Derivatives with Organic Halides. *Pure Appl. Chem.* **1991**, *63* (3), 419–422.

7. Bibliography

- [150] Suzuki, A. Recent Advances in the Cross-Coupling Reactions of Organoboron Derivatives with Organic Electrophiles, 1995–1998. *J. Organomet. Chem.* **1999**, 576 (1–2), 147–168.
- [151] Carey, F. A.; Sundberg, R. J. *Advanced Organic Chemistry: Part B: Reaction and Synthesis*, 5th ed.; Springer US, **2007**.
- [152] Peng, Y.-Y.; Liu, J.; Lei, X.; Yin, Z. Room-Temperature Highly Efficient Suzuki–Miyaura Reactions in Water in the Presence of Stilbazo. *Green Chem.* **2010**, 12 (6), 1072–1075.
- [153] Peris, E.; Crabtree, R. H. Recent Homogeneous Catalytic Applications of Chelate and Pincer *N*-Heterocyclic Carbenes. *Coord. Chem. Rev.* **2004**, 248 (21), 2239–2246.
- [154] Qiu, H.; Sarkar, S. M.; Lee, D.-H.; Jin, M.-J. Highly Effective Silica Gel-Supported *N*-Heterocyclic Carbene–Pd Catalyst for Suzuki–Miyaura Coupling Reaction. *Green Chem.* **2008**, 10 (1), 37–40.
- [155] Ma, J.; Cui, X.; Zhang, B.; Song, M.; Wu, Y. Ferrocenylimidazoline Palladacycles: Efficient Phosphine-Free Catalysts for Suzuki–Miyaura Cross-Coupling Reaction. *Tetrahedron* **2007**, 63 (25), 5529–5538.
- [156] Zhang, J.; Zhao, L.; Song, M.; Mak, T. C. W.; Wu, Y. Highly Efficient Cyclopalladated Ferrocenylimine Catalyst for Suzuki Cross-Coupling Reaction of 3-Pyridylboronic Pinacol Ester with Aryl Halides. *J. Organomet. Chem.* **2006**, 691 (6), 1301–1306.
- [157] Li, J.-H.; Liu, W.-J. Dabco as an Inexpensive and Highly Efficient Ligand for Palladium-Catalyzed Suzuki–Miyaura Cross-Coupling Reaction. *Org. Lett.* **2004**, 6 (16), 2809–2811.
- [158] Li, J.-H.; Liu, W.-J.; Xie, Y.-X. Recyclable and Reusable Pd(OAc)₂/DABCO/PEG-400 System for Suzuki–Miyaura Cross-Coupling Reaction. *J. Org. Chem.* **2005**, 70 (14), 5409–5412.
- [159] Bedford, R. B.; Cazin, C. S. J. Highly Active Catalysts for the Suzuki Coupling of Aryl Chlorides. *Chem. Commun.* **2001**, No. 17, 1540–1541.
- [160] Wu, K.-M.; Huang, C.-A.; Peng, K.-F.; Chen, C.-T. Palladacycles Bearing Pendant Benzamidinate Ligands as Catalysts for the Suzuki and Heck Coupling Reactions. *Tetrahedron* **2005**, 61 (41), 9679–9687.
- [161] Mukherjee, A.; Sarkar, A. New Pyrazole-Tethered Schiff's Bases as Ligands for the Suzuki Reaction. *Tetrahedron Lett.* **2005**, 46 (1), 15–18.
- [162] Shen, C.; Shen, H.; Yang, M.; Xia, C.; Zhang, P. A Novel D-Glucosamine-Derived Pyridyl-Triazole@palladium Catalyst for Solvent-Free Mizoroki–Heck Reactions and Its Application in the Synthesis of Axitinib. *Green Chem.* **2014**, 17 (1), 225–230.
- [163] Zhang, G.; Luan, Y.; Han, X.; Wang, Y.; Wen, X.; Ding, C.; Gao, J. A Palladium Complex with Functionalized β -Cyclodextrin: A Promising Catalyst Featuring Recognition Abilities for Suzuki–Miyaura Coupling Reactions in Water. *Green Chem.* **2013**, 15 (8), 2081–2085.
- [164] Silva, J. F. M. da; Perez, A. F. Y.; Almeida, N. P. de. An Efficient and New Protocol for Phosphine-Free Suzuki Coupling Reaction Using Palladium-Encapsulated and Air-Stable MIDA Boronates in an Aqueous Medium. *RSC Adv.* **2014**, 4 (53), 28148–28155.
- [165] Silva, J. F. M. da; Perez, A. F. Y.; Almeida, N. P. de. Phosphine-Free Suzuki Cross-Coupling Reaction Using an Efficient and Reusable Pd Catalyst in an Aqueous Medium Under Microwave Irradiation. *Synth. Commun.* **2015**, 45 (17), 1995–2004.
- [166] Badone, D.; Baroni, M.; Cardamone, R.; Ielmini, A.; Guzzi, U. Highly Efficient Palladium-Catalyzed Boronic Acid Coupling Reactions in Water: Scope and Limitations. *J. Org. Chem.* **1997**, 62 (21), 7170–7173.

- [167] Wallow, T. I.; Novak, B. M. Highly Efficient and Accelerated Suzuki Aryl Couplings Mediated by Phosphine-Free Palladium Sources. *J. Org. Chem.* **1994**, *59* (17), 5034–5037.
- [168] Arcadi, A.; Cerichelli, G.; Chiarini, M.; Correa, M.; Zorzan, D. A Mild and Versatile Method for Palladium-Catalyzed Cross-Coupling of Aryl Halides in Water and Surfactants. *Eur. J. Org. Chem.* **2003**, *2003* (20), 4080–4086.
- [169] Dupuis, C.; Adiey, K.; Charruault, L.; Michelet, V.; Savignac, M.; Genêt, J.-P. Suzuki Cross-Coupling of Arylboronic Acids Mediated by a Hydrosoluble Pd(0)/TPPTS Catalyst. *Tetrahedron Lett.* **2001**, *42* (37), 6523–6526.
- [170] Leadbeater, N. E. Fast, Easy, Clean Chemistry by Using Water as a Solvent and Microwave Heating: The Suzuki Coupling as an Illustration. *Chem. Commun.* **2005**, (23), 2881–2902.
- [171] Moore, L. R.; Shaughnessy, K. H. Efficient Aqueous-Phase Heck and Suzuki Couplings of Aryl Bromides Using Tri(4,6-Dimethyl-3-Sulfonatophenyl)Phosphine Trisodium Salt (TXPTS). *Org. Lett.* **2004**, *6* (2), 225–228.
- [172] Uozumi, Y.; Nakai, Y. An Amphiphilic Resin-Supported Palladium Catalyst for High-Throughput Cross-Coupling in Water. *Org. Lett.* **2002**, *4* (17), 2997–3000.
- [173] Abdel-Magid, A. F.; Mehrman, S. J. A Review on the Use of Sodium Triacetoxyborohydride in the Reductive Amination of Ketones and Aldehydes. *Org. Process Res. Dev.* **2006**, *10* (5), 971–1031.
- [174] Vollhardt, P.; Schore, N. *Organic Chemistry: Structure and Function*, 8th ed.; W. H. Freeman: New York, **2018**.
- [175] Cho, B. T.; Kang, S. K. Direct and Indirect Reductive Amination of Aldehydes and Ketones with Solid Acid-Activated Sodium Borohydride under Solvent-Free Conditions. *Tetrahedron* **2005**, *61* (24), 5725–5734.
- [176] Rylander, P. N. *Hydrogenation Methods*; Academic Press: New York, **1985**.
- [177] Tarasevich, V. A.; Kozlov, N. G. Reductive Amination of Oxygen-Containing Organic Compounds. *Russ. Chem. Rev.* **1999**, *68* (1), 55–72.
- [178] Schellenberg, K. A. The Synthesis of Secondary and Tertiary Amines by Borohydride Reduction. *J. Org. Chem.* **1963**, *28* (11), 3259–3261.
- [179] Borch, R. F.; Bernstein, M. D.; Durst, H. D. Cyanohydridoborate Anion as a Selective Reducing Agent. *J. Am. Chem. Soc.* **1971**, *93* (12), 2897–2904.
- [180] Abdel-Magid, A. F.; Carson, K. G.; Harris, B. D.; Maryanoff, C. A.; Shah, R. D. Reductive Amination of Aldehydes and Ketones with Sodium Triacetoxyborohydride. Studies on Direct and Indirect Reductive Amination Procedures. *J. Org. Chem.* **1996**, *61* (11), 3849–3862.
- [181] Abdel-Magid, A. F.; Harris, B. D.; Maryanoff, C. A. A Reductive Amination/Lactamization Procedure Using Borohydride Reagents. *Synlett* **1994**, *1*, 81.
- [182] Moya-Garzon, M. D. Síntesis de Derivados de *N*-Acil-4-Fenilnilina como Inhibidores de la Enzima Glicolato Oxidasa, Universidad de Granada, **2014**.
- [183] Katritzky, A. R.; Tala, S. R.; Lu, H.; Vakulenko, A. V.; Chen, Q.-Y.; Sivapackiam, J.; Pandya, K.; Jiang, S.; Debnath, A. K. Design, Synthesis, and Structure–Activity Relationship of a Novel Series of 2-Aryl 5-(4-Oxo-3-Phenethyl-2-Thioxothiazolidinylidene)methyl)Furans as HIV-1 Entry Inhibitors. *J. Med. Chem.* **2009**, *52* (23), 7631–7639.
- [184] Hosoya, T.; Aoyama, H.; Ikemoto, T.; Kihara, Y.; Hiramatsu, T.; Endo, M.; Suzuki, M. Dantrolene Analogues Revisited: General Synthesis and Specific Functions Capable of Discriminating Two Kinds of Ca²⁺ Release from Sarcoplasmic Reticulum of Mouse Skeletal Muscle. *Bioorg. Med. Chem.* **2003**, *11* (5), 663–673.
- [185] Moya-Garzón, M. D.; Martín Higuera, C.; Peñalver, P.; Romera, M.; Fernandes, M. X.; Franco-Montalbán, F.; Gómez-Vidal, J. A.; Salido, E.; Díaz-Gavilán, M.

- Salicylic Acid Derivatives Inhibit Oxalate Production in Mouse Hepatocytes with Primary Hyperoxaluria Type 1. *J. Med. Chem.* **2018**, *61* (16), 7144–7167.
- [186] Xie, Y.; Liu, Y.; Gong, G.; Rinderspacher, A.; Deng, S.-X.; Smith, D. H.; Toebben, U.; Tzilianos, E.; Branden, L.; Vidović, D.; et al. Discovery of a Novel Submicromolar Inhibitor of the Lymphoid Specific Tyrosine Phosphatase. *Bioorg. Med. Chem. Lett.* **2008**, *18* (9), 2840–2844.
- [187] Jones, H.; Fordice, M. W.; Greenwald, R. B.; Hannah, J.; Jacobs, A.; Ruyle, W. V.; Walford, G. L.; Shen, T. Y. Synthesis and Analgesic-Anti-inflammatory Activity of Some 4- and 5-Substituted Heteroarylsalicylic Acids. *J. Med. Chem.* **1978**, *21* (11), 1100–1104.
- [188] Hathway, T.; Chernyshov, D. L.; Jenks, W. S. Selectivity in the Photo-Fenton and Photocatalytic Hydroxylation of Biphenyl-4-Carboxylic Acid and Derivatives (Viz. 4-Phenylsalicylic Acid and 5-Phenylsalicylic Acid). *J. Phys. Org. Chem.* **2011**, *24* (12), 1151–1156.
- [189] Hunter, C. A.; Sanders, J. K. M. The Nature of π - π Interactions. *J. Am. Chem. Soc.* **1990**, *112* (14), 5525–5534.
- [190] Wang, M.; Xu, M.; Long, Y.; Fargue, S.; Southall, N.; Hu, X.; McKew, J. C.; Danpure, C. J.; Zheng, W. High Throughput Cell-Based Assay for Identification of Glycolate Oxidase Inhibitors as a Potential Treatment for Primary Hyperoxaluria Type 1. *Sci. Rep.* **2016**, *6*, 34060.
- [191] Brown, W. H.; Hutchinson, B. J. Intermediates in the Cycloanhydrotetramerization of Furan with Aliphatic and Alicyclic Ketones. *Can. J. Chem.* **1978**, *56* (5), 617–621.
- [192] Choura, M.; Belgacem, N. M.; Gandini, A. Acid-Catalyzed Polycondensation of Furfuryl Alcohol: Mechanisms of Chromophore Formation and Cross-Linking. *Macromolecules* **1996**, *29* (11), 3839–3850.
- [193] Sacia, E. R.; Balakrishnan, M.; Bell, A. T. Biomass Conversion to Diesel via the Etherification of Furanyl Alcohols Catalyzed by Amberlyst-15. *J. Catal.* **2014**, *313*, 70–79.
- [194] Kim, T.; Assary, R. S.; Pauls, R. E.; Marshall, C. L.; Curtiss, L. A.; Stair, P. C. Thermodynamics and Reaction Pathways of Furfuryl Alcohol Oligomer Formation. *Catal. Commun.* **2014**, *46*, 66–70.
- [195] Rücker, G.; Neugebauer, M.; Neugebauer, M. Zur chemischen Stabilität von Furfenorex und analogen Modells-substanzen. *Arch. Pharm. (Weinheim)* **1986**, *319* (4), 317–324.
- [196] Smith, E.; Collins, I. Photoaffinity Labeling in Target- and Binding-Site Identification. *Future Med. Chem.* **2015**, *7* (2), 159–183.
- [197] Sumranjit, J.; Chung, S. J. Recent Advances in Target Characterization and Identification by Photoaffinity Probes. *Molecules* **2013**, *18* (9), 10425–10451.
- [198] Moran, J. H.; Schnellmann, R. G. A Rapid β -NADH-Linked Fluorescence Assay for Lactate Dehydrogenase in Cellular Death. *J. Pharmacol. Toxicol. Methods* **1996**, *36* (1), 41–44.
- [199] Rupiani, S.; Buonfiglio, R.; Manerba, M.; Di Ianni, L.; Vettraino, M.; Giacomini, E.; Masetti, M.; Falchi, F.; Di Stefano, G.; Roberti, M.; et al. Identification of *N*-Acyldiazone Derivatives as Novel Lactate Dehydrogenase A Inhibitors. *Eur. J. Med. Chem.* **2015**, *101*, 63–70.
- [200] Dragovich, P. S.; Fauber, B. P.; Boggs, J.; Chen, J.; Corson, L. B.; Ding, C. Z.; Eigenbrot, C.; Ge, H.; Giannetti, A. M.; Hunsaker, T.; et al. Identification of Substituted 3-Hydroxy-2-Mercaptocyclohex-2-Enones as Potent Inhibitors of Human Lactate Dehydrogenase. *Bioorg. Med. Chem. Lett.* **2014**, *24* (16), 3764–3771.
- [201] Ramsay, R. R.; Popovic-Nikolic, M. R.; Nikolic, K.; Uliassi, E.; Bolognesi, M. L. A Perspective on Multi-Target Drug Discovery and Design for Complex Diseases. *Clin. Transl. Med.* **2018**, *7*.

- [202] Narumi, T.; Ochiai, C.; Yoshimura, K.; Harada, S.; Tanaka, T.; Nomura, W.; Arai, H.; Ozaki, T.; Ohashi, N.; Matsushita, S.; et al. CD4 Mimics Targeting the HIV Entry Mechanism and Their Hybrid Molecules with a CXCR4 Antagonist. *Bioorg. Med. Chem. Lett.* **2010**, *20* (19), 5853–5858.
- [203] Huang, C.; Yin, Q.; Meng, J.; Zhu, W.; Yang, Y.; Qian, X.; Xu, Y. Versatile Probes for the Selective Detection of Vicinal-Dithiol-Containing Proteins: Design, Synthesis, and Application in Living Cells. *Chem. – Eur. J.* **2013**, *19* (24), 7739–7747.
- [204] Zhang, Y.; Yang, X.; Yao, Q.; Ma, D. CuI/DMPAO-Catalyzed *N*-Arylation of Acyclic Secondary Amines. *Org. Lett.* **2012**, *14* (12), 3056–3059.
- [205] Matsukawa, S.; Yamamichi, H.; Yamamoto, Y.; Ando, K. Pentacoordinate Organoantimony Compounds That Isomerize by Turnstile Rotation. *J. Am. Chem. Soc.* **2009**, *131* (10), 3418–3419.
- [206] Liu, J.; Ma, R.; Bi, F.; Zhang, F.; Hu, C.; Venter, H.; Semple, S. J.; Ma, S. Novel 5-Methyl-2-Phenylphenanthridium Derivatives as FtsZ-Targeting Antibacterial Agents from Structural Simplification of Natural Product Sanguinarine. *Bioorg. Med. Chem. Lett.* **2018**, *28* (10), 1825–1831.
- [207] Kang, B.; Oh, J. A.; Lee, J. Y.; Rhim, H.; Yune, T. Y.; Park Choo, H.-Y. 3-Benzamides and 3,4,5-Trimethoxyphenyl Amines as Calcium Channel Blockers. *Bioorg. Med. Chem.* **2015**, *23* (18), 6166–6172.
- [208] Everett, R. K.; Wolfe, J. P. Aza-Wittig Rearrangements of *N*-Benzyl and *N*-Allyl Glycine Methyl Esters. Discovery of a Surprising Cascade Aza-Wittig Rearrangement/Hydroboration Reaction. *J. Org. Chem.* **2015**, *80* (18), 9041–9056.
- [209] Hofmann, J.; Jasch, H.; Heinrich, M. R. Oxidative Radical Arylation of Anilines with Arylhydrazines and Dioxygen from Air. *J. Org. Chem.* **2014**, *79* (5), 2314–2320.
- [210] Sato, K.; Miki, T.; Ueda, H. ビアリアル化合物の製造法. WO2007011005A1, January 25, **2007**.
- [211] Imaizumi, H.; Sekiguchi, S.; Matsui, K. Reactions of Aromatic Compounds in Molten Salts. I. Dimerization of Aromatic Amines in a Molten Mixture of AlCl₃–NaCl–KCl. *Bull. Chem. Soc. Jpn.* **1977**, *50* (4), 948–952.
- [212] Roy, P.-P.; D'Souza, K.; Cuperlovic-Culf, M.; Kienesberger, P. C.; Touaibia, M. New Atglistatin Closely Related Analogues: Synthesis and Structure-Activity Relationship towards Adipose Triglyceride Lipase Inhibition. *Eur. J. Med. Chem.* **2016**, *118*, 290–298.
- [213] Zhu, S.-E.; Liu, K.-Q.; Wang, X.-F.; Xia, A.-D.; Wang, G.-W. Synthesis and Properties of Axially Symmetrical Rigid Visible Light-Harvesting Systems Containing [60]Fullerene and Perylenebisimide. *J. Org. Chem.* **2016**, *81* (24), 12223–12231.
- [214] Wang, W.-L.; Chai, S. C.; Ye, Q.-Z. Synthesis and Biological Evaluation of Salicylate-Based Compounds as a Novel Class of Methionine Aminopeptidase Inhibitors. *Bioorg. Med. Chem. Lett.* **2011**, *21* (23), 7151–7154.
- [215] Levy, L. F.; Stephen, H. CXXIII.—4-Aminophthalide and Some Derivatives. *J. Chem. Soc. Resumed* **1931**, 867–871.
- [216] Franchi, L.; Rinaldi, M.; Vignaroli, G.; Innitzer, A.; Radi, M.; Botta, M. Arylation of 2-Furyl 4-Fluorophenyl Ketone: An Extension of Heck Chemistry towards Novel Integrase Inhibitors. *Synthesis* **2010**, *2010* (22), 3927–3933.
- [217] Kumar, K. A.; Raghavendra, K. R. Synthesis and Their Antifungal, Antihelmentic and Dying Properties of Some Novel Azo Dyes. *ResearchGate* **2013**, *3* (2), 275–280.
- [218] Korczynska, M.; Le, D. D.; Younger, N.; Gregori-Puigjané, E.; Tumber, A.; Krojer, T.; Velupillai, S.; Gileadi, C.; Nowak, R. P.; Iwasa, E.; et al. Docking and Linking of Fragments To Discover Jumonji Histone Demethylase Inhibitors. *J. Med. Chem.* **2016**, *59* (4), 1580–1598.

7. Bibliography

- [219] Border, E. C.; Blair, V. L.; Andrews, P. C. An Efficient Microwave Method for the Synthesis of Imines. *Aust. J. Chem.* **2015**, *68* (5), 844–848.
- [220] Jaysekhar, P.; Rao, S. B.; Santhakumari, G. Effect of 5-Substituted Benzylideneaminosalicylic Acid on Carrageenan-Induced Ulcerative Colitis. *Boll. Chim. Farm.* **2004**, *143* (8), 309–313.
- [221] van Veldhoven, J. P. D.; Blad, C. C.; Artsen, C. M.; Klopman, C.; Wolfram, D. R.; Abdelkadir, M. J.; Lane, J. R.; Brussee, J.; IJzerman, A. P. Structure–Activity Relationships of Trans-Substituted-Propenoic Acid Derivatives on the Nicotinic Acid Receptor HCA2 (GPR109A). *Bioorg. Med. Chem. Lett.* **2011**, *21* (9), 2736–2739.
- [222] Noberini, R.; De, S. K.; Zhang, Z.; Wu, B.; Raveendra-Panickar, D.; Chen, V.; Vazquez, J.; Qin, H.; Song, J.; Cosford, N. D. P.; et al. A Disalicylic Acid-Furanyl Derivative Inhibits Ephrin Binding to a Subset of Eph Receptors. *Chem. Biol. Drug Des.* **2011**, *78* (4), 667–678.
- [223] Li, X.; Li, L.; Tang, Y.; Zhong, L.; Cun, L.; Zhu, J.; Liao, J.; Deng, J. Chemoselective Conjugate Reduction of α,β -Unsaturated Ketones Catalyzed by Rhodium Amido Complexes in Aqueous Media. *J. Org. Chem.* **2010**, *75* (9), 2981–2988.
- [224] Salisbury, C. M.; Cravatt, B. F. Activity-Based Probes for Proteomic Profiling of Histone Deacetylase Complexes. *Proc. Natl. Acad. Sci.* **2007**, *104* (4), 1171–1176.
- [225] Zubkov, F. I.; Golubev, V. D.; Zaytsev, V. P.; Bakhanovich, O. V.; Nikitina, E. V.; Khrustalev, V. N.; Aysin, R. R.; Timofeeva, T. V.; Novikov, R. A.; Varlamov, A. V. Ring-Chain Tautomerism in the Products of the Reaction between 5-Substituted Furfurylamines and Anhydrides of α,β -Unsaturated Carboxylic Acids. *Chem. Heterocycl. Compd.* **2016**, *52* (4), 225–236.
- [226] Colpa, D. I.; Lončar, N.; Schmidt, M.; Fraaije, M. W. Creating Oxidase–Peroxidase Fusion Enzymes as a Toolbox for Cascade Reactions. *Chembiochem* **2017**, *18* (22), 2226–2230.
- [227] Salido, E. C.; Li, X. M.; Lu, Y.; Wang, X.; Santana, A.; Roy-Chowdhury, N.; Torres, A.; Shapiro, L. J.; Roy-Chowdhury, J. Alanine–Glyoxylate Aminotransferase-Deficient Mice, a Model for Primary Hyperoxaluria That Responds to Adenoviral Gene Transfer. *Proc. Natl. Acad. Sci.* **2006**, *103* (48), 18249–18254.
- [228] Ogasawara, D.; Deng, H.; Viader, A.; Baggelaar, M. P.; Breman, A.; Dulk, H. den; Nieuwendijk, A. M. C. H. van den; Soethoudt, M.; Wel, T. van der; Zhou, J.; et al. Rapid and Profound Rewiring of Brain Lipid Signaling Networks by Acute Diacylglycerol Lipase Inhibition. *Proc. Natl. Acad. Sci.* **2016**, *113* (1), 26–33.
- [229] Baggelaar, M. P.; Janssen, F. J.; van Esbroeck, A. C. M.; den Dulk, H.; Allarà, M.; Hoogendoorn, S.; McGuire, R.; Florea, B. I.; Meeuwenoord, N.; van den Elst, H.; et al. Development of an Activity-Based Probe and *In Silico* Design Reveal Highly Selective Inhibitors for Diacylglycerol Lipase- α in Brain. *Angew. Chem. Int. Ed.* **2013**, *52* (46), 12081–12085.
- [230] Baggelaar, M. P.; Chameau, P. J. P.; Kantae, V.; Hummel, J.; Hsu, K.-L.; Janssen, F.; van der Wel, T.; Soethoudt, M.; Deng, H.; den Dulk, H.; et al. Highly Selective, Reversible Inhibitor Identified by Comparative Chemoproteomics Modulates Diacylglycerol Lipase Activity in Neurons. *J. Am. Chem. Soc.* **2015**, *137* (27), 8851–8857.
- [231] Soethoudt, M.; Alachouzos, G.; van Rooden, E. J.; Moya-Garzón, M. D.; van den Berg, R. J. B. H. N.; Heitman, L. H.; van der Stelt, M. Development of a Cannabinoid-Based Photoaffinity Probe to Determine the $\Delta^{8/9}$ -Tetrahydrocannabinol Protein Interaction Landscape in Neuroblastoma Cells. *Cannabis Cannabinoid Res.* **2018**, *3* (1), 136–151.